Nasa CR 65580

GPO PRICE $ ____

CFSTI PRICE(S) $ ____

Hard copy (HC) 9.00

Microfiche (MF) .65

ff 653 July 65

An Introduction to Spacecraft Thermal Contro

CONTRACT NO. NAS 9-3349

Submitted to:
NASA MANNED SPACECRAFT CENTER
PRIMARY PROPULSION BRANCH
Houston, Texas

67-30163 (ACCESSION NUMBER)
____ (THRU)
469 (PAGES)
1 (CODE)
CR-65580 (NASA CR OR TMX OR AD NUMBER)
31 (CATEGORY)

[redacted]

FOREWORD

This report entitled "An Introduction to Spacecraft Thermal Control," LR 18901, was prepared by the Lockheed-California Company under NASA Contract NAS 9-3349. Some of the data contained in this report is based on work performed by the Lockheed-California and Lockheed Missiles and Space Companies over the past several years.

Other reports prepared under this contract are:

LR 18899	A Transient Heat Transfer and Thermodynamic Analysis of the Apollo Service Module Propulsion System - Final Report
LR 18900	A Transient Heat Transfer and Thermodynamic Analysis of the Apollo Service Module Propulsion System - Summary Report
LR 18902	Thermal Analyzer Computer Program for the Solution of General Heat Transfer Problems
LR 18903	Thermal Analyzer Computer Program for the Solution of Fluid Storage and Pressurization Problems
LR 18904	Computer Program for the Calculation of Incident Orbital Radiant Heat Flux
LR 18905	Computer Program for the Calculation of Three-Dimensional Configuration Factors.

This report was prepared by Messrs. B. A. Nevelli and H. D. Schultz of the Lockheed-California Company, with the exception of specific portions, which are herein acknowledged. In Section IV, the discussion of ascent heating was contributed by Mr. F. L. Guard of the Lockheed-California Company and the simplified analytical method for calculating orbital heating was developed by the Lockheed Missiles and Space Company. The discussion of fluid storage and pressurization in Section V was prepared by Messrs. P. S. Hirasawa and I. Shuldiner of the Lockheed-California Company. The Lockheed Missiles and

Space Company contributed the thermal control material data contained in Sections VI and VII. The propellant and pressurant properties data in Section VIII and structural materials data in Section IX were compiled by Dr. H. B. Wellman of the Lockheed-California Company.

TABLE OF CONTENTS

TABLE OF CONTENTS (Continued)

TABLE OF CONTENTS (Continued)

TABLE OF CONTENTS (Continued)

LIST OF FIGURES

LIST OF FIGURES (Continued)

LIST OF FIGURES (Continued)

LIST OF FIGURES (Continued)

LIST OF FIGURES (Continued)

LIST OF FIGURES (Continued)

LIST OF FIGURES (Continued)

LIST OF TABLES

LIST OF TABLES (Continued)

LIST OF TABLES (Continued)

I - INTRODUCTION

A typical spacecraft is subjected to ascent heating, direct insolation, planetary reflection and emission, and the extreme cold of deep space. A lunar spacecraft, for example, is exposed to lunar emission which has a maximum intensity at the subsolar point of approximately 400 Btu/hr-ft^2, nearly equivalent to the solar irradiation. Then, as the vehicle enters the lunar shadow, the external heat flux is essentially zero. This wide range of thermal environments creates a complicated temperature control problem, and a difficult challenge to those responsible for the design of the spacecraft thermal control system. The problem is further complicated by the narrow temperature tolerances of many spacecraft components. Also, the same vehicle might carry equipment which requires cryogenic temperatures and other equipment which must operate at refractory temperatures.

To ascertain that all vehicle systems will function within their allowable temperature range, it is necessary to perform a transient heat transfer and thermodynamic analysis of the vehicle, simultaneously accounting for the effects of external heating, internal power dissipation, heat exchange between vehicle components, and heat storage. For a new vehicle or during major modifications to an existing vehicle, the analysis must be performed in steps, with refinements made as the design progresses. Those responsible for spacecraft thermal performance must provide a large portion of data necessary to determine the type of thermal control system required, surface finishes, location of critical components, and even the primary structure.

The prediction of the thermodynamic performance of the propulsion and pressurization systems is particularly important, especially when engine restart capabilities are required. Engine performance varies with the propellant mixture ratio, mixture ratio distribution across the injector, and chamber pressure. Termperature variations in the feed systems, resulting in propellant density and ullage pressure changes, produce deviations in the flow rates and the resultant propellant mixture ratio. Extreme variations of propellant temperature may adversely affect normal injector operation, depending on the propellants used. These temperature variations can also result in a nonuniform mixture ratio distribution across the face of the injector, affecting combustion efficiency and stability. Engine operating life may be reduced by a nonuniform mixture ratio causing local hot spots along the walls of the thrust chamber. Engine valves, controls, and restart capabilities are also sensitive to temperature variations. Excessive temperatures in the region of the engine after shutdown may produce vaporization of residual propellants in the valves or in the feed lines.

The propellant feed system, consisting of the propellants, tankage, and controls, is strongly affected by the thermal environment. Temperature variations within the system determine pressurization utilization and regulation requirements for both pressure-fed and pump-fed propulsion systems. Pressurization requirements are also dependent on the ullage gas temperature and stratification within the propellant tanks.

This report discusses the problems associated with spacecraft thermal control, the currently employed techniques for achieving thermal control, and the analytical procedures required to perform a transient heat transfer and thermodynamic analysis of a space vehicle. Included are thermophysical properties of various structural and insulating materials, fluid thermodynamic properties, and surface finish radiative properties.

II - THE PROBLEM OF THERMAL CONTROL

Proper spacecraft thermal control is achieved when the vehicle and its components are maintained within allowable operating temperatures. These temperatures are influenced by the net thermal energy exchange with the environment, by internal heat sources, and by the heat stored within the spacecraft. The following paragraphs discuss component temperature requirements, the specific nature of the external environment, and the methods for predicting its effects.

SPACECRAFT COMPONENT TEMPERATURE REQUIREMENTS

All spacecraft contain certain components which function properly only if maintained within specific temperature ranges. Many of these components are characterized by narrow temperature tolerances. Storable propellants, for example, must be kept above their freezing point, which is about 20°F for typical fuels such as Aerozine 50. Certain specialized electronic components have temperature limits of 40 to 90°F. Cryogenic fluids must be maintained at or near their boiling point, which is -423°F for hydrogen. Currently typical temperature limits for a number of spacecraft components are shown in Figure 2-1. In the case of hardware, the limits are usually set by the manufacturer. A common procedure is to test the component only at the upper and possibly the lower temperature limits defined in the equipment Specification, and, as a result, the true temperature capabilities of the component are unknown. This is frequently a handicap to the engineer who must then design a thermal control system compatible with unreasonably narrow temperature tolerances.

It is important that components be temperature-qualified under realistic test conditions. Conventional techniques, such as testing in an oven, introduce a heat transfer mode not present in space, viz., free convection. Whenever possible, critical components should be temperature-qualified in a vacuum chamber to eliminate this problem. Another problem the heat transfer engineer encounters is that of obtaining details of "black box" electronic components. The total thermal capacity and heat dissipation of the component

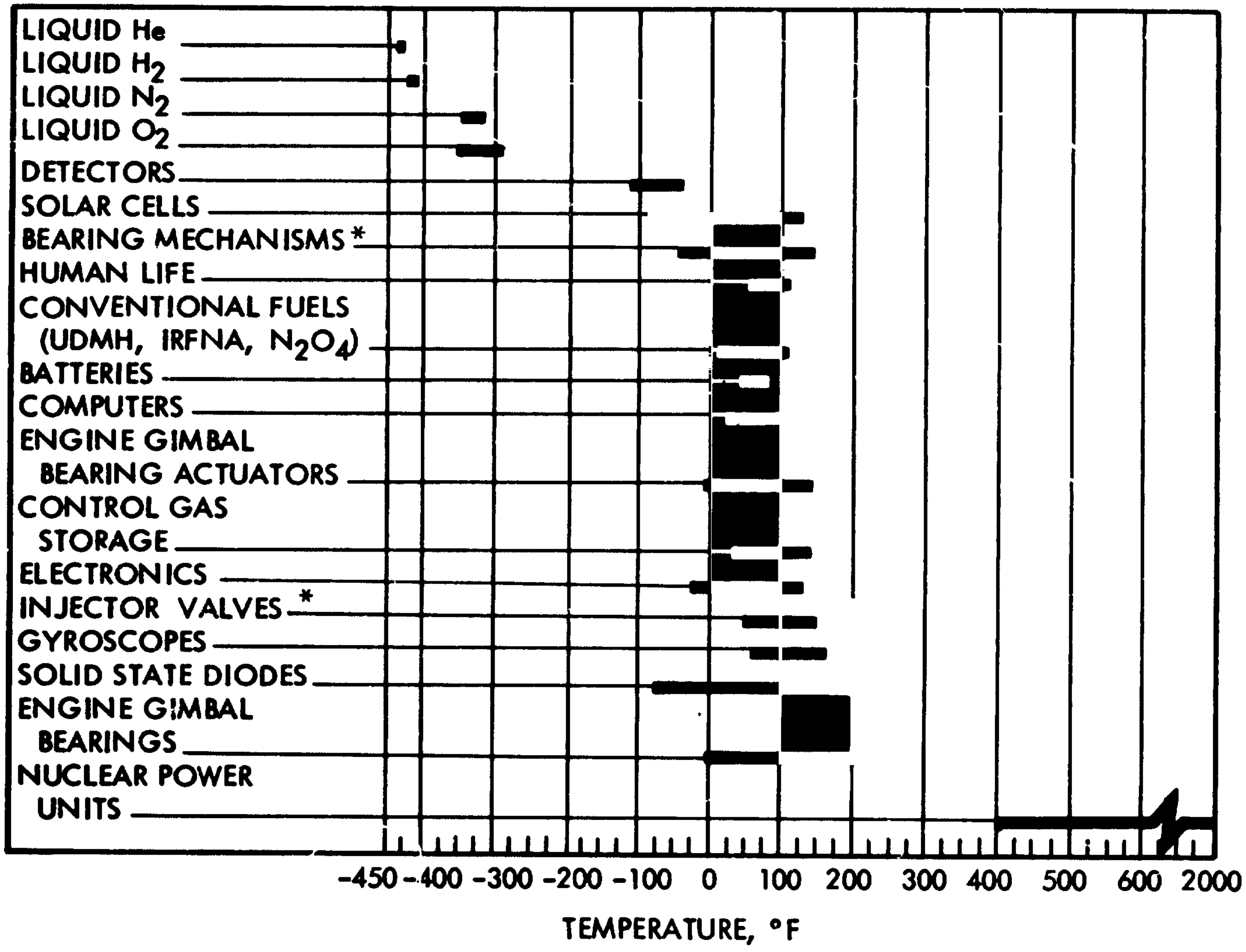

* APPLICABLE TO STORABLE PROPELLANTS

Figure 2-1. Temperature Tolerances of Typical Spacecraft Components are generally known, but not the internal arrangement. A substantial part of the power dissipation may occur in a localized area, and the assumption of a uniform temperature for the component may be grossly invalid. Unless details are available, the manufacturer should be consulted to discuss this problem.

THERMAL BALANCE IN SPACE

Spacecraft thermal balance is the relationship between the thermal energy received from external sources, internal power dissipation, energy reradiated from the exterior surfaces, and the heat stored within the spacecraft. Proper thermal control is achieved when the spacecraft and its components are maintained within allowable operating temperatures. To assure that satisfactory thermal control will be achieved, a complex three-dimensional transient thermal analysis must be performed with all significant modes of heat transfer included. The required thermal balance is illustrated in Figure 2-2.

An energy balance for a typical skin node yields

$$Q_{ER} + Q_{IR} + Q_{IC} + Q_A + P_N = C_N \frac{dT_N}{d\theta} \tag{2-1}$$

where

Q_{ER} = the net radiation interchange with the environment

Q_{IR} = the net radiation interchange with other segments of the vehicle

Q_{IC} = the net conduction exchange with adjacent segments of the vehicle

Q_A = the heat input from aerodynamic sources

P_N = the internal heat generation in the element

C_N = the thermal capacity of the element

T_N = the temperature of the element

θ = time

Aerodynamic heating is experienced only during periods of exit and entry through planetary atmospheres. During orbital and interplanetary phases,

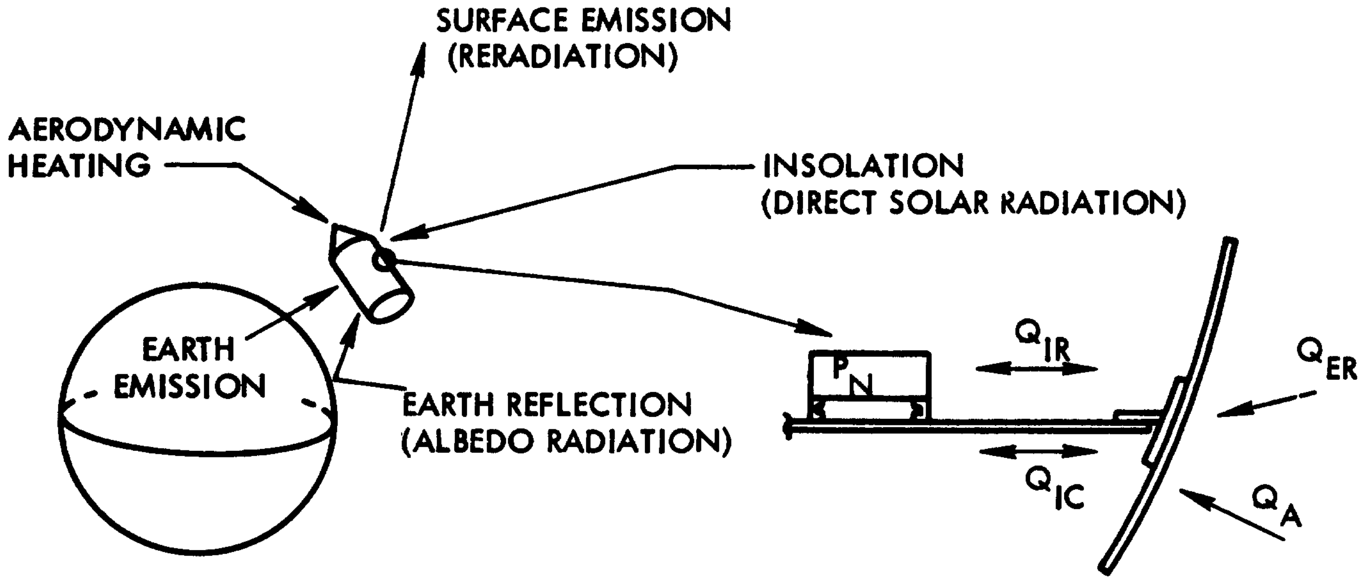

Figure 2-2. Spacecraft Thermal Balance

radiation is the only significant mode of heat transfer between the vehicle and its environment. The thermal analysis must consider radiation from the following sources:

1. Insolation (direct solar radiation)
2. Albedo radiation (solar energy reflected from the planet-atmosphere system)
3. Planetary and atmospheric emission

The magnitude of the incident radiation is essentially a geometry problem involving the relationships between the various sources and the vehicle. The magnitude of the absorbed radiation requires a knowledge of the spectral-energy distribution of the sources and the spectral-radiation characteristics of the vehicle surface.

The net radiant interchange with the environment, Q_{ER}, is given by:

$$Q_{ER} = \alpha_S F_S S + \alpha_E F_E E + \alpha_R F_R R - \epsilon \sigma T_N^4 \qquad (2\text{-}2)$$

where

$\alpha_S F_S S$ = the absorbed insolation

$\alpha_E F_E E$ = the absorbed planetary emission

$\alpha_R F_R R$ = the absorbed albedo radiation

$\epsilon \sigma T_N^4$ = the radiation emitted to space

$\alpha_S, \alpha_E, \alpha_R$ = the surface absorptivity for solar irradiation, planetary emission, and albedo

F_S, F_E, F_R = the configuration factor for solar irradiation, planetary emission, and albedo

S,E,R = the magnitude of the incident solar irradiation, planetary emission and albedo

ϵ, σ = the surface emissivity and the Stefan-Boltzmann constant

For simplified analyses, the surfaces are taken to be diffuse. In addition, it is normally assumed that $\alpha_R = \alpha_S$ and $\alpha_E = \epsilon$. By defining $P_I = Q_{IR} + Q_{IC} + P_N$, and neglecting Q_A, one obtains

$$C \frac{dT_N}{d\theta} = \alpha_S (F_S S + F_R R) + \epsilon (F_E E - \sigma T_N^4) + P_I \tag{2-3}$$

FACTORS GOVERNING SPACECRAFT TEMPERATURE

Temperatures experienced by the components of a given vehicle are controlled largely by the ability of the enternal surfaces to absorb, reflect, transmit, and emit thermal radiation. In most spacecraft designs, the two properties of predominant importance in describing these abilities are seen from equation (2-3) to be solar absorptivity, α_S, and emissivity, ϵ. The solar absorptivity is that fraction of the incident solar energy, including reflected solar energy, which is absorbed by a surface. The emissivity is the ratio of the energy emitted by the surface under consideration to that which would be emitted by an ideal radiator (black body) at the same temperature. For most calculations of radiant energy exchange it is convenient to use the total hemispherical value of emissivity. This is taken to be equivalent to the unmodified term, emissivity, and means that all energy emitted into the hemispherical space above the surface element is accounted for. Actually, the radiation behavior of a surface element is directional-dependent. Non-conductors have smaller emissivities with increasing emission angles, measured from the surface normal. For conductors, the emissivity first increases and then decreases with increasing emission angle. The ratio of normal emissivity to total hemispherical emissivity is approximately 1.2 for a bright metallic surface, and 0.95 for a non-conductor with a smooth surface finish. The directional dependence of emissivity can usually be ignored in radiation calculations with negligible error. However, if a primary heat transfer mode to a surface is radiation incident or emitted at an angle greater than 60° from the surface normal, it is advisable to investigate the directional emission characteristics of the surface material.

In addition to the surface radiation properties, the configuration factors for solar irradiation, planetary emission, and albedo must be computed before the magnitude of the absorbed radiation can be determined.

Because the sun's rays may be considered parallel, the configuration factor for direct isolation is simply the ratio of the surface area projected on a plane normal to the sun's rays to the total surface area. For an element of area small enough to be considered plane, the geometric factor for direct insolation is

$$F_S = \cos\delta \tag{2-4}$$

where δ is the solar incidence angle. Equations for the geometric factors for horizontal and vertical cones and cylinders are given in Section IV (equations 4-52 and 4-53) as a function of the body angle, cone half-angle, orbit angle, and orbit inclination.

The configuration factors for planetary emission and albedo are considerably more complicated. For a diffuse surface irradiated by a diffuse sphere of uniform emissive power, the configuration factor is given by the following equation:

$$F_E = \frac{1}{\pi} \int_{\gamma_1} \int_{\theta_1} \frac{\cos\gamma_{1n} \ \cos\gamma_{n1}}{r_{1n}^{2}} \, r_1^{2} \sin\gamma_1 \, d\theta_1 \, d\gamma_1 \tag{2-5}$$

The geometry is shown in Figure 2-3. The configuration factor for a diffuse surface irradiated by the reflection from a diffuse sphere exposed to parallel sun rays on one side is given by

$$F_R = \frac{1}{\pi} \int_{\gamma_1} \int_{\theta_1} \cos\gamma_{1S} \, \frac{\cos\gamma_{1n} \ \cos\gamma_{n1}}{r_{1n}^{2}} \, r_1^{2} \sin\gamma_1 \, d\theta_1 \, d\gamma_1 \tag{2-6}$$

The calculation of Earth emission and albedo is discussed in Section IV.

In addition to external heat sources, the spacecraft temperature is influenced by internal power generation, P_I. Most spacecraft have components on board which act as sources of thermal energy, such as electronic components thermally dissipating internal power. Although the internal power generation has a large effect on the internal components, it has little effect on the average temperature of the spacecraft as a whole.

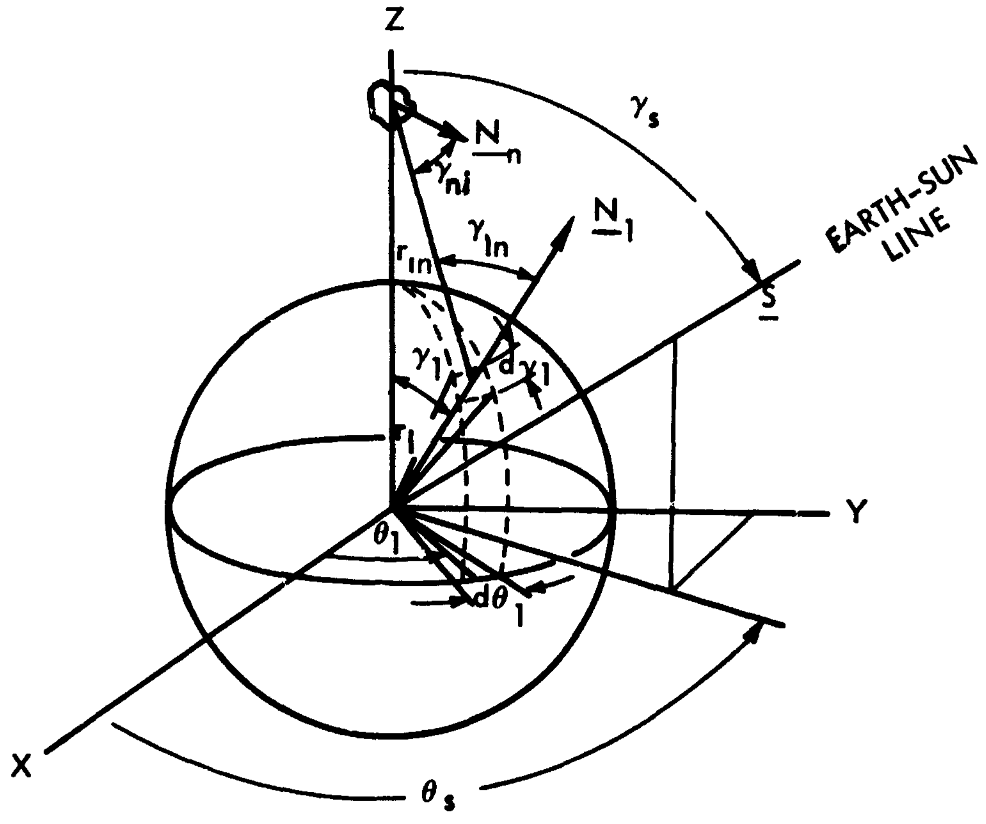

Figure 2-3. Geometric Relation Between Satellite Surface and Earth

The average temperature of a spacecraft in orbit can be obtained from equation (2-3) by setting $\frac{dT_N}{d\theta} = 0$ and rearranging:

$$\sigma \bar{T}_N^4 = \frac{\alpha_S}{\epsilon} (\bar{F}_S S + \bar{F}_R R) + \bar{F}_E E + \frac{1}{\epsilon} \bar{P}_I \tag{2-7}$$

This simplified equation shows the importance of the ratio α_S/ϵ in determining the average temperature.. A vehicle with low α_S/ϵ surfaces experiences relatively low temperatures, since it does not absorb solar energy very effectively (low α_S) in comparison to its ability to lose energy to space by thermal radiation (high ϵ). Conversely, high α_S/ϵ surfaces tend to become hot. This is illustrated by Figure 2-4, which shows the average temperature of a cylindrical Earth satellite orbiting at an altitude of 300 miles, with a vertical orientation. The three curves are for three types of orbits; β is the angle between the plane of the satellite's orbit and the Earth-sun line. As can be seen from this figure, the temperature increases with increasing α_S/ϵ.

The following table may be used as a general guide:

Type of Material	Approximate α_S/ϵ
White paints and ceramics	0.3
Black paints and ceramics	1.0
Metallic paints	0.8 - 1.2
Bare metals	>2

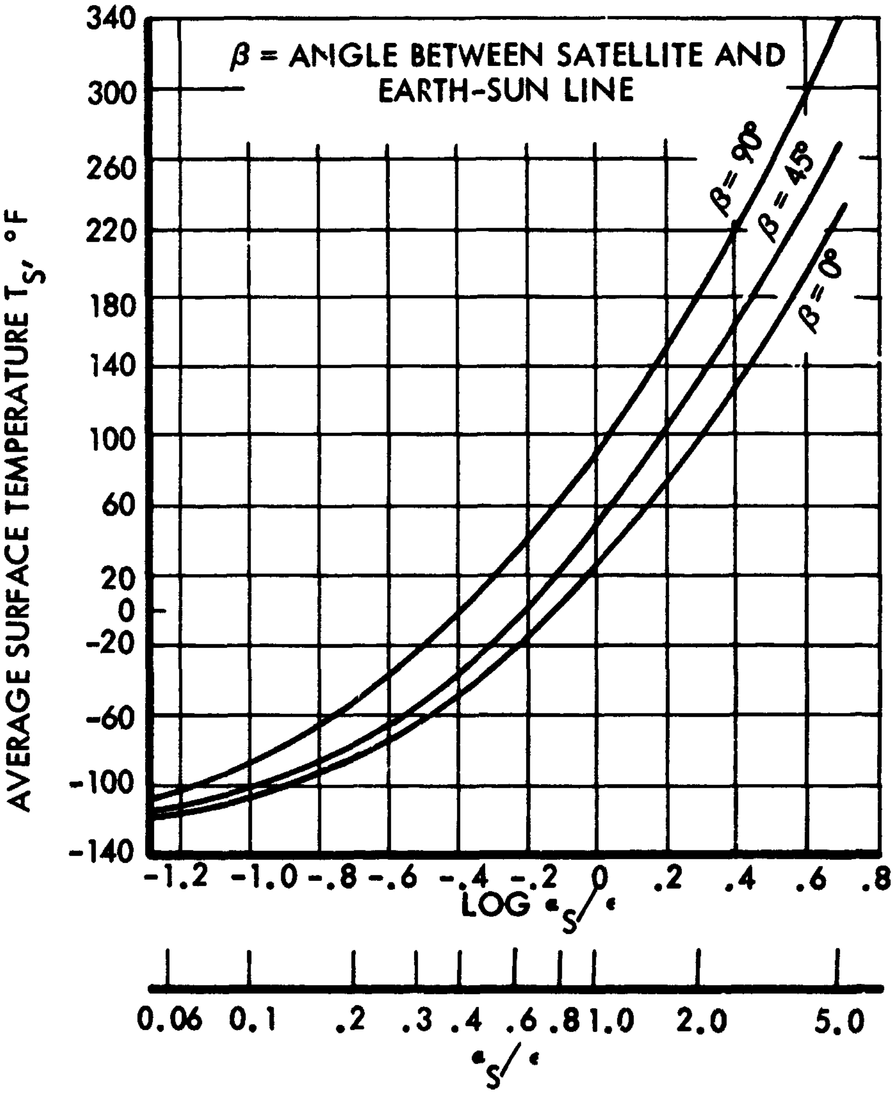

NOTE: VERTICALLY ORIENTED CYLINDRICAL SATELLITE IN A 300 SM POLAR EARTH ORBIT, NO INTERNAL POWER DISSIPATION

Figure 2-4. Average Satellite Surface Temperature

III - METHODS OF THERMAL CONTROL

There are two techniques for controlling spacecraft temperatures: passive thermal control and active thermal control. Passive control is the basis of all thermal control and it is often the sole means of controlling the amounts of energy absorbed and emitted. Active control generally is used in varying degrees to supplement passive control. Passive and active thermal control are discussed in relation to three general areas of importance:

1. External surface
2. Thermal resistance between the external surface and the internal environment
3. Internal environment

Problems associated with radiation to and from the vehicle are affected by external surface characteristics. Conduction, convection, radiation, and heat transfer loops are examples of thermal resistances between the external surface and the internal environment. Varying power input, storage of heat, and dissipation in expendable fluids are examples of controls which might be applied directly to the internal environment. Conductive "switches" and movable louvers are other devices which are becoming more common.

PASSIVE THERMAL CONTROL SYSTEMS

Passive control of the thermal behavior of a system and its components is attained wholly through geometrical design and the selection of materials with the requisite thermal properties. This method includes the static employment of temperature-induced physical changes in materials. Neither power nor moving parts are employed.

External Passive Control

External passive control is essentially the selection of surface pattern and finish to achieve a desired temperature level. It was shown in Section II that the temperatures of spacecraft which are dissipating internally generated heat are largely a function of α_S and ϵ of the outer surfaces. Selectively coating the surface can thus be used to establish an average sink temperature for internal components. In cases where no available surface coating exhibits the proper characteristics, paint can be applied in a striped or checkered pattern to achieve the desired effect.

Internal to External Thermal Resistance

The passive control of the thermal resistance between internal environment and the external surfaces is dependent on the conduction and radiation heat transfer paths afforded by the vehicle design. The thermal designer can exercise some control over the internal heat transfer.

If the equipment must dissipate a large amount of internal power, the internal structure should be designed to provide conduction paths of large cross-sectional area and high thermal conductivity to surfaces that have a relatively stable and low temperature. On the other hand, if the equipment has a low power output and requires temperature control, it may be desirable to insulate the equipment attachment points in order to keep the heat losses within the desired range. In addition, internal surfaces with high or low emissivities can be used to promote or retard radiation heat transfer.

For equipment highly sensitive to changes in temperature, a high thermal resistance between internal equipment and the external skin is generally required. In this way, a large time constant is provided for the entire internal system, which tends to damp out periodic external surface temperature changes. This large thermal resistance also tends to make internal temperatures more a function of average, rather than local or instantaneous, skin temperatures. One way of achieving this high resistance is the use of a heat shield with a low emissivity on both sides. An insulation blanket can also be used for this purpose. In some cases it may be more desirable to use a large thermal mass to damp out local temperature oscillations. A slab of material with a high specific heat, such as beryllium, can be used for this purpose.

The proper placement of temperature-sensitive equipment is very important. In general, the temperature is more stable in the interior of a satellite, away from the outer skin. Equipment can be mounted on brackets to reduce heat loss, or flush-mounted to promote conduction. The positioning of a component also affects the radiation configuration factor, and hence the radiation heat transfer. Therefore, a component with a large amount of heat dissipation is mounted with a good conduction path to a cool portion of the outer skin, and oriented in such a fashion as to also have a large radiation configuration factor. On the other hand a temperature-sensitive component, such as a primary battery, is located toward the center of the vehicle and thermally isolated insofar as possible. In this case, the average temperature of the surrounding portion of the vehicle must be in the proper range.

Internal Passive Control

An example of a method of internal passive control is the use of substances which are subject to a phase change at the desired control temperature. Phase-changing substances are useful in providing a constant temperature sink for a power source with a duty cycle. Some substances which could be used are paraffin, water, low-melting-point alloys, metals such as sodium and lithium, and certain organic substances.

ACTIVE THERMAL CONTROL SYSTEMS

Active thermal control of a system and its components is attained through a feedback control system, with temperature as the controlled variable. This method includes the dynamic employment of temperature-induced physical changes in materials. Generally, either power or moving parts are employed.

External Active Control

Active control methods involving the external surface are concerned with altering the net exchange of radiation between the surface and the surroundings. Examples of this type of system are:

1. Mechanical Variation of Surface Properties. The effective α_S/ϵ of the surface can be changed, for example, by louvers or a slotted or rotating shield which is moved across a pattern of alternating high and low α_S/ϵ. If a skin-mounted, temperature-sensitive actuator were used to move the shield, the skin temperature could be held within a narrow range even with large incident heat flux variations.

2. Variation of Surface Properties by Other Means. It is possible that surface coatings can be developed which exhibit reversible changes in α_S or ϵ, or both, due to the influence of an electrical current, electromagnetic field, or other stimuli. (Progress in this area, however, has been very slow.)

3. Fluid Circulation Through the Skin. This method is effective for maintaining the entire external surface at a nearby uniform temperature regardless of local internal or external heat input variations.

Variation of Internal to External Thermal Resistance.

The resistance between the external surface and the internal environment can also be used as a control parameter. It is analogous to the resistance term of the heat transfer equation $Q = \Delta T/R$. Some possible methods for varying the resistance are:

1. Variable Conduction. Various types of thermal switches have been proposed that utilize bimetallic or other thermal expansion actuating devices to vary physically the conduction path cross-sectional area between the internal environment and the external surface.

2. Variable Convection. In spacecraft where man is present, forced convection (a prime requirement for physiological reasons) can be utilized as an integral part of the thermal control system. Forced convection can also be used in unmanned vehicles.

3. Variable Radiation. Movable radiation shields or shutters placed between the temperature-sensitive equipment and the skin can provide a variable radiation resistance. The motion of shutters would be regulated by a temperature-sensitive actuator mounted on the equipment requiring control.

4. Heat Transfer Loops. A heat-transport loop, utilizing the vehicle skin as a heat sink can be used to maintain temperature control. A bypass valve in the fluid circuit would maintain a constant-temperature coolant supply to the equipment. A fluid which changes phase in the heat transport loop could be used to minimize the required circulation rate. An example would be a

water system in which boiling occurs during heat addition and condensation occurs during heat rejection.

5. Heat pumps. Heat pumps might allow a combination of components with incompatible temperature limits. Vapor compression, absorption, and thermoelectric systems are possible solutions. Primary problem areas with the vapor compression and absorption cycles are boiling and vapor separation under zero gravity. At the present time, the thermoelectric system results in excessive weight and power penalties, with the possible exception of systems with very small loads. Advantages of the thermoelectric system are the extremely close temperature control that can be achieved and the absence of moving parts.

Internal Active Control

The third or inner zone of the spacecraft involving thermal control has been defined as the internal environment. This includes man, the payload, and the equipment associated with the flight operation. Some of the methods previously discussed could be utilized directly in the control of the internal environment. For example, heat distribution between the internal components could be accomplished by the use of heat transport loops, heat pumps, thermal switches, variable radiation resistance, and forced convection. In addition, there are other methods of direct internal thermal control which possess varying degrees of potential usefulness, and therefore warrant some mention. Two possibilities are:

1. Varying Internal Power. Some satellite designs utilize variation of internal power to hold internal temperatures within a very small range, even with sizable variations in external radiation inputs.

2. Expendable Coolants. The use of expendable coolants is usually limited to short-term operation due to the weight penalties involved. Examples of short-term applications include the use of a water system in the Mercury capsule and the Polaris fleet ballistic missile.

PASSIVE VS ACTIVE CONTROL SYSTEMS

Passive thermal control systems have certain advantage over active systems with regard to reliability. They employ no moving parts or switches which may malfunction because of such factors as the cold-welding of bearing surfaces in the low pressures of space. Also, the passive solution to a design problem generally requires less weight.

Active thermal control systems, on the other hand, can correct for environmentally induced alterations in the thermal behavior of a vehicle. An example of such an alteration is the increase in the solar absorptivity of an exterior surface due to the influence of solar ultraviolet energy. These systems can also accept changes in the thermal environment, such as the increase in the solar constant experienced by a Venus probe. Extremely accurate knowledge of external thermal radiation characteristics is not mandatory for active systems, as it is for passive. Among other things, this means that successful operation of a given vehicle is less likely to be jeopardized by the various factors of the prelaunch environment. In addition, active control can provide much more precise control of temperature than is possible with passive control.

The choice of whether to use an active or a passive thermal control system depends on the particular application. The majority of unmanned satellites to date have utilized passive thermal control; some have used active systems in conjunction with passive. It should be noted that the design of active thermal control systems presupposes a knowledge of passive design techniques. The thermal environment and the fundamental analytical approaches are the same. The greater the accuracy with which one can predict the behavior of materials used for spacecraft thermal control, the smaller the heating and cooling capacities needed, and consequently, the less power and weight are required to solve a given design problem through active thermal control. A widening of temperature tolerances, of course, will help immensely in alleviating the thermal control problem.

THERMAL CONTROL SURFACES

It is seen from the foregoing discussion that the basic method of controlling spacecraft temperatures for both passive and active systems is by controlling the net thermal radiation exchange of the outer skin. This is achieved through use of materials that exhibit the necessary thermal radiation characteristics (α_S, ϵ); these materials cause the various surface areas of the vehicle to emit and absorb the correct amount of energy to ensure that the design temperatures of the interior of the vehicle are maintained. The four basic thermal control surfaces are shown in Figure 3-1, where monochromatic absorptance is plotted as a function of wave length. Note that 94% of the solar radiation is of wave lengths less than 2μ. The definitions of these surfaces are:

1. Solar Absorber -- a surface which absorbs solar energy far more effectively than it emits at spacecraft temperatures (high α_S/ϵ).
2. Solar Reflector -- a surface which is highly reflective to solar energy and emits well at spacecraft temperatures (low α_S/ϵ).
3. Flat Absorber -- a surface which absorbs all thermal energy incident upon it, including solar (high α_S and ϵ, $\alpha_S/\epsilon \approx 1.0$).
4. Flat Reflector -- a surface which reflects all thermal energy incident upon it, including solar (low α_S and ϵ, $\alpha_S/\epsilon \approx 1.0$).

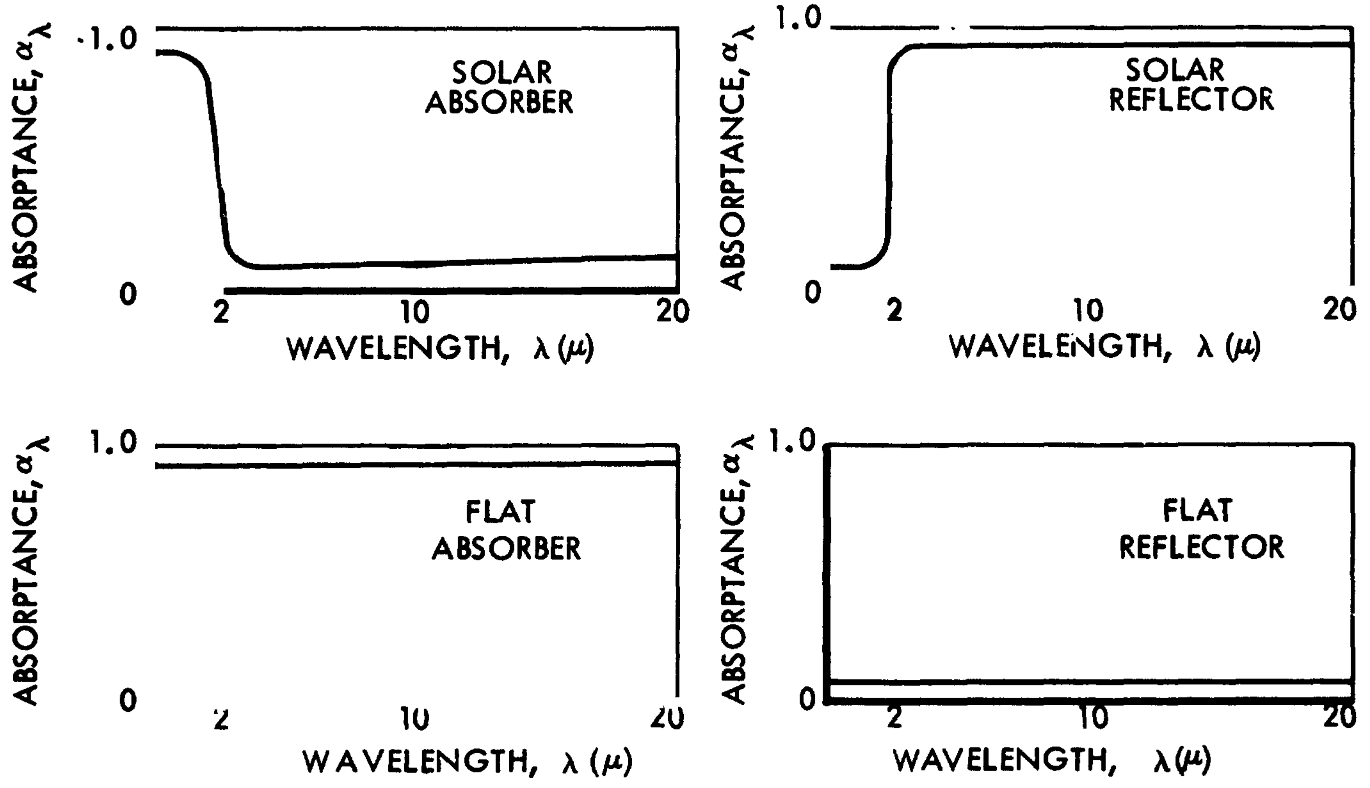

Figure 3-1. Four Basic Control Surfaces

IV - ANALYSIS OF EXTERNAL HEAT SOURCES

Although the external and internal heat balances are interrelated, it is convenient to separate the two, especially with regard to thermal loads. Furthermore, it is possible to obtain good first approximations to the external surface temperatures without considering all of the complications of internal heat transfer. This section describes methods for predicting ascent and orbital heating rates to the external skin. As the thermal analysis of the vehicle progresses, these external inputs eventually become boundary conditions for the spacecraft thermal analysis as discussed in Section V.

ASCENT HEATING

The accurate prediction of aerodynamic heating during the ascent phase of a space vehicle is of extreme importance. Generally, the heating rates and skin temperatures experienced during ascent will be more severe than those experienced during orbit. Thus, the temperature history and the loads during launch may be the criteria for the design of the vehicle primary structure and the requirements for the protection of internal equipment. Also, for orbit temperature control, the radiation characteristics of the external skin must be known, and these characteristics may be affected by the launch environment.

The nature of the ascent trajectory of satellite and space vehicles is such that a significant portion of the aerodynamic heating occurs above 100,000 ft. Because of the relatively low Reynolds number at this altitude, both laminar and turbulent boundary layers occur during boost. Experience has shown that laminar and turbulent heating are of equal importance. Laminar heating is more important in the stagnation region, but the large afterbody surfaces are more strongly affected by turbulent heating.

Flight parameters required in heating calculations include the airstream velocity, pressure, and temperature at the boundary-layer edge for the vehicle location in question. In addition, thermodynamic and transport properties of air are required at these conditions. Once the flow field and air properties have been obtained, the convective heating rate may be calculated. This assumes that a boundary-layer flow regime, i.e., laminar, turbulent, or transitory, has been established so that a heating theory corresponding to the particular flow conditions may be selected.

The following discussion describes methods for predicting local flow-field distributions and ascent heating rates. A list of symbols and a sample calculation for a typical launch configuration are included.

Ascent Heating and Flow-Field Nomenclature

a	velocity of sound, ft/sec
A	heated surface area, ft^2
c_p	specific heat, Btu/lb-R, or pressure coefficient
c_f	skin friction coefficient
D	diameter, ft
h	heat transfer coefficient, Btu/ft^2-sec-R
i	enthalpy, Btu/lb
J	mechanical equivalent of heat (778.26 ft-lb/Btu)
k	thermal conductivity, Btu/ft-sec-°R
M	Mach number
N_{Le}	Lewis number
N_{Nu}	Nusselt number
N_{Pr}	Prandtl number
N_{Re}	Reynolds number

N_{St}	Stanton number
P	pressure, lb/ft^2
q	heat flux, Btu/ft^2-sec
r	recovery factor
R	gas constant
R_b	nose radius, ft
s	distance along body surface
t	time
T	temperature, R
u, V	velocity, ft/sec
x	characteristic dimension, ft
Z	compressibility factor
α	shock wave angle, radians or degrees
β	stagnation point velocity gradient, sec^{-1}
γ	ratio of specific heats
δ	flow deflection angle, radians or degrees
θ	angle, radians or degrees
μ	absolute viscosity, $lb\text{-}sec/ft^2$
ρ	mass density, $lb\text{-}sec^2/ft^4$
τ	shear stress, lb/ft^2

Subscripts

aero	aerodynamic
aw	adiabatic wall
axi	axisymmetric

c	cone surface value
cond	conduction
conv	convection
cs	cross section
d	dissociation
l	boundary layer edge
i	based on enthalpy
iso	isothermal
max	maximum
o	reference value
rad	radiation
s	stagnation point
t	total
w	wall
2	behind normal shock
2-dim	two-dimensional
∞	freestream

Superscripts

*	evaluated at reference temperature or enthalpy

Flow-Field Calculations

Prediction of aerodynamic heat transfer depends first on determination of the applicable flow field. In practice, knowledge of the surface pressure distribution is essential for heat-transfer calculations. Figure 4-1 is a schematic representation of the flow field about a typical vehicle during supersonic flight and defines flow-field terms used in this section. In many instances, the concern is with the flow about blunted bodies or

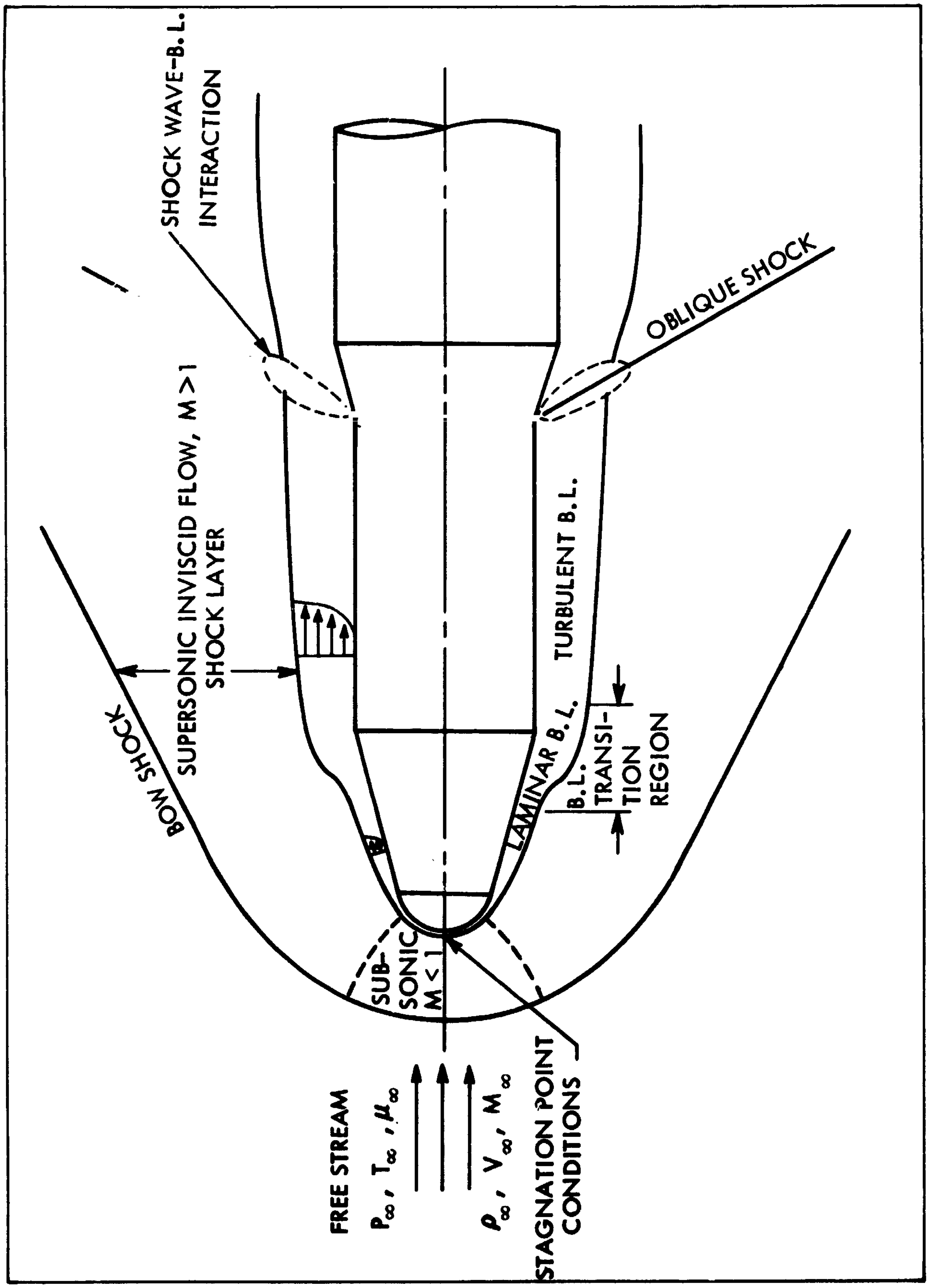

Figure 4-1. Typical Boost Vehicle Configuration and Flow Field Structure

bodies sufficiently blunt to produce a detached bow shock. Figure 4-1 indicates that in addition to the bow shock, other shock waves may be generated as a result of the vehicle geometry. Depending on the configuration, more than one oblique shock may exist.

The region bounded by the shock wave and the outer edge of the boundary layer shown in Figure 4-1 is called the shock layer. This region is important because its structure determines the distribution of surface pressures on the body. Because of the absence of significant viscous forces in this region, it is also commonly referred to as the inviscid flow field. The shock layer, or inviscid flow field, is further divided into subsonic and supersonic regions. The subsonic portion exists in the vicinity of the stagnation region, where the local velocities are low (relative to the freestream velocity). Static temperatures are high because of passage of the fluid through the strong, nearly normal shock wave. The combination of the relatively low-velocity and high-temperature levels leads to local Mach numbers below one in this region.

The flow, which is compressed as a result of the strong shock, expands as it moves around the body until a second shock is confronted. This expansion increases the velocity, lowers the static temperature, and, at some point, local Mach numbers in the shock layer exceed one. The dividing line between the subsonic and supersonic regions is called the sonic line.

Figure 4-1 also shows the development of a viscous boundary layer on the body. The boundary layer is initiated at the stagnation point, where it is laminar. It remains laminar for some distance downstream of the stagnation point until, at some location, various disturbances may cause the boundary layer to undergo transition from a laminar to a turbulent state. In general, this transition front moves aft on the vehicle during the boost phase of flight.

Configurations of the type shown in Figure 4-1, for the purpose of flow field analysis, may be divided into geometric sections to be solved by various theories. To obtain the pressure distribution on the entire vehicle, it is necessary to match the pressure and pressure gradient at the junction of two theories. Theoretical methods for calculating inviscid flow field quantities are discussed in the following sections. A sample calcuation illustrating the application of such theories is presented later.

Isentropic Relations - For approximate flow field calculations, it is customary to assume a thermally and calorically perfect gas, i.e., $P = \rho RT$ and $c_p = \text{Const.}$, respectively. In addition, with the exception of flow across shock waves, the flow is assumed isentropic. The term "isentropic" denotes a reversible adiabatic process. For these conditions, the following relations apply:

$$\frac{P_1}{P_2} = \left(\frac{\rho_1}{\rho_2}\right)^{\gamma} \tag{4-1}$$

$$\frac{T_1}{T_2} = \left(\frac{P_1}{P_2}\right)^{(\gamma - 1)/\gamma} \tag{4-2}$$

$$\left(\frac{T_t}{T}\right) = \left[1 + \frac{\gamma-1}{2} \;(M^2)\right] \tag{4-3}$$

$$\left(\frac{P_t}{P}\right) = \left[1 + \frac{\gamma-1}{2} \;(M^2)\right]^{\gamma/(\gamma-1)} \tag{4-4}$$

$$\left(\frac{\rho_t}{\rho}\right) = \left[1 + \frac{\gamma-1}{2} \;(M^2)\right]^{1/(\gamma-1)} \tag{4-5}$$

where subscripts 1 and 2 refer to any two points in the flow. The total temperature relation (equation (4-3)) is restricted to adiabatic flow only. Tabulations of these quantities may be found in Reference 4-1 for a perfect gas with $\gamma = 1.4$.

Normal Shock Relations - From the mass, momentum, and energy conservation equations and the perfect gas equation of state, the following useful relations may be obtained for flow across a normal shock wave:

$$\frac{P_2}{P_\infty} = \frac{2\gamma M_\infty^2 - (\gamma - 1)}{\gamma + 1} \qquad (4\text{-}6)$$

$$\frac{\rho_2}{\rho_\infty} = \frac{(\gamma+1)\, M_\infty^2}{(\gamma-1)\, M_\infty^2 + 2} \qquad (4\text{-}7)$$

$$\frac{T_2}{T_\infty} = \frac{\left[2\gamma M_\infty^2 - (\gamma-1)\right]\left[(\gamma-1)\, M_\infty^2 + 2\right]}{(\gamma+1)^2\, M_\infty^2} \qquad (4\text{-}8)$$

$$M_2^2 = \frac{(\gamma-1)\, M_\infty^2 + 2}{2\gamma M_\infty^2 - (\gamma-1)} \qquad (4\text{-}9)$$

$$\frac{P_{t2}}{P_\infty} = \left[\frac{(\gamma+1)\, M_\infty^2}{2}\right]^{\gamma/\gamma-1}\left[\frac{\gamma + 1}{2\gamma M_\infty^2 - (\gamma-1)}\right]^{1/\gamma-1} \qquad (4\text{-}10)$$

Tabulations of these quantities may also be found in Reference 4-1 for a perfect gas with $\gamma = 1.4$.

Oblique Shock Relations - With the exception of the static-to-total pressure ratio, the perfect-gas normal shock relations may be used for oblique shocks if M_∞ & M_2 are replaced by their normal components, $M_\infty \sin\alpha$ and $M_2\ (\alpha - \delta)$, where α is the shock-wave angle and δ is the flow-deflection angle. The application of this technique is also explained in Reference 4-1, and appropriate charts are provided for the determination of the shock-wave angle.

Real-Gas Normal and Oblique Shock Relations - At Mach numbers greater than about 6, dissociation effects become significant, and the normal and oblique shock relations for a perfect gas no longer hold. As an example, both the temperature and density ratios across a normal shock at $M_\infty = 20$ would be in error by over 100% using ideal gas shock relations.

Real-gas equilibrium quantities as a function of $M_\infty \sin \alpha$, where α is the oblique shock angle, are shown in Figures 4-2 through 4-6. These curves are reproduced from Reference 4-2 and are based on the 1959 ARDC atmosphere. The shock functions shown were calculated for the terminal points of the isothermal atmosphere regions. For a given freestream Mach number and two-dimensional flow deflection angle (δ), Figure 4-2 may be used to obtain the shock angle parameter ($M_\infty \sin \alpha$). This quantity and a known altitude allow the ratios T_2/T_∞, P_2/P_∞, ρ_2/ρ_∞, V_∞/V_2, and i_2/i_∞ to be read from Figures 4-3 through 4-6.

For the real-gas case of air in dissociated equilibrium, a useful relation between the pressure ratio and freestream Mach number is given by (Ref. 4-3).

$$\frac{P_{t_2}}{P_\infty} = 1.27\ M_\infty^{\ 2.02} \qquad (4\text{-}11)$$

For high Mach numbers the perfect-gas pressure ratio relation (Eqn. 4-10) reduces to

$$\frac{P_{t_2}}{P_\infty} = 1.289\ M_\infty^{\ 2} \qquad (4\text{-}12)$$

Thus, real-gas effects do not change the pressure ratio significantly from the perfect gas value.

The Newtonian Approximation - A common method for predicting surface pressure distributions is based on the Newtonian particle model. This model postulates discrete non-interacting particles impacting upon the body surface. The approaching stream loses all its normal momentum component to the body, but the tangential component remains unaltered. A momentum balance for a windward body element results in the following expression for the pressure coefficient:

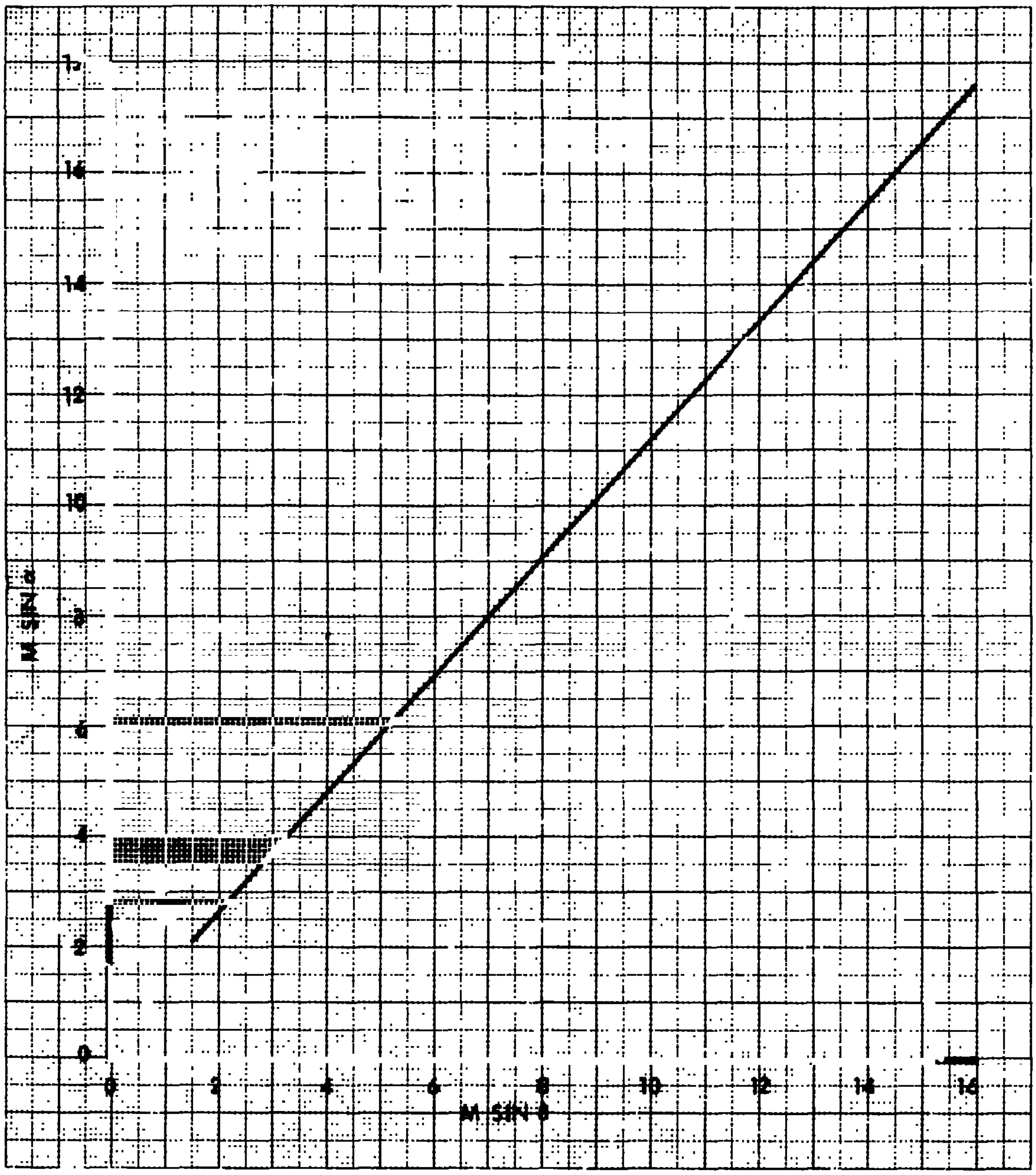

Figure 4-2. Two-Dimensional Flow Hypersonic Similarity Parameter vs Shock Angle Parameter

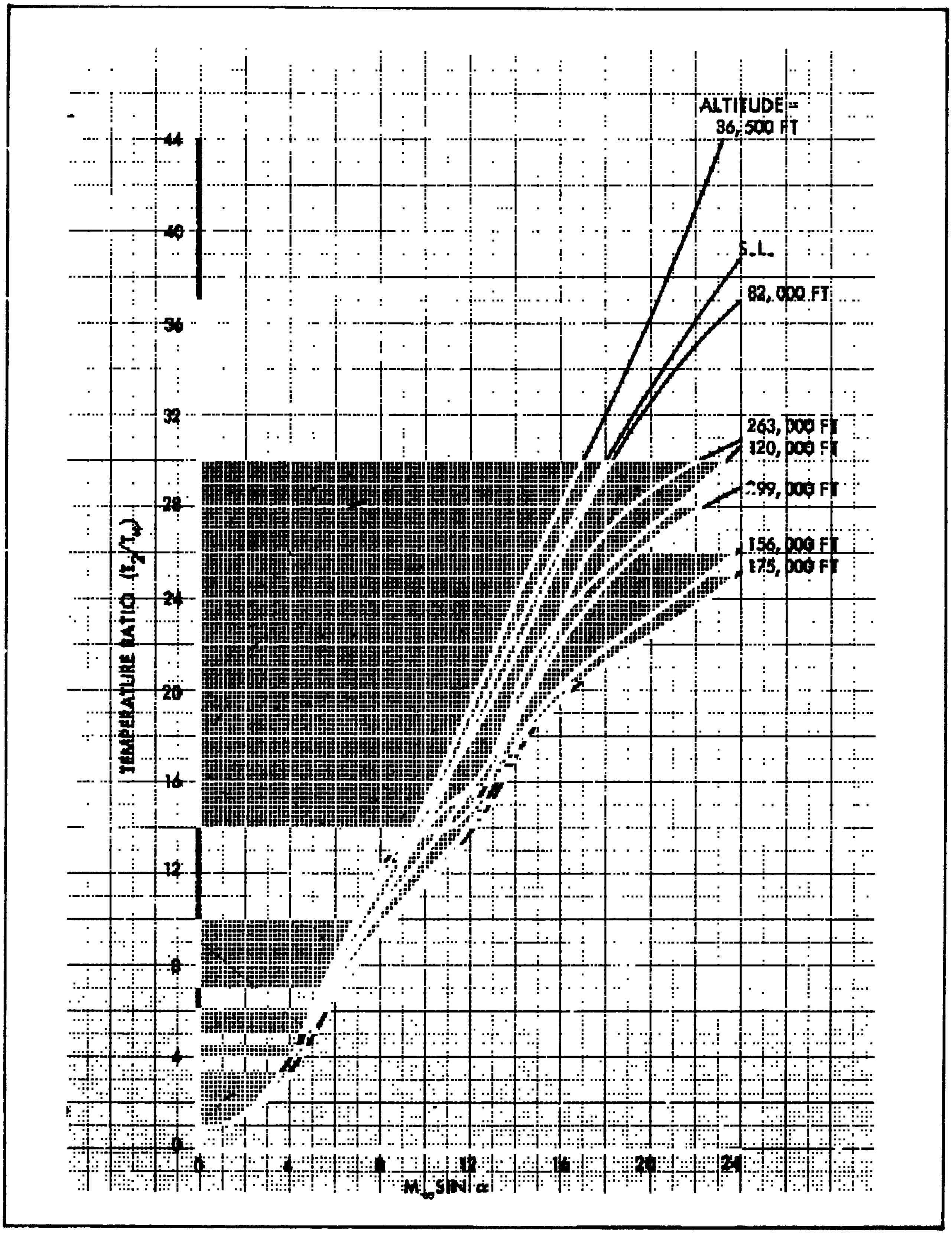

Figure 4-3. Real-Gas Temperature Ratio Across an Oblique Shock

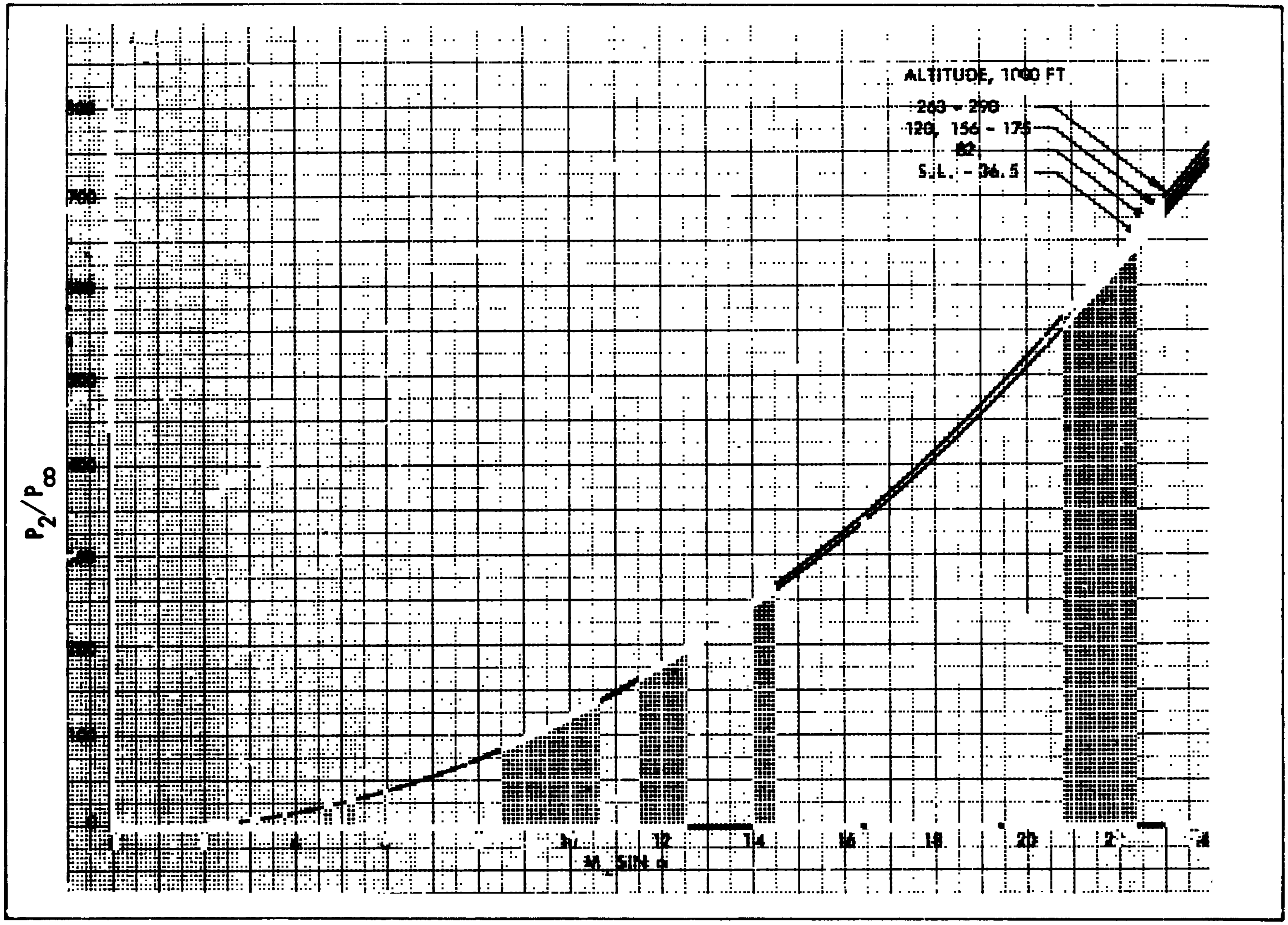

Figure 4-4. Real-Gas Pressure Ratio Across an Oblique Shock

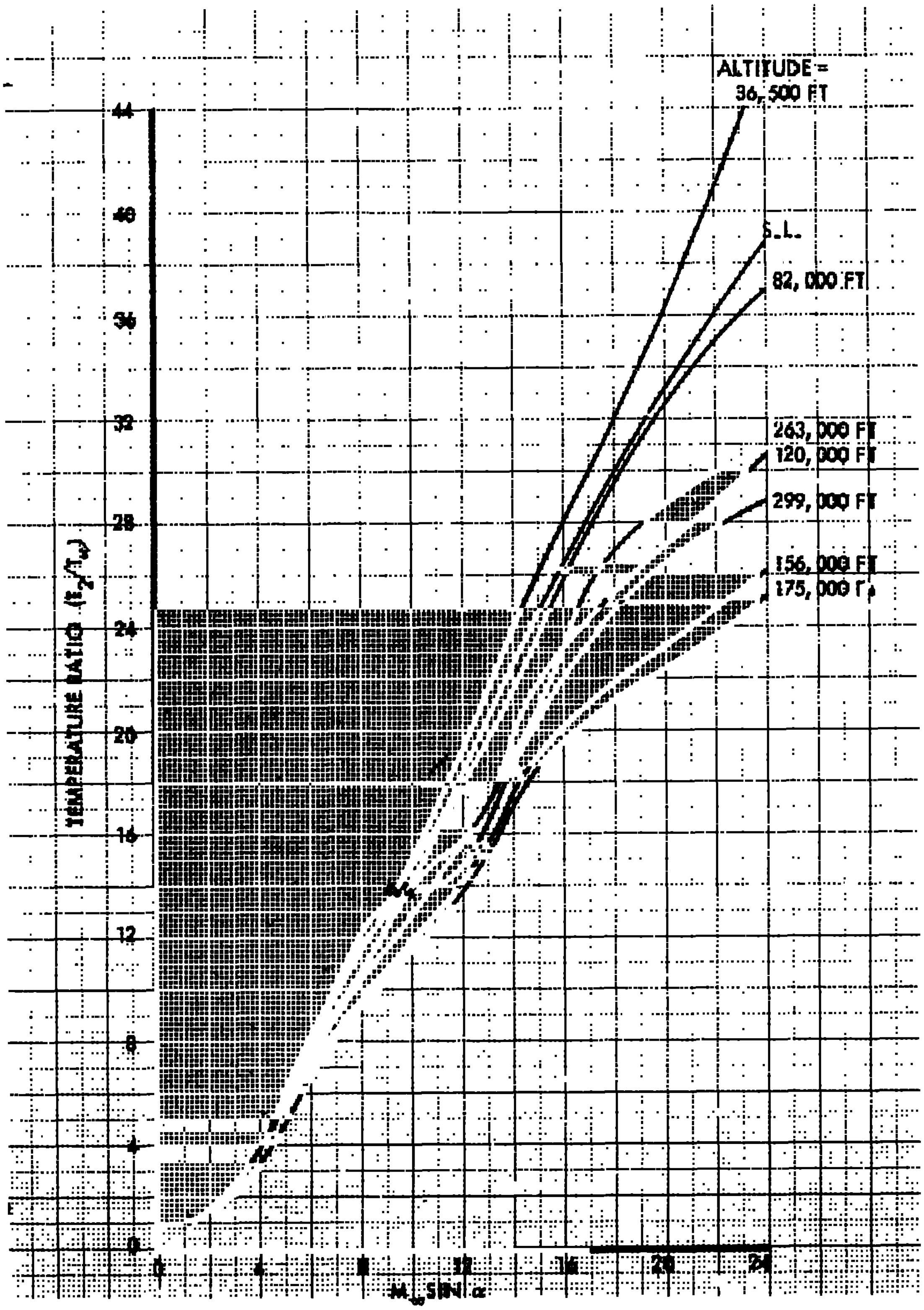

Figure 4-3. Real-Gas Temperature Ratio Across an Oblique Shock

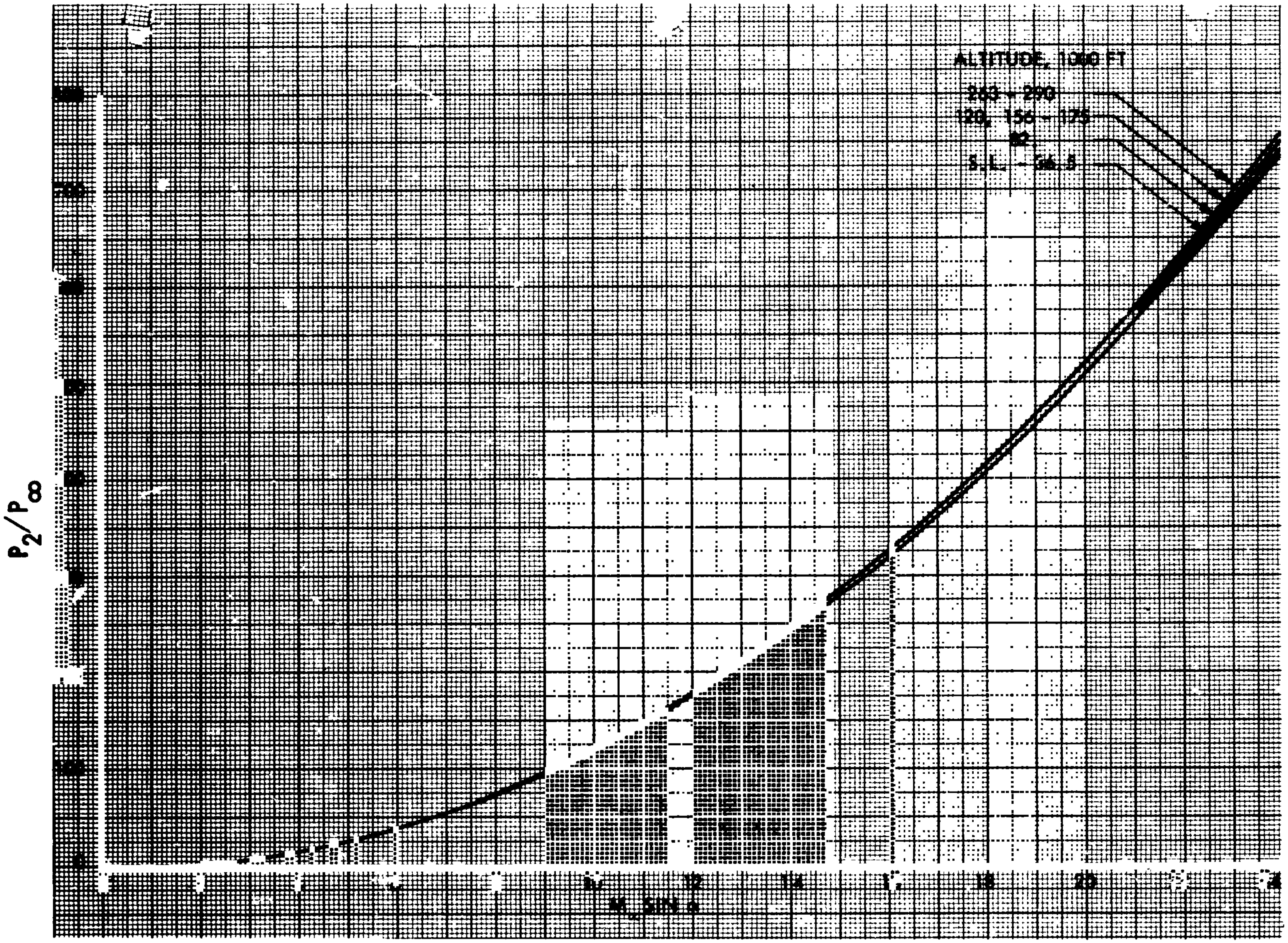

Figure 4-4. Real-Gas Pressure Ratio Across an Oblique Shock

$$c_p = 2 \sin^2 \Theta_b \tag{4-13}$$

where Θ_b is the angle between the freestream velocity and the local body surface inclination angle; i.e., at the stagnation point, $\Theta_b = 90°$.

Modified Newtonian - The pressure coefficient equation (4-13) is sometimes modified to match experimental data at the stagnation point. The resulting expression is known as the modified Newtonian approximation and is given by

$$c_p / c_{p_{max}} = \frac{P - P_\infty}{P_{t_2} - P_\infty} = \sin^2 \Theta_b \tag{4-14}$$

where:

$c_{p_{max}}$ = pressure coefficient at stagnation point.

This relation has been extensively compared with theory and adequately predicts the pressure in the vicinity of the stagnation point. Assuming the shock-layer fluid in the stagnation point vicinity to be incompressible, the normal-shock continuity and momentum equations provide an approximate $c_{p_{max}}$,

$$c_{p_{max}} = 2 - \frac{\rho_1}{\rho_2} \tag{4-15}$$

where the subscripts 1 and 2 denote conditions up and downstream from the detached shock wave. The modified Newtonian pressure distribution, combined with a Prandtl-Meyer expansion, for a hemisphere is presented in Figure 4-7.

The derivation of either the Newtonian or modified Newtonian equation makes the assumption, $M_\infty \phi \gg 1$, where ϕ is the angle between the surface tangent and the freestream velocity vector. This means that as the velocity decreases or the body becomes parallel to the flo , the method becomes increasingly inaccurate. The modified Newtonian method, however, has given good correlation with other methods even in the low supersonic regime.

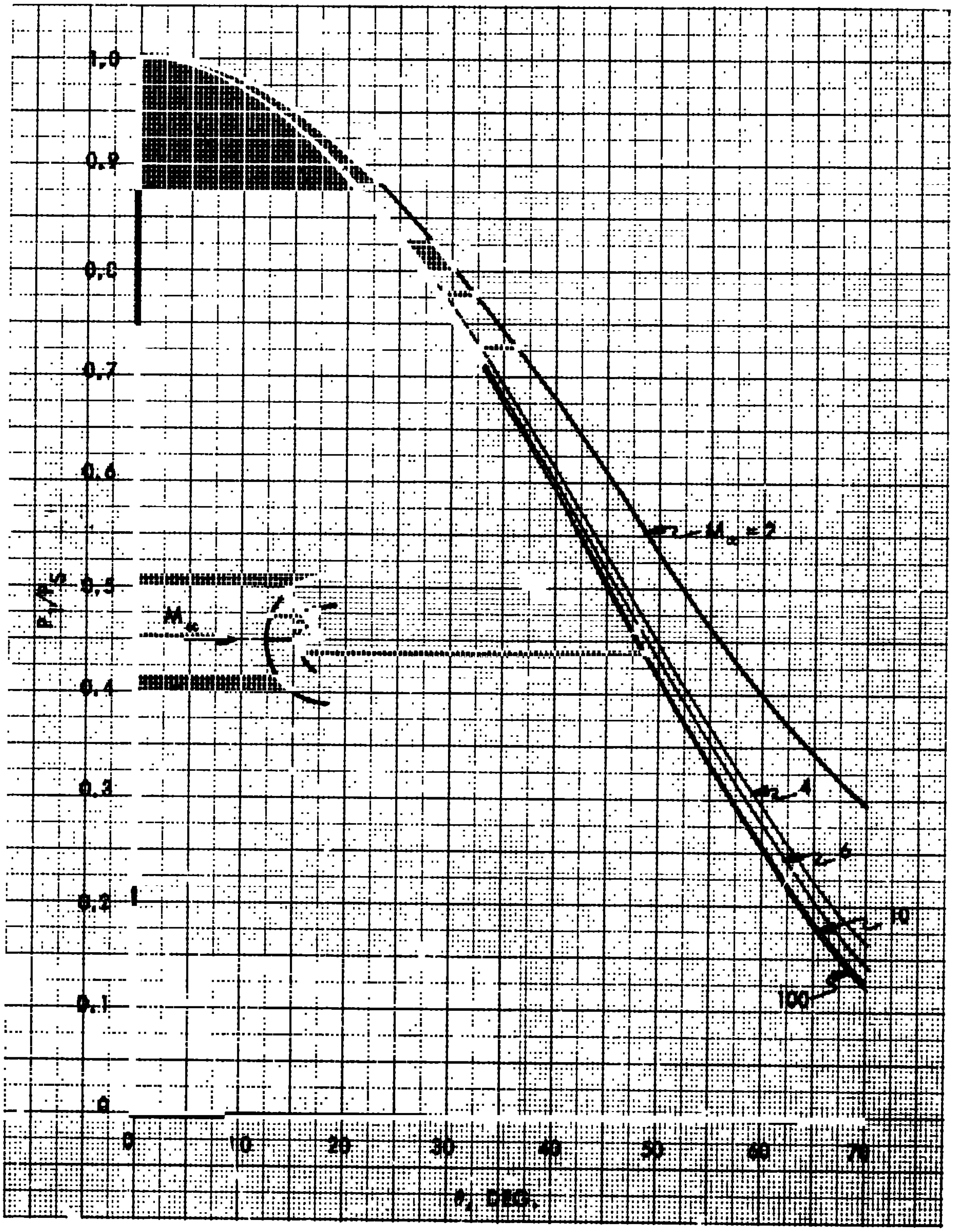

Figure 4-7. Modified Newtonian-Prandtl-Meyer Pressure Distribution on a Hemisphere

Prandtl-Meyer Flow - A solution for supersonic inviscid flow is available for corner-type flows. In such a flow, for given initial conditions, the magnitude of the Mach number at any point depends only on the flow direction at that point. Figure 4-8 illustrates the Prandtl-Meyer corner flow.

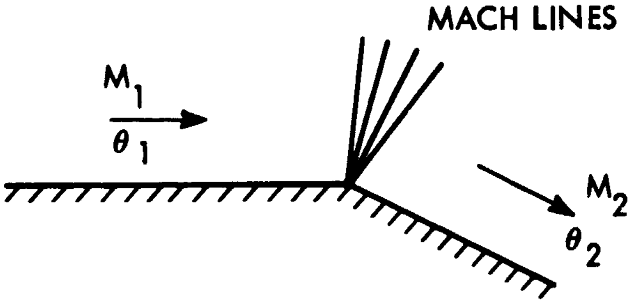

FIGURE 4-8 PRANDTL-MEYER EXPANSION

The results of the theory are easy to apply, since the direction of flow and the upstream Mach number are sufficient to determine the downstream Mach number, which in turn, determines all the local point functions of that Mach number.

The relation between the flow inclination Θ, and the Mach number M, in an isentropic two-dimensional compression, or expansion by turning, is

$$-\Theta + C = \left(\frac{\gamma+1}{\gamma-1}\right)^{\frac{1}{2}} \tan^{-1}\left[\left(\frac{\gamma-1}{\gamma+1}\right)(M^2-1)\right]^{\frac{1}{2}} - \tan^{-1}(M^2-1)^{\frac{1}{2}} \qquad (4\text{-}16)$$

where C is a constant of integration.

The right-hand side of equation (4-16) is called the Prandtl-Meyer function, $\nu(M)$. The constant of integration is chosen so that $\nu(1) = 0$. The resulting relations between the flow inclination angle (Θ) and the Prandtl-Meyer functions are then:

for expansion, $\nu_2 - \nu_1 = \left|\Theta_2 - \Theta_1\right|$

for compression, $\nu_2 - \nu_1 = -\left|\Theta_2 - \Theta_1\right|$

where subscripts 1 and 2 refer to conditions upstream and downstream from the expansion, respectively.

Although the Prandtl-Meyer theory applies only to a single boundary problem, it can be used to construct the flow in any plane symmetric problem by breaking the expansion zones into several regions of constant flow conditions. Each region is assumed to be separated by weak expansion shock boundaries. For a given initial Mach number and change in flow deflection angle, the resulting Mach number may be obtained from tabular values of $\nu(M)$. Such tables are contained in Reference 4-1 for $\gamma = 1.4$.

It has been amply demonstrated that the surface pressure distribution for a blunt body can be predicted by combining the modified Newtonian and Prandtl-Meyer expansion methods. The technique is to utilize modified Newtonian theory from the stagnation point to the point where the pressure gradient equals that computed using the Prandtl-Meyer method. Prandtl-Meyer solution is then introduced starting with the Newtonian pressure.

Taylor-Maccoll Cone Theory - The inviscid flow around a cone at zero angle of attack is axially symmetric and can therefore be described in terms of two independent space coordinates. Because of the axial symmetry, all stream properties are constant on conical surfaces having a common vertex. Taylor and Maccoll derived a non-linear differential equation describing the flow about a cone. By utilizing the energy equation derived from the mass conservation relations for steady, non-viscous flow, they arrived at the following differential equation:

$$\frac{d^2(u/c)}{d\theta^2}\left[\frac{\gamma+1}{2}\left(\frac{d(u/c)}{d\theta}\right)^2 - \left(\frac{\gamma-1}{2}\right)\left(1-\frac{u^2}{c^2}\right)\right] = (\gamma-1)\left(1-\frac{u^2}{c^2}\right)\frac{u}{c}$$

$$+\frac{\gamma-1}{2}\left(1-\frac{u^2}{c^2}\right)\cot\theta\,\frac{d(u/c)}{d\theta} + (-\gamma)\,\frac{u}{c}\left(\frac{d(u/c)}{d\theta}\right)^2 - \left(\frac{\gamma-1}{2}\right)\cot\theta\left(\frac{d(u/c)}{d\theta}\right)^3 \tag{4-17}$$

The constant c is the maximum attainable speed for a gas, i.e., the speed produced by expansion into a vacuum.

Results of this theory are plotted in Figures 4-9 through 4-11. Figures 4-9 and 4-10 present the cone surface pressure and temperature, respectively, ratioed to freestream values. Cone surface Mach number

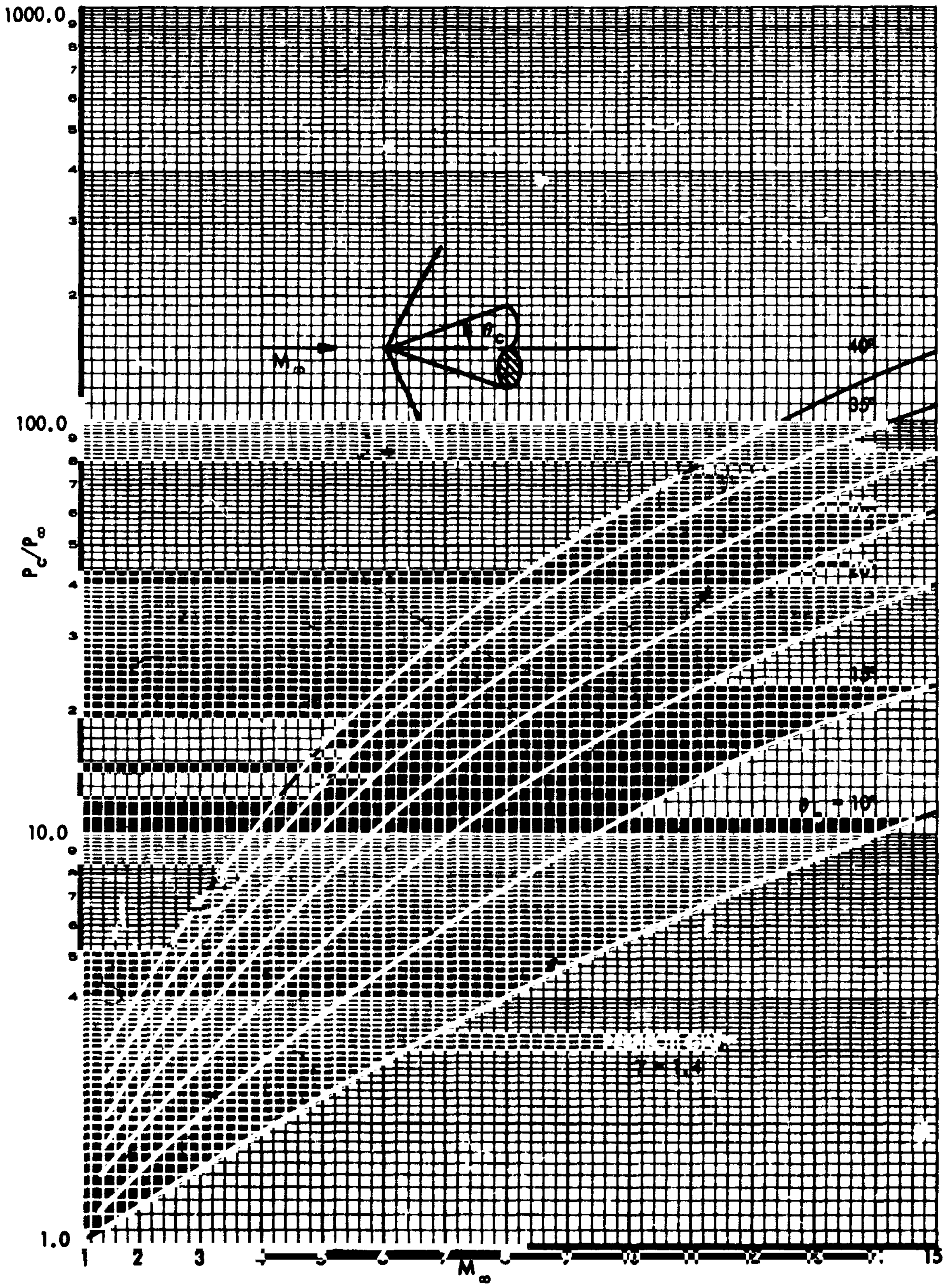

Figure 4-9. Cone Surface Pressure to Free Stream Pressure Ratio

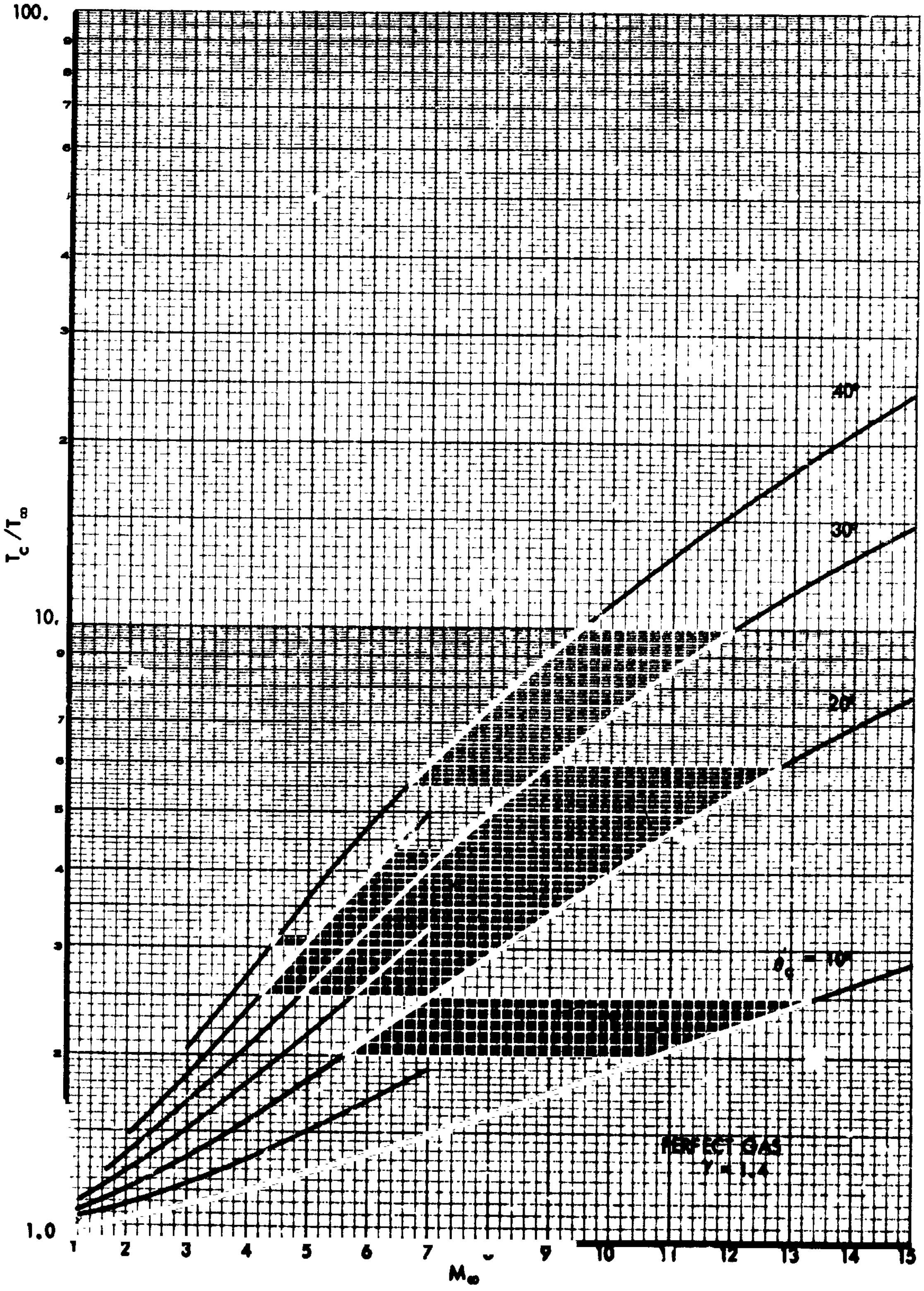

Figure 4-10. Cone Surface Temperature to Free Stream Temperature Ratio

variation is illustrated in Figure 4-11. From these curves, additional conical flow quantities may be determined using the isentropic flow relations. Additional presentation of the perfect gas results of this theory are contained in References 4-1 and 4-4.

For the real-gas case of air in dissociated equilibrium, Romig (Ref. 4-5) has calculated the cone flow quantities. These calculations are based on a constant freestream temperature of 490°R. A portion of Romig's results are plotted in Figures 4-12 and 4-13, showing the cone pressure ratio and velocity parameter as functions of the hypersonic similarity parameter ($V_\infty \sin \theta_c/10^4$). Also shown on these curves are approximate relations valid to about ± 2% for the pressure range shown.

Tangent Cone - The tangent cone approximation states that the pressure at any point on the surface of a body of revolution at arbitrary angles of pitch and yaw is identical with that on a semi-infinite unyawed circular cone of half-angle equal to the local inclination of the streamline with respect to the flight direction.

The equation for the local inviscid pressure is given by

$$\frac{P}{P_\infty} = 1 + \left(\frac{2\gamma}{\gamma+1}\right)\left(K_s^{\,2} - 1\right) + \gamma\left(K_s - K_c\right)^2 \left(\frac{\gamma+1}{\gamma-1+2/K_s^{\,2}}\right) \tag{4-18}$$

where

$$K_s = \left(\frac{\gamma+1}{\gamma+3}\right)K_c + \left[\left(\frac{\gamma+1}{\gamma+3}\right)^2 K_c^{\,2} + \frac{2}{\gamma+3}\right]^{1/2}$$

and $K_c = M_\infty\ \theta_c$

This method applies for angles only between 0 and 90°. Reference 4-1 contains graphs and equations of local pressure coefficient based on this method.

Tangent Wedge - This method is very similar to the tangent cone method, except that the local pressure coefficient calculation is based upon a two-dimensional oblique shock instead of a three-dimensional conical shock.

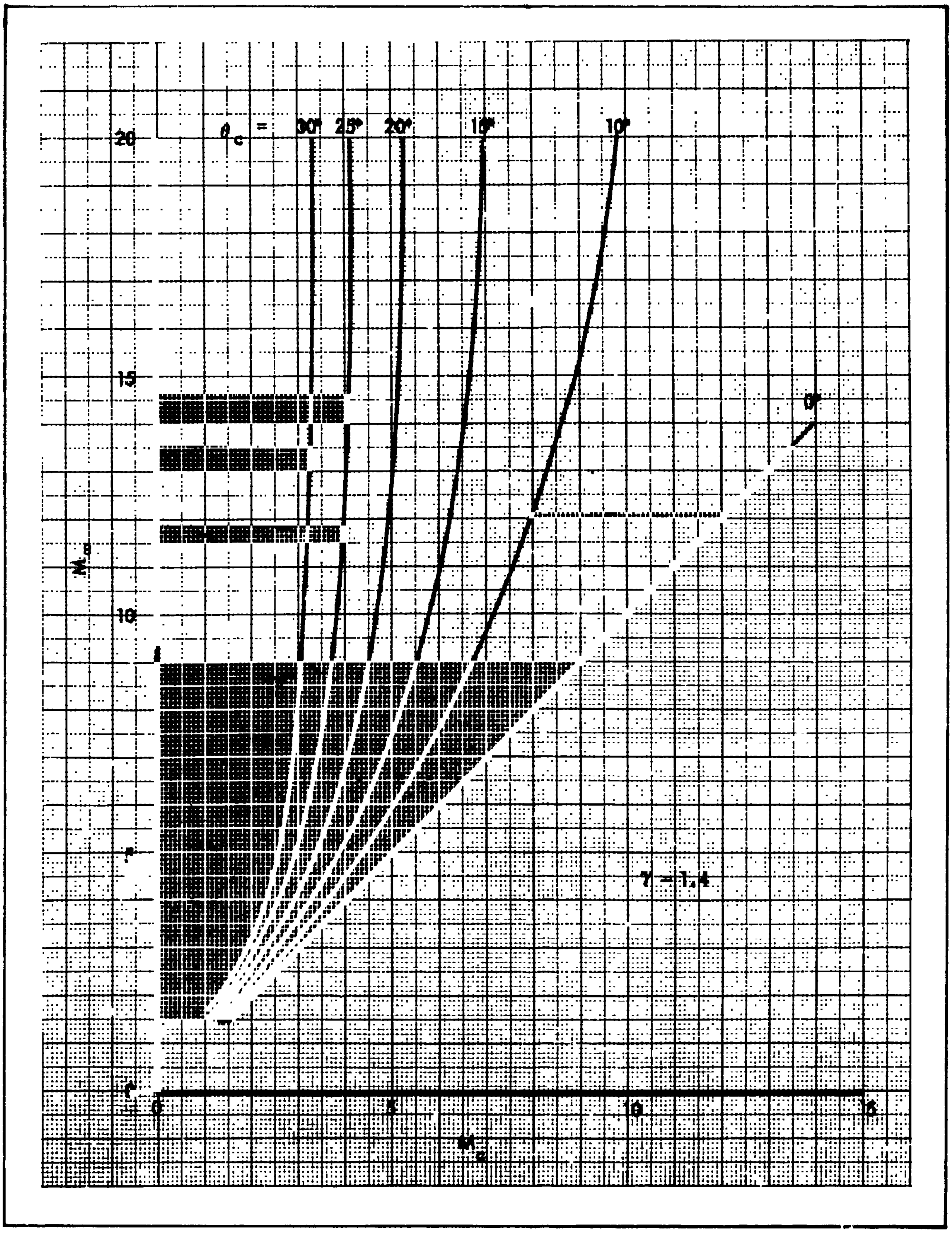

Figure 4-11. Mach Number at Cone Surface

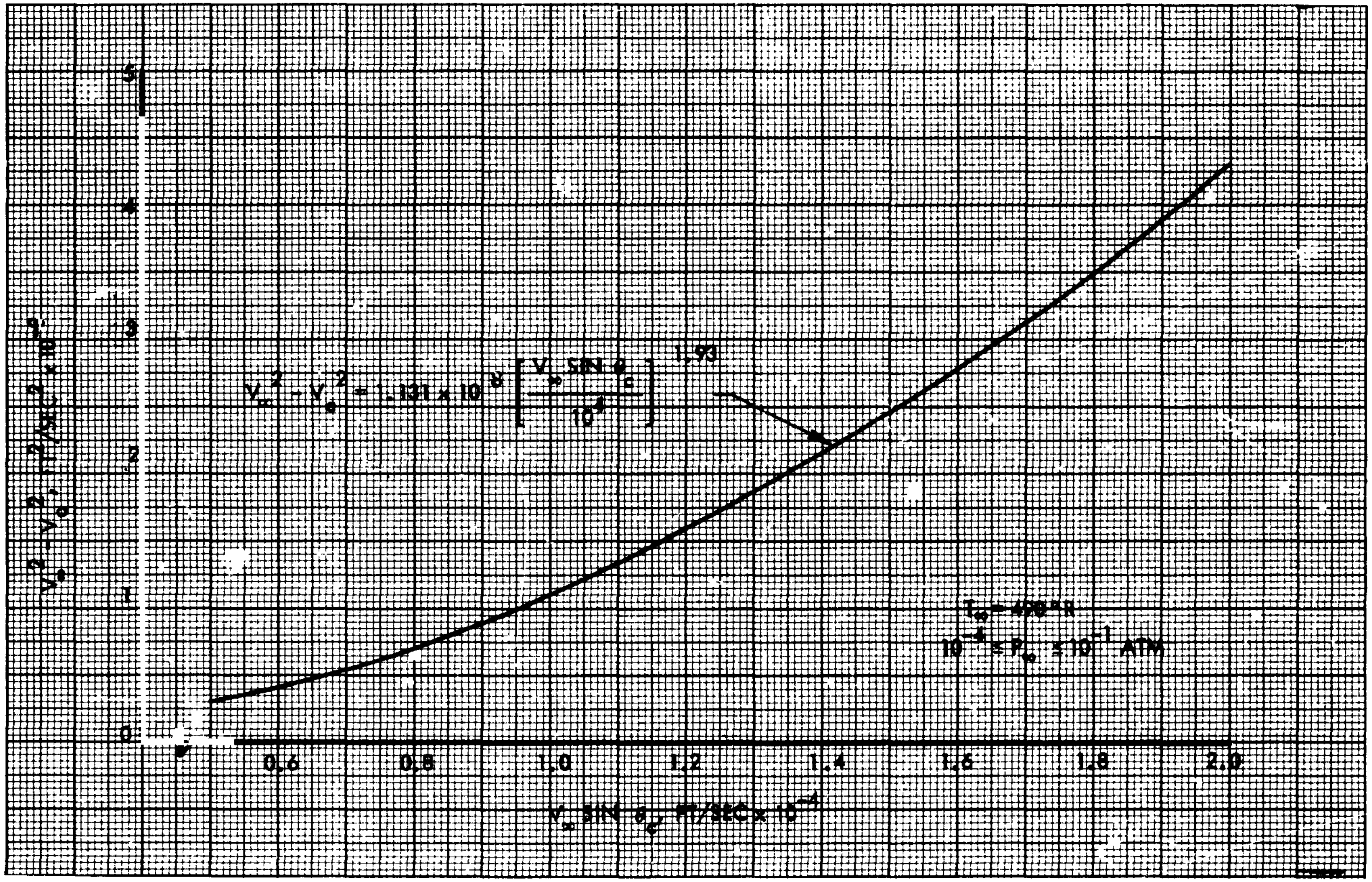

Figure 4-12. Real-Gas Cone Velocity Parameter

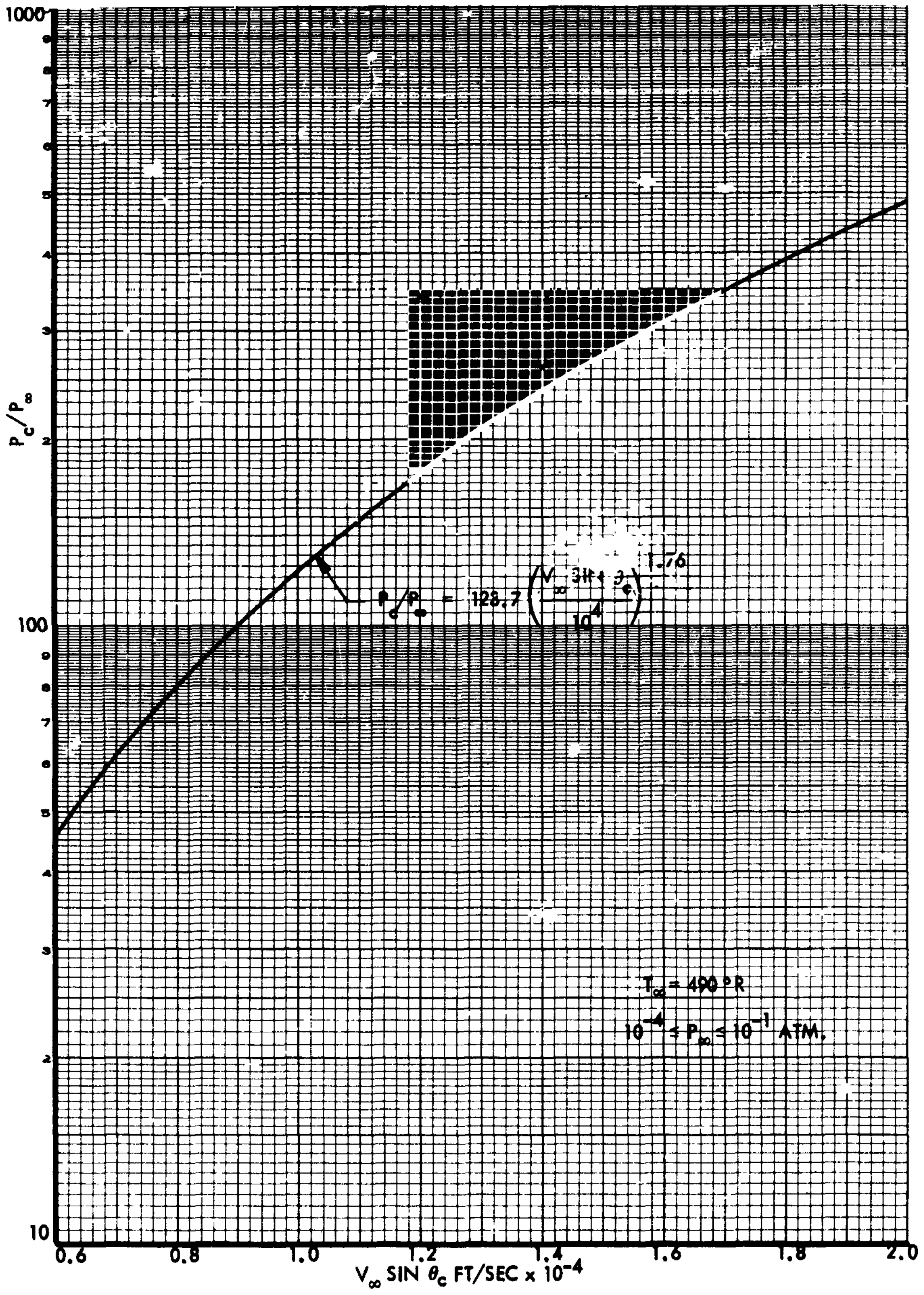

Figure 4-13. Real-Gas Cone Pressure Ratio

Equations and graphs of local pressure coefficient for the tangent wedge can also be found in Reference 4-1.

Expansions to Zero-Pressure Coefficient - At many vehicle locations it is possible to assume the local flow has passed through the bow shock wave and expanded to freestream static pressure, i.e.,

$$c_p = \frac{P_1 - P_\infty}{\frac{1}{2} \rho_\infty V_\infty^2} \approx 0$$

For most blunted vehicles with length-to-diameter ratios of about 5 or less, studies have shown that all of the fluid in the boundary layer passes through the near-normal portion of the shock wave (Ref. 4-6). Zero angle-of-attack blunted cylinders and flat plates are examples of such configurations. For these conditions, it is possible to calculate the inviscid flow quantities using the perfect-gas isentropic and normal shock relations discussed previously.

Shown in Figures 4-14 and 4-15 are the temperature, Mach number, and Reynolds number ratios for flow through a normal shock and expansion to zero pressure coefficient, i.e., $P_1 = P_\infty$. The Reynolds number curve assumes $\mu \sim T^{0.8}$

Expansion to zero pressure coefficient is also frequently assumed for cone-cylinder configurations. Local flow properites on the cylinder surface may be calculated using the isentropic relations and the cone flow solutions discussed previously. An example of one such calculation for a 15° semi-apex angle cone-cylinder is shown in Figure 4-16.

Applications - Various theories of predicting pressure can be used on a single vehicle. To obtain the inviscid pressure distribution on the entire vehicle, it is necessary to match the pressures and slope of the pressure at the junction of the two theories. An example of how a complicated composite body of revolution can be broken into sections to be solved by various theories and the various theories that can be used for each section is shown below:

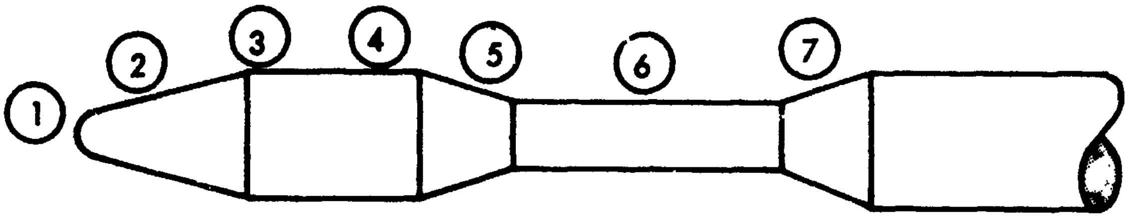

① Theories that can be used in the stagnation region are the Newtonian and Modified Newtonian.

② Theories that can be used in this region are the Taylor-Maccoll cone solution and the Tangent Cone.

③ At locations close to cone-frustum-cylinder intersections, the flow tends to overexpand to static pressures less than free stream. A two-dimensional Prandtl-Meyer expansion may be assuemd to occur at the cone-cylinder intersection.

④ For cylindrical vehicle sections at zero angle of attack, a common method used in obtaining the local static pressure is to assume a zero-pressure coefficient at the location in question. This approximation is usually made at locations downstream from cone-frustum-cylinder intersections so that overexpansions and recompressions of the flow have had sufficient distance to take place.

⑤ For small expansions the local problem of having separated flow at the aft end of this region should not affect the pressure obtained by using Prandtl-Meyer expansion.

⑥ The forward portion of this section is in separated flow with the flow reattaching somewhat aft of this region. In the region aft of the point of reattachment and in front of the point of separation due to surface 7, the assumption of a zero-pressure coefficient is reasonable.

⑦ At the cylinder-cone frustum intersection, an oblique shock is generated, due to the flow compression. Using the flow properties previously obtained for the cylindrical section, it is a simple matter to compute the change in these quantities across the oblique shock. Some variation in the computed properties will result, depending on whether a conical or wedge shock is assumed at the intersection.

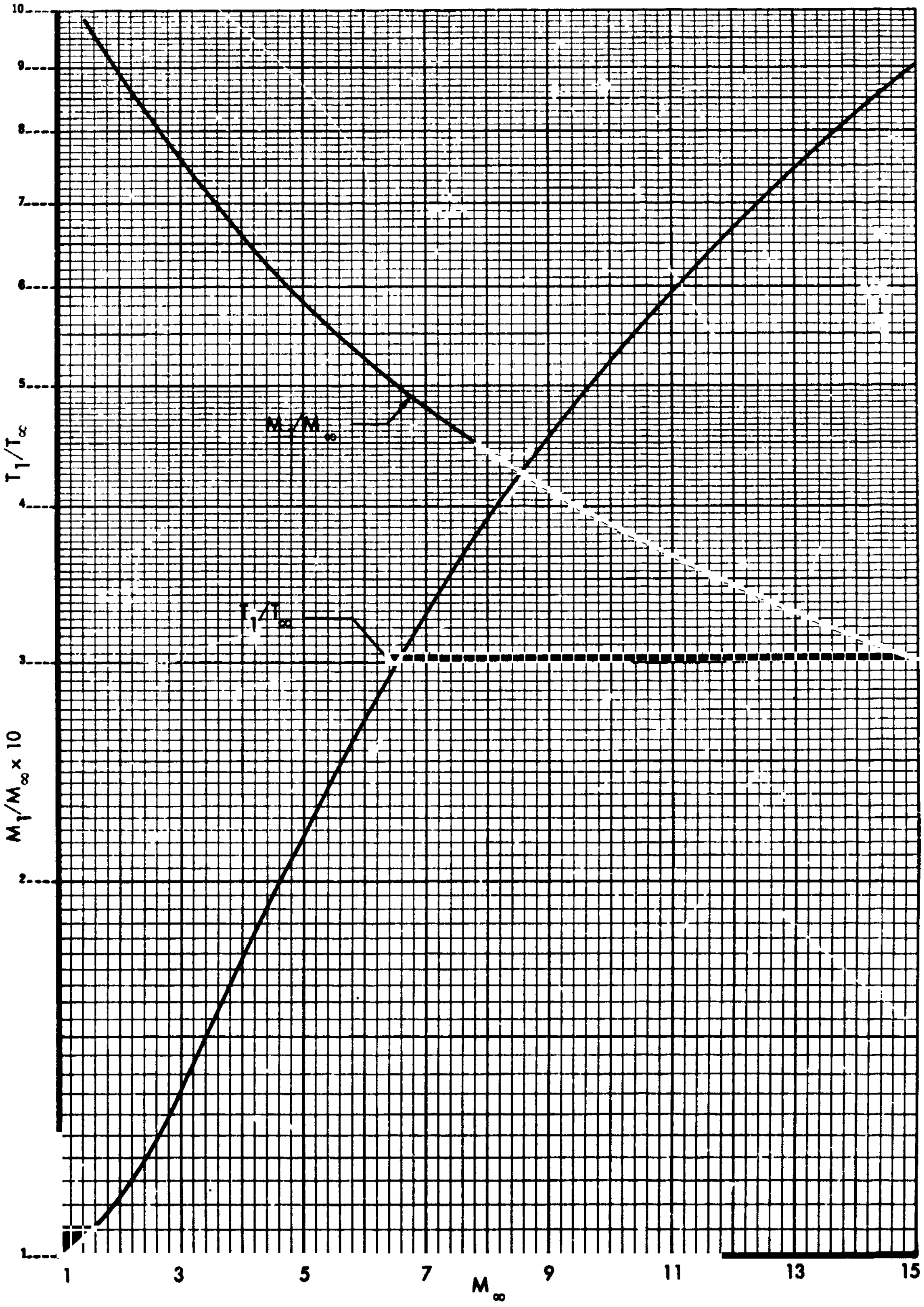

Figure 4-14. Property Ratios Across a Normal Shock Expanded to Free Stream Pressure

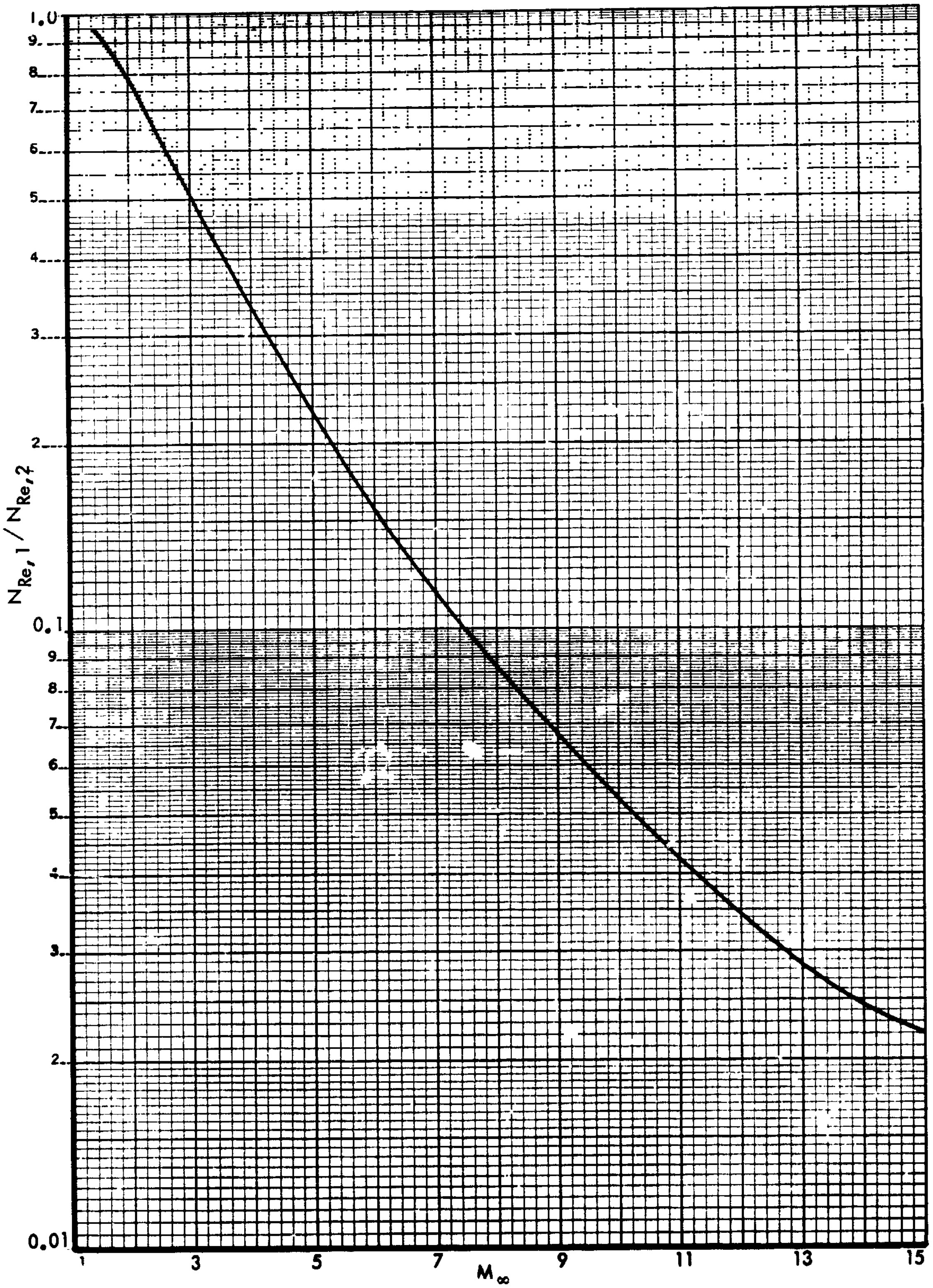

Figure 4-15. Reynolds Number Ratio Across a Normal Shock-Expanded to Free Stream Static Pressure

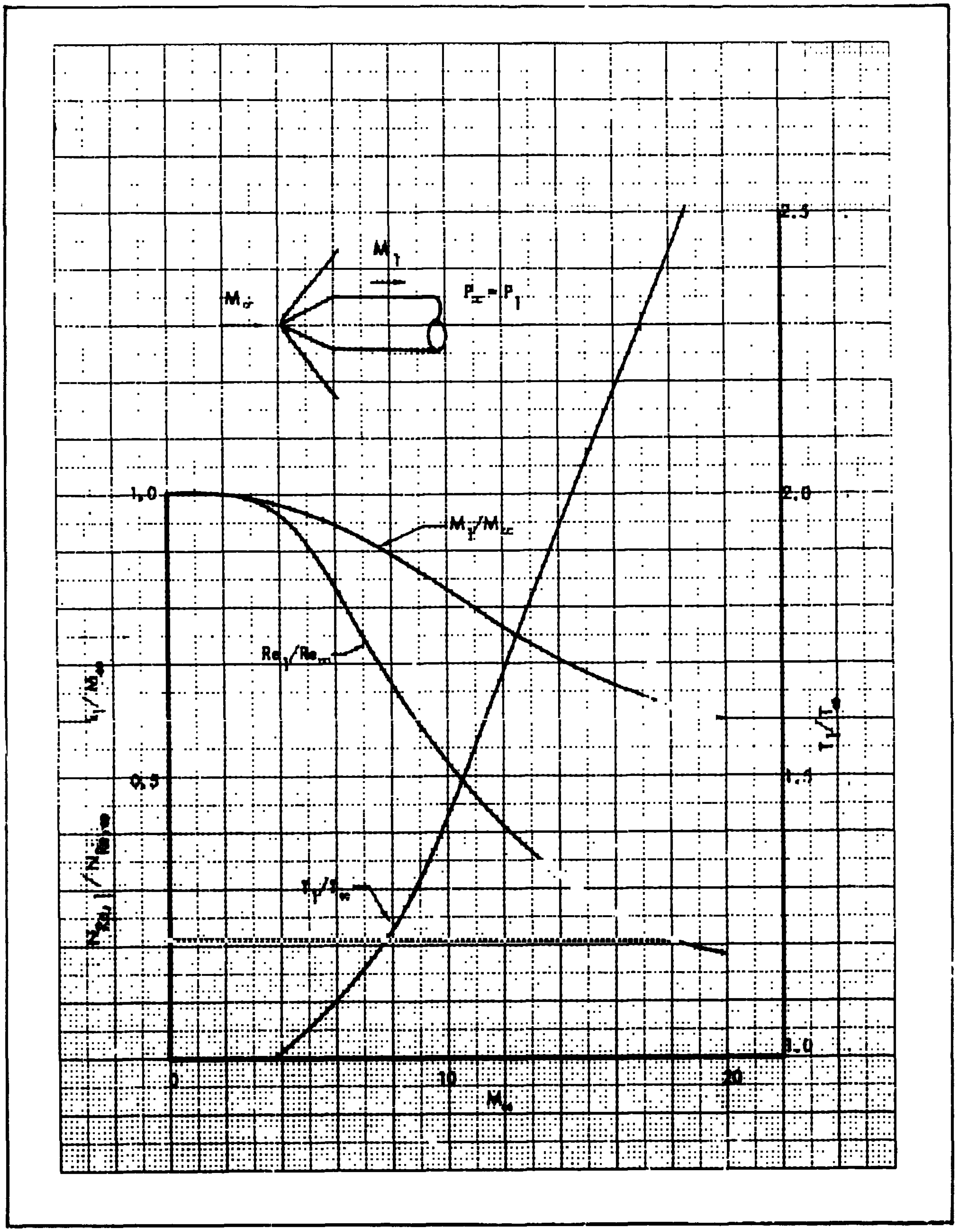

Figure 4-16. Flow Field Parameters for a 15° Half-Angle Sharp Cone Expanded to Free Stream Static Pressure

In addition to static pressure, a second local-flow property is required to fully determine the flow at the location of interest. At locations downstream of the nose shock only (locations 1 through 6), the local total pressure ratioed to the freestream total pressure should range between that computed across a normal shock wave and a conical shock generated by a pointed cone equal in cone angle to the nose cone value. The selection of the type of shock wave, i.e., normal or conical, which most nearly approximates the correct loss in total pressure is dependent on both the nose-bluntness ratio and distance downstream from the vehicle nose to the particular location. For length-to-nose diameter ratios of 5 or less, a normal nose shock is usually assumed.

In addition to the theories discussed in the previous paragraphs, which permit useful results to be obtained from hand calculations, additional analytical techniques are available which require the use of digital computers. Examples include the Van Dyke Blunt-Body Solution and the well-known Method of Characteristics. The primary justification for the use of approximate techniques in calculating inviscid flow fields is that results can be achieved in a relatively short time, however with some sacrifice in accuracy.

Air Property Relations

Once the velocity, static temperature, and pressure distribution around the body have been determined, boundary-layer edge thermodynamic and transport air property values may be obtained. At temperatures below about 3500°R, air may be considered a thermally perfect gas obeying the equation of state

$$P = \rho RT \qquad (4\text{-}19)$$

For the temperature range from 180 - 3500°R the well-known Sutherland viscosity relation may be used

$$\mu = 2.27 \times 10^{-8} \frac{T^{3/2}}{T + 198.6} \qquad (4\text{-}20)$$

This relation is shown in Figure 4-17. For approximate calculations the viscosity-temperature relation is often taken as $\mu \sim T^{0.7}$. Thermal conductivity values of air for the temperature range 200 to 1800°R are plotted in Figure 4-18. A reasonable assumption for the Prandtl number of air for the temperature range 180-3600°R is

$$N_{Pr} \simeq \text{Const} = 0.71$$

Aerodynamic Heating Definitions

Heat Transfer Coefficient - Similar to low-speed flows, the high velocity convection process is conventionally expressed through a heat transfer coefficient, h, which is defined by the following equation:

$$q = h \ (T_{aw} - T_w) \tag{4-21}$$

At very high temperatures, where real-gas effects become important, enthalpy is a better criterion of the energy potential than is temperature. This fact is accounted for through an alternate definition of the heat transfer coefficient based on enthalpy difference

$$q = h_i \ (i_{aw} - i_w) \tag{4-22}$$

Frequently, the heat transfer coefficient is expressed nondimensionally as either a Stanton or Nusselt number:

$$N_{St} = h/ \rho V c_p \tag{4-23}$$

$$N_{Nu} = hx/k \tag{4-24}$$

Adiabatic Wall Temperature and Enthalpy - The adiabatic wall temperature and enthalpy are the temperature and enthalpy, respectively, which the wall surface assumes for zero heat transfer. These quantities are expressed by a dimensionless parameter r, called the recovery factor and defined as

$$r = \frac{T_{aw} - T_1}{T_t - T_1} = \frac{i_{aw} - i_1}{i_t - i_1} \tag{4-25}$$

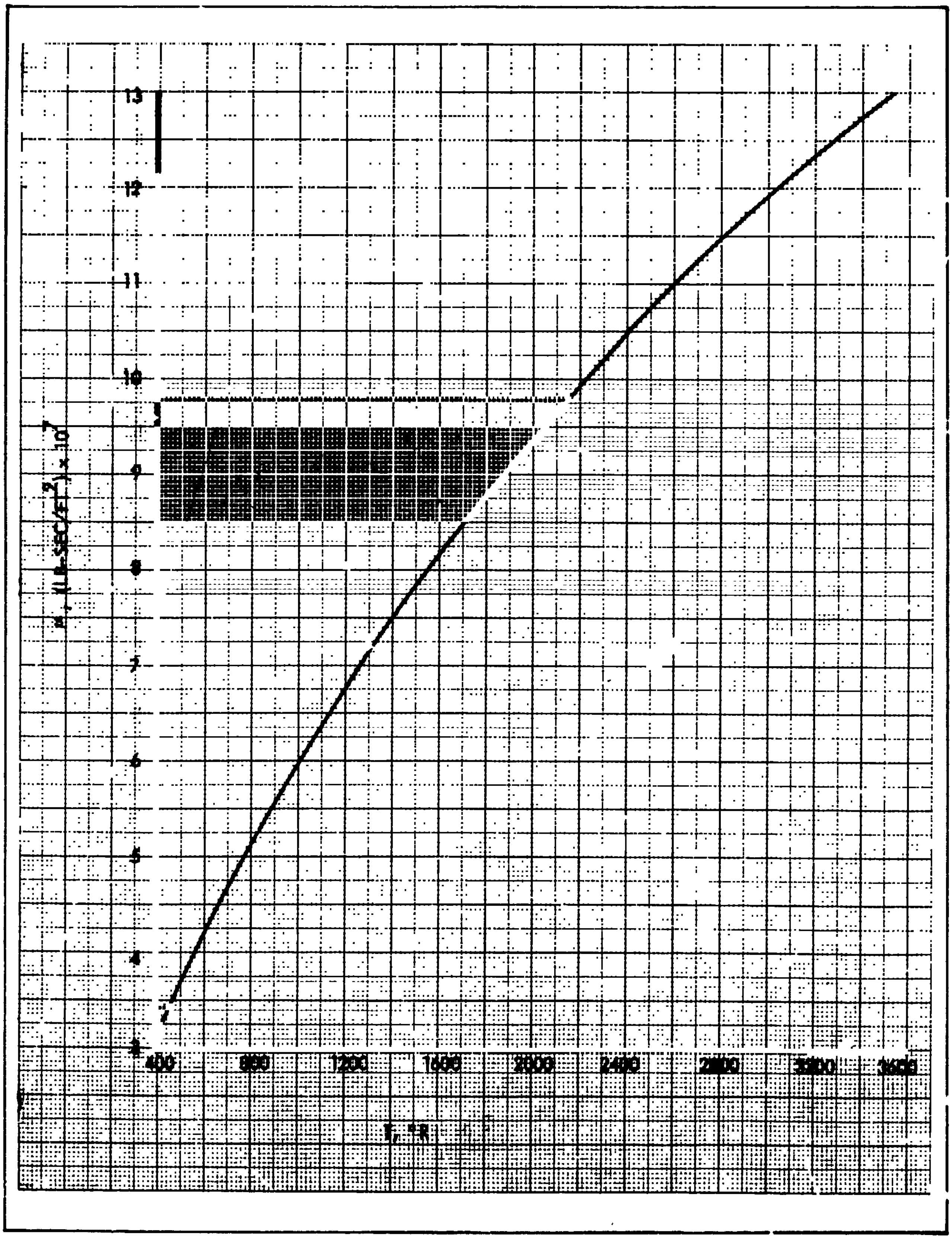

Figure 4-17. Viscosity of Air

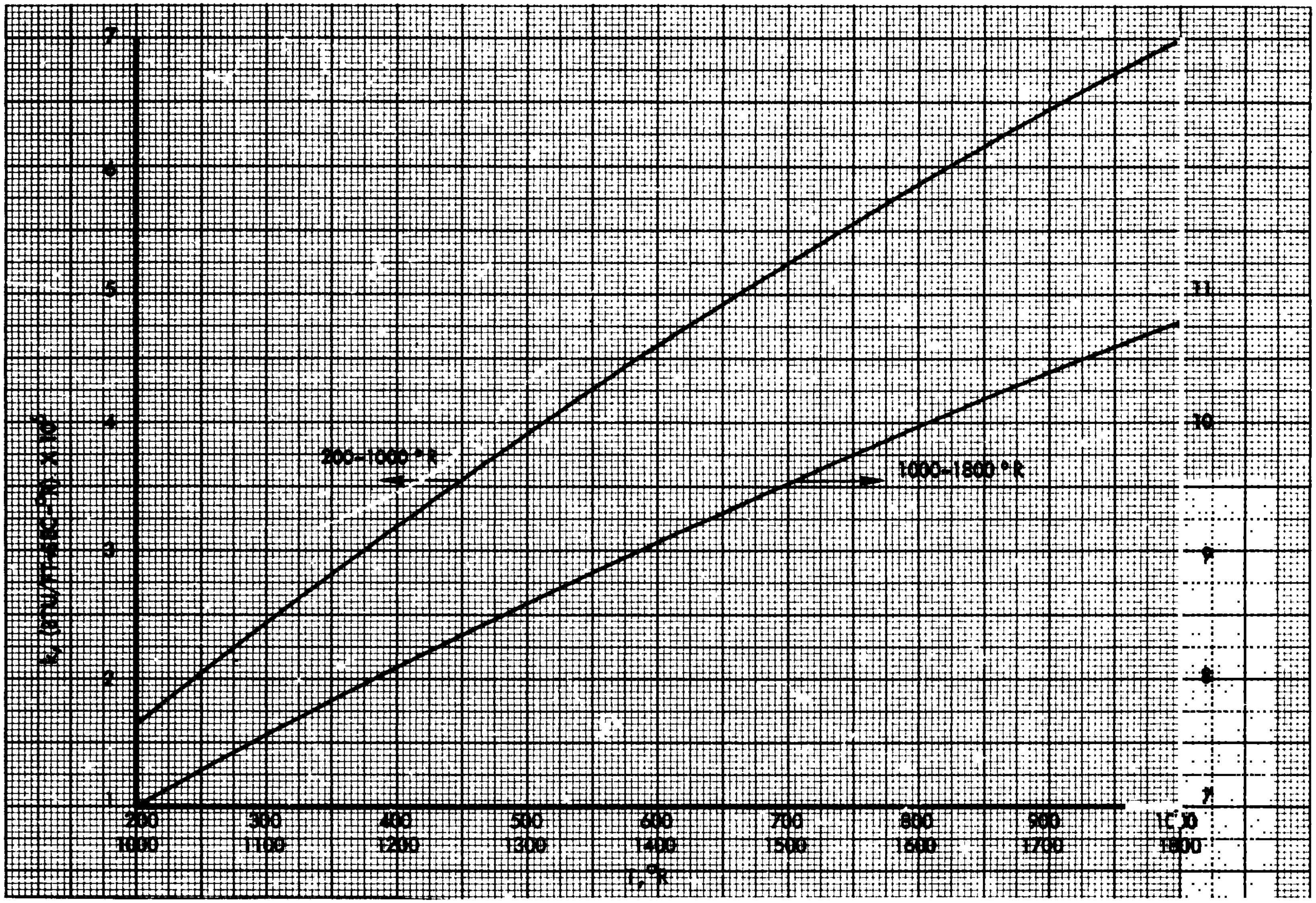

Figure 4-18. Thermal Conductivity of Air

where the subscripts t and l denote total and local (edge of boundary layer) conditions, respectively.

From the relations for total temperature and enthalpy, viz.

$$T_t = T_l + \frac{V_l^2}{2gJc_p} \tag{4-26}$$

$$i_t = i_l + \frac{V_l^2}{2gJ} \tag{4-27}$$

the expressions for adiabatic wall temperature and enthalpy become

$$T_{aw} = T_l + r\,\frac{V_l^2}{2gJc_p} \tag{4-28}$$

$$i_{aw} = i_l + r\,\frac{V_l^2}{2gJ} \tag{4-29}$$

For a perfect gas, the temperature relation is alternately

$$T_{aw} = T_l \left(1 + r\,\frac{\gamma - 1}{2} M_l^2 \right) \tag{4-30}$$

Generally, the recovery factor for air is taken as

$$r = N_{Pr}^{1/2} = 0.85 \text{ for laminar flow}$$

$$r = N_{Pr}^{1/3} = 0.90 \text{ for turbulent flow}$$

Local Skin Friction Coefficient - The local skin friction coefficient is, by definition, equal to the ratio of local shearing stress to the dynamic pressure, i.e.,

$$c_f = \frac{\tau_w}{\frac{1}{2}\rho_l u_l^2} \tag{4-31}$$

This quantity is of particular interest for heating calculation since it is related to the non-dimensional heat-transfer coefficient through the modified Reynolds analogy

$$N_{St} = \frac{h}{\rho_1 u_1 c_p} = \frac{c_f}{2} N_{Pr}^{-2/3} \qquad (4\text{-}32)$$

For incompressible flows, the local skin friction coefficient is a function of the local Reynolds number only, and may be obtained from the following relations:

$c_f = 0.664/N_{Re}^{0.5}$ (laminar flow-flat plate)

$c_f = 0.023/N_{Re}^{0.139}$ (turbulent flow-flat plate)

These equations are from Blasius (laminar) and Nikuradse (turbulent).

Reference Temperature-Enthalpy Concept

In addition to Reynolds number, the skin friction coefficient for high-velocity flow is a function of both the local Mach number and the wall-to-freestream static temperature ratio. Using a suitably defined reference temperature for evaluating the air-flow properties, it is possible to eliminate the skin friction coefficient's dependence on Mach number and temperature ratio (Ref. 4-7). This temperature allows the incompressible skin friction relations to be employed for high velocity compressible flow. The reference temperature relation for both laminar and turbulent flow is given by

$$T^* = 0.22\ T_{aw} + 0.28\ T_1 + 0.50\ T_w \qquad (4\text{-}33)$$

For a perfect gas, equation (4-33) may be written in terms of Mach number as

$$T^*/T_1 = 0.5\ (T_w/T_1 + 1) + 0.044\ r\ M_1^2 \qquad (4\text{-}34)$$

When the temperature variation within the boundary layer is so large that the specific heat of the air varies considerably, heating calculations should be based on enthalpies rather than temperatures. The Stanton number-skin friction relation becomes

$$N_{St} = \frac{h_i}{\rho u} \qquad (4\text{-}35)$$

and a reference enthalpy is used for the property evaluation, given by

$$i^* = 0.22\ i_{aw} + 0.28\ i_1 + 0.50\ i_w \tag{4-36}$$

Heating Relations

Flat Plates -

Laminar Flow - The recommended relation for calculation of laminar heat transfer on a uniform temperature flat plate is obtained from the modified Reynolds analogy and the Blasius equation for skin friction coefficient

$$N_{St}{}^* = 0.332\ (N^*_{Re})^{-1/2}\ (N_{Pr})^{-2/3} \tag{4-37}$$

where the Stanton number may be based on either temperature or enthalpy. The starred superscripts denote property evaluation at the reference temperature or enthalpy. An alternate expression, in terms of Nusselt number, may be written when the reference temperature is employed

$$N^*_{Nu} = 0.332\ (N^*_{Re})^{1/2}\ (N_{Pr})^{1/3} \tag{4-38}$$

Use of equations (4-37) and (4-38) should be restricted to the Reynolds number range, $N^*_{Re} \lesssim 10^5$.

Turbulent Flow - For Reynolds numbers greater than 10^6, the following reference temperature relation is recommended:

$$N^*_{Nu} = 0.0126\ (N^*_{Re})^{0.861}\ (N_{Pr})^{0.333} \tag{4-39}$$

This equation has been extensively verified by comparisons with flight data (Reference 4-8), and is valid for the Mach number range $1 \lesssim M_1 \lesssim 7$.

Transition Flow - For the Reynolds number range $10^5 \leq N^*_{Re} \leq 10^6$, the boundary-layer flow is usually transitory in nature. An equation for heating prediction for this N_{Re} range is given by

$$N^*_{Nu} = 5.85 \times 10^{-5}\ (N_{Re}{}^*)^{5/4}\ (N_{Pr})^{1/3} \tag{4-40}$$

The properties in this relation are evaluated at the reference temperature (Eqn. 4-33).

The above equations for flat plate heating may also be employed for cylindrical sections as long as the cylinder radius is large in comparison to the boundary layer thickness.

Cone and Cone Frustums - For equal boundary-layer edge flow conditions, the heating rate to a cone will be higher than a flat plate due to the thinner boundary layer associated with the conical flow. Using a Mangler transformation, it can be shown that the heating rate at a distance x from the apex of a cone with laminar boundary layer is equal to the heating rate at a distance x/3 from the leading edge of a flat plate, flow conditions immediately outside the boundary layer being the same. With the Blasius laminar skin friction relation, the equation for Stanton number on a cone becomes

$$N^*_{St} = \sqrt{3}\ 0.332\ (N^*_{Re})^{-1/2}\ (N_{Pr})^{-2/3} \qquad (4\text{-}41)$$

The heat transfer rates on a cone for turbulent flow at zero angle of attack can also be determined from flat-plate heating formulas. The heating rate at a distance x from the apex of a cone with turbulent boundary layer is equal to the heating rate on a flat plate at a distance $\frac{x}{2}$ from the leading edge of the plate, flow conditions immediately outside the boundary layer being the same. Thus, any of the formulas for predicting turbulent flat plate heating rates can be used to predict heating rates on a cone.

Stagnation Points - Due to the severity of stagnation heating rates, considerable investigation has been performed for this region. An exact solution for laminar stagnation point heat transfer was obtained by Fay and Riddell (Ref. 4-9), who considered both equilibrium and frozen flow. Numerical solutions were obtained for the range of variables, $540 \leq T_w \leq 5400°R$, $670 \leq i_t \leq 10{,}400$ Btu/lb (corresponding to $5800 \leq V_\infty \leq 22{,}800$ fps). The actual $\rho\mu$ variation through the boundary layer was determined. Their numerical solutions correlated with the following equation:

$$q_s = 0.763\, N_{Pr}^{-0.6} \; (i_t - i_w) \left(\frac{\rho_w \; \mu_w}{\rho_1 \; \mu_1} \right)^{0.1} \left(\rho_1 \, \mu_1 \beta \right)^{1/2} \left[1 + \left(N_{Le}^{\alpha} - 1 \right) \; i_d / i_t \right] \qquad (4\text{-}42)$$

where

$\alpha = 0.52$ for equilibrium flow

$\alpha = 0.63$ for frozen flow

Although this solution is based on the Sutherland formula for viscosity, a Prandtl number of 0.71 and a Lewis number constant through the boundary layer, the authors note that it should be valid for values of these parameters differing not too markedly from the values employed in the numerical solution.

Romig (Ref. 4-10) derived a simplified formula based on the reference enthalpy method, by assuming $M_\infty \gg 1$, $N_{Pr} = 1$, $T_\infty = 400$ R, and a highly cooled wall.

$$q_s = 0.0145\, M_\infty^{\,3.1} \; (P_\infty / R_b)^{1/2} \qquad (4\text{-}43)$$

Although Romig's reference enthalpy equation is an extrapolation of a low speed solution rather than a solution of the appropriate boundary layer equations, it has been shown to predict heating rates in fairly good agreement with the Fay-Riddell equation.

For a modified Newtonian flow, the stagnation point velocity gradient is given by

$$\beta = \frac{1}{R_b} \quad \left(\frac{2\,(P_t \; - \; P_\infty)}{\rho_t} \right)^{1/2} \qquad (4\text{-}44)$$

For air at hypervelocities, $N_{Le} \simeq 1.4$. The dissociation enthalpy, i_d, may be approximated by (Ref. 4-11).

$$1 \leq Z \leq 1.21, \; i_d = 8331\, Z - 8272 \qquad (4\text{-}45)$$

$$Z > 1.21, \; i_d = 14{,}032\, Z - 15{,}205 \qquad (4\text{-}46)$$

where Z is the compressibility factor defined by $Z = P/\rho RT$.

The ratio between stagnation-point heat transfer to bodies of revolution and two-dimensional bodies can be expressed as follows:

$$\frac{q_{s_{axi}}}{q_{s_{2\text{-dim}}}} \simeq 2^{1/2} \left(\beta_{axi}/\beta_{2\text{-dim}}\right)^{1/2} \tag{4-47}$$

For bodies of the same nose radius and freestream Mach numbers greater than approximately 2, equation (4-47) reduces to

$$q_{s_{axi}} \approx 2^{1/2}\, q_{s_{2\text{-dim}}} \tag{4-48}$$

Thus, the formulas given above for bodies of revolution may also be employed for two-dimensional bodies.

Heat-Transfer Distribution on a Blunt Body - The preferred method of calculating laminar boundary-layer heat-transfer distributions is that suggested by Lees in Reference(4-12). The fundamental input parameter in the calculation is the surface pressure distribution. Lees' results may be expressed as

$$\frac{q}{q_s} = \frac{\frac{1}{2}\left(\frac{P_1}{P_t}\right)\left(\frac{u_1}{u_\infty}\right) r \left(R_b\right)^{1/2}}{\left[\int_o^s \left(\frac{P_1}{P_t}\right)\left(\frac{u_1}{u_\infty}\right) r^2\, ds\right]^{1/2} \left[\frac{1}{u_\infty}\left(\frac{du_1}{d\theta}\right)_s\right]^{1/2}} \tag{4-49}$$

Figure 4-19 presents the heating distribution on a hemisphere for the case of a modified Newtonian-Prandtl-Meyer pressure distribution with free-stream Mach number as a parameter.

Heat transfer distributions for a family of blunted cones are presented in Figs. 4-20 through 4-24. These calculations utilized the modified Newtonian-Prandtl-Meyer method for estimating pressure variations.

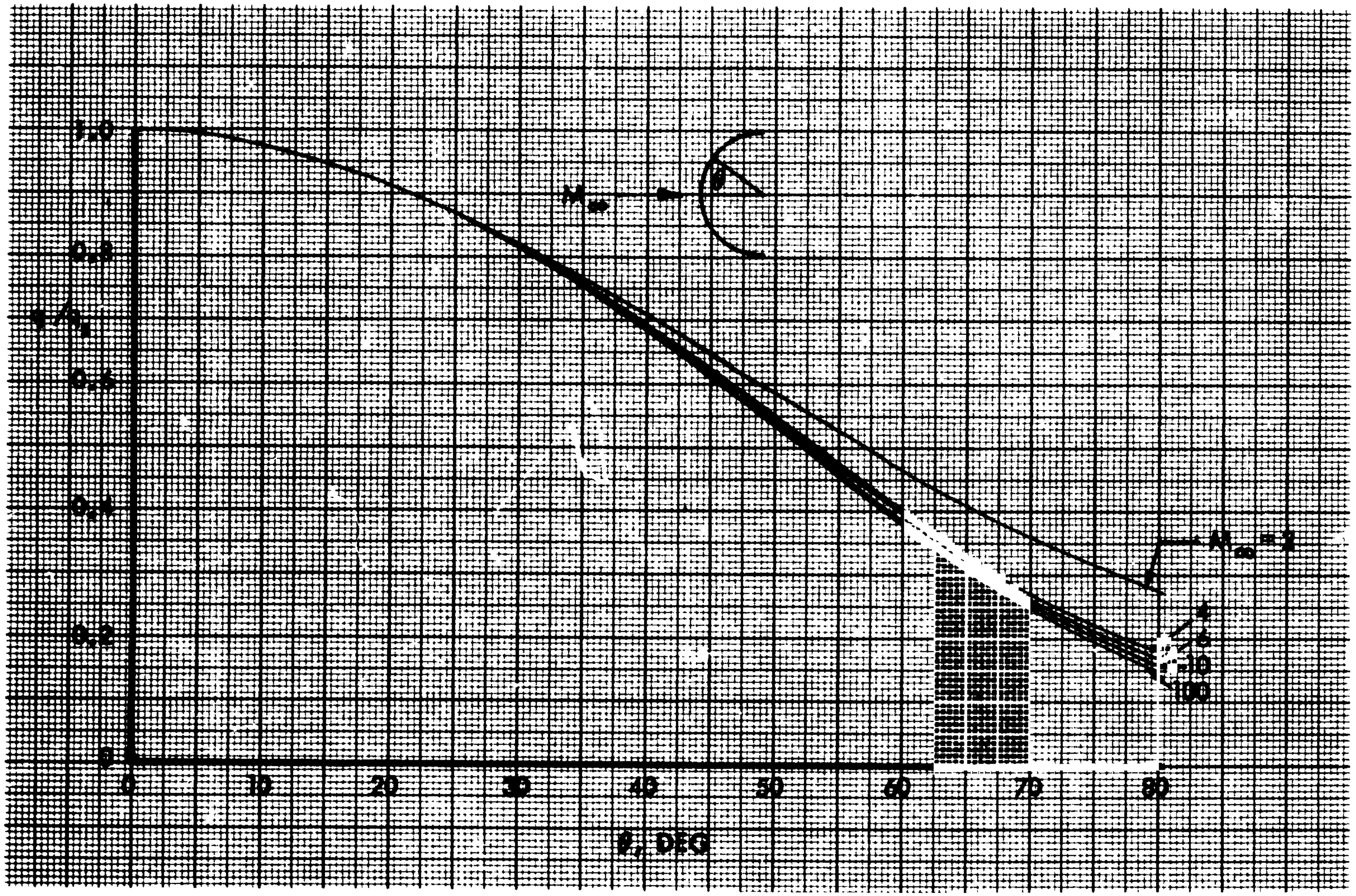

Figure 4-19. Laminar Heating Distribution on a Hemisphere

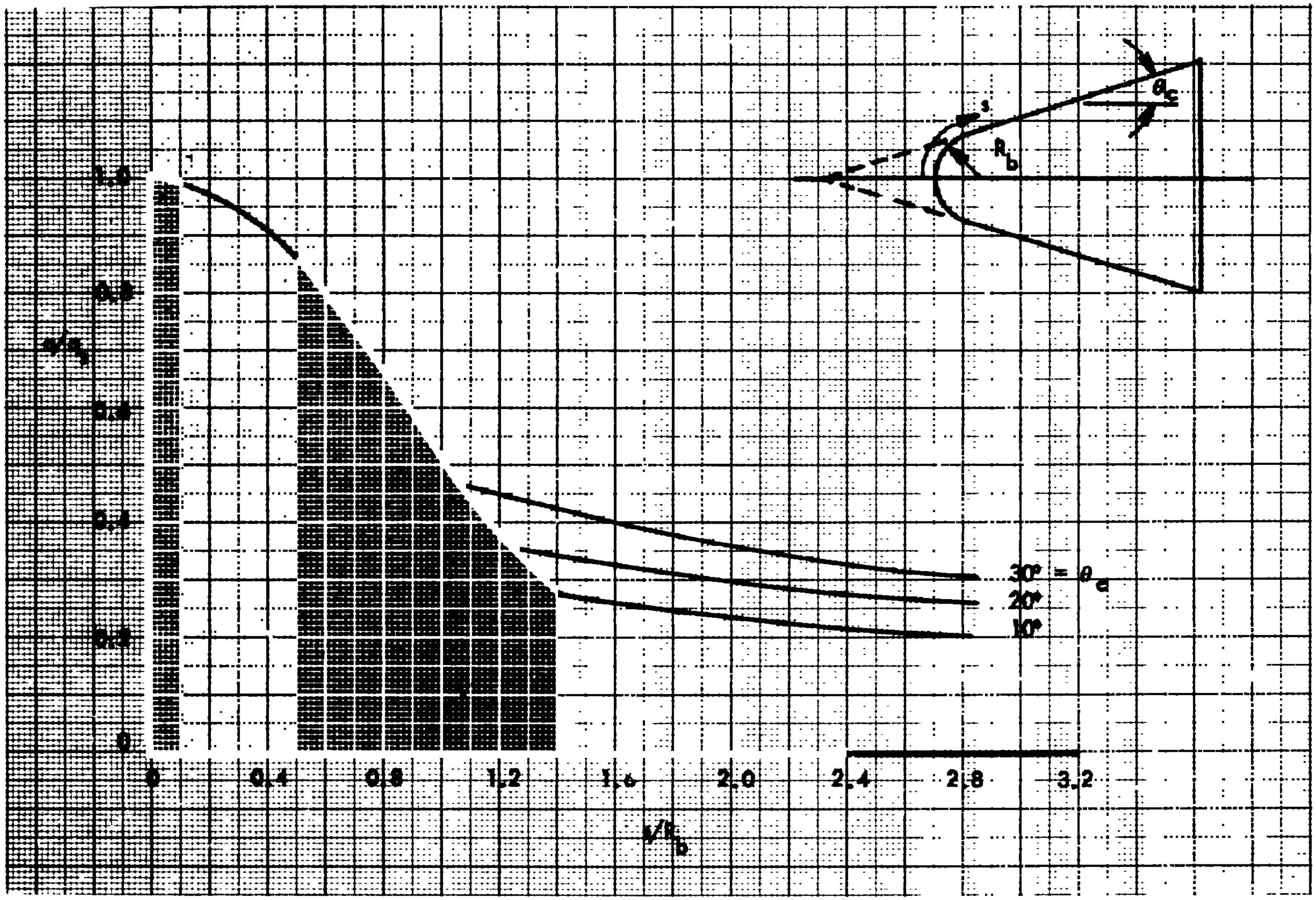

Figure 4-20. Blunted Cone Laminar Heating Distribution, $M_\infty = 2$

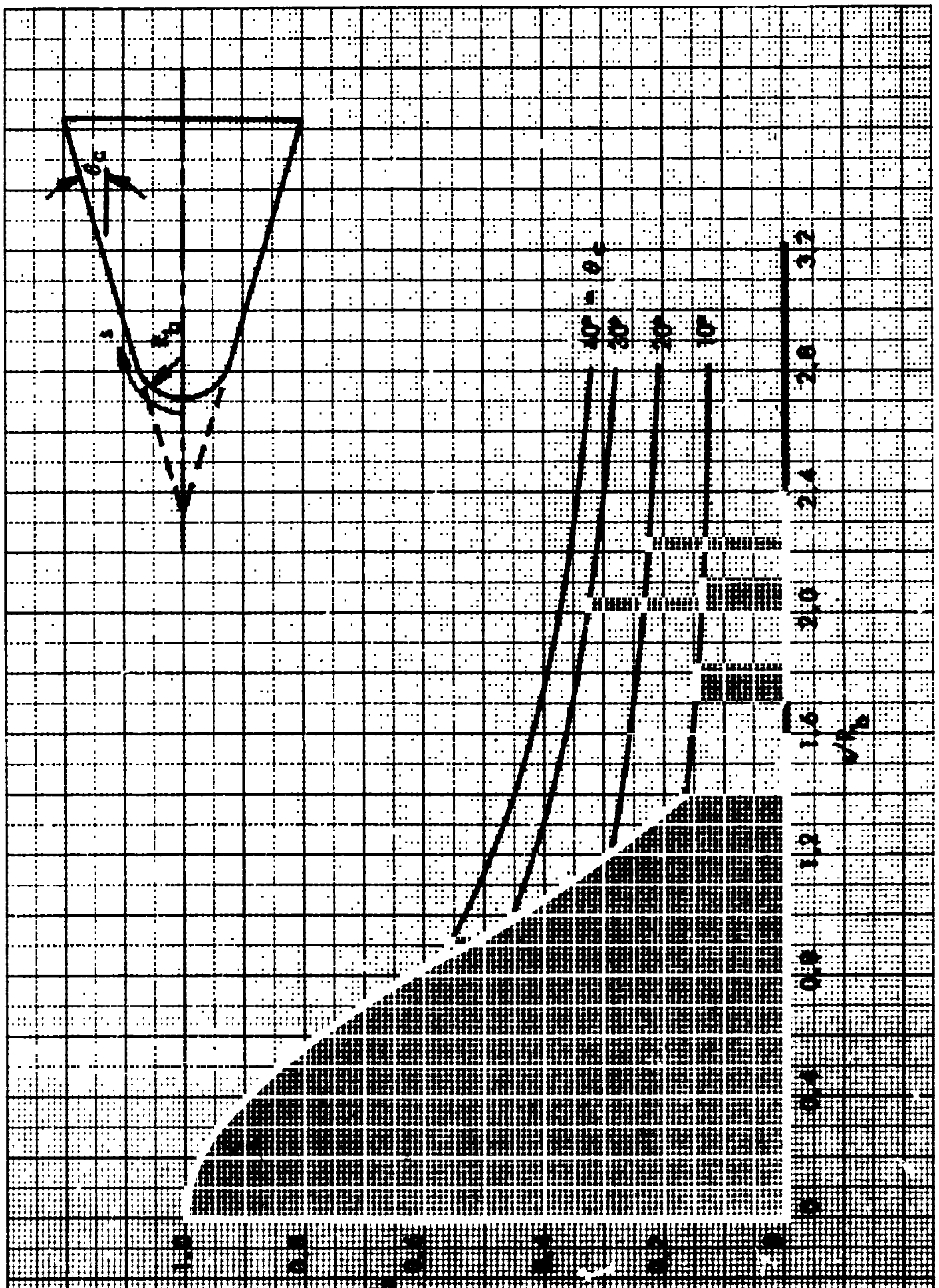

Figure 4-21. Blunted Cone Laminar Heating Distribution, $M_\infty = 4$

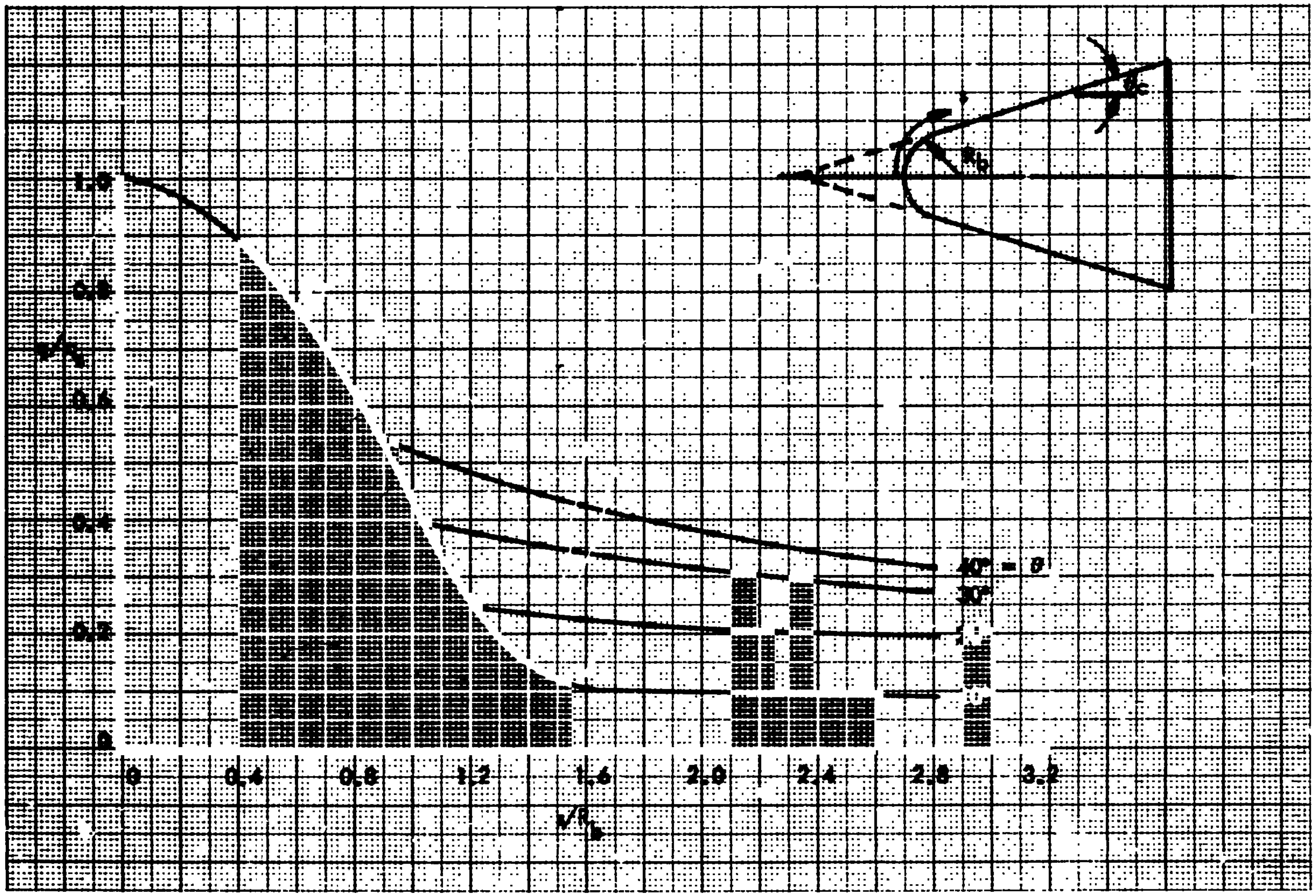

Figure 4-22. Blunted Cone Laminar Heating Distribution, $M_\infty = 6$

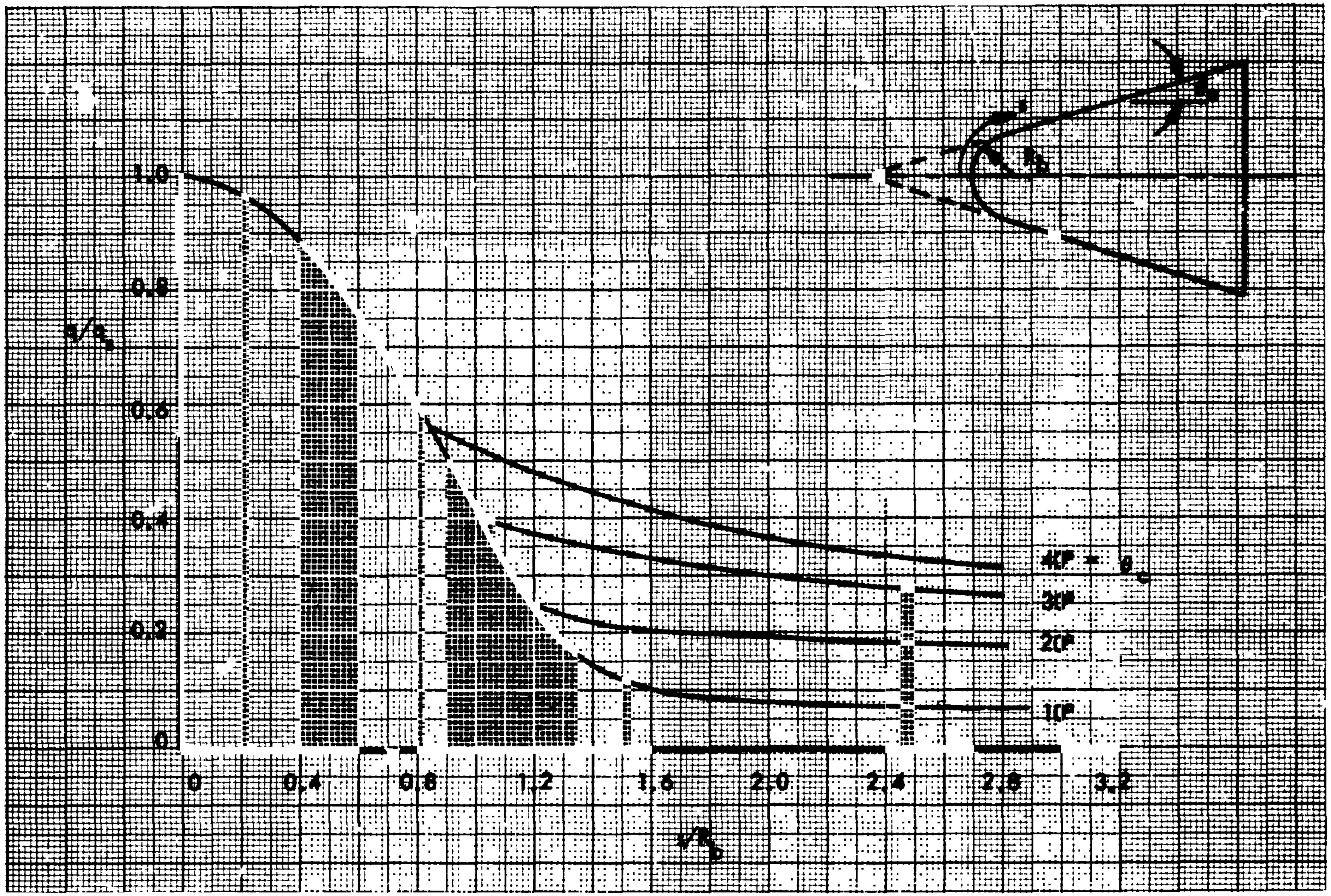

Figure 4-23. Blunted Cone Laminar Heating Distribution, $M_\infty = 10$

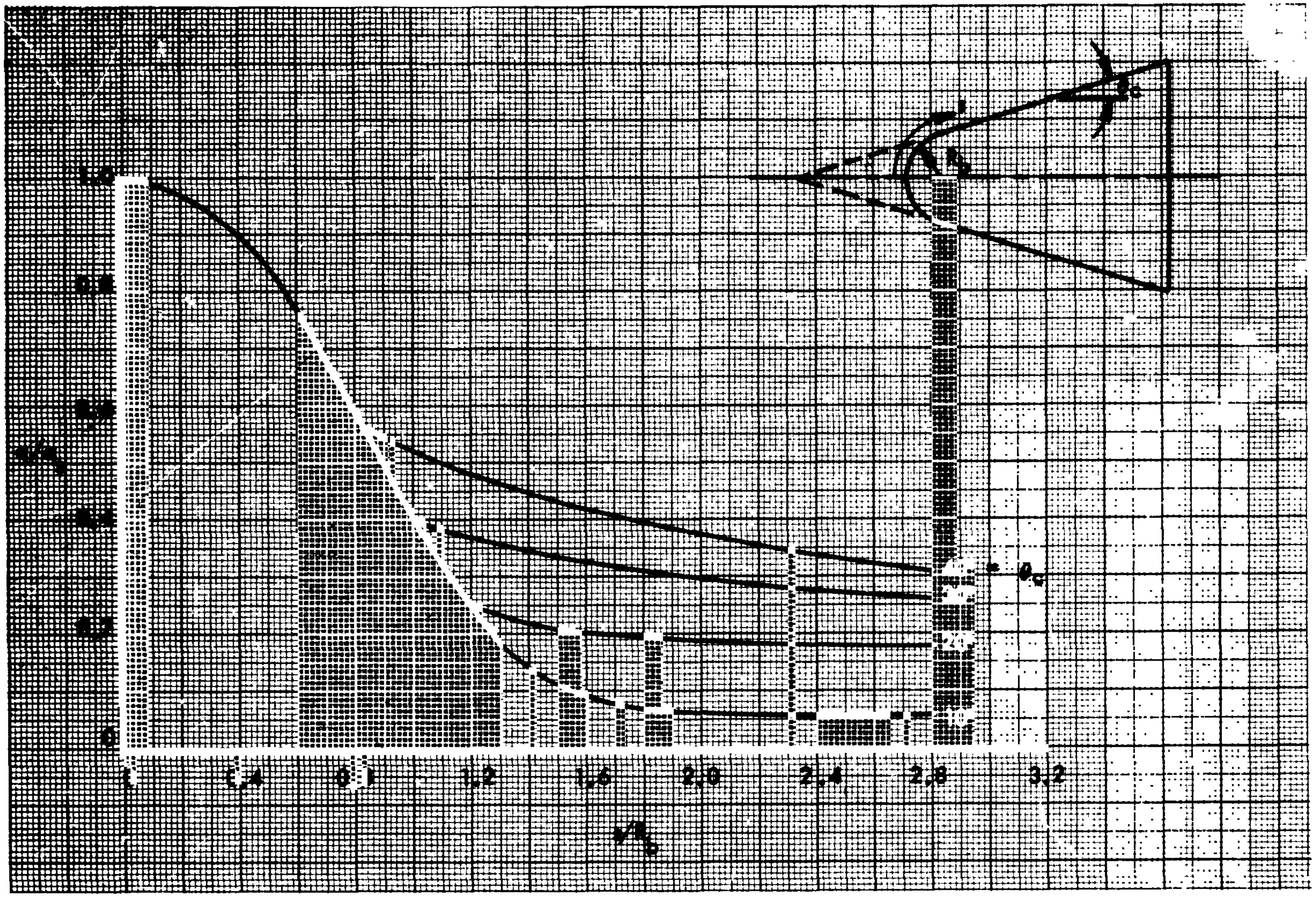

Figure 4-24. Blunted Cone Laminar Heating Distribution, $M_\infty = 100$

Sample Calculation

This section presents a sample calculation illustrating a portion of the recommended procedures for aerodynamic heating calculation. The vehicle configuration and location selected for this example are shown in the following sketch:

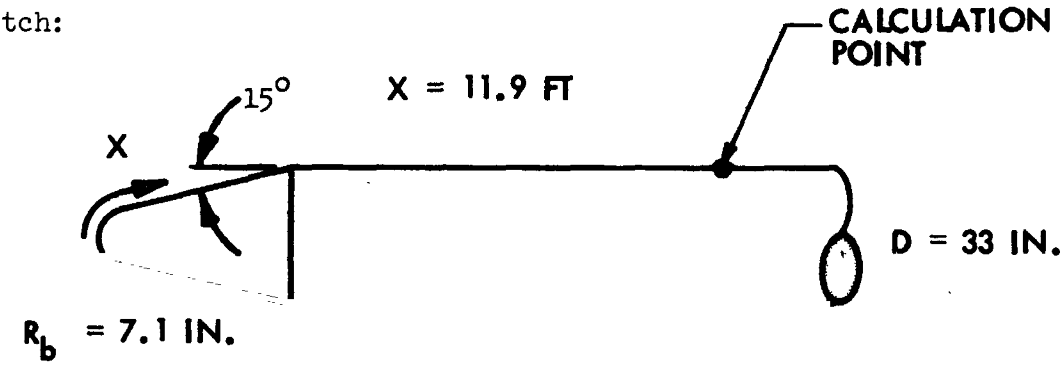

The nose configuration consists of a 15° blunted cone intersecting a 33-in. -diameter cylinder. At a particular trajectory time point (t = 80 sec), the freestream altitude and velocity are 100,000 ft and 6000 fps, respectively. The wall temperature is 625°R. It is desired to calculate the wall heating rate.

Using the 1962 ARDC atmosphere and the above trajectory data,

$$T_\infty = 408 \text{ R}$$

$$a_\infty = 991 \text{ fps}$$

$$\therefore \quad M_\infty = 6.05$$

Prior to calculation of the local aerodynamic heating rates, a determination of the inviscid flow parameters (M_1, P_1, T_1) at the boundary-layer edge is required. An approximate flow-field calculation method is utilized, which assumes the boundary-layer edge streamline passes through a shock wave generated by a 15° semi-apex angle sharp cone and expands to zero-pressure coefficient along the cylindrical section. Zero angles of attack, pitch, and yaw are assumed.

Inviscid Flow Field Calculation - The assumed configuration and shock shape used in the analysis is sketched below:

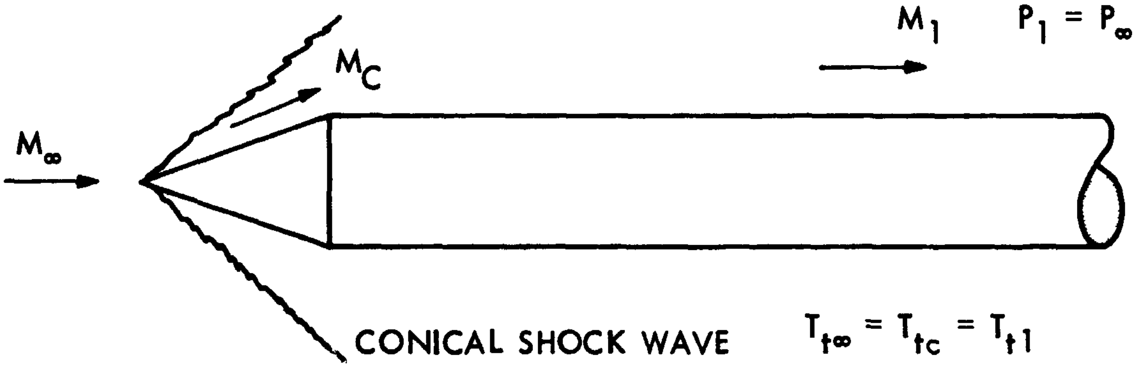

The ratios of the local Mach number and static temperature to the corresponding freestream values are plotted in Figure 4-16. However, to illustrate the computational method, these curves are not employed. The sharp cone-to-freestream property values are obtained from Figures 4-9 and 4-11 as

$$P_c/P_\infty = 4.80,\ M_c/M_\infty = 0.720\ \therefore M_c = 4.36$$

and from Table II of Reference 4-1:

$$P_c/P_{c_t} = 0.00412$$

The entire flow field downstream of the nose shock is assumed isentropic. Therefore,

$$P_\infty = P_1 \text{ and } P_{c_t} = P_{1_t}$$

$$\frac{P_1}{P_{1_t}} = \left(\frac{P_c}{P_{c_t}}\right)\left(\frac{P_\infty}{P_c}\right) = 0.00412/4.80 = 0.858 \times 10^{-3}$$

M_1 is obtained from Table II of Reference 4-1 as

$$M_1 = 5.71$$

Also

$$\frac{T_\infty}{T_{\infty_t}} = 0.120,\ \frac{T_1}{T_{1_t}} = 0.133$$

since

$$T_{\infty_t} = T_{1_t}$$

$$T_1 = (T_1/T_{1_t})\ (T_{\infty_t}/T_{\infty})\ (T_{\infty})$$

$$T_1 = \left(\frac{0.133}{0.120}\right)(408.) = 452.\text{R}$$

Heating Rate Calculation - Flat-plate heating relations are employed since the cylinder radius is large compared with the boundary layer thickness. To calculate the adiabatic wall temperature, turbulent flow is assumed. This assumption is checked later in the calculations. From equation (4-30)

$$T_{aw} = 452.\left(1 = 0.71^{1/3}\ \frac{1.4-1}{2}\ (5.71)^2\right)$$

$$T_{aw} = 3070.\ \text{R}$$

According to the Nusselt number definition

$$h = N^*_{Nu}\ \left(\frac{k^*}{x}\right)$$

The star superscript denotes property evaluation at the reference temperature, given by equation (4-33) ince $T_w = 652$ R

$$T^* = 0.22\ (3070) + 0.28\ (452.) + 0.50\ (652)$$

$$T^* = 1127.\ \text{R}$$

From equation (4-39)

$$h = 0.0126\ (k^*/x)\ \ N^*_{Re}\ 0.861\ \ N^*_{Pr}{}^{1/3}$$

The Reynolds number evaluated at the reference temperature is

$$N^*_{Re} = \frac{V_1 \rho^* x}{\mu^*}$$

Using the perfect-gas equation of state ($P = \rho RT$) and the speed of sound relation ($a = \sqrt{\gamma RT}$), this Reynolds number may be expressed as

$$N_{Re}{}^* = N_{Re_\infty}\left(\frac{M_1}{M_\infty}\right)\left(\frac{T_1}{T_\infty}\right)^{1/2}\left(\frac{P_1}{P_\infty}\right)\left(\frac{T_1}{T^*}\right)\left(\frac{\mu_\infty}{\mu^*}\right)$$

Assuming a viscosity-temperature relation of the form

$$\mu \sim T^{0.7}$$

and the condition, $P_1 = P_\infty$, yields

$$N_{Re}^* = N_{Re_\infty}\left(\frac{M_1}{M_\infty}\right)\left(\frac{T_1}{T_\infty}\right)^{1/2}\left(\frac{T_\infty}{T^*}\right)^{1.7}$$

The heat-transfer coefficient is, then,

$$h = \frac{0.0126}{X^{0.139}} \cdot \left[\frac{N_{Re_\infty}}{X}\left(\frac{M_1}{M_\infty}\right)\left(\frac{T_1}{T_\infty}\right)^{1/2}\left(\frac{T_\infty}{T^*}\right)^{1.7}\right]^{0.861} k^* N_{Pr}^{1/3}$$

where

x is taken as the wetted distance from the stagnation point to the location in question.

N_{Re_∞}/x is the freestream Reynolds number per foot and is simply a function of the vehicle altitude and velocity.

k* is the temperature dependent thermal conductivity of air and may be obtained from Figure 4-18.

A constant Prandtl number equal to 0.71 is recommended for the heating rate calculation.

The freestream Reynolds number is, by definition,

$$N_{Re} = \frac{V_\infty x}{\nu_\infty}$$

From the configuration sketch, the wetted distance x is given as

$$x = 11.9 \text{ ft}$$

From the '62 atmosphere table at 100,000 ft

$$\nu_\infty = 9.30 \times 10^{-3}\ \text{ft}^2/\text{sec}$$

then

$$N_{Re_\infty} = \frac{(6000)\ (11.9)}{(9.30 \times 10^{3})}$$

$$N_{Re_\infty} = 7.0 \times 10^{6}$$

The local Reynolds number, evaluated at T* is thus

$$N^*_{Re} = (7.0 \times 10^{6}) \left(\frac{5.71}{6.05}\right)\left(\frac{452}{408}\right)^{0.5}\left(\frac{408.}{1127.}\right)^{1.7}$$

$$N^*_{Re} = 1.23 \times 10^{6}$$

Since $N^*_{Re} > 10^6$, the turbulent flow assumption is probably correct. The heat-transfer coefficient for turbulent flow is, then, from equation (4-39)

$$h = 0.0126\ \left(\frac{7.75 \times 10^{-6}}{11.9}\right)\ (1.23 \times 10^{6})^{0.861}\ \ (0.71)^{1/3}$$

$$h = 1.26 \times 10^{-3}\ \ \frac{\text{Btu}}{\text{ft}^2\text{-sec-}^\circ\text{R}}$$

where k (T*) was obtained from Figure 4-18

From equation (4-21), the wall heating rate is

$$q_w = 1.26 \times 10^{-3}\ \ (3070-652)$$

$$q_w = 3.04\ \text{Btu/ft}^2\text{-sec}$$

ORBITAL HEATING

The absorbed thermal radiation in orbit above the Earth's atmosphere at any body angle, altitude, and orbit angle, can be found from the following equation:

$$\dot{q} = \alpha_S(\dot{q}_S + \dot{q}_A) + \epsilon(\dot{q}_E) \quad \text{Btu/sec ft}^2 \tag{4-50}$$

where α_S = solar absorptivity

ϵ = infrared emissivity

$\dot{q}_S$ = incident solar radiation

$\dot{q}_A$ = albedo, reflected solar radiation from Earth and its atmosphere

$\dot{q}_E$ = Earthshine, radiation emitted from the Earth

This section describes the method of determining the incident thermal radiation, $\dot{q}$, on a spacecraft in Earth orbit, using a simplified procedure suitable for preliminary hand computation. Charts are included to assist in the calculation of albedo and Earthshine. A more rigorous approach to the computation of orbital radiation, including lunar orbits and non-uniform radiosity of the Earth, and a computer program to perform the calculations are presented in Ref. 4-13. The concept of effective sink temperature, which is useful in simplified analyses of orbiting spacecraft, is introduced in Section V.

The location of orbit and body angles is illustrated in Figure 4-25 and the various terms are defined in the following section. The thermal radiation incident on a spacecraft in orbit can be obtained by dividing the surface into a number of "flat" segments. To ensure that the heating rate at the center of the surface element is a good approximation for the whole segment, the body angles included by the surface should be no larger than 30°.

Orbital Radiation Nomenclature

ψ **Body angle, measured clockwise around the vehicle when looking forward. (ψ=0° at the point furthest from the Earth in a horizontal flight, or at the leading edge in a vertical flight.)**

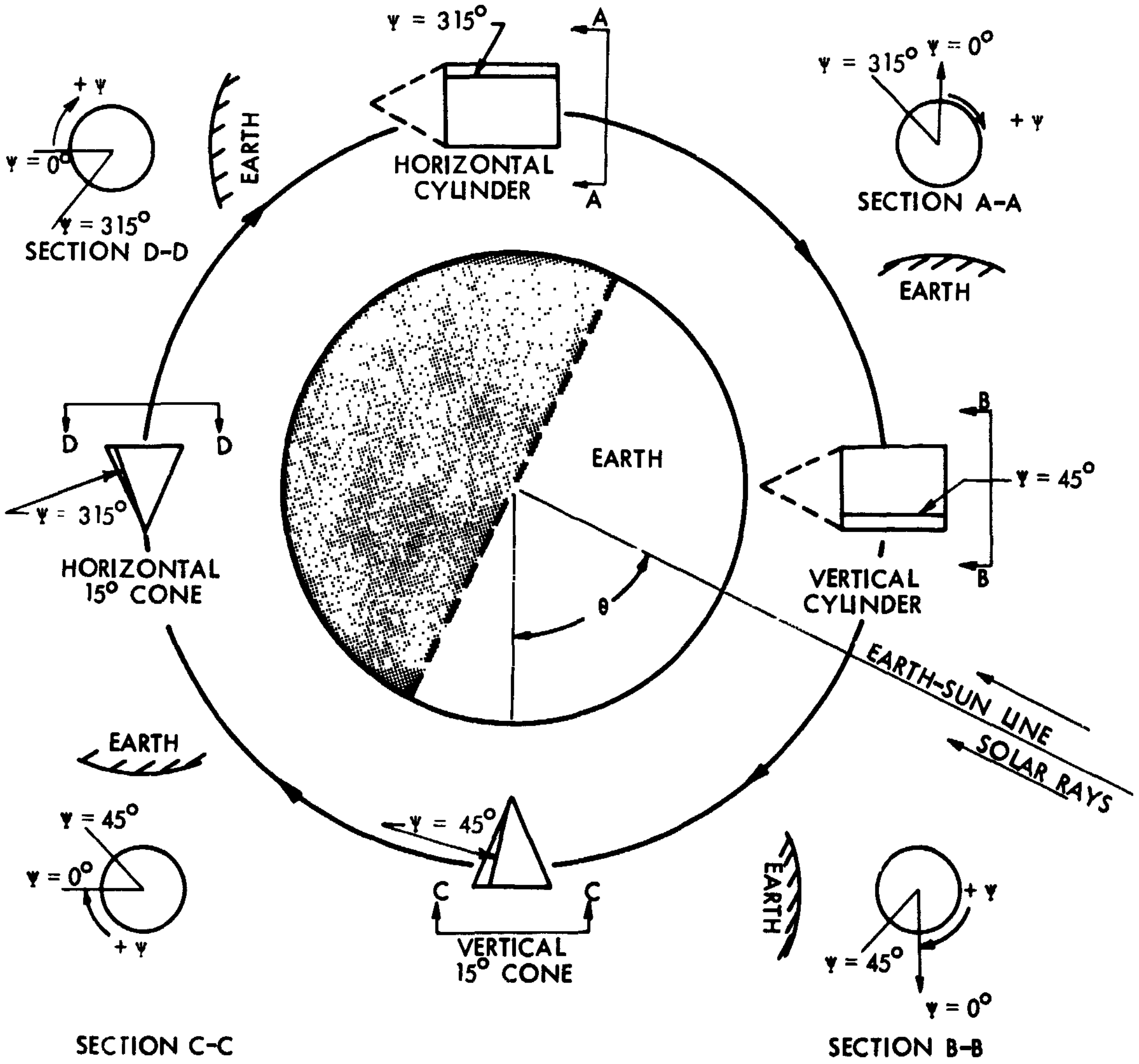

NOTE: THE BODY ANGLES ARE ALWAYS MEASURED CLOCKWISE WHEN LOOKING TOWARD THE NOSE OF THE VEHICLE.

IN A NOON ORBIT, THE ORBIT ANGLE IS MEASURED FROM THE EARTH-SUN AXIS IN THE DIRECTION OF MOTION OF THE VEHICLE.

Figure 4-25. Location of Orbit and Body Angles

λ	Cone half-angle, the angle between the axis of the cone and any element. (λ is positive for a vertical cone with the vertex toward the Earth, and for a horizontal cone with the vertex in the direction of motion.)
θ	Orbit angle, measured in the direction of flight from the point closest to the sun and in the orbit plane. ($\theta = 0°$ at the Earth-sun line for a "noon" orbit.
β	Orbit inclination, the angle between the Earth-sun line and the orbit plane. β is positive if an increase in θ produces counter-clockwise motion when the orbit plane is viewed from the sun. ($\beta = 0°$ for a "noon" orbit.)
δ	Angle between the sun's rays and a line normal to the surface.
ρ	Angle between the zenith and a line normal to the surface, always positive and less than 180°. ($\rho = 0°$ on the top of a horizontal flat plate and 180° on the bottom.)
α_S	Solar absorptivity
ϵ	Surface emissivity
h	Orbit altitude, miles
R_e	Mean radius of Earth, 3,960 miles
F_p	View factor from spacecraft surface element to Earth's surface.
S	Solar constant, the irradiation from the sun intercepted by a plane surface normal to the sun's rays at a distance equivalent to the mean distance between the Earth and the sun, 0.123 Btu/sec ft^2.
$\dot{Q}$	Total irradiation absorbed per ft^2, Btu/sec ft^2.
$\dot{q}$	Incident thermal radiation, Btu/sec ft^2.

Subscripts

S	Solar, direct radiation from the sun.
A	Albedo, reflected radiation from Earth and atmosphere.
E	Earthshine, radiation emitted from Earth.

Solar Irradiation

Solar irradiation is calculated from the following equation:

$$\dot{q}_S = S \cos \delta \text{ Btu/sec ft}^2 \qquad (4\text{-}51)$$

where cos δ is evaluated as follows:

1. Horizontal Cone

$$\cos \delta = \cos \lambda \cos \psi \cos \beta \cos \theta - \sin \lambda \cos \beta \sin \theta - \cos \lambda \sin \psi \sin \beta \qquad (4\text{-}52)$$

For a 15° half-angle horizontal cone, vertex trailing, and in a "noon" orbit, $\lambda = -15°$, $\beta = 0°$.

$$\cos \delta = \cos 15° \cos \psi \cos \theta + \sin 15° \sin \theta \qquad (4\text{-}52a)$$

For a horizontal cylinder in a "noon" orbit, $\lambda = 0°$, $\beta = 0°$.

$$\cos \delta = \cos \psi \cos \theta \qquad (4\text{-}52b)$$

2. Vertical Cone

$$\cos \delta = \cos \lambda \sin \psi \sin \beta - \sin \lambda \cos \beta \cos \theta - \cos \lambda \cos \psi \cos \beta \sin \theta \qquad (4\text{-}53)$$

For a 15° half angle vertical cone, vertex toward Earth, and in a "noon" orbit, $\lambda = 15°$, $\beta = 0°$.

$$\cos \delta = -\sin 15° \cos \theta - \cos 15° \cos \psi \sin \theta \qquad (4\text{-}53a)$$

For a vertical cylinder in a "noon" orbit, $\lambda = 0°$, $\beta = 0°$.

$$\cos \delta = -\cos \psi \sin \theta \qquad (4\text{-}53b)$$

The solar inputs occur when cos δ is positive, where the angle between the sun's rays and the normal to the surface is given by $270° < \delta < 90°$. For any given body angle, ψ, the appropriate equation for cos δ can be solved for the orbit angles, θ, where cos δ becomes either zero or negative. These orbit angles indicate when the orientation is such that the spacecraft itself shades the surface. At low altitudes, however, the spacecraft may pass into the shadow of the Earth before this happens. The maximum range of orbit angles during which the spacecraft can receive solar irradiation is given by:

$$\left(90° + \cos^{-1}\frac{R_e}{R_e+h}\right) \geq \theta \geq \left(270° - \cos^{-1}\frac{R_e}{R_e+h}\right) \qquad (4\text{-}54)$$

This relation is illustrated in Figure 4-26. Both the maximum range of solar irradiation and the orbit angles when cos δ is negative must be considered when determining the duration of solar input at any body angle.

Albedo Irradiation

The albedo irradiation may be expressed as:

$$\dot{q}_A = 0.38 \text{ S } F_p \cos\theta \cos\beta \text{ Btu/sec ft}^2 \qquad (4\text{-}55)$$

where 0.38 is the average reflectivity of the Earth. Figure 4-27 presents the albedo irradiation as a function of the angle between the surface normal and the zenith, ρ, orbit angle, θ, orbit inclination, β, and altitude, h. A family of curves of $\dot{q}_A$ vs F_p is plotted with θ as a parameter. Another family of curves of F_p as a function of ρ is plotted on the same figure with altitude as a parameter. Since F_p is a function of ρ and h, and q_A is a function of F_p, θ, and β, it is possible to find albedo irradiation for various combinations of ρ, θ, and h by plotting both families of curves with F_p as the abscissa. For inclination angles other than $\beta = 0°$, the effect is the same as shifting the F_p scale by cos β. Albedo irradiation for any inclination can be found by using the F_p scale corresponding to the orbit inclination under consideration. The procedure for use of Figure 4-27 to compute the albedo irradiation is as follows:

1. Enter the right-hand scale at the angle between the normal and the zenith, ρ.
2. Project a horizontal line intersecting the appropriate altitude line.
3. Find the planetary view factor, F_p, on the lower scale for $\beta = 0°$.

4a. For orbit inclination $\beta = 0$, project a vertical line intersecting the appropriate orbit angle, θ.

4b. For orbit inclination $\beta \neq 0$, enter lower scale with reduced scale F_p for correct value of β, then project a vertical line intersecting the appropriate orbit angle, θ.

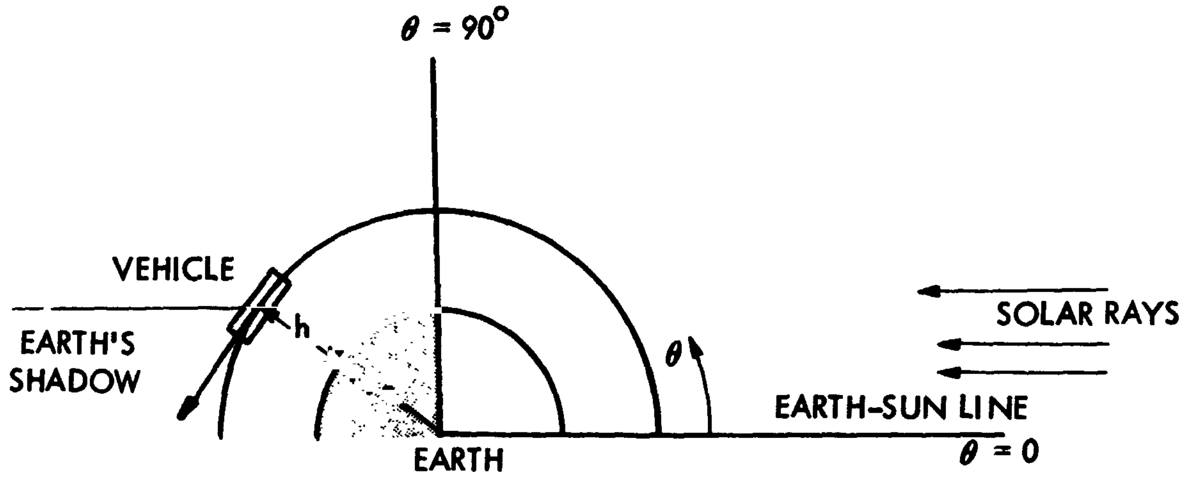

NOTE: VEHICLE RECEIVES SOLAR IRRADIATION FOR

$$\left(90^\circ + \cos^{-1}\frac{R_e}{R_e + h}\right) \geq \theta \geq \left(270^\circ - \cos^{-1}\frac{R_e}{R_e + h}\right)$$

Figure 4-26. Orbit Angles for Receiving Solar Irradiation

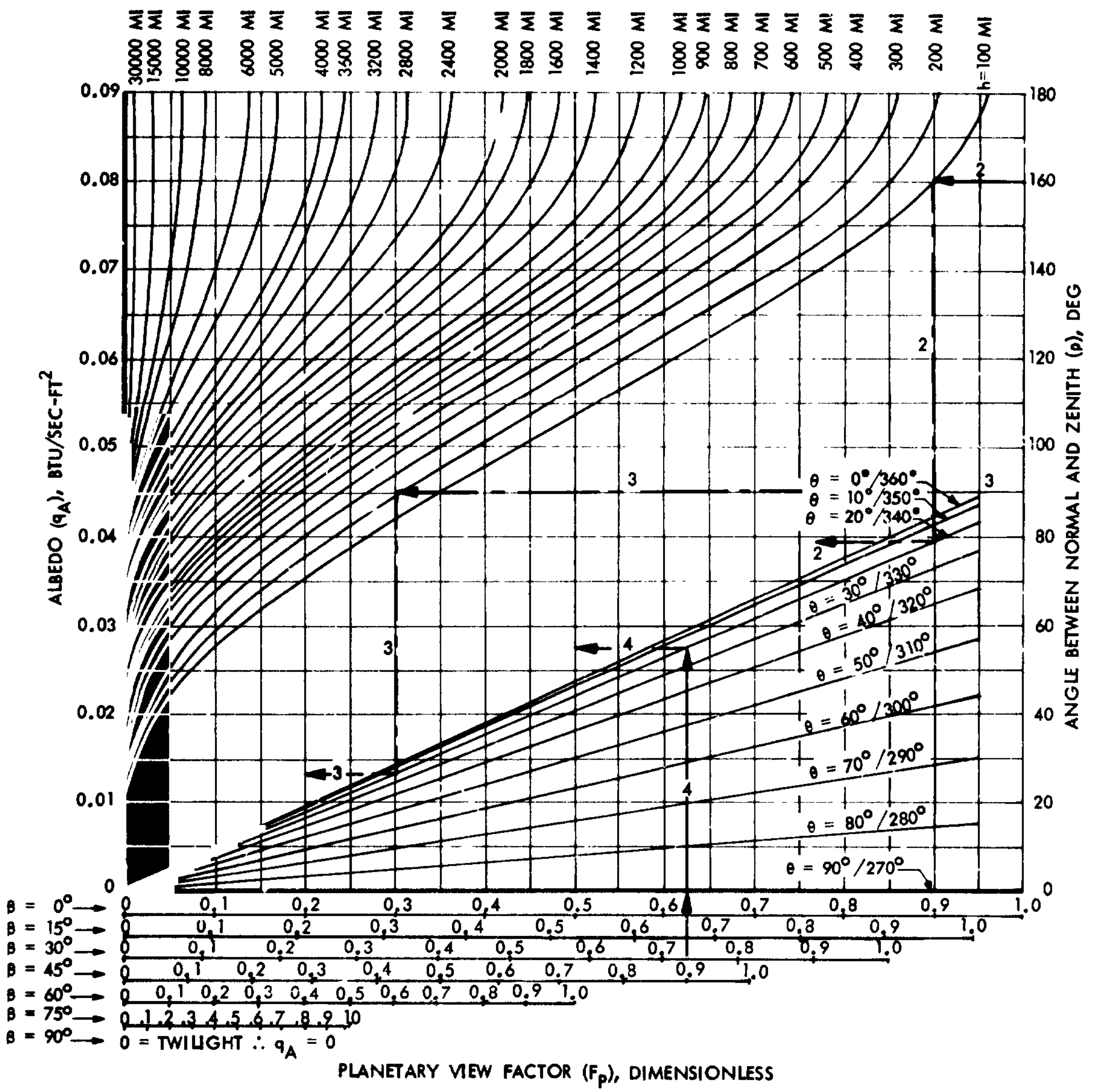

Figure 4-27. Incident Albedo Irradiation on a Surface Element in an Earth Orbit

5. Read the albedo value on the left-hand scale.

The lines labeled 2, 3, and 4 on Figure 4-27 refer to Examples 2, 3, and 4, which illustrate the use of this chart.

Earthshine Irradiation

The Earthshine irradiation, which does not vary with orbit angle or inclination, is given by:

$$\dot{q}_E = \frac{0.62}{4} SF_p \quad \text{Btu/sec ft}^2 \tag{4-56}$$

where 0.62 is assumed to be the average solar absorptivity of the Earth (1 - 0.38), the surface temperature of the Earth is assumed to be constant, and the Earth is assumed to radiate uniformly over its entire surface (4 times the projected area receiving solar radiation). Figure 4-28 presents the Earthshine irradiation as a function of the angle between the surface normal and the zenith, ρ, and altitude, h. A curve of $\dot{q}_E$ vs F_p is plotted on the same figure as a family of curves of ρ vs F_p with altitude as a parameter. Since F_p is a function of ρ and h, and $\dot{q}_E$ is a function of F_E, it is possible to find Earthshine irradiation for various combinations of ρ and h by having F_p as the abscissa. The procedure for the use of Figure 4-28 to compute the Earthshine irradiation is as follows:

1. Enter the right-hand scale at the angle between the normal and the zenith, ρ.
2. Project a horizontal line intersecting the appropriate altitude line.
3. Project a vertical line intersecting the diagonal line labeled q_E.
4. Read the Earthshine value on the left-hand scale.
5. The planetary view factor, F_p is given on the lower scale.

The lines labeled 5 and 6 on Figure 4-28 refer to Examples 5 and 6, which illustrate the use of this chart.

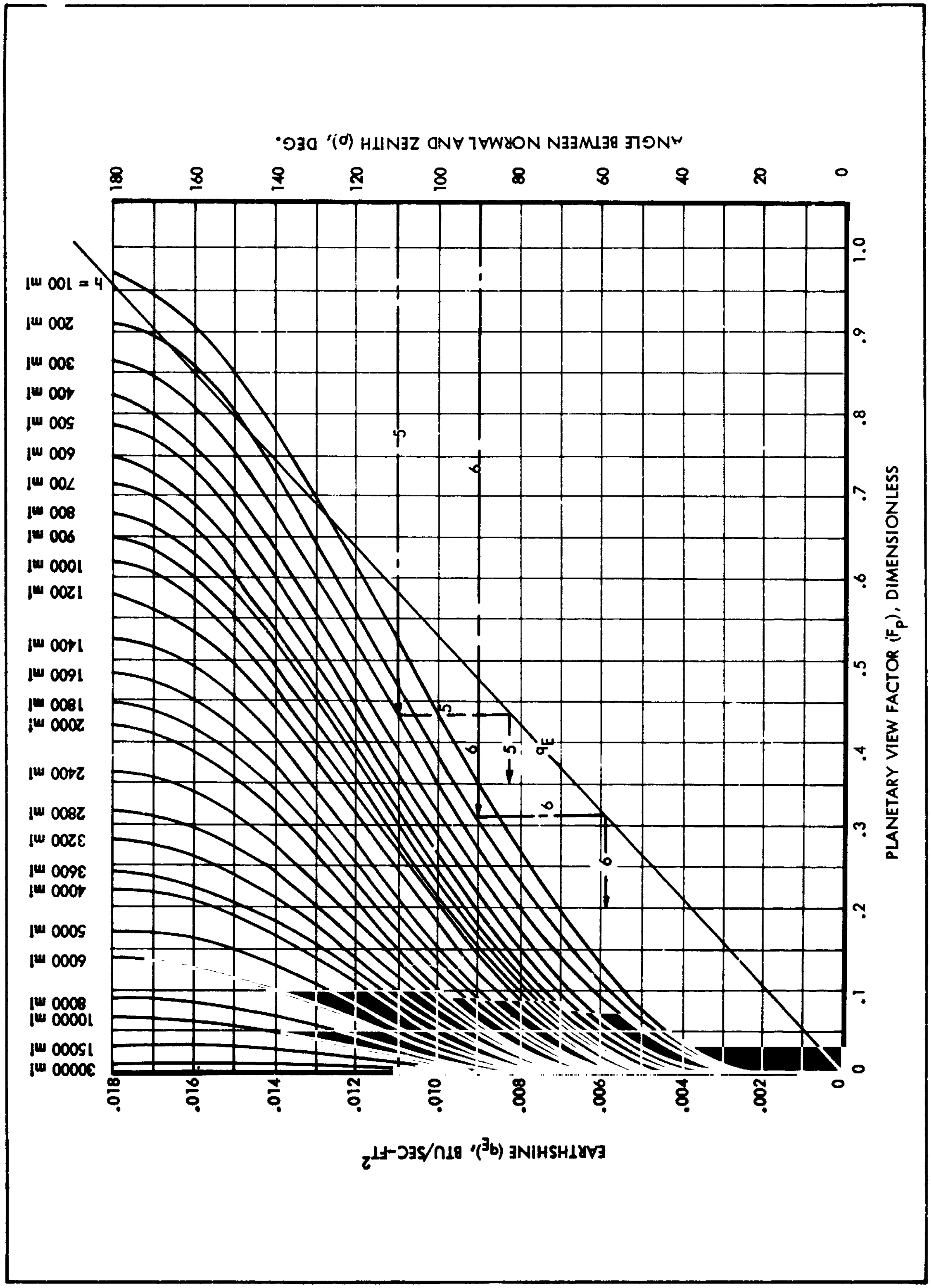

Figure 4-28. Incident Earthshine Irradiation on a Surface Element in an Earth Orbit

Sample Orbital Radiation Calculations

Example 1: Horizontal, 15° Half-angle Cone, Vertex Trailing

Given: $\beta = 0°$ ("noon" orbit), $h = 2300$ miles, $\psi = 105°$, $\lambda = -15°$

Determine: solar, albedo, and Earthshine vs θ.

Solution: From equation (4-52a):

$$\cos\delta = \cos 15° \cos 105° \cos\theta + \sin 15° \sin\theta$$

$$= -.25 \cos\theta + .259 \sin\theta$$

From equation (4-51):

$$\dot{q}_S = S\cos\delta = .123(-.25\cos\theta + .259\sin\theta)$$

$$\text{Btu/sec ft}^2$$

It appears that at $\psi = 105°$, the surface could receive solar radiation from $44° < \theta < 224°$, since $\cos\delta$ is positive for these orbit angles. However, from equation (4-54), it is found that the vehicle is in the Earth's shadow from $140.6° \leq \theta \leq 219.4°$. The solar input will therefore occur for $44° < \theta \leq 140.6°$ and $219.4° \leq \theta < 224°$. From Figure 4-27 or Figure 4-28, $F_p = 0.115$ at $\rho = \cos^{-1}(\cos\psi\cos\lambda) = 104.5°$. From equation (4-55):

$$\dot{q}_A = 0.38(.123)0.115 \cos\theta \text{ Btu/sec ft}^2$$

From equation (4-56):

$$\dot{q}_E = \frac{.62}{4}(.123)(0.115) = .0022 \text{ Btu/sec ft}^2$$

Table 4-1 summarizes the resulting heat rates.

TABLE 4-1

INCIDENT THERMAL RADIATION ON A 15° HORIZONTAL CONE

Vertex Trailing, 2300-Mile Altitude, in a "Noon" Orbit

Orbit Angle θ	$\dot{q}_S$ Btu/sec ft^2	$\dot{q}_A$ Btu/sec ft^2	$\dot{q}_{S+A}$ Btu/sec ft^2	$\dot{q}_E$ Btu/sec ft^2
0°	0	.0051	.0051	.0022
15	0	.0050	.0050	.0022
30	0	.0044	.0044	.0022
44	0	.0037	.0037	.0022
60	.0123	.0026	.0149	.0022
75	.0228	.0013	.0241	.0022
90	.0320	0	.0320	.0022
105	.0387	0	.0387	.0022
120	.0430	0	.0430	.0022
134	.0442	0	.0442	.0022
140.6	.0436	0	.0436	.0022
↑	0	0	0	.0022
In Shadow	0	0	0	.0022
↓	0	0	0	.0022
219.4	.0034	0	.0034	.0022
224	0	0	0	.0022
270	0	0	0	.0022
285	0	.0013	.0013	.0022
300	0	.0026	.0026	.0022
315	0	.0037	.0037	.0022
330	0	.0044	.0044	.0022
345	0	.0050	.0050	.0022
360°	0	.0051	.0051	.0022

Example 2: Horizontal Cylinder ("Noon" Orbit)

Given: $\beta = 0°$, h = 100 miles, $\theta = 20°$, $\psi = 160°$ ($\rho = 160°$)

Determine: Albedo irradiation, $\dot{q}_A$

Solution: Using Figure 4-27, at the intersection of $\rho = 160°$ and h = 100 miles, find $F_p = 0.9$. Project $F_p = 0.9$ to $\theta = 20°$, and read $\dot{q}_A = .0395$ Btu/sec ft^2 on left-hand scale.

Example 3: Vertical Cylinder ("Noon" Orbit)

Given: $\beta = 0°$, h = 200 miles, $\theta = 20°$ ($\rho = 90°$ for all ψ)

Determine: Albedo irradiation, $\dot{q}_A$

Solution: Using Figure 4-27, at the intersection of $\rho = 90°$ (constant for vertical cylinder) and h = 200 miles, find $F_p = 0.307$. Project $F_p = 0.307$ to $\theta = 20°$, and read $\dot{q}_A = 0.0132$ Btu/sec ft^2 on left-hand scale.

Example 4: Horizontal Cylinder (Non-"Noon" Orbit)

Given: Same as Example 2, except that $\beta \doteq 45°$

Determine: Albedo irradiation, $\dot{q}_A$

Solution: From Example 2, $F_p = 0.9$. Since $\beta = 45°$, use the $\beta = 45°$ scale for F_p. Project $F_p = 0.9$ to $\theta = 20°$, and read $\dot{q}_A = .0272$ Btu/sec ft^2 on left-hand scale.

Example 5: Horizontal Cylinder

Given: h = 300 miles, $\psi = 110°$ ($\rho = 110°$)

Determine: Earthshine irradiation, $\dot{q}_E$

Solution: Using Figure 4-28, at the intersection of $\rho = 110°$ and h = 300 miles, find $F_p = 0.432$. Project $F_p = 0.432$ to the line labeled $\dot{q}_E$ and read $\dot{q}_E = 0.0082$ Btu/sec ft^2.

Example 6: Vertical Cylinder

Given: h = 200 miles ($\rho = 90°$ for all ψ)

Determine: Earthshine irradiation, $\dot{q}_E$

Solution: Using Figure 4-28, at the intersection of $\rho = 90°$ (constant for vertical cylinder) and h = 200 miles, find $F_p = 0.307$. Project $F_p = 0.307$ to the line labeled $\dot{q}_E$, and read $\dot{q}_E = 0.0058$ Btu/sec ft^2.

Orbital Period

To perform a transient skin-temperature analysis using the curves presented in Figures 4-27 and 4-28, the orbit period is required. For circular orbits:

$$t_o = 2\pi\sqrt{\frac{R_e}{g_o}}\left(\frac{R_e + h}{R_e}\right)^{\frac{3}{2}} = 1.41 \left(\frac{R_e + h}{R_e}\right)^{\frac{3}{2}} \tag{4-57}$$

where:

t_o = orbital period, hr

R_e = radius of Earth = 20.9×10^6 ft

g_o = acceleration of gravity at surface of Earth = 32.17 ft/sec^2

h = orbit altitude, mi

The vehicle is in the Earth's shadow t_d hours per orbit where:

$$\frac{t_d}{t_o} = \frac{\sin^{-1}\left(\frac{R_e}{R_e + h}\right)}{\pi} \tag{4-58}$$

The orbit period is plotted as a function of orbit altitude in Figure 4-29.

Transient Skin Temperatures

An example of the temperature oscillations a vehicle skin section may experience during Earth orbit is shown in Figures 4-30, 4-31, and 4-32. These figures show the transient temperature histories of the faces of a cube

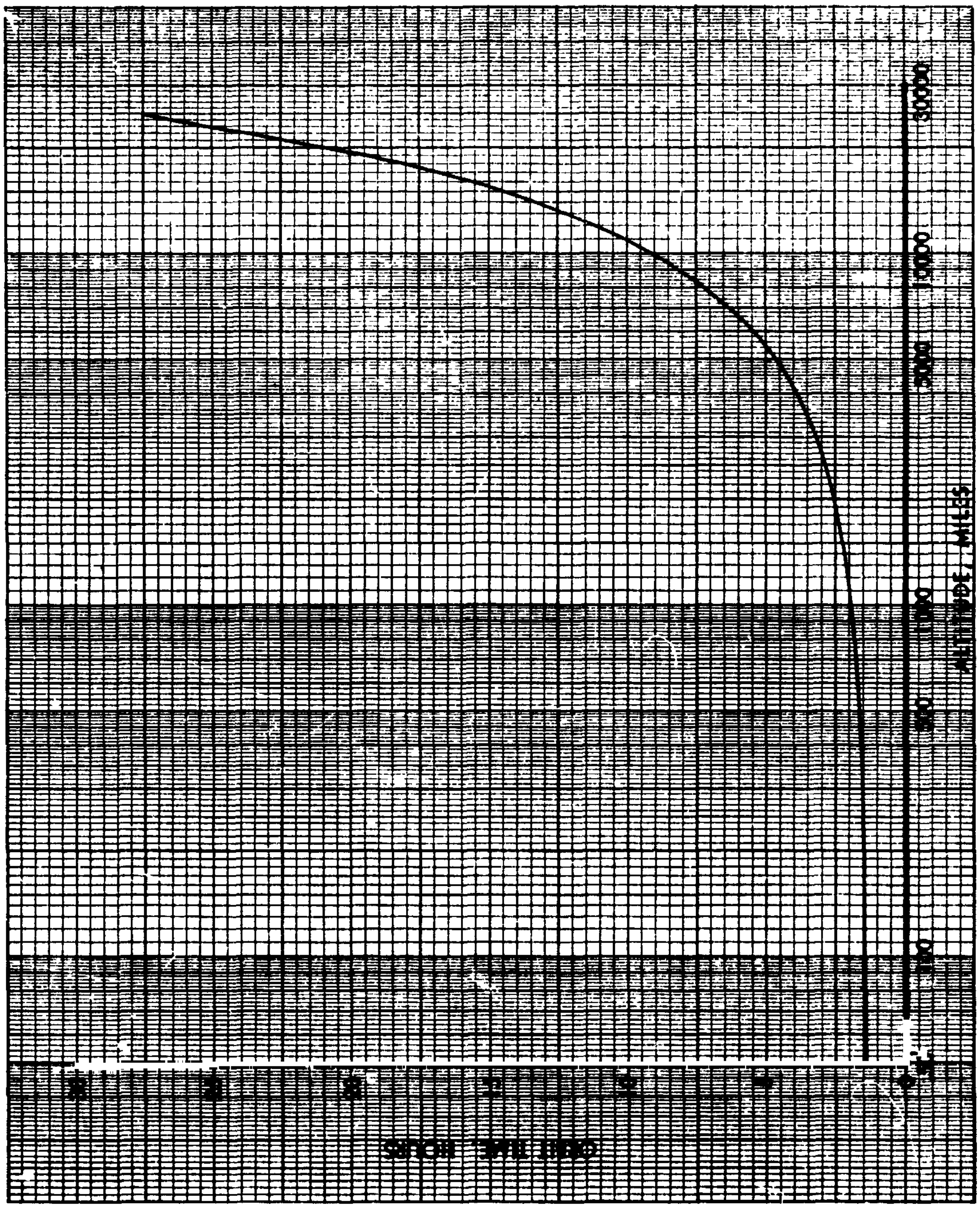

Figure 4-29. Orbit Period for Circular Earth Orbit

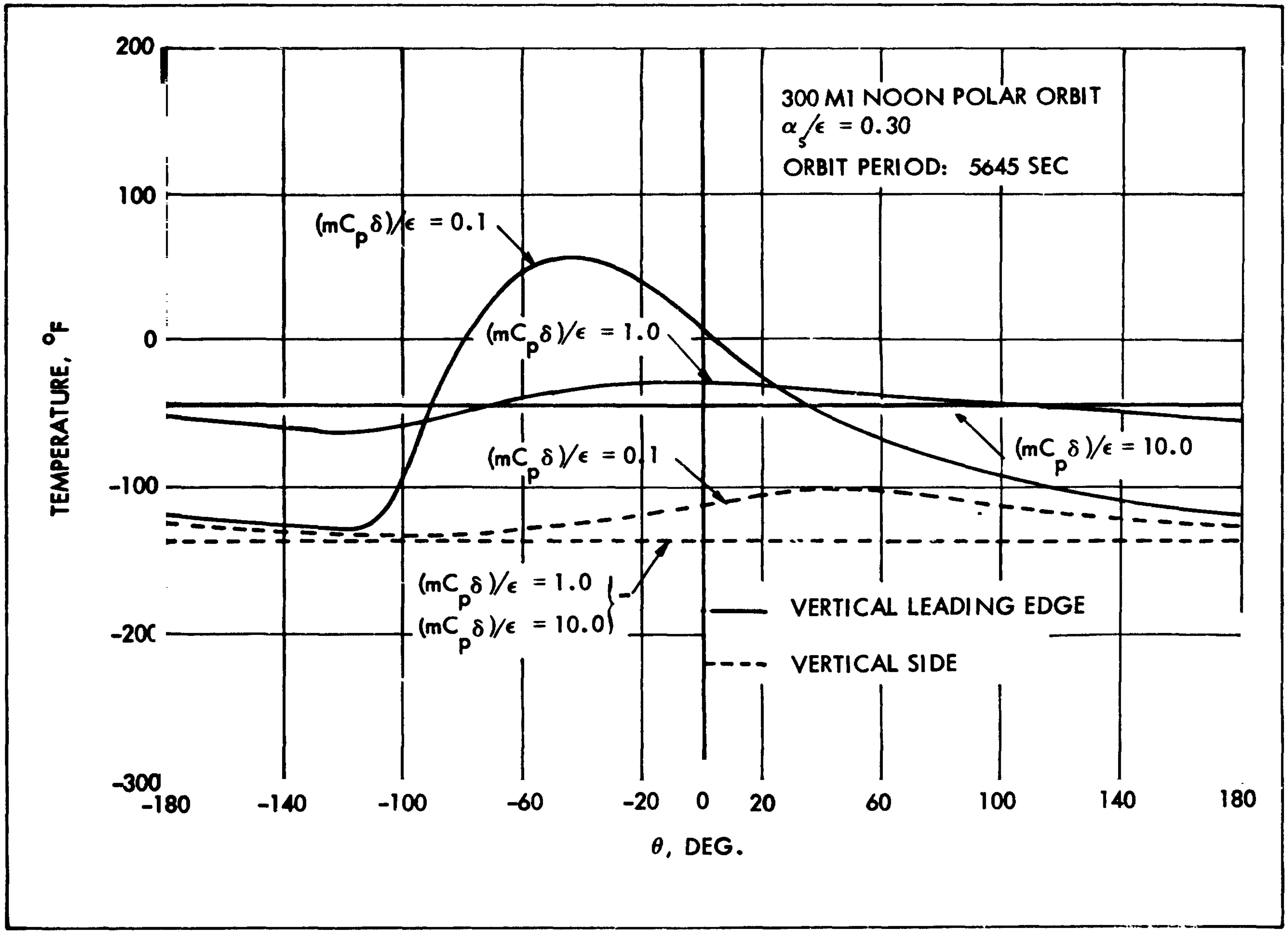

Figure 4-30. Satellite Skin-Temperature Oscillations - Vertical Surfaces of Cubical Satellite

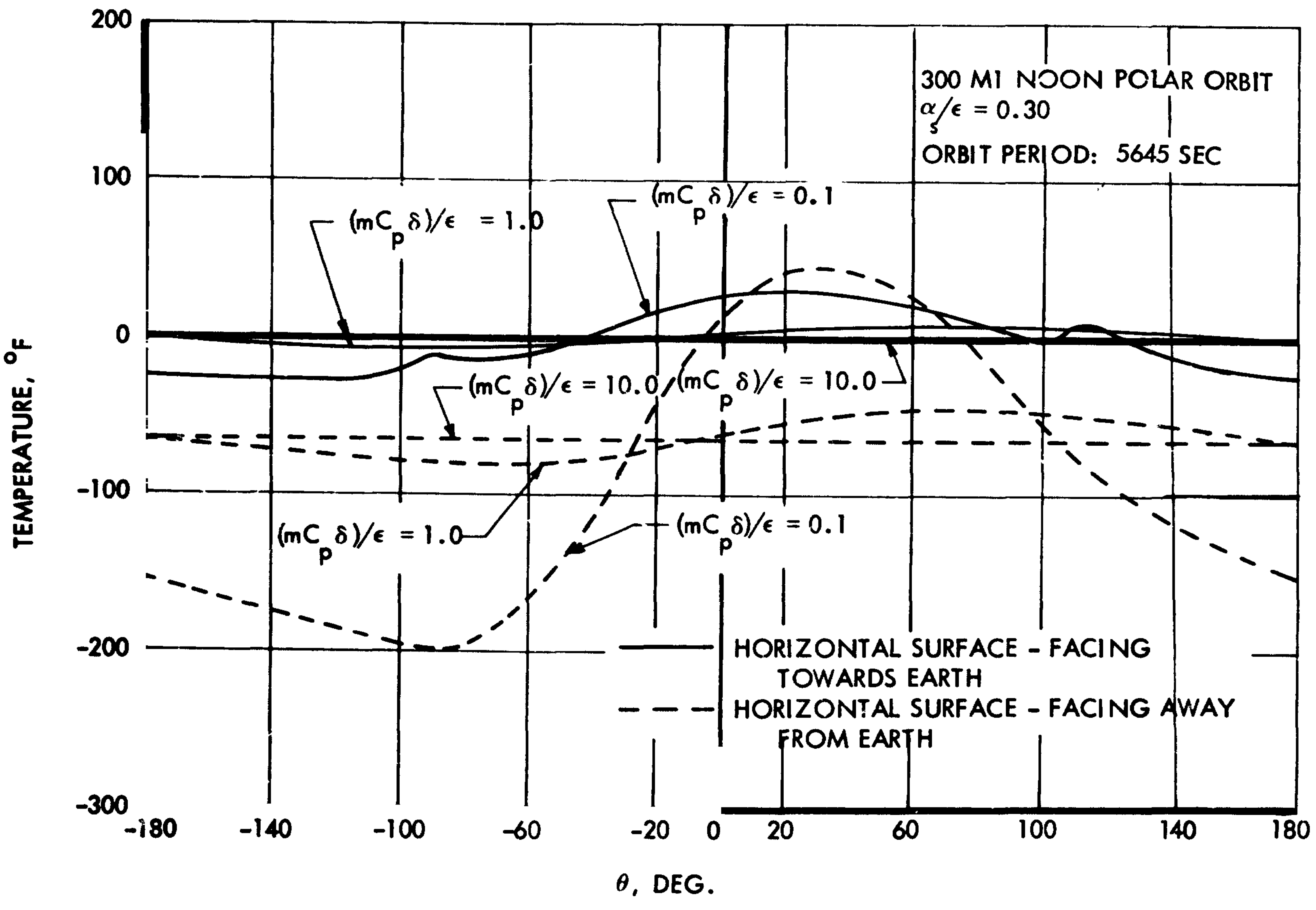

Figure 4-31. Satellite Skin-Temperature Oscillations - Horizontal Surfaces of Cubical Satellite

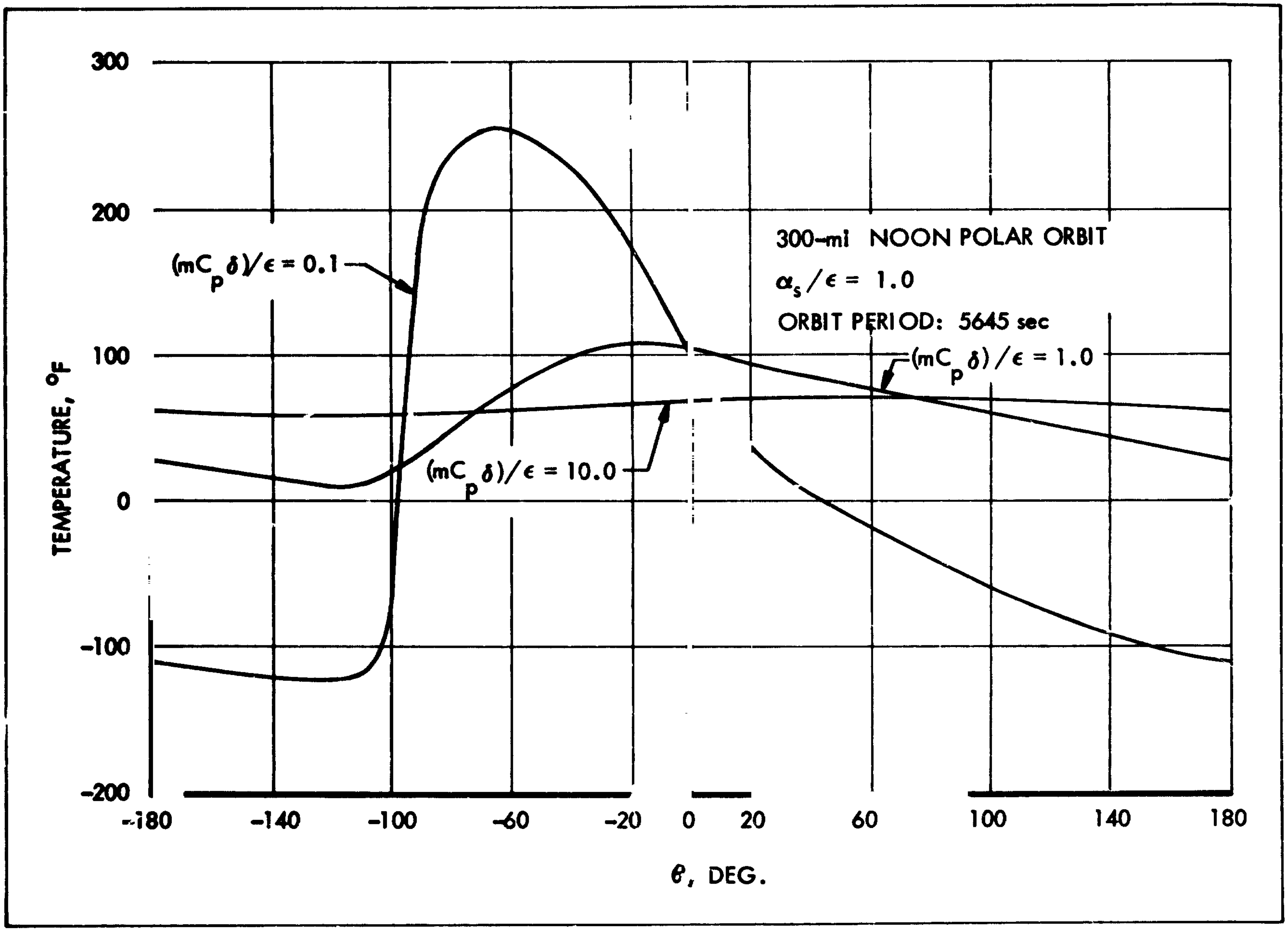

Figure 4-32. Satellite Skin-Temperature Oscillations - Vertical Leading Surface of Cubical Sattellite

(Figure 4-33) in a 300-mile noon circular orbit. Each face of the cube has $\alpha_s/\epsilon = 0.30$ and is assumed to be isolated from the other faces. The temperature histories are plotted as a function of orbit angle with the ratio of thermal capacitance to surface emissivity as a parameter. This ratio is approximately 0.5 for an 0.10-inch aluminum skin with $\epsilon = 0.5$. In general, the temperature fluctuations experienced by internal components are much less than those of the vehicle skin.

HEATING FROM OTHER SOURCES

In addition to ascent and orbital heating, a typical spacecraft may experience external heat loads from the main propulsion system, from the reaction control system, from other parts of the vehicle, and from other nearby vehicles

During operation of the main propulsion engine, the vehicle base receives radiant heating from the nozzle extension, and both radiant and convective heating from the exhaust gases. For a single nozzle configuration, convective heating is not particularly severe. In clustered rocket configurations, however, recirculation of the exhaust gases between the nozzles may require the addition of heavy heat shields to maintain the vehicle's structural integrity and to protect the vehicle components in the base area. This, of course, adds weight and results in reduced overall spacecraft performance. Typical base heating rates for a multirocket configuration are on the order of 5-20 Btu/sec ft^2, considerably more severe than the ascent heating to the majority of the spacecraft external surfaces. On some practical configurations, local heating rates on the order of 100 Btu/sec ft^2 are not uncommon. On single nozzle configurations base heating results primarily from radiation exchange with the nozzle extension, since most exhaust gases have low emittance, and the view factor from the base to the high-temperature portion of the plume is small. Typical base heating rates for single nozzle configurations are on the order of 1-4 Btu/sec ft^2.

Heat transfer to the vehicle skin during reaction control system engine firings is extremely difficult to analyze. In addition to radiant heating from the nozzle, convective heating from the impinging exhaust gases

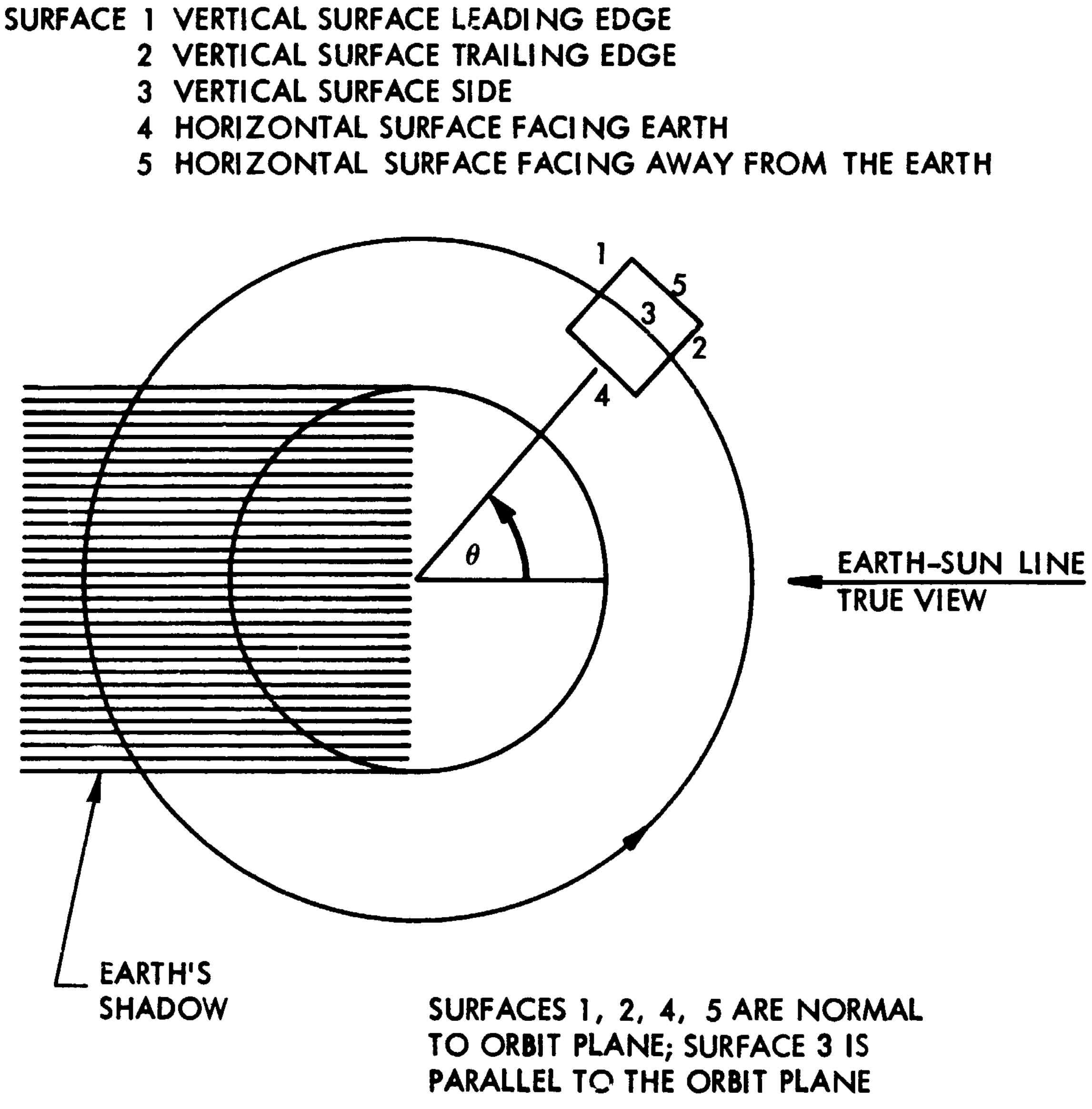

Figure 4-33. Position of Cube-Shaped Satellite Surfaces with Respect to Earth and Earth-Sun Line

must be considered. Furthermore, the possibility of changing the surface radiation characteristics due to the plume impingement should be investigated. The practical method to investigate these problems is to test a model of the RCS and adjacent structure in a vacuum chamber.

REFERENCES

4.1. Equations, Tables, and Charts for Compressible Flow, Ames Aeronautical Laboratory, NACA Report 1135, 1953

4.2. Walburn, A.B. and P. Harner — Real Gas Oblique Shock Functions for Air in Chemical Equilibrium, Fairchild Stratos Corporations, DM 63-1, December 1962.

4-3. Meyer, M.G. — Real Gas Equilibrium Properties Behind a Normal Shock in Air, Lockheed Missiles and Space Company Report 399791, 13 July 1961

4-4. Dailey, C.L. and F.C. Wood — Computation Curves for Compressible Fluid Problems, John Wiley and Sons, Inc., 1949

4-5. Romig, M. — On Heat Transfer to Cones at High Velocities, Convair Laboratory Report, August 1958

4-6. Dunn, M.G., — Boost-Phase Aerodynamic Heat Transfer Calculation Techniques, Lockheed Missiles and Space Company Report A381550, July 1963

4-7. Eckert, E.R.G. — Survey of Boundary Layer Heat Transfer at High Velocities and High Temperatures, Wright Air Development Center, WADC Tech. Report 59-624, April 1960

4-8. Guard, F.L., et al — Compilation of Structural Inflight Heating Data Applicable to Large Launch Vehicles, Lockheed-California Company Report, LR 17562, February 1964

4-9. Fay, J.A. and F.R. Riddell — "Theory of Stagnation-Point Heat Transfer in Dissociated Air," Journal of Aeronautical Sciences, February 1958

4-10. Romig, M. — Stagnation Point Heat Transfer for Hypersonic Flow, Jet Propulsion, December 1956

REFERENCES (Continued)

4-11. Murphy, J.D., and R.A. Rindal — Enthalpy of Dissociation for Air in Thermodynamic Equilibrium, Visdya Technical Note 2T, 12 January 1962

4-12. Lees, L. — Laminar Heat Transfer Over Blunt-Nosed Bodies at Hypersonic Speeds, Jet Propulsion Laboratory, April 1956.

4-13. Nevelli, B.A. — Computer Program for the Calculation of Incident Orbital Radiant Heat Flux, Lockheed-California Company Report LR 18904, June 1965

V - SPACECRAFT THERMAL ANALYSIS

The problem of controlling the thermal environment within a space vehicle differs from the external radiation problem largely because of the existence of other modes of heat transfer. Conduction of heat through structural members and other vehicle components is always present. If pressurized systems are used, convective heating will be introduced. Internal radiation is of great importance and is usually the most difficult mode to accurately account for because of the complex geometries for which configuration factors must be computed, and the inherent problems of multiple interreflections.

During preliminary design, simplified analyses are used to obtain first-order approximations to the required surface properties and the temperature distributions on the shell, primary structure, and critical components. Many of these computations can be done by hand. The depth and complexity of the thermal analysis increases, however, as the design progresses. Eventually it is necessary to perform a detailed three-dimensional transient thermal analysis of the spacecraft to ascertain that all component temperatures will operate within their allowable temperature range. Such a complex solution must be obtained through the use of automatic computing machines. Of the several methods to accomplish this, the one most commonly employed is the electrical resistance-capacitance (R-C) analog, with the heat transfer equations solved by the finite differences approach to obtain the temperature history of the system.

This section describes some simplified analytical techniques applicable to preliminary design, and how the physical problem is later converted to an equivalent R-C network in order to perform a detailed transient-temperature analysis. Because of its importance in computing internal heat transfer, a description of various methods for computing radiation configuration factors and emissivity factors is included. Finally, some of the problems associated with fluid storage are discussed.

SIMPLIFIED THERMAL ANALYSES

The heat-transfer engineer responsible for the thermal analysis of a space vehicle must make a major contribution to decisions regarding the type of thermal control system to be used, surface finishes, location of critical components, vehicle attitude in space, and even the primary structure since the conductive paths are very important for internal temperature control. Many tentative decisions must be made rapidly to provide ground rules on which the design may proceed. Because of the time element and the absence of design details to justify detailed analyses, many preliminary decisions are based on hand calculations, using simplified analytical techniques.

Effective Sink Temperature

A very useful concept in simplified analyses is the effective sink temperature, T_S, computed by assuming radiation equilibrium conditions at the external skin. In other words, it is the temperature which a zero capacitance skin element would assume if it were insulated from the rest of the vehicle. Assuming integrated (over time) average external radiant inputs, the effective sink temperature is given by

$$T_S = \left[\frac{\bar{q}_E + \frac{\alpha_S}{\epsilon} \bar{q}_{S+A}}{\sigma} \right]^{1/4} \qquad (5\text{-}1)$$

This expression is useful in preliminary studies of the α_S/ϵ ratio required to maintain a specified average skin temperature, T_S.

Figures 5-1 and 5-2 show the average orbital sink temperatures as a function of the α_S/ϵ ratio for two common spacecraft orientations. Figure 5-1 is applicable to an Earth-oriented horizontal cylinder with the cylinder axis tangent to the flight path, in a near-Earth (100 to 300-mile) orbit. A "noon" orbit (orbit whose plane contains the Earth-sun line) is assumed and thus the heating rates are symmetrical about the Earth-vehicle-sun line as shown. The actual temperature fluctuation of the higher numbered nodes, which face the Earth, is much less than that of the lower numbered nodes, which receive a sinusoidal solar input for half an orbit.

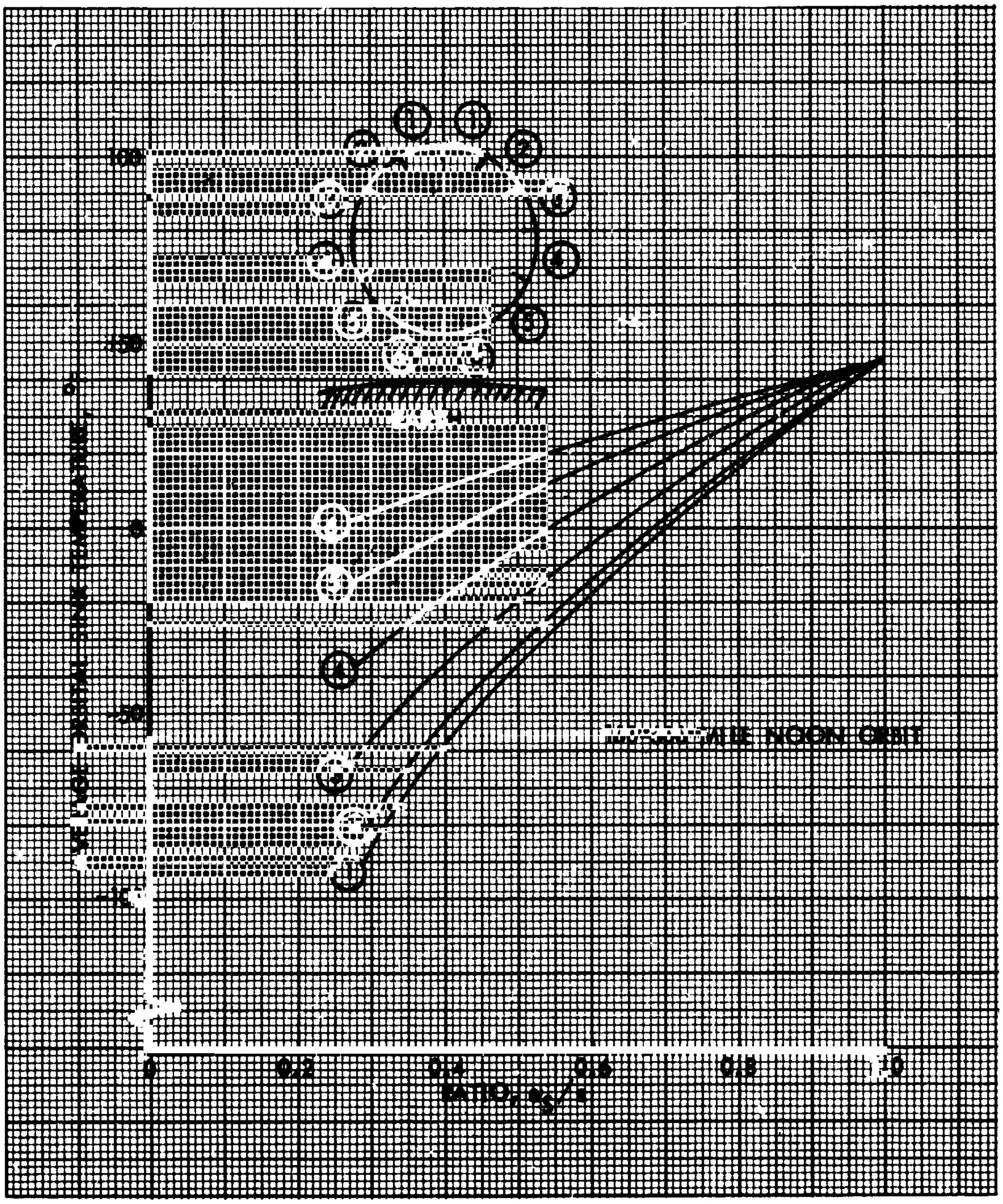

Figure 5-1. Orbital Average Sink Temperature for an Earth-Oriented Horizontal Cylinder Aligned with the Flight Path

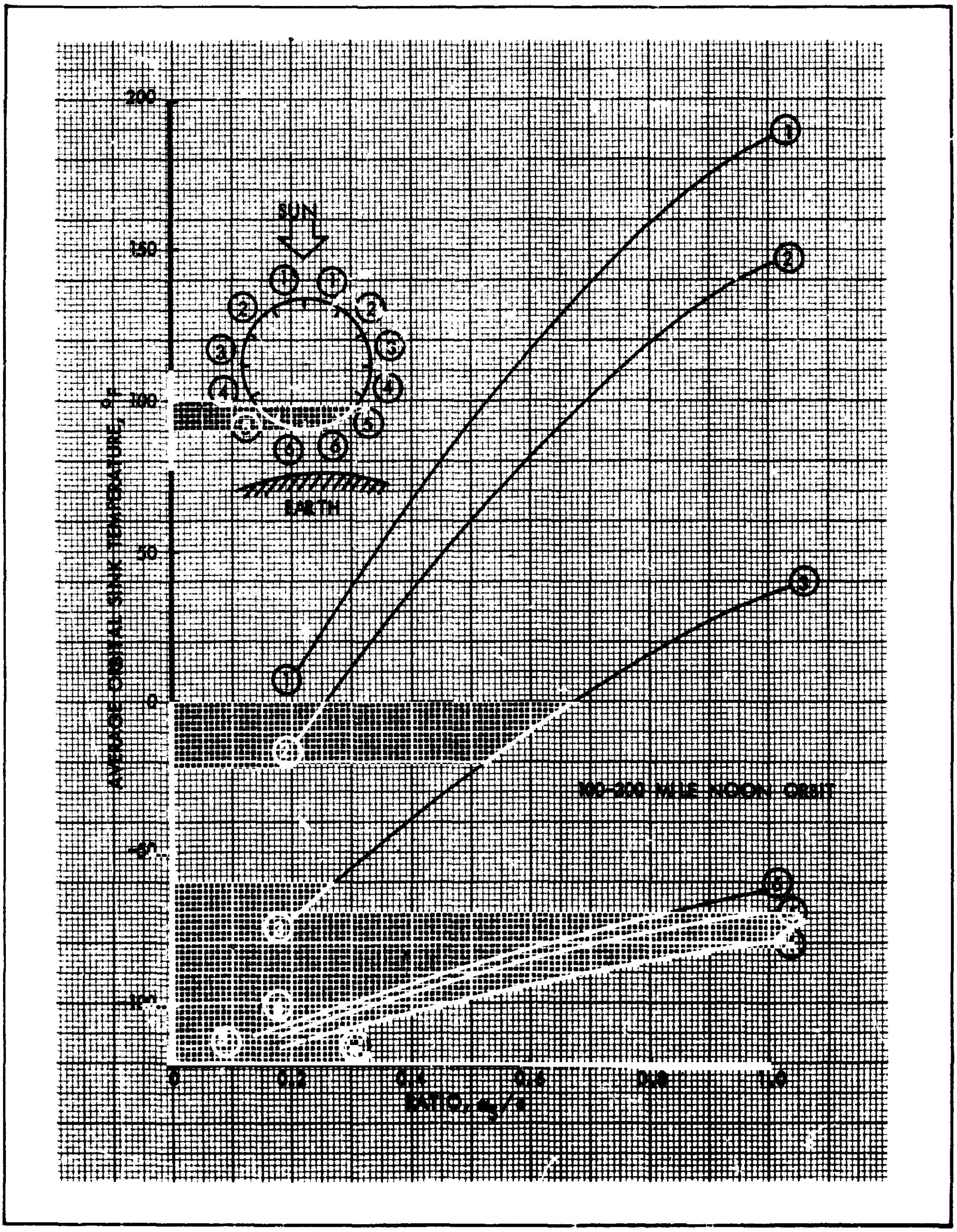

Figure 5-2. Orbital Average Sink Temperature for a Solar-Oriented Cylinder Normal to the Solar Vector

Figure 5-2 shows the average orbital sink temperature as a function of the α_S/ϵ ratio for a solar oriented cylinder with the axis normal to the solar vector. A launch into a near Earth noon orbit is again assumed, and thus the heating rates are symmetrical about the vehicle-sun line. The lower numbered nodes receive a one-sun heat flux for slightly more than half an orbit, and Earthshine on the dark side of the Earth. The higher numbered nodes absorb Earthshine and albedo on the illuminated side of the Earth, but receive no radiant inputs on the dark side; thus, their average temperatures are extremely low.

Figure 5-3 shows the maximum orbital sink temperature for the Earth oriented horizontal cylinder described above. These temperatures were computed by assuming radiation equilibrium conditions based on the instantaneous heat flux at the subsolar point or where the spacecraft enters and leaves the Earth's shadow.

Figure 5-4 shows the absorbed (or emitted) radiant energy as a function of surface temperature using surface emissivity as a parameter.

Use of Sink Temperature in Preliminary Analyses

The concept of space sink temperature is frequently used in preliminary estimates of the surface properties required so that the heat rejected by an internal component may be dissipated to space directly through the skin. As an example, consider the arrangement shown below where a heat dissipating component is mounted to the skin and insulated on the backside to protect other internal components:

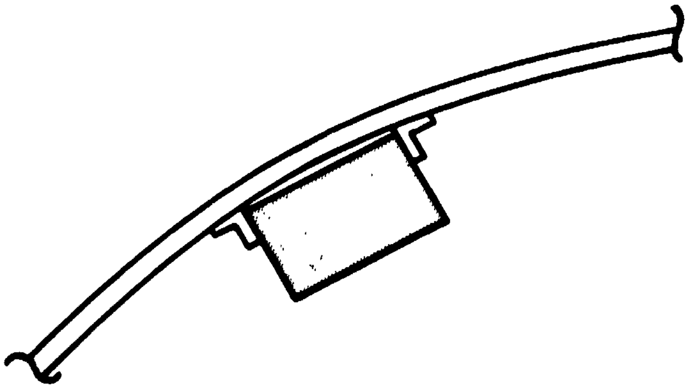

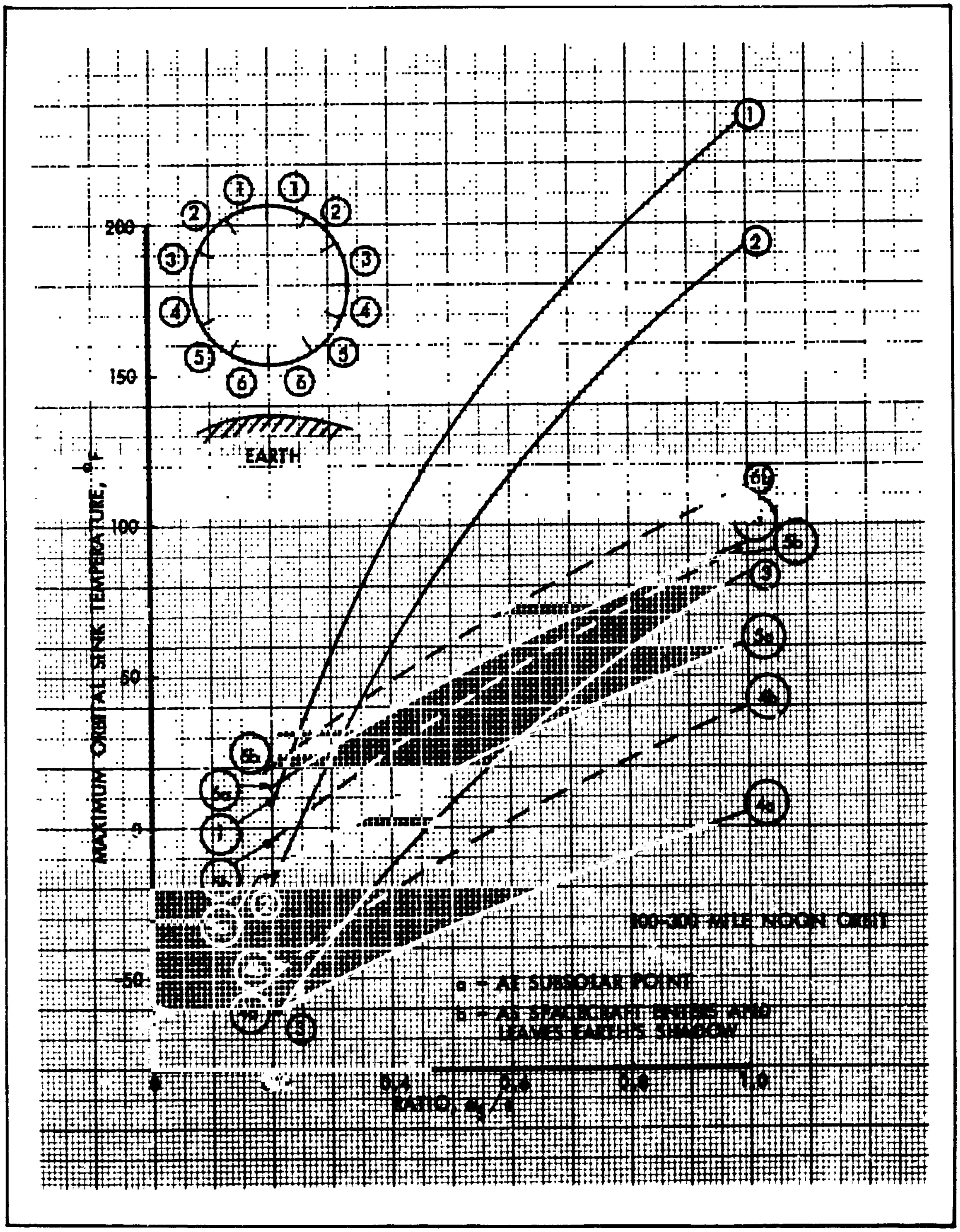

Figure 5-3. Maximum Orbital Sink Temperature for an Earth-Oriented Horizontal Cylinder Aligned with the Flight Path

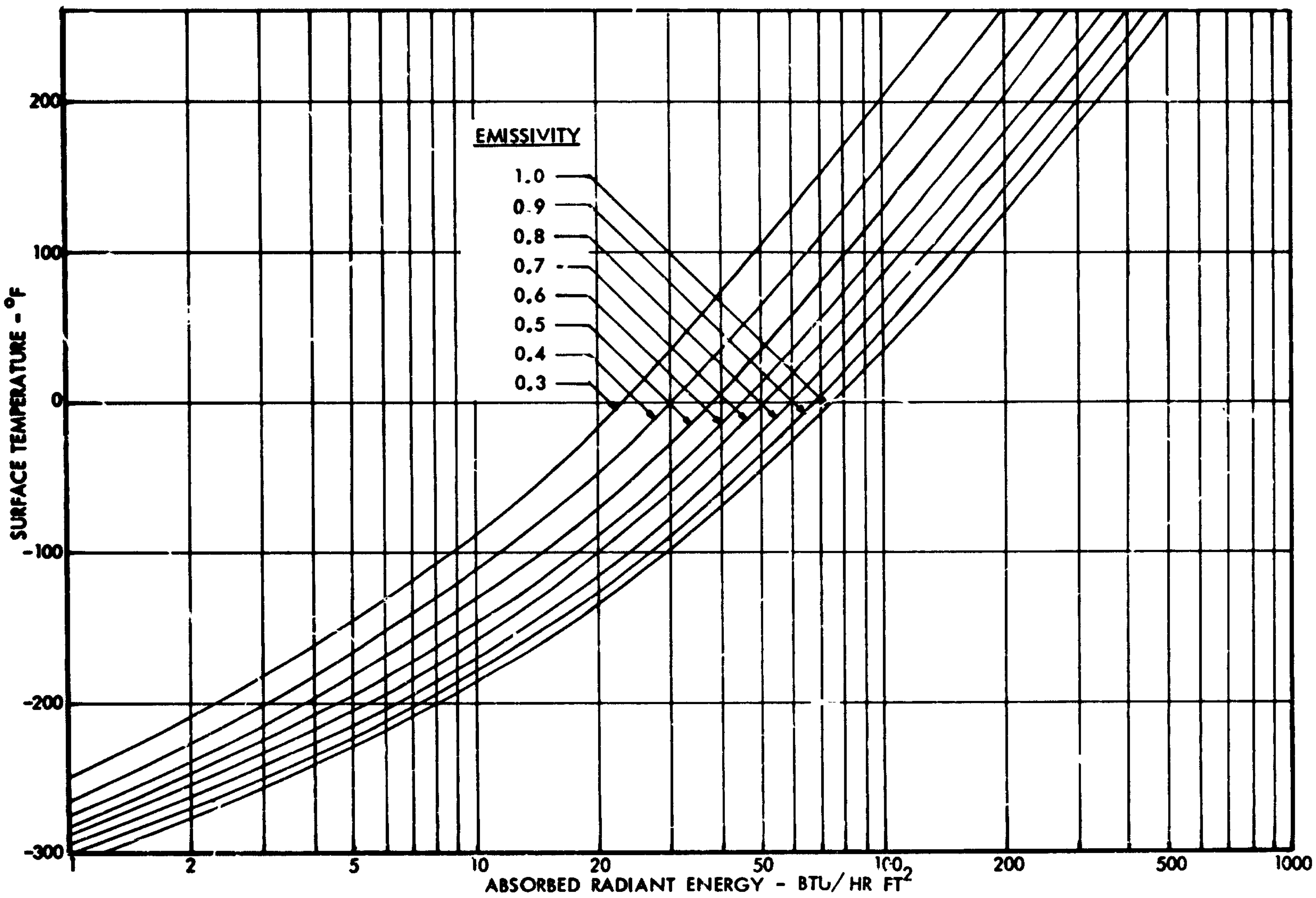

Figure 5-4. Surface Temperature as a Function of the Absorbed Radiant Energy

It is assumed that the component has sufficient mass to damp out temperature oscillations caused by orbital variations of the skin temperature and/or periodic heat rejection. Using integrated average values of the external radiant energy inputs, the component, skin and sink temperatures can be related in steady state as follows:

$$T_C = T_O + \sigma \epsilon R_{CR} \left[T_O{}^4 - T_S{}^4 \right] \qquad (5\text{-}2)$$

$$P_C = \frac{T_C - T_O}{R_{CR}} \qquad (5\text{-}3)$$

These equations are obtained from the simple thermal network given below:

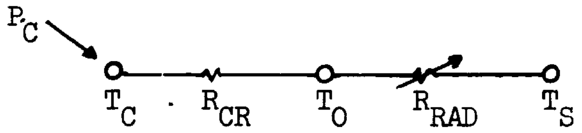

where

T_C = component temperature, °R

T_O = average outside wall temperature, °R

R_{CR} = conduction resistor through the mounting bracket and the radiation resistor between the component and the skin (in parallel), $\frac{hr\,°R}{Btu}$

T_S = external effective sink temperature given by equation 5-1, °R

P_C = component heat rejection, Btu/hr

R_{RAD} = radiation resistor to space, $\frac{hr\,°R}{Btu}$

Equations 5-2 and 5-3 may be solved simultaneously to determine the necessary α_S/ϵ ratio, and the corresponding wall temperature.

The effective sink temperature concept can also be used to perform an energy balance on a composite wall, accounting for internal heat transfer.

To illustrate, consider the structure shown below, which might represent the wall construction of a manned space station:

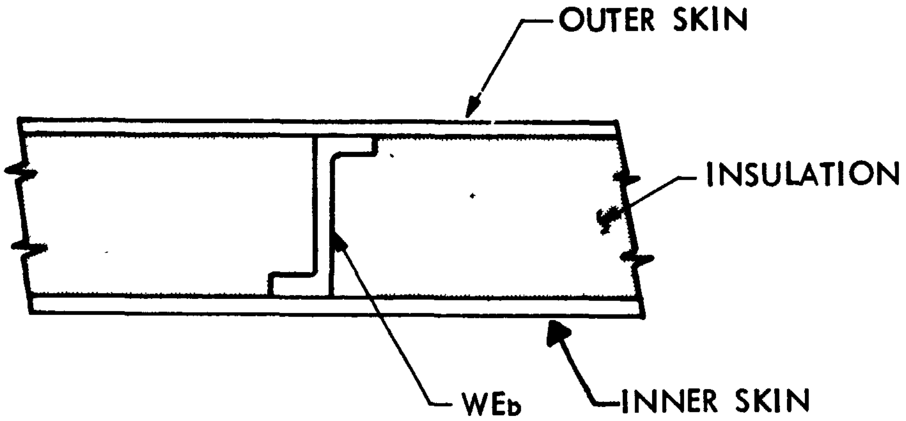

The problem is to make a preliminary estimate of the insulation thickness required to maintain the temperature of the inner skin above the cabin dew temperature. The wall thermal performance is influenced by geometry, insulation design, external surface finish, and inside film coefficient (assuming the station is rotating and hence natural convection is present). Using integrated average values of the external radiant energy inputs, the various parameters can be related in steady state as follows:

$$T_I = T_o + \sigma \epsilon R_w \left[T_o^4 - T_s^4 \right] \qquad (5\text{-}4)$$

and

$$T_I = \frac{R_h T_o + R_w T_c}{R_h + R_w} \qquad (5\text{-}5)$$

where

T_I = average inside wall temperature, °R

T_o = average outside wall temperature, °R

R_w = wall thermal resistance, hr°R/Btu

R_h = resistance across inside film coefficient, hr°R/Btu

T_s = external effective sink temperature given by equation (5-1), °R

T_c = cabin bulk air temperature , °R

The wall thermal resistance, R_w, is the parallel hook-up of the resistance across the insulation and across the web. Since all parameters are known except the wall resistance R_w and the temperature T_o, equations (5-4) and (5-5) can be solved simultaneously for R_w. The required insulation thickness is then computed as the product of the resistance, thermal conductivity, and cross-sectional area.

As a simple numerical example of the space sink concept, consider the problem of computing the average inside skin temperature for the composite wall shown above. The following parameters are assumed:

Cabin temperature = 70°F

Inside film coefficient = 0.5 Btu/hr ft^2 °R

Insulation conductivity = 0.2 Btu in/hr ft^2 °R

External surface emissivity = 0.3

External surface solar absorptivity = 0.8

Web thickness = 0.10 in.

Web spacing = 6.0 in.

Web conductivity = 2.0 Btu in/hr ft^2 °R

The wall is assumed to be a portion of a horizontal, 15° half-angle cone, with vertex trailing, in a 2300-mile noon circular orbit. The Earth orbit heating rates to such a configuration are computed in Section IV. The body angle ψ, measured clockwise from the point furthest from the Earth, is 105°. The heating rates given in Table 4-1 are plotted as a function of orbit angle in Figure 5-5. The integrated average solar spectrum radiant inputs are determined as the area under the curve divided by 360. The approximate value is

$$\bar{q}_{S+A} = 0.0096 \text{ Btu/sec ft}^2$$

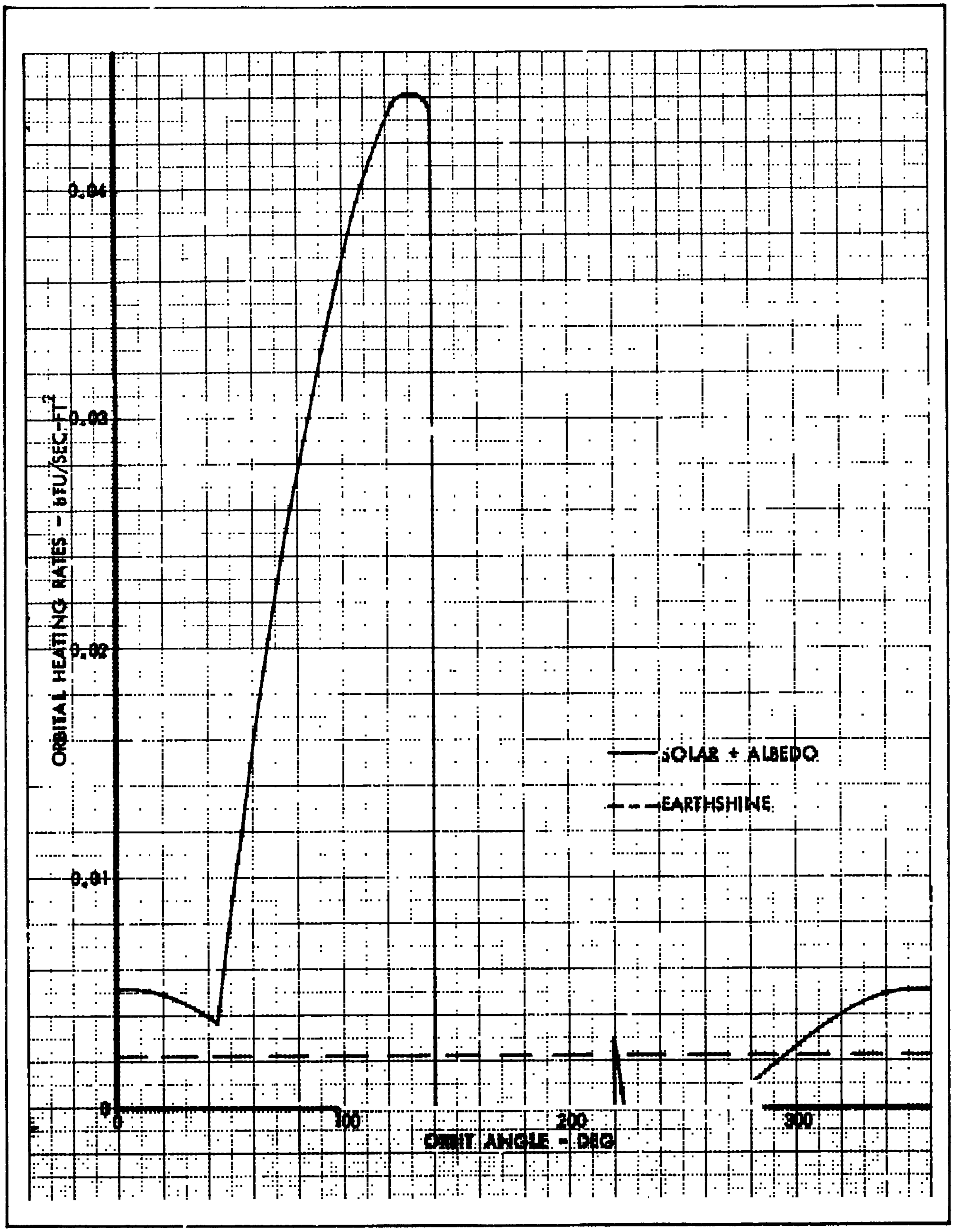

Figure 5-5. Earth Orbital Radiation to a Horizontal 15° Half-Angle Cone in a 2300-Mile Noon Circular Orbit, $\Psi = 105°$

Earthshine radiation is comparatively small at 2300 miles and is assumed to have a uniform value,

$$\bar{q}_E = 0.0022 \text{ Btu/sec ft}^2$$

The effective sink temperature is computed from equation (5-1).

$$T_s = \left[\frac{0.0022 + \left(\frac{0.8}{0.3}\right)(0.0096)}{(0.1713 \times 10^{-8})\ \left(\frac{1}{3600}\right)}\right]^{1/4} = 490°\text{R} = 30°\text{F}$$

The resistors through the insulation and web are

$$R_{ins} = \frac{\ell}{kA} = \frac{\ell \text{ in.}}{0.2 \dfrac{\text{Btu in.}}{\text{hr ft}^2\ °\text{R}} \times 1 \text{ ft}^2} = 5.0\ell \frac{\text{hr }°\text{R}}{\text{Btu}}$$

and

$$R_{web} = \frac{\ell}{kA} = \frac{\ell \text{ in.}}{2.0 \dfrac{\text{Btu in.}}{\text{hr ft}^2\ °\text{R}} \times 1 \text{ ft} \times \dfrac{2(0.1)}{12} \text{ ft}} = 30.0\ell \frac{\text{hr }°\text{R}}{\text{Btu}}$$

The insulation and web resistors, in parallel, give the wall resistance, i.e.,

$$R_w = \frac{R_{ins}\ R_{web}}{R_{ins} + R_{web}} = \frac{(5\ell)(30\ell)}{5\ell + 30\ell} = 4.29\ell \frac{\text{hr }°\text{R}}{\text{Btu}}$$

The internal convection resistor is

$$R_h = \frac{1}{h\ A} = \frac{1}{0.5 \dfrac{\text{Btu}}{\text{hr ft}^2\ °\text{R}} \times 1 \text{ ft}^2} = 2.0 \frac{\text{hr }°\text{R}}{\text{Btu}}$$

The average inside wall temperature, T_I, is computed as a function of wall resistance by the following equation, which is obtained by combining equations (5-4) and (5-5):

$$T_I = T_I\left(1 + \frac{R_w}{R_h}\right) - T_c \frac{R_w}{R_h} + \sigma \epsilon R_w \left[\left(T_I\left(1 + \frac{R_w}{R_h}\right) - T_c \frac{R_w}{R_h}\right)^4 - T_s^4\right]$$

The results are shown in Figure 5-6 where T_I is plotted as a function of the wall thickness, ℓ.

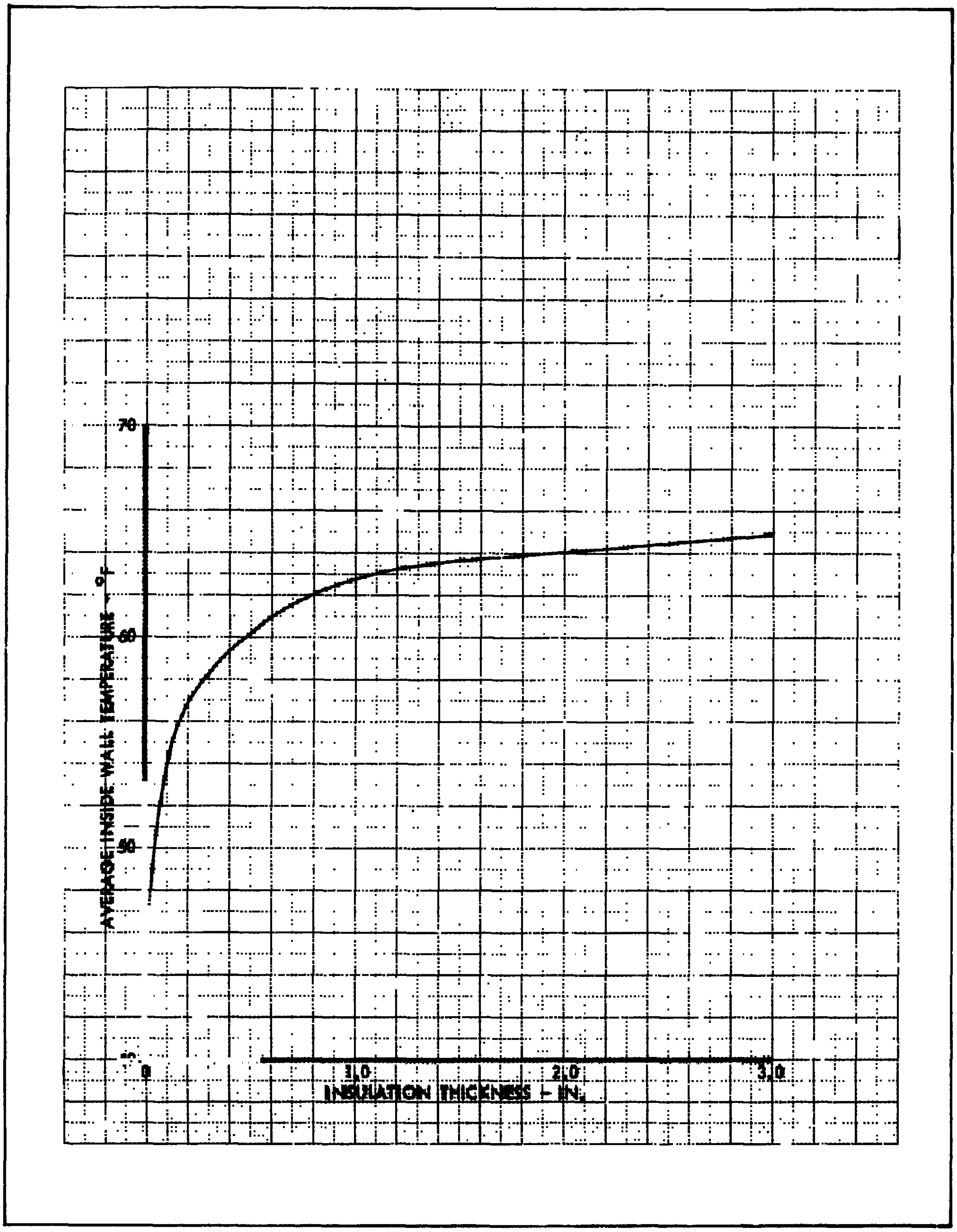

Figure 5-6. Inside Wall Temperature vs Wall Insulation Thickness

DETAILED THERMAL ANALYSES

As the design progresses, it eventually becomes necessary to perform a more sophisticated analysis, in which the interrelationship of all significant sources of thermal energy are accounted for. As noted previously, this is accomplished by setting up the thermal problem as an R-C network and solving for the temperature history of the system on an electronic computer. There are two primary reasons for this choice of solution:

1. The equations describing any general heat transfer problem are of the same form as those describing an equivalent electrical R-C network. The electrical equations are simple to set up in finite difference form, and consequently the heat transfer problem may be solved to any degree of accuracy.

2. The network setup is easy to visualize in relation to a schematic diagram of the physical problem.

Analytical Procedures

To facilitate the solution of complex transient heat-transfer problems, the Lockheed-California Company has developed a computer program (Ref. 5-1) to solve thermal resistance – capacity analog networks. The steps required to perform a detailed thermal analysis of a space vehicle using the Thermal Analyzer Program, are as follows:

1. The physical problem must be completely defined. This requires that the vehicle structure and component arrangement be known in detail. All materials, surface finishes, internal power generation, engine firing schedule, propellant flow rates and properties, etc., must be known or assumed. Generally these data are not available as early as desired, and the thermal analysis must be performed in stages, as described below.

2. A preliminary model layout is established, following the general rules given later in this section under "Dividing the Physical Problem into Lumps." This is the initial step in the process of converting the physical problem into an equivalent R-C network. Much consideration should be given to the location of the nodes,

since this is the key to the accuracy to the analysis. Occasionally the network generation process requires side analyses to estimate, for example, the temperature gradient in a particular area of the vehicle.

3. After the node layout is established, the network resistor and capacitor values must be computed. This is generally the most time-consuming phase of the analysis. The calculation of capacitors and conduction resistors is usually straightforward but tedious due to the complex geometries involved. The proper accounting for internal radiation is a difficult problem. Obviously, radiation resistors cannot be placed between all nodes which view each other because of the large number of calculations involved, and the possibility of exceeding the computer storage capacity. Therefore, the radiation problem must be grossly simplified. For example, if the temperature of an electronic component is strongly influenced by its radiation to the surroundings, but the temperature of the surroundings is not greatly affected by absorbing this flux, the radiation network for the system might consist simply of a resistor between the electronic component and a sink node, whose temperature is specified as the average temperature of the surroundings.

   If a large temperature variation is anticipated at a particular node, it may be necessary to account for the effects of variable resistors and capacitors. This is handled in the Thermal Analyzer Program by inputting curves showing the resistor (or capacitor) value as a function of temperature, or by directing the program to compute its own resistor and capacitor values, after interpolating the curves for the value of the appropriate thermodynamic property.

4. The ascent and orbital heating rates are determined at any convenient time prior to submitting the problem to the computer. For a complete vehicle, the accuracy requirements and the large number of orbital heating calculations involved generally

preclude the use of hand computations, and the Orbital Radiation Program (Ref. 5-2) is used. This program has an output option to provide the heating rate history at any particular vehicle location in the form of punched IBM cards in proper format for the Thermal Analyzer Program.

5. Once the network parameters and all internal and external heating rates have been determined, this data is described in detail in a form which allows it to be accepted by the computer program and solved. This involves writing up the program on data input sheets in a certain standard format, described in detail in Reference 5-1.

As noted above, an iterative procedure is used in the planning of a new vehicle or major modifications to an existing design. Preliminary layouts are made on the basis of previous experience and hand calculations of boundary conditions. The thermal analysis is then performed in stages, starting with the basic structure. As the detailed design proceeds, refinements and additions are made to the thermal network. Parameters of the basic program are varied to study the effectiveness of the selected thermal control system, internal and external surface finish requirements, and the general location of equipment. Such factors as equipment duty cycles and orbital variables may then be introduced.

The complete network is solved on a trial basis. It is usual, at this point, to discover problems in equipment temperature. Solutions are proposed by means of internal structural modifications (insulators, conduction straps, relocation) and/or changes to the external surface finish, and the effects ascertained by reanalysis. Equation (5-1) demonstrates how local surface temperature may be controlled by choice of surface finishes to provide the requisite values of solar absorptance and infrared emittance. The resulting vehicle surface pattern may consist of one or more paints, in any desired arrangement. A mosaic is used when the required characteristics are not available in a single paint or metallic surface.

The following subsections discuss the relationship between the physical problem and its electrical analog, and some general rules pertinent to converting the physical system into an R-C network. The equations used by the Thermal Analyzer Program to compute the transient temperature response of the system are also presented.

Basic Thermal System and Electrical Analog

The electrical analog solution requires that the problem be described as an equivalent network using resistance, capacity, and temperature to define the heat-transfer situation. The comparable values in the thermal and electrical systems are as follows:

THERMAL	ELECTRICAL
Temperature	Voltage
Heat Flux	Current
Resistance	Resistance
Capacity	Capacity

In any case involving heat transfer between two points, at temperatures T_j and T_k, the heat flow is given by an equation (analogous to Ohm's electrical law) as follows:

$$q = \frac{T_j - T_k}{R} \tag{5-6}$$

where, for conduction

$$q = kA\frac{\Delta T}{\Delta X} \quad \text{and} \quad R = \frac{\Delta X}{kA}$$

for simple convection

$$q = hA\,\Delta T \quad \text{and} \quad R = \frac{1}{hA}$$

for simple radiation

$$q = \epsilon_{12}A_1F_{12}\,\sigma\left[(T_1 + 460)^4 - (T_2 + 460)^4\right]$$

and $$R = \frac{1}{\epsilon_{12}A_1F_{12}\,\sigma\left[(T_1 + 460)^2 + (T_2 + 460)^2\right]\left[(T_1 + 460) + (T_2 + 460)\right]}$$

Transient analyses differ from steady-state analyses in that heat storage in a material undergoing a heating or cooling process is accounted for, thus causing a time lag in the temperature response of the material. The quantity of heat thus stored, and the description of the temperature response, will depend on the properties of the material itself. The combination of these properties determines the quantity called "thermal capacity," which will behave in the thermal network in the same manner as electrical capacity behaves in an electrical network. Thermal capacity must be in the units of heat quantity per degree of temperature (e.g., Btu/°F) and is a function of the material's density, specific heat and volume. Physically, the thermal capacity of a material represents the amount of heat stored in a given volume for each degree of temperature rise experienced by the material.

The thermal problem in a space vehicle is typified by the system shown in Figure 5-7. The basic elements of thermal capacity, heat-transfer paths, and an external radiating surface are shown together with the analogous electrical circuit. The dots in the lower sketch represent discrete portions of the structure or equipment. Each of these "lumped" nodes has an associated thermal capacity equal to the capacity of that portion of the physical problem which the lump represents. A space vehicle may be represented by many systems like that shown in Figure 5-7, all interconnected to form a single network.

Dividing the Physical Problem Into Lumps

To transform the physical problem into a form suitable for the computer, it must be converted into an equivalent network. This is accomplished by dividing the physical system into sections, called "lumps," and calculating the resistance and capacity of these lumps. A "lump," then, is any portion of the physical problem which (though not necessarily physically disconnected) will not be connected to any other portion of the problem except by resistors. The use of the lumping process implies that a given block of material is at a uniform average temperature.

In lumping a problem, several factors influence the size, shape, and number of lumps to be used. Among these are the nature of the physical

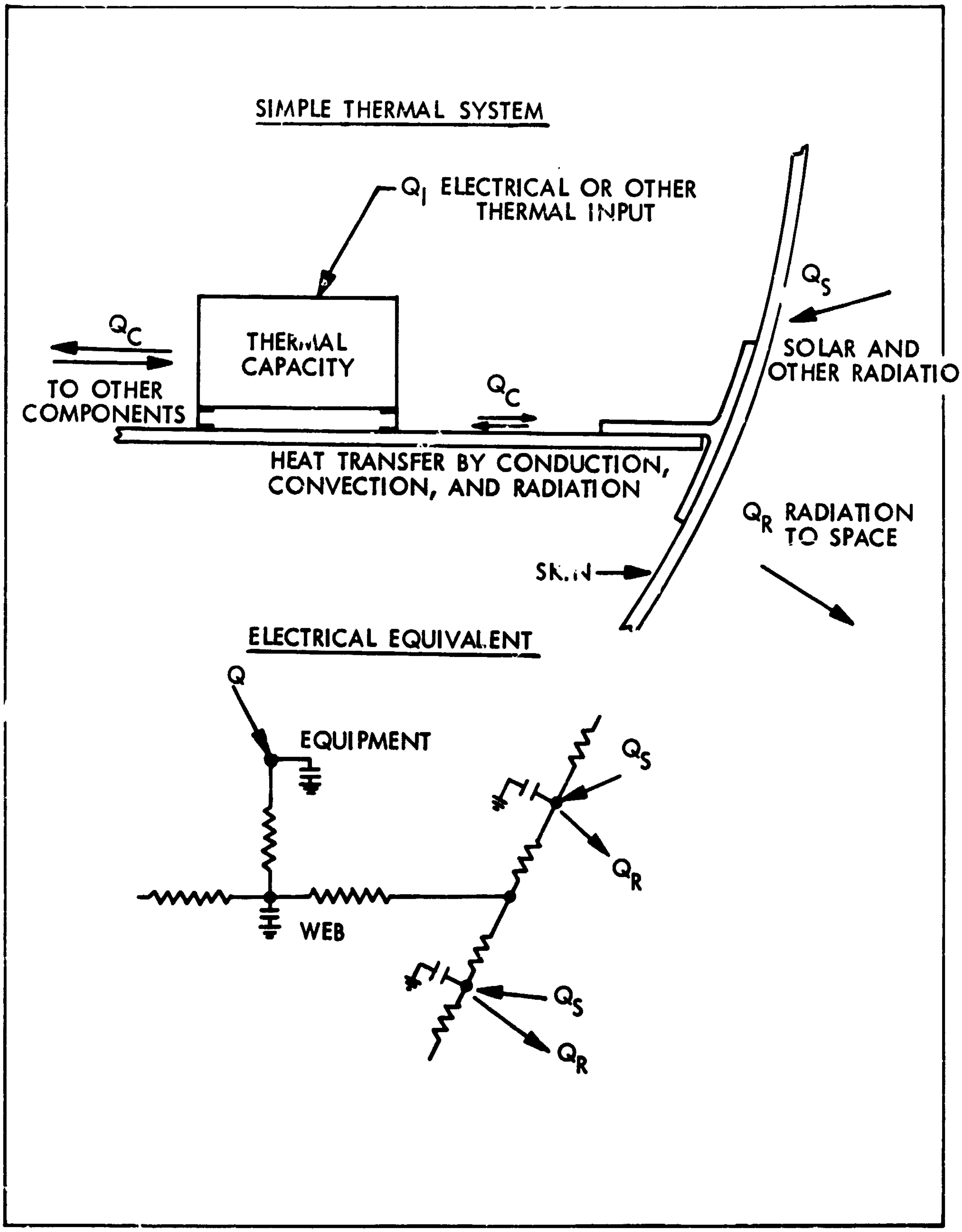

Figure 5-7. Basic Thermal System

problem, the amount of detailed information desired, and the anticipated transient response rates, and temperature gradients. Some of the considerations involved in problem lumping are outlined in the following discussion.

Location of Lumps - Although the lumps may take any size or shape, it is best that they bear a simple relationship to the physical problem. As a general rule, the nodes (the points where the lump capacities are assumed to be concentrated) should be located at those points where temperature data are desired, and these in turn are dictated by the nature of the problem itself. This is illustrated in the examples which follow. In each instance, the node locations are determined first and the lump boundaries located afterwards.

Example 1, Section of the Outer Wall of a Space Vehicle

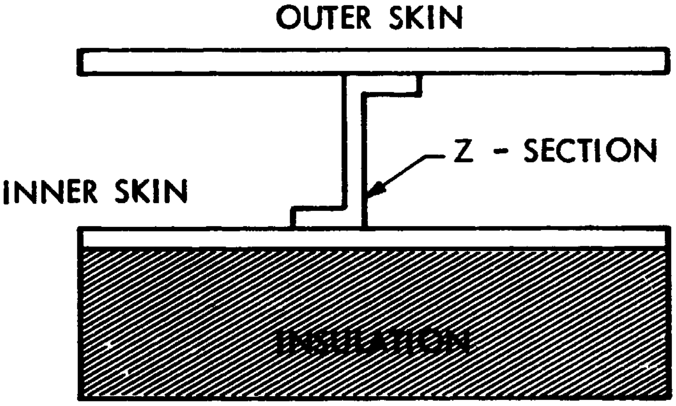

It is assumed that the problem is two-dimensional, i.e., no heat flows in or out of the plane of the drawing. However, it is a simple matter to connect many such sections into a complex three-dimensional problem. For this example, the net heat transfer through the wall and the temperature of the internal surface of the insulation are of primary importance. It is assumed that the latter exchanges heat by radiation with the interior components. Also, it is assumed that large lateral temperature gradients exist near the Z-section, with smaller gradients further out. With these points in mind, the resulting network is shown below:

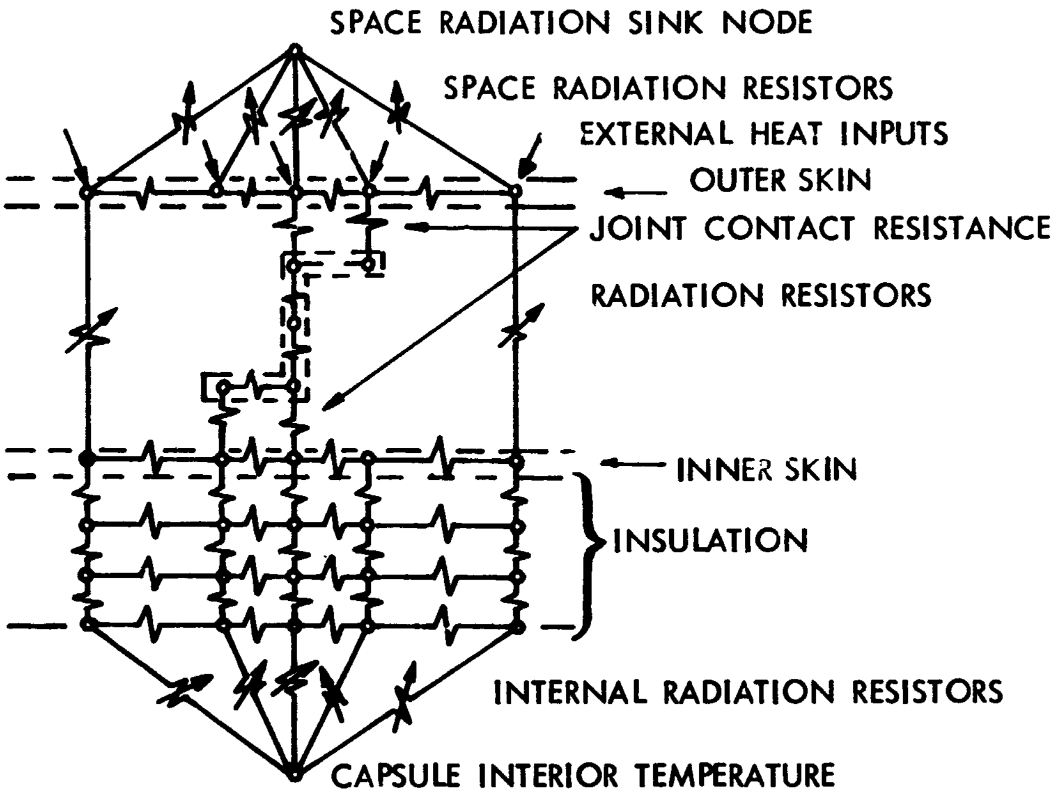

With regard to lump boundaries, the usual procedure is to place them so that the nodes are approximately in the center of the lumps except, of course, at the boundaries of the various layers. Nodes are usually placed at the boundaries in order to properly account for radiation or convection, both of which depend on the surface temperature. A large solid slab, such as the insulation, is normally represented as a series of rectangular parallelepipeds interconnected in three dimensions by conduction resistors. Each interior node is then connected to 6 other nodes.

Example 2, Electronic Equipment Rack Consisting of Several Intersecting Webs

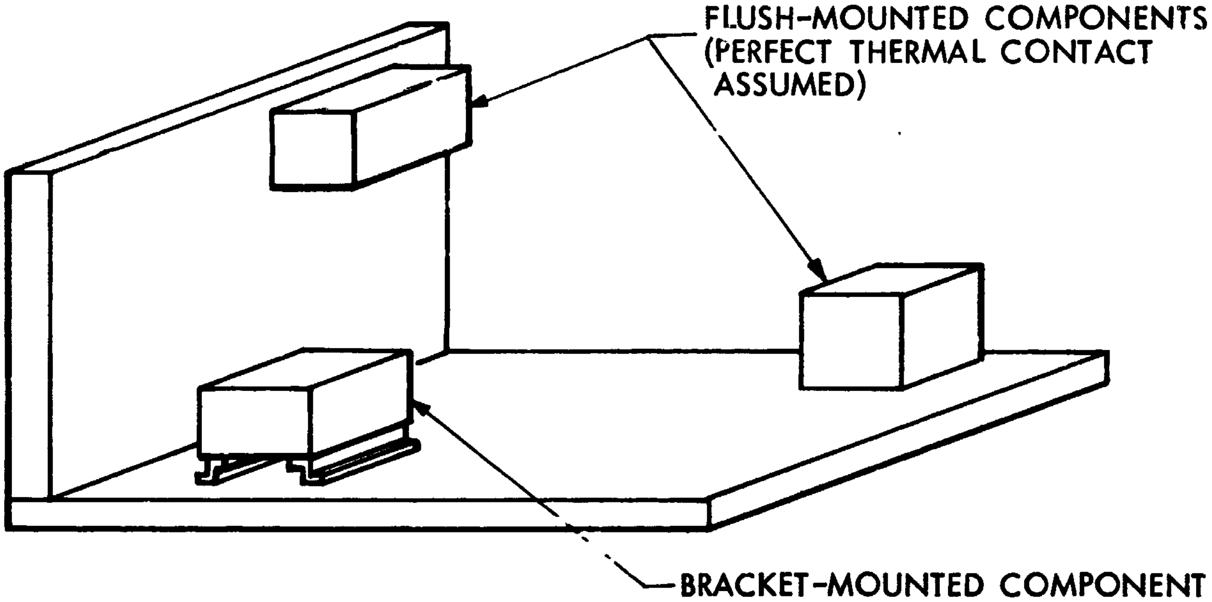

The corresponding network is shown below.

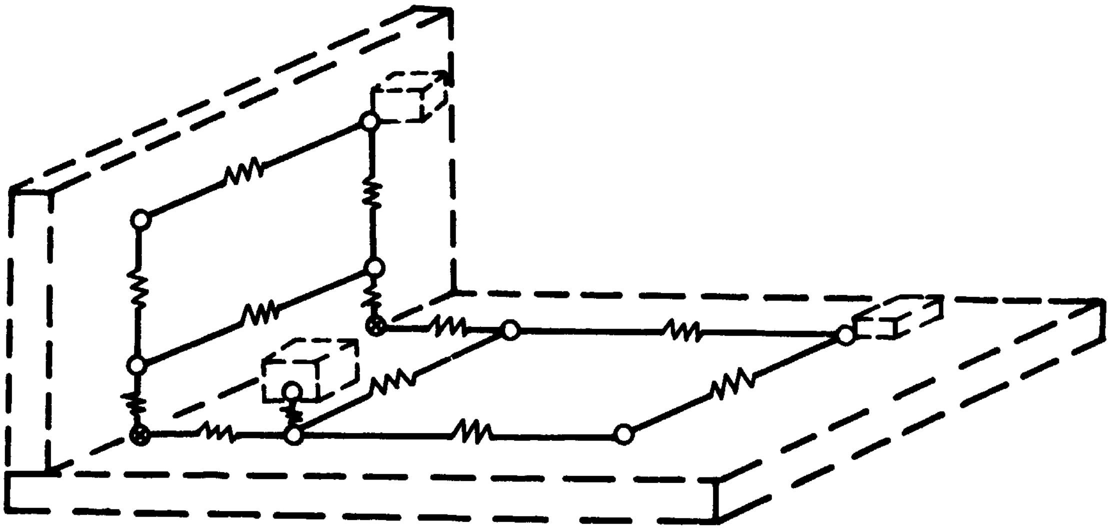

Since component temperatures are of primary interest here, the various capacities are assumed to be concentrated at points corresponding to equipment locations. However, this places the nodes inside the web boundaries as shown at the free ends of the two webs. At the juncture between the two webs, a string of zero capacitance nodes (designated by ⊗ in the preceding sketch and sometimes referred to as "dummy" nodes) is required to affect a connection between webs. This technique is particularly useful in a complex network where many such interconnecting webs are involved, since it allows each web to be treated separately and then connected to other such webs at the various "dummy" nodes.

Example 3, Conduction Network for Spacecraft Structure

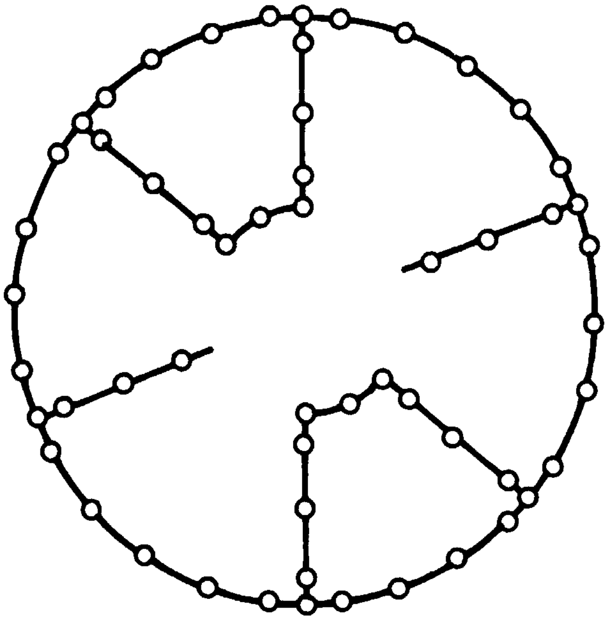

This is a cross-section of the conduction network used in a thermal analysis of the Apollo Service Module. The structure consists of an aluminum honeycomb outer shell, 6 radial beams, and center webs in two bays. The 26 circumferential nodes on the shell is an unusually large number but was dictated by the temperature gradients caused by radiator panels in 4 bays and by 16 external heat shields which protect the shell from the Reaction Control System engine firings. The nodes at the shell-beam intersection represent a large "T" section at the end of the beam plus two "Z" sections at the edge of each shell panel. Allowance is made for emission and absorption of radiation from a 3-inch-wide strip at each of these nodes. The network shown in this sketch, of course, is interconnected with others to represent the entire vehicle. The final network for this analysis consisted of approximately 850 nodes and 2200 resistors.

Normally, sufficient accuracy is obtained by placing an external shell node approximately every 20 degrees around the circumference of a spacecraft. The spacing depends, of course, on the accuracy required, the number and location of internal webs, the magnitude of the shell temperature variations, and the relative importance of the shell temperatures on the thermal behaviour of internal components.

The preceding illustrations are of but a few of the many lumping situations which arise. Probably the most important factor in problem lumping is past experience. Also, since no two situations are identical, it is impossible to cover all conceivable situations in a single report. It is hoped, however, that the examples presented here provide some insight into the problems involved.

Choice of Lump Size - In selecting the optimum lump size, recourse must be made to logical reasoning, and, most of all, experience. Here again, the nature of the physical problem dictates to a great extent the final decisions. Generally, the choice of lump size is based upon these factors:

1. Consideration of inaccuracies introduced into the system resulting from the finite difference method of solution. These inaccuracies decrease (not necessarily linearly) as lump size decreases. About the only definite statement which can be made is that lump size should be as large as possible without causing excessive inaccuracies.

2. Anticipated temperature gradients and relative rates of transient response. Where it is suspected that large temperature gradients will occur, nodes should be placed closer together than those where these gradients are smaller. This is especially true when the thermal diffusivity of a particular layer is very small, with the resulting temperature gradients across it being highly nonlinear.

3. Convenience in visualizing the network and making calculations.

4. Program capacity. Ordinarily the capacity of the computer is not approached; on occasion, for extremely large and complex problems, this becomes an important consideration.

5. Consideration of machine time. Not only do small lumps increase the number of nodes to be computed, but also they result in a smaller computing interval (difference in real time between successive steps), thus greatly increasing machine time.

Method of Solution by the Thermal Analyzer Program

As previously indicated, the Thermal Analyzer Program solves equations in finite difference form. At a given node point k,

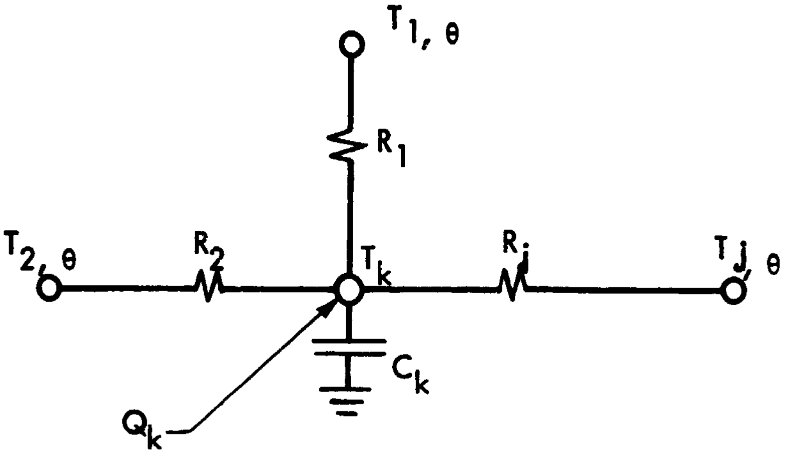

the solution is obtained by applying the linear form of Kirchhoff's law at a point, i.e.,

$$T_{k,\theta+\Delta\theta} = \frac{\Delta\theta}{C_k}\left[\sum_j \frac{T_{j,\theta} - T_{k,\theta}}{R_j} + q_k\right] + T_{k,\theta} \tag{5-7}$$

where

$T_{k,\theta+\Delta\theta}$ = temperature of node k after time increment $\Delta\theta$.

$T_{k,\theta}$ = temperature of node k at time θ.

C_k = thermal capacity of node k.

$T_{j,\theta}$ = Temperature at time θ of any arbitrary node j connected to node k by a resistor R_j.

$T_{k,\theta}$ = Temperature of node k at time θ.

R_j = resistor connecting nodes j and k.

q_k = arbitrary heat input into node k.

If the value of a capacity C_k is zero, e.g., in a steady-state problem, the temperature of node k is computed as

$$T_{k,\theta+\Delta\theta} = \frac{\sum_j \frac{T_{j,\theta}}{R_j} + q_k}{\sum_j \frac{1}{R_j}} \tag{5-8}$$

To obtain the computing interval, $\Delta\theta$, the computer searches the network to find the minimum R-C product and compares this value with the printing interval (the real-time increment for which the output is desired). The computer then takes the smaller of the two values and multiplies it by some fraction, normally 0.25, to obtain $\Delta\theta$.

CONFIGURATION FACTORS

One of the most tedious jobs in any spacecraft thermal analysis is the computation of radiation configuration factors. Unfortunately, closed-form solutions for configuration factors exist only for a small number of simple shapes with restrictions on the boundary surfaces and the orientation of the elements. The following paragraphs discuss the available closed form solutions, the concept of shape factor algebra, a digital computer program to compute shape factors between complex configurations including interfering surfaces, and a very useful optical projection technique.

Closed-Form Solutions

The configuration factor, F_{12}, is defined as the fraction of the radiation leaving black surface A_1 in all directions which is intercepted by surface A_2. In Figure 5-8, dA_1 and dA_2 represent surface elements of two radiating bodies A_1 and A_2. The distance between the surface elements is S, and the angles between the normals to the surfaces and the connecting line S are β_1 and β_2, respectively. The heat radiated per unit time from surface dA_1 within the solid angle under which dA_2 is seen from dA_1 is

$$dQ_{1\to 2} = I_{1n} \cos \beta_1 \; dA_1 \; d\omega_1 \qquad (5\text{-}9)$$

where I_{1n} is the radiation intensity of dA_1 in the normal direction and $d\omega_1$ is the solid angle under which dA_2 is seen from dA_1. This angle is given by

$$d\omega_1 = \frac{dA_2 \cos \beta_2}{S^2}$$

Equation (5-9) becomes

$$dQ_{1\to 2} = I_{1n} \frac{\cos \beta_1 \cos \beta_2}{S^2} \; dA_1 \, dA_2 \qquad (5\text{-}10)$$

This heat is absorbed by black surface dA_2.

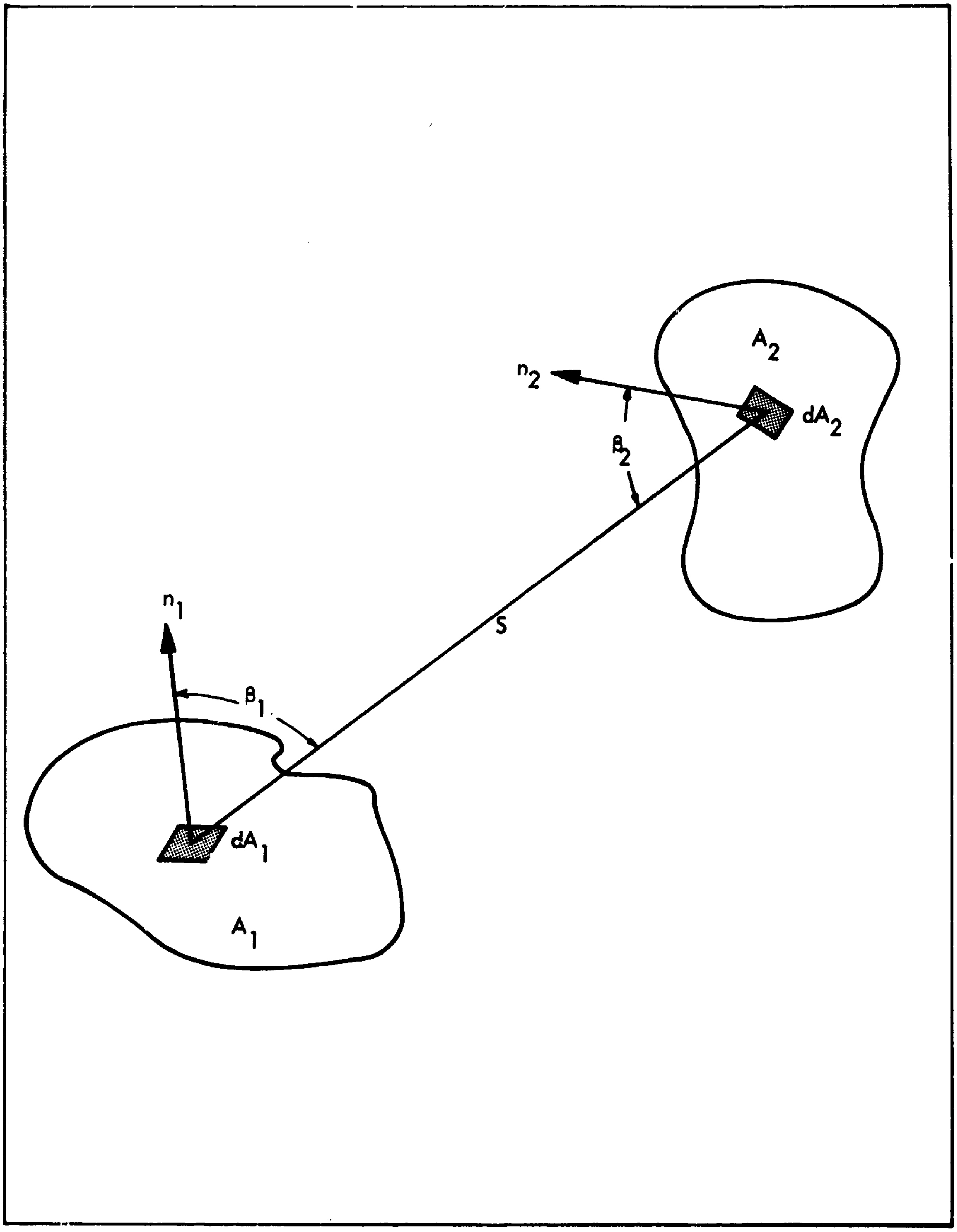

Figure 5-8. Geometry for Radiation Heat Transfer Between Two Small Surface Elements

By the same reasoning, the heat radiated from dA_2 to dA_1 is

$$dQ_{2\rightarrow 1} = I_{2n} \frac{\cos\beta_1 \ \cos\beta_2}{s^2} \ dA_1 \ dA_2 \tag{5-11}$$

The configuration factor was defined above as the heat radiated per unit area from dA_1 to dA_2, divided by the emissive power I of dA_1. The latter is $I = \pi I_n = \sigma T^4$. Then, from equation (5-10)

$$dF_{12} = \frac{\cos\beta_1 \ \cos\beta_2}{\pi s^2} \ dA_2 \tag{5-12}$$

The configuration factor is strictly a geometrical relation. The heat radiated from dA_1 and intercepted by dA_2 is given by

$$dQ_{1\rightarrow 2} = \sigma T_1^4 \ dF_{12} \ dA_1 \tag{5-13}$$

By the same reasoning

$$dQ_{2\rightarrow 1} = \sigma T_2^4 \ dF_{12} \ dA_1 \tag{5-14}$$

and the net heat exchange becomes

$$dQ = dQ_{1\rightarrow 2} - dQ_{2\rightarrow 1} = \sigma(T_1^4 - T_2^4) \ dF_{12} \ dA_1 \tag{5-15}$$

The calculations can be referenced in the same way to the surface element dA_2 to obtain the following expression:

$$dQ = \sigma(T_1^4 - T_2^4) \ dF_{21} \ dA_2 \tag{5-16}$$

where the configuration factor dF_{21} of dA_2 with respect to dA_1 is

$$dF_{21} = \frac{\cos\beta_1 \ \cos\beta_2}{\pi \ s^2} \ dA_1 \tag{5-17}$$

The radiant heat exchange between a surface element and a surface whose size is not small compared with their distance apart can be determined by integration of equation (5-15). The result is the equation

$$Q = \sigma \ (T_1^4 - T_2^4) \ F_{12} \ dA_1 \tag{5-18}$$

where the configuration factor is given by

$$F_{12} = \int_{A_2} \frac{\cos \beta_1 \cos \beta_2}{\pi S^2} dA_2 \qquad (5\text{-}19)$$

For radiation exchange between two surfaces of finite area according to the equation

$$Q = \sigma(T_1^4 - T_2^4) F_{12} A_1 \qquad (5\text{-}20)$$

the configuration factor is obtained by integrating over both surface areas. The resulting expression is

$$F_{12} = \frac{1}{A_1} \int_{A_1} F_{12}(A_1)\, dA_1 = \frac{1}{\pi A_1} \int_{A_1} \int_{A_2} \frac{\cos \beta_1 \cos \beta_2}{S^2} dA_1\, dA_2 \qquad (5\text{-}21)$$

where F_{12} (A_1) denotes the shape factor of an element dA_1 of A_1. F_{12} is the mean value of all local shape factors with which any differential element on surface A_1 irradiates surface A_2. The same reasoning can be applied to derive the following configuration factor from surface A_2 to surface A_1:

$$F_{21} = \frac{1}{A_2} \int_{A_2} F_{21}(A_2)\, dA_2 = \frac{1}{\pi A_2} \int_{A_2} \int_{A_1} \frac{\cos \beta_1 \cos \beta_2}{S^2} dA_1\, dA_2 \qquad (5\text{-}22)$$

where

$$Q = \sigma(T_1^4 - T_2^4) F_{21} A_2 \qquad (5\text{-}23)$$

By comparing equations (5-20) and 5-23), it is apparent that the following relation holds:

$$F_{12} A_1 = F_{21} A_2 \qquad (5\text{-}24)$$

This is a convenient relation since, in most problems, one configuration factor is simpler to compute than the other. For example, if surface A_1 is completely surrounded by surface A_2, it can be stated immediately that F_{12} is equal to 1, since all radiant flux leaving surface A_1 will impinge on A_2.

Closed-form solutions to equations (5-19, 5-21), and (5-22) are available only for a small number of simple shapes. A selected group of practical interest in aerospace applications is given below. Reference 5-3 contains solutions for these and other configurations, with the more complicated equations presented as families of curves.

Plane-Surface Element to a Circular Disk:

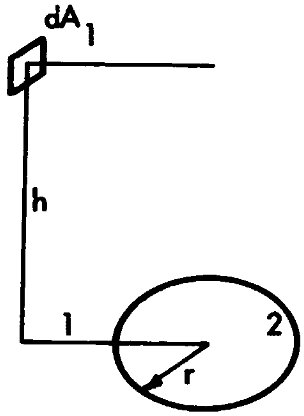

$$F_{12} = \frac{h}{2}\left[\frac{h^2 + r^2 + 1}{\sqrt{(h^2 + r^2 + 1)^2 - 4r^2}} - 1\right]$$

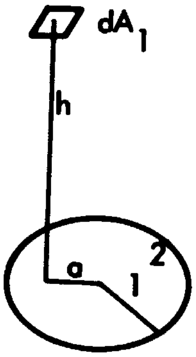

$$F_{12} = \frac{1}{2}\left[1 - \frac{h^2 + a^2 - 1}{\sqrt{(h^2 + a^2 + 1)^2 - 4a^2}}\right]$$

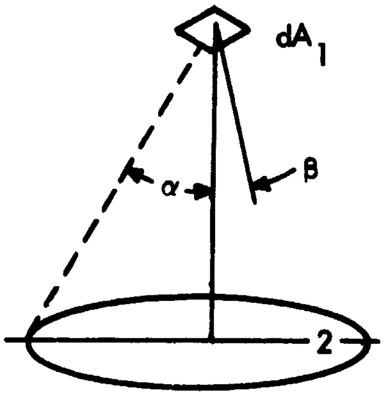

$$F_{12} = \sin^2\alpha \cos\beta$$

Plane Surface Element to a Rectangle:

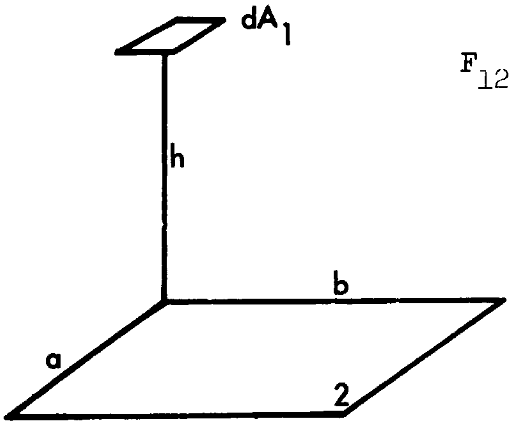

$$F_{12}\ (\text{parallel}) = \frac{1}{2\pi}\left[\frac{a}{\sqrt{a^2+h^2}}\tan^{-1}\frac{b}{\sqrt{a^2+h^2}} + \frac{b}{\sqrt{b^2+h^2}}\tan^{-1}\frac{a}{\sqrt{b^2+h^2}}\right]$$

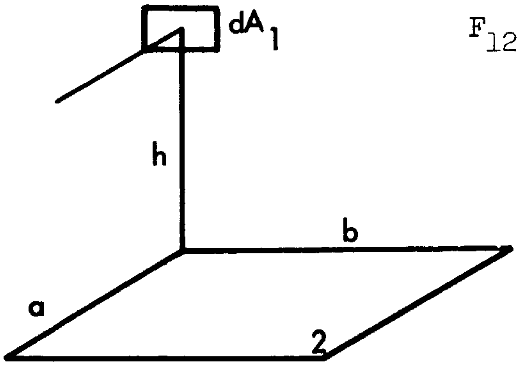

$$F_{12}\ (\text{normal}) = \frac{1}{2\pi}\left[\tan^{-1}\frac{b}{h} - \frac{h}{\sqrt{a^2+h^2}}\tan^{-1}\frac{b}{\sqrt{a^2+h^2}}\right]$$

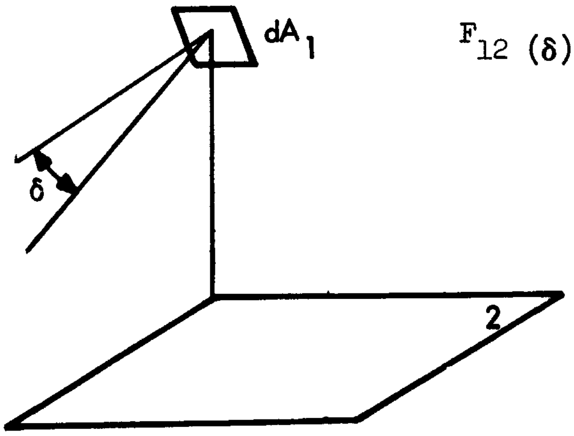

$$F_{12}\ (\delta) = F_{12}\ (\text{parallel})\cos\delta + F_{12}\ (\text{normal})\sin\delta$$

Plane Surface Element dA_1 to Any Surface A_2 Generated by an Infinitely Long Line Moving Parallel to Itself and to the Plane of dA_1:

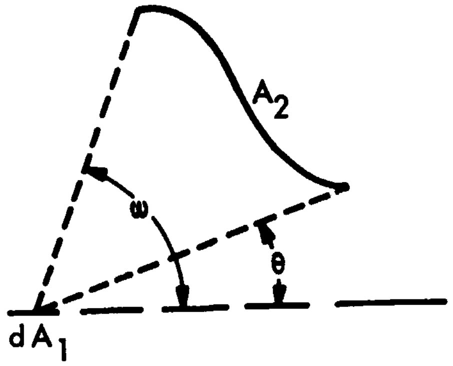

$$F_{12} = \frac{1}{2}\left[\cos\theta - \cos\omega\right]$$

Plane Surface Element dA_1 to Any Infinite Plane A_2 with the Planes of dA_1 and A_2 Intersecting at an Angle θ:

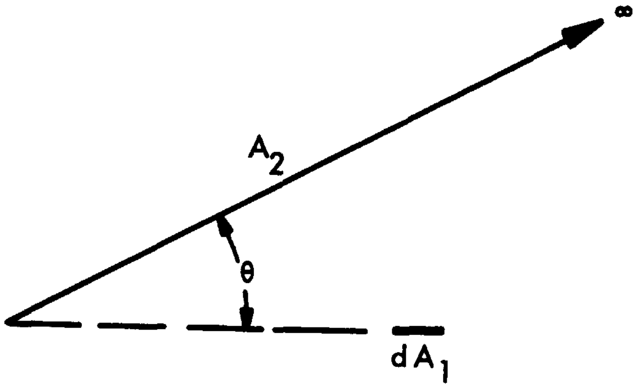

$$F_{12} = \frac{1}{2}\left(1 - \cos\theta\right)$$

Two Infinitely Long Planes with One Common Edge:

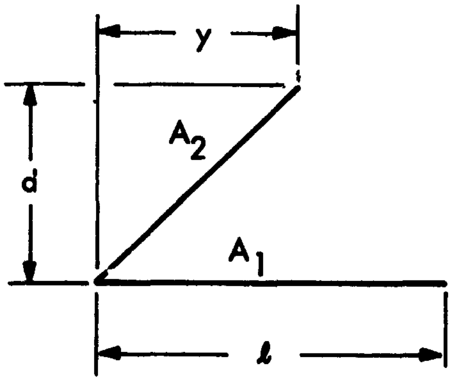

$$F_{12} = \frac{1}{2}\left[1 + \sqrt{\left(\frac{d}{\ell}\right)^2 + \left(\frac{y}{\ell}\right)^2} - \sqrt{\left(\frac{d}{\ell}\right)^2 + \left(\frac{y}{\ell} - 1\right)^2}\,\right]$$

Two Infinitely Long Parallel Planes of Unequal Width:

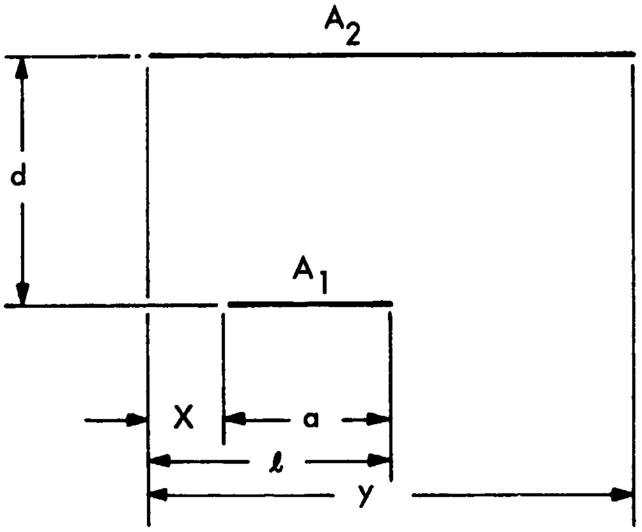

$$F_{12} = \frac{1}{2(\ell - x)} \left[\sqrt{d^2 + \ell^2} - \sqrt{d^2 + x^2} + \sqrt{d^2 + (y - x)^2} - \sqrt{d^2 + (y - \ell)^2} \right]$$

Identical, Parallel, Directly Opposed Rectangles A_1 and A_2:

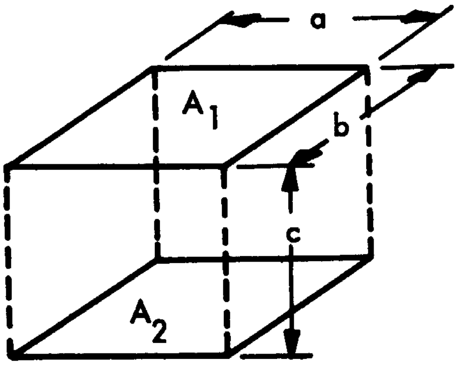

$$F_{12} = \frac{2}{\pi x y} \left\{ \ln \left[\frac{(1 + x^2)(1 + y^2)}{1 + x^2 + y^2} \right]^{1/2} + y\sqrt{1 + x^2} \tan^{-1}\left(\frac{y}{\sqrt{1 + x^2}} \right) + x\sqrt{1 + y^2} \tan^{-1}\left(\frac{x}{\sqrt{1 + y^2}} \right) - y \tan^{-1} y - x \tan^{-1} x \right\}$$

$$\lim_{x \to \infty} F_{12} = \sqrt{1 + \frac{1}{y^2}} - \frac{1}{y}$$

$$\lim_{y \to \infty} F_{12} = \sqrt{1 + \frac{1}{x^2}} - \frac{1}{x} \qquad \lim_{x,y \to \infty} F_{12} = 1$$

where $x = \frac{b}{c}$ $\qquad y = \frac{a}{c}$

This configuration factor is plotted in Figure 5-9.

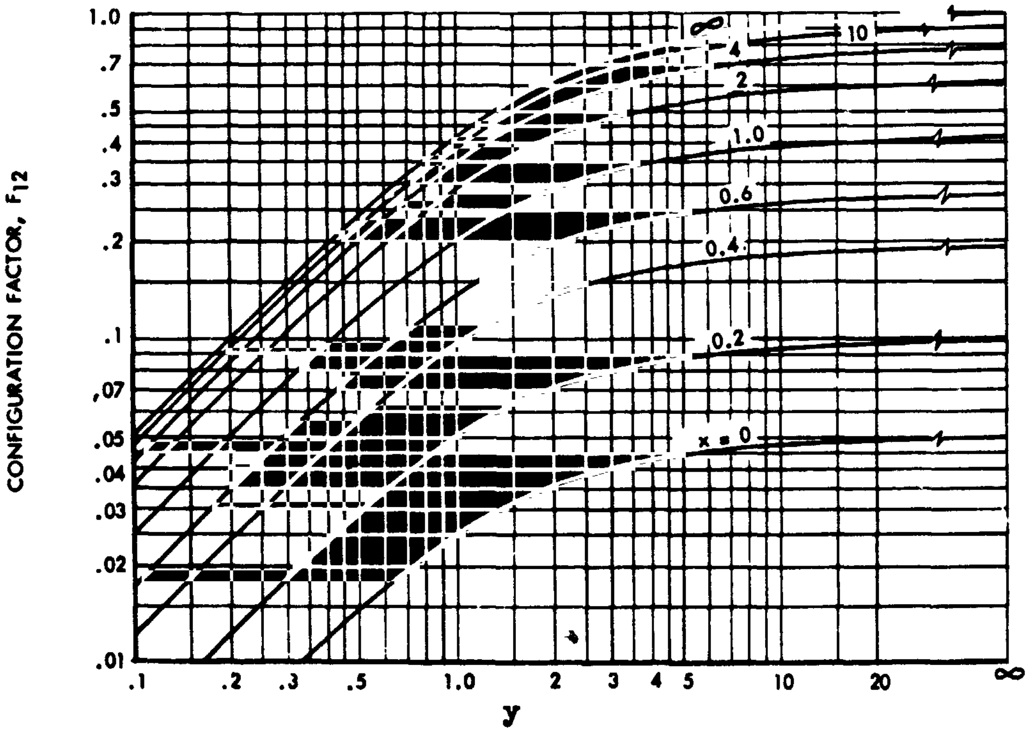

FIGURE 5-9 CONFIGURATION FACTOR FOR TWO IDENTICAL, PARALLEL, DIRECTLY OPPOSED RECTANGLES

Two Rectangles A_1 and A_2 with One Common Edge and Included Angle ϕ :

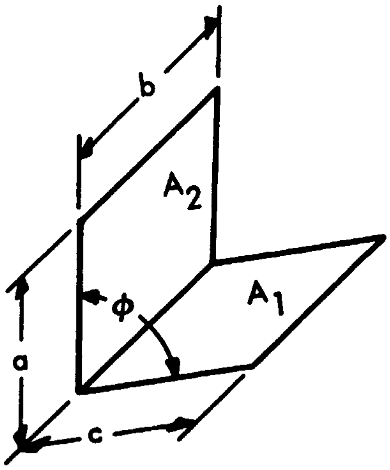

for $\phi = 90°$

$$F_{12} = \frac{1}{\pi L}\left(L \tan^{-1}\left(\frac{1}{L}\right) + N \tan^{-1}\left(\frac{1}{N}\right) - \sqrt{N^2 + L^2}\ \tan^{-1}\frac{1}{\sqrt{N^2 + L^2}}\right.$$

$$+ \frac{1}{4}\ \ln\left\{\left[\frac{(1 + L^2)\ (1 + N^2)}{(1 + L^2 + N^2)}\right]\left[\frac{L^2\ (1 + L^2 + N^2)}{(1 + L^2)\ (L^2 + N^2)}\right]^{L^2}\right.$$

$$\left.\left.\left[\frac{N^2\ (1 + L^2 + N^2}{(1 + N^2)\ (L^2 + N^2)}\right]^{N^2}\right\}\right)$$

where

$L = \frac{c}{b}$ $\qquad$ $N = \frac{a}{b}$

This configuration factor is plotted in Figures 5-10a, 5-10b, and 5-10c, for ϕ = 30°, 60°, and 90°, respectively.

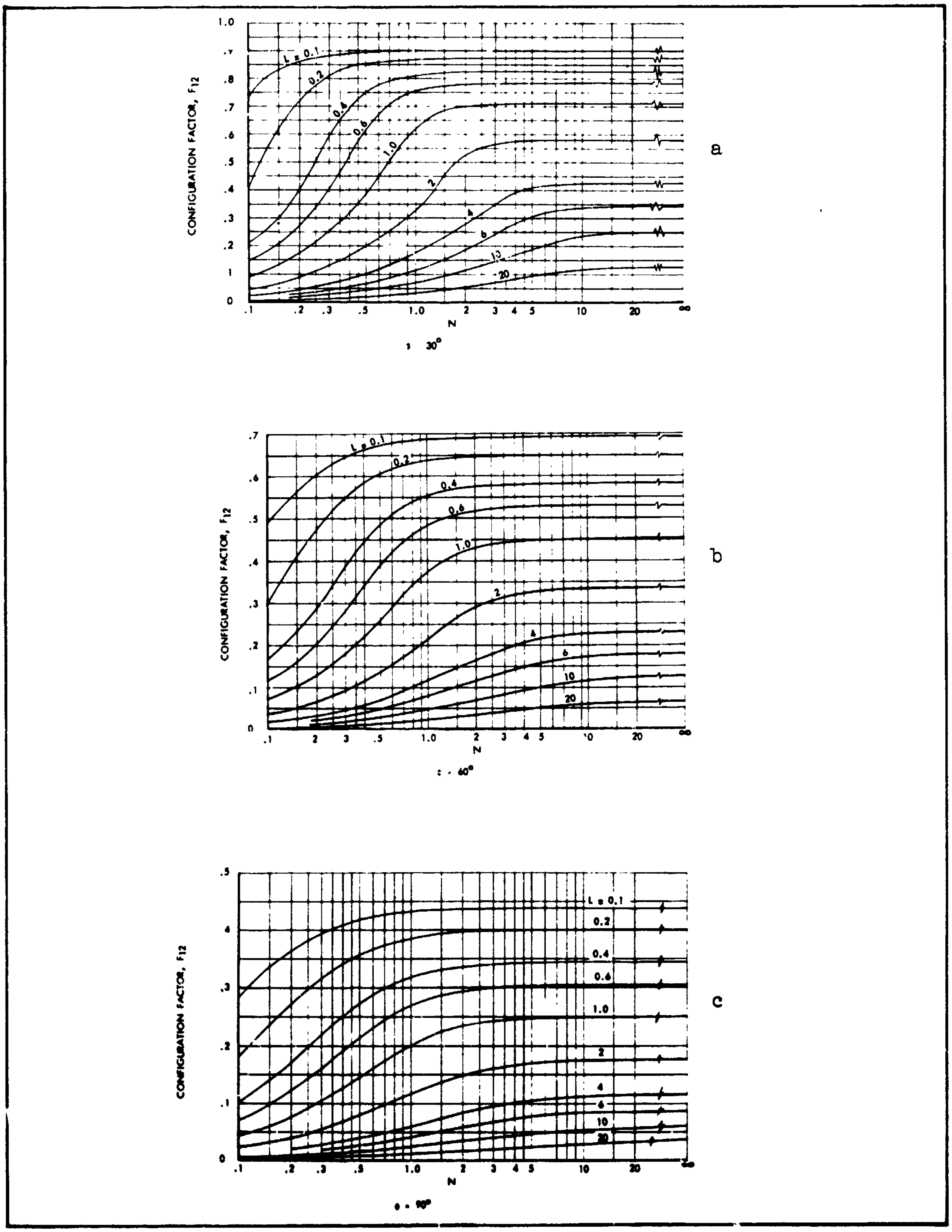

Figure 5-10. Configuration Factor for Two Rectangles with One Common Edge and Included Angle ϕ

Parallel, Directly Opposed, Plane Circular Disks:

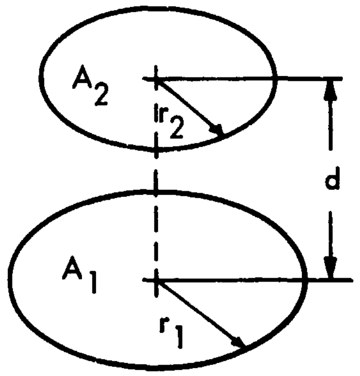

$$F_{12} = \frac{1}{2}\left(x - \sqrt{x^2 - 4E^2D^2} \right)$$

Where $x = 1 + (1 + E^2)D^2$

$E = r_2/d$

$D = d/r_1$

The configuration factor is plotted in Figure 5-11.

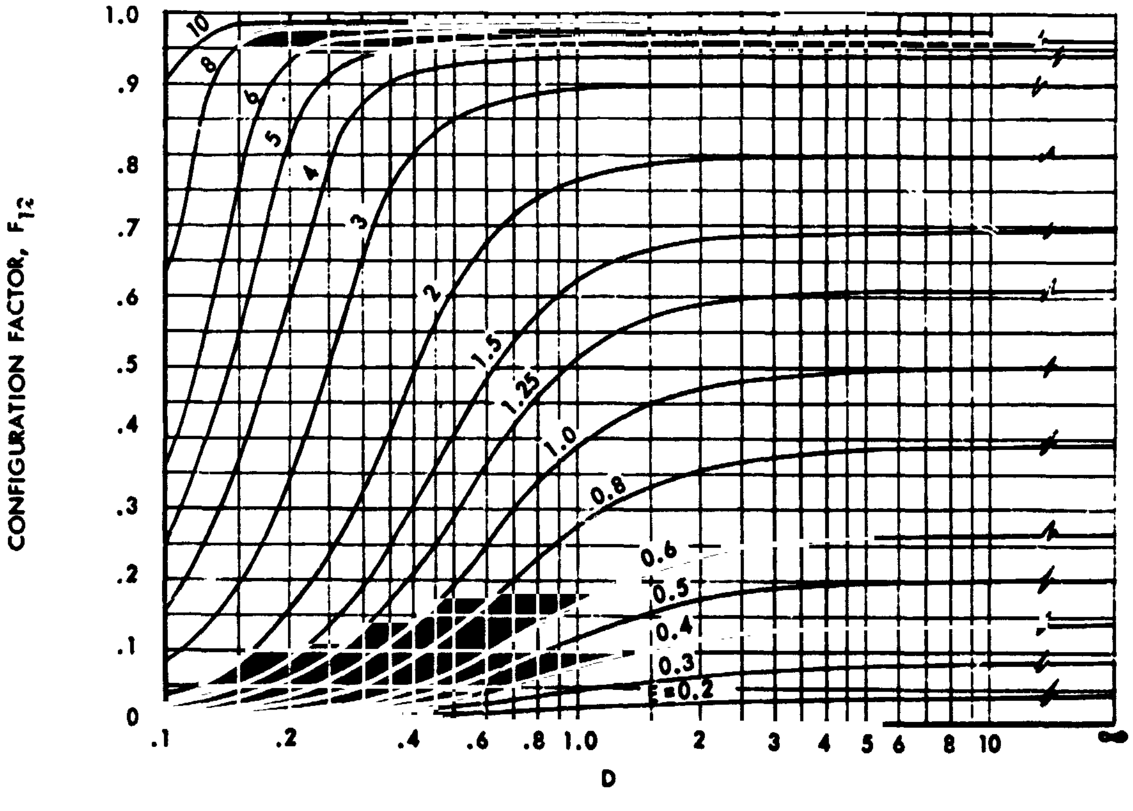

Figure 5-11. Configuration Factor for Parallel, Directly Opposed, Plane Circular Disks

Two Parallel, Concentric Cylinders A_1 and A_2 of Radius r_1 and r_2 and Infinite Length:

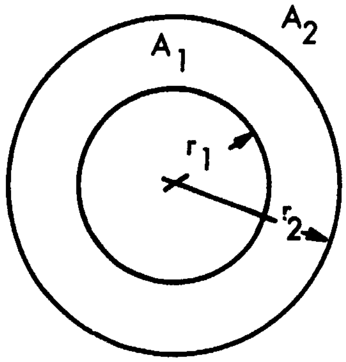

$$F_{12} = 1$$

$$F_{21} = r_1/r_2$$

Two Concentric Spheres A_1 and A_2 of Radius r_1 and r_2:

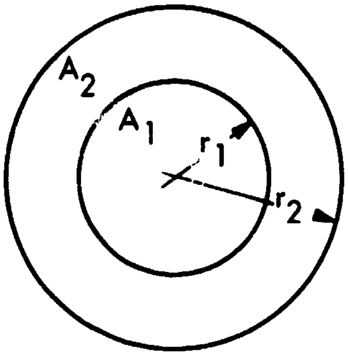

$$F_{12} = 1$$

$$F_{21} = (r_1/r_2)^2$$

An Infinite Cylinder Parallel to the Plane of an Infinitely Long Rectangle of Width ℓ-m.

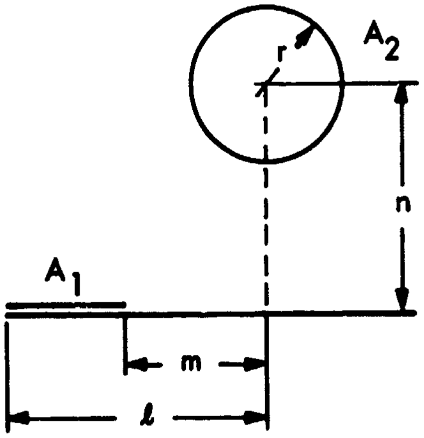

$$F_{12} = \left[\frac{1}{(L - M)}\right] \tan^{-1}\left(\frac{L}{N}\right) \tan^{-1}\left(\frac{M}{N}\right)$$

For M = 0 :

$$F_{12} = \left(\frac{1}{L}\right) \tan^{-1} \left(\frac{L}{N}\right)$$

where $N = \frac{n}{r}$ $M = \frac{m}{r}$ $L = \frac{\ell}{r}$

Configuration Factor Algebra

Configuration factor algebra can be used in conjunction with the preceding equations to compute shape factors for many additional geometries. This concept is based on the following simple rules which should be apparent from the geometric interpretation of the shape factor:

1. For any radiating body the sum of the configuration factors to all surrounding bodies is equal to unity.
2. $A_1 F_{12} = A_2 F_{21}$ as discussed above.
3. AF products follow the laws of arithmetic.

Several examples are given below. For brevity, the symbol (AB) (C) is used to represent $A_{AB} F_{AB-C}$, etc.

Example 1, AF Product (AC) Between a Surface Element and a Finite Area:

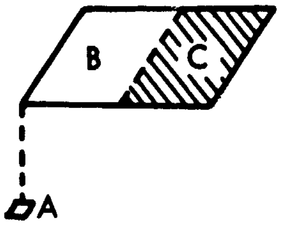

$$(A)(C) = (A)(BC) - (A)(B)$$

Example 2, AF Product (AD) Between Finite Surface Areas on Two Intersecting Planes:

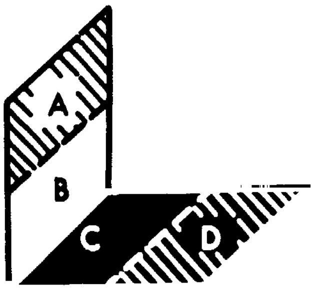

$$(AB)(CD) = (A)(C) + (A)(D) + (B)(C) + (B)(D)$$

$$\therefore (A)(D) = (AB)(CD) - (A)(C) - (B)(C) - (B)(D)$$

$$= (AB)(CD) - (AB)(C) - (B)(CD) + (B)(C)$$

Example 3, AF Product (AD) Between Finite Surface Areas on Two Parallel Planes:

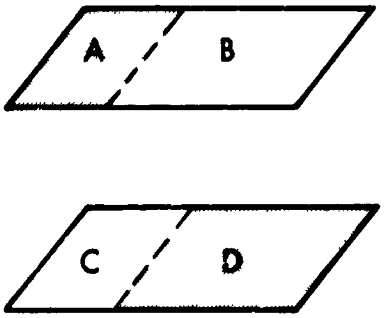

$$(AB)(CD)=(A)(C)+(A)(D)+(B)(C)+(B)(D)$$

$$\therefore (A)(D)=(AB)(CD)-(A)(C)-(B)(C)-(B)(D)$$

But, $(B)(C)=(A)(D)$

$$\therefore (A)(D) = \frac{1}{2}\left|(AB)(CD)-(A)(C)-(B)(D)\right|$$

The expressions become increasingly complex as the geometries become more involved. The mathematics, however, are simple, and solutions can generally be obtained without difficulty.

Configuration Factor Program

The Lockheed-California Company has developed a Configuration Factor Program (Reference 5-4) for use on the IBM 7094 Digital Computer. The program computes geometrical configuration factors between any two bodies whose surfaces and boundary surfaces can be represented as a general quadratic, i.e., as surfaces defined by equations of the form

$$Ax^2 + By^2 + Cz^2 + Dxy + Exz + Fyz + Gx + Hy + Iz + J = 0$$

This permits eleven different surface types:

One plane

Two parallel or intersecting planes

Elliptic cylinders

Parabolic cylinders

Hyperbolic cylinders

Elliptic cones

Ellipsoids

Elliptic paraboloids

Hyperboloids of one sheet

Hyperboloids of two sheets

Hyperbolic paraboloids

Since a circle is a special kind of ellipse, the list includes spheres, right circular cones, and right circular cylinders, as well as the surfaces obtained by rotating ellipses, parabolas, or hyperbolas around an axis of the curve.

The surfaces may be input in the form of coefficients of the quadratic equation, a set of points over the surface, coefficients of the equations of a simpler surface such as a plane or a sphere, or as a set of points on the simpler surface. Every primary surface must be bounded. Up to 100 surfaces can be handled in one run.

The configuration factor is computed from equation (5-21) by numerical methods. The size of the grid used for the integration process is specified by the user in the input.

An outstanding feature of the program is that the shading effects of interfering surfaces is accounted for. The interfering surfaces and their boundaries are input in the same manner as the primary surfaces.

Optical Projection Technique

The Lockheed-California Company has developed an optical projection technique to compute radiation configuration factors from a plane point source to any object. The method employs a point light source to cast the shadow of a scale model of the viewed object on a wall, marked in a pattern so that the view factor is obtained directly from the number of sectors shaded by the object. The method is similar to the familiar double-projection method of Nusselt, but it avoids the necessity of constructing a hemispherical surface and the conversion of configuration factor to units of area. This is done by projecting the object onto a plane which is parallel to the point source instead of projecting the object to the surface of the hemisphere and then reprojecting the image to the base of the hemisphere. The requirement of relating the configuration factor to units of area is eliminated by accounting for the area integration in the mathematics which describes the wall pattern.

The apparatus consists of a small lamp (a 75- or 100-watt projection lamp is satisfactory), a scale model, and surfaces marked in the pattern described below. The lamp and scale model represent the plane point source from which the configuration factor is taken and the object to which it is taken, respectively. The marked surfaces consist of the end wall, floor, ceiling and side walls of a small room. These surfaces are subdivided into p sectors, each representing an area which intercepts 1/p of the total radiant flux leaving the point source. By definition, each sector, therefore, has a configuration factor of 1/p from the point source. The pattern that is drawn is somewhat arbitrary, but a pattern constructed of circles and radials has been found to be most convenient.

A Lambertian plane point source can be considered to emit radiant flux along concentric cones whose axes coincide with the normal to the emitter. No flux will penetrate the surface of the cones. A number n of such concentric cones can be visualized so that each will enclose 1/n of the radiant flux leaving the point source. If a plane is passed normal to the axis of these cones (parallel to the emitter), the intersection of the cone with the plane forms a series of concentric circles whose enclosed areas intercept the same fraction of the radiant flux as enclosed by the cones. This is the basis for establishing the wall pattern. The end wall, which is parallel to the point source, is marked with a series of concentric circles whose areas intercept 1/n of the total radiant flux leaving the point source. The radii of these circles is determined from the expression for the shape factor from a plane point source to a parallel disk whose center lies along the normal to the emitting element. From the solutions presented above, the expression is seen to be

$$F_{12} = \frac{r^2}{r^2 + d^2} = \frac{1}{1 + (\frac{d}{r})^2}$$

where r is the radius of the disk and d is the distance between the parallel surfaces dA_1 and A_2. This expression can be rewritten as follows:

$$r = d\sqrt{\frac{F_{12}}{1 - F_{12}}}$$

F_{12} is taken at convenient fractions such as .1, .2, .3 ... 1.0 to define the pattern circles $r_{.2}$, $r_{.3}$, etc. The areas between each circle will intercept 0.1 of the flux leaving the point source.

If the side walls, floor, and ceiling are parallel to the axis of the emission cones, they intersect the cones as hyperbolas. The equation of the hyperbolas is given by

$$y = d \left[1 - \frac{\sqrt{X^2 + a^2}}{r} \right]$$

The symbols are defined by the sketch in Figure 5-12. The distance r would be the radius of the circle if the end wall were extended to infinity in all directions.

To further subdivide the wall pattern so that each sector represents a configuration factor of 0.01, ten planes, 30° apart are passed through the axis of the emission cones. These planes intersect the end wall to form radial lines through the circle origin, and intersect the floor, ceiling, and side walls to form straight lines normal to the end wall. Figure 5-13 is a perspective drawing of the marked walls. Of course, the exact pattern depends on the size and shape of the room, and on the distance d.

To measure the configuration factor from the point source to any object the lamp is placed at a distance d from the end wall along the normal to the origin of the circles. The scale model is located between the lamp and the wall with suitable model holders. The size of the model and its location relative to the point source must be scaled to the physical configuration. The configuration factor is obtained from the shadow cast by the model on the wall. Each completely shaded sector represents a value of 0.01. The value of a partially shaded sector can generally be estimated within 0.001.

Two photographs of the wall pattern and projection lamp used at Lockheed are shown in Figure 5-14. The dimensions of the end wall are 9 ft x 12 ft. The lamp is placed 4 ft from the end wall and 4 ft from the floor. These distances are satisfactory to accommodate most full-scale mockup components and models. For additional accuracy the pattern has been further subdivided within the innermost and outermost rings such that each shaded sector represents a configuration factor of 0.001.

Figures 5-15 and 5-16 show two objects projecting shadows upon the end wall grid. The object in Figure 5-15 is a scale model of the Lunar Excursion Module (LEM) and the objects in Figure 5-16 are ordinary balloons, representing

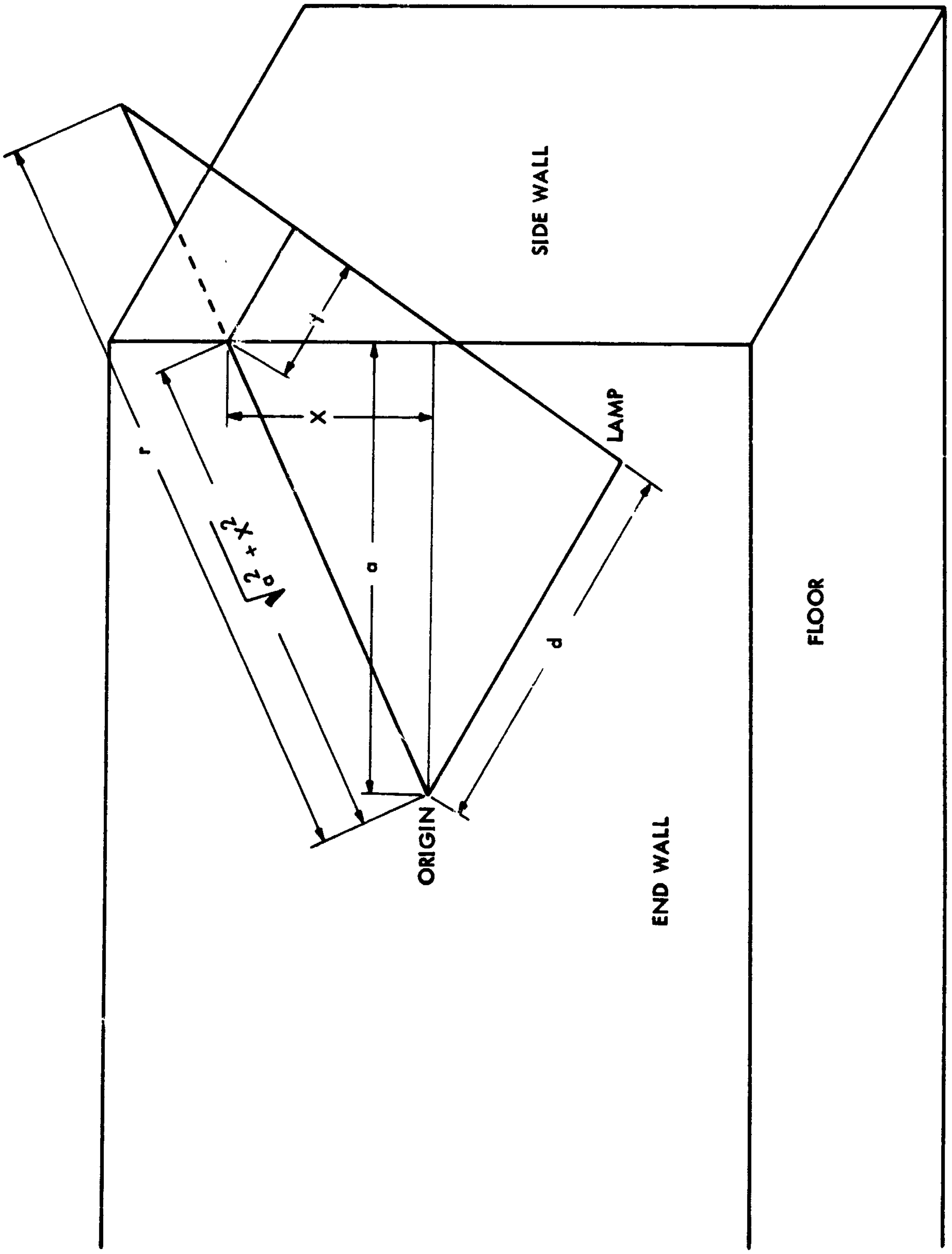

Figure 5-12 Intersection of Emission Cone with Side Wall

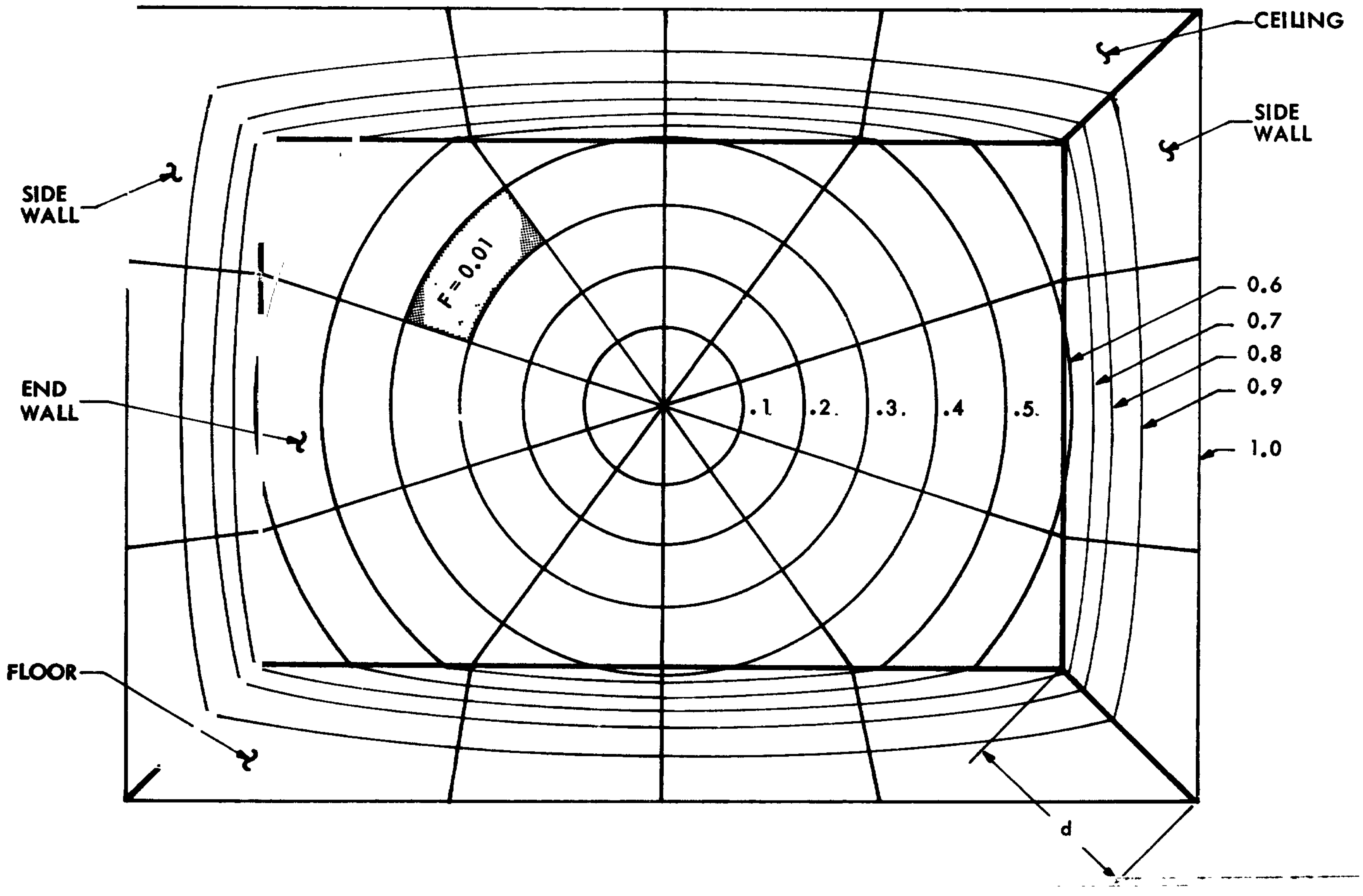

Figure 5-13 Configuration Factor Room Wall Pattern

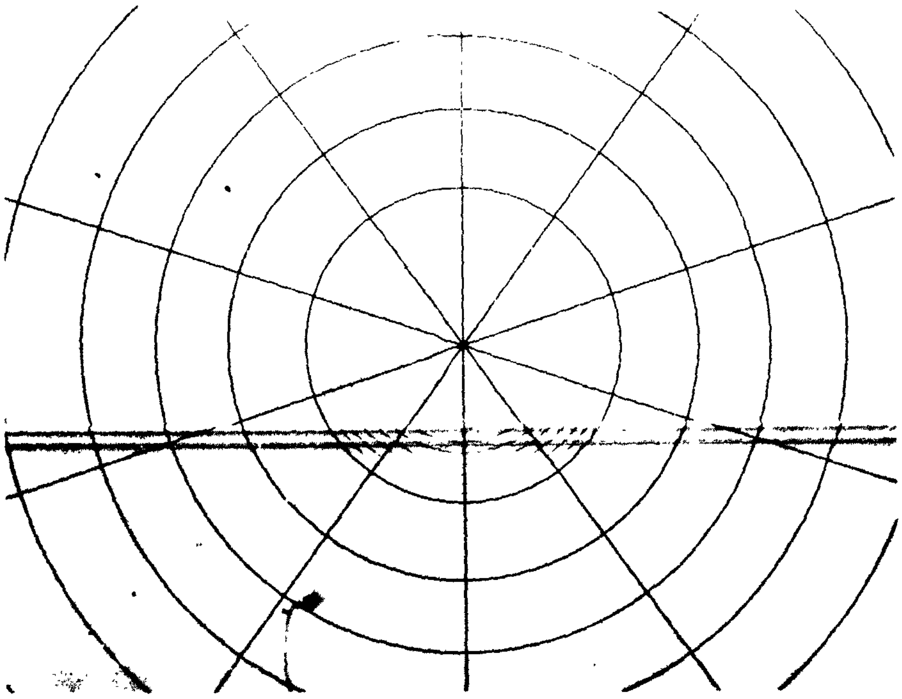

(a) End Wall

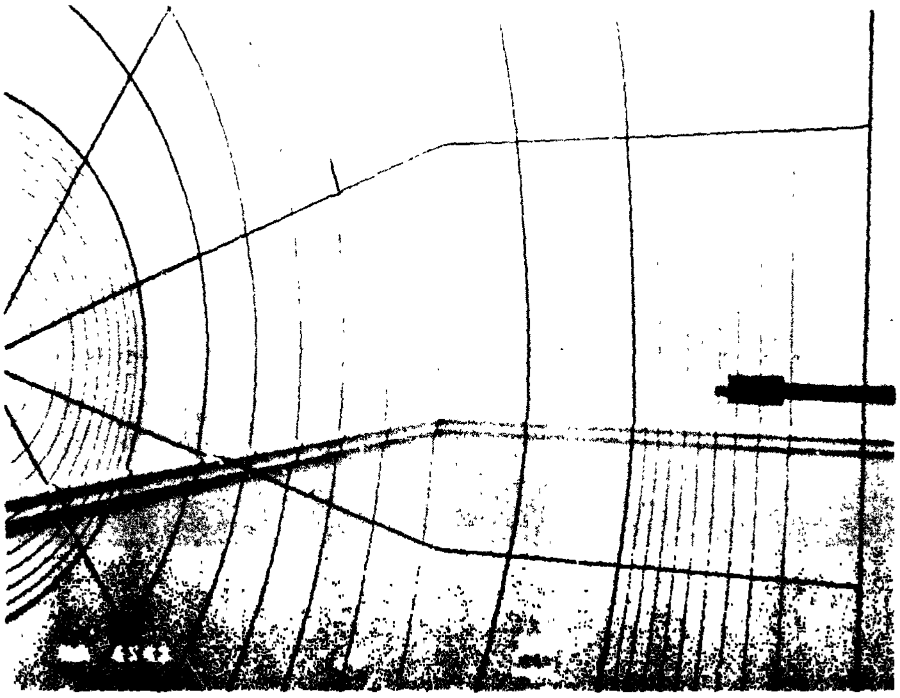

(b) Side Wall Showing Projection Lamp

FIGURE 5-14 CONFIGURATION FACTOR WALL PATTERN AND PROJECTION LAMP

FIGURE 5-15 LEM SHAPE FACTOR SETUP

FIGURE 5-16 HELIUM BOTTLES SHAPE FACTOR SETUP

two adjacent high-pressure helium bottles in the Apollo Service Module. The models and lamp in the photographs are positioned so as to most clearly show the method used and shadows obtained, and not the acquisition of actual configuration factors. The lamp holder consists of an insulated socket, an aluminum tube holding the wires, and a heavy steel base. The model holder in Figure 5-16 is a camera tripod.

Configuration factors in Figure 5-15 and 5-16 can be evaluated from an inspection of their shadows. For the LEM it can be seen that approximately 66 small segments are shadowed yielding 0.066, and 1.5 of the large sectors are shadowed, yielding 0.015. Thus the total configuration factor for this example would be approximately 0.081. The configuration factor for the helium bottles in Figure 5-16 is approximately 0.075.

The optical projection method is extremely useful for obtaining rapid data and for analyzing complex shapes which are difficult to solve by analytical means. Where available, real or mockup components of the viewed object are used, but experience has shown that good results can be obtained with relatively crude models constructed of cardboard or papier-mâché.

EMISSIVITY FACTOR

According to the Stefan-Boltzmann law, black body radiation is proportional to the fourth power of the absolute temperature, i.e.,

$$I_b = \sigma T^4 \qquad (5\text{-}25)$$

where the constant σ was determined theoretically as 0.1714×10^{-8} Btu/hr ft^2 °R^4. In practice, however, perfectly black surfaces do not exist. The ratio of the emissive power I of a surface at temperature T to the emmissive power I_b of a black surface at the same temperature is defined as the emissivity, i.e.,

$$\epsilon = \frac{I(T)}{I_b(T)} \qquad (5\text{-}26)$$

The heat radiated by a non-black body at temperature T is then given by

$$I = \sigma \epsilon T^4 \qquad (5\text{-}27)$$

In engineering calculations, the data for the total radiation as obtained by integration over the entire wavelength range are usually the most important. For this reason the properties listed in engineering handbooks are generally the total hemispherical values.

If the surfaces which exchange heat by radiation are not black, computation of the net heat transfer becomes more complicated since part of the incident radiation is reflected by the surfaces. Some of the radiation travels in this way back and forth between the surfaces until it is finally absorbed. The influence of reflected radiation on the net heat transfer is studied by tracing the travel of heat rays emitted by the two surfaces. To illustrate, consider the problem of two concentric spheres or cylinders whose surfaces reflect diffusely. The total radiative flux leaving the smaller surface (1) consists of both emitted and reflected radiation and is given by

$$q_1 = \sigma \epsilon_1 T_1^4 + (1 - \alpha_1) q_2 \tag{5-28}$$

q_2 is the total radiation leaving surface 2 and consists of emitted radiation, of reflected radiation coming from A_1, and of reflected radiation from A_2.

$$q_2 = \sigma \epsilon_2 T_2^4 + (1 - \alpha_2) F_{21} q_1 + (1 - \alpha_2)(1 - F_{21}) q_2 \tag{5-29}$$

The net heat flow between surfaces is given by

$$q = q_1 - q_2 \tag{5-30}$$

Combining the last three equations with the configuration factor $F_{21} = A_1/A_2$ yields

$$q = \frac{\alpha_2 \sigma \epsilon_1 T_1^4 - \alpha_1 \sigma \epsilon_2 T_2^4}{\alpha_2 + (A_1/A_2)(\alpha_1 - \alpha_1 \alpha_2)} \tag{5-31}$$

Then, assuming $\alpha = \epsilon$ (Kirchhoff's law applied to a gray surface) the following expression is obtained:

$$q = \frac{\sigma\left(T_1^4 - T_2^4\right)}{\frac{1}{\epsilon_1} + \left(\frac{A_1}{A_2}\right)\left(\frac{1}{\epsilon_2} - 1\right)} \tag{5-32}$$

The heat flux is per unit area of the smaller surface A_1. For engineering calculations it is convenient to introduce the emissivity factor ϵ_{12} so that the radiation heat transfer between surfaces 1 and 2 will assume the form

$$q = \epsilon_{12} A_1 F_{12} \sigma (T_1^4 - T_2^4) \qquad (5\text{-}33)$$

The emissivity factors for several geometries are given below:

For two concentric cylinders or spheres (A_1 is the smaller body):

$$\epsilon_{12} = \frac{1}{\frac{1}{\epsilon_1} + \frac{A_1}{A_2}\left(\frac{1}{\epsilon_2} - 1\right)}$$

For two infinite parallel plates:

$$\epsilon_{12} = \frac{1}{\frac{1}{\epsilon_1} + \frac{1}{\epsilon_2} - 1}$$

For two surfaces whose size is small compared to their distance apart:

$$\epsilon_{12} = \epsilon_1 \epsilon_2$$

For surface 1 much smaller than, and completely enclosed by, surface 2 :

$$\epsilon_{12} = \epsilon_1$$

MULTIPLE INTERREFLECTING SURFACES

Problems involving radiation interchange between several nonparallel absorbing and reflecting gray surfaces are very complex. Unfortunately, this is the type of problem most fequently encountered in spacecraft applications. If several surfaces are involved, the numerical complexity precludes the use of hand calculations, and the solution must be obtained on a computer. Such problems are usually solved by the network method of Oppenheim (Reference 5-5) or the matrix solution by Hottel (Reference 5-6).

Oppenheim Radiation Network

Oppenheim's technique involves the solution of an electrical network composed of resistances determined by the surface configuration factors, emissivities, and areas. In describing this network it is first convenient to determine an expression for the net radiation leaving a surface in terms of its irradiation G (total incident energy in Btu/hr ft^2) and radiosity J (total energy leaving in Btu/hr ft^2). For a gray opaque surface the radiosity is the sum of the emitted and reflected radiation and is given by

$$J = \epsilon I_b + (1 - \epsilon) G \tag{5-34}$$

By definition of G and J the net radiation leaving the surface is

$$q_{net} = A (J - G) \tag{5-35}$$

Combining equations (5-34) and (5-35) gives

$$q_{net} = \frac{\epsilon}{1 - \epsilon} A (I_b - J) \tag{5-36}$$

Thus the net radiation leaving the surface can be regarded as the current flow when a potential of $I_b - J$ is impressed across a resistance of $(1 - \epsilon)/\epsilon A$. In terms of a system network, the effect of the surface emissivity and reflectivity can be taken into account by connecting a potential $I_b = \sigma T^4$ through a resistance $(1 - \epsilon)/A\epsilon$ to a potential J, which is determined by the surface and the rest of the enclosure. Figure 5-17 shows the network for an enclosure consisting of two heat transfer surfaces. The resistance of the center element is determined by observing that the net heat flow is the difference of the radiosities, modified to account for the geometry of the system, i.e., $q_{net} = A_1 F_{12} (J_1 - J_2)$. For two infinite parallel walls $F_{12} = 1$ and the network solution is

$$q_{net} = \left[\frac{1}{\frac{1 - \epsilon_1}{A_1 \epsilon_1} + \frac{1}{A_1} + \frac{1 - \epsilon_2}{A_2 \epsilon_2}} \right] (I_{b1} - I_{b2}) \tag{5-37}$$

which reduces to the parallel plate formula given above.

Figure 5-18 represents an enclosure consisting of three heat transfer surfaces. This method of analysis may be extended to any number of isothermal bodies provided that the black body configuration factors are known. Each heat transfer surface n is connected to a floating node n' through a resistor $(1 - \epsilon_n)/A_n \epsilon_n$. The floating nodes are interconnected by the black body thermal resistance between the respective surfaces (1/AF). The net heat transfer between the various nodes is obtained from simple circuit theory or from computer techniques. Such a network is easily solved by the Thermal Analyzer Program. Minor modifications to the resistor values are required since the driving potential for the Thermal Analyzer is T, rather than σT^4. Figure 5-19 shows the appropriate network parameters, using the three-surface problem of Figure 5-18 as an example. The values shown are the radiation K factors, which are used by the program to compute the radiation resistors between nodes m and n by the formula

$$R_{m-n} = \frac{1}{\sigma K_{rad_{mn}} \left[(T_m^2 + T_n^2)(T_m + T_n) \right]} \qquad (5\text{-}38)$$

The K factors are input to the program in the FUNCT subroutine as described in Reference 5-1. Also, the thermal capacitance of the floating nodes (1', 2', and 3') must be specified as zero.

Hottel Radiation Matrix

The Thermal Analyzer Program also has a special subroutine to compute radiation interchange by the matrix solution proposed by Hottel. The heat flux between radiating surfaces m and n is computed by an equation of the form

$$q_{m-n} = A_m \mathfrak{F}_{mn} \sigma (T_m^4 - T_n^4) = A_n \mathfrak{F}_{nm} \sigma (T_n^4 - T_m^4) \qquad (5\text{-}39)$$

where the overall shape factor $\mathfrak{F}$ includes the effects of both system geometry and surface emissivities. The problem is to evaluate $A\mathfrak{F}$. It cannot depend on any system temperature. Consequently, if all surfaces except A_1 are kept at absolute zero, and q_{m-n} is evaluated and used to determine $\mathfrak{F}$ in equation (5-39), that value of $\mathfrak{F}$ will be generally applicable regardless of the particular combination of surface temperatures. In addition to the assignment

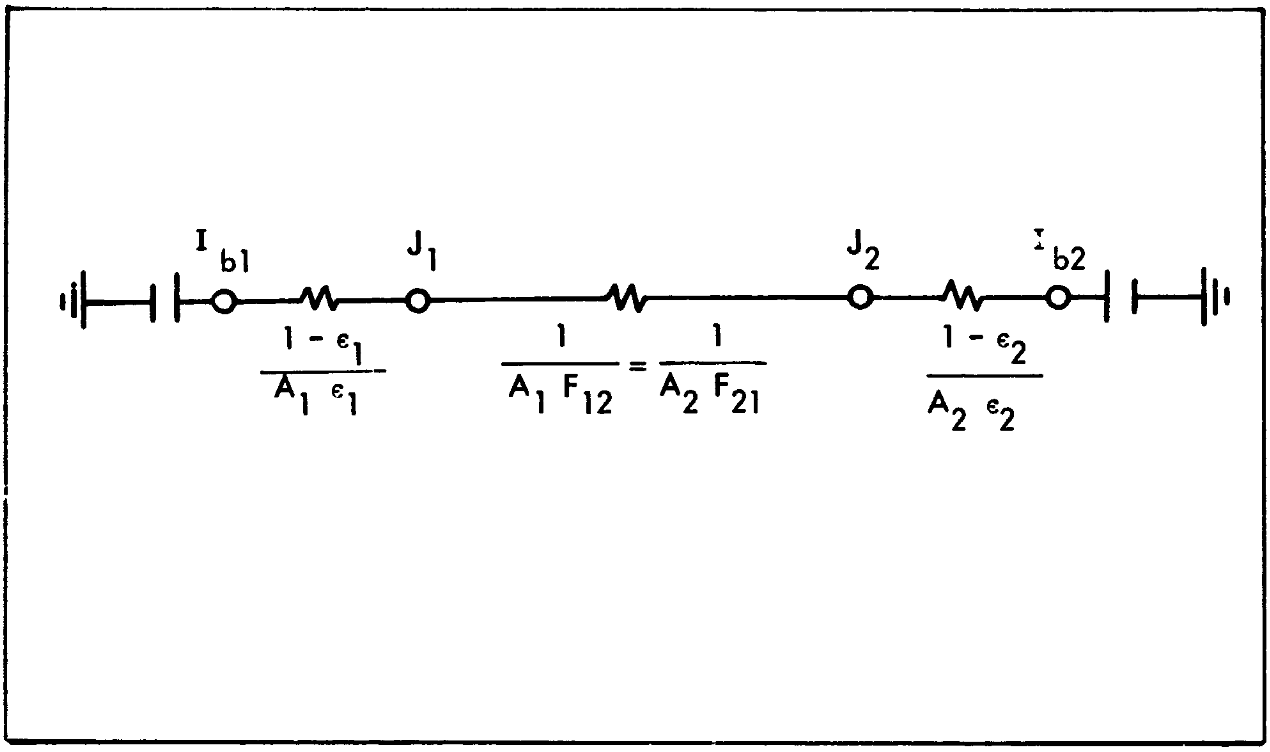

Figure 5-17 Oppenheim Radiation Network for a System Consisting of Two Heat Transfer Surfaces

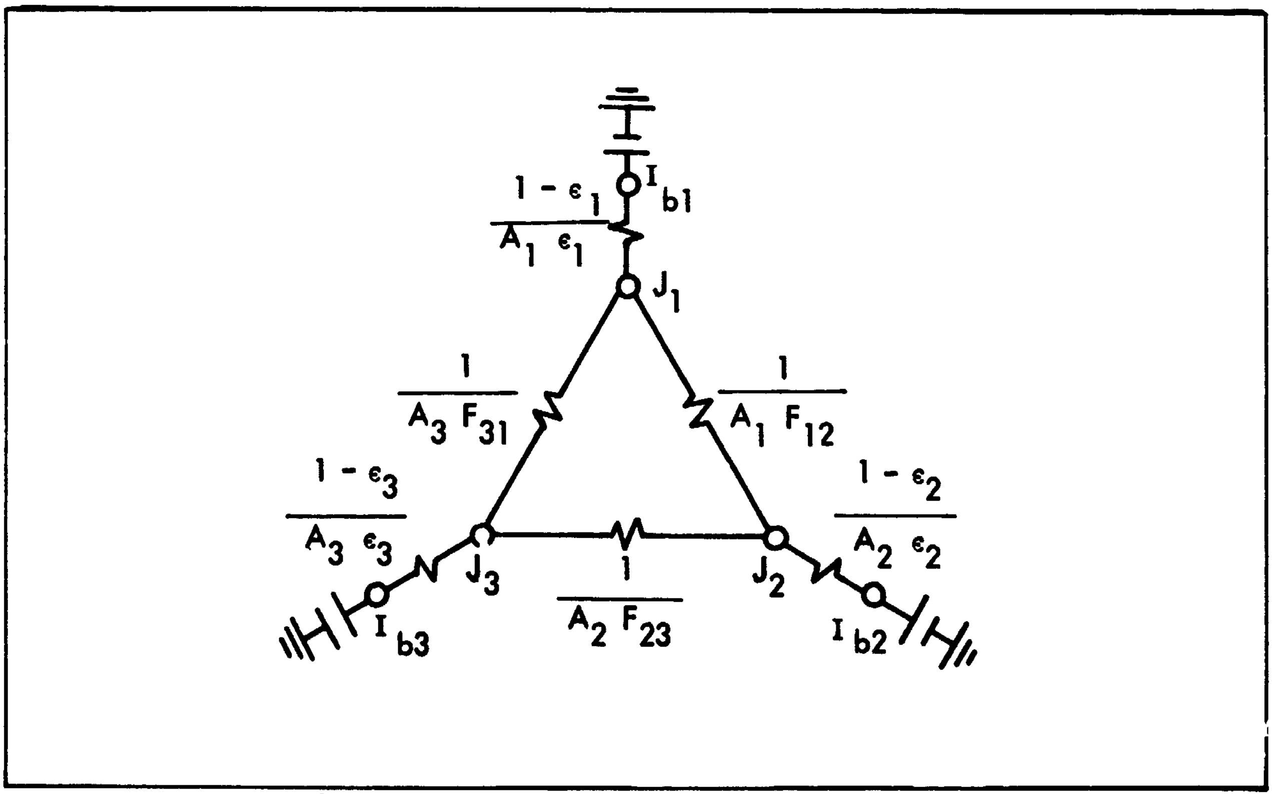

Figure 5-18 Oppenheim Radiation Network for a System Consisting of Three Heat Transfer Surfaces

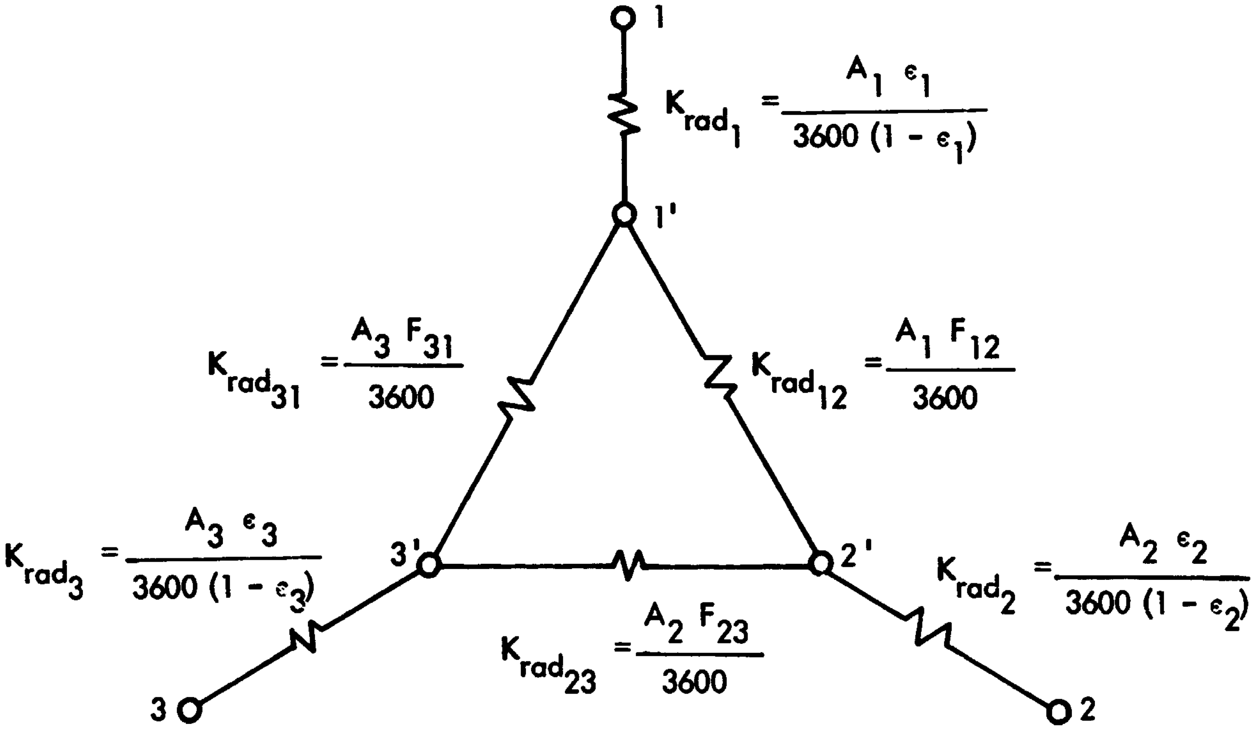

Figure 5-19 Radiation Parameters Required to Solve an Oppenheim Network on the Thermal Analyzer Program

of zero temperatures to all surfaces except A_1, one more simplification is introduced. The temperature of A_1 is specified such that if black, it would have an emissive power of unity. At each surface there will be radiant flux toward and away from the surface due to reflection of radiation initially emitted by A_1 and involving multiple reflections between surfaces. For surface A_m the radiant flux per unit area is designated ${}_1R_m$. The presubscript is a reminder of the original source of the flux, and the R indicates that the quantity is a relative flux density scaled down in the ratio $1/\sigma T_1^4$ because of the assumed value of the emissive power of A_1. The flux densities streaming away from A_2, A_3,... will be ${}_1R_2$, ${}_1R_3$,... , geometrically analogous to emissive powers in their fractional interception by various black surfaces, but due exclusively to reflection; they would be zero in a black system. The flux density from A_1 is ${}_1R_1 + \epsilon_1$, to include its own original emission ϵ_1 as well as its contribution due to mutual reflection within the system.

The radiation absorbed by surface A_2 is due to beams from the various surfaces seen by it. Each incident beam is partially absorbed and partially relected, in the ratio $\epsilon_2/(1 - \epsilon_2)$. Then, since the flux away from A_2 is $A_2\ {}_1R_2$, the total rate of absorption at A_2 is $A_2\ {}_1R_2\ \epsilon_2/(1 - \epsilon_2)$. Since this absorption is the result solely of emission originating at A_1 when σT_1^4 is 1, it follows that

$$A_1 \mathcal{F}_{12} = {}_1R_2\ A_2 \frac{\epsilon_2}{1 - \epsilon_2} \tag{5-40}$$

In general,

$$A_1 \mathcal{F}_{1n} = {}_1R_n\ A_n \frac{\epsilon_n}{1 - \epsilon_n} \tag{5-41}$$

The problem is to find the values of the R's for use in equation (5-41) by setting up energy balances on all the surfaces. The incidence of radiation on A_1 includes that from itself and from A_2, A_3, etc. Their sum is represented by the bracketed term below. The fraction $1 - \epsilon_1$ is reflected and therefore equals the flux leaving A_1 exclusive of its original emission, or $A_1\ {}_1R_1$. Equating these two gives

$$\left[A_1\ F_{11}\ (\epsilon_1 + {}_1R_1) + A_2\ F_{21}\ {}_1R_2 + \cdots\right]\ (1 - \epsilon_1) = A_1\ {}_1R_1 \tag{5-42}$$

Similar relations may be formulated for A_2, A_3, etc. One thus obtains as many equations as there are unknown flux densities R, permitting a solution for the latter and correspondingly an evaluation of any interchange factor $A_1 \mathcal{F}_{1n}$ by equation 5-41. After replacing the reflectivity $1 - \epsilon$ by the symbol ρ and dividing both sides of the equation by it, the system of energy balances becomes

$$\begin{array}{lllll}
\left[A_1 F_{11} - \dfrac{A_1}{\rho_1}\right] {}_1R_1 & + A_2 F_{21}\, {}_1R_2 & + A_3 F_{31}\, {}_1R_3 & + \cdots = & -A_1 F_{11} \epsilon_1 \\
A_1 F_{12}\, {}_1R_1 & + \left[A_2 F_{22} - \dfrac{A_2}{\rho_2}\right] {}_1R_2 & + A_3 F_{32}\, {}_1R_3 & + \cdots = & -A_1 F_{12} \epsilon_1 \\
A_1 F_{13}\, {}_1R_1 & + A_2 F_{23}\, {}_1R_2 & + \left[A_3 F_{33} - \dfrac{A_3}{\rho_3}\right] {}_1R_3 & + \cdots = & -A_1 F_{13} \epsilon_1 \\
\vdots & \vdots & \vdots & & \vdots
\end{array}$$

To obtain a solution, the following matrix is set up:

$$\begin{array}{llll}
A_1 F_{11} - \dfrac{A_1}{\rho_1} & A_2 F_{21} & A_3 F_{31} & \cdots \\
A_1 F_{12} & A_2 F_{22} - \dfrac{A_2}{\rho_2} & A_3 F_{32} & \cdots \\
A_1 F_{13} & A_2 F_{23} & A_3 F_{33} - \dfrac{A_3}{\rho_3} & \cdots \\
\vdots & \vdots & \vdots &
\end{array}$$

The solution for ${}_1R_n$ is

$${}_1R_n = \frac{{}_1D_n}{D} \tag{5-43}$$

in which D is the determinant of the above matrix, and ${}_1D_n$ is the determinant of the matrix formed by replacing the n - th column of the matrix by the quantities on the right side of the system of energy balances, i.e., by $-A_1 F_{11} \epsilon_1$, $-A_1 F_{12} \epsilon_1$, etc. Then, from equation 5-41,

$$A_1 \mathcal{F}_{1n} = \frac{\epsilon_n A_n}{\rho_n} \frac{{}_1D_n}{D} \qquad (5\text{-}44)$$

More generally,

$$A_m \mathcal{F}_{mn} = \frac{\epsilon_n A_n}{\rho_n} \frac{{}_mD_n}{D} \qquad (5\text{-}45)$$

On formulation of ${}_1D_2$ for insertion into equation (5-44), the first and second columns, after factoring $-\epsilon_1$ out of the second column, will be found alike except for the top members $A_1 F_{11} - A_1/\rho_1$ and $A_1 F_{11}$, respectively. Since the value of a determinant is unchanged by replacing any column (or row) by a new one whose members are formed by subtracting any other column from the one in question, column 1 may be replaced by the values $-A_1/\rho_1$, 0, 0, 0, ... The determinant then equals $-A_1/\rho_1$ times the minor determinant formed by crossing out the first row and column. Then

$$A_1 \mathcal{F}_{12} = \frac{\epsilon_1 \epsilon_2}{\rho_1 \rho_2} A_1 A_2 \frac{\begin{vmatrix} A_1 F_{12} & A_2 F_{23} & \cdot\ \cdot \\ A_1 F_{13} & A_3 F_{33} - \dfrac{A_3}{\rho_3} & \cdot\ \cdot \\ \vdots & \vdots & \end{vmatrix}}{D} \qquad (5\text{-}46)$$

More generally,

$$A_m \mathcal{F}_{mn} = \frac{\epsilon_m \epsilon_n}{\rho_m \rho_n} A_m A_n \frac{{}_mD'_n}{D} \qquad (5\text{-}47)$$

where ${}_mD'_n$ is the minor of the element (m, n), i.e., the determinant formed by removing the m - th row and the n - th column. The radiant exchange between nodes m and n is then computed from equations (5-39).

Practical Application of the Oppenheim and Hottel Techniques

The Oppenheim and Hottel techniques give nearly identical results and the choice of solution is usually based on the numerical complexity involved.

The Oppenheim solution requires a larger network because of the floating nodes. On the other hand, the resistor values are straightforward, whereas in the Hottel procedure they must be computed from the matrix. The determinants become quite complicated when a large number of surfaces are involved. Although the methods are undoubtedly accurate, it is usually impractical to apply these techniques to radiant exchange between all internal nodes in a spacecraft. Such a network would take an enormous amount of time to set up (black body configuration factors would be required for each set of viewing nodes) and the amount of computer core storage would be prohibitive. For example, a system of 50 radiating nodes solved by the Hottel method on the Thermal Analyzer would require a 50 x 100 matrix of input data, and the 5,000 storage locations required would exceed the 3,500 storages currently available for the data block. As a result, the radiation network used for spacecraft analyses must be simplified, and should be carefully selected. Frequently, it is possible to isolate a portion of a vehicle, such as an enclosed equipment bay, or the interior of an engine thrust chamber and analyze it separately by either the Oppenheim or Hottel methods. If this is impractical, the radiation network should include only those surfaces whose temperatures are largely affected by the emission or absorption of radiation. The number of radiation resistors required can often be decreased by adding a fictitious node to the network to represent several nodes of nearly equal temperature, which act as a radiation sink for a particular component. This approach is applicable only if the temperature of the component is strongly influenced by radiation to the surroundings, but the temperature of the surroundings is not greatly affected by the absorption of this energy.

The relative importance of radiation to a particular node can be estimated by assuming a temperature for the component and its surroundings, computing the radiation resistor by equation (5-38), and comparing this value with the parallel combination of all conduction resistors into the node. Such calculations often justify a further reduction in the size of the radiation network required for a particular analysis.

FLUID STORAGE AND PRESSURIZATION

This section discusses the analysis of pressurization systems for storable or cryogenic propellants using either the fluids own vapor or a non-condensable pressurant to expell the propellant from the tank.

In general, a fluid storage system is comprised of a complex series of time and temperature dependent processes. The fluid in the tank is heated through the container walls by radiation and convection from the environment, by conduction through attached structure, plumbing and miscellaneous penetrations, by conduction, convection and radiation through insulation, by conduction and convection from the tank wall to the fluid phases, and by radiation to the liquid through the vapor space. Mass and energy are transferred at the gas-liquid interface by evaporation or condensation and by fluid transport at the tank wall by gravity induced convection; liquid is drained from the tank; liquid or vapor is replenished; condensable or non-condensable pressurant gas is added; and gas is vented to relieve over-pressure. Additionally, extended periods under very low gravity conditions, where fluid internal forces (surface tension) are substantial in comparison to the system external forces (gravity and acceleration) and where a switch from a very low gravity to non low gravity situations where internal forces are negligible, and vice versa, must be considered.

Variables which influence the pressurization system are:

1. Heat and mass transfer between the liquid and gas regions.
2. Heat transfer through the tank walls to the fluid.
3. Magnitude of the net accelerating vector (gravity).

Nomenclature For Fluid Storage and Pressurization

A	Area
C	Specific Heat
e	Total energy
F	Overall view factor
g	Acceleration due to gravity
H	Enthalpy, total
h	Enthalpy, specific

J	Mechanical equivalent of heat
M	Molecular weight
m	Mass
$\dot{m}$	Mass flow rate
N_{BO}	Bond number
P	Pressure
Q	Heat
q	Heat flow rate
R	Gas constant
T	Temperature
U	Internal energy, total
u	Internal energy, specific
V	Volume
v	Velocity
Z	Compressibility factor
z	Elevation above datum plane
γ	Heat capacity ratio
Δ	Difference
θ	Time
ρ	Density
σ	Control Volume or Stefan-Boltzmann constant
ϵ	Emissivity

Subscripts

G	Gas phase
L	Liquid phase
P	Constant pressure
V	Constant volume
1	Previous value
2	Present value
TW	Tank wall
S	Fluid Surface

Simplified Analysis

Thermodynamic Analysis - The equations describing these variables through a mission are complex and non-linear, and require numerical solution under even the simplest mission conditions.

Certain assumptions can be made which will permit approximate analysis of the pressurization system. These assumptions are:

1. The ullage gas is non viscous
2. The ullage gas is always uniformly mixed
3. The tank pressure does not vary spatially
4. The ullage gas temperature does not vary spatially
5. The liquid temperature does not vary spatially
6. No condensation or evaporation occurs
7. No heat is transferred from the gas to the liquid
8. Gravitational forces are greater than the fluid body forces ($g \gg o$)

Assumptions 1, 2, 3 and 4 reduce the problem to a simple thermodynamic open system

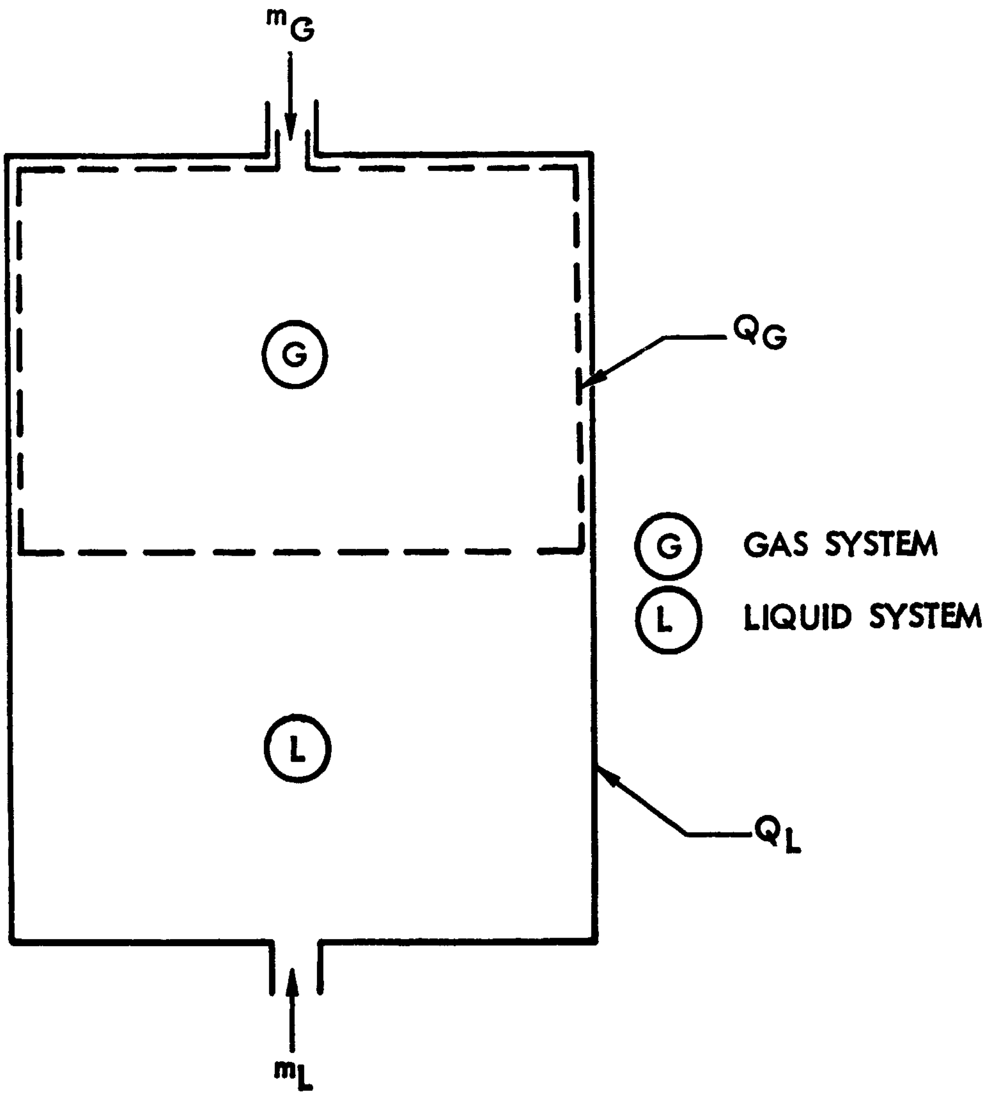

Within a differential discharge time d θ the following relationship holds:

$$\frac{dQ}{d\theta} = \frac{d}{d\theta}\int_{\sigma} \rho e d\sigma - \left[\rho \ A \ v \ (e + \frac{P}{\rho})\right]_{L} + \left[\rho \ A \ v \ (e + \frac{P}{\rho})\right]_{G} + \frac{Pdv}{Jd\theta} \qquad (5\text{-}48)$$

where $\frac{d}{d\theta}\int_{\sigma} \rho e d\sigma$ = internal energy change

$\rho \ A \ v \ (e + \frac{P}{\rho})$ = Energy change due to mass entering or leaving the system

and $\left[\rho \ A \ v\right]_{L} = \dot{m}_{L} = \frac{dm_{L}}{d\theta}$ = Propellant use rate

$\left[\rho \ A \ v\right]_{G} = \dot{m}_{G} = \frac{dm_{G}}{d\theta}$ = pressurant addition rate

PdV = flow work done in extending the vapor system boundary

From the definition of energy

$$e = U + \frac{v^2}{2} + gz = \text{energy} \qquad (5\text{-}49)$$

$$h = U + \frac{P}{\rho} = \text{enthalpy} \qquad (5\text{-}50)$$

Neglecting mechanical and potential energy terms $(\frac{v^2}{2} = gz = o)$

$$h = e + \frac{P}{\rho}$$

From assumptions 3, 4 and 5

$$\int_{\sigma} \rho e d\sigma = d \ U \qquad (5\text{-}51)$$

and equation 5-48 becomes

$$dQ = dU - h_{L} \ dm_{L} + h_{G} \ dm_{G} + PdV \qquad (5\text{-}52)$$

From the definition of enthalpy

$$dH = dU + d(PV) \tag{5-53}$$

For a constant pressure process $(d(PV) = PdV)$

$$dQ = dH - h_L \, dm_L + h_G \, dm_G \tag{5-54}$$

Using assumptions 6 and 7 the phases become thermodynamically separable and

$$dH = dH_L + dH_G \tag{5-55}$$

Equation 5-54 can then be written:

In the gas region

$$\begin{aligned} dQ_G &= dH_G + h_G dm_G \\ dm_G &= \frac{dQ_G - dH_G}{h_G} \end{aligned} \tag{5-56}$$

In the liquid region

$$\begin{aligned} dQ_L &= dH_L - h_z dm_z \\ dm_G &= \frac{dH_L - dQ_L}{h_L} \end{aligned} \tag{5-57}$$

To determine the amount of pressurant required, equation 5-56 can be solved for the two cases involved in typical spacecraft missions:

1. No flow, thermal soak
2. No heating, high flow

In case 1, the propellant and pressurant tankage are subject to heating under no-flow conditions such as in a planetary orbit.

During this period $dm_1 = dm_2 = 0$

$$\therefore d\,Q_G = d\,H_G = dU_G = m_G C_{VG}\,d\,T_G \qquad (5\text{-}58)$$

and $$d\,Q_L = d\,H_L = dU_L = m_L\,C_{PL}\,d\,T_L \qquad (5\text{-}59)$$

Where dQ is determined from analysis of the external system covered in Ref. 5-1.

The temperature change of the fluid is the quantity of interest, so that:

$$T_{G2} = T_{G1} + \Delta\,Q_G/m_G\,C_{VG} \qquad (5\text{-}60)$$

$$T_{L2} = T_{L1} + \Delta\,Q_L/m_L\,C_{PL} \qquad (5\text{-}61)$$

Case 2 occurs whenever the engine is fired and fluid flows. In the typical spacecraft case, the firings are of relatively short duration, lasting on the order of a few seconds to, at most, a few minutes. Under these conditions it can be assumed that:

$$dQ_L = dQ_G = 0$$

$$\therefore dH_G = h_G dm_G \qquad (5\text{-}62)$$

$$\Delta(hm_G) = \int dH_G = \Big[H_2 - H_1\Big]_G = (m_2h_2 - m_1h_1)_G \qquad (5\text{-}63)$$

The pressurant control problem is usually minimized by passing the pressurant through a propellant outlet - pressurant gas heat exchanger prior to entering the propellant tank. The pressurant temperature at the propellant tank inlet is computed as a function of the exchanger effectiveness, ϵ, described by:

$$\epsilon = \frac{(m\,C)_G \left[T_{G_{out}} - T_{G_{in}}\right]}{(m\,C)_{min} \left[T_L - T_{G_{in}}\right]} \tag{5-64}$$

where $(m\,C)_{min}$ is the smaller value of either $(mC_v)_G$ or $(m\,C_p)_L$

In the usual case $(m\,C_V)_G << (m\,C_P)_L$ and

$$\epsilon = \frac{\left[T_{G_{out}} - T_{G_{in}}\right]}{\left[T_L - T_{G_{in}}\right]} \tag{5-65}$$

As a first approximation, the pressurant heat exchanger inlet temperature during fluid expulsion is assumed equal to the pressurant temperature at the beginning of the firing. Using a heat exchanger effectiveness determined from the characteristic of the exchanger, the propellant tank incoming pressurant temperature ($T_{G_{out}}$) can be determined from equation 5-65.

For a constant pressurant inlet temperature and a constant ullage pressure:

$$h_2 = h_1 = h_G$$

and $m_2 - m_1 = \Delta m_G = -\rho_G \Delta m_L/\rho_L$ (5-66)

That is, the mass of gas required to maintain a constant pressure is a function of the volume change due to liquid outflow.

A similar analysis of the pressurant gas system would yield:

Case 1 · Heating under a non-flow condition

$$dQ = mC_V\, dT \tag{5-67}$$

$$T_2 = T_1 + \Delta Q/mC_V \tag{5-68}$$

where ΔQ is the heat input to the pressurant tank as determined from the external system analysis.

Case 2 - During discharge, the gas within the pressure vessel expands from the initial tank pressure to a final pressure. In the approximate analysis of the problem it is necessary to assume no heat interchange between the gas and the walls of the container. Actually, such interchange of heat cannot be avoided and the results of these calculations are to be regarded only as a limiting value which is approched as a condition of zero heat interchange is approached.

The mass removed from the pressurant tank is equal to the mass of pressurant required by the propellant tank during firing, which is computed as a function of the mass of liquid removed as

$$m_2 - m_1 = \Delta m = \rho_G \Delta m_L / \rho_L \tag{5-69}$$

The temperature of the gas remaining in the pressurant tank is determined from the following relationship:

$$T_2 = T_1 \left(\frac{m - \Delta m}{m}\right)^{\gamma - 1} \tag{5-70}$$

where $\gamma = C_P/C_V$

The pressure change is given by the real gas law.

$$P_2 = P_1 + \frac{R}{MV} T_2 \left[Z_2 m_2 - Z_1 m_1 \frac{T_1}{T_2} \right] \tag{5-71}$$

Example Problem - The following example demonstrates the use of the analytical procedures specified above:

Problem Statement: Compute the quantity of pressurant required to expell 275 lbs of fluid under 50 psia pressure from a propellant tank containing 555 lb of propellant (N_2O_4). Prior to firing, the system is exposed for 12 hours to a constant environmental heat flux of 3 Btu/hr ft^2. The pressurant (He) is supplied through a propellant - pressurant heat exchanger having an exchanger effectiveness of 0.9.

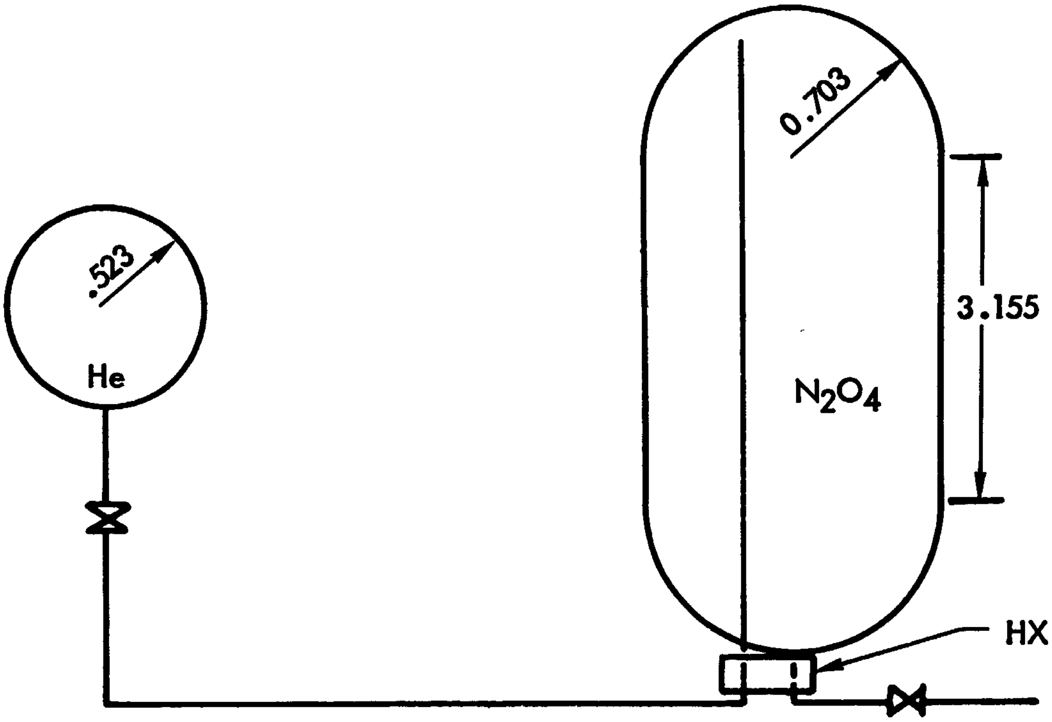

Initial Conditions

He Tank Vol = 0.6 ft^3
Pressure = 1500 psia
Temperature = 70°F
Mass He = 0.63 lb
Mass tank = 74.0 lb

$C_{V,He}$ = 0.74 Btu/lb °F

Z_{He} = 1.0

$C_{P_{tank}}$ = 0.11

N_2O_4 Tank Vol = 6.35 ft^3

Liquid Weight = 555 lb $\qquad C_{P,\,N_2O_4} = 0.37$

Temperature = 70°F

Mass Tank = 125 lb

Operating Pressure = 50 psia

Heat Input $\dot{q} = 3$ Btu/hr ft^2

Final Conditions

N_2O_4 Liquid Weight = 275 lb

Calculation of Ullage

$$\rho_{(N_2O_4),\ 70^\circ F} = 92.7 \text{ lb/ft}^3$$

$$V_{(N_2O_4),\ 70^\circ F} = 555/92.7 = 5.98 \text{ ft}^3$$

$$\text{Ullage} = \frac{6.35 - 5.98}{6.35} = .0583$$

Calculation of Heat Input During the 12 hr Soak (No Outflow)

Helium Bottle

$$\text{Heat transfer area} = 4\pi r^2 = 4\pi(.525)^2 = 3.44 \text{ ft}^2$$

$$\text{Heat input} = \Delta Q_{TOT} = 3.0\,(3.44)(12) = 124 \text{ Btu}$$

For a long term soaking period under a relatively low heat input rate, the change in gas temperature can be assumed to equal the change in gas container temperature. Utilizing this approximation with equation (5-68), we have:

$$T_2 - T_1 = \left[\Delta Q/m\, C_V\right]_{He} = \left[\Delta Q/m\, C_P\right]_{He\ tank}$$

and $\Delta Q_{TOT} = \Delta Q_{He} + \Delta Q_{He\ Tank}$

rearranging:

$$T_2 - T_1 = \frac{\Delta Q_{TOT}}{\left[mC_V\right]_{He} + \left[mC_P\right]_{He\ Tank}}$$

and $$T_2 = T_1 + \frac{\Delta Q_{TOT}}{\left[mC_V\right]_{He} + \left[mC_P\right]_{He\ Tank}}$$

$$= 532 + \frac{124}{(0.63)(0.74) + (74)(0.11)} = 544.4\ ^{o}R$$

Propellant Tank

Heat Transfer Area $= 4\pi r^2 + 2\pi r\ell$

$A = 4\pi(.703)^2 + 2\pi(.703)\ (3.155) = 20.1\ ft^2$

Heat input $= \Delta Q_{TOT} = 3.0\ (20.1)\ (12) = 723$ Btu

Again, for a long-term soak under a low heating rate, the temperature rise of the container is considered equivalent to the temperature rise of the fluid. Also, since the ullage region is small (5.8%), all of the heat input is absorbed in the liquid and the tank wall. Using these assumptions and equation (5.61):

$$T_2 - T_1 = \frac{\Delta Q_{TOT}}{\left[mC_P\right]_{N_2O_4} + \left[mC_P\right]_{N_2O_4\ Tank}}$$

$$T_2 = 532 + \frac{723}{(555)\ (0.37) + (125)\ (.11)} = 535.3\ ^{o}R$$

Calculation of Mass Transferred During Firing Period

Propellant Tank

The change of energy in the N_2O_4 tank during fluid expulsion is shown in equation (5-48). Since the firing time is relatively short (~ 4 min), the liquid (N_2O_4) temperature remains constant. The change in gas region temperature is determined from the integrated average temperature of the incoming pressurant gas which, in turn, is a function of the heat exchanger effectiveness.

From equation (5-65) with $\epsilon = 0.90$:

$$T_{He,\ out} = 0.90 \left[T_{N_2O_4} - T_{He,\ in} \right] + T_{He,\ in} = 0.9\ T_{N_2O_4} + 0.1\ T_{He,\ in}$$

As a first approximation, assume $T_{He,\ in} = T_{He}$ at end of 12 hr soak period.

$$T_{He,\ out} = 0.9\ (555.5) + 0.1\ (544.4) = 536.4\ ^{O}R$$

Assuming adiabatic transfer of the gas from the heat exchanger to the propellant tank:

$$T_{He,\ out} = T_{G,\ \text{propellant tank}}$$

For an operating pressure of 50 psia and invoking assumption 6, the helium pressure in the propellant tank after firing is 50 psia. (The error introduced by the assumption that no evaporation or condensation occurs becomes large when the initial ullage space is large and/or low operating pressures are required, i.e., liquid vapor pressure is significant).

The density of Helium at 554.4 ^{O}R and 50 psia is

$$\rho = \frac{MP}{RT} = \frac{4\ (50)}{10.73\ (536.4)} = .0346\ \text{lb/ft}^3$$

From equation (5-69), the mass of pressurant required is computed as:

$$\Delta m_{He} = \rho_{He}\ \Delta m_{N_2O_4} / \rho_{N_2O_4} = \frac{.0346(275)}{92.7} = 0.1\ \text{lb}_{He}$$

Calculations of Pressurant Conditions at End of Firing

Based on the assumption that the firing time is short, the expansion of the gas in the pressurant bottle during firing is considered to be approximated by a reversible, adiabatic (isentropic)expansion, and is computed using equations 5-70 and 5-71.

$$T_2 = 544.4 \left(\frac{0.63 - 0.1}{0.63}\right) = 466 \text{ °R}$$

$$P_2 = 1500 + \frac{10.73(466)}{4(.6)} \left[.53 - .63 \frac{(544.4)}{466}\right] = 1082 \text{ psia}$$

Supercritical Fluid Storage

Storage of cryogenic fluids under conditions of zero or low gravity is complicated by the problems of handling or separating vapor-liquid phases. A type of storage which avoids low gravity phase separation problems is supercritical fluid storage.

The tank is initially incompletely filled with cryogenic liquid at atmospheric pressure. Heat is applied to increase the pressure at constant density until supercritical fluid conditions are achieved. Fluid delivery is started after the supercritical pressure is reached and continues at constant pressure during system operation. The pressure is maintained by heat addition to the tank during fluid withdrawal. After the fluid temperature exceeds the fluid critical temperature, the pressure may be allowed to drop. Phase separation will not occur as long as the temperature is maintained above the critical temperature permitting reduction in heating requirements during the final fluid discharge stage.

In order to analyze the heat input and fluid outflow requirements, a curve of the "specific heat input" must be developed for that particular pressure. Specific heat input is the amount of heat required to expel a pound of fluid at a constant pressure. Conversely, it also determines the mass of fluid to be removed, due to a given heat input, in order to maintain a constant pressure. The working relationship is developed as follows.

Heat added to the fluid results in fluid expulsion plus a change in fluid internal energy. The enthalpy of the fluid leaving the tank is assumed equal to that of the fluid in the storage space at any instant. The heat balance is

$$\frac{dQ}{d\theta} = q = \frac{d}{d\theta}(mu) + h\dot{m} \qquad (5\text{-}72)$$

in terms of enthalpy

$$u = h - PV$$

$$q = \frac{d}{d\theta}(mh) - \frac{144V}{J}\frac{dp}{d\theta} + h\dot{m} \qquad (5\text{-}73)$$

$$= m\frac{dh}{d\theta} + h\frac{dm}{d\theta} - \frac{144V}{J}\frac{dp}{d\theta} + h\dot{m} \qquad (5\text{-}74)$$

since $\dot{m} = -\frac{dm}{d\theta}$ and thus, for constant pressure operation

$$q = m\frac{dh}{d\theta} \qquad (5\text{-}75)$$

$$\frac{dh}{d\theta} = \frac{dm}{d\theta}\left(\frac{\partial h}{\partial m}\right)_P = -\dot{m}\left(\frac{\partial h}{\partial m}\right)_P \qquad (5\text{-}76)$$

Substituting (5-76) into (5-75) yields

$$q = -m\dot{m}\left(\frac{\partial h}{\partial m}\right)_P \qquad (5\text{-}77)$$

Since $m = V_f\,\rho$, equation (5-77) can be rewritten as

$$q = -\dot{m}\left[\rho\left(\frac{\partial h}{\partial \rho}\right)_P\right] \qquad (5\text{-}78)$$

The quantity $\left[-\rho\left(\frac{\partial h}{\partial \rho}\right)_P\right]$ is the specific heat input and is a function of fluid density at a given pressure, and thus varies during operation. This is usually plotted as ordinate versus percent of fluid weight remaining in the tank. As can be noted in Fig. 5-20, the curve passes through a minimum.

For example, at the minimum point, if the flow rate, $\dot{m}$, is known, then multiplying $\dot{m} \times \frac{q}{\dot{m}}$ will give the heat requirement to maintain that flow rate. At any other time, a larger heat input is required to maintain the same flow rate. For a given vessel heat leak, q, a flow rate out of the tank, $\dot{m}$, is obtained by dividing q by $q/\dot{m}$. If this flow rate is greater than the required flow, the excess may have to be vented.

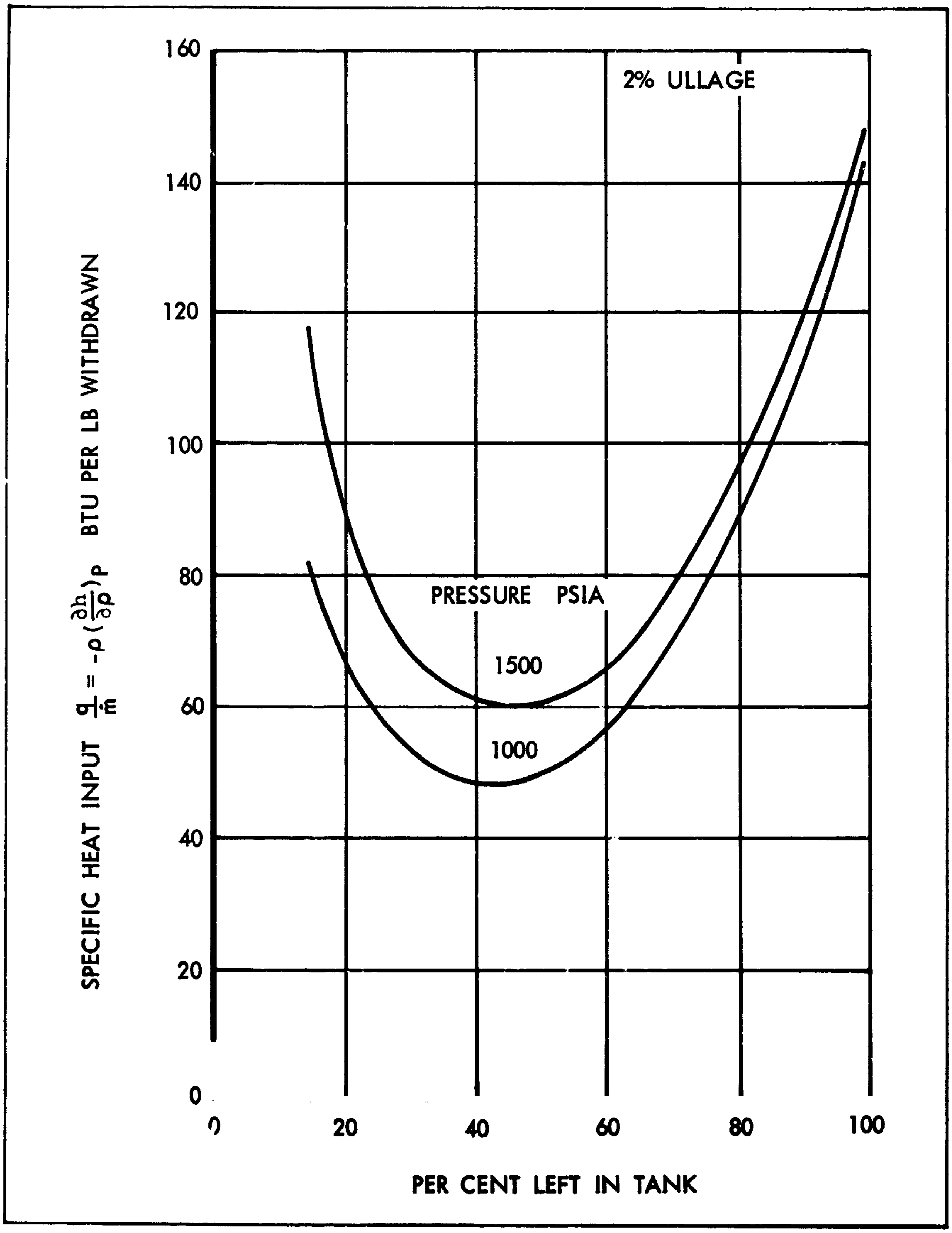

Figure 5-20 Specific Heat Input for Constant Pressure Delivery - Supercritical Nitrogen Storage

Example - The following example will demonstrate the use of the methods specified for the compilation of supercritical storage requirements.

Problem: Compute the heater power required for the supercritical storage of 100 lbs of nitrogen for 14 days at a constant use rate of 6 lb/day. The initial ullage is 2% and pressure is maintained at 1000 psia.

Practical design of supercritical storage tankage dictates that the heat leak into the fluid from the environment be less than the minimum heat input required for constant pressure delivery. Referring to figure 5-20,

$$\left.\frac{q}{m}\right)_{\text{min, 1000 psia}} = 48 \text{ Btu/lb}$$

From the problem statement

$$\dot{m} = \frac{6}{24} = 0.25 \text{ lb He/hr}$$

and the tank heat leak requirement is

$$q_{HL} \leq 48\ (.25) = 12 \text{ Btu/hr}$$

For a conservative design, allowing for tolerances in material properties and manufacturing, this allowable heat leak is reduced by a factor of 2 resulting in a system heat input rate of 6 Btu/hr.

The final percent left in tank is

$$100 - \frac{6 \times 14 \times 100}{100} = 16\%$$

Referring again to figure 5-20:

$$\left.\frac{q}{m}\right|_{\text{initial (100\%)}} = 142 \text{ Btu/lb}$$

$$\left.\frac{q}{m}\right|_{\text{final (10\%)}} = 82 \text{ Btu/lb}$$

$\frac{q}{\dot{m}}$ min (42%) = 48 Btu/lb

At a constant withdrawal rate of 0.25 lb N_2/hr the power input required varies from an initial value of 142 (.25) - 6.0 = 32 Btu/hr to a final value of 82(.25) - 6.0 = 14.5 Btu/hr. The nominal maximum operational power requirement is calculated to be 32/3.416 = 9.35 watts.

The average q/ṁ at a constant pressure of 1000 psia is approximately 75 Btu/lb.

The total power required to expel 6 lb/day for 14 days is:

75 (6)(14) = 6300 Btu = 1.84 kw-hrs.

Standby Capability - Standby capability or no loss storage capacity is another area of interest in the design of storage systems for the extended storage of cryogenic liquids.

The tankage is filled on the ground with saturated or subcooled liquid at 1 atmosphere pressure and maintained in this condition with ground service equipment during groundhold. At lift off, the tank is capped and slowly pressurized by tank heat leakage to supercritical operating conditions. The time required to become operational is a measure of the no-loss standby capability of the system.

The energy input during no-loss storage is determined by the relationship:

$$dE = dH - d(PV) \qquad (5\text{-}79)$$

where $$dE = C_V dT + \left(\frac{\partial E}{\partial V}\right)_T dV \qquad (5\text{-}80)$$

For a constant volume conditions:

$$dE = C_V dT = dQ \qquad (5\text{-}81)$$

substituting: $$dQ = dH - VdP \qquad (5\text{-}82)$$

and $$\Delta Q = \int dH - \int VdP \qquad (5\text{-}83)$$

From tabulated values of fluid enthalpy and system operational parameters, the heat input required (ΔQ) can be computed.

The standby term is then determined by dividing the energy input required by the heat leak rate for the system.

In a similar manner, computation of the extension in system standby time achieved by storage of the cryogenic fluids as subcooled liquids or liquid-solid mixtures (slush) can be accomplished.

Computer Analysis

For a detail study of fluid storage and pressurization problems, a generalized IBM 7094 digital computer program is available which will provide pressure-time and temperature-time histories, fluid mass transfer rates, and pressurization requirements for complex fluid storage systems. The program input specifications have been generalized to permit maximum applicability to current and projected aerospace vehicle and spacecraft storage systems. A complete, detailed description of the program is found in Reference 5-7.

For the computer program, mathematical models have been written which depict the fluid dynamics and the mass and energy transfer mechanisms typically encountered in a storage and pressurization system designed for space applications. These models, discussed briefly below, are covered in detail in Reference 5-7.

Heat Transfer Model - The steady state and transient heat flow in the system is approximated by means of an analogous resistance-capacitance network simulating the actual physical system. This network consists of discrete volumes or nodes interconnected by thermal resistors. The state and properties of the material within each element is assumed to be uniform throughout the element. Nodal properties are treated as functions of time and of axial and radial distance. The temperature distribution throughout the system is obtained by computer solution of the total network using the lumped parameter, numerical method.

Effect of Variations in Gravity Level - Two liquid/vapor configurations are considered in the program:

1. A zero or low gravity configuration in which the liquid surrounds a centrally located vapor space.
2. The normal non-low gravity configuration.

Judgment as to which configuration to use is based on evaluation of the system Bond number (N_{BO}) which is the ratio of the system external forces to the fluid internal forces. This ratio is represented as:

$$N_{BO} = \frac{\rho L^2 g}{\sigma} \tag{5-84}$$

The program contains an input variable such that whenever $N_{BO} < 1.0$, configuration 1 (zero gravity) is used to determine the shape and location of the vapor-liquid interface for heat and mass transfer computations.

Mass and Energy Transfer at the Gas-Liquid Interface - The mass and energy transferred due to condensation or evaporation is computed as a function of the average temperature in the gas space, the partial pressure of the liquid vapor based on the maximum liquid temperature, the volume of the gas space and the fluid latent heat of vaporization. The rate of change in the mass of vapor in the gas region is computed as:

$$\dot{m} = \frac{d}{d\theta}\left[\frac{144\ P_c\ M_c\ V_G}{z_c R T_{L\ MAX}}\right] \tag{5-85}$$

Mass and Energy Transfer Within a Phase (Stratification) - When the magnitude of the system external forces (gravity, acceleration) is large compared to the fluid internal forces (surface tension), heat flow through the tank wall will set up a density gradient in the fluid. Because of the thermal resistance of the fluid, the density gradient is greatest at the wall of the tank. This provides a driving force for fluid transport up the wall of the tank. The warm fluid spreads over the upper level of the fluid, building up successive warmer layers of fluid (strata) as the heating continues. The process is depicted schematically in Figure 5-21.

The mass and energy transferred within a phase due to gravity induced fluid circulation (convection) is computed as a function of fluid depth, the fluid Grashof and Prandtl numbers and the tank wall heating rate.

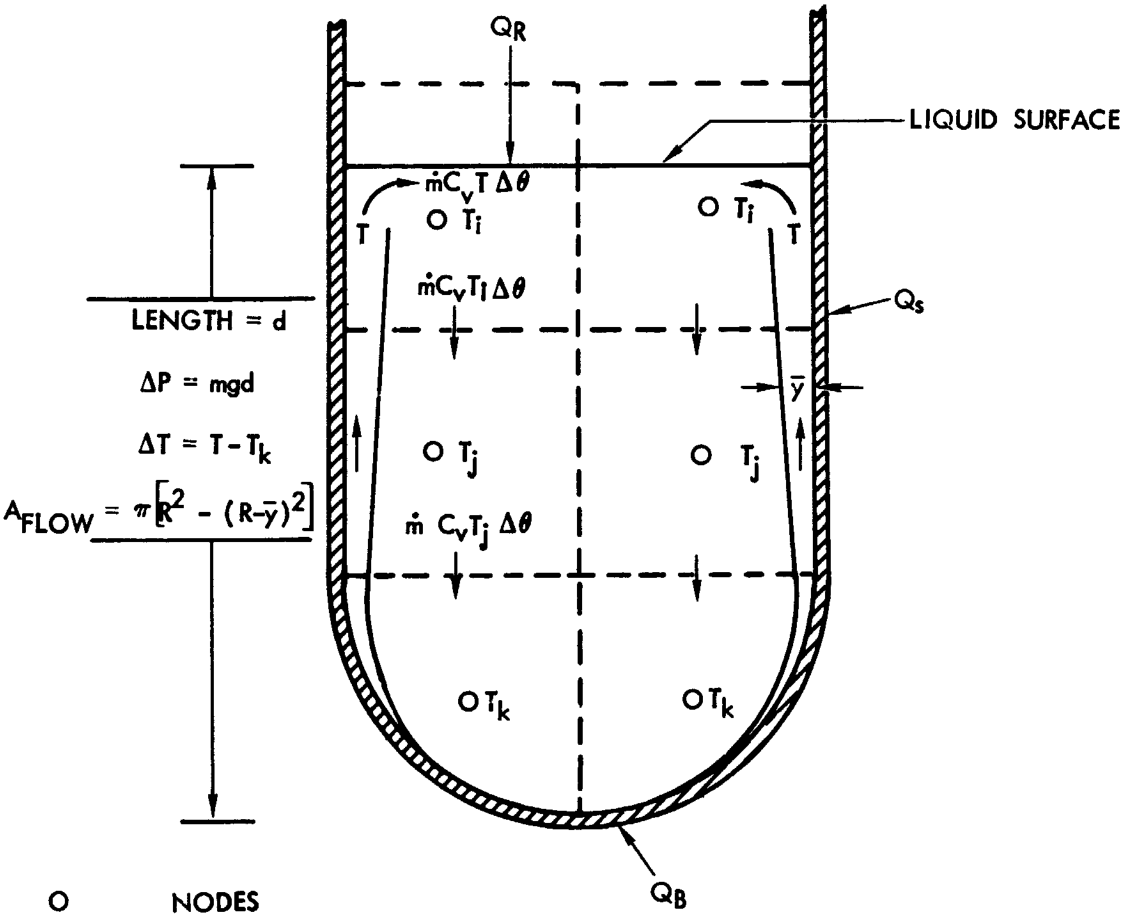

O	NODES		
---	NODE BOUNDARIES	Q_R	RADIATION HEAT FLUX
$\bar{y}$	BOUNDARY LAYER THICKNESS	Q_S	SIDEWALL HEAT FLUX
R	TANK RADIUS	Q_B	BOTTOM HEAT FLUX
$T_{i,j,k}$	NODE TEMPERATURES	m	MASS = W/g
C_v	HEAT CAPACITY	g_o	GRAVITATIONAL CONSTANT
Δ	COMPUTING INTERVAL	g	LOCAL GRAVITY VECTOR
$\dot{m}$	WEIGHT FLOW RATE		

Figure 5-21 Schematic of Fluid Stratification Analytical Model

The existence of mass transfer within a phase is also determined from the value of the system Bond number (N_{BO}).

In the computer program, the inception of convective heat transfer is assumed to occur when $N_{BO} = 1.0$. For $N_{BO} < 1.0$, surface tension forces predominate and, in the case of container wetting fluids, the only mechanism of heat transfer through the fluid is by conduction. For $N_{BO} \geq 1.0$, convection is assumed to exist in the system and the magnitude of the fluid Rayleigh number (N_{Ra}) is used to determine:

a. Whether convection is laminar or turbulent.

b. The wall boundary layer thickness.

c. The fluid film heat transfer coefficient.

d. Whether bottom heating is great enough to destroy stratification.

Tank Wall Radiation - Radiation heat transfer between the tank wall and the liquid surface through a gas space is incorporated into the program as:

$$q_R = F \sigma A \frac{\left(\overline{T_{TW}^4} - \overline{T_s^4}\right)}{\frac{1}{\epsilon_{TW}} + \frac{1}{\epsilon_L} - 1} \qquad (5\text{-}86)$$

$$\text{where } \overline{T^4} = \frac{1}{n} \sum_{i=1}^{n} T_i^4 \qquad n = \text{No. of nodes affected} \qquad (5\text{-}87)$$

During very low gravity conditions, the walls are assumed to be wetted by liquid and, as a consequence, radiation heat transfer is negligible.

Pressurant Supply Tank Analysis - Analysis of the pressurant supply tank is accomplished in two parts:

a. Thermal soak during non-flow periods.

b. Gas expansion during flow periods.

During non-flow periods the heat balance determines the heat input to the gas. The temperature and pressure change are the result of assuming a constant volume heat addition process.

Flow periods are considered to be brief so that an adiabatic expansion process is used during each computing interval to describe the temperature and pressure changes. Short computing intervals are used and a heat balance is calculated at the end of each interval to account for heat transfer to the gas.

REFERENCES

5-1. Schultz, H.D. *Thermal Analyzer Computer Program for the Solution of General Heat Transfer Problems*, Lockheed-California Company Report LR 18902, 16 July 1965

5-2. Nevelli, B.A. *Computer Program for the Calculation of Incident Orbital Radiant Heat Flux*, Lockheed-California Report LR 18904, 18 June 1965

5-3. Hamilton, D. and W. Morgan *Radiant-Interchange Configuration Factors*, NACA TN 2836, December 1962

5-4 Linneman, E.R. *Computer Program for the Calculation of Three-Dimensional Configuration Factors*, Lockheed-California Company Report LR 18905, 30 June 1965

5-5. Oppenheim, A.K. *Radiation Analysis by the Network Method*, Transactions of the ASME, May 1956

5-6. Hottel H.C. "*Radiant Heat Transmission*" *Heat Transmission* by W. C. McAdams, McGraw-Hill, 1954

5-7 Hirasawa, P.S., I. Shuldiner, and Josephine Laue *Thermal Analyzer Computer Program for the Solution of Fluid Storage and Pressurization Problems*, Lockheed-California Company Report LR 18903, 10 August 1965

VI - EFFECTS OF THE SPACECRAFT ENVIRONMENT ON THERMAL-CONTROL MATERIALS

In this section, factors of the spacecraft environment which are either known or thought to be significant sources of damage for thermal-control materials are discussed in terms of present estimates of their effects on these substances. More thorough treatments, both of the environment and the behavior of materials in general, are found in References 6-1 through 6-4. The general remarks of this section are supplemented by the discussions of stability of specific materials found in Section VII.

PRELAUNCH ENVIRONMENTAL EFFECTS

The prelaunch environment of a space vehicle material includes its entire history up to launch. Major problems of manufacturing and quality control, handling techniques, and protection of thermal-control surfaces have become increasingly obvious. The difficulties are intensified in the case of large satellites, such as the Agena. The production of the thermal-control surface must be carefully controlled, whether the surface be a paint or ceramic film, polished metal, or conversion coating. If the bulk radiative characteristics of a given paint or ceramic coating are to be achieved by a coated surface, care must be taken to assure that adequate film thicknesses are obtained. For the materials evaluated at Lockheed Missiles and Space Company (LMSC), it has been found that thicknesses required for opacity varies from 0.001 in. or less for some black paints (flat absorbers) to 0.005 in. for some white paints. Rokide A, a flame-sprayed aluminum oxide coating produced by Norton Abrasive Company, was found to require thickness in excess of 0.015 in (Ref. 6-5). In the case of metals used as solar absorbers, the surface condition achieved is as important as the material.

Once the desired thermal-control surface is achieved, still more problems are encountered. Fingerprints have been known to cause localized corrosion of aluminum and gold-plated surfaces which resulted in a doubling of emittance. Atmospheric corrosion and contamination of bright metal surfaces involve so many different parameters (time, salinity, temperature, moisture condensation or precipitation, wind current, and dirt) that it is preferable to protect a surface rather than attempt to predict its behavior.

Identical aluminum specimens were exposed out of doors throughout June, 1961 in two different locations. The results are summarized in terms of radiation characteristics at room temperature:

	Solar Absorptance, α_s		Emittance, ϵ	
Location	Initial	Final	Initial	Final
San Francisco	0.17	0.30	0.11	0.15
LMSC Palo Alto	0.17	0.18	0.11	0.14

Attemps to clean the specimens did not significantly alter these values. The fog and salinity conditions encountered at San Francisco were generally more severe than those at Palo Alto. At San Francisco, α_s/ϵ increased by 30%; at Palo Alto a decrease of about 15% was incurred. The quantitative results, though not important in themselves, indicate that effects of atmospheric exposure are not only significant but unpredictable. Even if daily, seasonal, and regional meteorological variations are ignored, the general unpredictability of spacecraft prelaunch exposure time necessitates the use of protective measures.

In summary, the prelaunch environment merits the same detailed consideration as the ascent and space environments. Practical manufacturing considerations must be included in the selection and development of spacecraft thermal-control materials.

ASCENT ENVIRONMENT

As the space vehicle enters the ascent phase of its history, it is exposed simultaneously to aerodynamic heating and aerodynamic pressure and shear forces, to the possible presence of ionized and dissociated gas particles, and to vibration and shock forces arising mainly from engine ignition shocks, acoustic pressures, aerodynamic forces, and stage-separation shocks. Of these factors, aerodynamic heating apparently has the most significant effect on the subsequent thermal-control problem. Often surfaces which are external during ascent must perform as thermal-control surfaces upon reaching space. Such surfaces may be subjected to temperature histories as those in Figure 6-1; the peak temperatures shown are followed by a slow radiative decay. The exact temperature history experienced depends primarily on ascent trajectory, vehicle geometry, vehicle material properties, and location of the particular surface on the vehicle. This thermal behavior is accompanied by a rapid decrease in local air pressure and density. A typical local pressure history for the cylindrical section is 5 mm Hg at 100 sec after liftoff, 10^{-1} mm Hg at 160 sec, and 10^{-2} mm Hg at 180 sec.

The ascent heating damage most difficult to circumvent is the darkening of white paints which results in increased α_s. Iorganic films generally possess stability in ascent superior to that of organic materials.

In addition to the direct effect on thermal-control materials, a secondary source of damage in the ascent environment results from the outgassing, volatilization, or pyrolysis of materials during ascent and subsequent recondensation on and contamination of adjacent thermal-control materials. The most noteworthy example is damage which might be caused by such material as adhesives, wire insulation, or potting compounds located in a space vehicle nose cone.

The other important constituents of the ascent phase are shear and vibration. However, tests performed to date indicate damage caused by these constituents to be of second order as compared to the effects of heating and reduced pressure.

In summary, the most serious effects of the ascent environment on thermal-control materials are the discoloration of white paints, the bubbling and adhesion failures experienced by paints in general, and the potential contamination of surfaces through recondensation of substances evolved from adjacent materials.

SPACE ENVIRONMENT

In the space environment, the vehicle encounters a large assortment of environmental constituents. Only those potentially damaging to thermal-control materials are discussed.

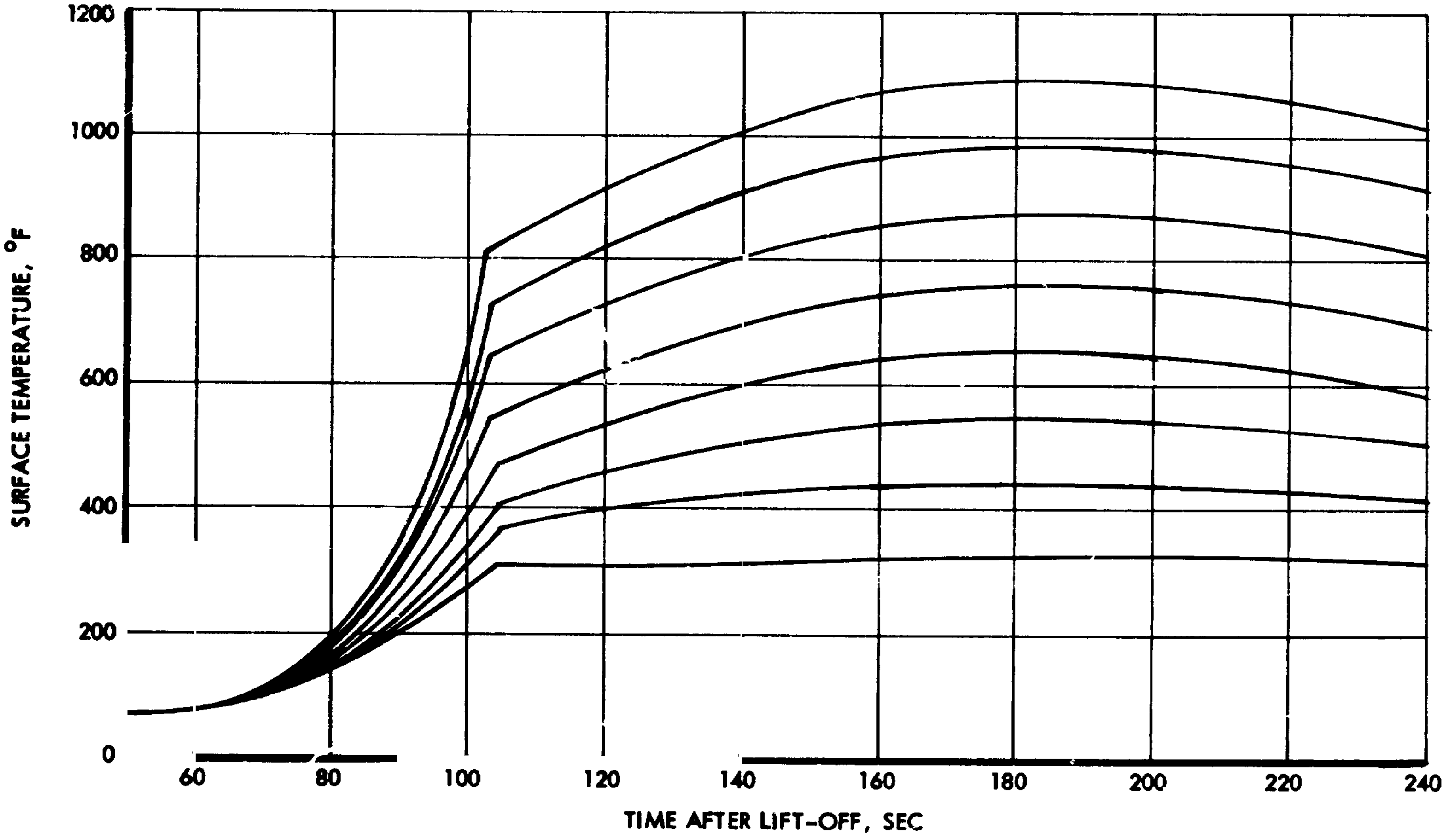

Figure 6-1. Representative Agena Ascent Temperature Histories

Planetary Atmospheres - Vacuum

Planetary atmospheres at artificial satellite altitudes are best described in terms of particles species, kinetic energies, and concentrations, rather than by the continuum concept of pressure. Johnson, in a description of the Earth's atmosphere (Ref. 6-1), estimates that concentrations of $\sim 10^9$ particles/cm^3 exists at an altitude of 200 miles above the earth, with the particles consisting of approximately 70 to 85% atomic oxygen, 5% atomic nitrogen, and the remainder molecular nitrogen. This corresponds to a pressure of roughly 10^{-7} mm Hg. Lower concentrations are estimated for greater altitudes. The most significant aspect of these numbers from a thermal-control standpoint is simply their small size. Particles leaving a surface will not return; volatilization is therefore a potential problem. In addition, participation in reactions by the atmospheric constituents, particularly oxygen, may be much less than is the case in the presence of air at 1 atmosphere pressure.

Volatilization of metals is not an expected source of damage to thermal design. Numerous treatments of this subject are available (Ref. 6-2 through 6-6). All conclude that evaporation at modest temperatures of all metals except tin, cadmium and zinc will be insignificant. Pure magnesium might present a problem if operated continuously above 250°F. Because of its susceptibility to corrosion in the prelaunch environment, however, bare magnesium is not employed as a thermal-control surface. Whenever such a surface is desired, the metal is invariably covered with a coating or film which inhibits evaporation of the underlying magnesium. Sublimation of magnesium, therefore, is not a problem to thermal design.

The question of the stability of dielectric materials in a vacuum has not proved to be amenable to so simple an answer (Ref. 6-1 and 6-2). Mechanisms of degradation are generally more complex than those of metals. As an example of this complexity, a substance can decompose to simpler materials, which may subsequently volatilize; and the loss of more volatile components of a complex material may be governed by diffusion rates rather than the subsequent volatilization process. Organic compounds are generally less stable in vacuum than are inorganic ones. Organic coatings used for thermal control [illegible] LMSC spacecraft are the acrylics (Kemacryl), silicones, and vinyl-phenolics (Micobond) discussed in Section VII. These coatings have been extensively studied under vacuum conditions in various environmental tests; no indications of vacuum instability at temperature levels to be encountered in service have been noted.

It must be remarked that for thermal-control surfaces operating at elevated temperatures, with 600- 1400°F nuclear reactor radiators, for example, the volatilization problem must be reexamined.

One phenomenon caused by the presence of atmospheric particles is sputtering, which is the removal or ejection of one or more atoms from a surface due to collision with a high-velocity particle. The kinetic energy of surface atoms of an orbiting satellite, relative to that of an atmospheric particle, is high enough for some sputtering to occur. The question, of course, is how much. Measurements made by R. Stein (Ref. 6-7) indicate that the energies of these collisions are about an order of magnitude too low to cause significant sputtering on an exposed surface. Stein exposed thermal-control surface specimens to sputtering caused by the impingement of argon or Xenon ions; such exposure had negligible effect on their radiation characteristics. Here again, the paucity of adequate environmental information makes these results open to question. All that can be said is that the information indicates that sputtering due to the particles of planetary atmospheres is not a significant problem for thermal control of spacecraft with lifetimes of two years or less.

Solar Electromagnetic Radiation

The present knowledge of extraterrestrial solar radiation is summarized in References 6-1 and 6-2. Only 0.02% is estimated to be of wavelengths less than 2,200 Å; 9% is estimated to be between 2,200 and 4,000 Å (near-ultraviolet energy). Although the shorter-wavelength radiation is more energetic, the much greater flux density in the 2,200 to 4,000-Å region, together with the known effects of this wavelength region on materials, point to this portion of the solar spectrum as a likely source of severe environmental damage. Possible effects of energy of wavelengths longer than 4,000 Å have not received much attention, since materials under consideration are not known to alter significantly their radiation characteristics due to incident terrestrial solar radiation. It is known, however, that terrestrial solar radiation has considerable flux density at wavelengths of 4,000 Å and longer. It should be noted that not all ultraviolet energy received by surfaces of a space vehicle is direct insolation; artificial earth satellites, for example, receive significant albedo rediation, i,e., ultraviolet irradiation via solar energy reflected from the earth-atmosphere system (Ref. 6-2).

The effects of ultraviolet are felt most strongly by organic materials, which undergo such structural alterations as molecular cross-linking and decomposition through scission. Pigments and other inorganic materials may be affected by the formation of color centers - a phenomenon connected with the presence of defect sites in the materials. The practical significance of these effects is that white dielectric materials turn brown and suffer an increase in α_s. However, black surfaces do not appear to be significantly affected. If an extremely stable white surface is required, it appears that very carefully prepared inorganic materials must be used (Refs. 6-2, 6-4, and 6-8). Metals should be unaffected by ultraviolet energy (Refs. 6-1 through 6-3), although the oxide film found on metals may be altered

Penetrating Radiation

Summaries of present information on penetrating radiation have been presented by Dessler (Ref. 6-1) and Lee (Ref. 6-2). Lee estimates the most important sources of damage to be natural trapped radiation(Van Allen radiation), auroral radiation, solar flare radiation, and cosmic radiation. However, there are order-of-magnitude uncertainties in present estimates of the amount, distribution, and energy spectra of radiation fluxes in space. This problem is heightened by the artificial trapped radiation belts caused by recent high-altitude nuclear detonations.

Even if the radiation environment of space were clearly defined, it would be difficult to quantitatively assess the behavior of thermal-control materials in that environment through theory and experiment. It is not possible to obtain in laboratories the full range of energies and flux levels desired for the difference species individually, not to mention the various combinations encountered in space. Thus, material stability must be qualitatively estimated. This has been done by J. C. Lee (Ref. 6-2). Expected radiation doses have been calculated and compared to known tolerance data. Indications are that many materials, especially organics, are potentially vulnerable to the low energy electron components of the auroral, Van Allen, and artificial radiation belts. Inorganic dielectric materials are expected to be less affected, while the optical properties of metals should be affected least of all.

Results of sputtering due to solar-flare and solar-wind protons have been estimated by several different workers (Refs. 6-1 through 6-3). The general conclusion derived from these studies is that such sputtering is not likely to be a real problem to thermal design of earth satellites, except possibly for thin-film control surfaces. Such surfaces should receive special attention if used on vehicles likely to encounter solar-flare protons. Since solar-flare proton fluxes are thought to increase as one approaches the sun from the orbit of the earth, possible damage may be incurred by surfaces of probes to the interior planets. Before final approval for design use, it would be wise to subject candidate surfaces to low-energy proton (<20 Mev) bombardment if they are to be used for such missions.

In addition to the penetrating radiation of the natural environment, spacecraft with nuclear devices will create an induced environment of penetrating radiation. The induced penetrating radiation will consist primarily of neutron and gamma radiation, as contrasted to the electron and proton radiation of the space environment. The induced environment will generally be more severe than the natural environment (i.e., higher local flux rates). Also, the effects of neutron and gamma radiation are different from those of electron and proton radiation. The prediction of damage effects in either case must be based on experimental data from vacuum irradiation tests on the material in question. Such tests are underway at various facilities in support of LMSC/USAF space programs. Preliminary results indicate the damage to be of equivalent importance to that incurred by exposure to solar ultraviolet energy.

Meteoroids

The available information on size, mass, velocity, spacial distribution, and number densities of meteoroids has been presented in References 6-1, 2, 3, 9, 10, and 11. The various values of particle fluxes presented in each reference vary by at least four orders of magnitude. Estimates of damage are generally theoretical, since particles with meteoric mass and velocity have not been produced in the laboratory in a controlled fashion. Jaffe and Rittenhouse (Ref. 6-3), among others, have estimated the effect on aluminum over a period of one year, based on the work of Bjork (Ref. 6-9). The general conclusion is that thermal-control surfaces of deep-space vehicles with lifetimes of two years or less will not be significantly affected by meteoroid impact. Surfaces of vehicles in earth orbits of less than 300-mile altitude may experience some degradation. Greater difficulties can be anticipated for very thin structures and optical systems. If care is not exercised in design, penetration may seriously damage active thermal-control systems.

CONCLUSIONS

Results of investigations on effects of the spacecraft environment indicate the most important sources of damage to thermal control materials to be ascent heating, solar ultraviolet energy, penetrating radiation, and the entire prelaunch environment.

The materials most susceptible to damage during ascent are the white dielectric films used as solar reflectors; these generally tend to darken and suffer increases in α_s.

In addition, secondary damage can be caused during ascent through the contamination of surfaces due to recondensation of substances evolved by the outgassing, volatilization, or pyrolysis of adjacent materials.

For practical thermal-control purposes, solar ultraviolet energy produces the same macroscopic effect on white materials as does ascent heating, i.e., turning brown with resulting increases in α_s. The behavior of candidate thermal materials in penetrating radiation fluxes has yet to be adequately determined. However, as a consequence of the results of the ascent and ultraviolet tests, and the anticipated results of radiation exposures, inorganic materials are recommended where a highly stable solar reflector is desired for use on a spacecraft with a desired lifetime of one to two years.

A major obstacle to the achievement of reliable thermal control of sophisticated spacecraft is the lack of definition of the space environment. Considerable uncertainty exists as to the kinetic or quantum energy spectra and spatial distribution of such constituents as micrometeorites, Van Allen radiation, and solar protons. The factors constituting the actual thermal energy inputs to a spacecraft also need better evaluation - the Earth's albedo, the Earth emission, and the ultraviolet component of solar radiation are three that require further study.

Information is also needed on the behavior of materials in the total spacecraft environment. An attempt is being made to infer such information from experimental and theoretical studies of the effects of individual constituents. It is far more desirable and reliable, however, to base stability estimates upon data of material behavior in space. For this reason, the utilization of spacecraft-borne experiments designed for this specific purpose is urgently needed.

Since the space environment cannot be controlled, concentration on the selection or development of stable materials with predictable characteristics is necessary to achieve reliable thermal design. The prelaunch environment of a thermal-control surface, on the other hand, is potentially controllable. The approach adopted at Lockheed, therefore, is to concentrate on prelaunch protection, enforced by inspection. An inspection device and protective handling procedures and devices have been developed; production personnel are receiving indoctrination in the handling and care of thermal-control surfaces.

REFERENCES

6-1. Johnson, F.S., ed. Satellite Environment Handbook, Stanford University Press, Stanford, California, 1961

6-2. Goetzel, C.G., and J.B. Singletary, ed. Space Materials Handbook, Lockheed Missiles & Space Co., Sunnyvale, California, January 1962

6-3. Jaffe, L.D. and J.B. Rittenhouse Behavior of Materials in Space Environments, JPL 32-150, Jet Propulsion Laboratory, Pasadena, California, 1 November 1961

6-4. Allen, J.M. Environmental Factors Influencing Metals Applications in Space Vehicles, DMIC 142, Defense Metals Information Center, Battelle Memorial Institute, Columbia, Ohio, 28 December 1960

6-5. Gaumer, R.E. and L.A. McKellar Thermal Radiactive Control Surfaces for Spacecraft, Lockheed Missiles & Space Co. Report 704014, Sunnyvale, California, March 1961

6-6. Dushman, S. Vacuum Techniques, John Wiley and Sons, New York, 1949

6-7. Stein, R.P. "Atomic and Molecular Sputtering," Surface Effects on Spacecraft Materials, ed., F.J. Clauss, John Wiley and Sons, New York, N.Y.

6-8. Gaumer, R.E., F.J. Clauss, M.E. Sibert, and C.C. Shaw Materials Effects in Spacecraft Thermal Control, Lockheed Missiles & Space Co. Report 704019, Sunnyvale, California, November 1960

6-9. Bjork, R.L. Meteoroids Versus Space Vehicles, RAND P-1963, 4 April 1960; included in Paper No. 1200-60, Semi-Annual Meeting and Astronautical Exhibition, Los Angeles, California, 9-12 May, 1960

REFERENCES (Continued)

6-10. Whipple, F.L. "Solid Particles in the Solar System," *J. Geophys, Research*, Vol. 64, 1959

6-11. Beard, D.B. "Interplanetary Dust Distribution," *Astrophys, J.*, Vol. 129, No. 2, March 1959

VII - PROPERTIES OF REPRESENTATIVE THERMAL-CONTROL SURFACES

The thermophysical properties data contained in this section were obtained by the Lockheed Missiles and Space Company Thermophysics Laboratory. Table 7-1 summarizes the properties of a number of surfaces reported in References 7-1 and 7-2. These references contain a more complete discussion of thermal-control surfaces, the methods of measuring properties, and properties of additional surfaces. Representative surfaces of each of the four types, solar absorber, solar reflector, flat absorber, and flat reflector, are discussed on the following data sheets, which were obtained from Reference 7-2.

The following code is used on the data sheets to specify the source of radiation property data (the equipment is described in Ref. 7-2):

A. Cary integrating sphere and spectrophotometer

B. Hohlraum and spectrophotometer

C. Standard calorimetric emittance devices

D. Direct α_s/ϵ device

E. Emissometer unit of Optical Surface Comparator
(Lion Research Corporation)

F. Elevated temperature directional emittance device

G. Radiometric total normal emittance apparatus

H. Reflectometer unit of Optical Surface Comparator
(Lion Research Corporation)

The process bulletins, PB-35, -38, -55, and -59, referred to on the data sheets are contained in Reference 7-3.

TABLE 7-1
THERMAL CONTROL SURFACES

MATERIAL DESCRIPTION	α_S	ϵ	α_S/ϵ
SOLAR ABSORBERS			
6061 ALUMINUM SHEET (WELD AREA)	0.18	0.10	1.8
6061 ALUMINUM SHEET (NON CLAD)	0.16	0.06	2.7
2024 ALUMINUM SHEET (NON CLAD)	0.20	0.06	3.3
2024 ALUMINUM SHEET (CLAD)	0.22	0.06	3.7
FASSON FOIL	0.12	0.04	3.0
DRY ANNEALED ALUMINUM FOIL	0.12	0.04	3.0
MYSTIK 7402 ALUMINUM FOIL	0.12	0.04	3.0
INCONEL FOIL	0.38	0.12	3.2
INCONEL X FOIL	0.66	0.15	4.4
QMV BERYLLIUM ALLOY			
MILLED FROM SINTERED BLOCK	0.45	0.11	4.1
ROLLED PLATE, CHEMICALLY MILLED	0.48	0.11	4.4
MILLED-SINTERED BLOCK & CHEM. POLISH	0.48	0.08	6.0
ROLLED PLATE, CHEM. MILLED, CHEM. POLISH	0.50	0.09	5.6
MOLYBDENUM			
AS RECEIVED	0.48	0.12	4.0
OXIDE COATING	0.84	0.26	3.3
RENE 41 ALLOY			
AS RECEIVED	0.73	0.39	1.4
MECHANICALLY POLISHED	0.63	0.23	2.7
RENE 41 FOIL (0.006")	0.55	0.22	2.5
302 STAINLESS STEEL (MECH POLISHED)	0.38	0.19	2.0
347 STAINLESS STEEL (DEGREASED & SANDBLASTED)	0.65	0.45	1.4
410 STAINLESS STEEL (DEGREASED & SANDBLASTED)	0.71	0.41	1.7
STAINLESS STEEL (CORRUGATED FOIL)	0.38	0.16	2.4
ALODYNE TYPE 1200T on 6061 ALUM. ALLOY	0.47	0.06	7.8
6 AL4VA TITANIUM ALLOY	0.66	0.20	3.3
ALUMINUM (DEPOSITED FILM)			
ON MAGNESIUM, SILICONE UNDERCOAT	0.13	0.04	3.3
ON MAGNESIUM, EPOXY UNDERCOAT	0.13	0.07	1.9
ON HM21A MAGNESIUM ALLOY	0.24	0.11	2.2

TABLE 7-1 (Continued)

MATERIAL DESCRIPTION	α_S	ϵ	α_S/ϵ
SOLAR ABSORBERS			
GOLD (DEPOSITED FILM)			
ON TITANIUM, SILICONE RESIN BASE	0.34	0.05	6.8
ON ALUMINUM WITH RESIN UNDERCOAT	0.24	0.04	6.0
PLATED ELECTROLYTICALLY ON POLISHED NICKEL STEEL	0.28	0.10	2.8
GOLD FOIL	0.29	0.23	1.3
NICKEL (DEPOSITED FILM)			
ELECTROLESS NICKEL	0.45	0.17	2.6
ELECTROLESS NICKEL ON QE-22 MAGNESIUM CASTING ALLOY			
SURFACE POLISHED	0.40	0.09	4.4
SURFACE UNPOLISHED	0.46	0.15	3.1
138 SILVER (DEPOSITED FROM SOLUTION)			
ON DOW 15 - SURFACED HM21 MAGNESIUM ALLOY	0.30	0.24	1.3
ON DOW 17 - SURFACED MAGNESIUM ALLOY	0.30	0.34	0.88
ALUMINUM (METAL FOILS AND FILMS)			
FASCAL CHROME ALUMINIZED MYLAR FILM	0.25	0.09	2.8
MIL-A-148 FOIL, SLICK ANNEALED	0.19	0.06	3.2
MAGNESIUM			
MODIFIED DOW 1	0.33	0.06	5.5
HM21A (DOW 15 COATED)	0.19	0.08	2.4
SOLAR REFLECTORS			
WHITE KEMACRYL PAINT	0.28	0.86	0.33
WHITE SILICONE PAINT	0.25	0.90	0.28
WHITE SKYSPAR PAINT	0.22	0.91	0.24
ALZAK ON ALUMINUM ALLOY	0.19	0.76	0.25
ROKIDE A (ALUMINUM ALLOY, .010")	0.26	0.71	0.37
ADHESIVE-BACKED DIELECTRIC NO. 3650 WHITE SCOTCH CAL FILM ON ALUM. 6061-T6	0.24	0.83	0.29
FLAT ABSORBERS			
BLACK KEMACRYL PAINT	0.93	0.88	1.06
BLACK SILICONE PAINT	0.89	0.88	1.01
ROKIDE C (NICHROME ON RENE)	0.90	0.85	1.06

TABLE 7-1 (Continued)

MATERIAL DESCRIPTION	α_S	ϵ	α_S/ϵ
FLAT ABSORBERS			
PLATINUM BLACK ON BERYLLIUM	0.94	0.85	1.11
DOW 17 ON HM21A	0.78	0.70	1.11
HEAVY HAE MAGNESIUM	0.75	0.77	0.97
MAGNESIUM (DOW 10)	0.89	0.85	1.05
FLAT REFLECTORS			
ALUMINUM SILICONE (FULLER 172-A-1)	0.25	0.28	0.89
ALUMINUM SILICONE (FULLER 171-A-1)	0.22	0.24	0.92
NON-LEAFING ALUMINUM KEMACRYL	0.41	0.48	0.85
GRAY-ANODIZED ALUMINUM	.50-.62	.44-.76	.67-1.4

SOLAR ABSORBERS

MATERIAL	6061 Aluminum Alloy
SUBSTRATE	Not applicable
MATERIAL DESCRIPTION	6061 Aluminum sheet (nonclad), forging and weld area chemically cleaned per PB-35 Method I

THERMOPHYSICAL PARAMETERS

Sample Temperature (°R)	Radiant Source	α	Tolerance	Date Source	Remarks
530	Sun	0.16[a]	±0.04	A	Nonclad sheet as processed per PB-35 Method I[c]
530	Sun	0.19[b]	±0.06	A	Sheet sanded before processing[c]
530	Sun	0.18[b]	±0.06	A, H	Agena fuel tank. Sanded before processing per PB-35 Method I[c,d]

Sample Temperature (°R)	ϵ	Tolerance	Data Source	Remarks
530	0.06[a]	±0.03	B, E	Nonclad sheet as processed per PB-35 Method I[c]
530	0.08[b]	+0.03 -0.05	B, E	Sheet or Agena fuel tanks. Sanded before processing per PB-35 Method I[c,d]
500 600	0.09 0.10	±0.06 ±0.06	B	Forging
400 500 600	0.10 0.10 0.11	±0.06 ±0.06 ±0.06	B	Weld Area

(a) Values of α_s = 0.12 to 0.27 and $\epsilon \leq 0.12$ have been observed on samples improperly processed.

(b) Values of α_s = 0.13 to 0.33 and $\epsilon \leq 0.18$ have been observed on samples sanded and improperly processed.

(c) Surfaces that are critical for thermal control purposes must be inspected with the Lion Optical Surface Comparator.

(d) Agena fuel tanks must be sanded before processing per PB-35 Method I. If external surfaces are to be thermal-control surfaces, the Optical Surface Comparator inspection is required.

SOLAR ABSORBERS (Continued)

ENVIRONMENTAL BEHAVIOR

Prelaunch

Aluminum surface is very susceptible to increases in α_s and ϵ caused by contamination. The surface must be protected from physical abuse, atmospheric exposure, and caustic contaminants; cleanliness must be assured.

Postlaunch

There are no known restrictions, other than structural.

REMARKS

The surface characteristics of the sheet materials are subject to variations depending on fabricating operations.

SOLAR ABSORBERS (Continued)

MATERIAL	6061 Aluminum Alloy
SUBSTRATE	Not applicable
MATERIAL DESCRIPTION	6061 Aluminum sheet (nonclad) chemically cleaned per PB-35 Method II

THERMOPHYSICAL PARAMETERS

Sample Temperature (°R)	Radiant Source	α	Tolerance	Data Source	Remarks
530	Sun	0.16(a)	±0.05	A	(b)

Sample Temperature (°R)	ϵ	Tolerance	Data Source	Remarks
530	0.06	±0.03	B, E	(b)

(a) Values of 0.11 to 0.40 for α_s have been observed where the instructions of PB-35 were not followed or were improperly applied.

(b) Surfaces that are critical for thermal control purposes must be inspected with the Lion Optical Surface Comparator.

ENVIRONMENTAL BEHAVIOR

Prelaunch

Aluminum surface is very susceptible to increases in α_s and ϵ caused by contamination. The surface must be protected from physical abuse, atomspheric exposure, and caustic contaminants; cleanliness must be assured.

Postlaunch

There are no known restrictions, other than structural.

REMARKS

The surface characteristics of the sheet materials are subject to variations depending on fabricating operations. These values are given for the as-rolled condition.

SOLAR ABSORBERS (Continued)

MATERIAL	2024 Aluminum Alloy Sheet (nonclad)
SUBSTRATE	Not applicable
MATERIAL DESCRIPTION	2024 Aluminum alloy sheet (nonclad) chemically cleaned per PB-35 Method II

THERMOPHYSICAL PARAMETERS

Temperature (°R)	Radiant Source	α	Tolerance	Data Source	Remarks
535	Sun	0.20(a)	±0.05	A	(b)

Sample Temperature (°R)	ϵ	Tolerance	Data Source	Remarks
535	0.06	±0.03	B, E	(b)

(a) Values of 0.15 to 0.36 for α_s have been observed where the instructions of PB-35 were not followed or were improperly applied.

(b) Surfaces that are critical for thermal control purposes must be inspected with the Lion Optical Surface Comparator.

ENVIRONMENTAL BEHAVIOR

Prelaunch

Aluminum surface is very susceptible to increases in α_s and ϵ caused by contamination. The surface must be protected from physical abuse, atmospheric exposure, and caustic contaminants; cleanliness must be assured.

Postlaunch

There are no known restrictions, other than structural.

REMARKS

The surface characteristics are subject to variations depending on prior fabrication operations. These values are given for the as-rolled condition.

SOLAR ABSORBERS (Continued)

MATERIAL	2024 Aluminum Alloy Sheet (Clad)
SUBSTRATE	Not applicable
MATERIAL DESCRIPTION	2024 Aluminum alloy sheet (clad) chemically cleaned per PB-35 Method II

THERMOPHYSICAL PARAMETERS

Sample Temperature (°R)	Radiant Source	α	Tolerance	Data Source	Remarks
535	Sun	0.22(a)	±0.05	A	(b)

Sample Temperature (°R)	ϵ	Tolerance	Data Source	Remarks
535	0.06	±0.03	B, E	(b)

(a) Values of $\alpha_s \simeq 0.28$ have been observed where the instructions of PB-35 were not followed or were improperly applied.

(b) Surfaces that are critical for thermal control purposes must be inspected with the Lion Optical Surface Comparator.

ENVIRONMENTAL BEHAVIOR

Prelaunch

Aluminum surface is very susceptible to increases in α_s and ϵ caused by contamination. The surface must be protected from physical abuse, atmospheric exposure, and caustic contaminants; cleanliness must be assured.

Postlaunch

There are no known restrictions, other than structural.

REMARKS

The surface characteristics are subject to variations depending on prior fabrication operations. The cladding can be removed by abrasives, caustics, etc. These values are given for the as-rolled condition with cladding intact.

SOLAR ABSORBERS (Continued)

MATERIAL	Fasson Foil
SUBSTRATE	Any clean rigid surface
MATERIAL DESCRIPTION	Adhesive-backed bright aluminum foil. Type I has a clear protective coating, Type II is bare.

THERMOPHYSICAL PARAMETERS

Sample Temperature (°R)	Radiant Source	α	Tolerance	Data Source	Remarks
530	Sun	0.12	±0.04	A, D	This is Type II with no protective film on the surface.

Sample Temperature (°R)	ϵ	Tolerance	Data Source	Remarks
530	0.04	+0.02 -0.01	B,C,D,E	This is Type II with no protective film on the surface. Type I with the film properly removed is essentially equivalent. The aluminum surface has been exposed to air and has the thin oxide layer characteristic of aluminum.

ENVIRONMENTAL BEHAVIOR

Prelaunch

The surface of Type II or Type I with the film removed is very susceptible to increases in α_s and ϵ caused by contamination. The surface must be protected from physical abuse, atmospheric exposure, and caustic contaminants; cleanliness must be assured.

Postlaunch

This material should be used only in areas where the peak ascent temperatures are not expected to exceed 375°F: it must not be external during ascent.

SOLAR ABSORBERS (Continued)

REMARKS

Type II fasson foil is supplied bare, with nothing to protect the bright surface from handling and application damage to the thermal properties. Any film, such as oil or fingerprints, may increase ϵ to 0.15 or higher. Type I fasson foil, with the nitrocellulose lacquer protection, may be used in place of Type II, provided the lacquer is completely removed prior to application of the foil. The coating may be removed by wiping with a soft clean cloth, using the following solvents in this order:

a) Lacquer thinner or methyl-ethyl-ketone (MEK)
b) Isopropyl or ethyl alcohol

To avoid localized lifting of the foil from the substrate in vacuum or high-temperature applications due to gas evolved from the underlying adhesive the foil should be perforated. Holes approximately 1/32 in. in diameter on 1/2 in. centers are recommended.

Cleaning and removing of the protective lacquer must be done prior to perforation of the foil to avoid introducing solvents within the adhesive.

The lacquer coating on Type I fasson is almost invisible to the eye. If any doubt exists whether the foil is Type I or Type II, or whether the lacquer has been removed, the following technique is recommended. Place the probes of ohmmeter lightly against the foil surface: if electrical continuity is observed the foil is bare; if electrical resistance is indicated, the probes are on the dielectric lacquer coating. Fasson foil for spacecraft or missile use should be ordered with S-277 adhesive. Nylon gloves should be worn by all persons working on or near this thermal-control surface.

SCLAR ABSORBERS (Continued)

MATERIAL	Dry Annealed Aluminum Foil (MIL-A-148C)
SUBSTRATE	Not applicable
MATERIAL DESCRIPTION	MIL-A-148C Aluminum Foil vapor degreased

THERMOPHYSICAL PARAMETERS

Sample Temperature (°R)	Radiant Source	α	Tolerance	Data Source	Remarks
530	Sun	0.12	±0.04	A, D	--

Sample Temperature (°R)	ϵ	Tolerance	Data Source	Remarks
530	0.04	+0.02 -0.01	B,C,D,E	--

ENVIRONMENTAL BEHAVIOR

Prelaunch

Foil surface is very susceptible to increases in α_s and ϵ caused by contamination. The surface must be protected from physical abuse, atmospheric exposure, and caustic contaminants; cleanliness must be assured.

Postlaunch

There are no known restrictions other than structural.

SOLAR ABSORBERS (Continued)

MATERIAL	Mystik 7402 Pressure-Sensitive Aluminum Foil
SUBSTRATE	Any clean rigid surface
MATERIAL DESCRIPTION	Aluminum foil tape with a pressure-sensitive silicone adhesive

THERMOPHYSICAL PARAMETERS

Sample Temperature (°R)	Radiant Source	α	Tolerance	Data Source	Remarks
530	Sun	0.12	±0.04	A, D	
530	1200° blackbody	0.07	±0.05	B	—

Sample Temperature (°R)	ϵ	Tolerance	Data Source	Remarks
530	0.04	+0.02 -0.01	B,C,D,E	—

ENVIRONMENTAL BEHAVIOR

Prelaunch

Aluminum surface is very susceptible to increases in α_s and ϵ caused by contamination. The surface must be protected from physical abuse, atmospheric exposure, and caustic contaminants; cleanliness must be assured.

Postlaunch

The tape, if applied externally, should have mechanical fastening on both ends to prevent ascent forces from peeling the tape away from its substrate.. This tape may be used internally where peak temperatures of up to 800°F are anticipated and externally for temperatures up to 750°F.

SOLAR ABSORBERS (Continued)

MATERIAL	Chemically Polished Beryllium
SUBSTRATE	Not applicable
MATERIAL DESCRIPTION	The beryllium tested to date is known as QMV which is a Brush Co. designation that refers to the processing technique. QMV is a sintered product and is supplied in four different minimum purities (87, 98, 98.5 and 99.0 percent). Lockheed-purchased beryllium has a minimum purity of 98 percent.

THERMOPHYSICAL PARAMETERS

Sample Temperature (°R)	Radiant Source	α	Tolerance	Data Source	Remarks
530	Sun	0.50	±0.06	A	PB-59
530	2100° R blackbody	0.18	±0.05	B	
530	1500° R blackbody	0.15	±0.05	B	
530	800° R blackbody	0.11	±0.06	B	
530	Sun	0.50	±0.06	A	Not chemically polished. As machined, but free of corrosion and fingerprints.

Sample Temperature (°R)	ϵ	Tolerance	Data Source	Remarks
530	0.10	±0.06	B,E	PB-59
530	0.10	±0.06	B	Not chemically polished. As machined, but free of corrosion and fingerprints.
530	0.10	±0.06	B	A previously chemically polished piece of beryllium wet sanded with #400 silicone carbide paper.

SOLAR ABSORBERS (Continued)

ENVIRONMENTAL BEHAVIOR

Prelaunch

Oxidation in air at room temperature is negligible due to formation of a nonporous protective oxide film approximately 10^{-6} cm thick. In this respect, beryllium is similar to aluminum. Samples have been left outdoors in the Palo Alto environment for an entire month (June 1961) with no observable changes in optical properties. However, similar samples left out in the San Francisco environment (10 blocks from the ocean) for the same month suffered permanent corrosive damage. Following residue removal, α_s increased by 0.10 and ϵ by 0.05. Corrosion damage due to fingerprints has been observed although the chemically polished surfaces appear to be less susceptible to this type of damage than are as-machined surfaces.

Postlaunch

Normal ascent temperatures do not affect the optical properties of this material. Oxidation rates below 1400°F are negligible. Heating to 1600°F within 3 minutes followed by normal cooling in a one-atmosphere environment resulted in an increase of ϵ of only 0.04. Heating to 1700°F within five minutes in a 0.05-mm HG environment resulted in a 0.01 increase in ϵ.

REMARKS

As the above measurements indicate, machined or sanded beryllium surfaces have the same nominal optical properties as the chemically polished surfaces. However, it is not always possible to adequately protect as-machined surfaces, and sanding can be a health hazard. The PB-59 chemical polishing process is not difficult and will ensure a surface finish with known optical properties. Additionally, the chemically-polished surfaces appear to resist corrosion better than the machined surfaces, although there is no quantitative data to support this observation.

SOLAR ABSORBERS (Continued)

MATERIAL — Inconel Foil (Hitco Specification Number TPS-0101B, H. I. Thompson Company)

SUBSTRATE — Not applicable

MATERIAL DESCRIPTION — Nickel-chrome alloy, a nonmagnetic heat- and corrosion-resisting alloy which will withstand temperatures up to 2200°F with high-temperature strength and resistance to progressive oxidation and fatigue. This foil has been "quilted." The general appearance is of a foil that has been corrugated twice with the directions of the corrugations perpendicular to each other.

THERMOPHYSICAL PARAMETERS

Sample Temperature (°R)	Radiant Source	α	Tolerance	Data Source	Remarks
530	Sun	0.38	±0.05	A	—
530	800°R blackbody	0.32	±0.05	B	

Sample Temperature (°R)	ϵ	Tolerance	Data Source	Remarks
400	0.11	±0.05	B, E	—
500	0.12	±0.05		
600	0.13	±0.05		

ENVIRONMENTAL BEHAVIOR

Prelaunch

Highly polished foil is very susceptible to increases in α_s and ϵ by fingerprinting and oxidation of surface. Permanent damage may ensue unless contamination is removed immediately and the surface protected.

Postlaunch

Ascent heating is very likely to increase α_s and ϵ. Measurements performed on samples scorched during a test-engine firing have given α_s values as high as 0.91 and room-temperature emittances as high as 0.27.

SOLAR ABSORBERS (Continued)

REMARKS

Chemical polish may be performed on sheet material only; it is not suitable for completed assemblies.

SOLAR ABSORBERS (Continued)

MATERIAL	Inconel X Foil
SUBSTRATE	Not applicable
MATERIAL DESCRIPTION	Age-hardened nickel-chromium alloy which has high strength and low creep rate at temperatures up to 1500°F, after suitable thermal treatment. The material has high resistance to chemical corrosion and oxidation.

THERMOPHYSICAL PARAMETERS

Sample Temperature (°R)	Radiant Source	α	Tolerance	Data Source	Remarks
530	Sun	0.66	±0.09	A	
530	800° R blackbody	0.18	±0.04	B	—
	1800° R blackbody	0.25			
	2100° R blackbody	0.27			

Sample Temperature (°R)	ϵ	Tolerance	Data Source	Remarks
500	0.15	±0.05	B, E	—
900-2, 000° R	see Fig. 8-1		G	

ENVIRONMENTAL BEHAVIOR

Prelaunch

The higly polished foil is very susceptible to increases in α_s and ϵ by fingerprinting and oxidation of surface. Permanent damage may ensue unless contamination is removed imediately and the surface protected.

Postlaunch

Ascent heating is very likely to increase α_s and ϵ by 100 percent or more. Results of total normal-emittance measurements performed in air are shown in Fig. 7-1. Data were obtained with the Radiometric Total Normal Emittance apparatus "G." Each ϵ value was obtained with

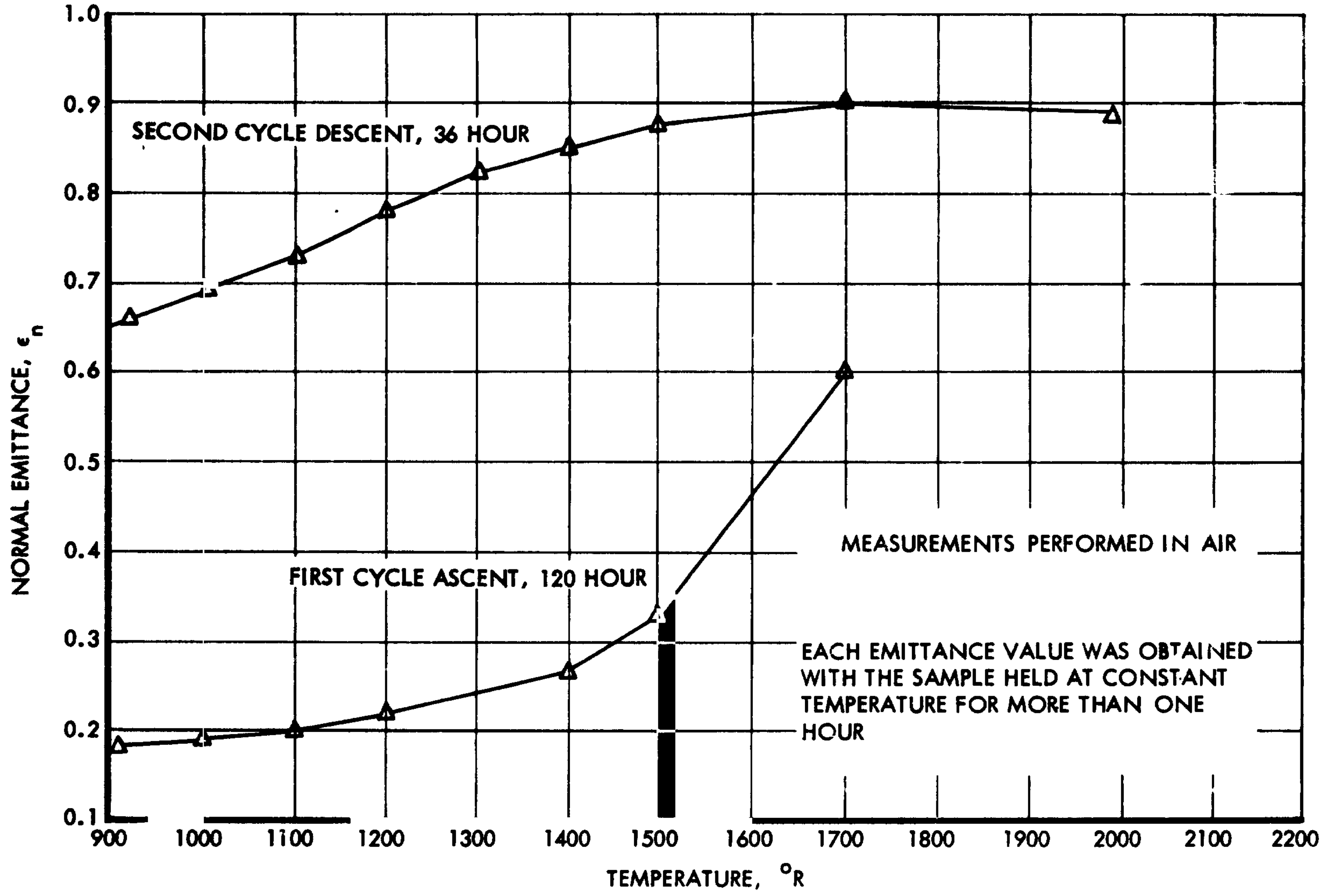

Figure 7-1. Normal Emittance of Inconel X Foil

SOLAR ABSORBERS (Continued)

the sample held at constant temperature for over one hour. The figure shows data from the first test-cycle ascent with progressive increases in temperature and a second successive cycle descent with progressive decreases in temperature.

Note that the lowest data point in Fig. 7-1 (ϵ = 0.16) is not an initial room-temperature value but a value of ϵ for Inconel X after more than one hour at 900°R in air. The primary cause for the increased ϵ values for Inconel X in air is oxidation. At a given temperature in air, 85 percent or more of the expected change in emittance will occur within the first hour of exposure.

REMARKS

Chemical polish PB-38 may be performed on sheet material only; it is not suitable for completed assemblies.

SOLAR REFLECTORS

MATERIAL	Tinted White Kemacryl Lacquer (Sherwin Williams M49WC17)(a)
SUBSTRATE	Any clean, rigid substrate; primer required
MATERIAL DESCRIPTION	White acrylic flat paint, room-temperature cured

THERMOPHYSICAL PARAMETERS

Sample Temperature (°R)	Radiant Source	α	Tolerance	Data Source	Remarks
530	Sun	0.28	±0.04	A,D	Tinted(a)

Sample Temperature (°R)	ϵ	Tolerance	Data Source	Remarks
530	0.86	±0.03	B,C,D,E	-

(a) Only tinted Kemacryl is approved for thermal control use.

ENVIRONMENTAL BEHAVIOR

Prelaunch

The surface is porous and requires protection from contamination.

Postlaunch

This material requires a minimum of 14 days of room-temperature curing to remove volatile materials sufficiently to minimize blistering during ascent heating.

Ascent. The affect of ascent heating is shown in Fig. 7-2, where α_s at room temperature is plotted as a function of the peak temperature experienced during ascent heating. Time held at peak temperatures and ambient pressures are as indicated. At peak temperatures less than 450-500°F, the most serious stability problem results from outgassing or bubbling of the surface. Bubble height was <0.04 in.; bubble diameter 0.1 in. Bubbling commenced at peak temperatures of 205°F and above. This material may be used in locations where maximum temperatures encountered during ascent are less than 450°F, provided the alterations in surface finish and solar absorptance due to the bubbling discussed herein and

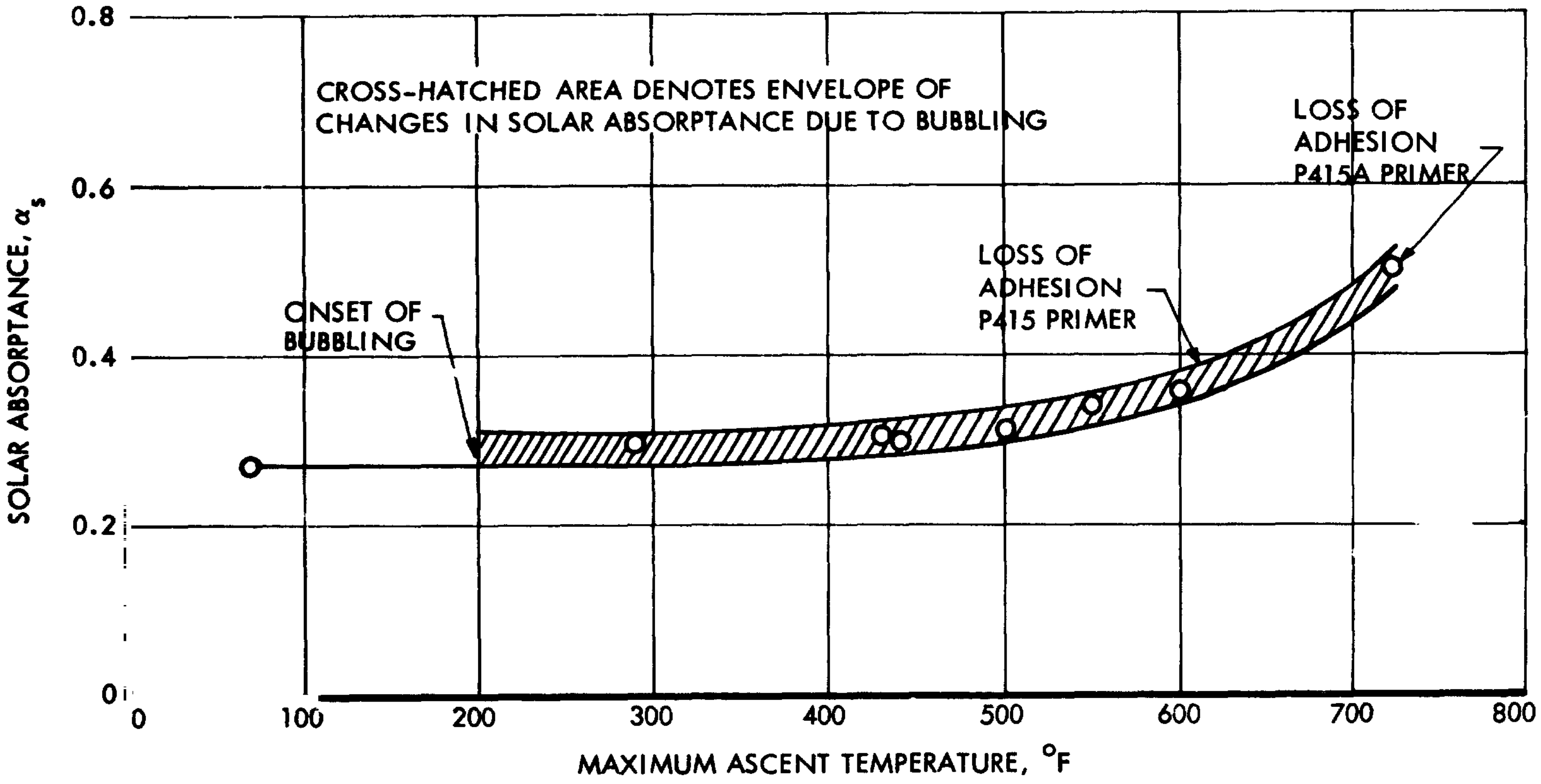

Figure 7-2. Effect of Ascent Heating on Solar Absorptance of Sherwin-Williams White Kemacryl Lacquer

SOLAR REFLECTORS (Continued)

shown in Fig. 7-2 can be tolerated. If no change in surface finish or solar absorptance is allowable, the maximum temperature encountered must be less than 200°F.

Orbital. The primary source of degradation appears to be the near-ultraviolet portion of incident solar and albedo radiation. Presently available data on ultraviolet damage are summarized in Fig. 7-3.

The following half-cylinder specimens successfully survived 385 temperature cycles between 150°F and 70°F with a 12-15 min. cycling period in a vacuum of 10^{-5}mm Hg:

- White Kemacryl Lacquer (Sherwin-Williams M49WC17); 3.0 to 4.0 mil thick; over one coat pretreatment primer P40GCI; on Dow-17 coated HM21 magnesium alloy.
- The same coating system as above on a 6061-aluminum alloy substrate.

No serious flaking, cracking, or loss of adhesion was observed. The results are interpreted as demonstrating the behavior of Kemacryl-base paints on the substrates specified above during orbital temperature cycling.

REMARKS

For internal applications, where emittance is the value of interest, a minimum thickness of 1.0 mil should be maintained (PB-55 Method I Class A). For external surfaces, where both α_s and ϵ are important, the minimum thickness for opacity is 5.0 mil (PB-55 Method II Class A).

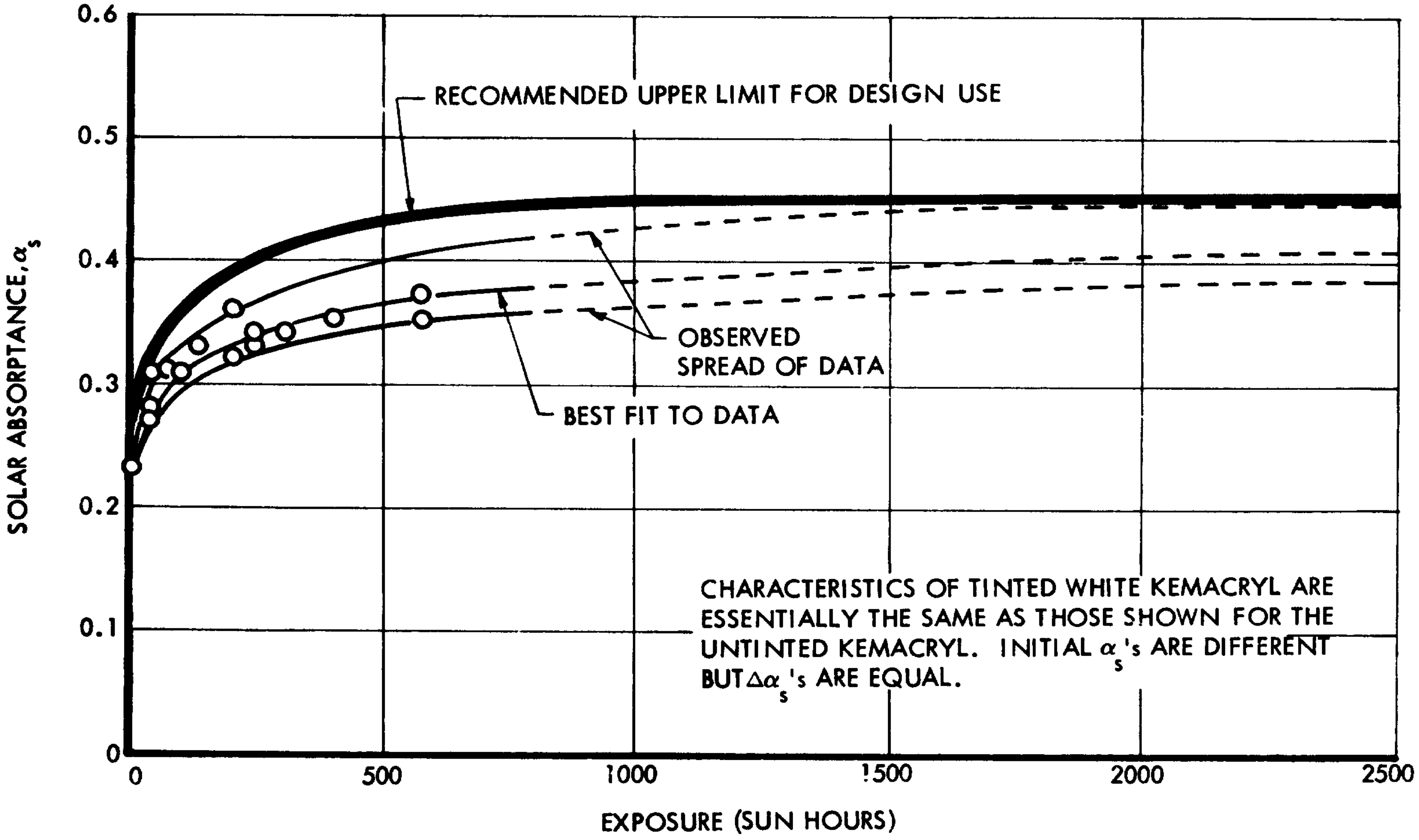

Figure 7-3. Effect of Near Ultraviolet Radiation in Vacuum on Solar Absorptance of Untinted White Kemacryl Lacquer

SOLAR REFLECTORS (Continued)

MATERIAL	Fuller Gloss White Silicone Paint (517-W-1)
SUBSTRATE	HM21A-T8 magnesium annealed (-0) magnesium and aluminum, titanium, stainless steels and super alloys, and any other rigid substrate capable of withstanding the cure cycle.
MATERIAL DESCRIPTION	TiO_2 pigment in silicone-modified alkyd vehicle. Cured by baking at 465°F (see PB-55).

THERMOPHYSICAL PARAMETERS

Sample Temperature (°R)	Radiant Source	α	Tolerance	Data Source	Remarks
530	Sun	0.25	±0.03	A	-

Sample Temperature (°R)	ϵ	Tolerance	Data Source	Remarks
530	0.90	+0.03 -0.06	B,E	-

ENVIRONMENTAL BEHAVIOR

Prelaunch

The surface must be protected from contamination.

Postlaunch

Ascent. The effect of ascent heating is shown in Figs. 7-4 and 7-5, where α_s at room temperature is plotted as a function of the peak temperature experienced during ascent. Time held at peak temperatures and ambient pressures are as indicated. This paint is not recommended for general use in locations reaching temperatures above 650°F during ascent, for at temperatures from 690°F to 775°F, the paint surface cracks.

Orbital. The primary source of degradation appears to be the near-ultraviolet portion of incident solar and albedo radiation. Presently available data on ultraviolet damage are summarized in Fig. 7-6. The results recorded in Table 7-2 were observed during cycling tests with 12 to 15-minute periods at a vacuum of 10^{-5}mm Hg.

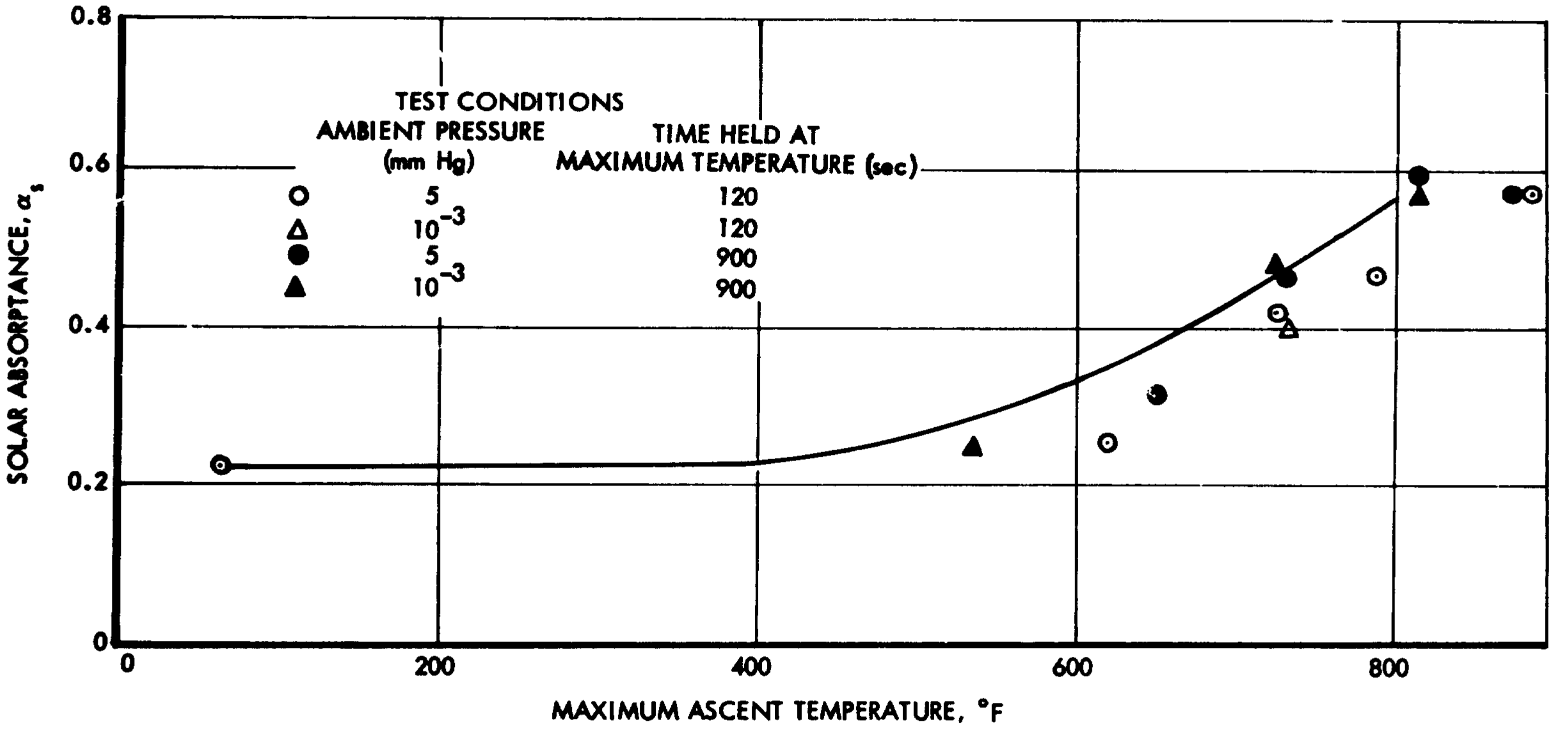

Figure 7-4. Effect of Ascent Heating on Solar Absorptance of Fuller Gloss White Silicone Paint on 6061 Aluminum

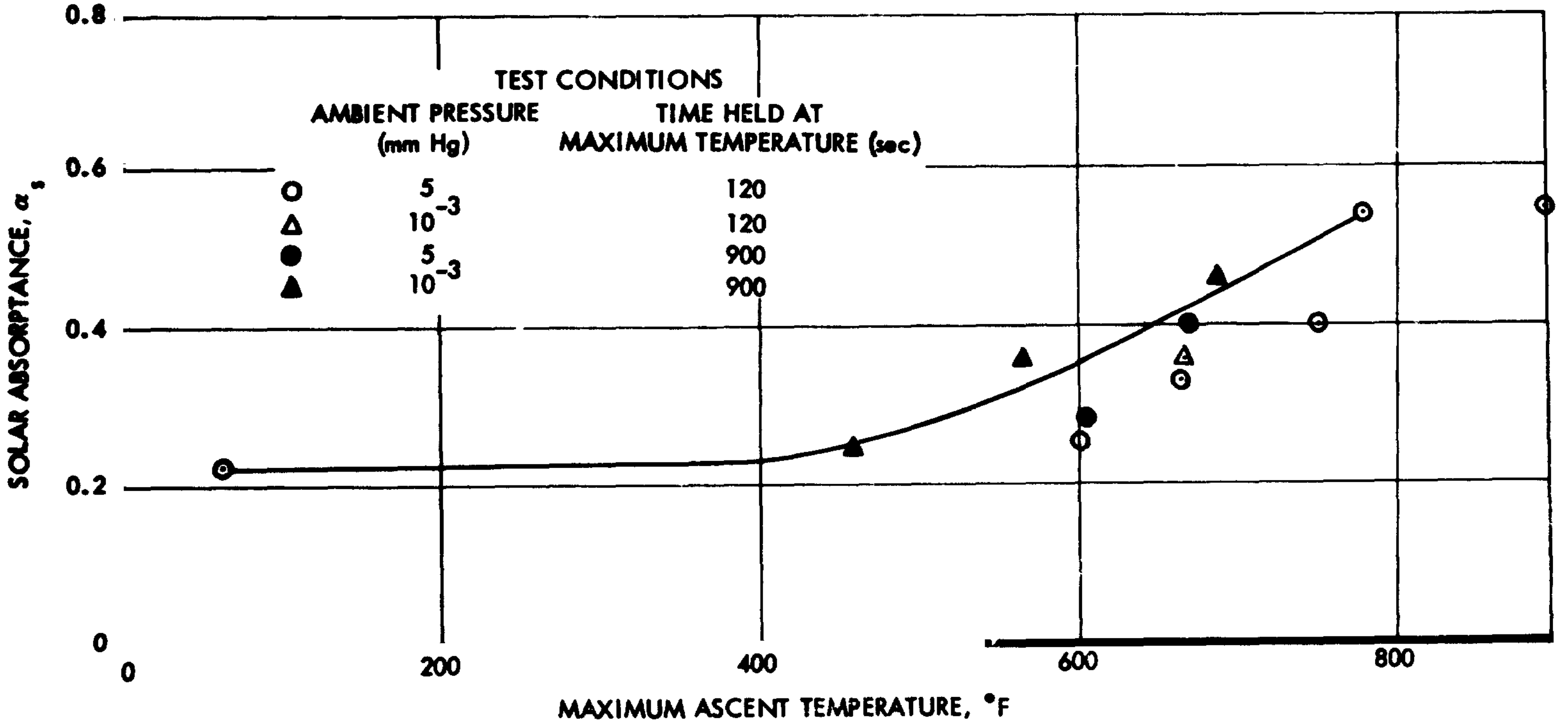

Figure 7-5. Effect of Ascent Heating on Solar Absorptance of Fuller Gloss White Silicone Paint on Dow-17 Coated HM 21A Magnesium

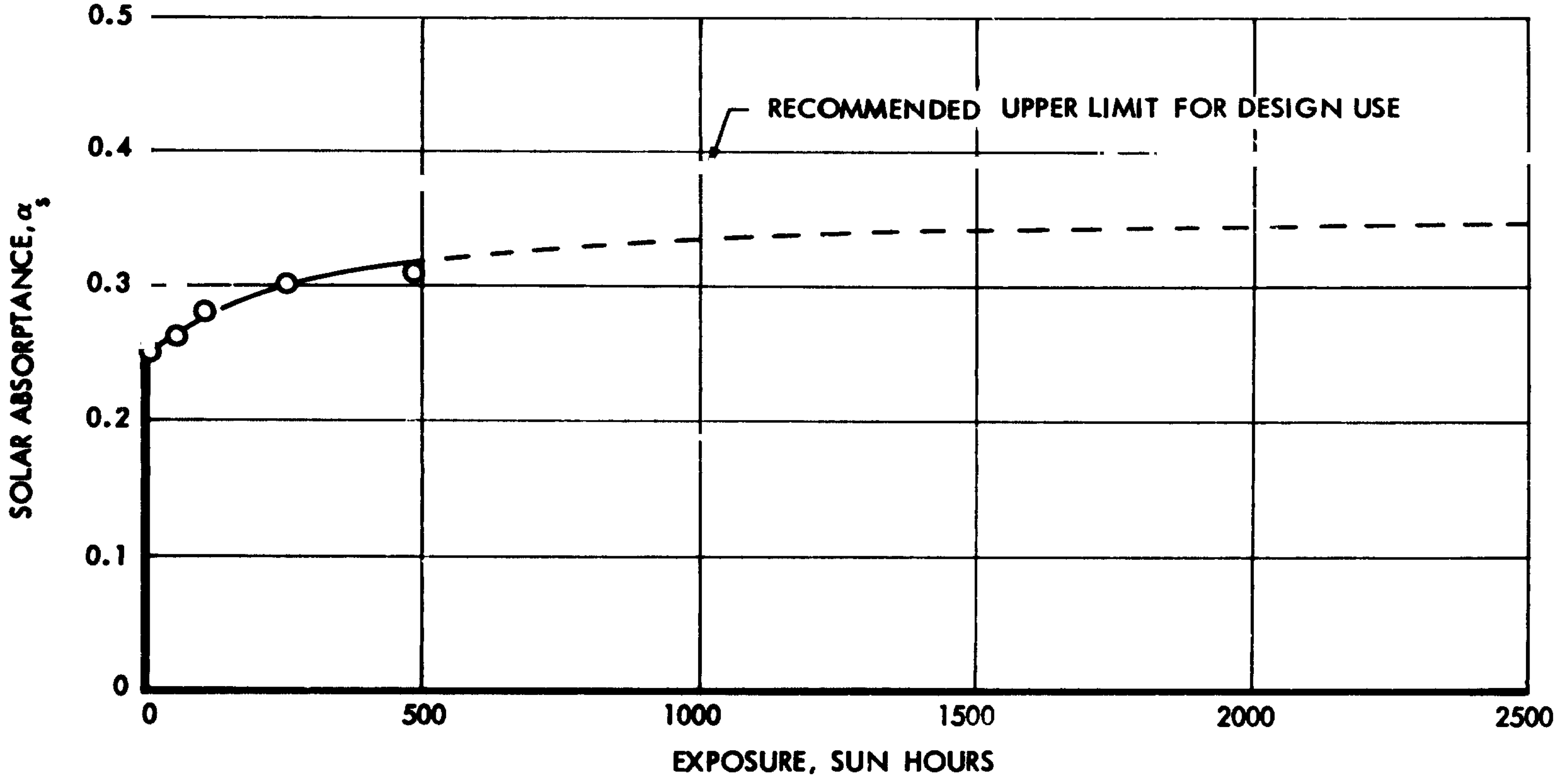

Figure 7-6. Effect of Near-Ultraviolet Radiation in Vacuum on the Solar Absorptance of Fuller Gloss White Silicone Paint on 6061 Aluminum

SOLAR REFLECTORS (Continued)

TABLE 7-2

THERMAL CYCLING RESULTS FOR GLOSS WHITE SILICONE PAINT (FULLER 517-W-1)

Material	Temp. Range	No. of Cycles	Results
517-W-1 White Silicone on Dow 17-coated flat plate of HM21A magnesium alloy, 1-1/4 in. x 2-1/2 in. x 0.060 in.	-240°F + 70°F	170	Severe cracking occurred on first cycle. As test progressed, cracks increased both in number and severity. Testing was terminated at the 170th cycle because large sections of paint (≈1/8 in. strips) began to peel back.
517-W-1 White Silicone on Dow-17 coated half cylinder of HM21A magnesium alloy, 2-1/2 in. long, 5/8 in. radius	-240°F + 70°F	1210	Three fine cracks extending around circumference appeared after 45 cycles. After 170 cycles, six cracks were visible. At 332 cycles, the surface had become covered with cracks ranging from hairline to fairly wide, through which the substrate was visible. At 433 cycles two small specks fell off the surface. No major visual change occurred from this point to the end of the test.

REMARKS

These results are interpreted as demonstrating the behavior of all approved Fuller silicone thermal-control paints during orbital thermal cycling. Evaluation is continuing.

For internal applications, where emittance is the value of interest, a minimum thickness of 1.0 mil should be maintained (PB-55 Method 5, Class C). For external surfaces, where both α_s and ϵ are important, the minimum thickness for opacity is 5.0 mil, (Method 6, Class C).

SOLAR REFLECTORS, (Continued)

MATERIAL	White Skyspar Enamel (A. Brown A423 Color SA 9185)
SUBSTRATE	Any rigid substrate
MATERIAL DESCRIPTION	TiO_2 pigmented epoxy-base paint, room-temperature cured

THERMOPHYSICAL PARAMETERS

Sample Temperature (°R)	Radiant Source	α	Tolerance	Data Source	Remarks
530	Sun	0.22	±0.04	A,D	-

Sample Temperature (°R)	ϵ	Tolerance	Data Source	Remarks
530	0.91	+0.03 -0.06	B,C,D,E	-

ENVIRONMENTAL BEHAVIOR

Prelaunch

The resistance to ultraviolet degradation is low. Sufficient ultraviolet energy is radiated by the common flourescent lights used throughout the fabrication areas to measureably change the α_s values after several months of exposure. Samples exposed within six inches of these lights for 60 days displayed an increase in α_s of 0.06. Epoxy paints are generally resistant to most chemical environments anticipated. Protection from contamination is required.

Postlaunch

Ascent. The effect of ascent heating is shown in Fig. 7-7, where α_s at room temperature is plotted as a function of the peak temperature experienced during ascent. Time held at peak temperatures is two minutes: ambient pressure is 10^{-3} mm Hg. This paint is not recommended for general use in locations reaching temperatures above 450° F during ascent.

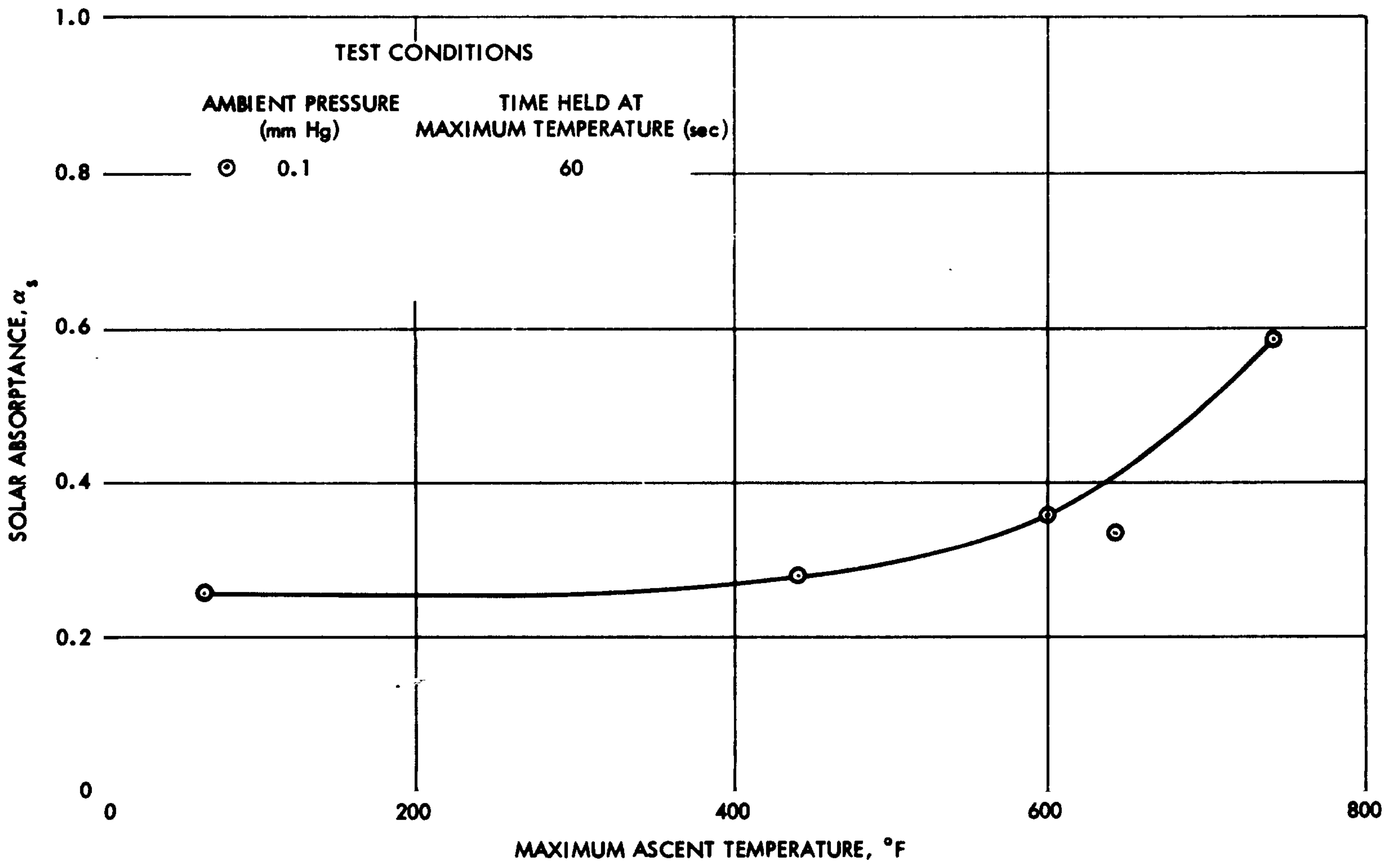

Figure 7-7. Effect of Ascent Heating on Solar Absorptance of White Skysper Enamel on Dow-15 Coated HM21A Magnesium

SOLAR REFLECTORS, (Continued)

Orbital. The primary source of degradation appears to be the near-ultra-violet portion of incident solar and albedo radiation. Presently available data on ultra-violet damage are summarized in Fig. 7-8.

REMARKS

For internal application, where emittance is the value of interest, a minimum thickness of 1.0 mil should be maintained (PB-55 Method 3, Class B). For external surfaces where both α and ϵ are important, the minimum thickness for opacity is 4.0 mil (PB-55 Method 4, Class B).

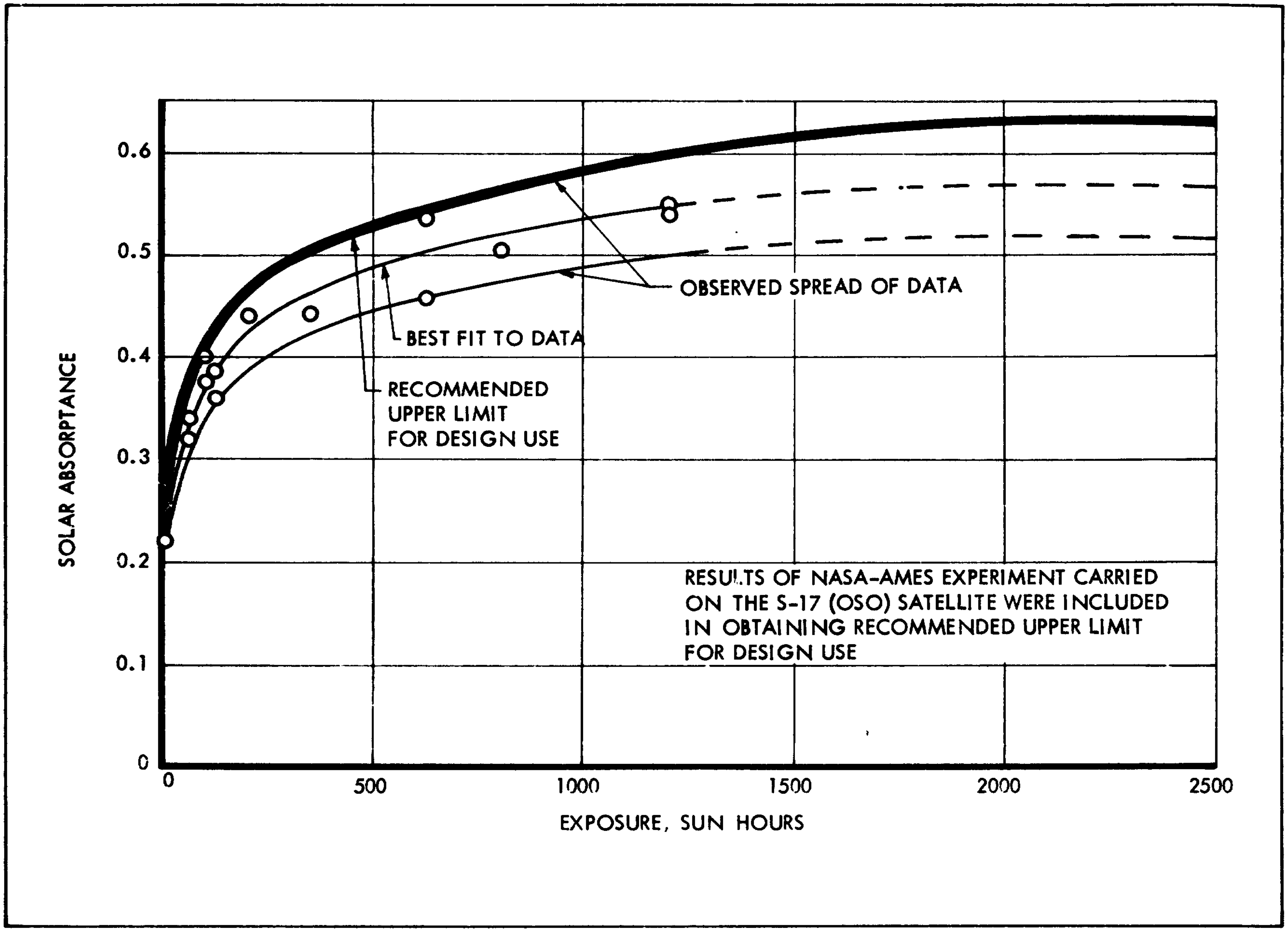

Figure 7-8. Effect of Near-Ultraviolet Radiation in Vacuum on Solar Absorptance of White Skyspar Enamel

FLAT ABSORBERS

MATERIAL	Black Kemacryl Lacquer (Sherwin-Williams M49BC12)
SUBSTANCE	Any clean, rigid substrate; primer required
MATERIAL DESCRIPTION	Room-temperature cured black acrylic flat paint

THERMOPHYSICAL PARAMETERS

Sample Temperature (°R)	Radiant Source	α	Tolerance	Data Source	Remarks
530	Sun	0.93	±0.03	A	-

Sample Temperature (°R)	ϵ	Tolerance	Data Source	Remarks
530	0.88	±0.03	B, E	-

ENVIRONMENTAL BEHAVIOR

Prelaunch

The surface is porous and requires protection from contamination.

Postlaunch

Ascent. This paint requires a minimum of 14 days of room-temperature curing to remove volatile materials sufficiently to minimize blistering during ascent heating. It is not recommended for general use in locations reaching temperatures above 450°F; at temperatures less than this, α_s, ϵ, and adhesives are unaffected. At peak temperatures above 470°F, the paint blisters.

Orbital. No orbital degradation has been observed in tests of the natural space environment. The following half-cylinder specimens successfully survived 385 temperature cycles between -150°F and 70°F with cycling periods of from 12 to 18 minutes in a vacuum of 10^{-5} mm Hg.

- White Kemacryl Lacquer (Sherwin-Williams M49WC12); 3.0 to 4.0 mil thick; over one coat pretreated primer P40GC1; or Dow 17 on HM21 magnesium alloy
- The same coating system as above on a 6061 aluminum alloy substrate. No serious flaking, cracking, or loss of adhesion was observed.

FLAT ABSORBERS (Continued)

These results are interpreted as demonstrating the behavior of Kemacryl-base paints on the substrate specified above, during orbital temperature cycling.

REMARKS

For both internal and external applications, the minimum thickness for opacity is 1.5 mil (PB-55 Method, Class A).

FLAT ABSORBERS (Continued)

MATERIAL	Fuller Black Silicone Paint (517-B-2)
SUBSTRATE	HM21A-T8 Magnesium, annealed (-0) magnesium and aluminum, titanium, stainless steels and superalloys, and any other rigid substrate capable of withstanding the cure cycle
MATERIAL DESCRIPTION	Lamp black pigment in silicone vehicle; cured by baking at 465°F

THERMOPHYSICAL PARAMETERS

Sample Temperature (°R)	Radiant Source	α	Tolerance	Data Source	Remarks
530	Sun	0.89	±0.05	A	-

Sample Temperature (°R)	ϵ	Tolerance	Data Source	Remarks
530	0.88	±0.05	B, E	-

ENVIRONMENTAL BEHAVIOR

Prelaunch

Requires protection from contamination.

Postlaunch

Ascent. Adhesion, α_s and ϵ are unaffected by ascent-heating histories with peak temperatures $\leq$1070°F. The material has not been evaluated at higher temperatures.

Orbital. In tests simulating exposure to extraterrestrial solar near-ultraviolet energy in vacuum, changes in α_s of 0.05 or less were observed after 600 "sun-hours." It is suspected that even changes as small as 0.05 may not be real. Simulated orbital thermal-cycling tests were performed on white silicone paint (Fuller 517-W-1). Results observed during cycling tests with 12 to 15-minute periods in a vacuum of 10^{-5} mm Hg are shown in Table 7-1.

FLAT ABSORBERS (Continued)

REMARKS

These results are interpreted as demonstrating the behavior of all approved Fuller silicone thermal-control paints during orbital thermal cycling. For both internal and external application, the minimum thickness for opacity is 1.0 mil (PB-55 Method 5, Class C).

FLAT ABSORBERS (Continued)

MATERIAL	Rokide C
SUBSTRATE	René 41 with a two-mil coating of nichrome
MATERIAL DESCRIPTION	Rokide C is essentially chromic oxide (85 percent Cr_2O_3), flame sprayed by Norton Abrasive Company

THERMOPHYSICAL PARAMETERS

Sample Temperature (°R)	Radiant Source	α	Tolerance	Data Source	Remarks
530	Sun	0.90	±0.04	A	-
530	2100°R blackbody	0.84	±0.04	B	
530	1500°R blackbody	0.84	±0.04	B	
530	800°R blackbody	0.82	±0.04	B	

Sample Temperature (°R)	ε	Tolerance	Data Source	Remarks
400	0.85	±0.04	C, B	See Fig. 7-9
600	0.85	±0.04	C, B	
800	0.85	±0.04	C, B	
1,000	0.86	±0.04	C	
1,300	0.86	±0.04	C	
1,600	0.86	±0.04	C	
1,900	0.86	±0.04	C	
2,100	0.86	±0.04	C	

ENVIRONMENTAL BEHAVIOR

Prelaunch

The Rokide-C coating is extremely hard and is very inert chemically. Consequently, no problem with the prelaunch environment is anticipated.

Postlaunch

There is no degradation of optical properties resulting from ultraviolet exposure. Because of the differential in thermal expansion between typical oxide coating and metal substrates, there is always concern about the

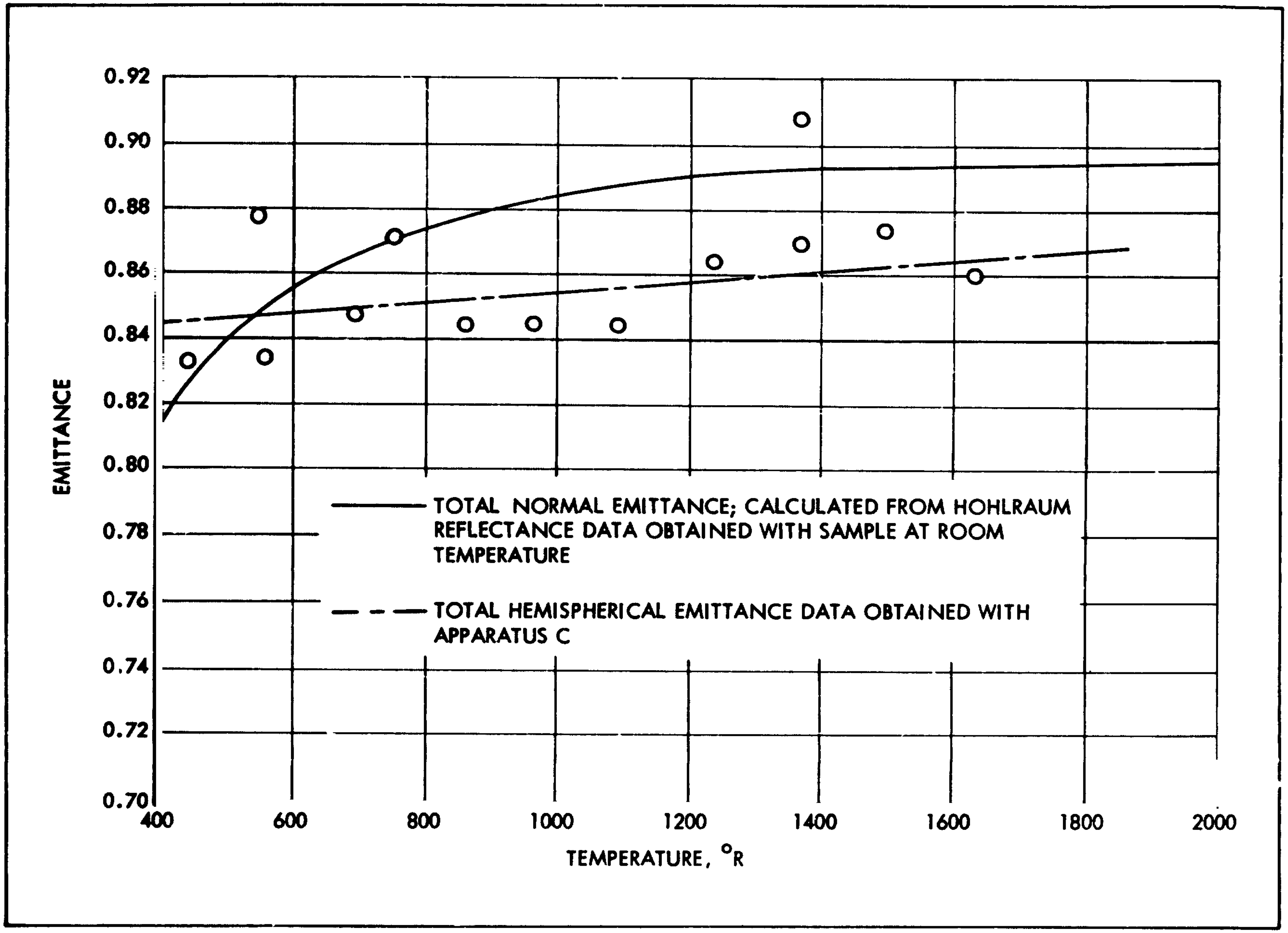

Figure 7-9. Emittance of Rokide C

FLAT ABSORBERS (Continued)

adhesion of such coatings during rapid changes of temperature. The René 41-nichrome-Rokide C combination thermal control system has been checked for possible thermal shock damage. Heating complex shapes to 2100°R within 5 minutes followed by a 5-minute cooling period has resulted in no coating failures.

REMARKS

The bonding between the substrate material, nichrome, and the Rokide C is purely mechanical. Rokide C may be used on other metallic substrates; however, thermal shock stability should always be checked experimentally for any new substrate. Because of the mechanical bonding requirement, all substrates must be grit blasted before coating application.

FLAT ABSORBERS (Continued)

MATERIAL Dow-17 Anodize on HM21A Magnesium Alloy

SUBSTRATE HM21A-T8 Magnesium Alloy Sheet

MATERIAL DESCRIPTION An anodic conversion coating for magnesium alloys - a proprietary process of the Dow Chemical Company

THERMOPHYSICAL PARAMETERS

Sample Temperature (°R)	Radiant Source	α	Tolerance	Data Source	Remarks
530	Sun	0.78	±0.08	A	-

Sample Temperature (°R)	ϵ	Tolerance	Data Source	Remarks
530	0.70	±0.06	B, E	-

ENVIRONMENTAL BEHAVIOR

Prelaunch

The surface is porous and requires protection from contamination.

Postlaunch

There are no unusual restrictions other than structural requirements of the substrate. Thermal stability above 500°F is in doubt.

REMARKS

The surface can be cleaned with most inert solvents.

FLAT REFLECTORS

MATERIAL Fuller Aluminum Silicone Paint (172-A-1)

SUBSTRATE HM21A-T8 Magnesium, annealed (-0) magnesium and aluminum, titanium, stainless steels and super alloys, and any other rigid substrate capable of withstanding the cure cycle

MATERIAL DESCRIPTION Leafing aluminum pigment in silicone vehicle; baked on at 465°F

THERMOPHYSICAL PARAMETERS

Sample Temperature (°R)	Radiant Source	α	Tolerance	Data Source	Remarks
530	Sun	0.25	±0.07	A, D	—

Sample Temperature (°R)	ϵ	Tolerance	Data Source	Remarks
530	0.28	±0.07	B, C, D, E	—

ENVIRONMENTAL BEHAVIOR

Prelaunch

Requires protection from contamination.

Postlaunch

Ascent. No change was observed in α_s and ϵ as a result of ascent heating with peak temperatures $\leq 885°F$.

Orbital. The primary source of degradation appears to be the near-ultraviolet portion of incident solar and albedo radiation. Present data indicate that α_s increases by $\Delta\alpha_s = 0.09 \pm 0.04$ after 600 "sun-hours"; ϵ is unaffected. Simulated orbital thermal-cycling tests were performed on white silicone paint (Fuller 517-W-1). The results observed during cycling tests with 12 to 15- minute periods at a vacuum of 10^{-5} mm Hg are shown in Table 7-1.

FLAT REFLECTORS (Continued)

REMARKS

These results are interpreted as showing the behavior of all approved Fuller silicone thermal-control paints during orbital thermal cycling. For internal applications, where emittance is the value of interest, a minimum thickness of 1.0 mil should be maintained (PB- 55 Method 5, Class C). For external sources, both α_s and ϵ are important. The minimum thickness for opacity is 3.0 mil (PB-55 Method 6, Class C).

FLAT REFLECTORS (Continued)

MATERIAL	Fuller Aluminum Silicone Paint (171-A-152)
SUBSTRATE	HM21A-T8 Magnesium, annealed (-0) magnesium and aluminum titanium, stainless steels, and super alloys, and any other rigid substrate capable of withstanding the cure cycle.
MATERIAL DESCRIPTION	Leafing aluminum pigment in silicone vehicle; baked on at 465°F

THERMOPHYSICAL PARAMETERS

Sample Temperature (°R)	Radiant Source	α	Tolerance	Data Source	Remarks
530	Sun	0.22	±0.04	A, D	

Sample Temperature (°R)	ϵ	Tolerance	Data Source	Remarks
530	0.24	±0.04	B, C, D, E	

ENVIRONMENTAL BEHAVIOR

Prelaunch

Requires protection from contamination.

Postlaunch

Ascent. Ascent heating histories with peak temperatures $\leq$ 880°F cause an increase in α_s of 0.01 or less; ϵ is unaffected.

Orbital. The primary source of degradation appears to be the near-ultraviolet portion of incident solar and albedo radiation. Present data indicate that α_s increases by $\Delta\alpha_s = 0.09 \pm 0.04$ after 600 "sunhours"; ϵ is unaffected. The results observed during cycling tests with 12 to 15-minute periods at a vacuum of 10^{-5} mm Hg are shown in Table 7-1.

FLAT REFLECTORS (Continued)

REMARKS

These results are interpreted as showing the behavior of the stability of all approved Fuller silicone thermal-control paints during orbital thermal cycling.

For internal application, where emittance is the value of interest, a minimum thickness of 1.0 mil should be maintained (PB-55 Method 5 Class C). For external surfaces, where both α_s and ϵ are important, the minimum thickness for opacity is 3.0 mil (PB-55 Method 6, Class C).

FLAT REFLECTORS (Continued)

MATERIAL	Nonleafing Aluminum Acrylic Paint
SUBSTRATE	Any clean substrate; primer required
MATERIAL DESCRIPTION	Room-temperature cured flat acrylic-based aluminum paint

THERMOPHYSICAL PARAMETERS

Sample Temperature (°R)	Radiant Source	α	Tolerance	Data Source	Remarks
530	Sun	0.38- 0.52	—	A, D	Prepared per PB-55
530	Sun	0.41	±0.03	A	Prepared per PB-55 controlled with OSC[(a)]

Sample Temperature (°R)	ϵ	Tolerance	Data Source	Remarks
530	0.36-0.58	—	B, D, E	Prepared per PB-55
530	0.48	±0.05	E	Prepared per PB-55 controlled with OSC[(a)]

(a) OSC = Optical Surface Comparator (Lion Research Corp.)

ENVIRONMENTAL BEHAVIOR

Prelaunch

The surface is porous and requires protection from contamination.

Postlaunch

Ascent. This material requires a minimum of 14 days of room-temperature curing to remove volatile materials sufficiently to minimize blistering during ascent heating. The affect of ascent heating is shown in Fig. 7-10 where α_s at room temperature is plotted as a function of the peak temperature experienced during ascent heating.

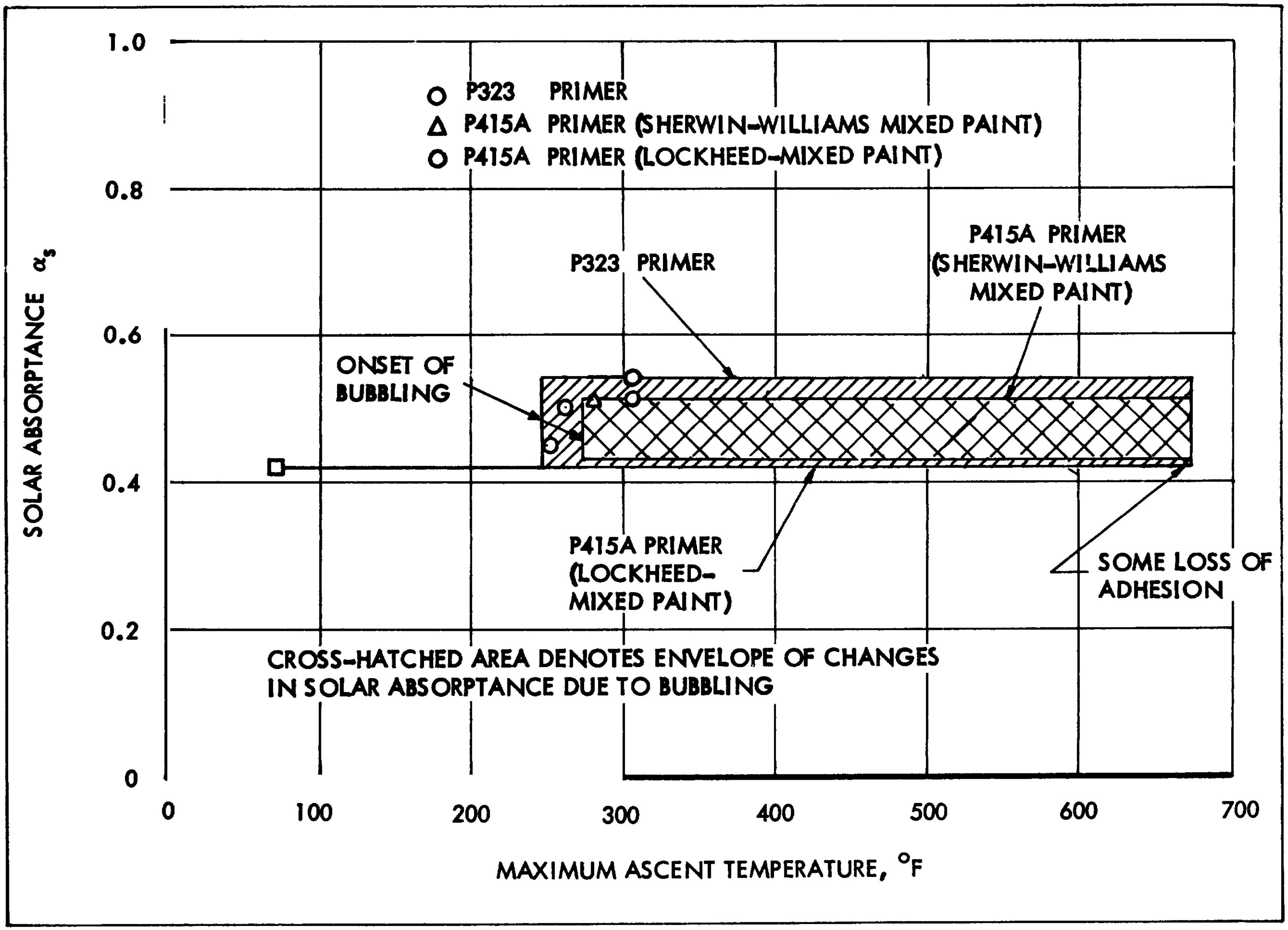

Figure 7-10. Effect of Ascent Heating on Solar Absorptance of Sherwin-Williams Non-leafing Aluminum Acrylic Paint

FLAT REFLECTORS (Continued)

Time held at peak temperatures and ambient pressures are as indicated. At peak temperatures less than 650°F, the most serious stability problem is caused by outgassing or bubbling of the surface. Bubble height ≤0.015 in.; bubble diameter ≤0.04 in. Bubbling commenced at temperatures of 245°F and above. The material may be used in locations where maximum temperatures encountered during ascent are less than 650°F, provided the alteration in surface finish and solar absorptance due to bubbling discussed herein and shown in Fig. 7-10 can be tolerated. If no change in surface finish or solar absorptance is allowable, the maximum temperature allowable must be less than 240°F.

The following half-cylinder specimens successfully survived 385 temperature cycles between 150 and 70°F with an 18-minute cycling period in a vacuum of 10^{-5} mm Hg.

- White Kemacryl Lacquer (Sherwin-Williams M49WC17) 3.0 to 4.0 mil thick over one coat pretreatment primer P40GC1; or Dow 17 on HM21 magnesium alloy
- The same coating system as above on a 6061-aluminum alloy substrate.

No serious flaking, cracking, or loss of adhesion was observed. The results are interpreted as demonstrating the behavior of Kemacryl-base paints on the substrates specified above, during orbital temperature cycling.

REMARKS

For internal applications, where emittance is the value of interest, a minimum thickness of 1.0 mil should be maintained (PB-55 Method I, Class A). For external surfaces where both α_s and ϵ values are important, the minimum thickness for opacity is 3.0 mil (PB-55 Method II Class A). This material is mixed at LMSC per PB-55. The base is Sherwin-Williams Kemacryl clear acrylic vehicle and the pigment is aluminum paste.

REFERENCES

7-1. Gaumer, R.E. and L.A. McKellar — Thermal Radiative Control Surfaces for Spacecraft, Lockheed Missiles and Space Company Report 704014, March 1961

7-2. Thermophysics Design Handbook, Lockheed Missiles and Space Company Report LMSC-8-55-63-3, July 1963

7-3. Space Systems Process Bulletins, Lockheed Missiles and Space Company, 1 October 1964

BLANK PAGE

VIII - THERMAL PROPERTIES OF PROPELLANTS AND PRESSURANTS

PROPERTIES OF LIQUIDS

The following physical properties of liquids were sought for five oxidizers, five fuels, two pressurants, and two typical test fluids:

- Specific Gravity
- Vapor Pressure
- Viscosity
- Specific Heat
- Thermal Conductivity
- Heat of Vaporization
- Surface Tension

Wherever data were available, a chart was drawn to show the variation of the liquid property with temperature from the freezing point to the critical temperature. From these charts it was then possible to derive the minimum number of point pairs to encompass all the data in tabular form within the 5% accuracy desired for the thermal properties library (Section XI). Table 8-1 indicates the figures and tables of physical properties prepared for the 14 liquids. In a few cases, as indicated, only a single value at one temperature, or no data, could be found in the literature search. Table 8-1 also indicates each reference source from which the data were obtained. A convenient summary of physical properties of all fourteen liquids is provided in Table 8-2. Where the liquid is cryogenic, with critical temperature below 77°F, the normal boiling point at atmospheric pressure is the temperature selected for properties in this table. The properties of storable liquids, whose critical temperatures are well above 77°F, are listed at 77°F. For a few exceptions the temperature for the property measurement is shown in parenthesis.

In general, all estimated or extrapolated data are indicated by dashed lines, which in most cases are taken from the chosen source. It is desirable to plot these liquid properties from freezing point to critical temperature. The available surface tension data for all these liquids were found to be simple linear relations with temperature. For each liquid a nearly straight line extrapolation was made to pass through zero surface tension at the critical temperature. A short straight line extrapolation was made to the freezing point also. This linear extrapolation in either direction could also be used where only a single surface tension measurement is available.

PROPERTIES OF GASES

The following physical properties of gases were sought for the two pressurants and the more volatile propellants:

- Compressibility Factor
- Specific Heat
- Thermal Conductivity

In the gas phase these properties are dependent on both pressure and temperature. It was not attempted to draw the complex family of curves to express this bivariant relationship in most cases. The point pairs were derived directly from available tabular data and charts. Table 8-1 indicates the tables of properties so derived and the reference sources. Again, data for only one pressure, or sometimes no data, were found for the property. The vapor properties of 50:50 UDMH:hydrazine, of monomethyl hydrazine, and of Hybaline A-5 were omitted on account of the low vapor pressure of these liquids in comparison with the operating pressures to be obtained with the pressurant gas.

SELECTION OF DATA

The 1963 report by Stanford Research Institute (Ref. 8-3) was a useful initial reference for the gaseous and liquid properties of nitrogen, helium, hydrogen, oxygen, nitrogen tetroxide and chlorine triflouride. Comparisons were made however, with other published data, particularly with data measurements and correlations reported most recently by the National Bureau of Standards. Preference was given to the NBS data, because they represent the most careful assessments and the most consistent correlations of physical properties. The most nearly complete information on properties was found for nitrogen, helium, hydrogen and oxygen, which have been most studied. Somewhat incomplete information was obtained for all the other fluids, for which the properties have hitherto been of less interest in the laboratory.

TABLE 8-1

PROPELLANT AND PRESSURANT DATA STATUS AND SOURCES

	LIQUID PROPERTIES							GAS PROPERTIES		
	Specific Gravity	Vapor Pressure	Viscosity	Specific Heat	Thermal Conductivity	Heat of Vaporization	Surface Tension	Compressibility Factor	Specific Heat	Thermal Conductivity
OXIDIZERS										
Nitrogen Tetroxide	F8-1 (8-4)	F8-2 (8-4)	F8-3 (8-4)	F8-4 (8-8)	F8-5 (8-4)	P (8-4)	P (8-4)	T8-4 (8-16)	F8-6 (8-4)	F8-7 (8-4)
Oxygen	F8-8 (8-20)	F8-9 (8-20,2)	F8-10 (8-2)	F8-11 (8-20)	F8-12 (8-2)	F8-13 (8-20,3)	F8-14 (8-6)	T8-5 (8-20)	T8-6 (8-20)	T8-7 (8-2)
Fluorine	F8-15 (8-11)	F8-16 (8-23,6)	F8-17 (8-5,2)	F8-18 (8-11)	F8-19 (8-5)	F8-20 (8-23,2)	F8-21 (8-2)	NA -	F8-22 (8-2)	T8-8 (8-2)
Oxygen Difluoride	F8-23 (8-10)	F8-24 (8-10)	F8-25 (8-10)	P (8-6)	F8-26 (8-6)	P (8-10)	NA -	NA -	T8-9 (8-13)	NA -
Chlorine Trifluoride	F8-27 (8-25,5)	F8-28 (8-25,5)	F8-29 (8-26,6)	F8-30 (8-25,5)	F8-31 (8-5)	P (8-5,6)	F8-32 (8-26)	P (8-6)	T8-10 (8-13)	NA -
FUELS										
50:50 Hydrazine, UDMH	F8-33 (8-7)	F8-34 (8-7)	F8-35 (8-7)	F8-36 (8-8,5)	F8-37 (8-28)	P (8-7)	P (8-28)	NR -	NR -	NR -
Monomethyl Hydrazine	F8-38 (8-5)	F8-39 (8-5,28)	F8-40 (8-12,6,5)	F8-41 (8-12)	F8-42 (8-5)	P (8-12)	F8-43 (8-29)	NR -	NR -	NR -
Diborane	F8-44 (8-9)	F8-45 (8-9)	F8-46 (8-9)	F8-47 (8-28,5)	F8-48 (8-5)	P (8-9)	NA -	NA -	T8-11 (8-13)	NA -
Hydrogen	F8-49 (8-15)	F8-50 (8-15)	F8-51 (8-14)	F8-52 (8-22)	F8-53 (8-14)	F8-54 (8-15)	F8-55 (8-2)	T8-12 (8-1)	T8-13 (8-2)	T8-14 (8-2)
Hybaline A-5	F8-56 (8-28)	F8-57 (8-28)	F8-58 (8-28)	F8-59 (8-28)	F8-60 (8-28)	NA -	NA -	NR -	NR -	NR -
PRESSURANTS										
Nitrogen	F8-61 (8-24,3)	F8-62 (8-24,23)	F8-63 (8-3)	F8-64 (8-24)	F8-65 (8-3)	F8-66 (8-24,23,3)	F8-67 (8-3)	T8-15 (8-24)	T8-16 (8-24)	T8-17 (8-1)
Helium	F8-68 (8-19,3)	F8-69 (8-19,3)	F8-70 (8-3)	F8-71 (8-3)	F8-72 (8-3)	F8-73 (8-3)	F8-74 (8-3)	T8-18 (8-18,19)	T8-19 (8-19,3)	T8-20 (8-3)

TABLE 8-1 (Continued)

	LIQUID PROPERTIES							GAS PROPERTIES		
	Specific Gravity	Vapor Pressure	Viscosity	Specific Heat	Thermal Conductivity	Heat of Vaporization	Surface Tension	Compressibility Factor	Specific Heat	Thermal Conductivity
TEST FLUIDS										
Freon 11	T8-21 (8-30)	T8-21 (8-30)	T8-21 (8-30)	T8-21 (8-30)	T8-21 (8-30)	T8-21 (8-30)	T8-21 (8-30)	T8-22 (8-30)	T8-23 (8-30)	T8-24 (8-30)
60% **Ethylene Glycol**	T8-25 (8-31)	T8-25 (8-31)	T8-25 (8-31)	T8-25 (8-31)	T8-25 (8-31)	T8-25 (8-31)	T8-25 (8-31)	NR -	NR -	NR -

NOTE: Figures and tables are denoted by F and T, respectively; single point values are denoted by P; reference numbers are enclosed in parentheses; NA and NR denote data not available and data not required, respectively. Data denoted by P are shown in Table 8-2.

TABLE 8-2

SUMMARY OF PROPELLANT AND PRESSURANT PHYSICAL PROPERTIES

LIQUID	Storable or Cryogenic	Freezing Point	Boiling Point	Critical Temp.	Critical Press.	Density*	Vapor Pressure*	Viscosity*	Specific Heat*	Thermal Conductivity*	Heat of Vaporization*	Surface Tension*
	S or C	°F	°F	°F	psia	gm/cm^3	psia	lb/ft-sec x10^4	Btu/lb-°F	Btu/hr-ft-°F	Btu/lb	lb/ft x10^4
OXIDIZER												
Nitrogen Tetroxide	S	11.8	70.1	316.8	1469	1.43	17.5	2.7	0.37	0.075	178	17.9
Oxygen	C	-361.8	-297.4	-181.1	737	1.14	14.7	1.27	0.40	0.084	92	9.0
Fluorine	C	-363.3	-306.4	-200.6	808	1.51	14.7	1.60	0.37	0.162	71	9.3
Oxygen Difluoride	C	-370.9	-229.5	-75.5	728	1.53	14.7	1.80	0.35 (-260°F)	0.12	89	-
Chlorine Trifluoride	S	-107.1	53.2	345	838	1.80	24	2.77	0.31	0.13	128 (53°F)	15.6
FUEL												
50:50 Hydrazine	S	18.8	158.2	634	1696	0.90	2.7	5.4	0.69	0.13	426	20.4
Monomethyl Hydrazine	S	-62.3	189.2	609	1195	0.87	0.9	5.7	0.70	0.14	377	23.2
Diborane	C	-265.9	-134.5	62.1	581	0.43	14.7	0.9	0.67	0.061	222	-
Hydrogen	C	-434.8	-423.2	-400.3	188	0.071	14.7	0.090	2.3	0.070	191	1.32
Hybaline A-5	S	-59	Decomposes		-	0.73	0.06	42	0.64	0.10	-	-
PRESSURANT												
Nitrogen	C	-346	-320.4	-232.7	492	0.81	14.7	1.06	0.49	0.081	86	6.1
Helium	C	NONE	-452.1	-450.2	33.3	0.125	14.7	0.020	1.09	1.57	9.1	0.063
TEST FLUID												
Freon 11	S	-168	74.8	388.4	635	1.47	15.3	2.8	0.21	0.055	78	13
60:40 glycol:water	S	-65	232	-	-	1.07	21.2 (250°F)	29	0.745	0.227	-	-

* Properties at 77°F for storable liquid or at normal boiling point at 14.7 psia for cryogenic liquid unless otherwise noted.

PROPELLANT AND PRESSURANT PROPERTIES

Nitrogen Tetroxide

Both the liquid and the vapor of nitrogen tetroxide have exceptional physical properties due to the very rapid reactions to form or dissociate nitrogen tetroxide from or to nitrogen dioxide.

$$2NO_2 \rightleftharpoons N_2O_4 \qquad \Delta H_{77°F} = 271 \text{ Btu/lb}$$

Shock tube experiments have shown less than 1-μsec relaxation time to equilibrium at 77°F and at pressures from 4.0 to 14.7 psia. Table 8-3 shows the effects of temperature and pressure on the amount of dissociation.

TABLE 8-3

EQUILIBRIUM PERCENTAGE DISSOCIATION OF NITROGEN TETROXIDE VAPOR

	Temperature, °F				
Pressure, psia	68	104	140	176	212
7.35	19.5	38.7	66.0	85.0	93.7
14.7	15.8	31.0	50.4	73.8	88.0
73.4	7.2	15.1	28.2	46.7	66.5

$$\text{Percentage Dissociation} = \frac{P_{NO_2} \times 100}{P_{NO_2} + 2P_{N_2O_4}}$$

A profound effect of both the shift in equilibrium with temperature and the associated heat of reaction, is a sevenfold increase in the thermal conductivity of the vapor at 77°F and 14 psia, over the value for the vapor with frozen equilibrium. Under the same conditions the specific heat of the vapor is sixfold higher than it would be for frozen equilibrium. Of course, both pressure and temperature changes shift the equilibrium in the vapor, while temperature changes also shift the liquid equilibrium. The compressibility factor for the vapor is based on the molecular weight of 46.008 for nitrogen dioxide as in Reference 8-16. This factor then also reflects the degree of association to nitrogen tetroxide over all the range of pressures and temperatures in the point pair matrix for the compressibility factors. All other properties are based on unit weight, not molecular weight, and therefore do not involve calculation of the degree of association. All properties have to take account of shifting equilibrium. Furthermore, the properties of liquid nitrogen tetroxide, as for other volatile liquids, are for saturated liquid under its normal vapor pressure. Under the much higher pressures at a rocket injector the propellant liquids exhibit different physical properties. Although nitrogen tetroxide boils at 70°F at 14.7 psia, slightly below room temperature, it is considered fully storable. The critical pressure and temperature are 1469 psia and 317°F, respectively.

Chlorine Trifluoride

This liquid oxidizer combines high bulk density and high performance capability with storability. The critical pressure and temperature are 838 psia and 345°F, respectively. In the rocket engine the associated fuel usually serves as a regenerative coolant. If the fuel is carbonaceous, perchloryl fluoride may be added to the oxidizer to oxidize this carbon, and to avoid formation of carbon tetrafluoride (mol. wt. = 88) in the rocket.

50:50 Hydrazine—UDMH

This propellant also has exceptional properties because it is a solution of two hydrazines with wide differences, particularly in freezing points and in vapor pressures. It represents a convenient compromise, intended to reduce the high freezing point of pure hydrazine (35.1°F), as well as to improve thermal stability and to reduce the explosive nature of pure hydrazine. Mixing with about 50% UDMH (unsymmetrical dimethylhydrazine) accomplishes these purposes to some extent. It was not practical to use pure UDMH on account of its lower performance, or to use MMH (monomethyl hydrazine) on account of a delay in obtaining sufficient production. Addition of UDMH to hydrazine (50:50) reduces the freezing point to 18.8°F, stabilizes the fuel to higher temperatures, and noticeably raises the vapor pressure. The higher volatility of UDMH produces more than 90% UDMH content (molal) in the vapor phase above the propellant mixture at 77°F. Moreover, hydrazine gradually crystallizes out of the mixture from the initial 18.8°F freezing point over a downward range in temperature, unlike the complete solidification of pure hydrazine at 35.1°F. The properties of this mixed propellant were obtained from reports by Aerojet-General Corp. (References 8-5, 8-7), Bell Aerosystems (Reference 8-8) and from other material furnished by NASA (Reference 8-28)

Monomethyl Hydrazine (MMH)

This hydrazine derivative is a pure compound with freezing point of -62.3°F, boiling point of 188°F, and estimated critical pressure and temperature of 1195 psia and 609°F. Since it has not only a lower freezing point and a lower vapor pressure, but also matches the performance of the mixed hydrazines just discussed, the pure compound (MMH) is preferred as a fuel. The properties were derived from several of the same sources.

Hybaline A-5

This is an aluminum borohydride amine derivative with higher theoretical performance capability than the hydrazines. However, it has not been found possible to realize the performance increase in actual rocket engines, due to difficulties with inefficient combustion and expansion. There is also the added disadvantage of high cost of synthesis of this fuel. The physical properties of the liquid were derived from charts furnished by NASA (Reference 8-28). The vapor pressure of Hybaline A-5 and of the two hydrazine fuels is low enough to neglect the vapor phase contribution to the pressurant gas properties in the fuel tank.

Diborane

This high energy fuel has a low boiling point of -134.5°F, and critical pressure and temperature of 581 psia and 62°F, respectively. The "space-storable" propellant system of diborane with oxygen difluoride offers both high performance and high density. However, regenerative cooling is not feasible with either fuel or oxidizer, while the flame temperature is above 8000°F with 1000-psia chamber pressure. The properties of diborane were obtained from reports by Callery Chemical (Reference 8-9), Aerojet-General Corp. (Reference 8-5) and from NASA (Reference 8-28).

Cryogenic Pressurants and Propellants

As stated earlier, the physical properties of nitrogen, helium, hydrogen and oxygen were readily obtained from recent NBS publications, also from the NASA report (Reference 8-3). Less complete information was available for fluorine and oxygen difluoride for which the properties have been of interest more recently. The difficulty of working with highly corrosive fluids such as these has naturally been a deterrent to laboratory measurements.

Test Fluids

It is considered more economical, practical and safe for the heat transfer tests under the simulated space environment to prove out design analysis by using two test fluids with some important properties to match those of the real fuel and oxidizer, such as nitrogen tetroxide and 50:50 hydrazine:UDMH. Freon 11 and 60:40 ethylene glycol:water could be satisfactory substitutes for the respective liquid propellants. Therefore, the physical properties of the two liquids and of the vapor of Freon 11 are included in Table 8-2 and appropriate references in Table 8-1.

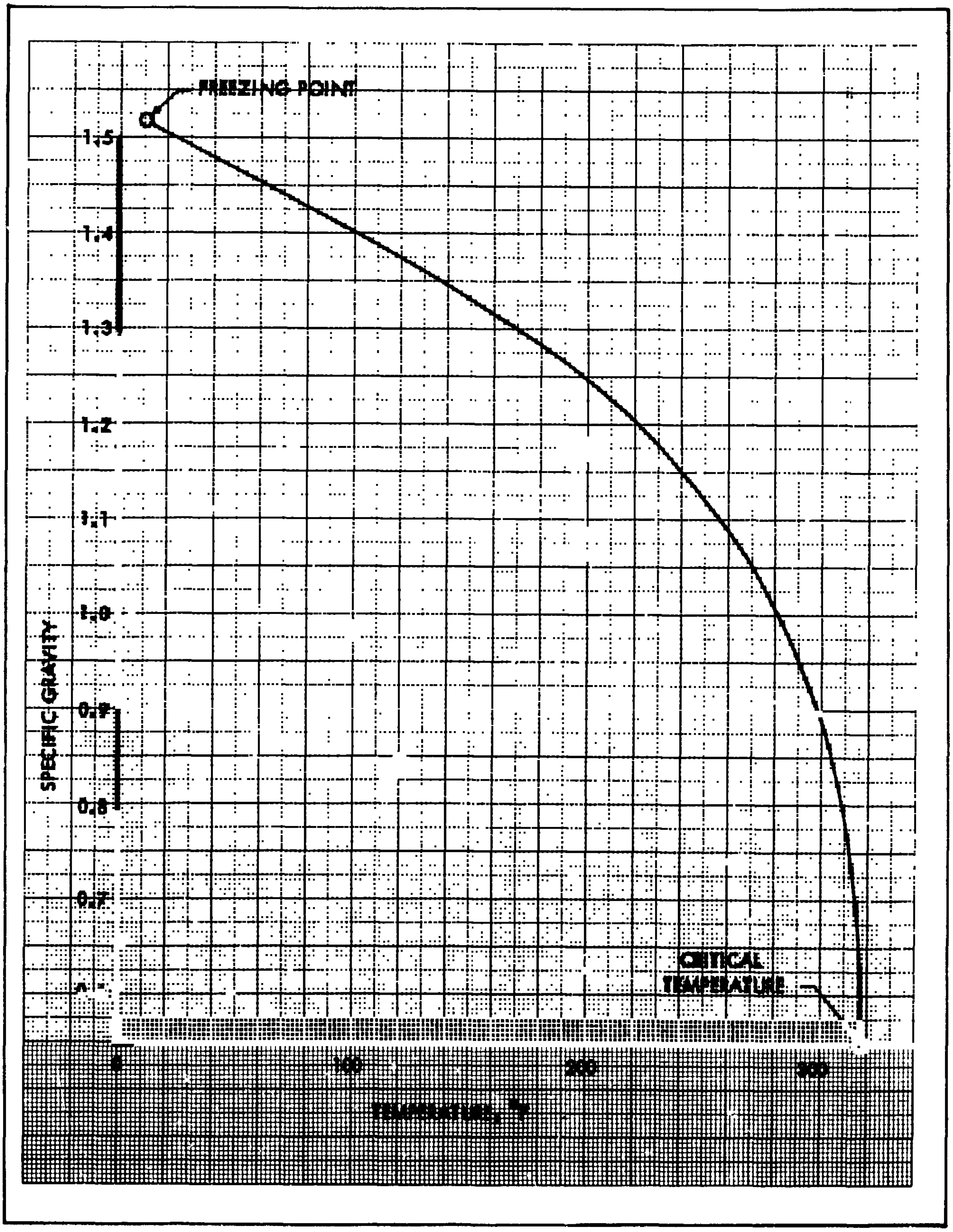

Figure 8-1. Liquid Nitrogen Tetroxide Specific Gravity vs Temperature

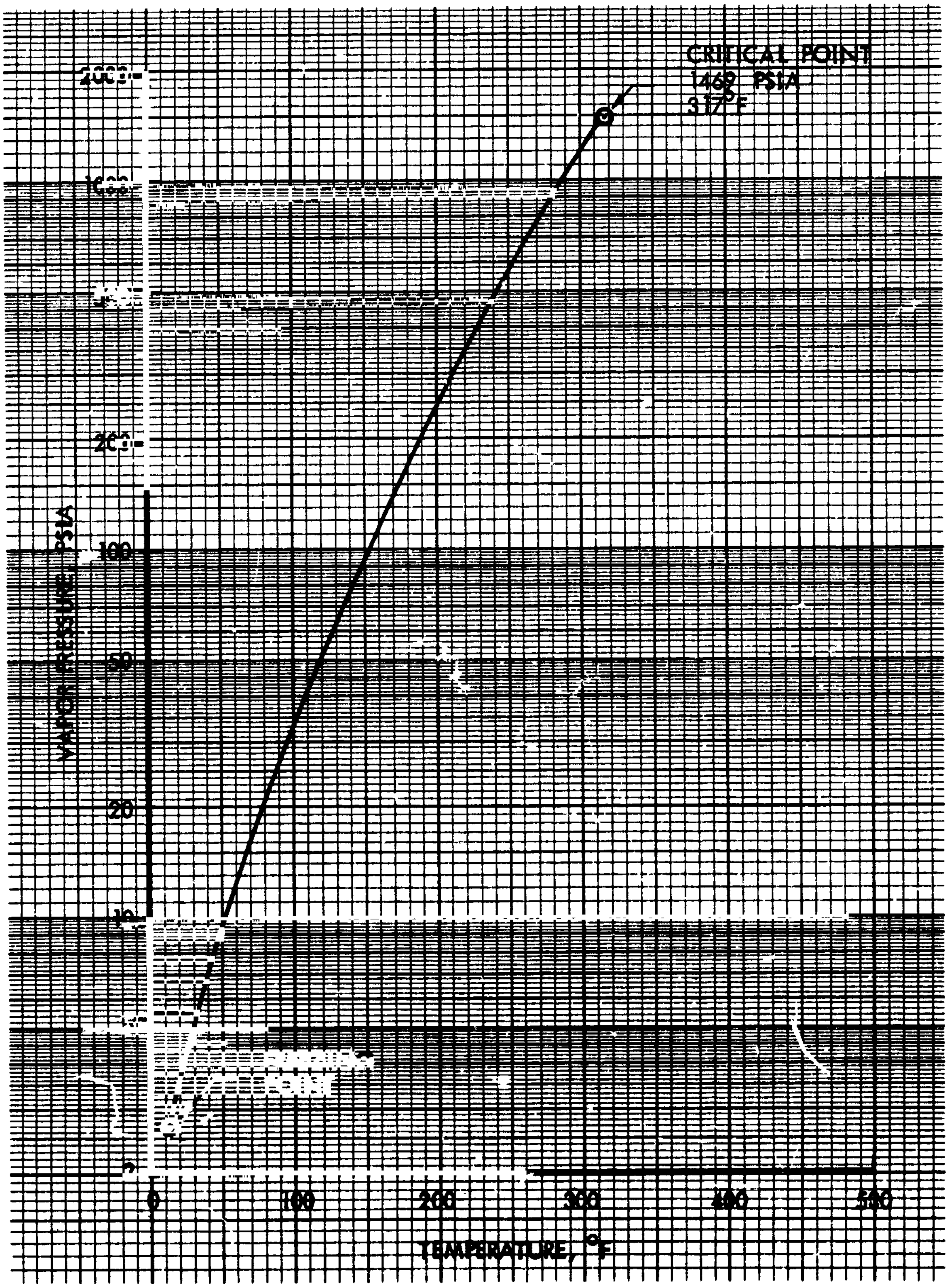

Figure 8-2. Liquid Nitrogen Tetroxide Vapor Pressure vs Temperature

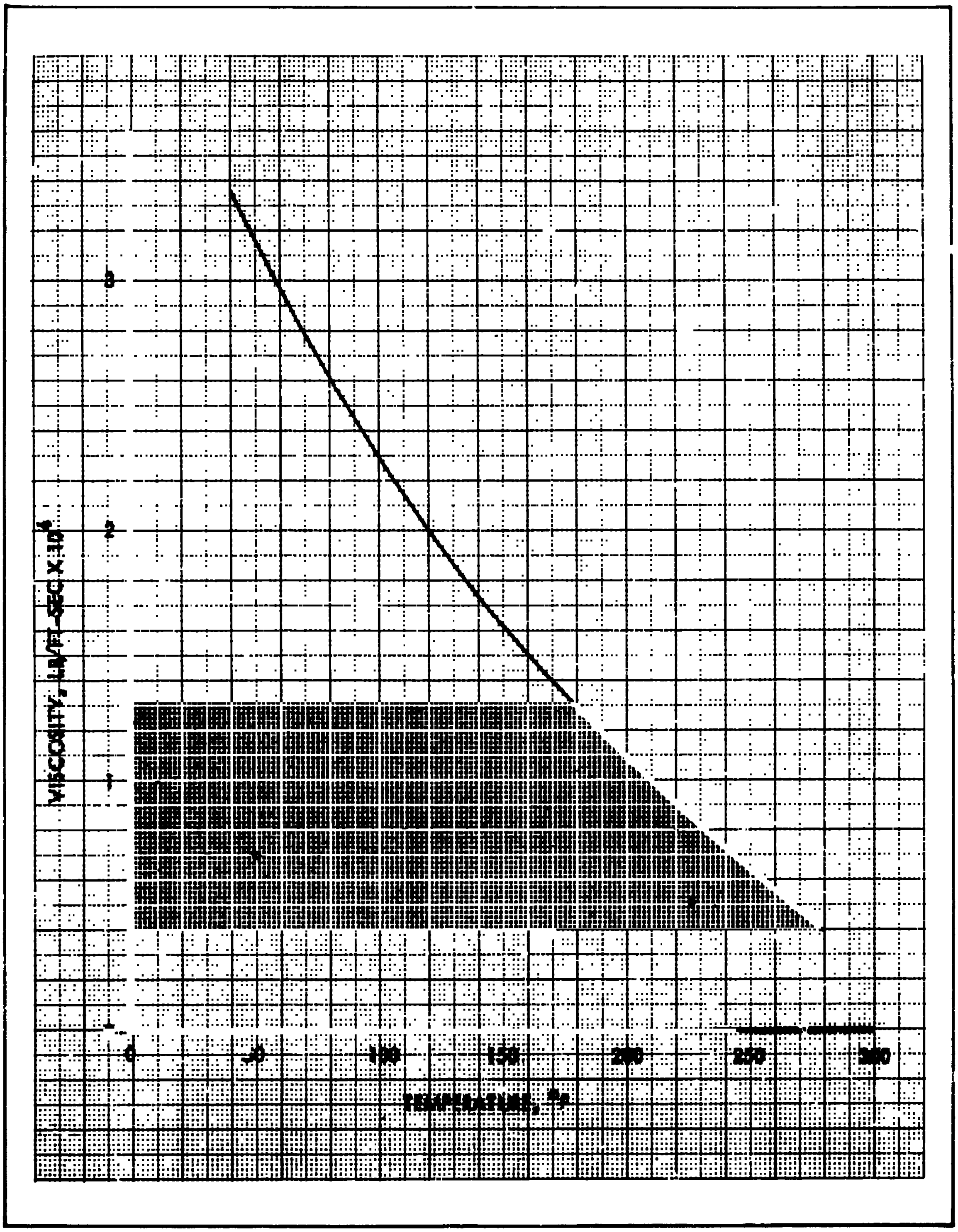

Figure 8-3. Liquid Nitrogen Tetroxide Viscosity vs Temperature

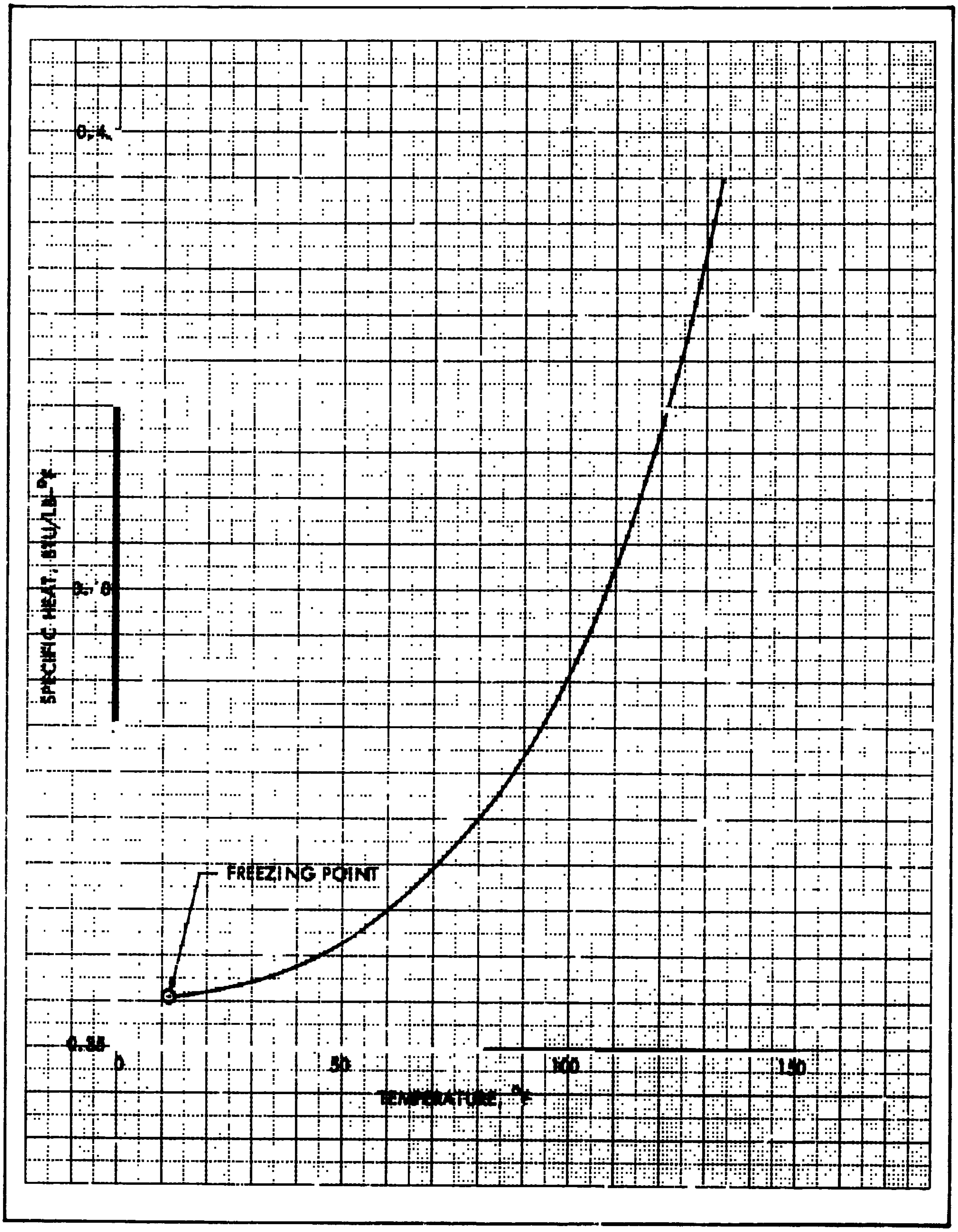

Figure 8-4. Liquid Nitrogen Tetroxide Specific Heat vs Temperature

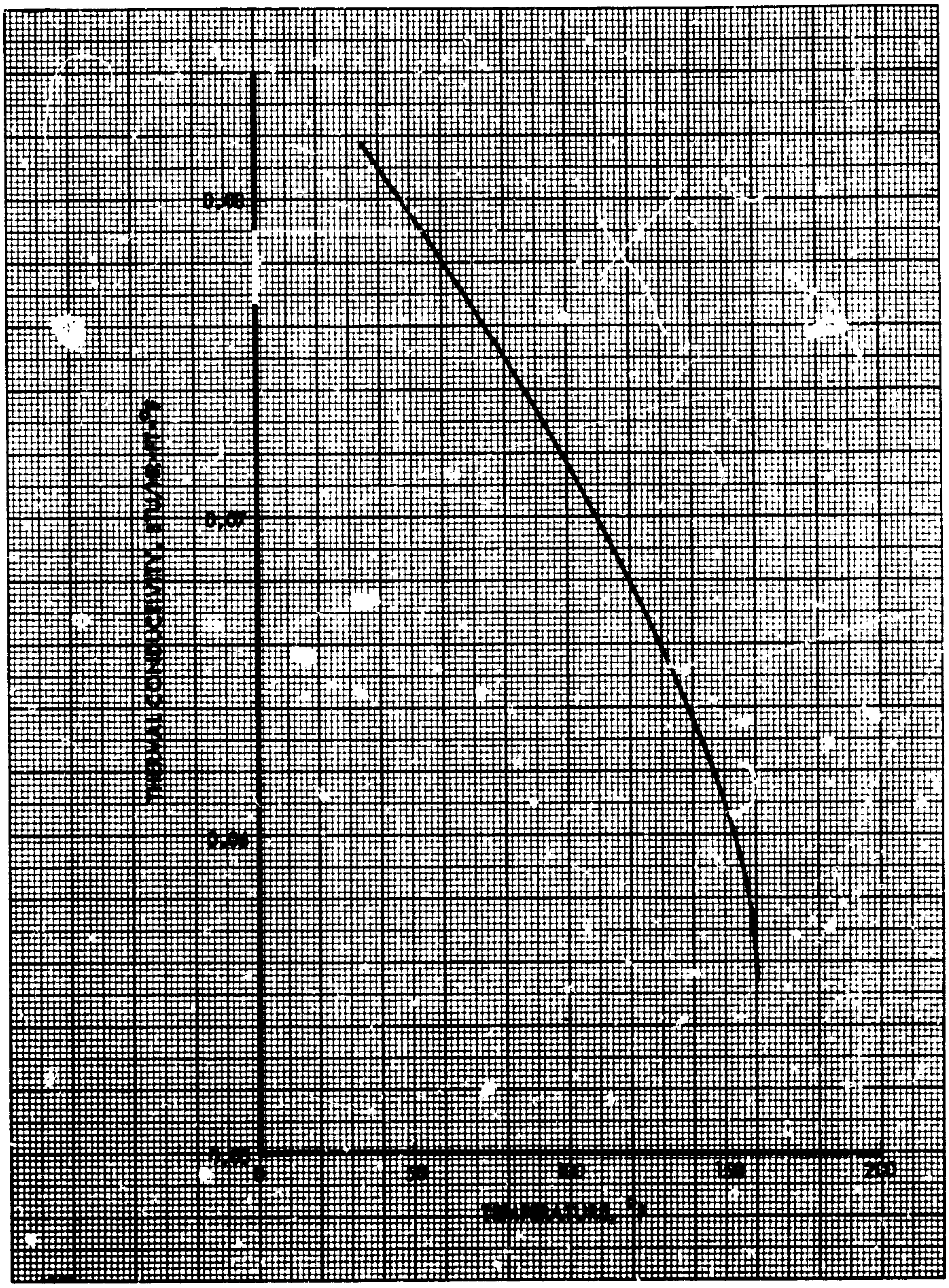

Figure 8-5. Liquid Nitrogen Tetroxide Thermal Conductivity vs Temperature

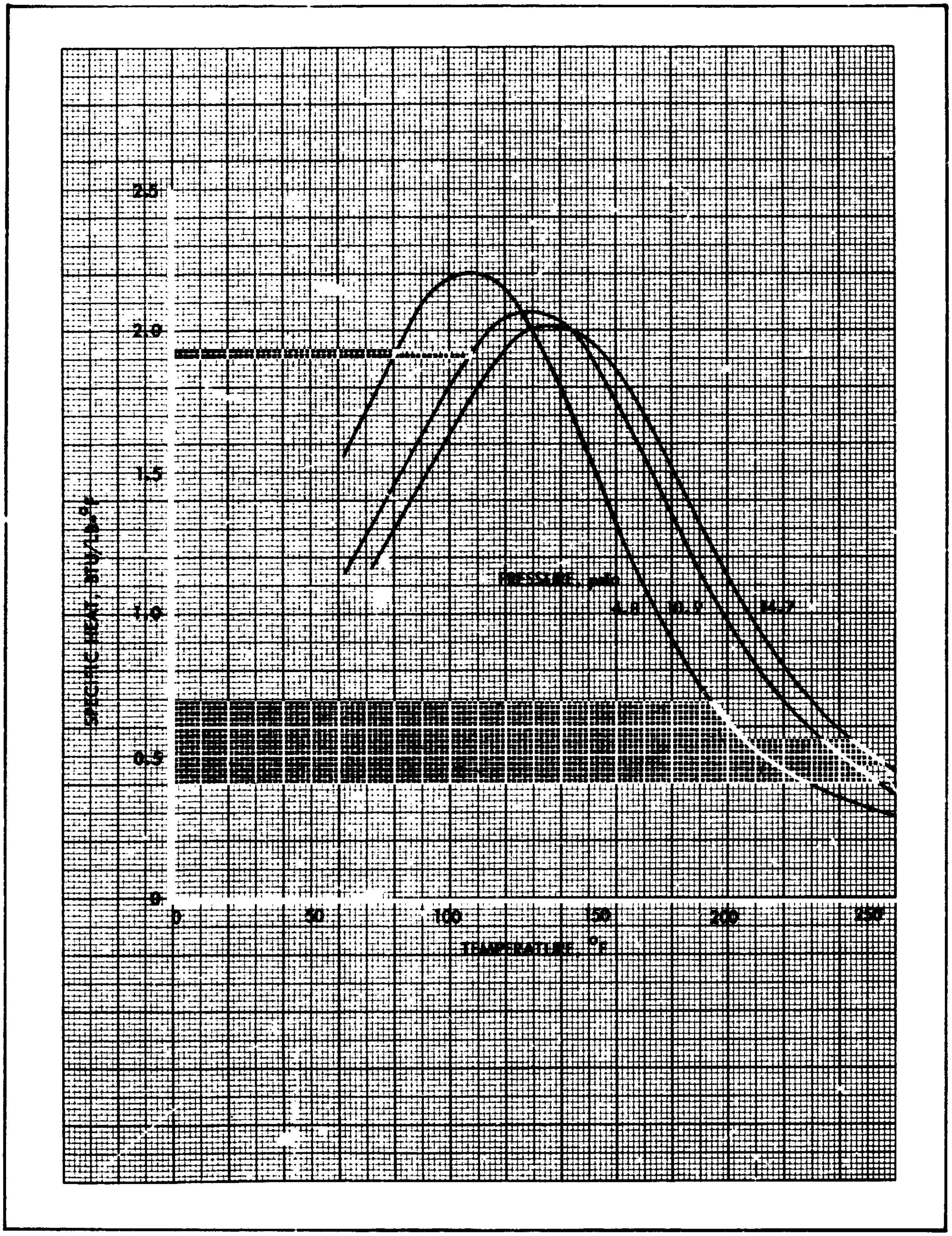

Figure 8-6. Nitrogen Tetroxide Gas Specific Heat vs Temperature

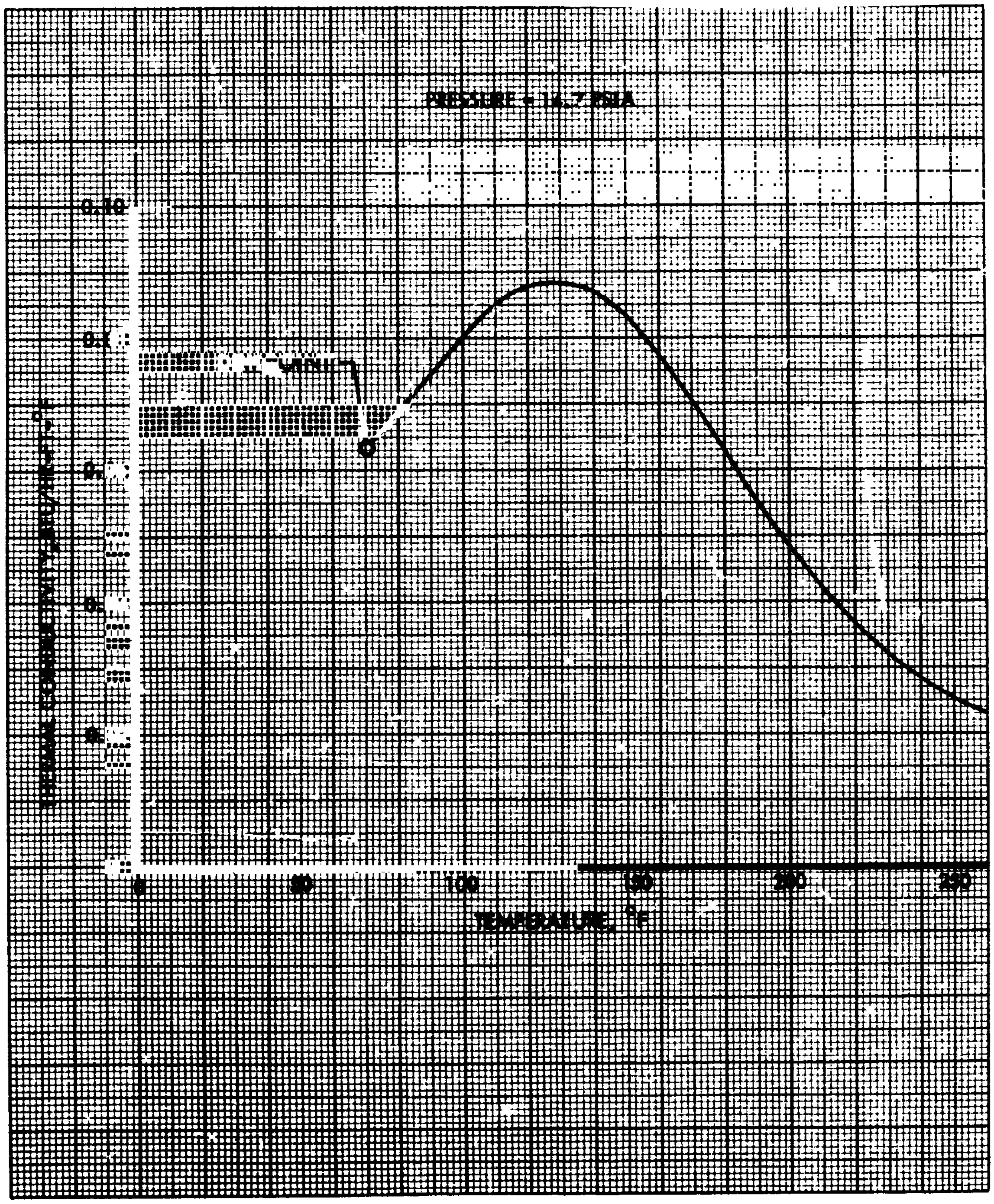

Figure 8-7. Nitrogen Tetroxide Gas Thermal Conductivity vs Temperature

TABLE 8-4

GASEOUS NITROGEN TETROXIDE COMPRESSIBILITY FACTOR
(BASIS M = 46.008)

	Temperature, °F					
Pressure, psia	70	100	130	160	190	220
14.7	.566	.640	.728	.830	.913	.957
20	L	.620	.698	.800	.889	.942
30		.594	.659	.755	.851	.917
40		L	.632	.722	.821	.894
50			.612	.695	.792	.872
60			.597	.673	.767	.855
80			L	.637	.725	.824
100				.609	.693	.797
125				L	.660	.768
150					.632	.742
200					L	.696
250						.653
300						.608

NOTE: $\frac{M}{R} = \frac{46.008}{10.7314} = 4.287$

$Z = \frac{M}{R} \frac{P}{\rho T}$

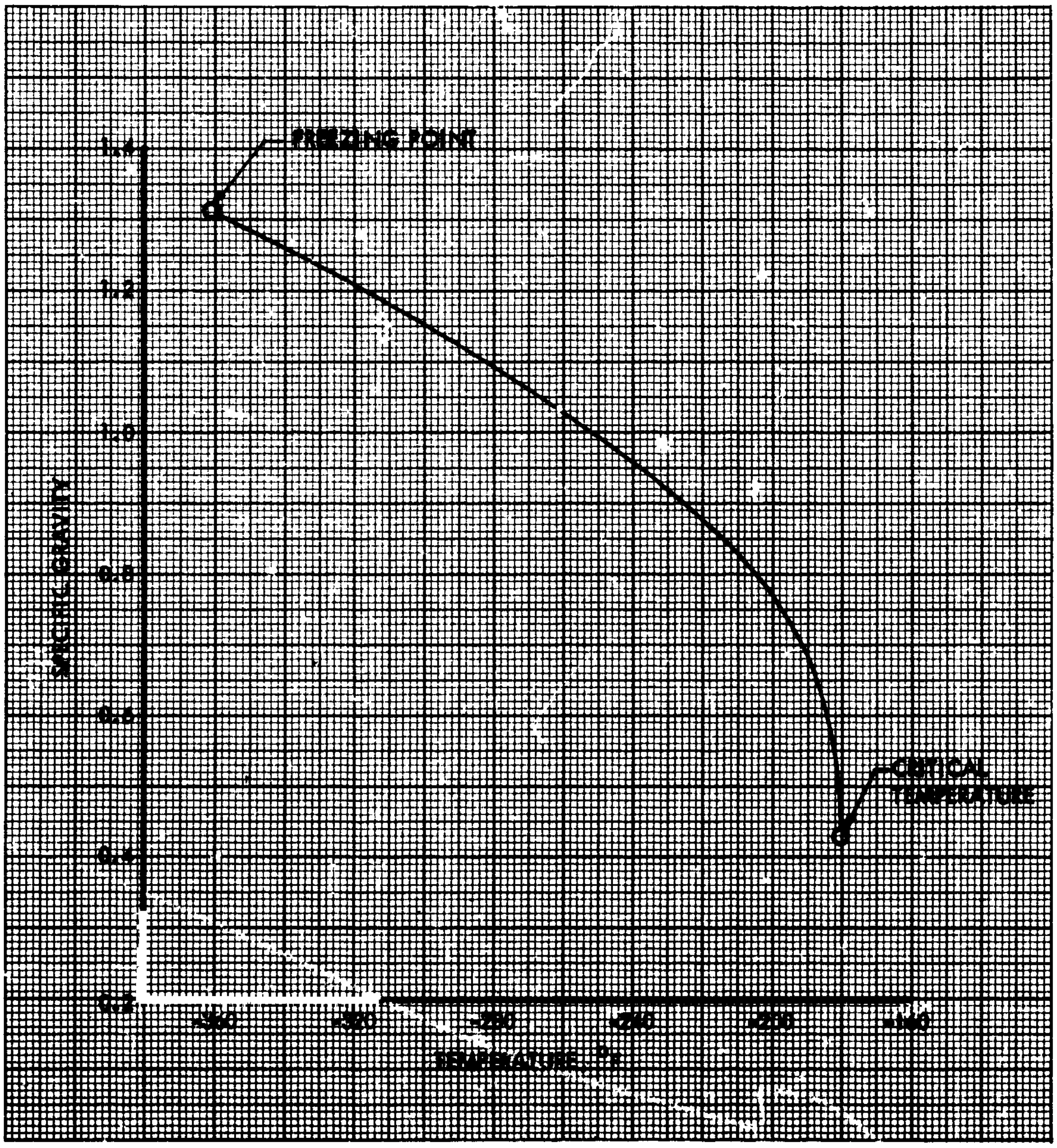

Figure 8-8. Liquid Oxygen Specific Gravity vs Temperature

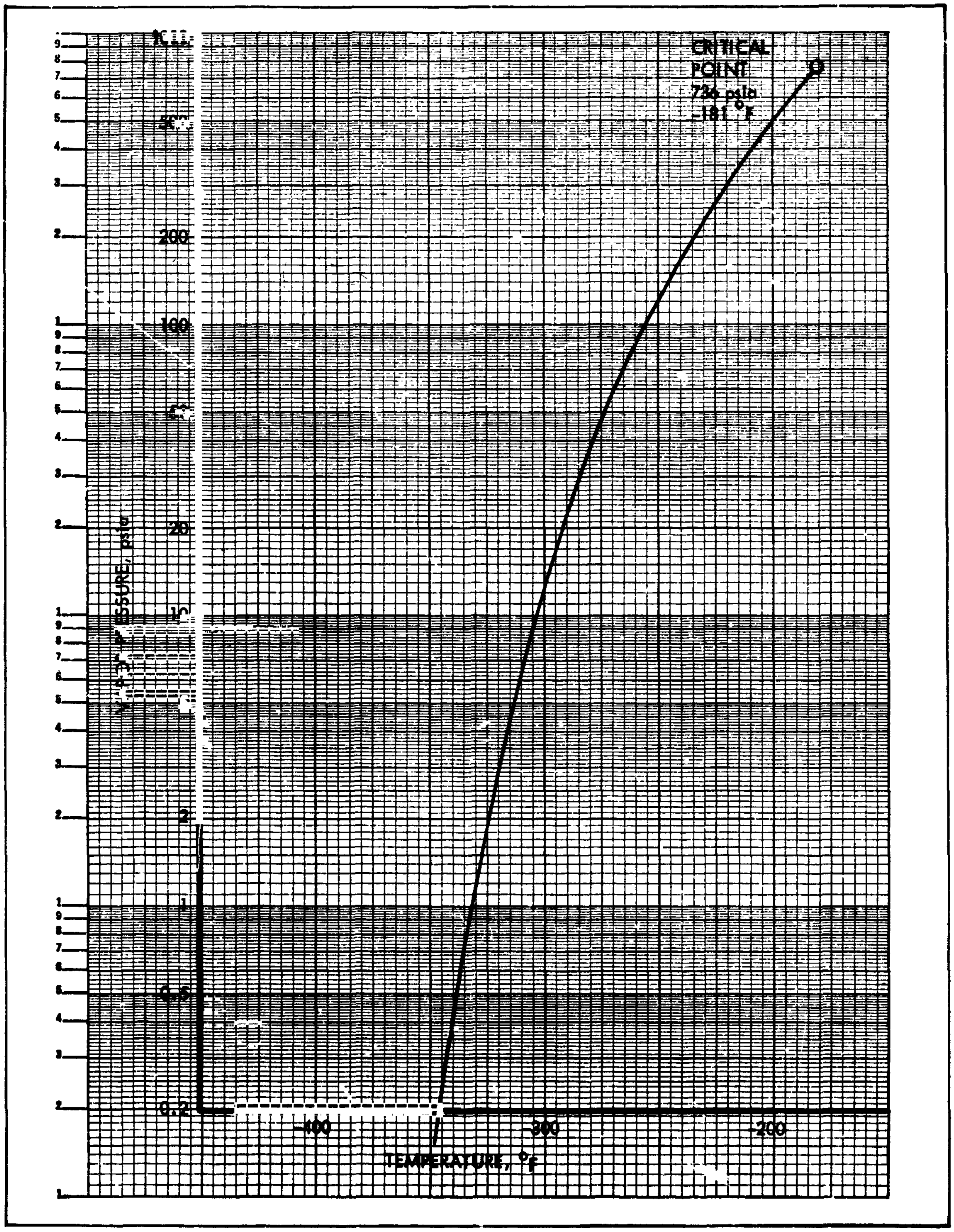

Figure 8-9. Liquid Oxygen Vapor Pressure vs Temperature

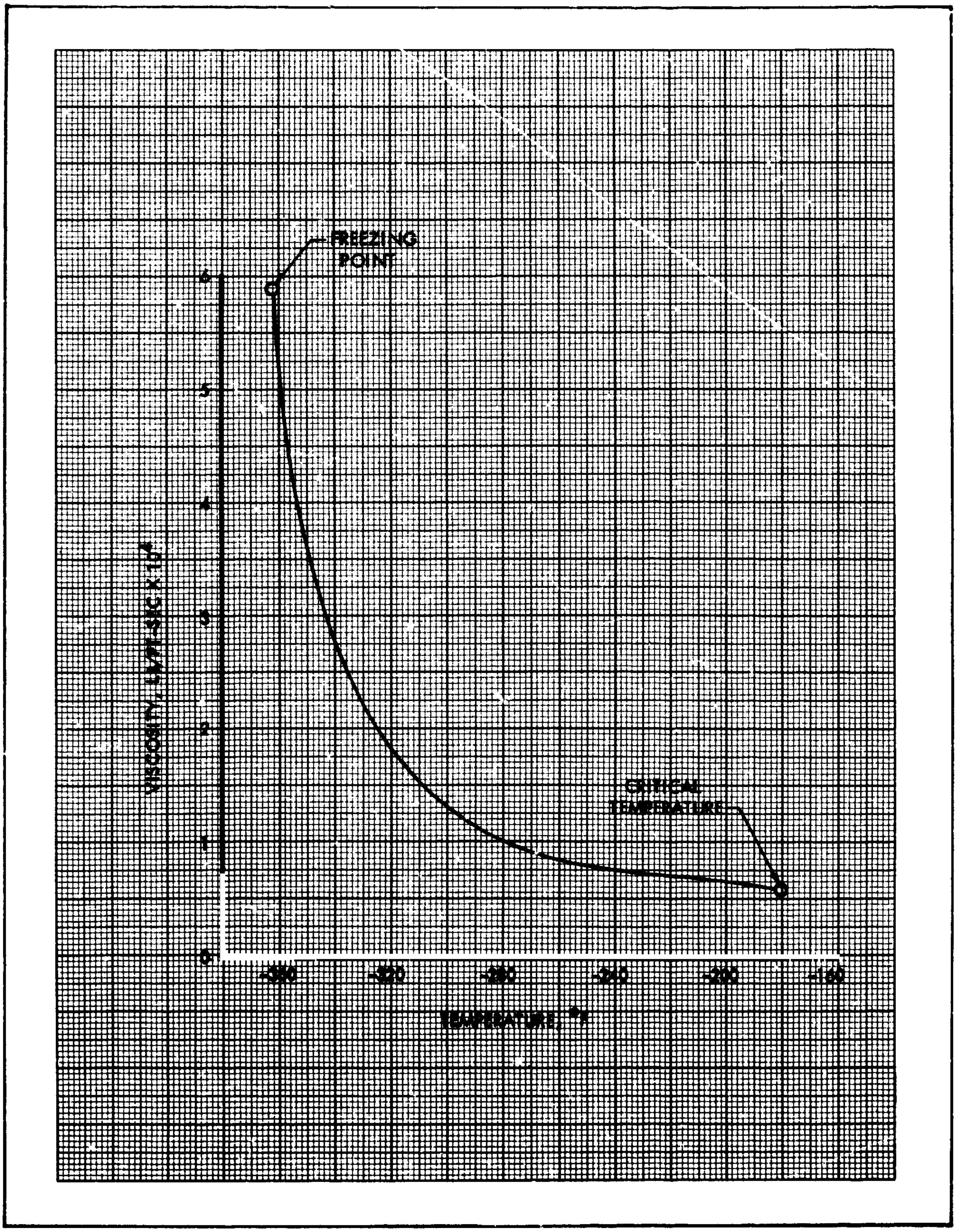

Figure 8-10. Liquid Oxygen Viscosity vs Temperature

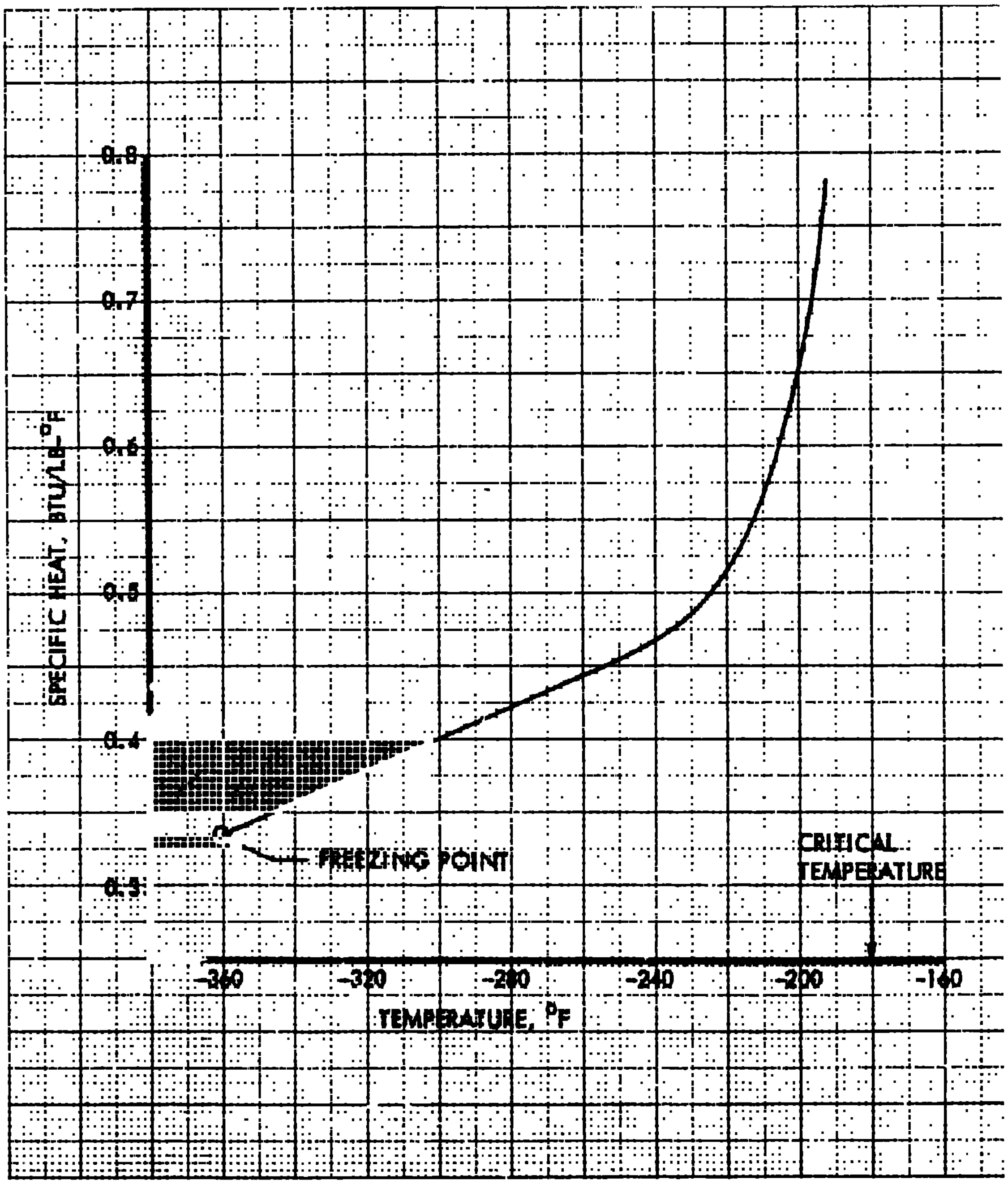

Figure 8-11. Liquid Oxygen Specific Heat vs Temperature

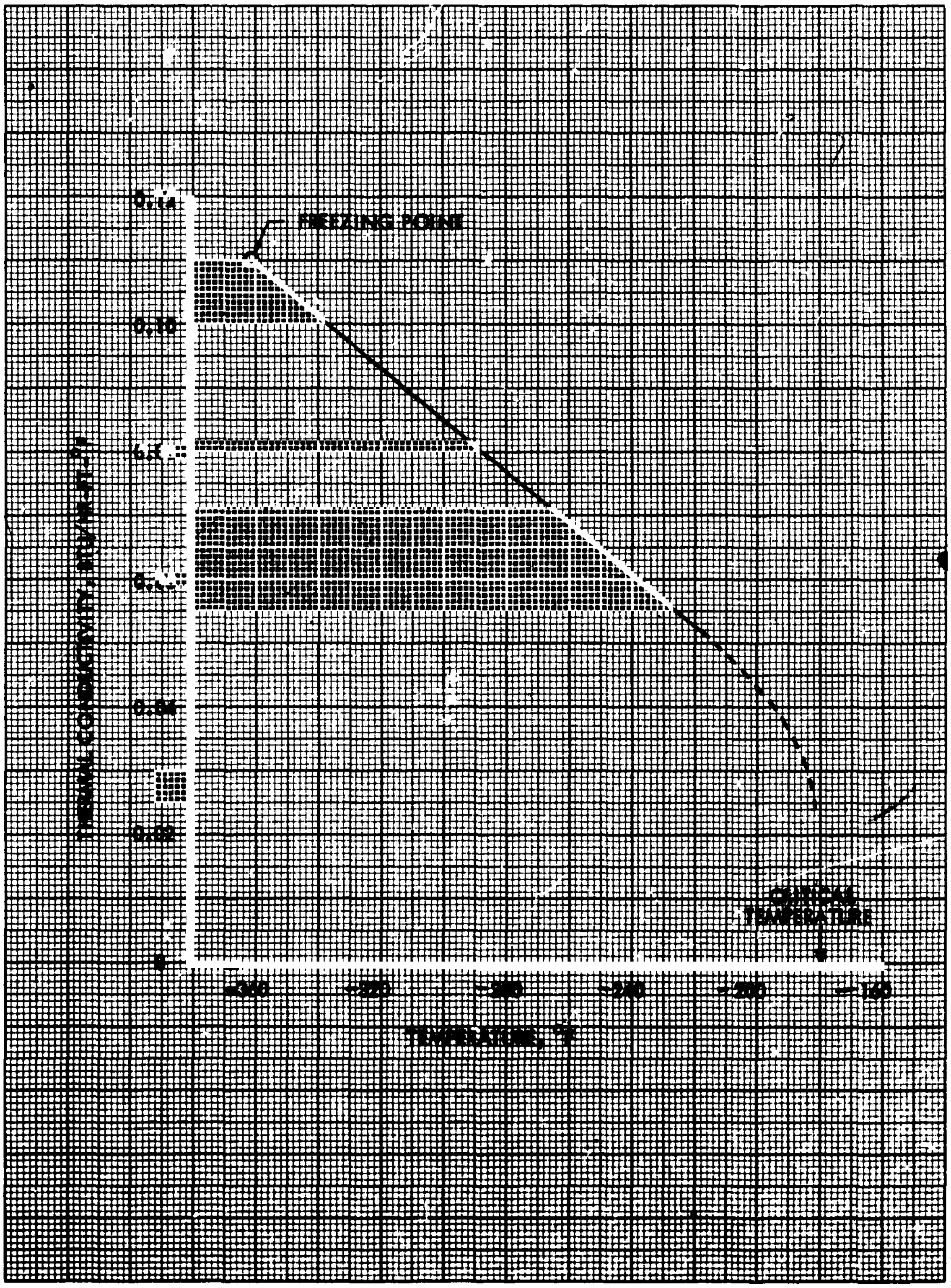

Figure 8-12. Liquid Oxygen Thermal Conductivity vs Temperature

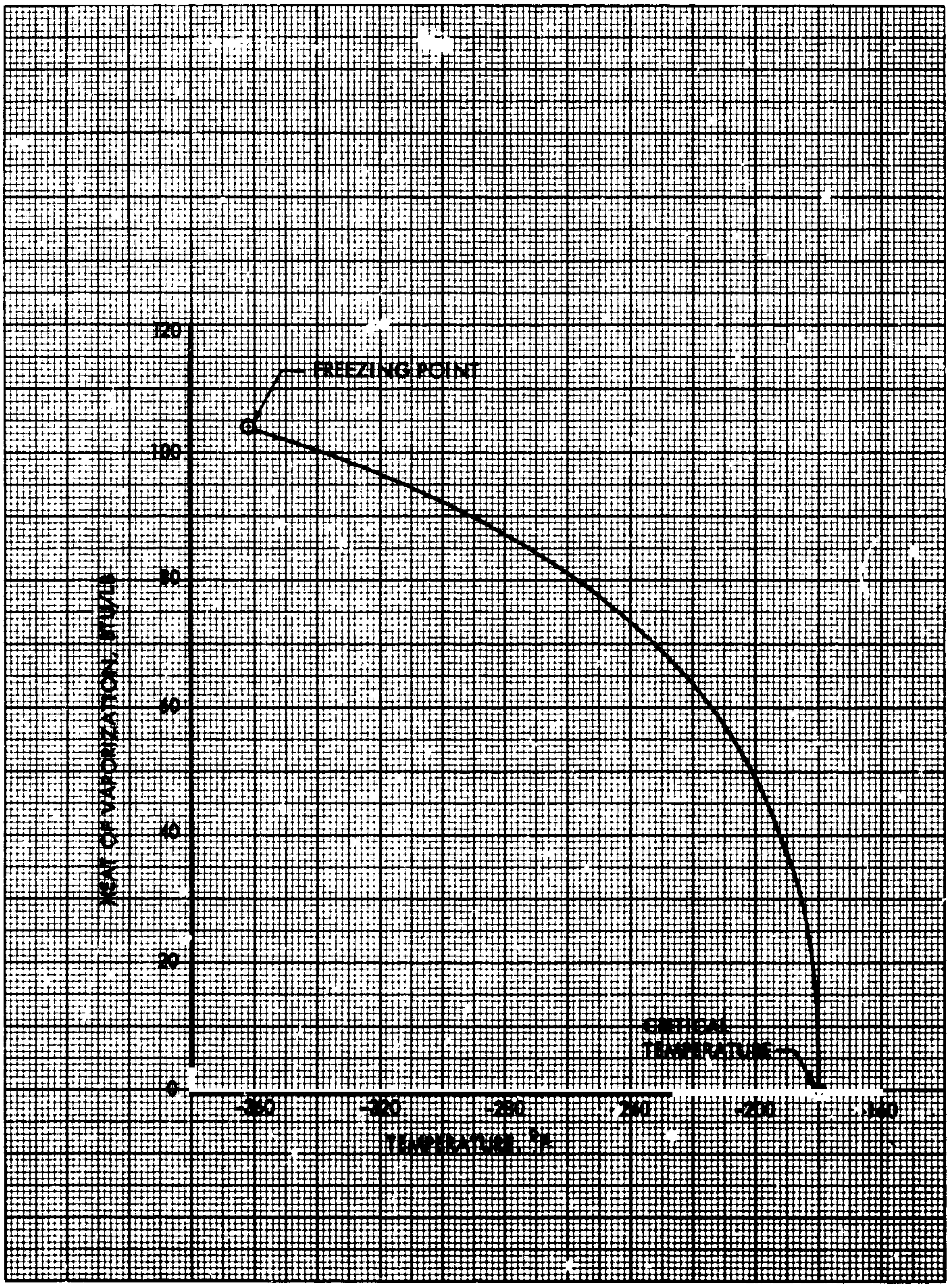

Figure 8-13. Liquid Oxygen Heat of Vaporization vs Temperature

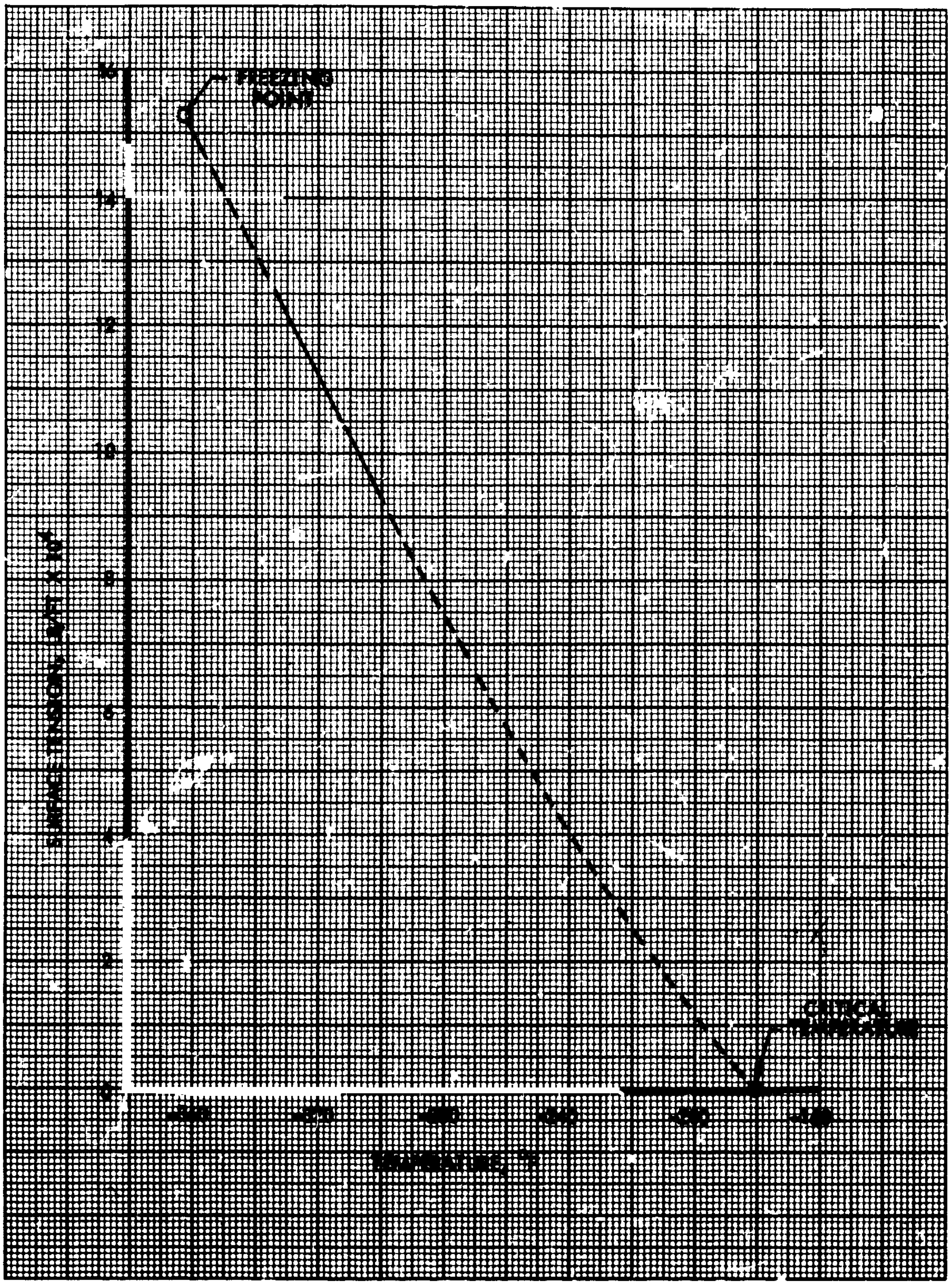

Figure 8-14. Liquid Oxygen Surface Tension vs Temperature

TABLE 8-5

GASEOUS OXYGEN COMPRESSIBILITY FACTOR

Temperature, °F

Pressure, psia	-296	-280	-260	-240	-220	-200	-100	0	80	300
14.7	.969	.976	.982	.987	.990	.992	.997	.999	1.000	1.000
29.4	L	.951	.964	.973	.979	.983	.994	.998	.999	1.000
44.1		L	.945	.959	.968	.975	.992	.997	.999	1.000
73.5			.905	.929	.946	.958	.985	.994	.997	1.000
147			L	.846	.866	.912	.971	.988	.995	1.000
221				L	.817	.862	.955	.982	.992	1.000
294					.734	.807	.940	.976	.989	1.000

TABLE 8-6

GASEOUS OXYGEN SPECIFIC HEAT

(Btu/lb-°F)

Pressure, psia	Temperature, °F									
	-296	-280	-260	-240	-220	-200	-150	-100	80	800
14.7	.225	.225	.222	.220	.220	.220	.220	.220	.220	.228
29.4	L	.232	.229	.225	.222	.222	.220	.220	.220	.228
44.1		L	.234	.229	.229	.225	.222	.220	.220	.228
73.5			.251	.244	.236	.234	.225	.222	.222	.229
147			L	.282	.263	.251	.236	.229	.222	.229
221				L	.303	.277	.248	.234	.225	.232
294					L	.315	.260	.241	.227	.234

TABLE 8-7

GASEOUS OXYGEN THERMAL CONDUCTIVITY

(Btu/hr-ft-°F)

Pressure, psia	Temperature, °F -292	 -220	 +104
14.7	.0048	.0070	.0160
294	L	.0089	.0165

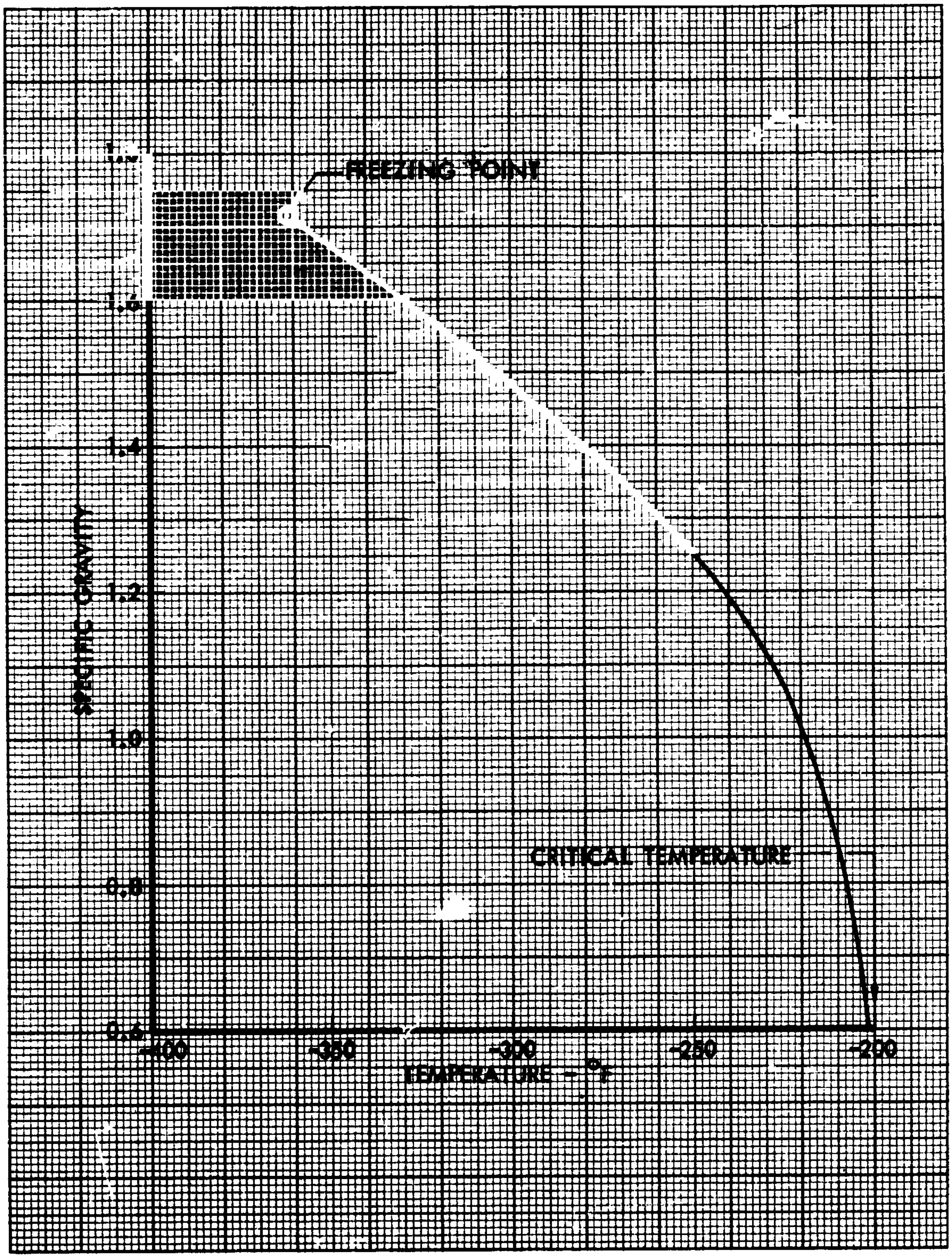

Figure 8-15. Liquid Fluorine Specific Gravity vs Temperature

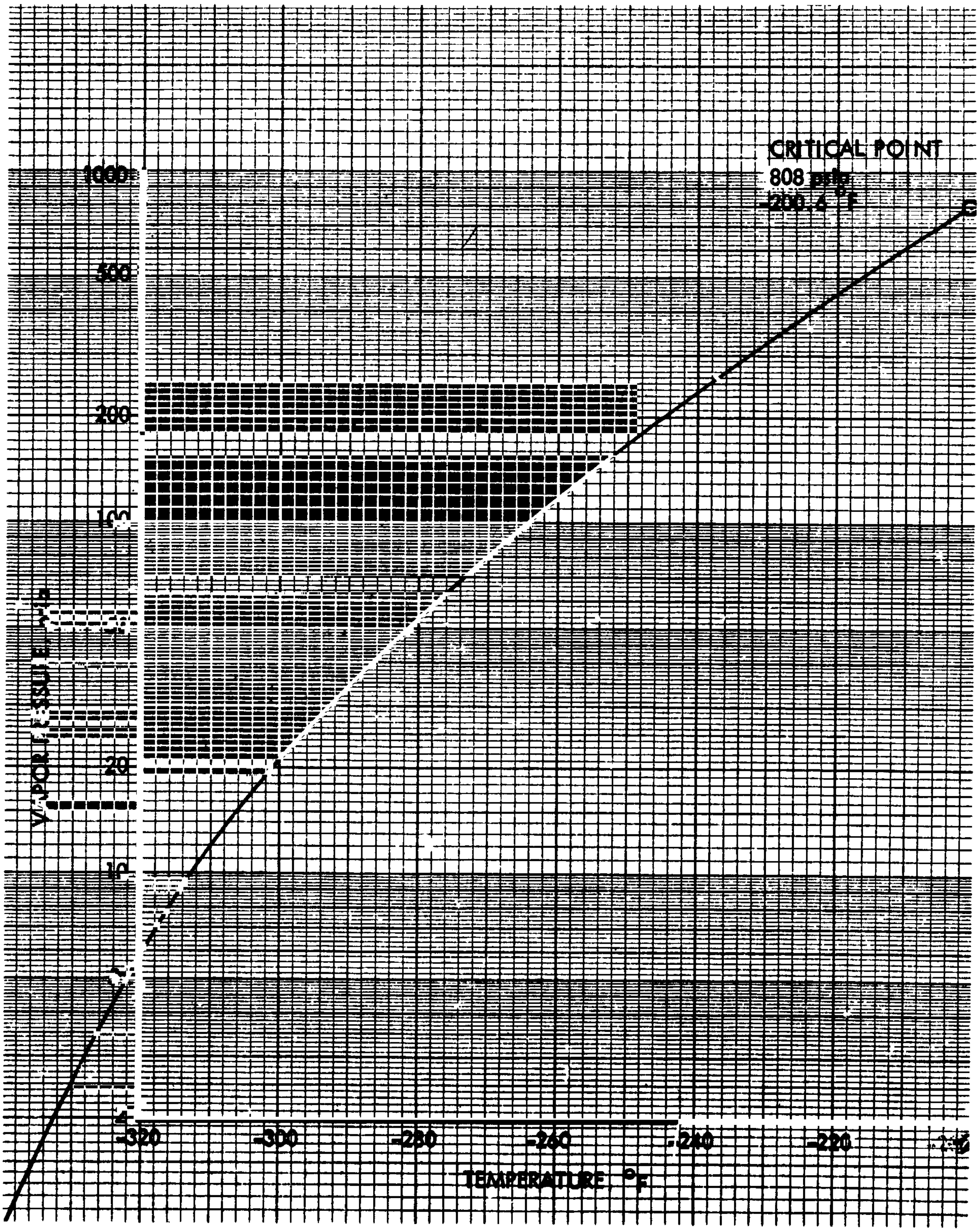

Figure 8-16. Liquid Fluorine Vapor Pressure vs Temperature

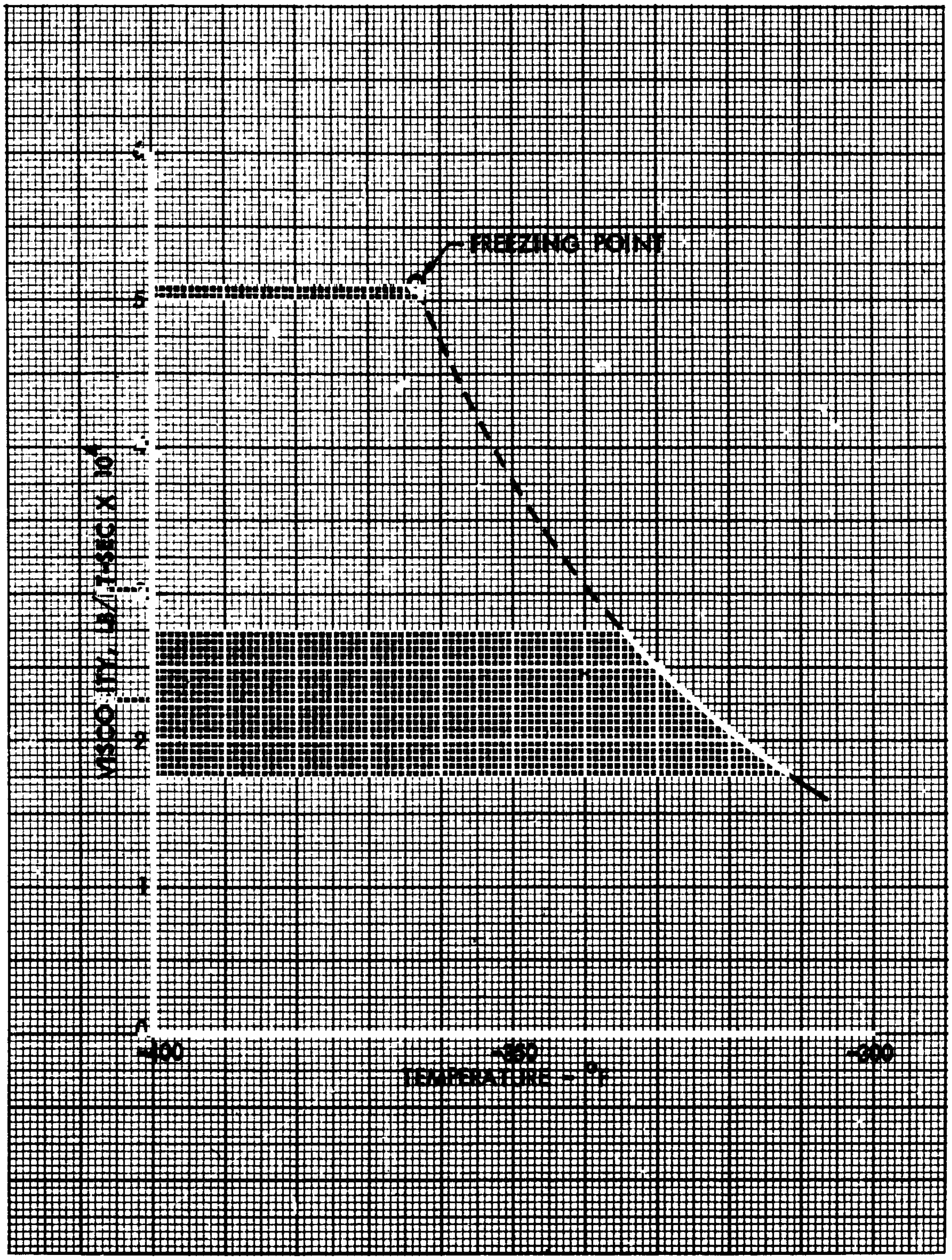

Figure 8-17. Liquid Fluorine Viscosity vs Temperature

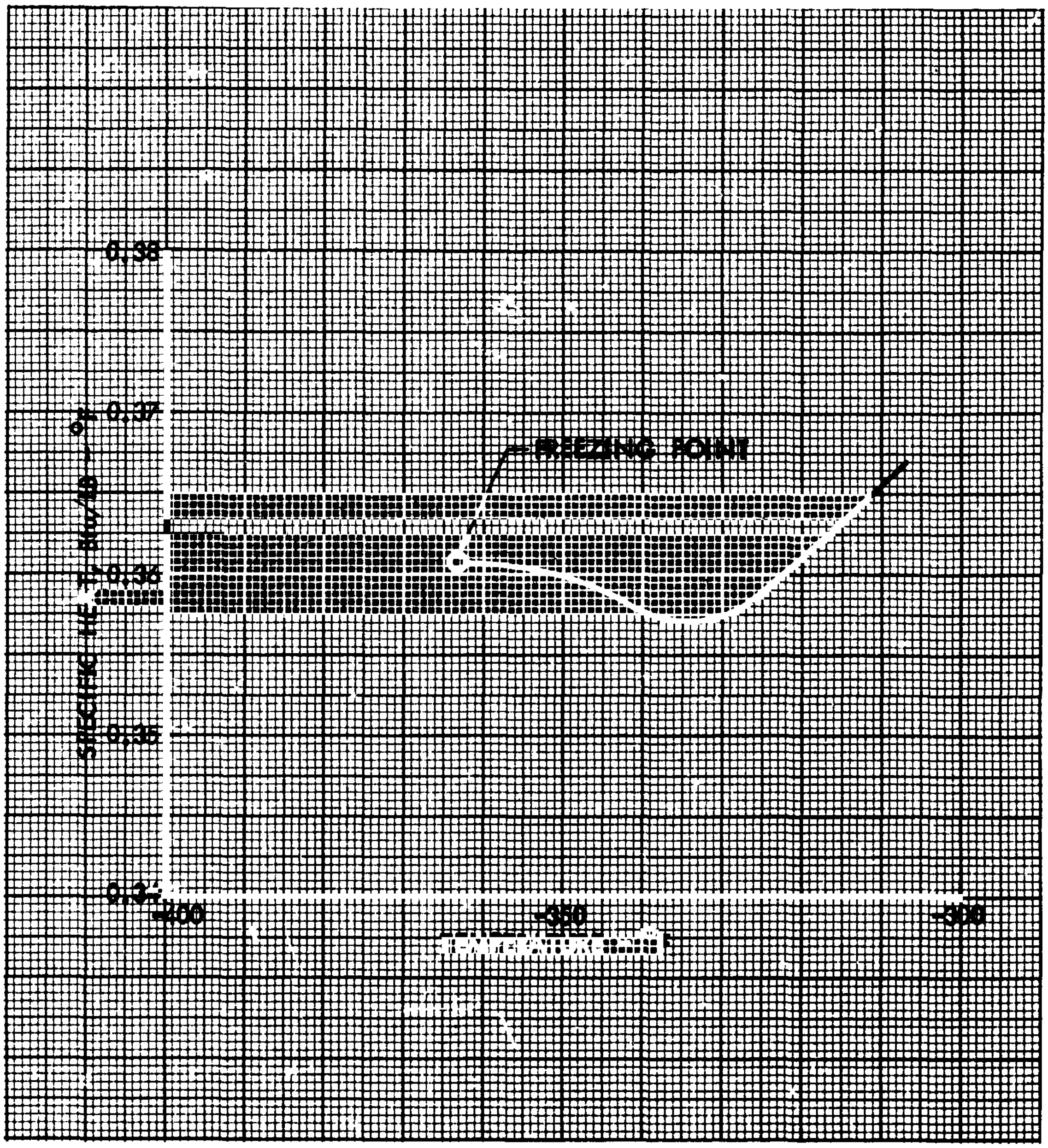

Figure 8-18. Liquid Fluorine Specific Heat vs Temperature

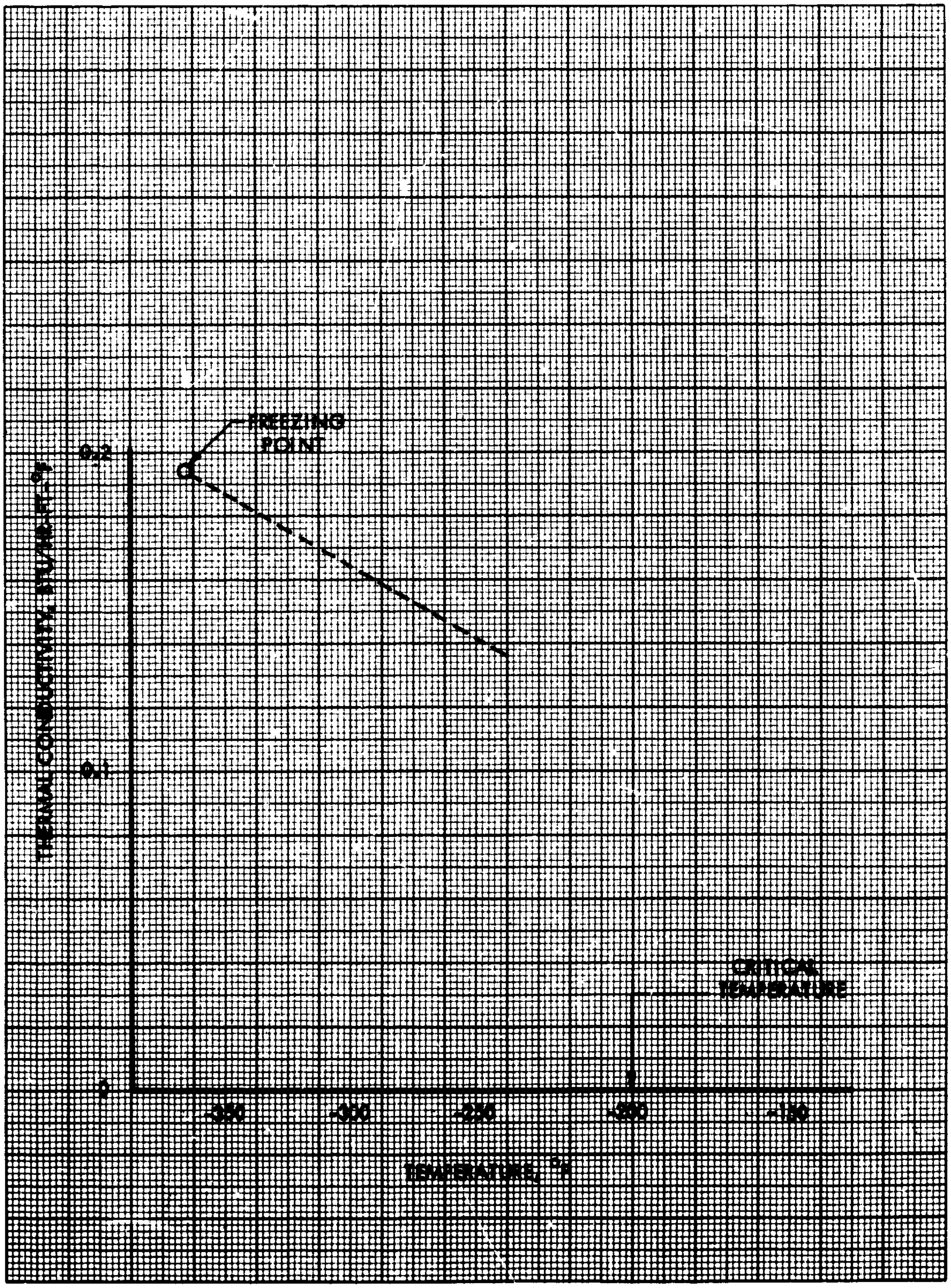

Figure 8-19. Liquid Fluorine Thermal Conductivity vs Temperature

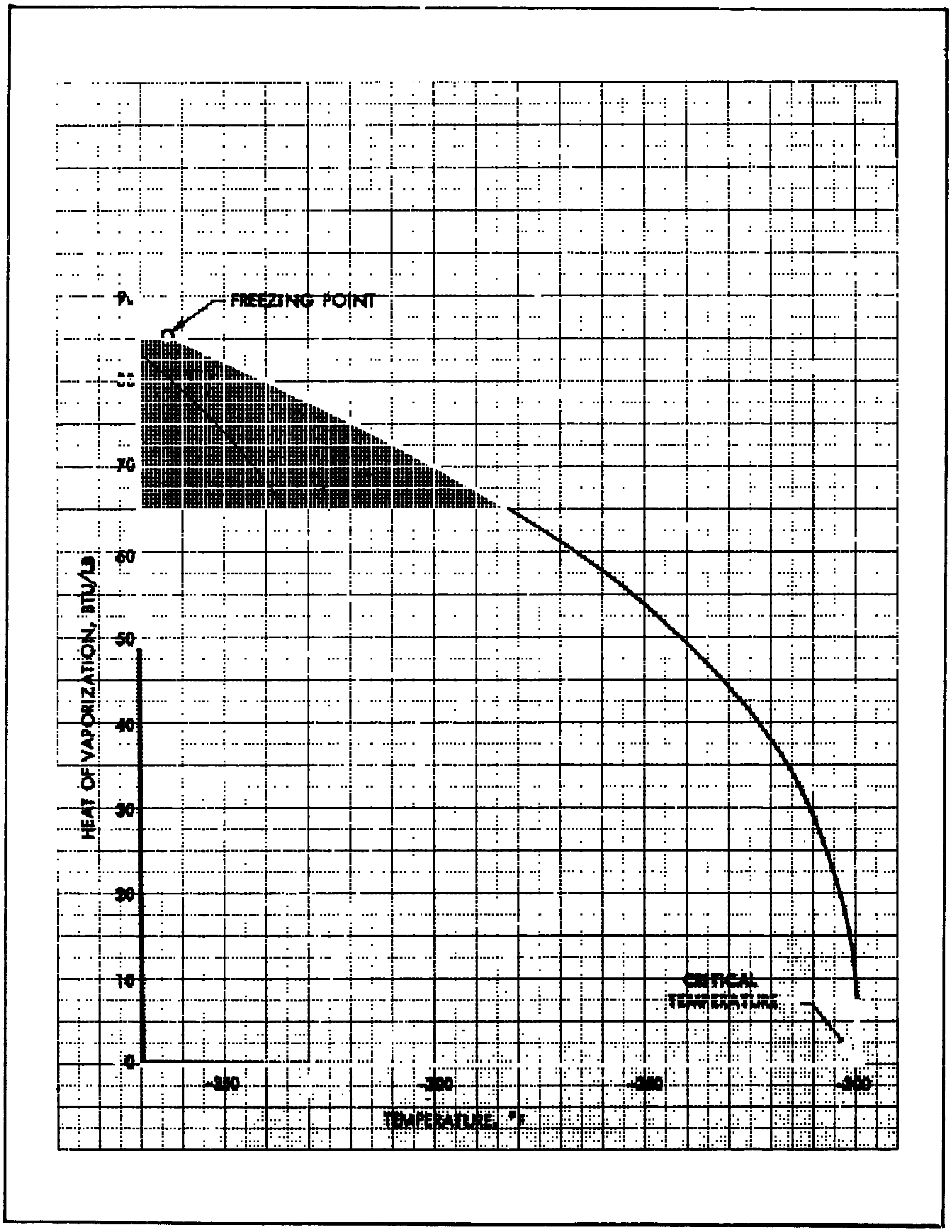

Figure 8-20. Liquid Fluorine Heat of Vaporization vs Temperature

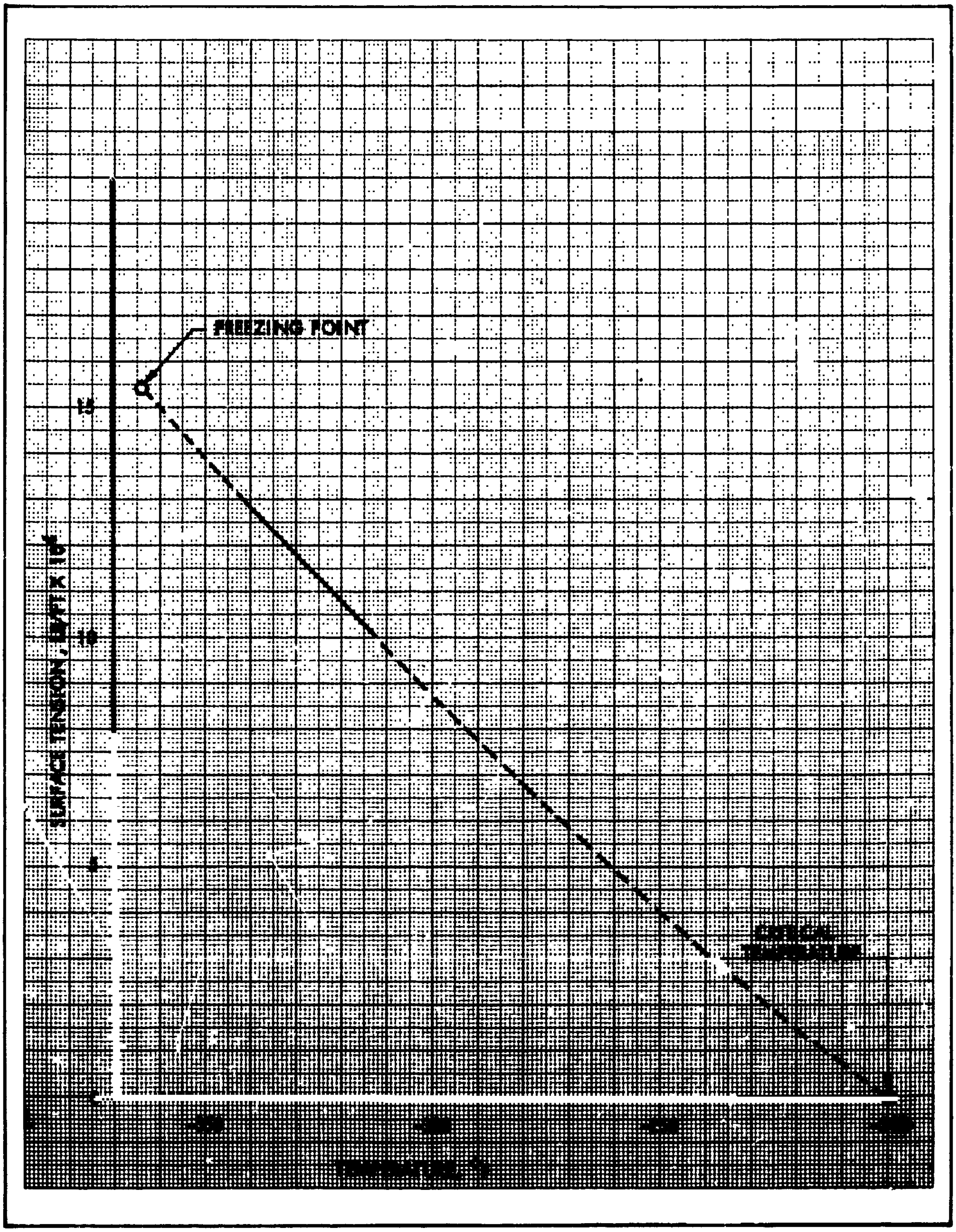

Figure 8-21. Liquid Fluorine Surface Tension vs Temperature

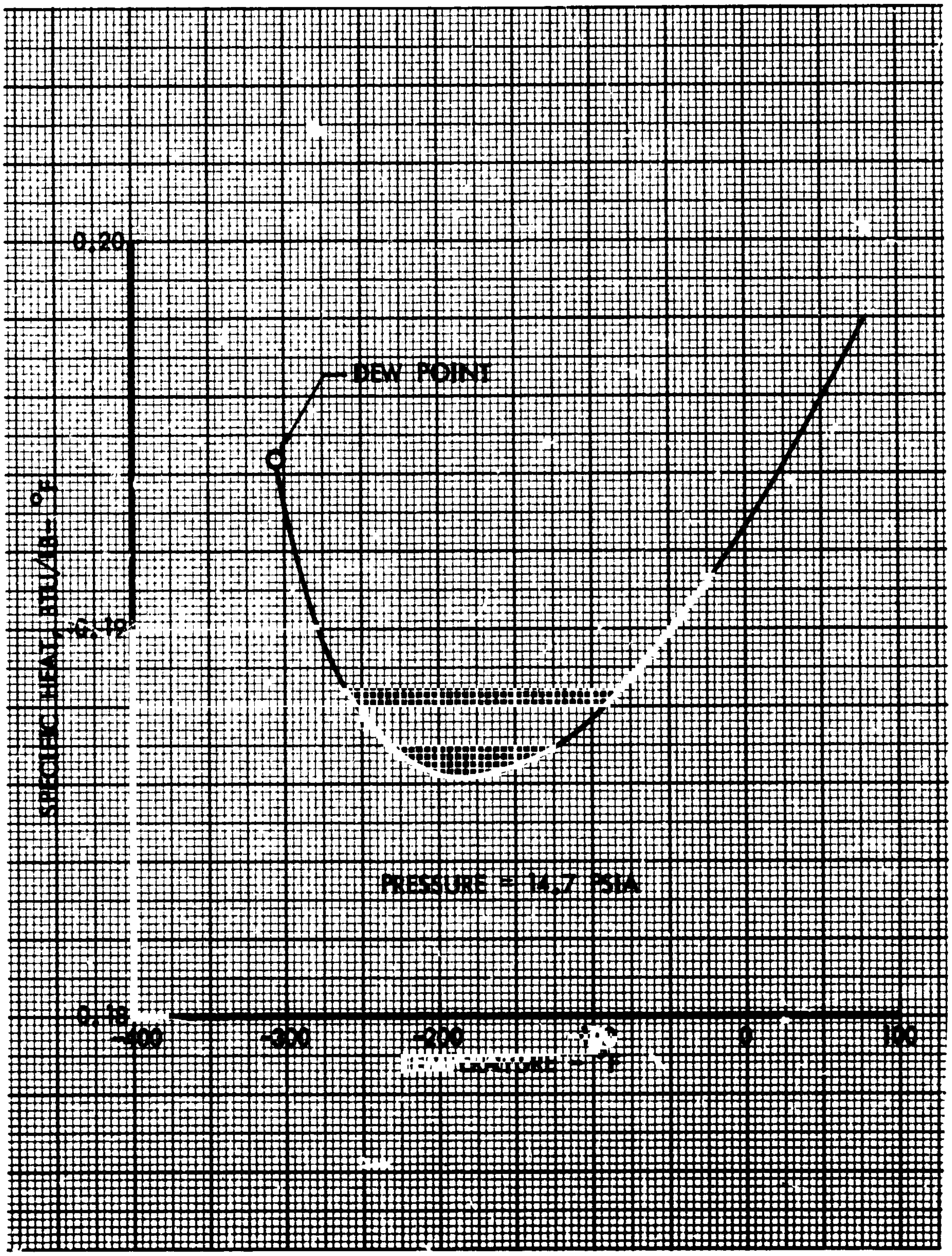

Figure 8-22. Fluorine Gas Specific Heat vs Temperature

TABLE 8-8
GASEOUS FLUORINE THERMAL CONDUCTIVITY

(Pressure = 14.7 psia)

Temperature (°F)	Conductivity (Btu/hr-ft·°F)
-280	.00498
-100	.0105
+ 31	.0143
+170	.0178

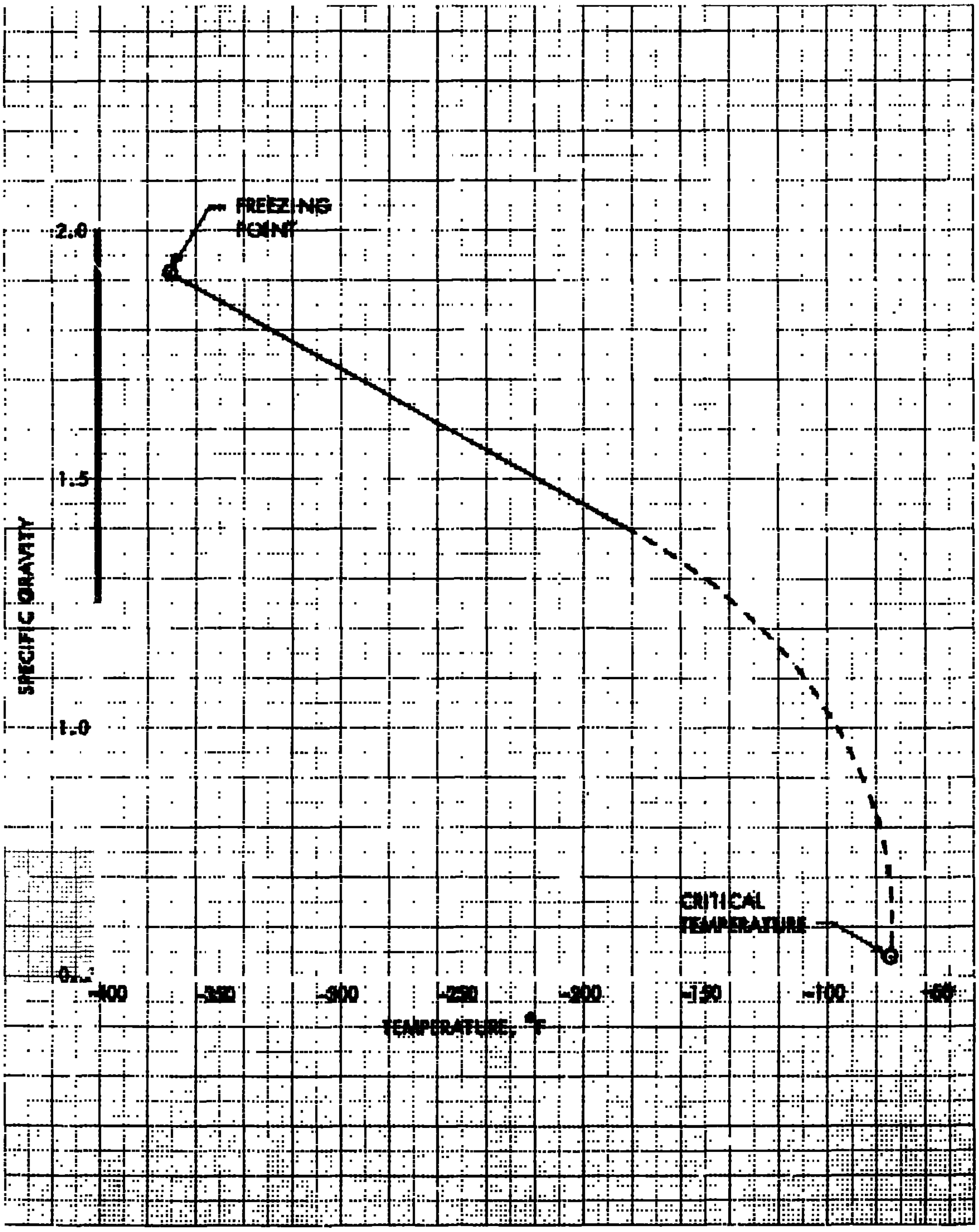

Figure 8-23. Liquid Oxygen Difluoride Specific Gravity vs Temperature

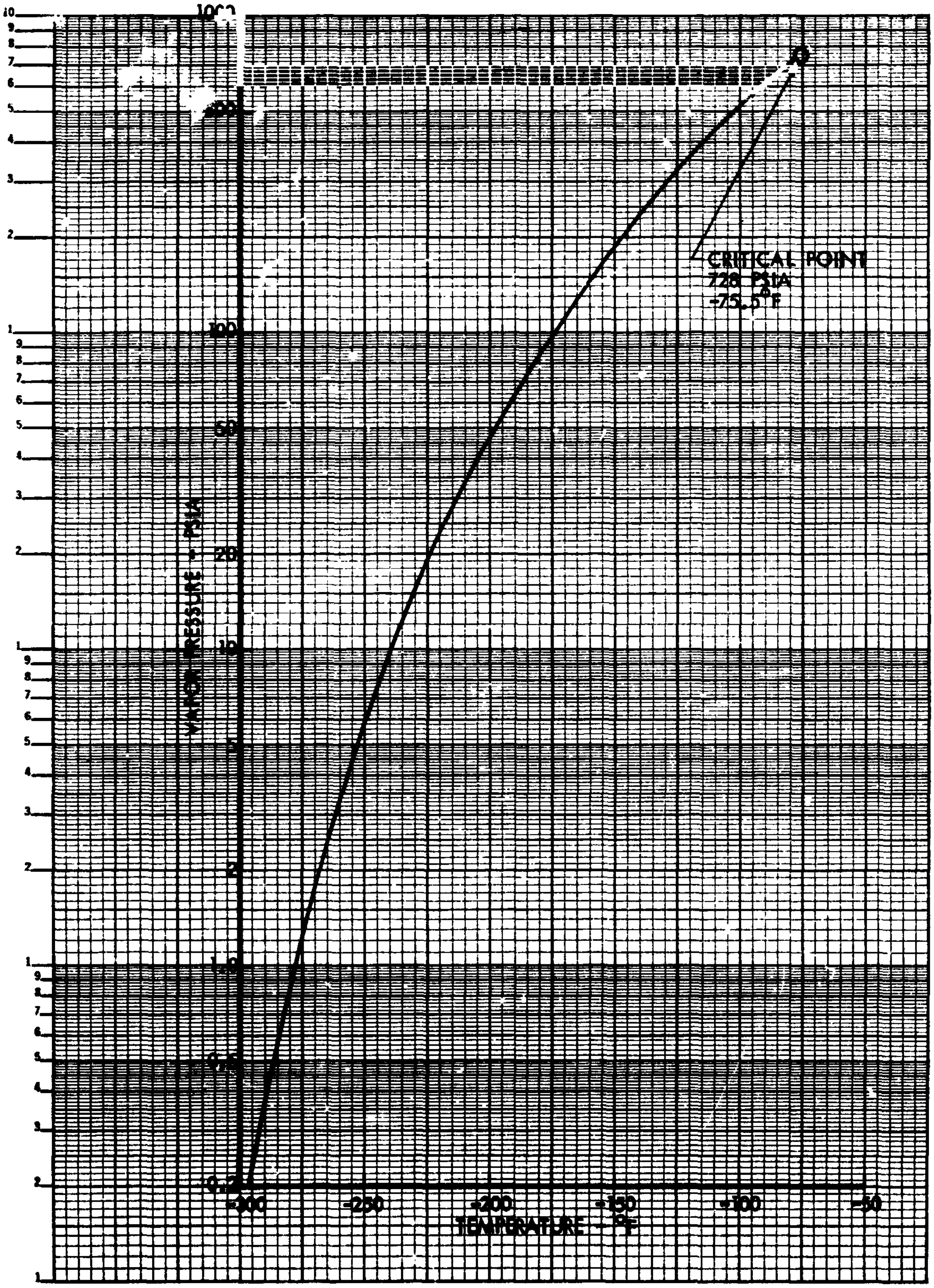

Figure 8-24. Liquid Oxygen Difluoride Vapor Pressure vs Temperature

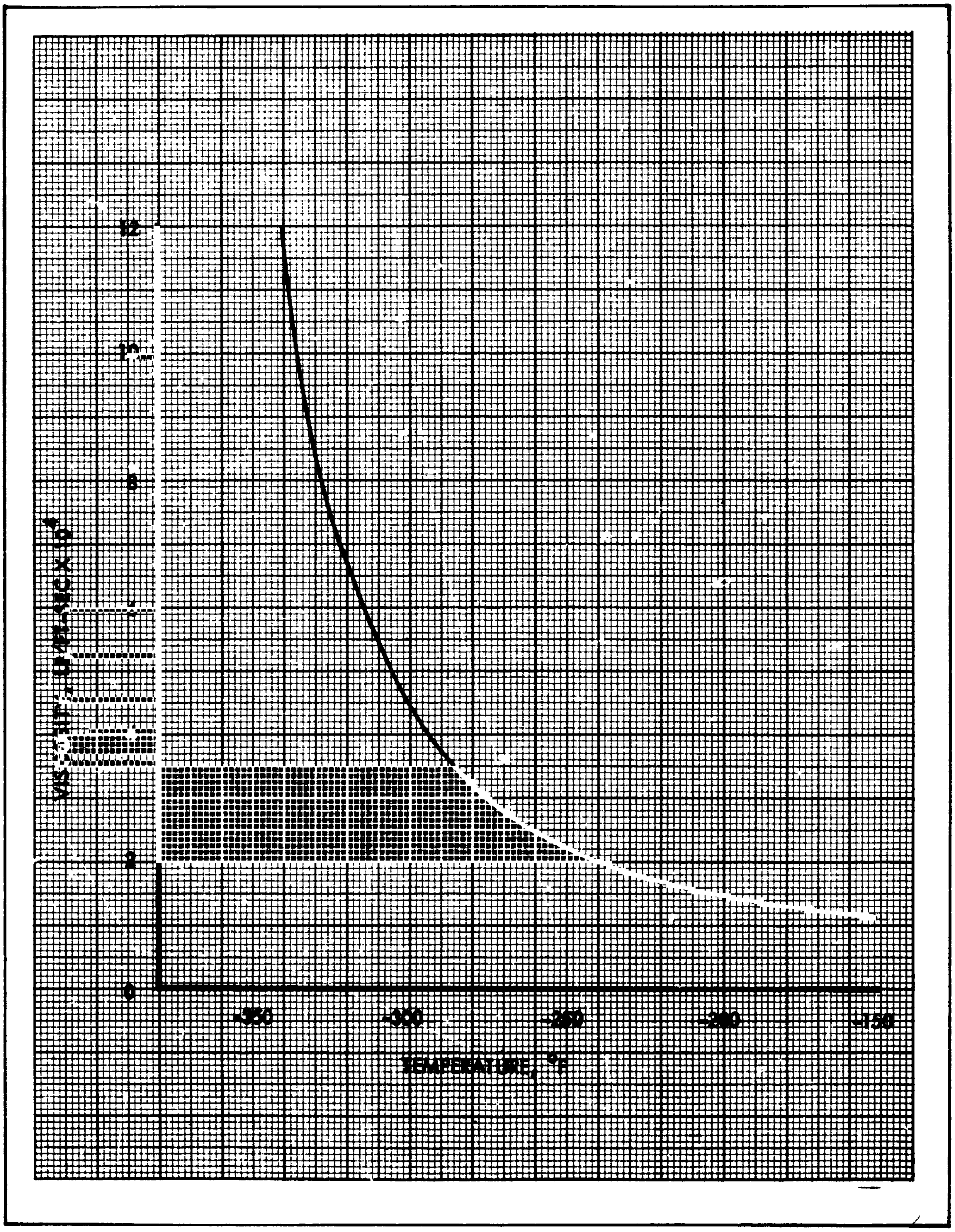

Figure 8-25. Liquid Oxygen Difluoride Viscosity vs Temperature

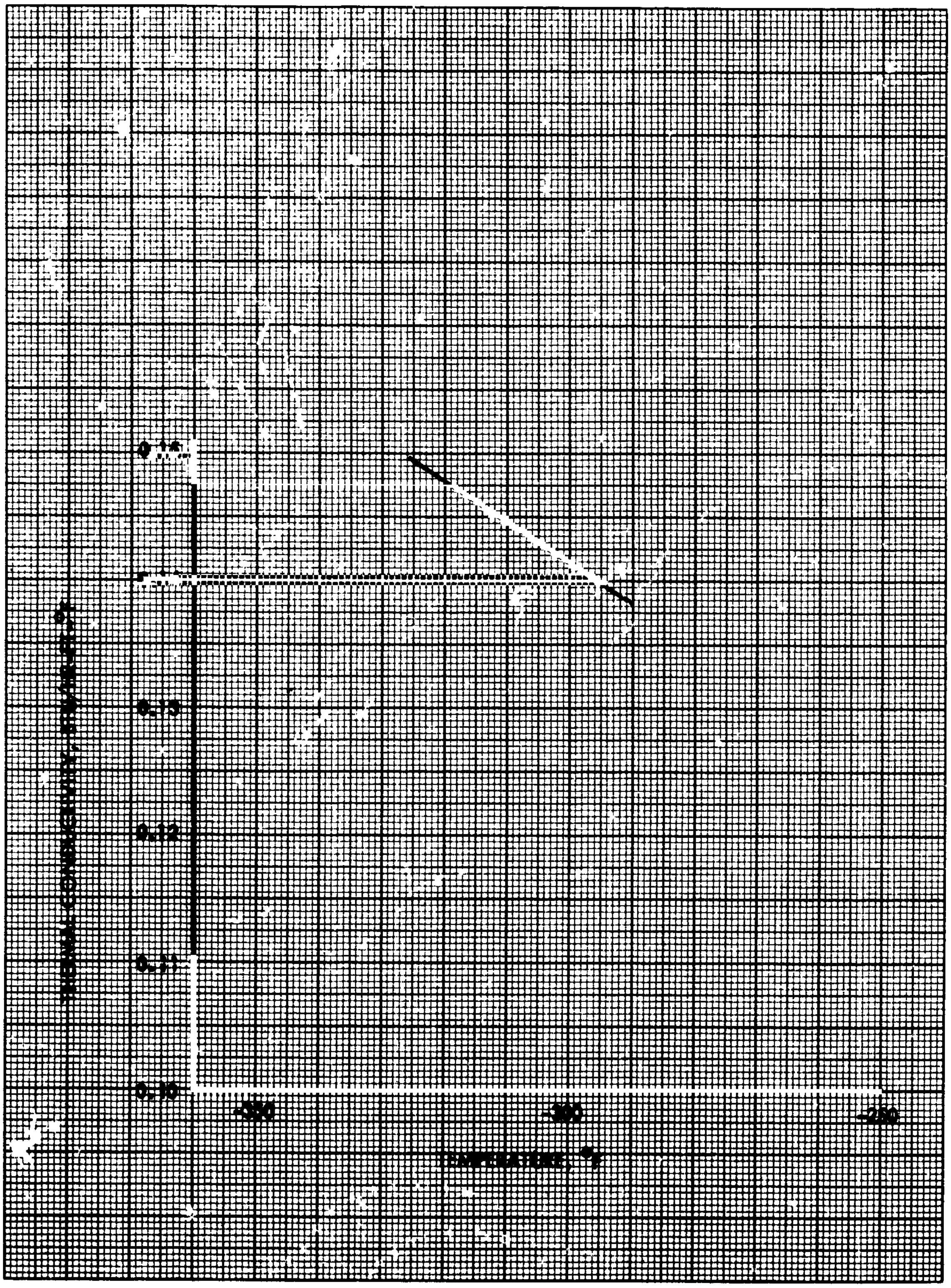

Figure 8-26. Liquid Oxygen Difluoride Thermal Conductivity vs Temperature

TABLE 8-9

GASEOUS OXYGEN DIFLUORIDE SPECIFIC HEAT

(Pressure = 14.7 psia)

Temperature (°F)	Specific Heat (Btu/lb-°F)
-229.5	.150
+ 80	.192
+300	.215

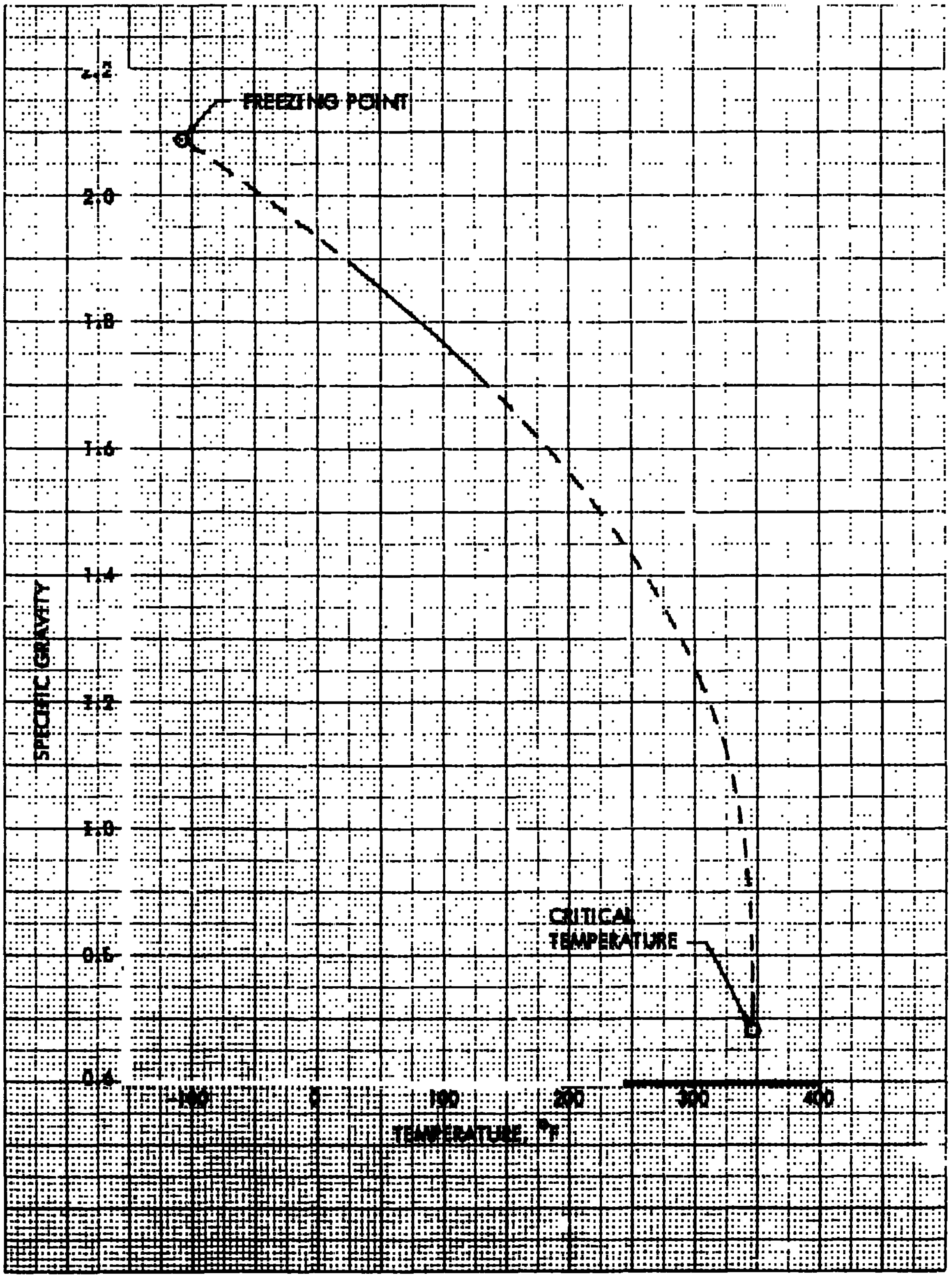

Figure 8-27. Liquid Chlorine Trifluoride Specific Gravity vs Temperature

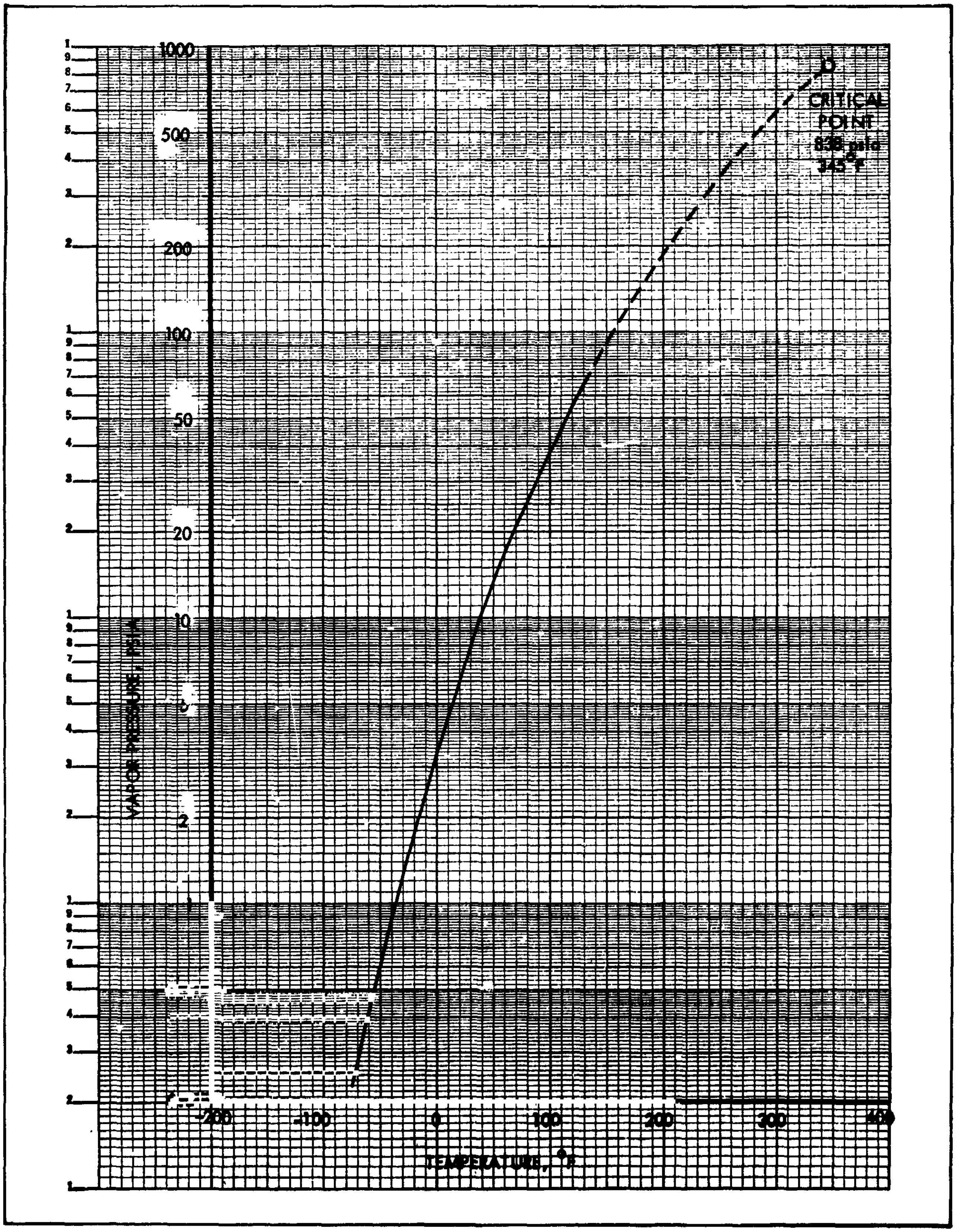

Figure 8-28. Liquid Chlorine Trifluoride Vapor Pressure vs Temperature

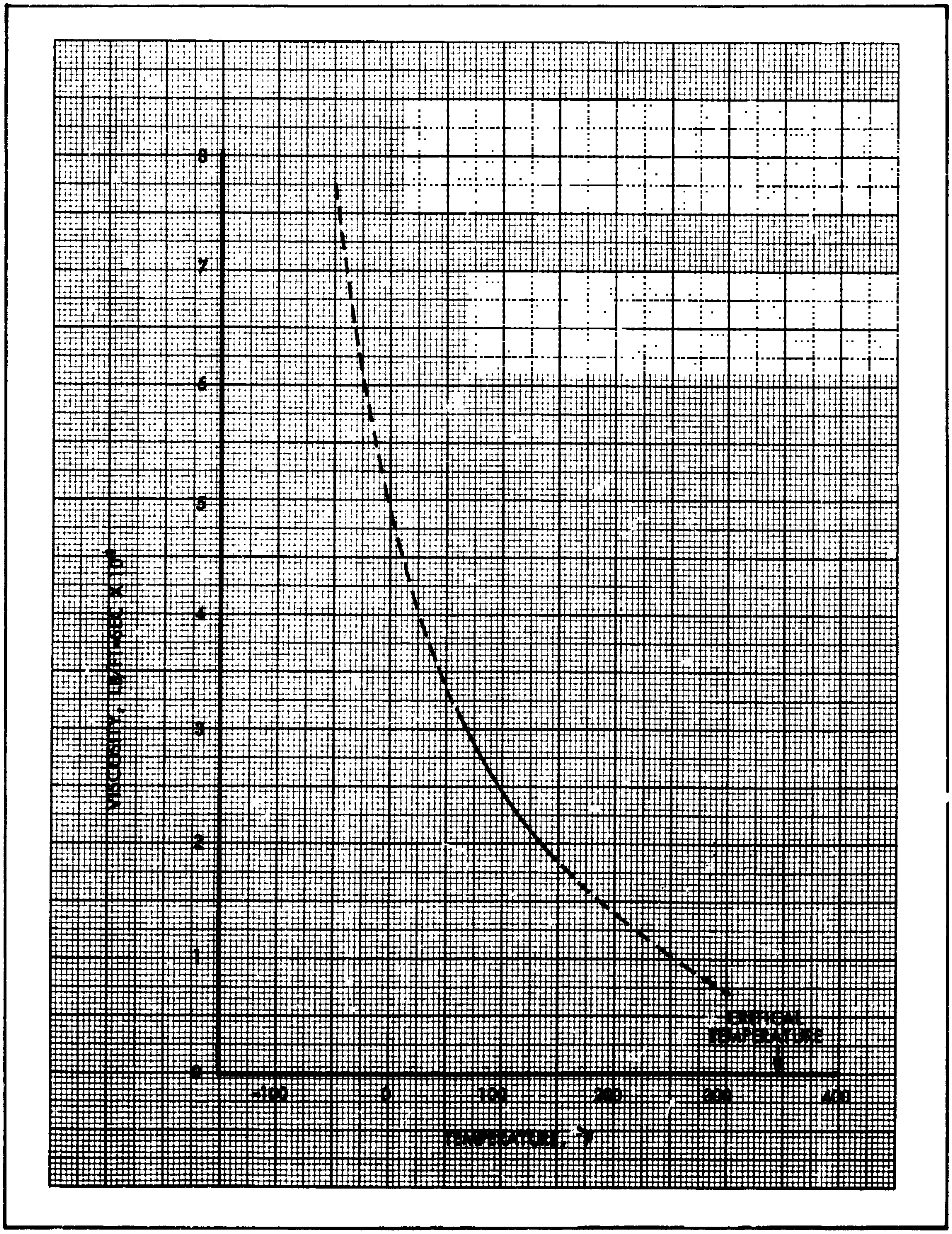

Figure 8-29. Liquid Chlorine Trifluoride Viscosity vs Temperature

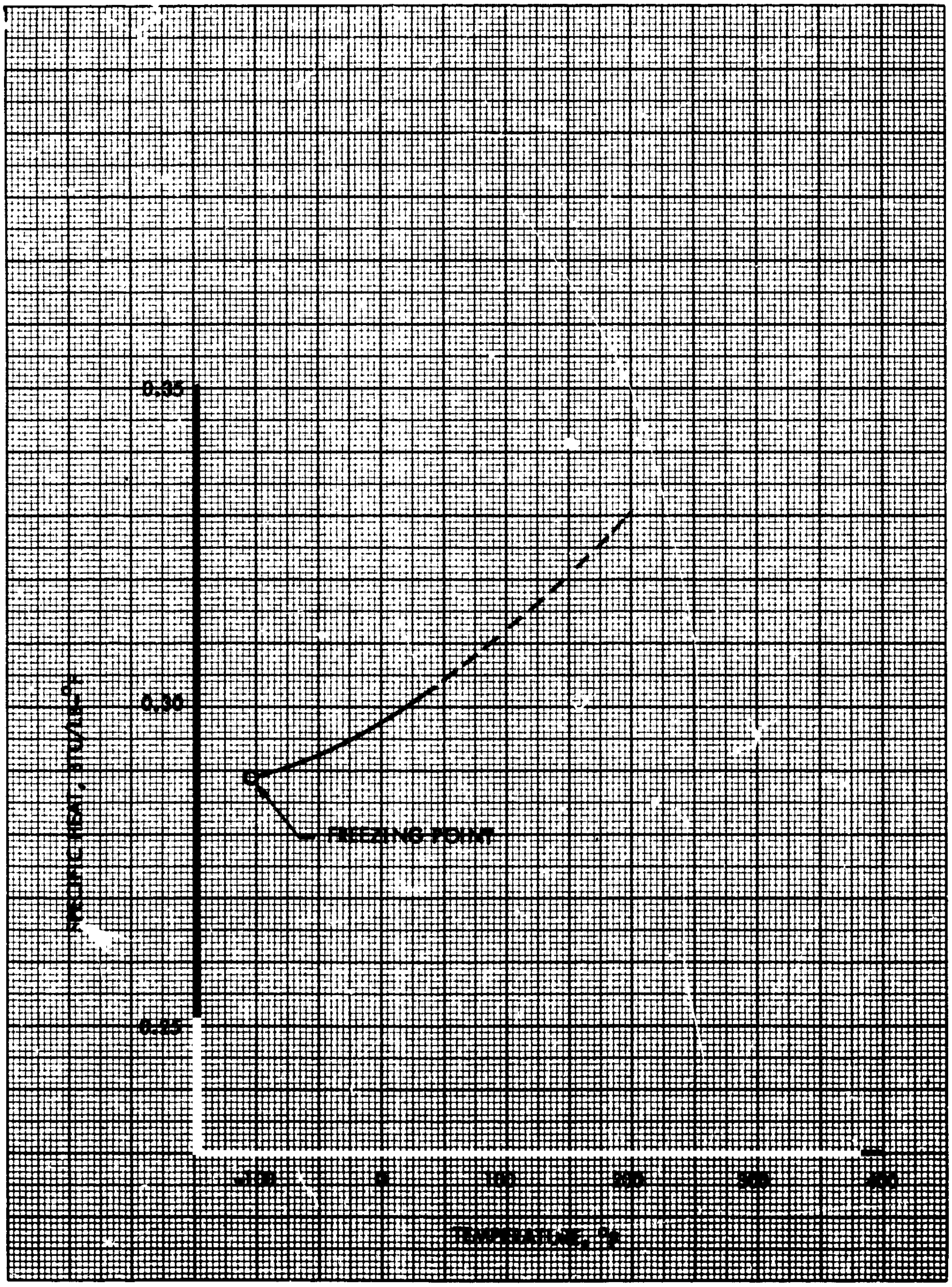

Figure 8-30. Liquid Chlorine Trifluoride Specific Heat vs Temperature

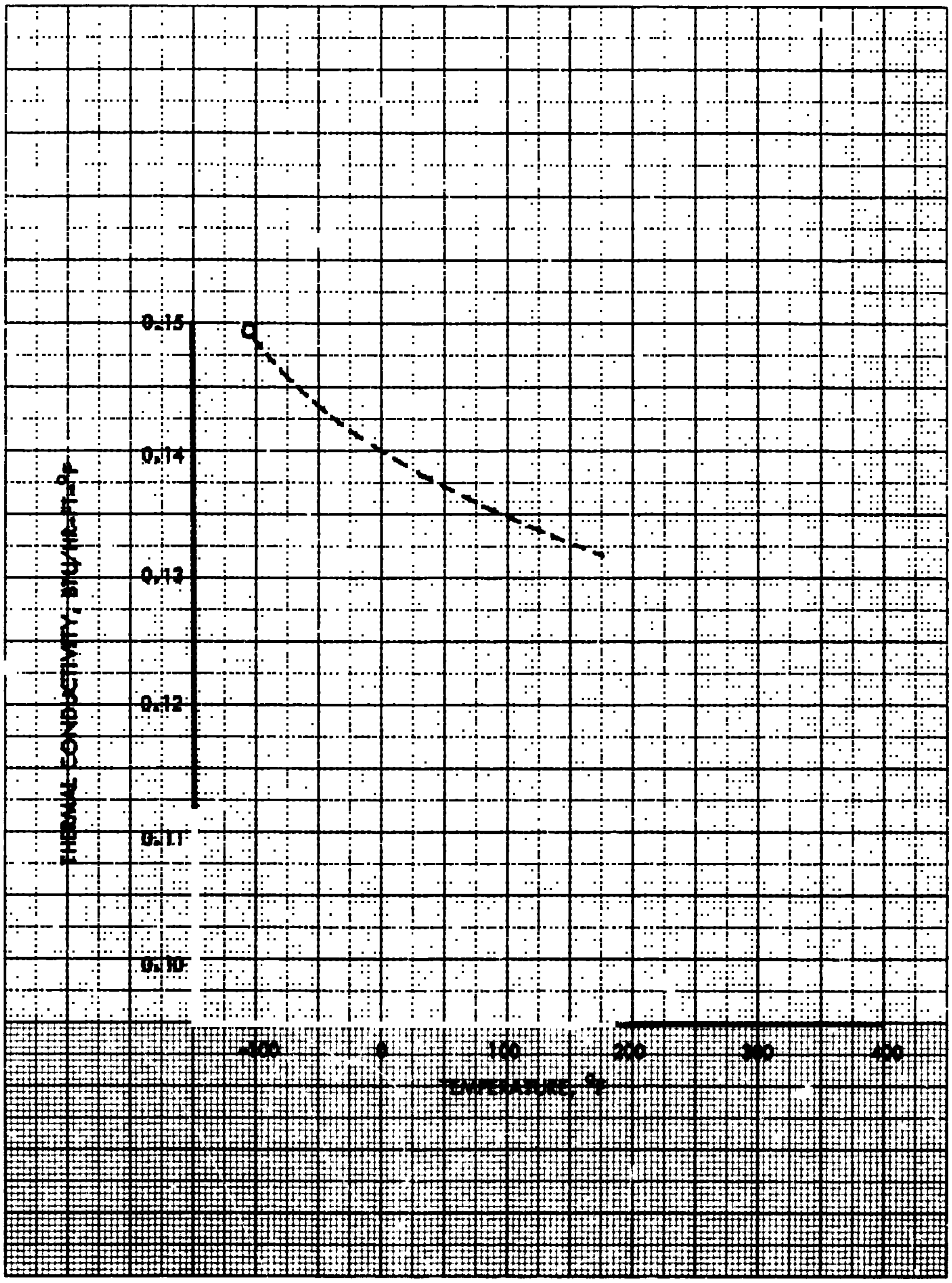

Figure 8-31. Liquid Chlorine Trifluoride Thermal Conductivity vs Temperature

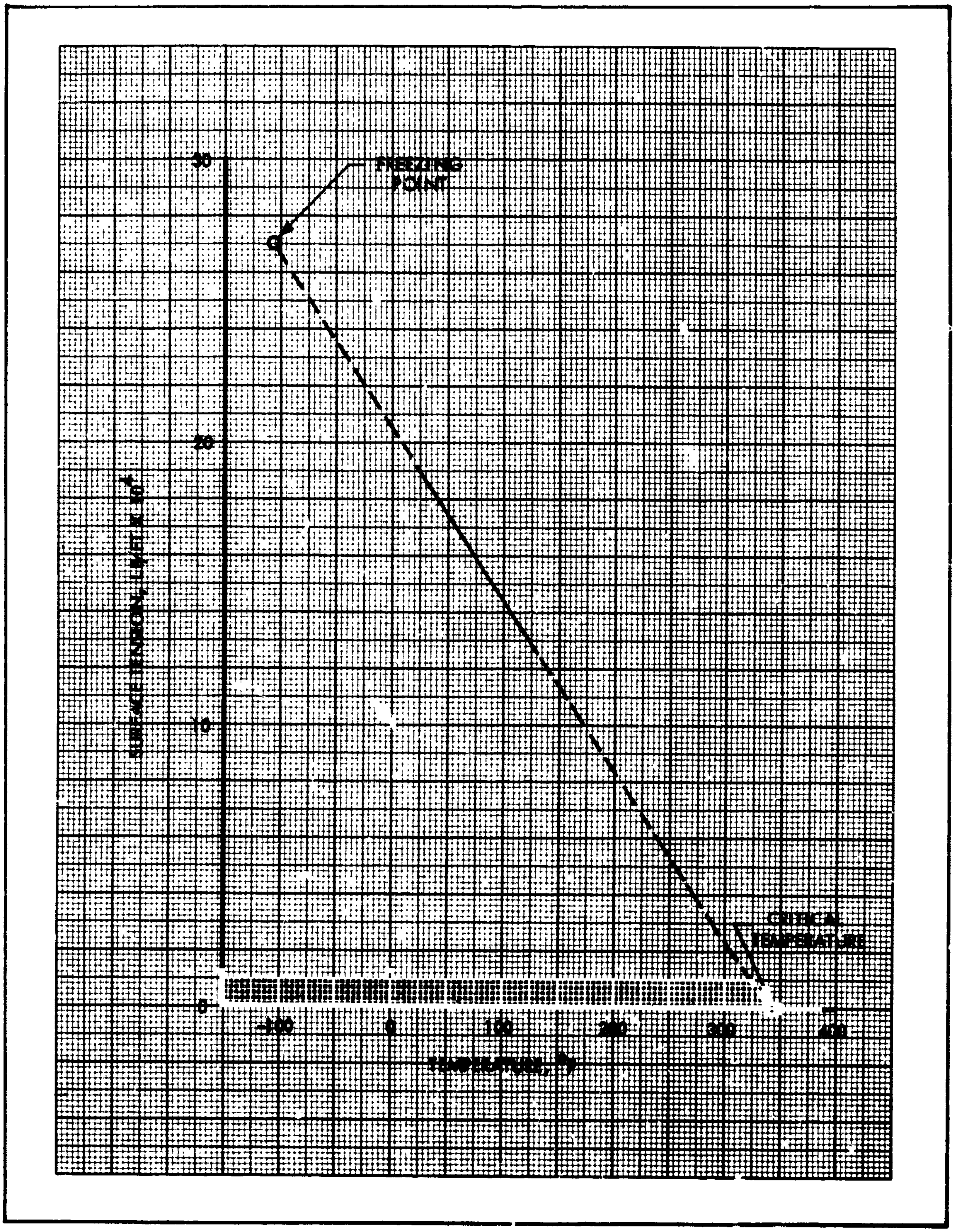

Figure 8-32. Liquid Chlorine Trifluoride Surface Tension vs Temperature

TABLE 8-10

GASEOUS CHLORINE TRIFLUORIDE SPECIFIC HEAT

(Pressure = 14.7 psia)

Temperature (°F)	Specific Heat (Btu/lb-°F)
-100	.141
+ 80	.168
260	.184
440	.194

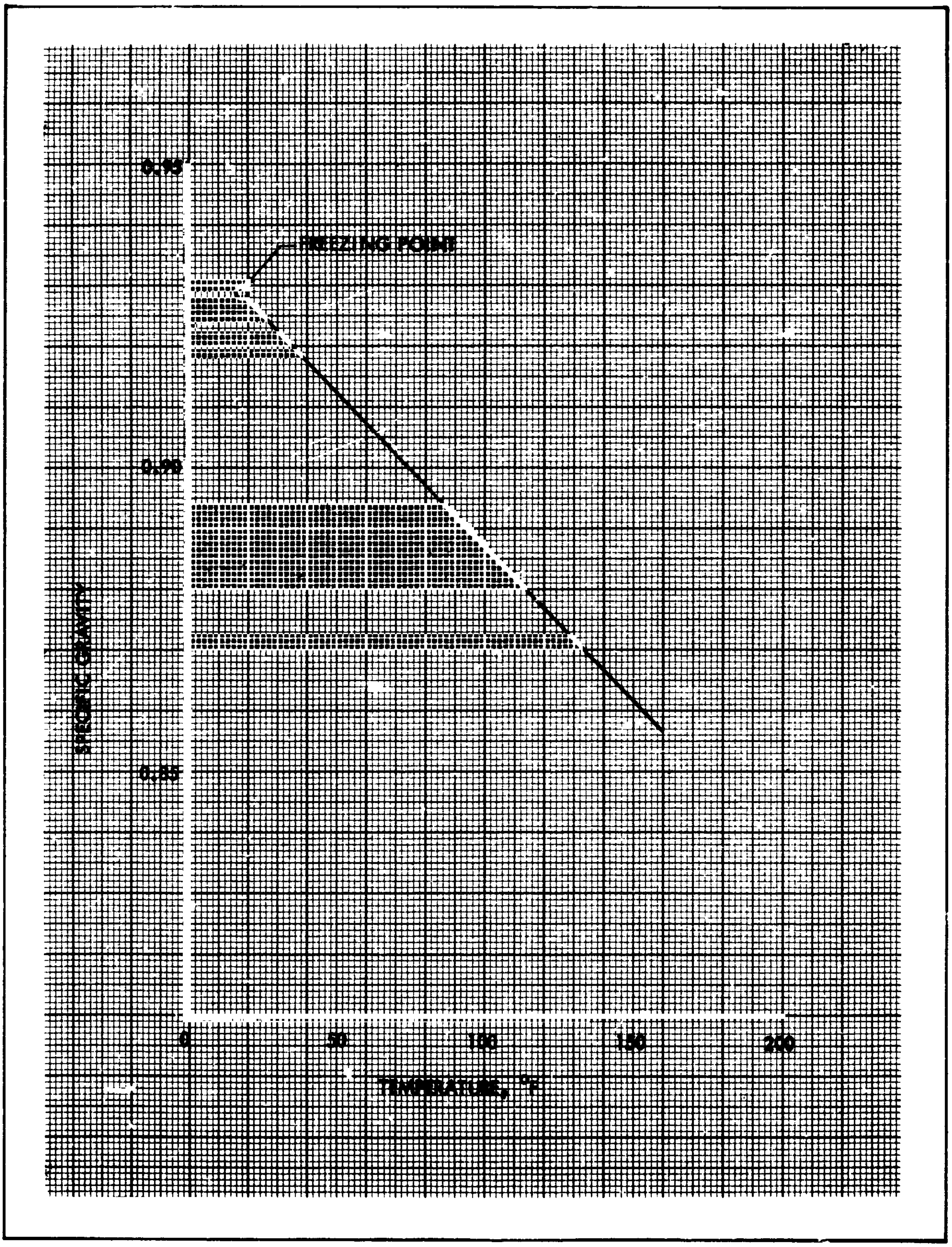

Figure 8-33. Mixed Hydrazine Specific Gravity vs Temperature

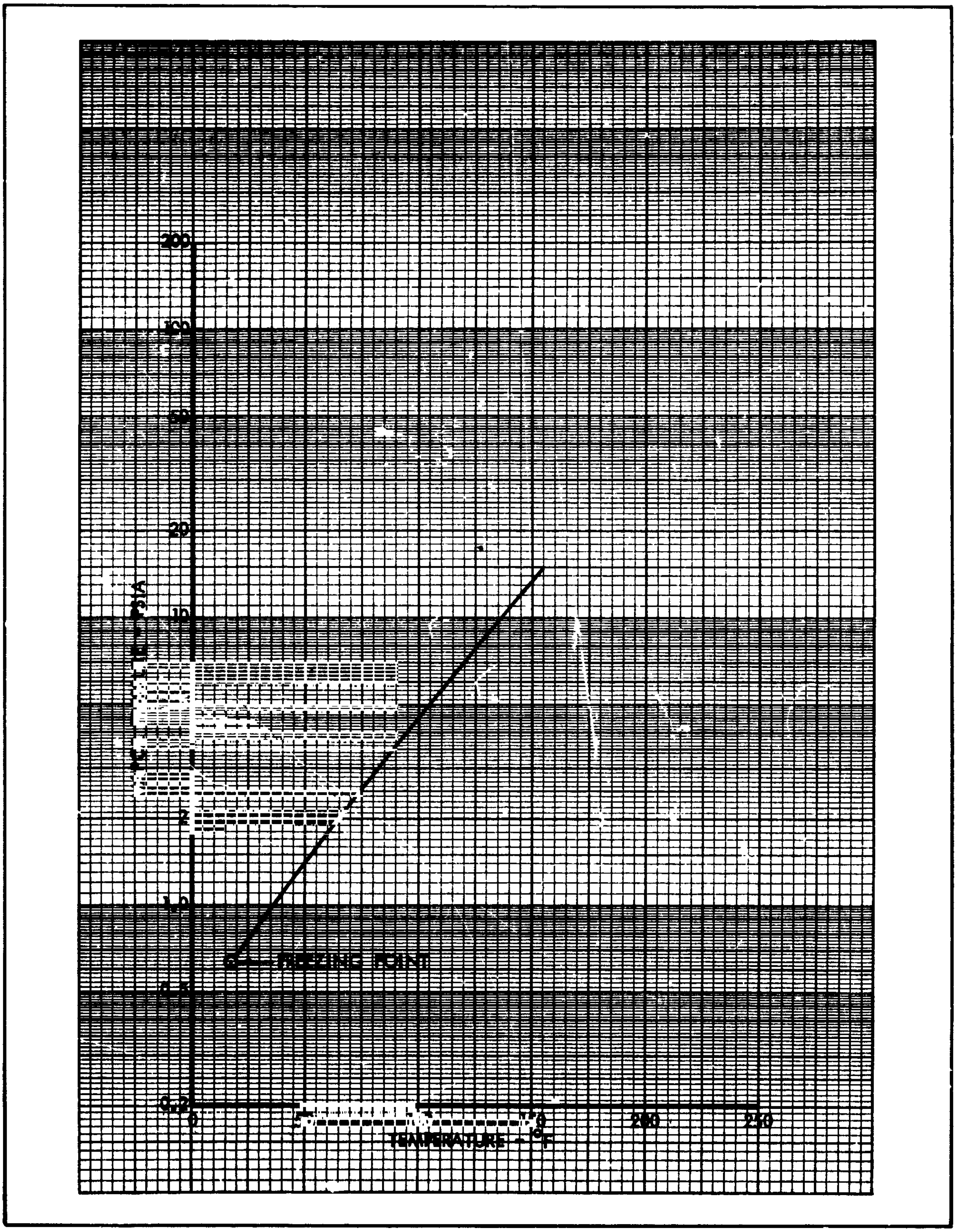

Figure 8-34. Mixed Hydrazine Vapor Pressure vs Temperature

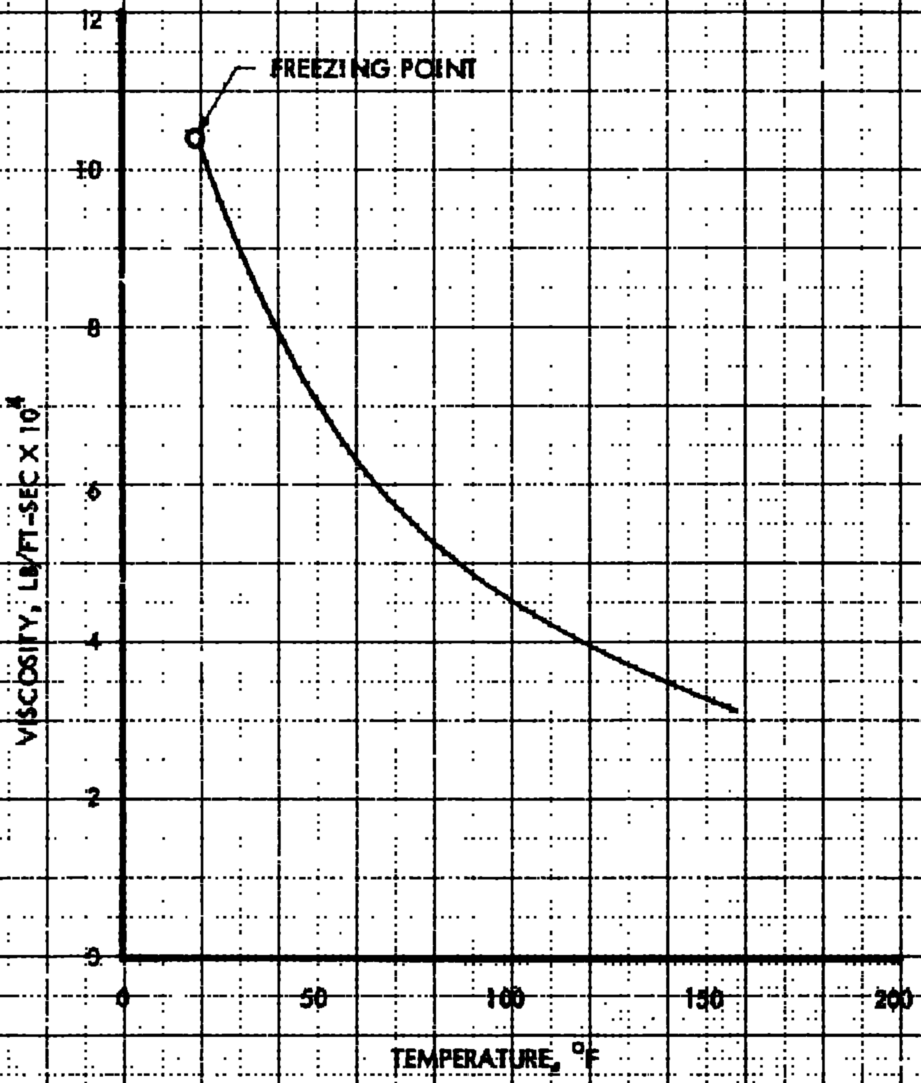

Figure 8-35. Mixed Hydrazine Viscosity vs Temperature

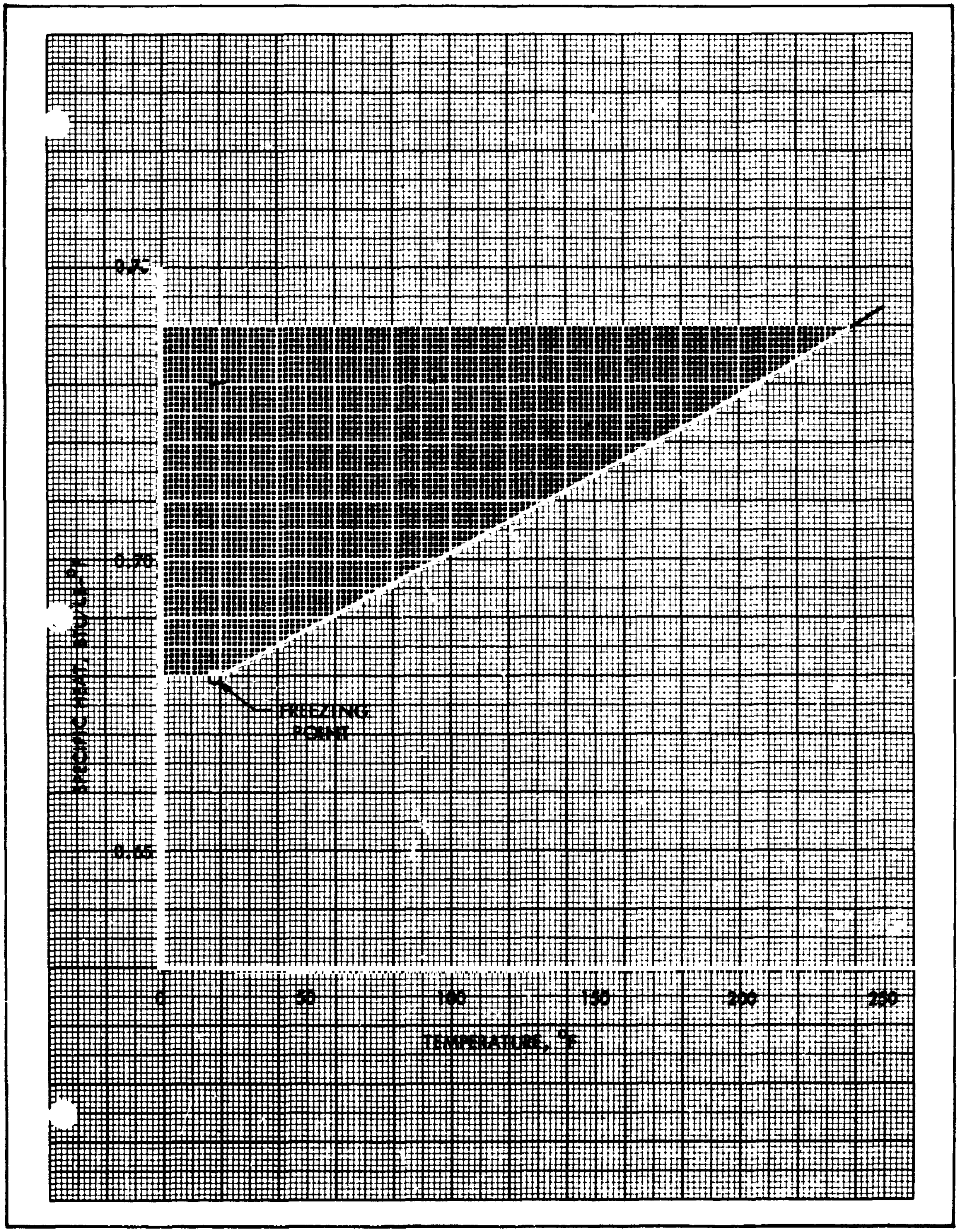

Figure 8-36. Mixed Hydrazine Specific Heat vs Temperature

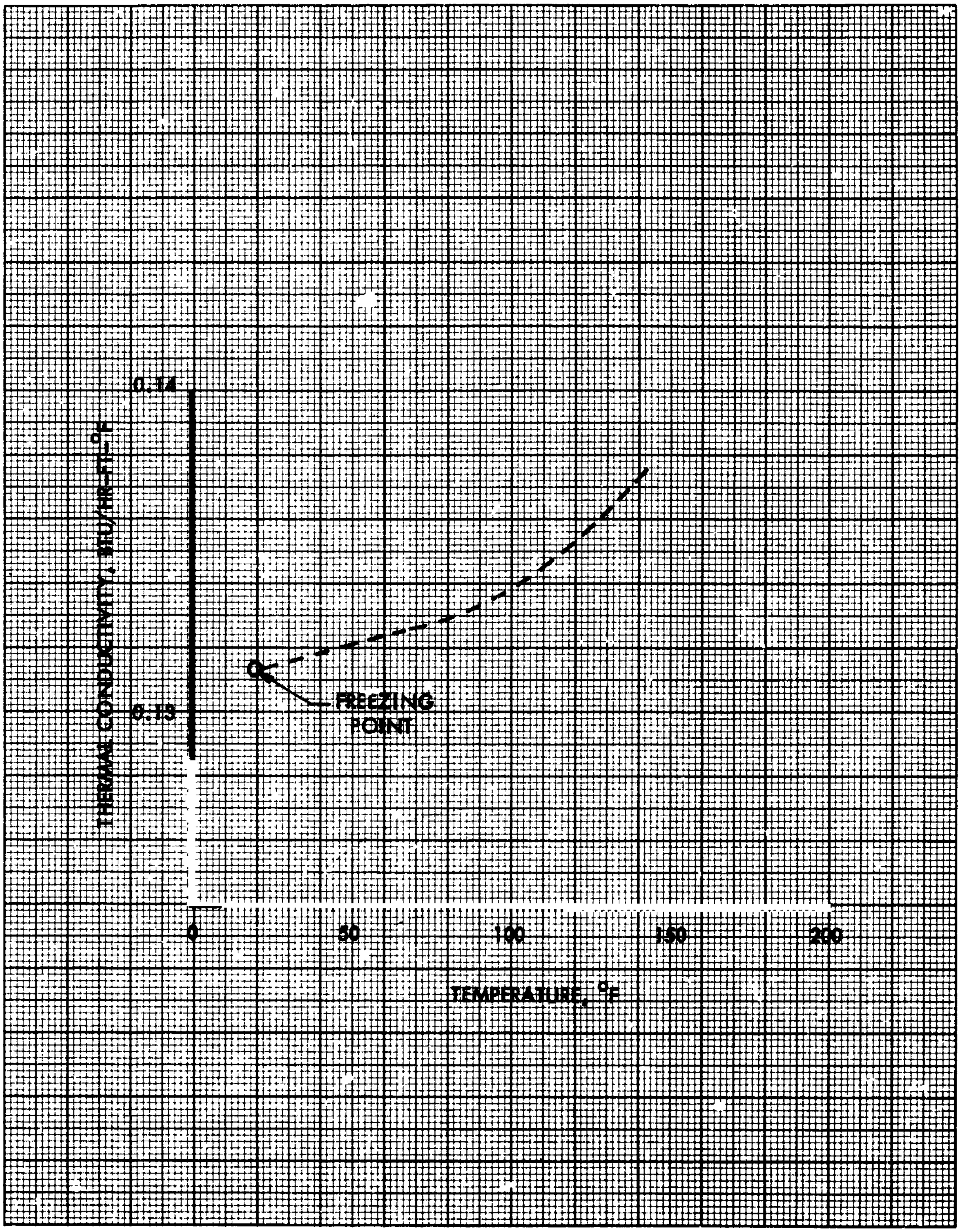

Figure 8-37. Mixed Hydrazine Thermal Conductivity vs Temperature

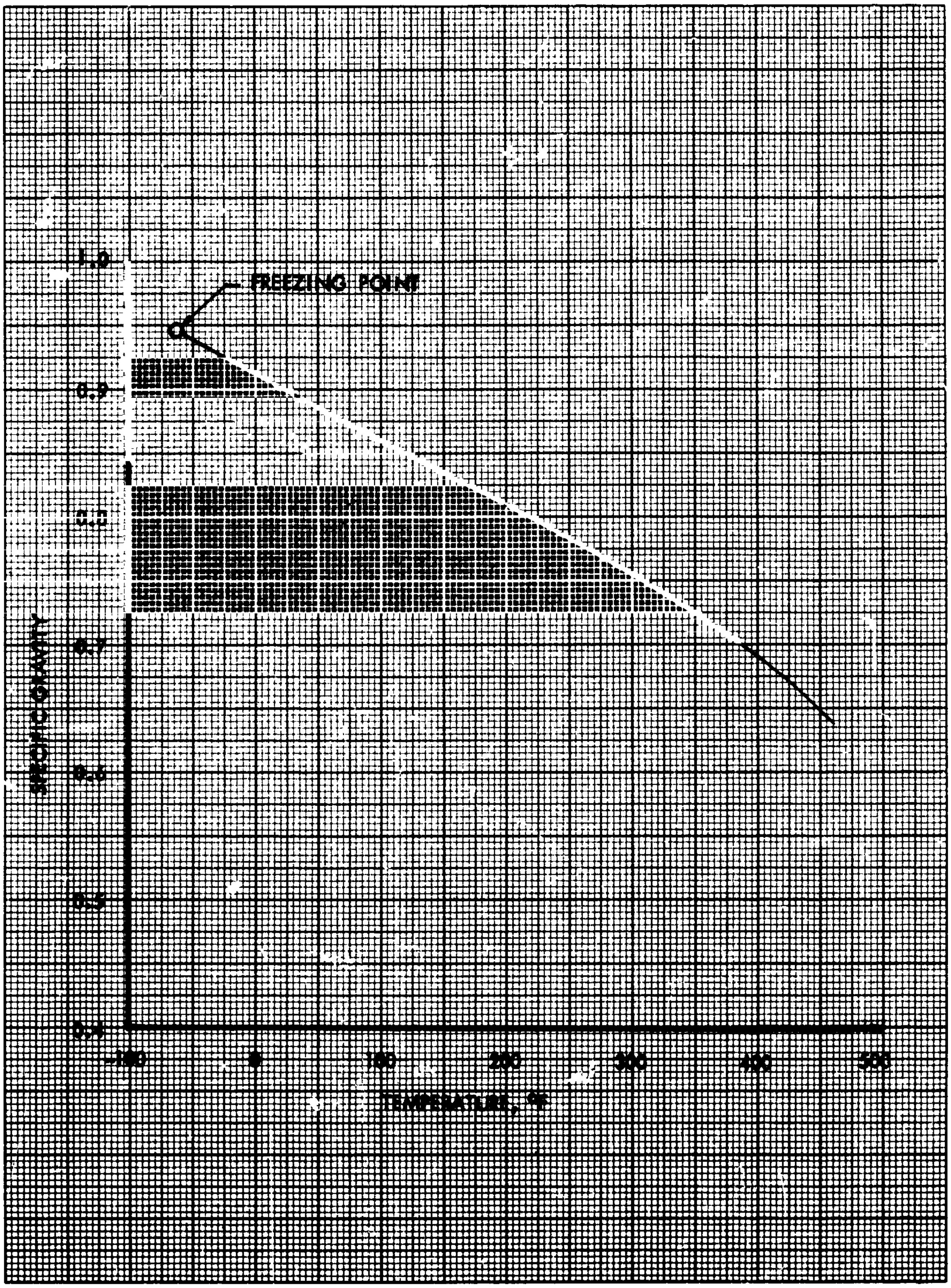

Figure 8-38. Monomethyl Hydrazine Specific Gravity vs Temperature

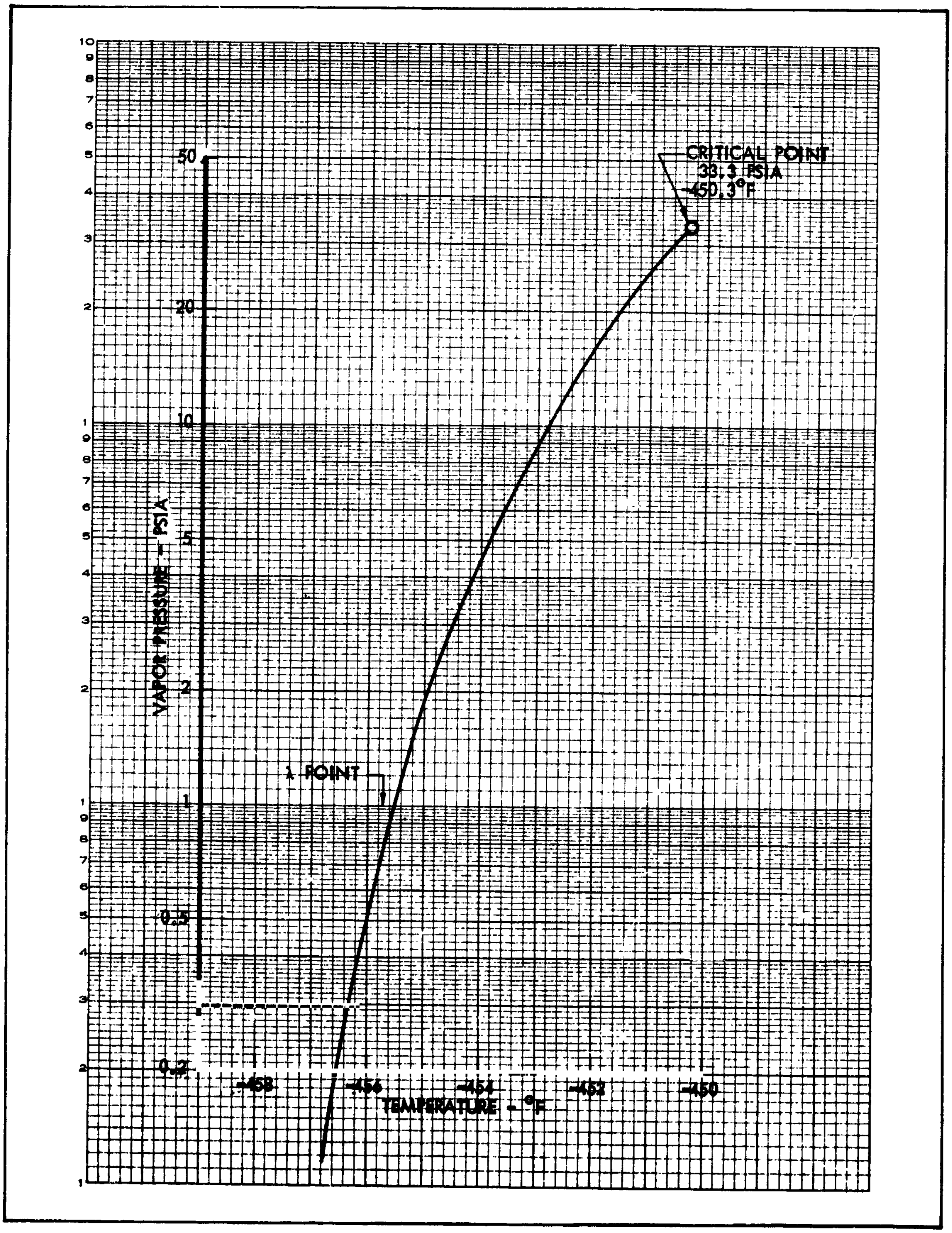

Figure 8-39. Monomethyl Hydrazine Vapor Pressure vs Temperature

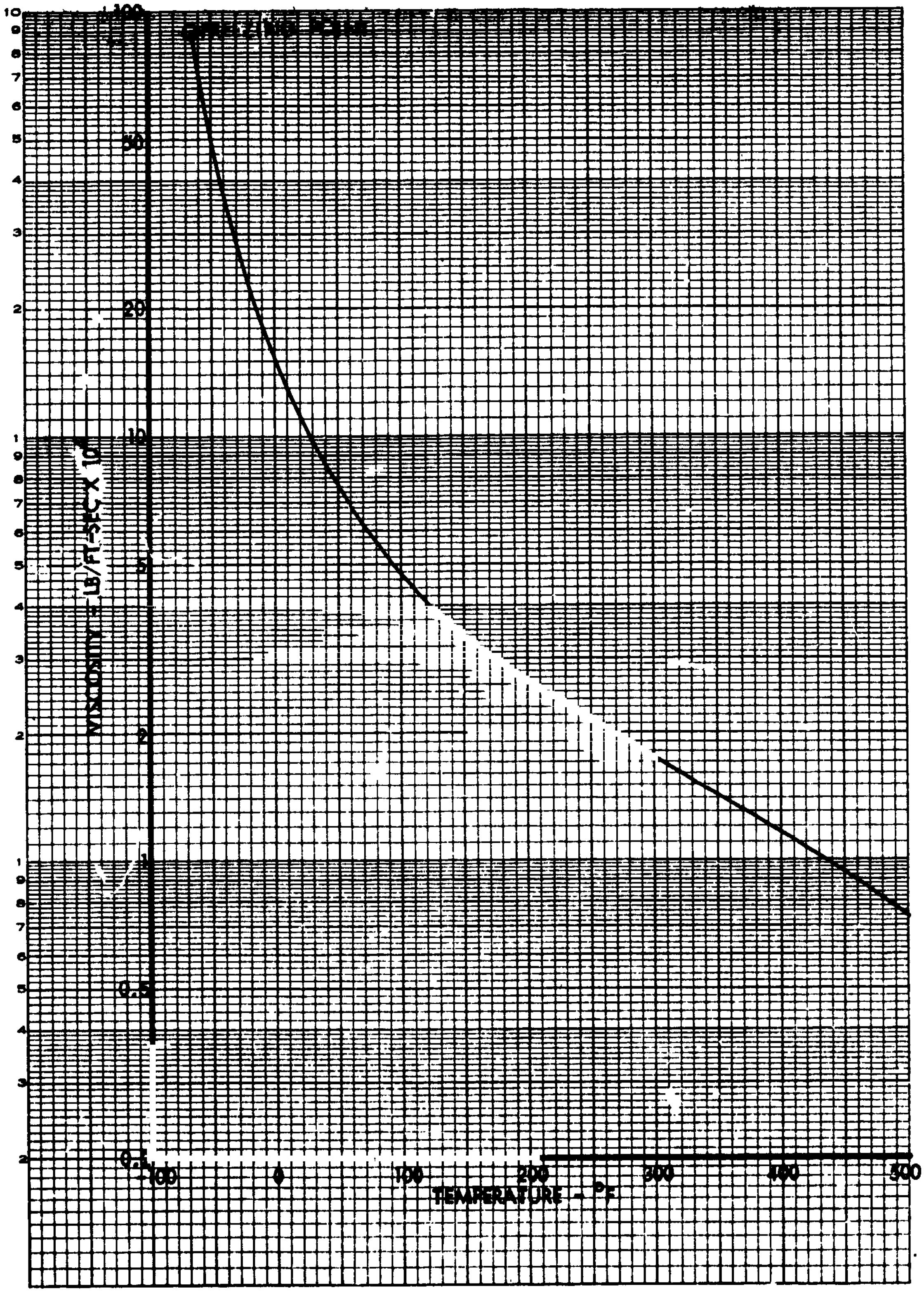

Figure 8-40. Monomethyl Hydrazine Viscosity vs Temperature

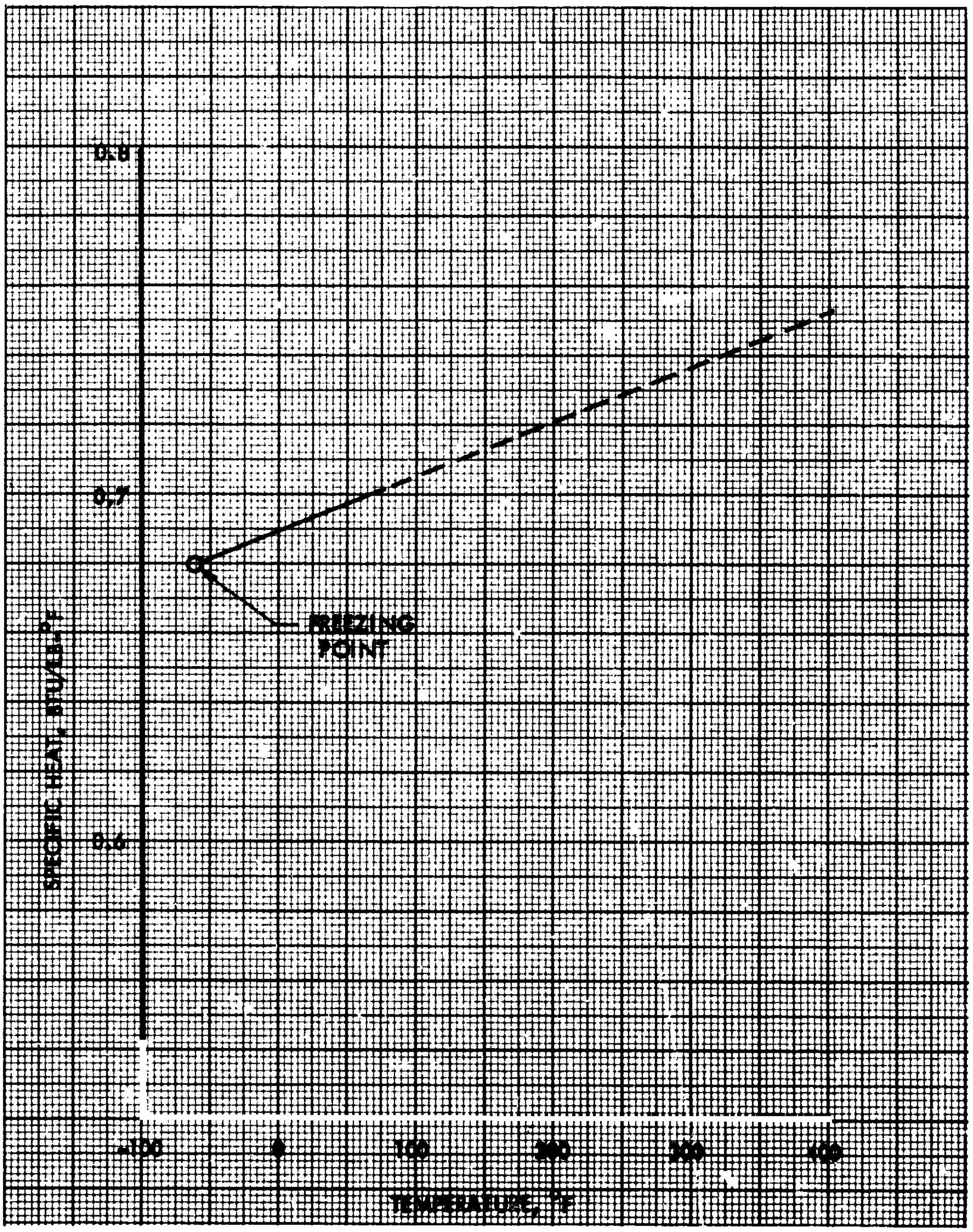

Figure 8-41. Monomethyl Hydrazine Specific Heat vs Temperature

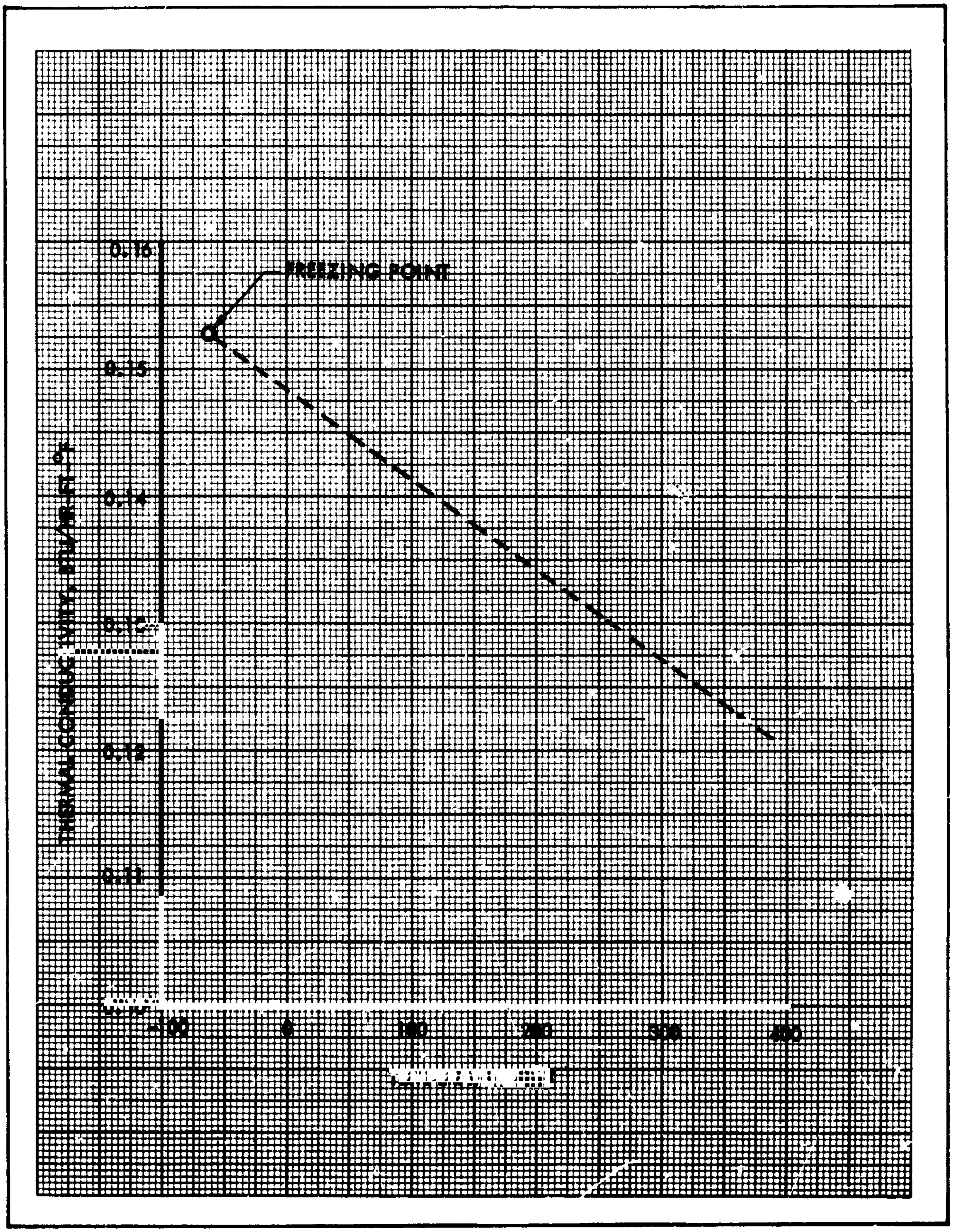

Figure 8-42. Monomethyl Hydrazine Thermal Conductivity vs Temperature

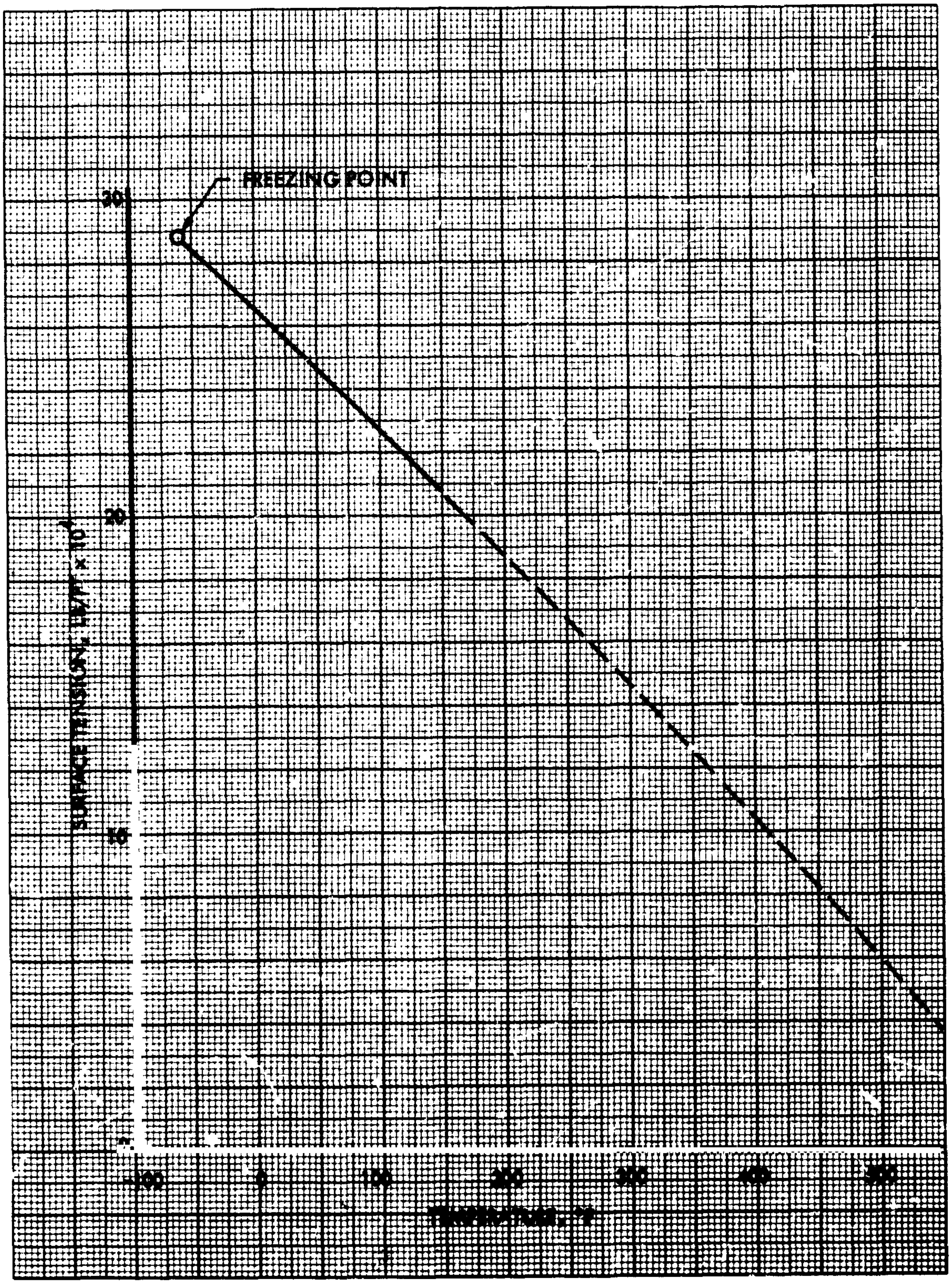

Figure 8-43. Monomethyl Hydrazine Surface Tension vs Temperature

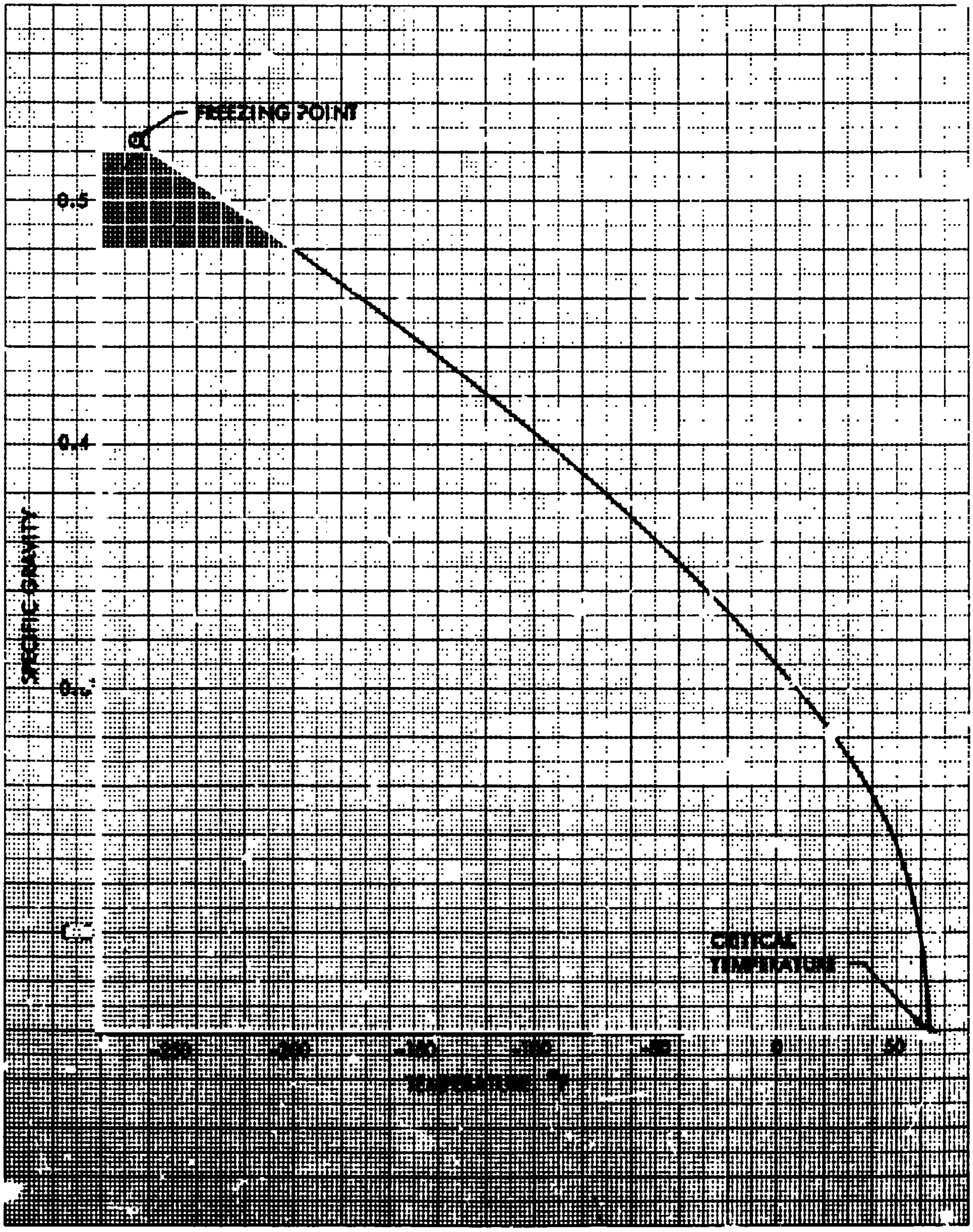

Figure 8-44. Liquid Diborane Specific Gravity vs Temperature

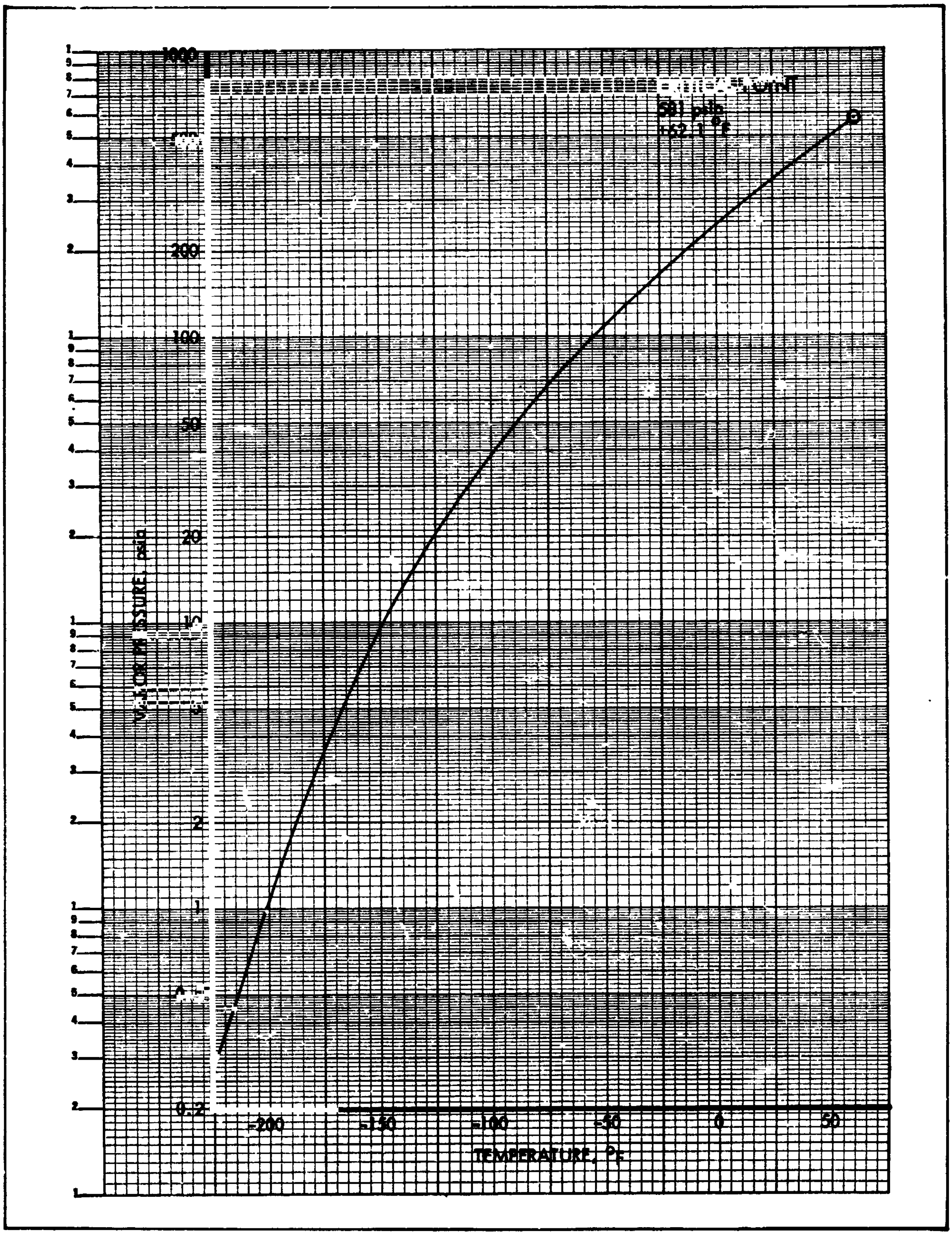

Figure 8-45. Liquid Diborane Vapor Pressure vs Temperature

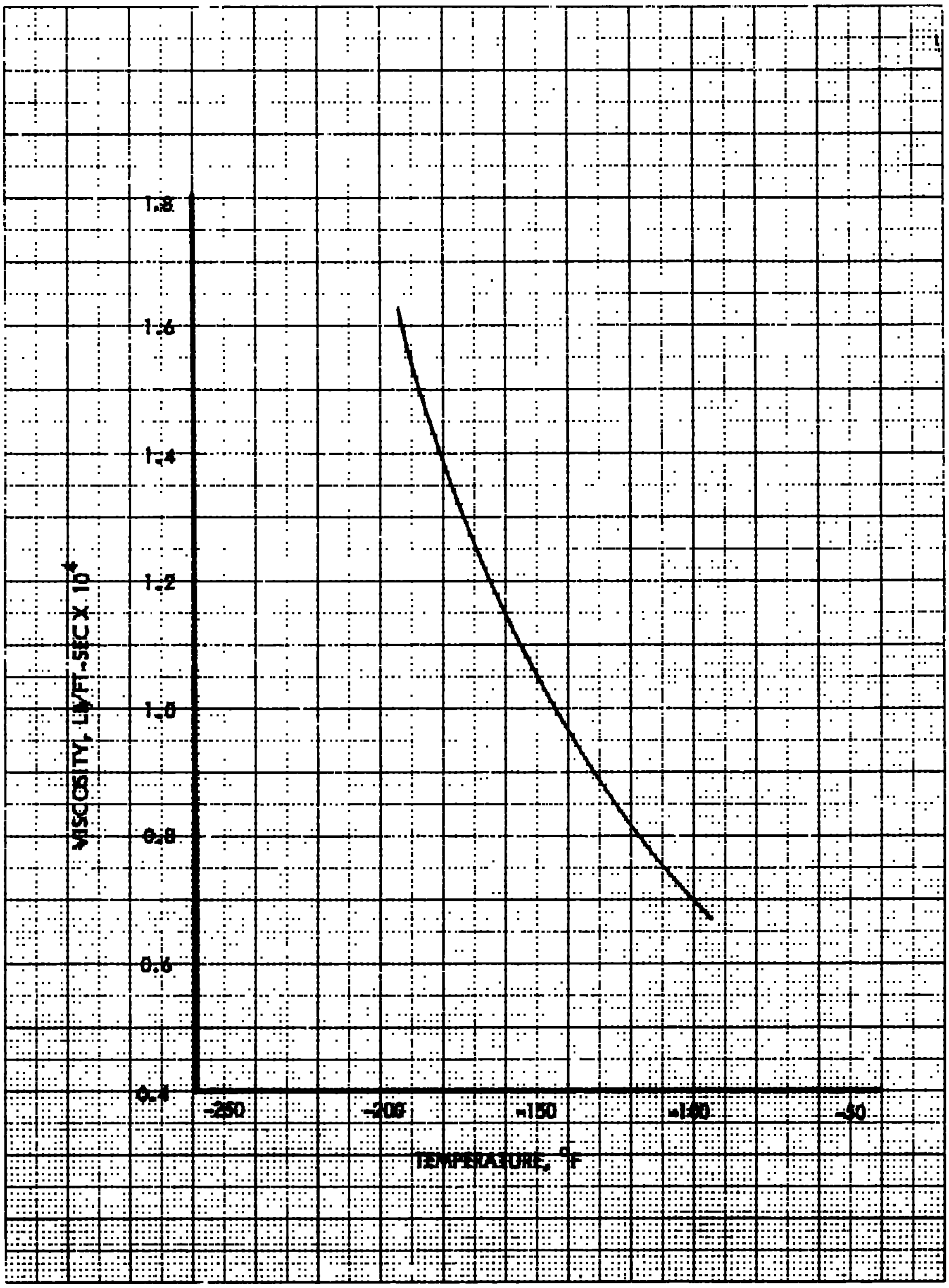

Figure 8-46. Liquid Diborane Viscosity vs Temperature

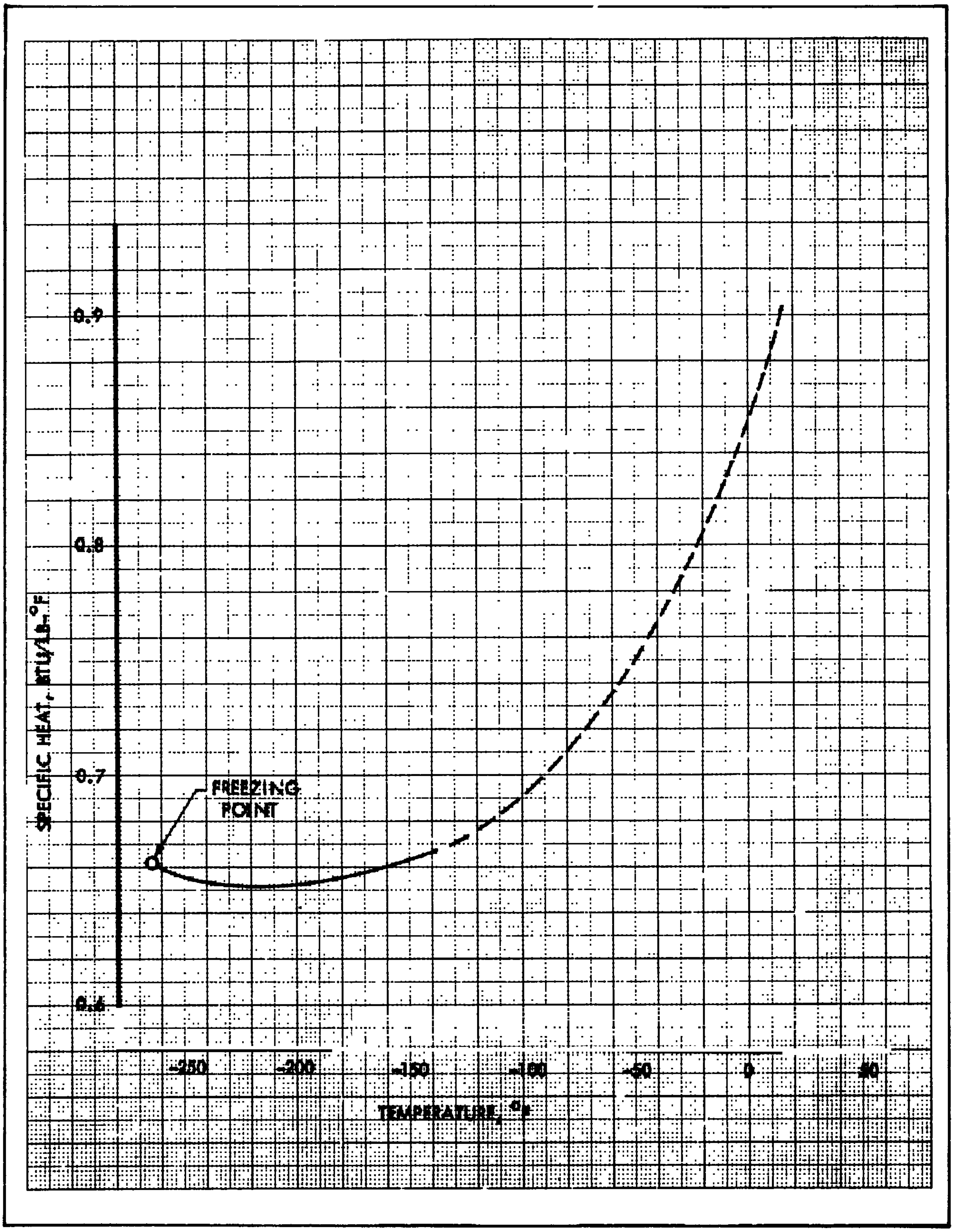

Figure 8-47. Liquid Diborane Specific Heat vs Temperature

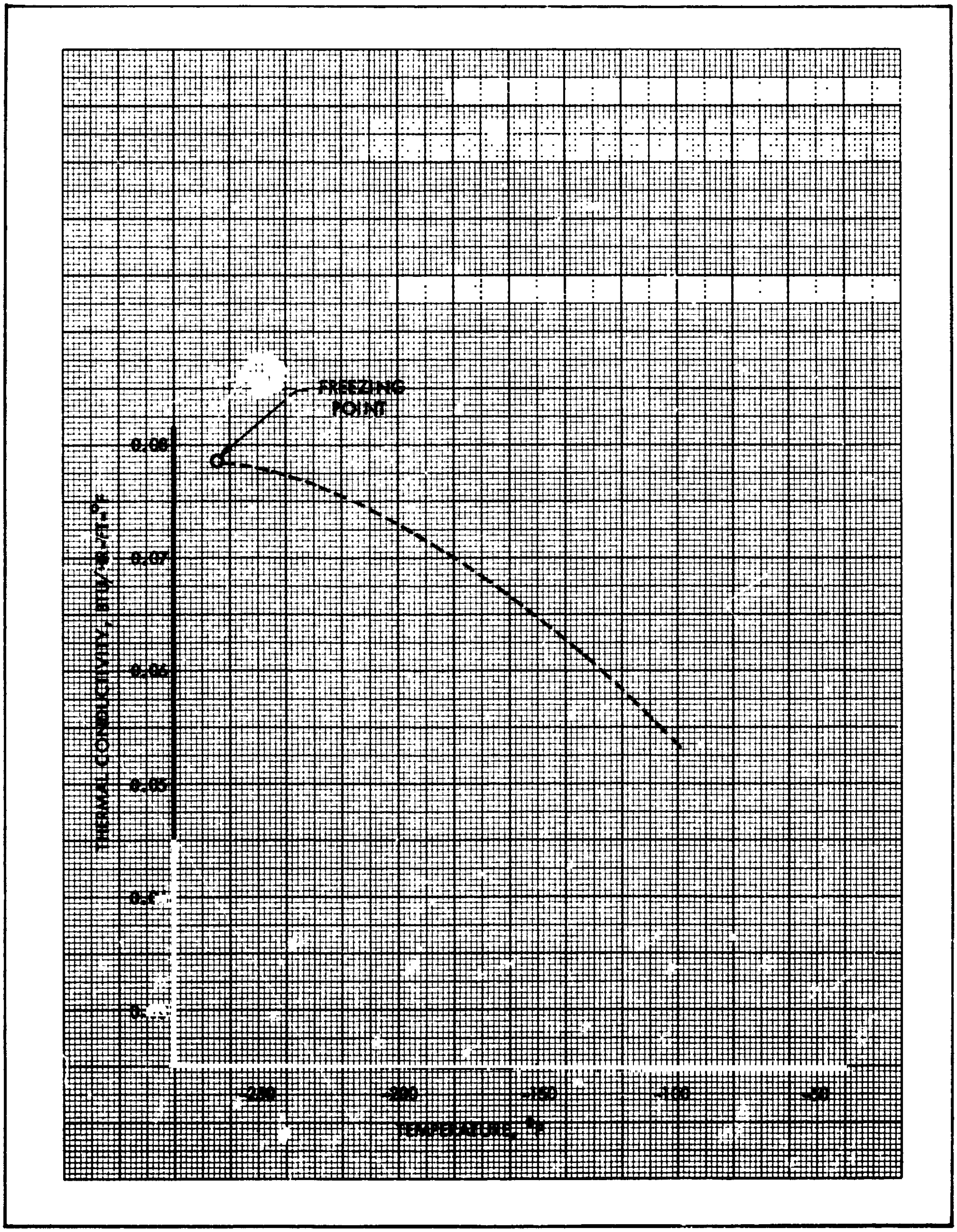

Figure 8-48. Liquid Diborane Thermal Conductivity vs Temperature

TABLE 8-11

GASEOUS DIBORANE SPECIFIC HEAT

(At Saturation Pressure)

Temperature (°F)	Specific Heat (Btu/lb-°F)
-100	.361
+ 80	.483
260	.621
440	.749

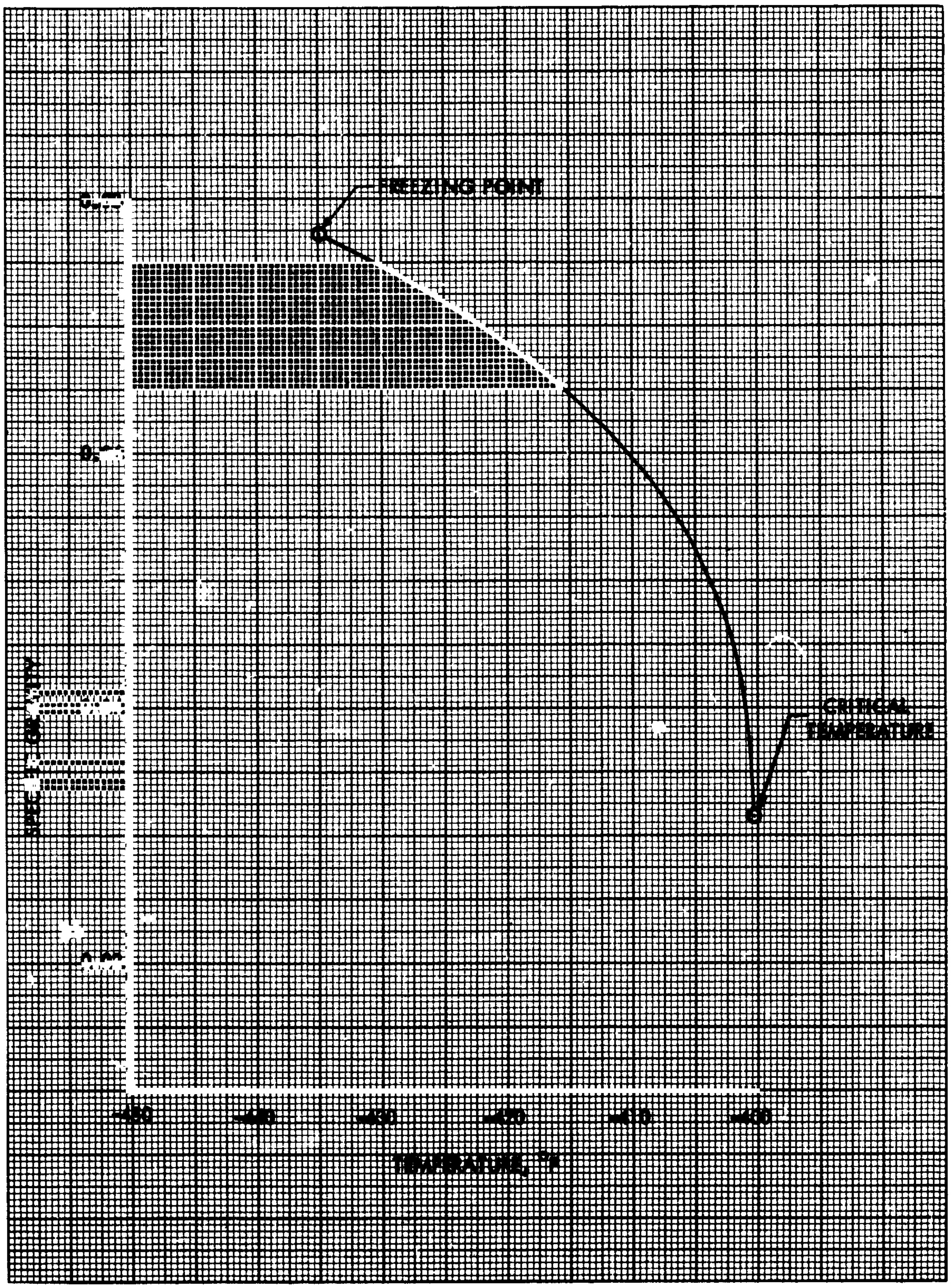

Figure 8-49. Liquid Hydrogen Specific Gravity vs Temperature

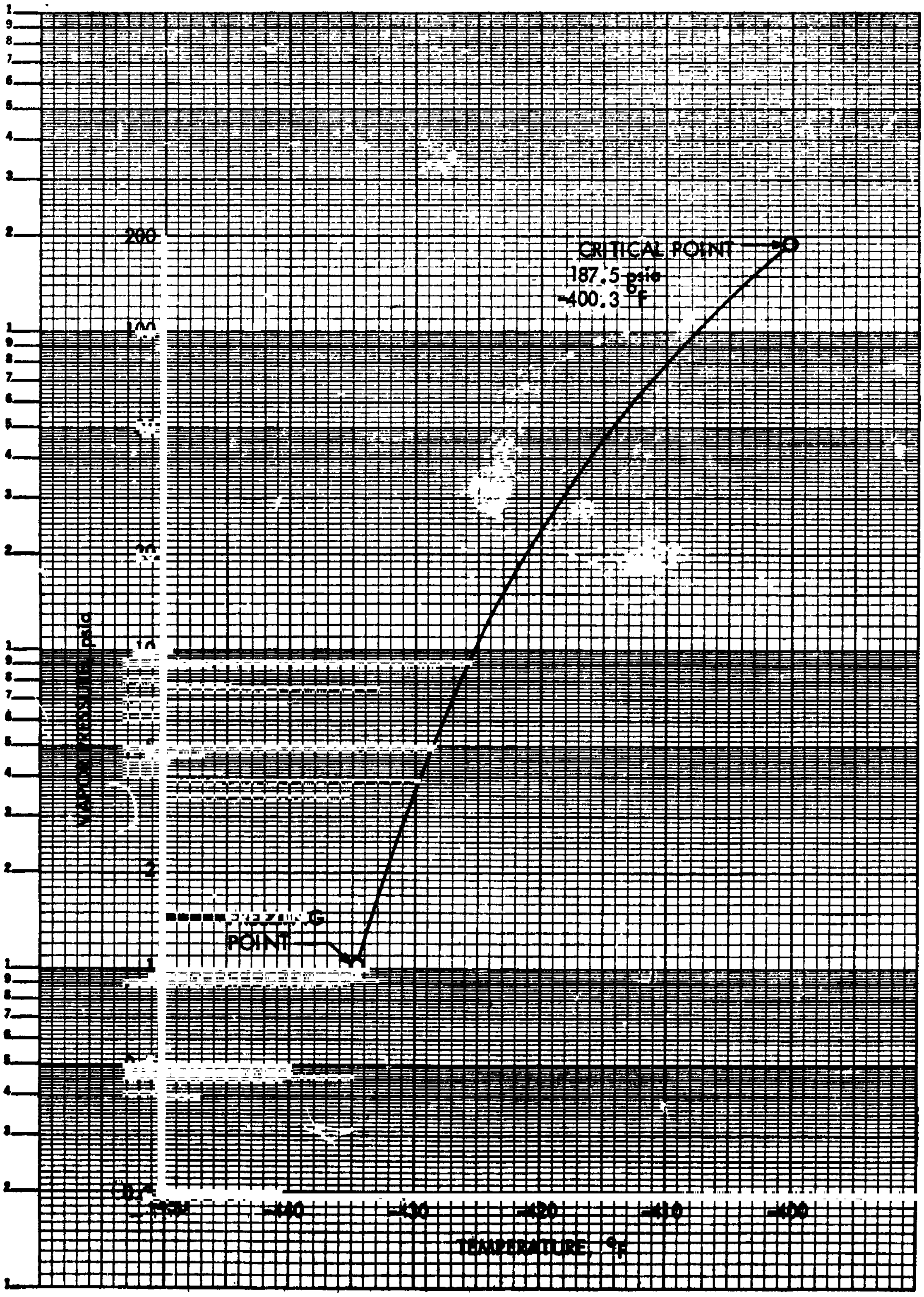

Figure 8-50. Liquid Hydrogen Vapor Pressure vs Temperature

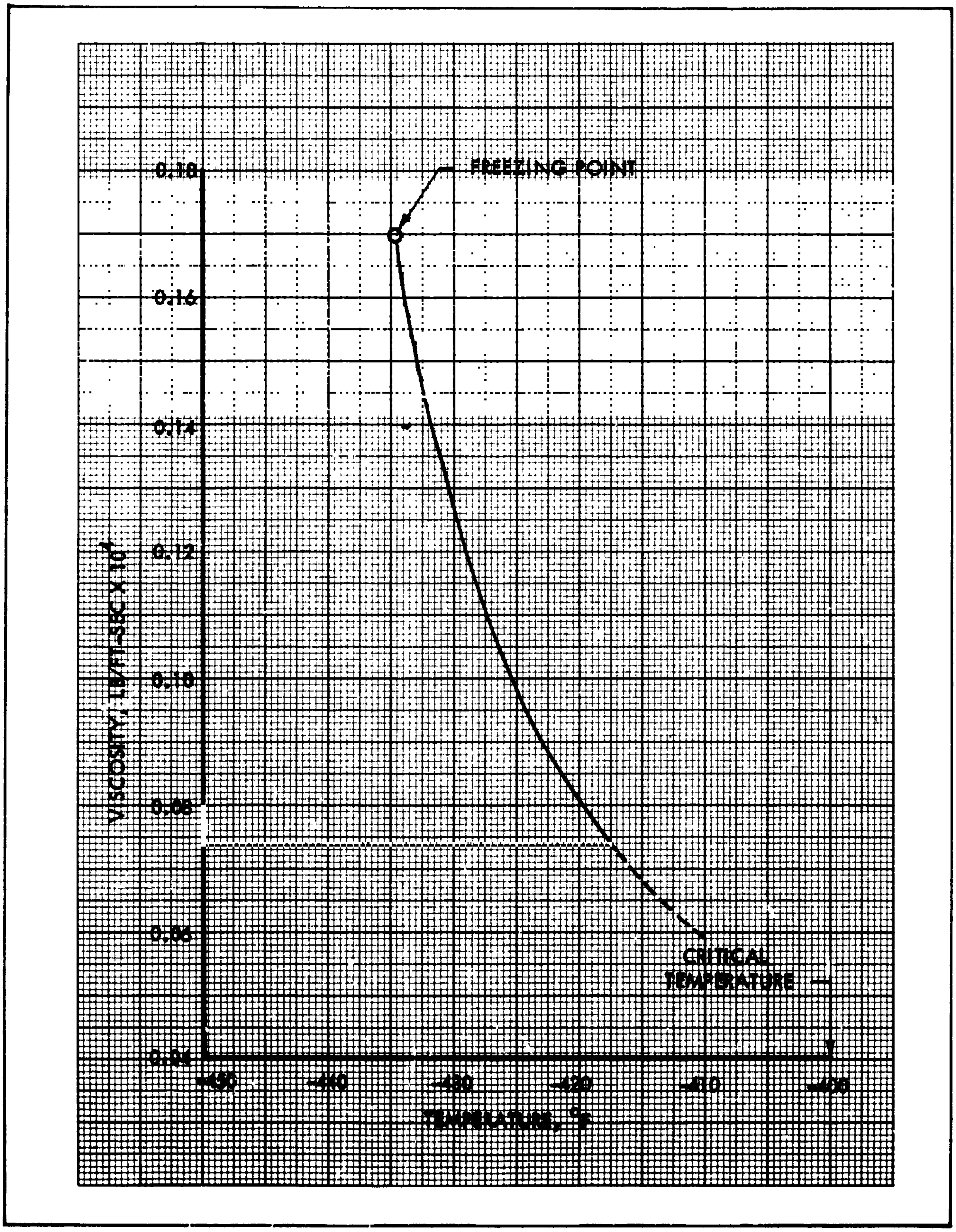

Figure 8-51. Liquid Hydrogen Viscosity vs Temperature

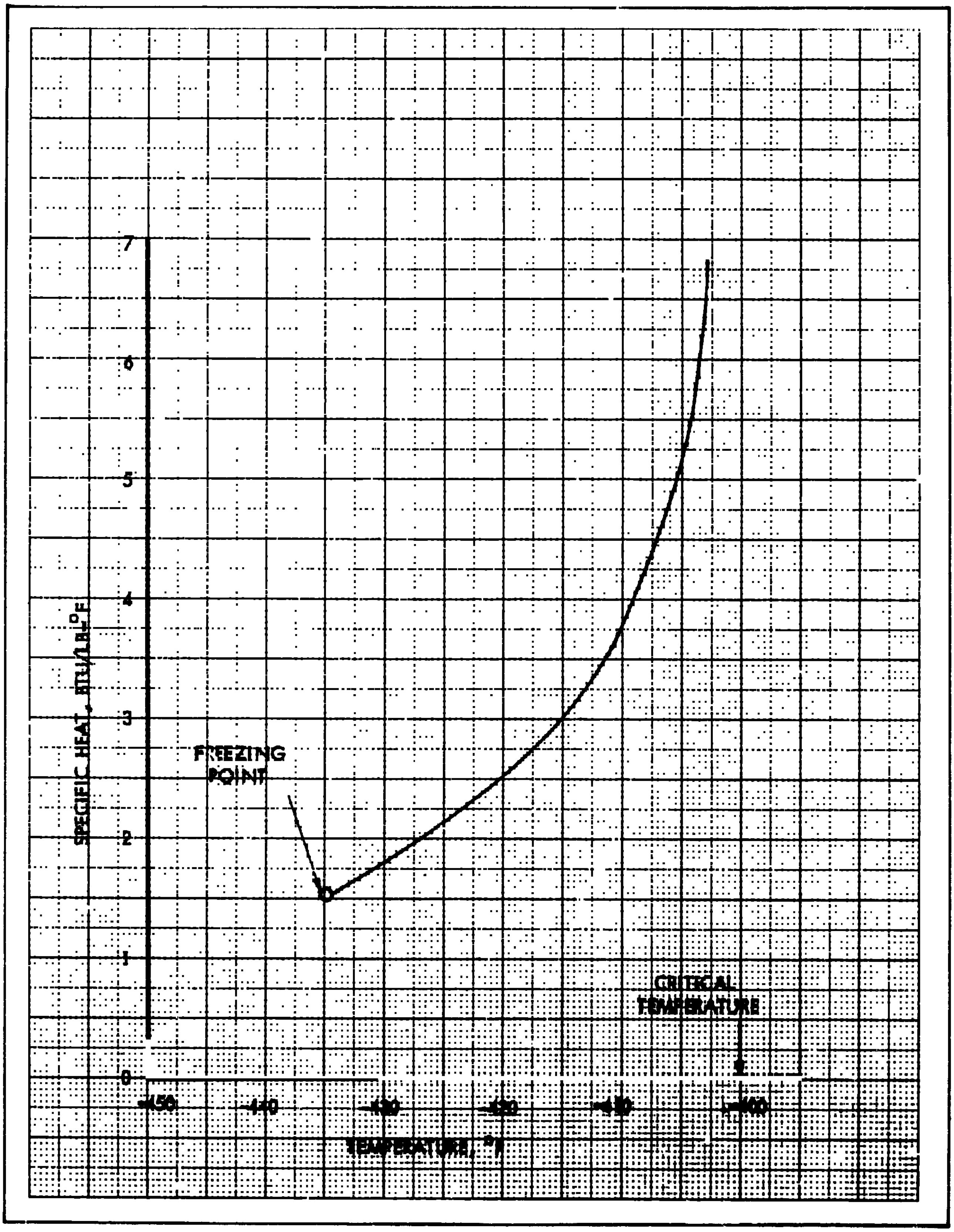

Figure 8-52. Liquid Hydrogen Specific Heat vs Temperature

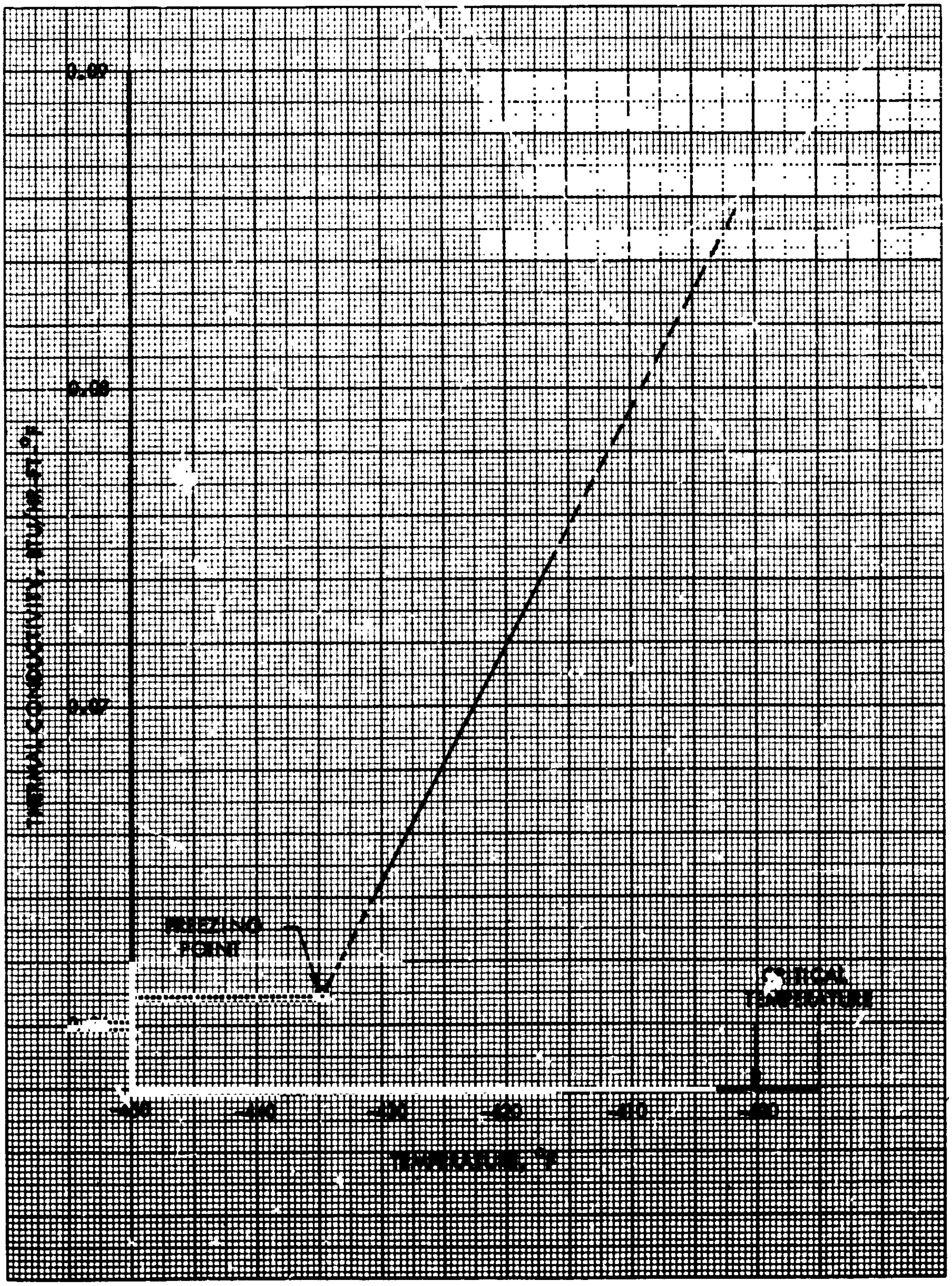

Figure 8-53. Liquid Hydrogen Thermal Conductivity vs Temperature

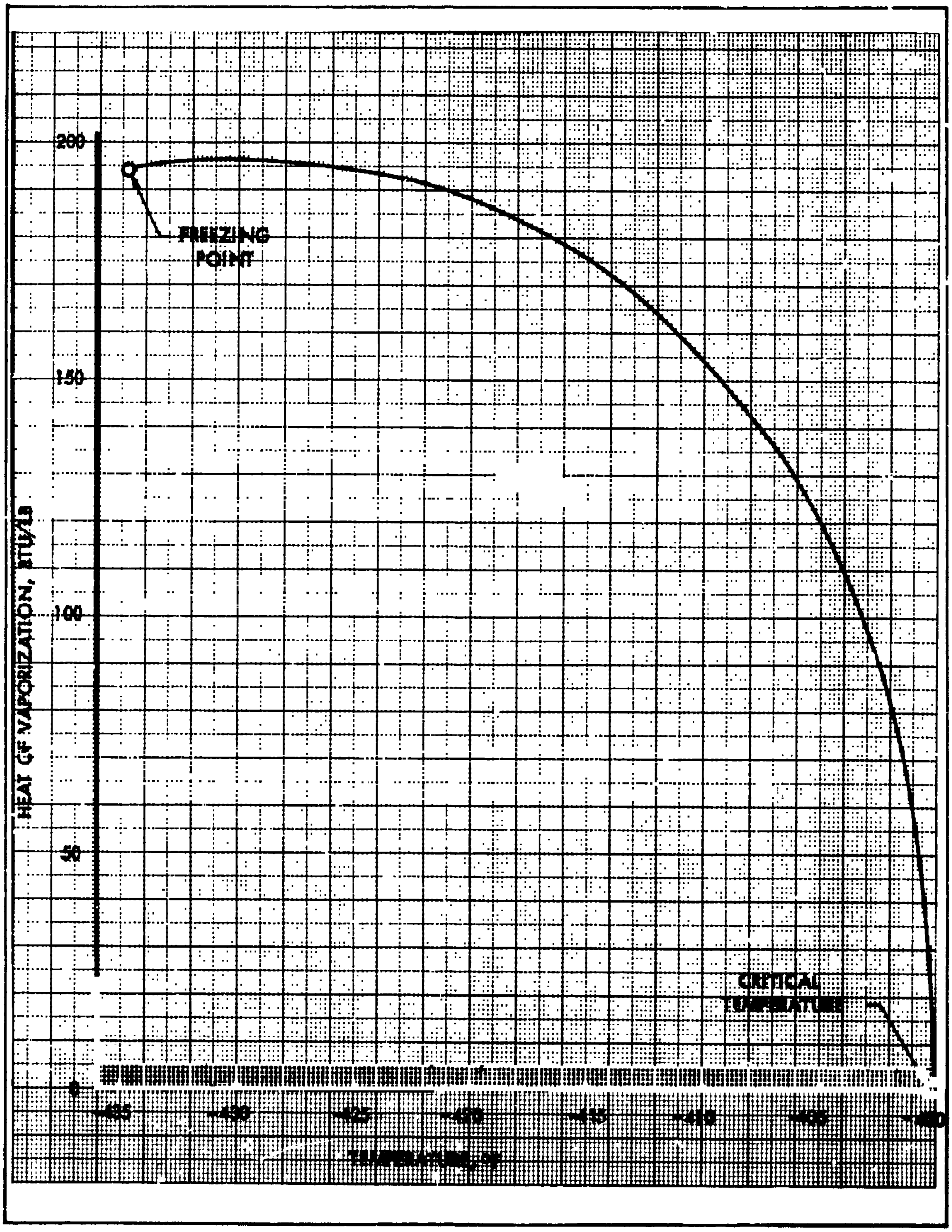

Figure 8-54. Liquid Hydrogen Heat of Vaporization vs Temperature

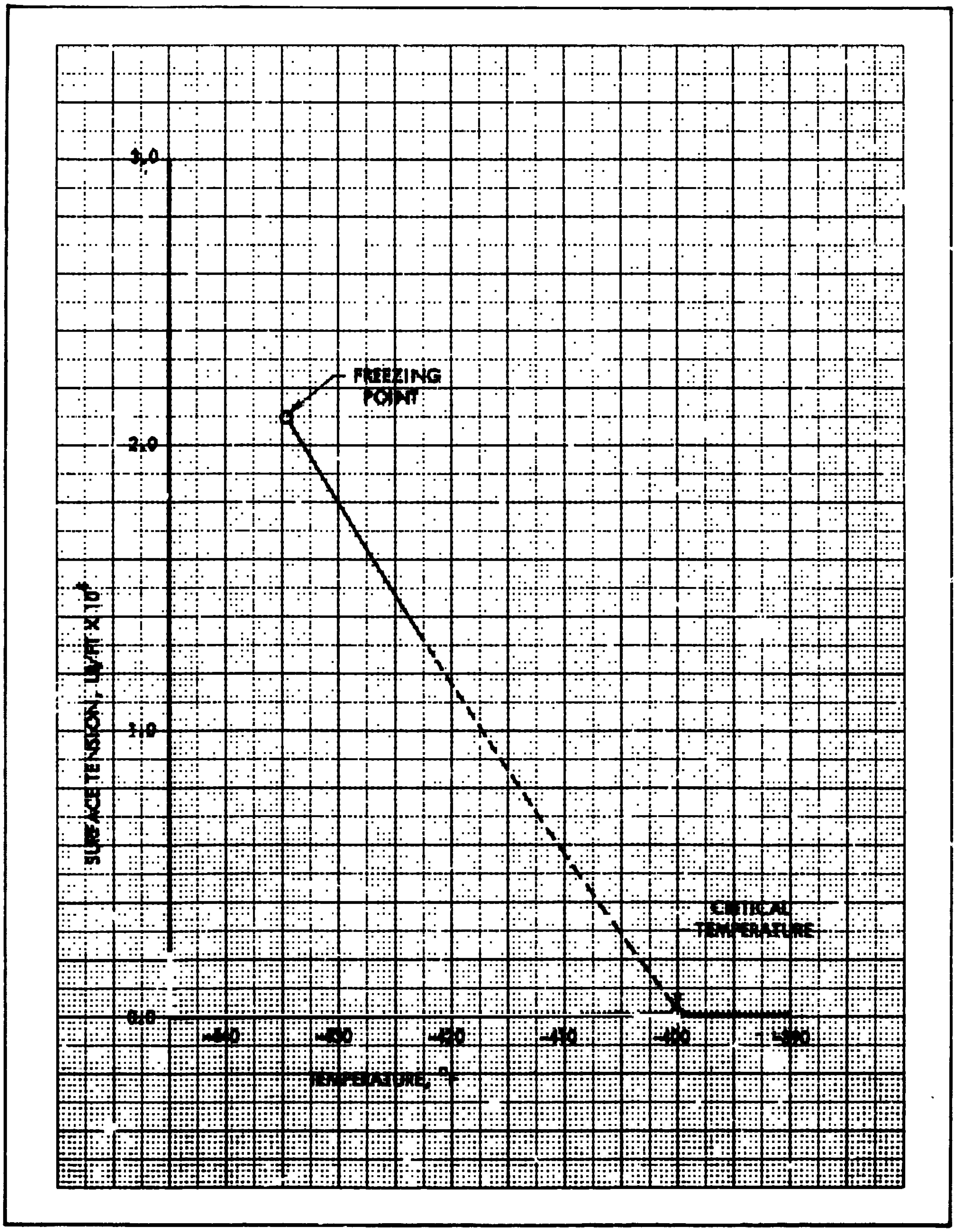

Figure 8-55. Liquid Hydrogen Surface Tension vs Temperature

TABLE 8-12

GASEOUS PARA HYDROGEN COMPRESSIBILITY FACTOR

Temperature, °F

Pressure, psia	-429.7	-419.7	-409.7	-399.7	-395	-390	-385	-380	-370	-360	-310	-260	+340
1	.990	.995	.997	.998	.998	.999	.999	.999	.999	.999	1.000	1.000	1.000
6	.939	.969	.982	.990	.991	.993	.994	.995	.996	.997	1.000	1.000	1.000
14.7	L	.918	.949	.976	.983	.988	.989	.989	.987	.991	.999	1.000	1.000
30		L	.895	.948	.965	.971	.975	.979	.980	.986	.998	1.000	1.001
60			L	.890	.915	.932	.944	.954	.966	.975	.995	1.000	1.002
100				.796	.847	.883	.907	.925	.945	.957	.992	1.001	1.003
150				.664	.775	.826	.862	.883	.908	.934	.989	1.002	1.004
200				.263	.647	.765	.802	.802	.887	.923	.986	1.002	1.005
300				.285	.385	.554	.669	.748	.839	.885	.981	1.004	1.008

LOCKHEED
CALIFORNIA COMPANY

TABLE 8-13

GASEOUS NORMAL HYDROGEN SPECIFIC HEAT
(Btu/lb-°F)

Temperature, °F

Pressure, psia	-423	-410	-405	-402.5	-400	-397.5	-395	-392.5	-390	-387.5
0	2.46	2.46	2.46	2.46	2.46	2.46	2.46	2.46	2.46	2.46
14.7	2.86	2.67	2.6	2.6	2.59	2.57	2.56	2.55	2.54	2.53
71	L	4.3	3.5	3.4	3.25	3.1	3.0	2.95	2.9	2.9
147		L	L	8.5	6.2	4.9	4.3	4.0	3.8	3.4
191				L	Critical	8.5	6.0	4.9	4.4	4.0
220						16	8.4	6.6	5.3	4.5
294							34.5	12.4	8.6	6.5

Pressure, psia	-385	-380	-370	-360	-350	-300	-200	-100	-10	+80
0	2.46	2.47	2.47	2.48	2.48	2.6	2.95	3.23	3.35	3.42
14.7	2.53	2.5	2.5	2.5	2.5	2.6	2.95	3.23	3.35	3.42
71	2.9	2.8	2.7	2.65	2.6	2.65	2.95	3.23	3.35	3.42
147	3.3	3.15	3.0	2.85	2.75	2.7	3.0	3.25	3.36	3.42
191	3.85	3.55	3.2	3.0	2.85	2.7	3.0	3.3	3.4	3.45
220	4.1	3.8	3.4	3.1	2.9	2.7	3.0	3.3	3.4	3.45
294	5.5	4.5	3.6	3.2	3.0	2.7	3.05	3.3	3.4	3.46

NOTE:

	Hydrogen Normal	Hydrogen Para
Critical temperature	-399.9	-400.3
Pressure	190.8	187.5

TABLE 8-14

GASEOUS PARA HYDROGEN THERMAL CONDUCTIVITY

(Pressure = 14.7 psia)

Temperature (°F)	Conductivity (Btu/hr-ft-°F)
-420	.010
-330	.030
-190	.070
- 60	.090
+ 80	.165

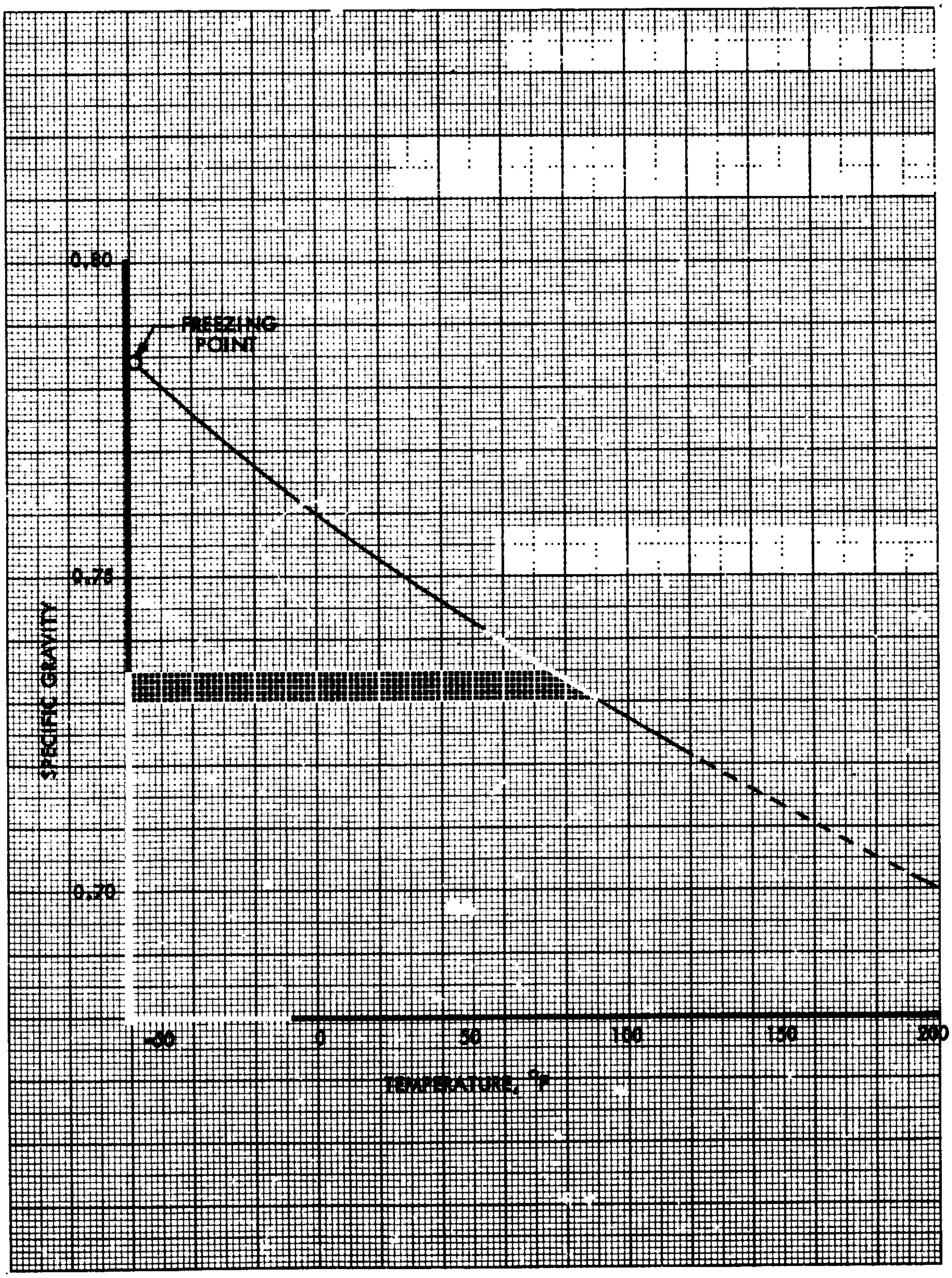

Figure 8-56. Liquid Hybaline A-5 Specific Gravity vs Temperature

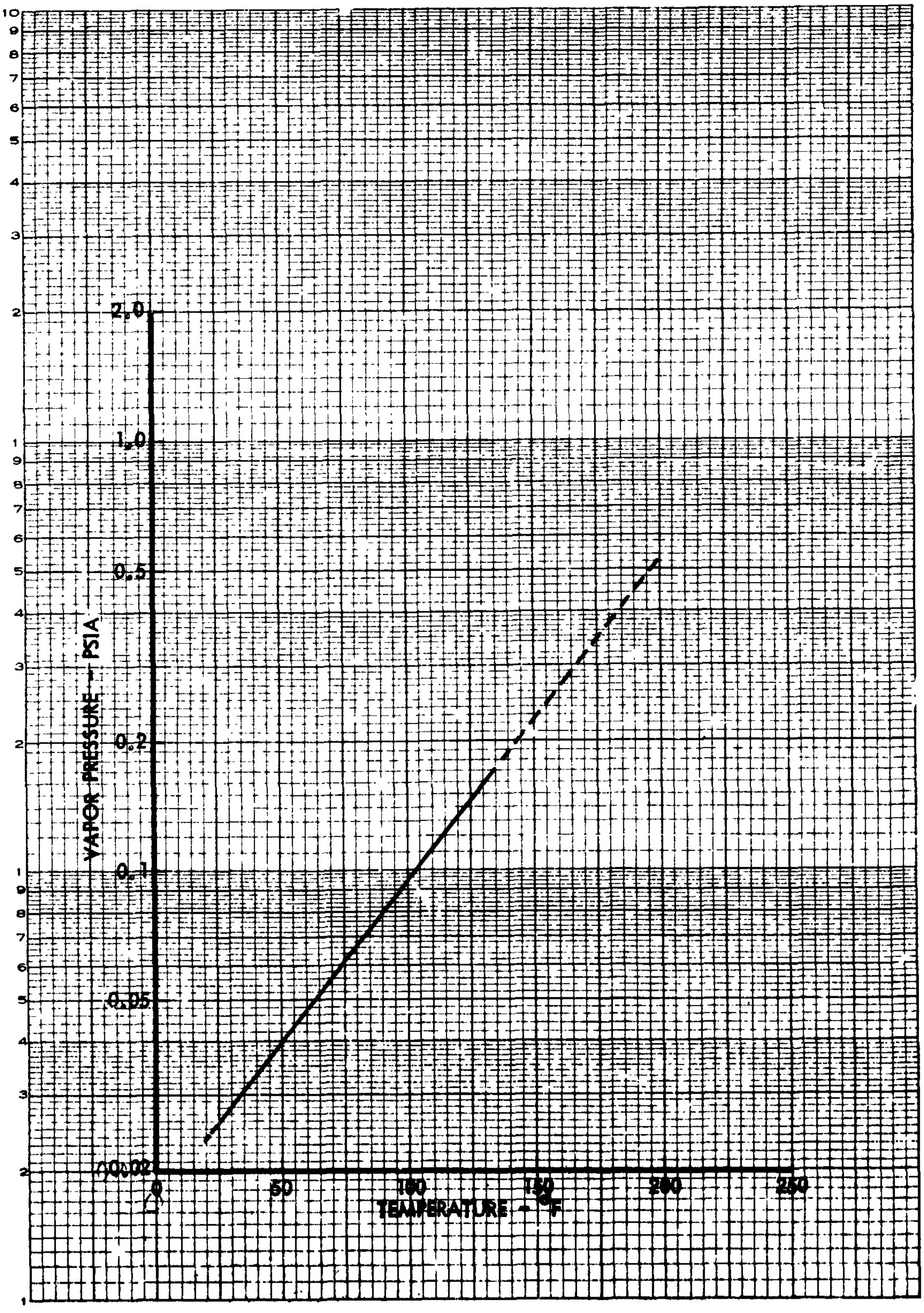

Figure 8-57. Liquid Hybaline A-5 Vapor Pressure vs Temperature

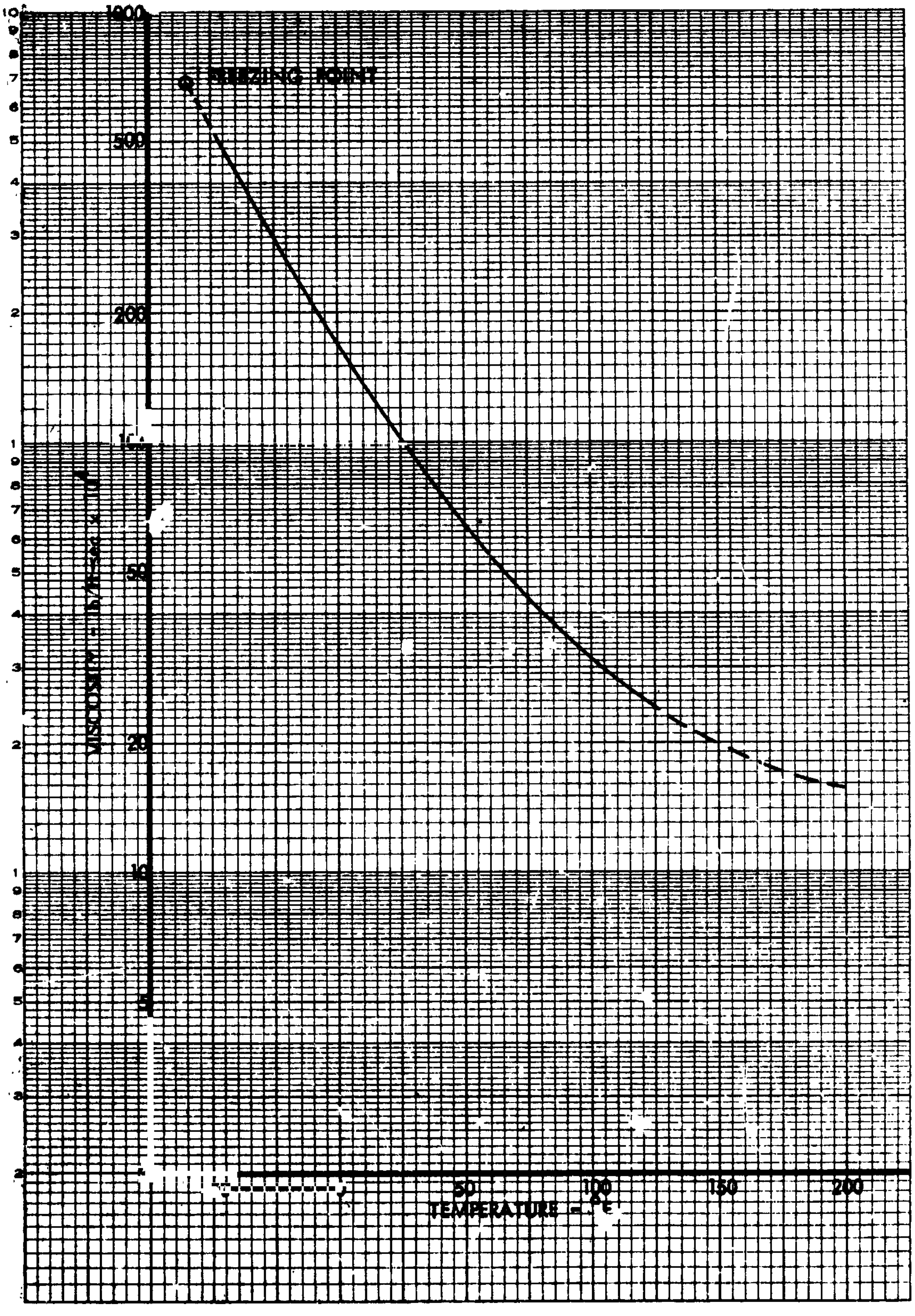

Figure 8-58. Liquid Hybaline A-5 Viscosity vs Temperature

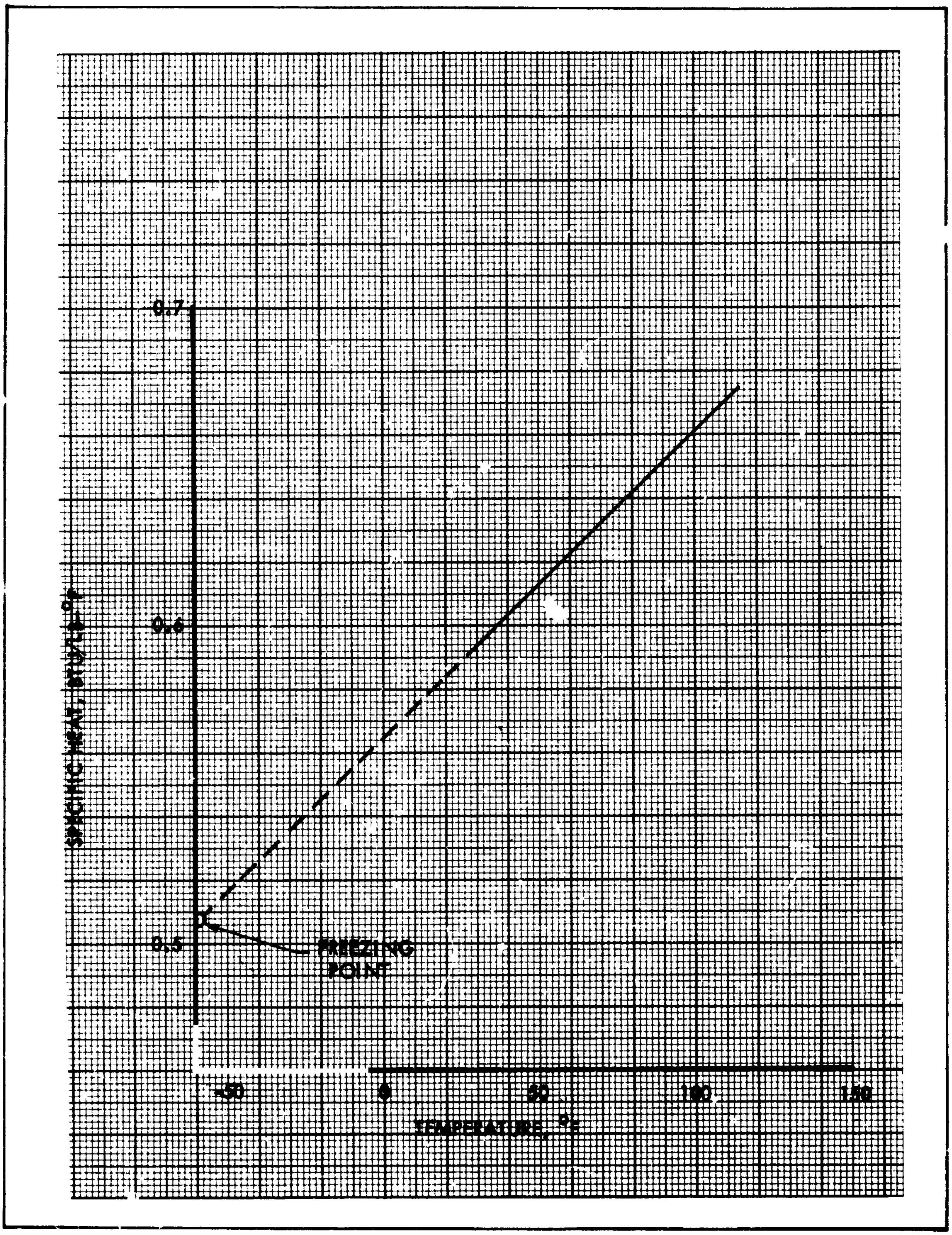

Figure 8-59. Liquid Hybaline A-5 Specific Heat vs Temperature

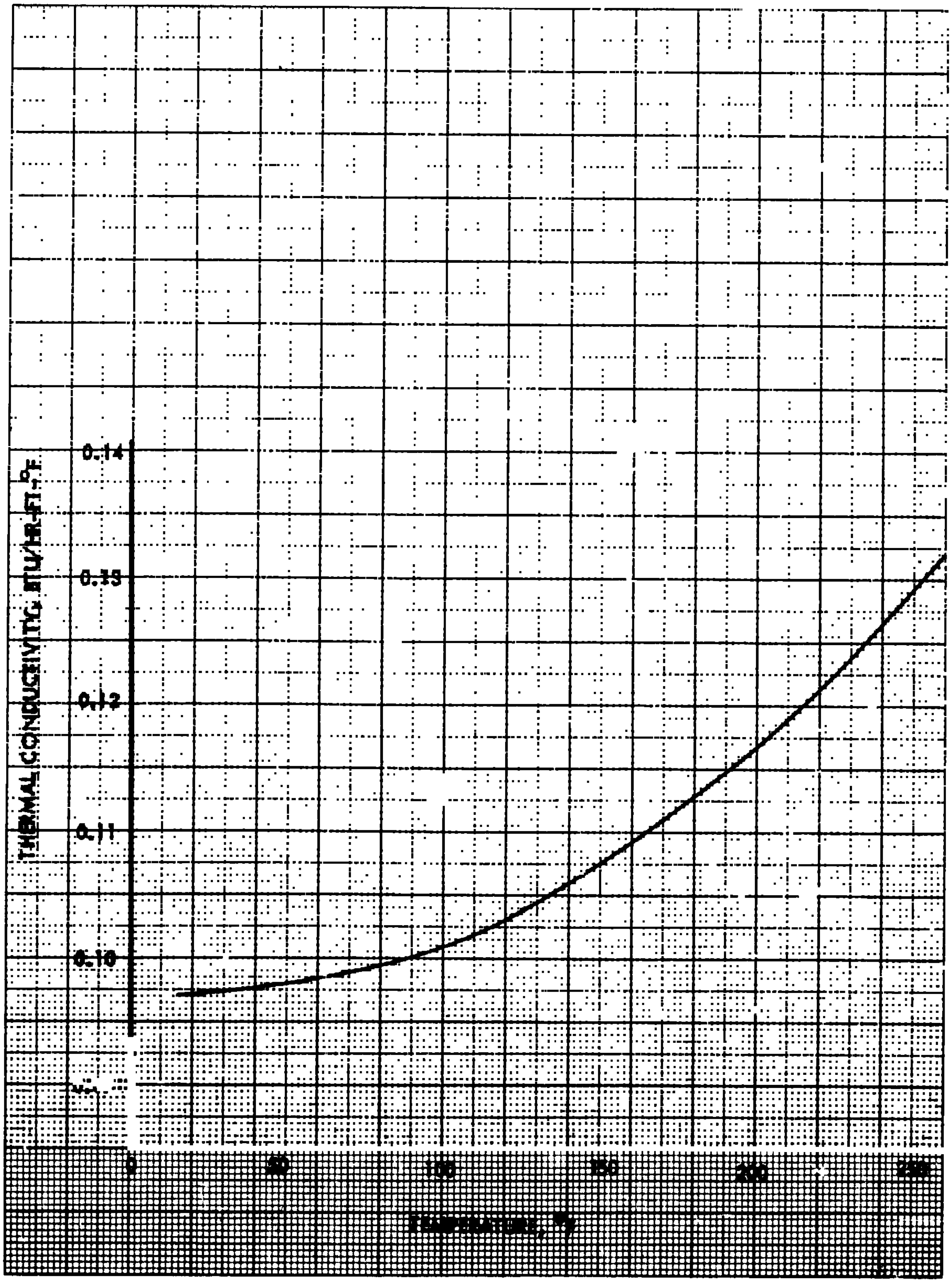

Figure 8-60. Liquid Hybaline A-5 Thermal Conductivity vs Temperature

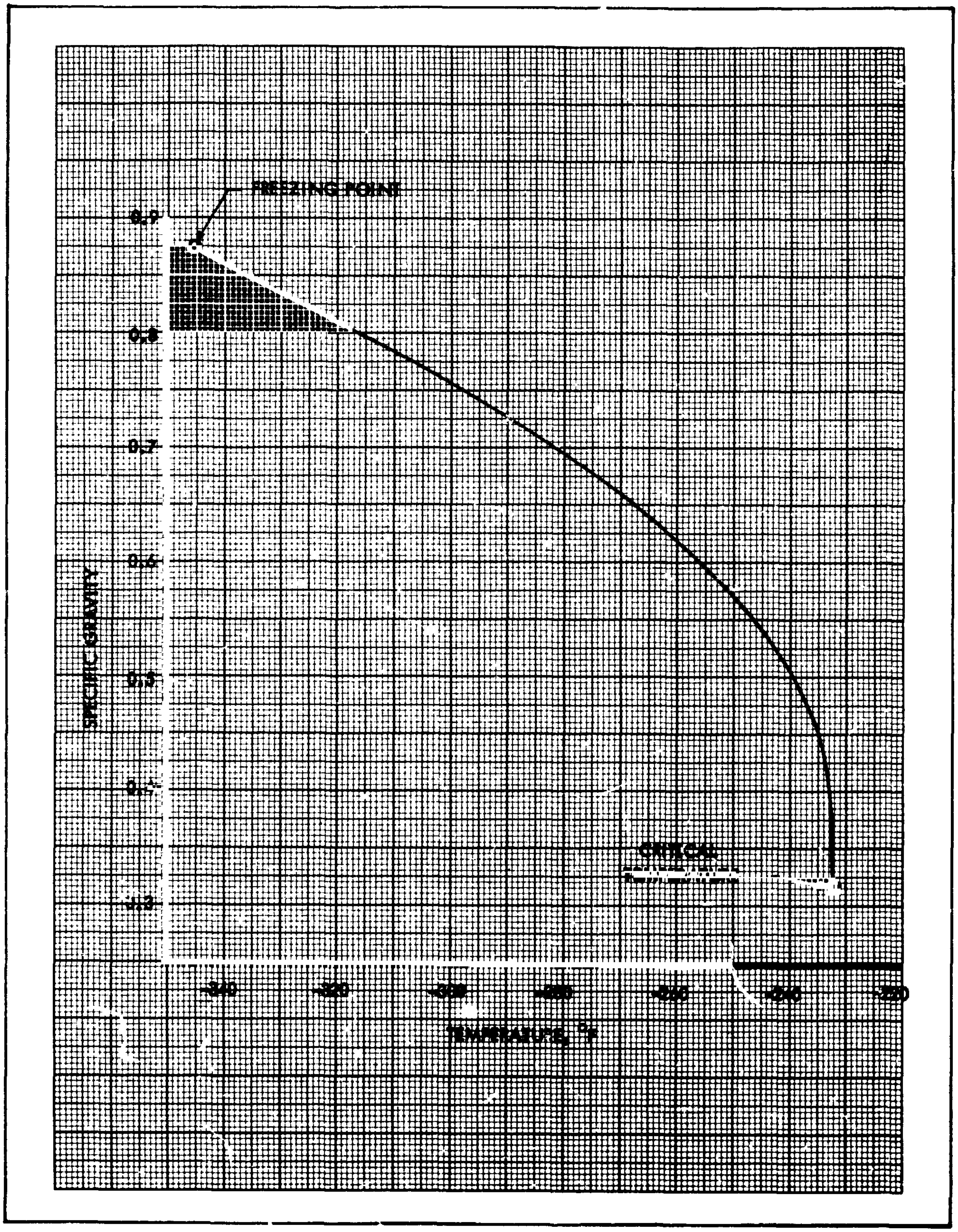

Figure 8-61. Liquid Nitrogen Specific Gravity vs Temperature

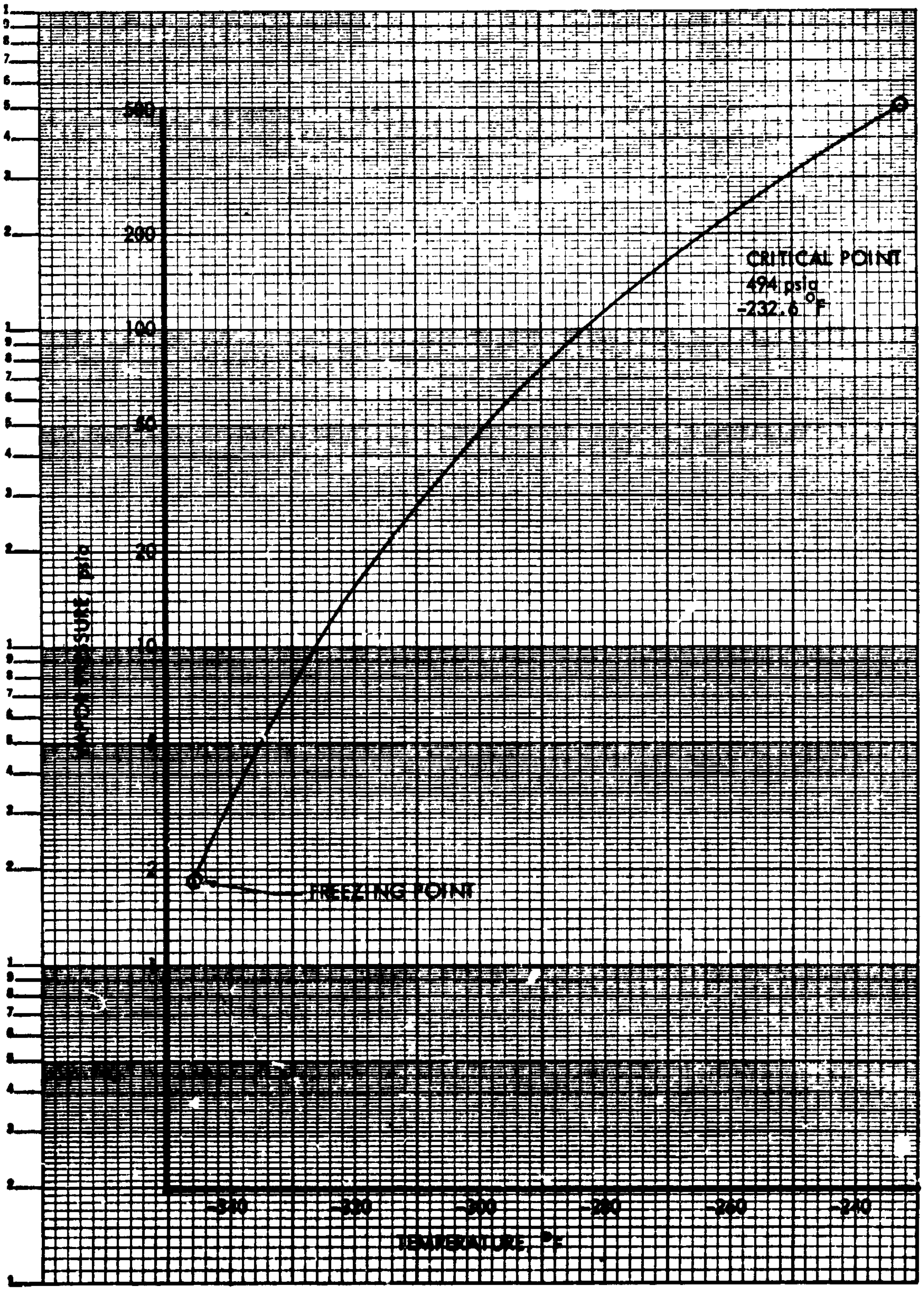

Figure 8-62. Liquid Nitrogen Vapor Pressure vs Temperature

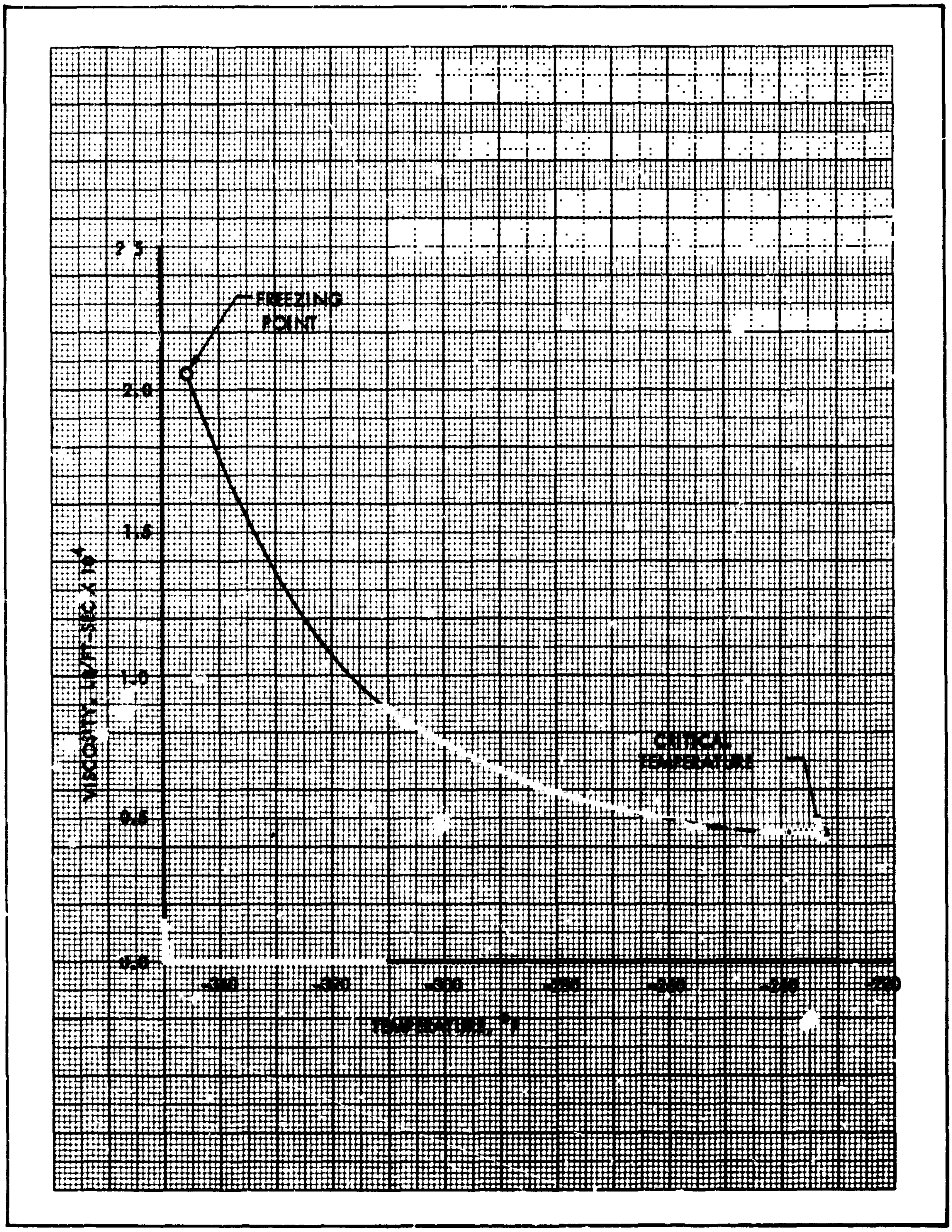

Figure 8-63. Liquid Nitrogen Viscosity vs Temperature

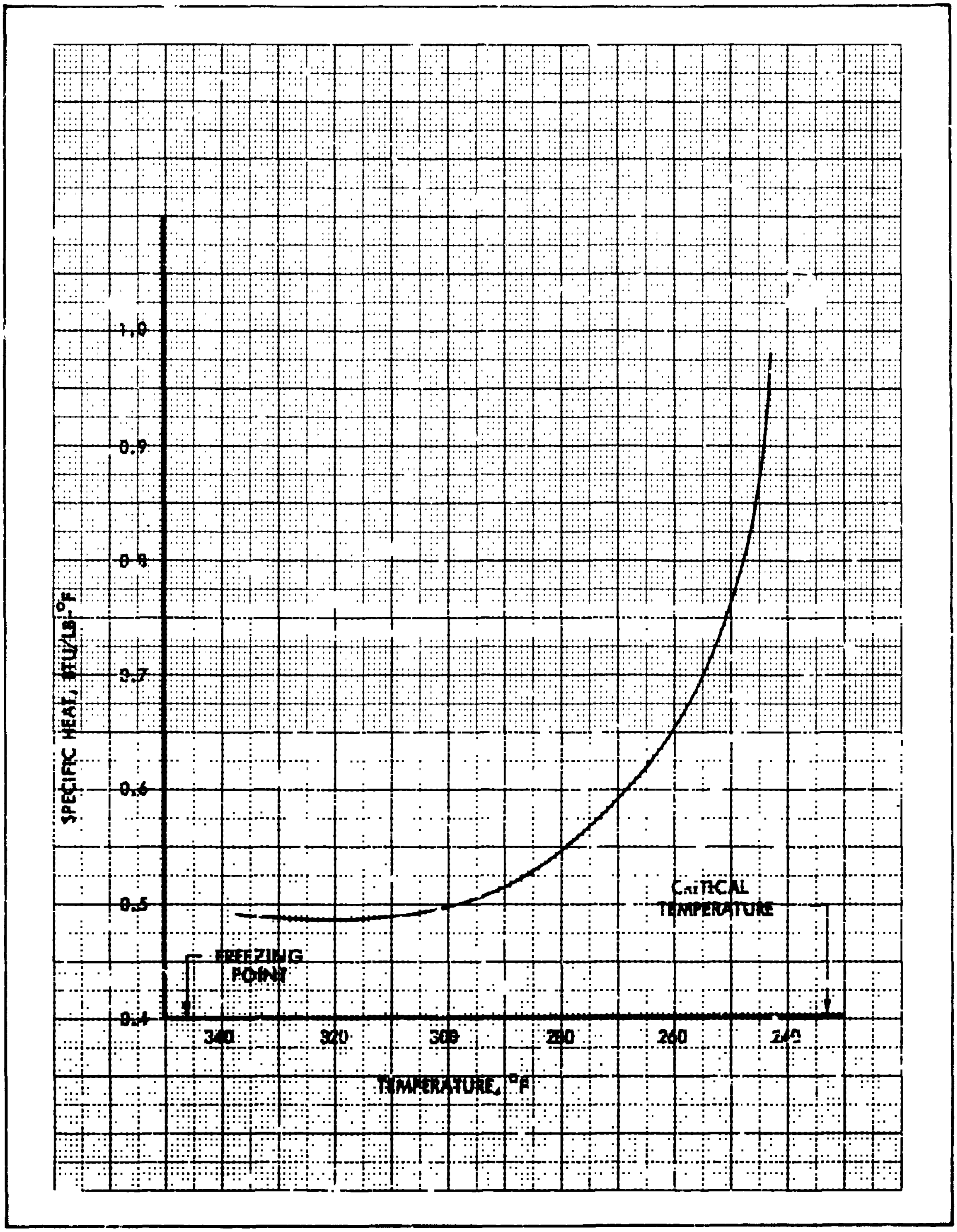

Figure 8-64. Liquid Nitrogen Specific Heat vs Temperature

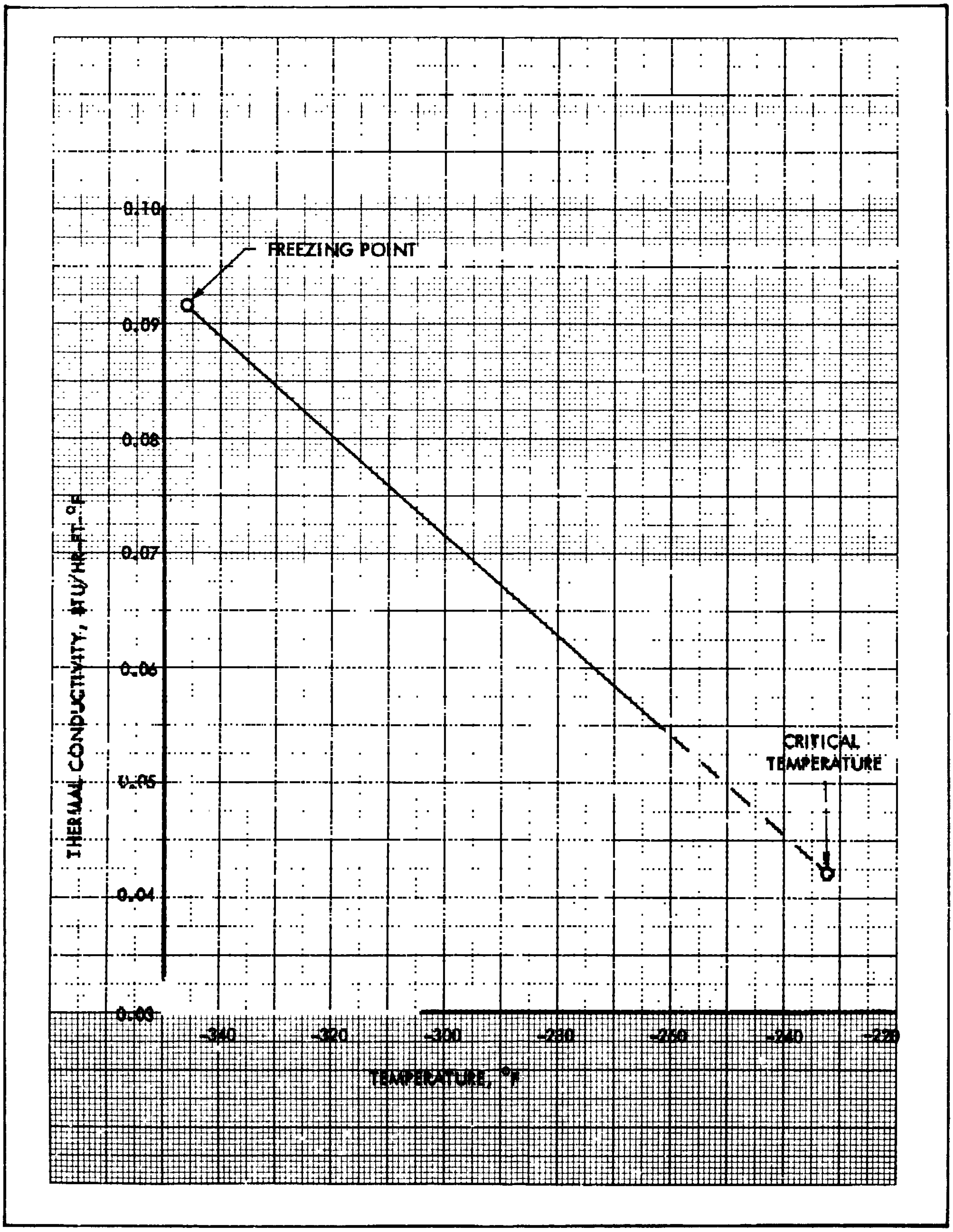

Figure 8-65. Liquid Nitrogen Thermal Conductivity vs Temperature

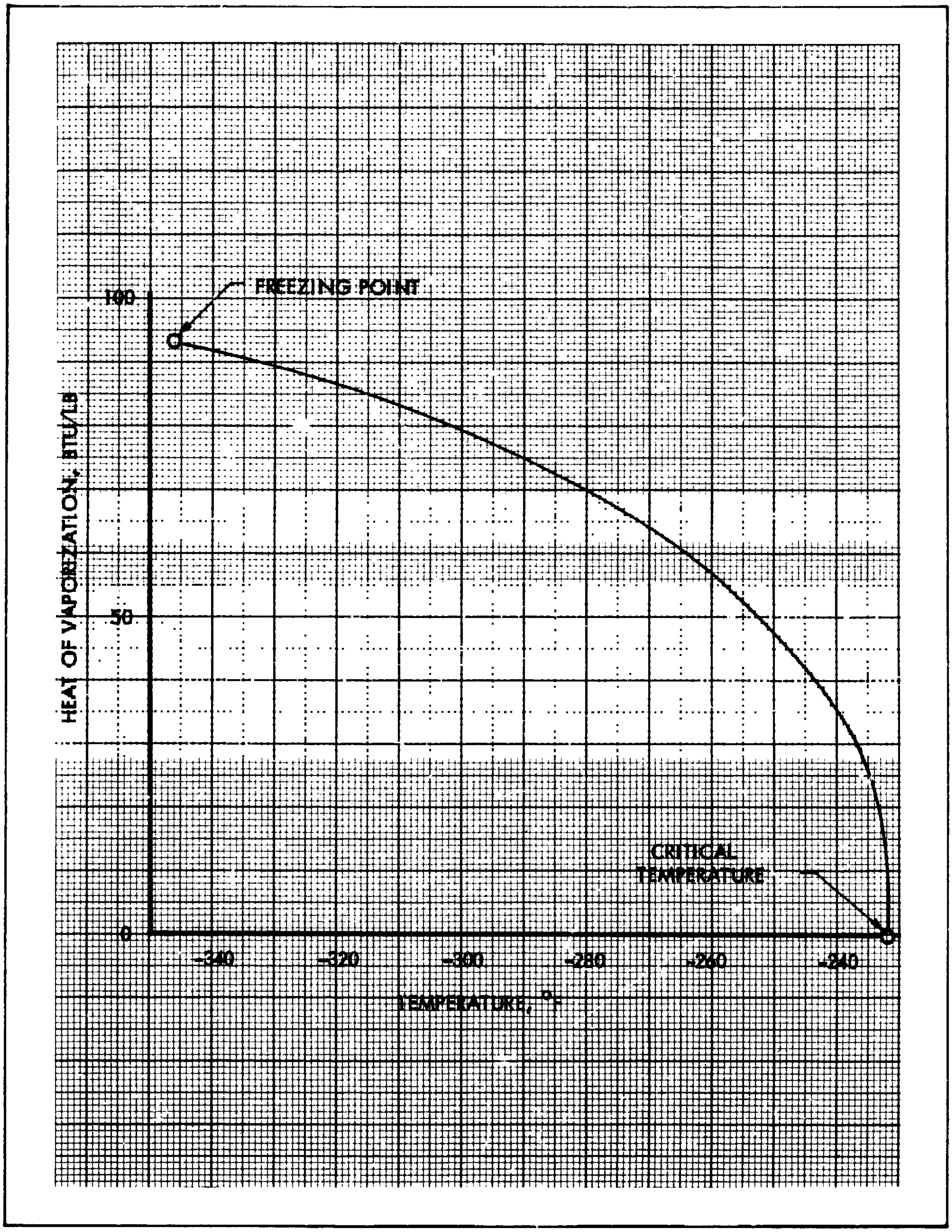

Figure 8-66. Liquid Nitrogen Heat of Vaporization vs Temperature

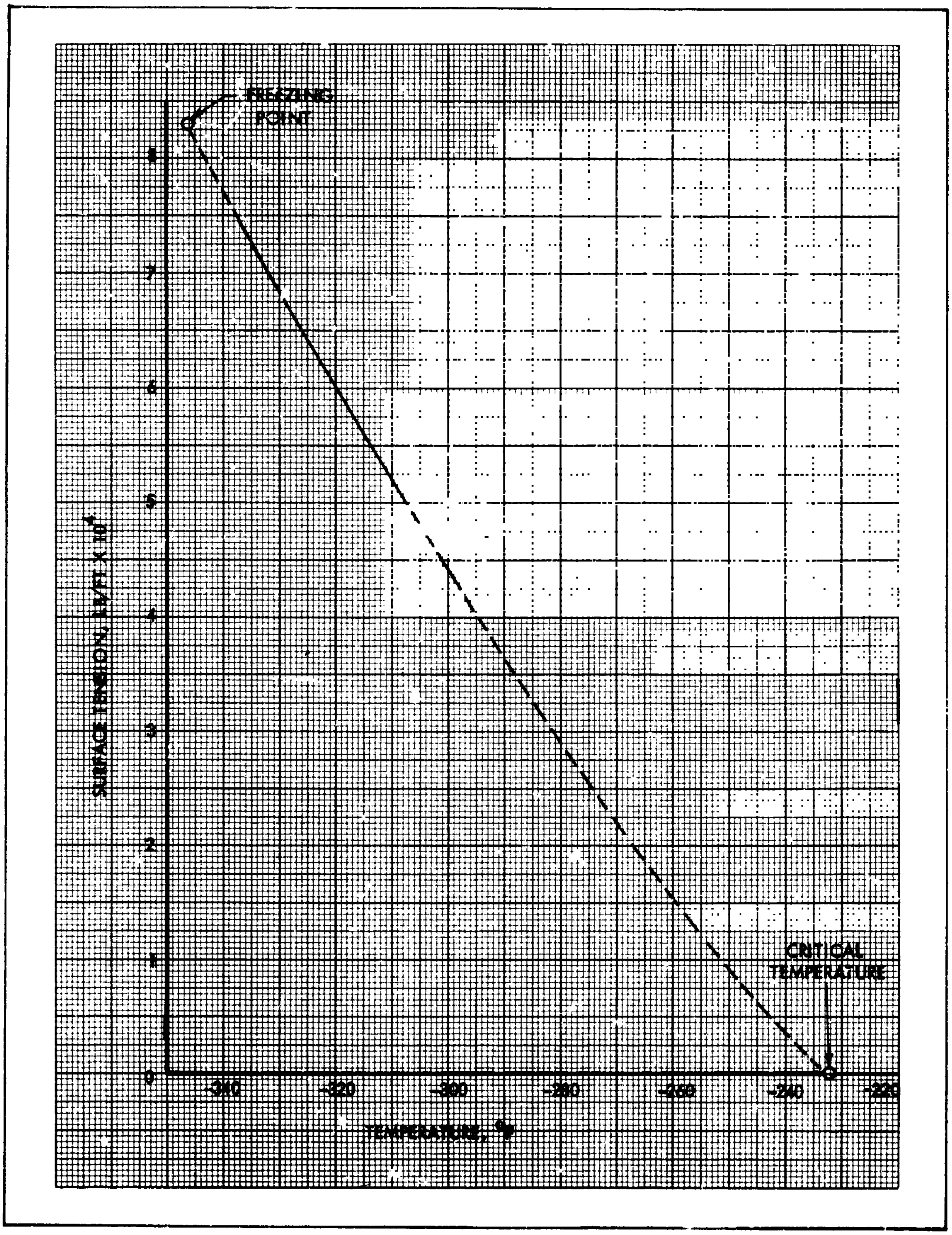

Figure 8-67. Liquid Nitrogen Surface Tension vs Temperature

TABLE 8-15
GASEOUS NITROGEN COMPRESSIBILITY FACTOR

Temperature, °F

Pressure, psia

	-300	-280	-260	-240	-230	-220	-210	-190	-160	-110	-60	+80
14.7	.97	.98	.99	.99	.99	.99	.99	1.00	1.00	1.00	1.00	1.00
50	L	.93	.95	.96	.97	.97	.98	.98	.99	.99	1.00	1.00
100		.85	.89	.92	.93	.94	.95	.96	.97	.98	.99	1.00
200		L	L	.83	.86	.88	.89	.92	.94	.97	.98	1.00
400				.54	.65	.72	.76	.83	.89	.94	.96	1.00
600				L	.244	.48	.60	.73	.83	.91	.95	1.00
800					.284	.327	.43	.63	.77	.88	.94	1.00
1000					.334	.358	.40	.55	.72	.86	.93	1.00
1400					.44	.45	.47	.53	.67	.83	.91	1.00
2000					.59	.59	.60	.62	.69	.82	.91	1.02
3000					.83	.82	.82	.76	.84	.90	.96	1.06

TABLE 8-16

GASEOUS NITROGEN SPECIFIC HEAT

(Btu/lb-°F)

Temperature, °F

Pressure, psia	-320	-280	-230	-210	-190	-160	-130	-100	-60	0	+80
14.7	.246	.255	.252	.251	.250	.250	.249	.249	.249	.249	.248
150	L	L	.296	.284	.276	.293	.263	.260	.257	.254	.252
400		L	.59	.415	.351	.314	.294	.282	.273	.264	.209
500			2.28	.52	.398	.336	.308	.292	.280	.269	.262
600			1.62	.72	.462	.363	.324	.304	.286	.273	.264
1000			.72	.96	.80	.494	.393	.347	.315	.290	.224
1400			.61	.66	.70	.576	.455	.388	.342	.306	.284
3000			.52	.50	.47	.468	.456	.433	.393	.349	.314

TABLE 8-17

GASEOUS NITROGEN THERMAL CONDUCTIVITY

(Btu/hr-ft-°F)

Temperature, °F

Pressure, psia	-280	-270	-243	-226	-210	-190	-170	-140	-100	+106
14.7	.00546	.0057	.0062	.0070	.0075	.0080	.0087	.0094	.0105	.0156
123	L	.0085	.0080	.0080	.0085	.009	.0095	.0105	.0115	
247		L	.0128	.0090	.0090	.0095	.010	.011	.012	
492			L	.0145	.0115	.0115	.0115	.012	.0125	
739				.026	.0195	.015	.013	.013	.0135	.0168
985				.035	.0265	.020	.017	.015	.015	.0173
1477				.040	.034	.0275	.023	.0195	.0175	.0184
1969				.0435	.038	.0325	.0285	.0235	.0205	.0199
3020										.0222

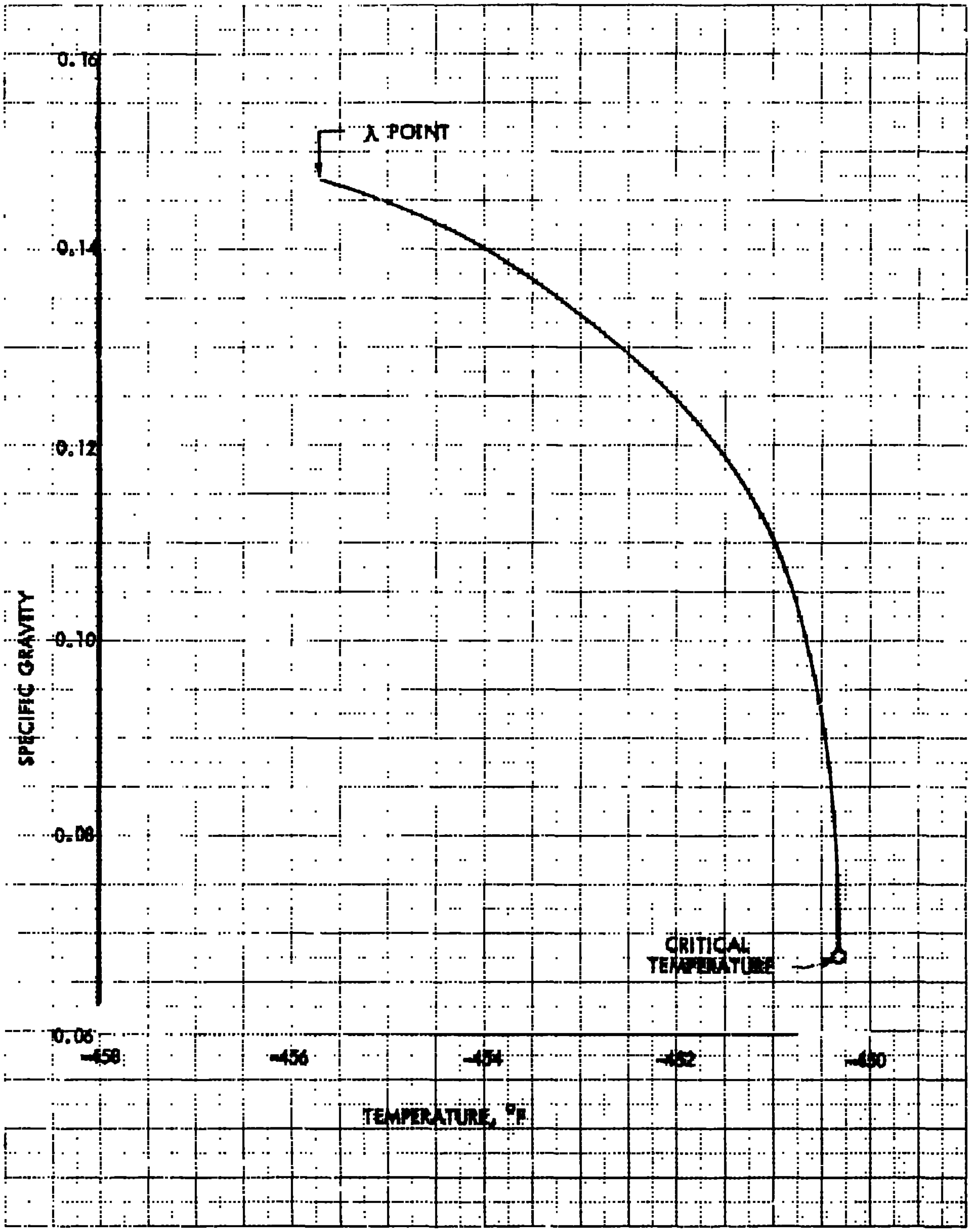

Figure 8-68. Liquid Helium Specific Gravity vs Temperature

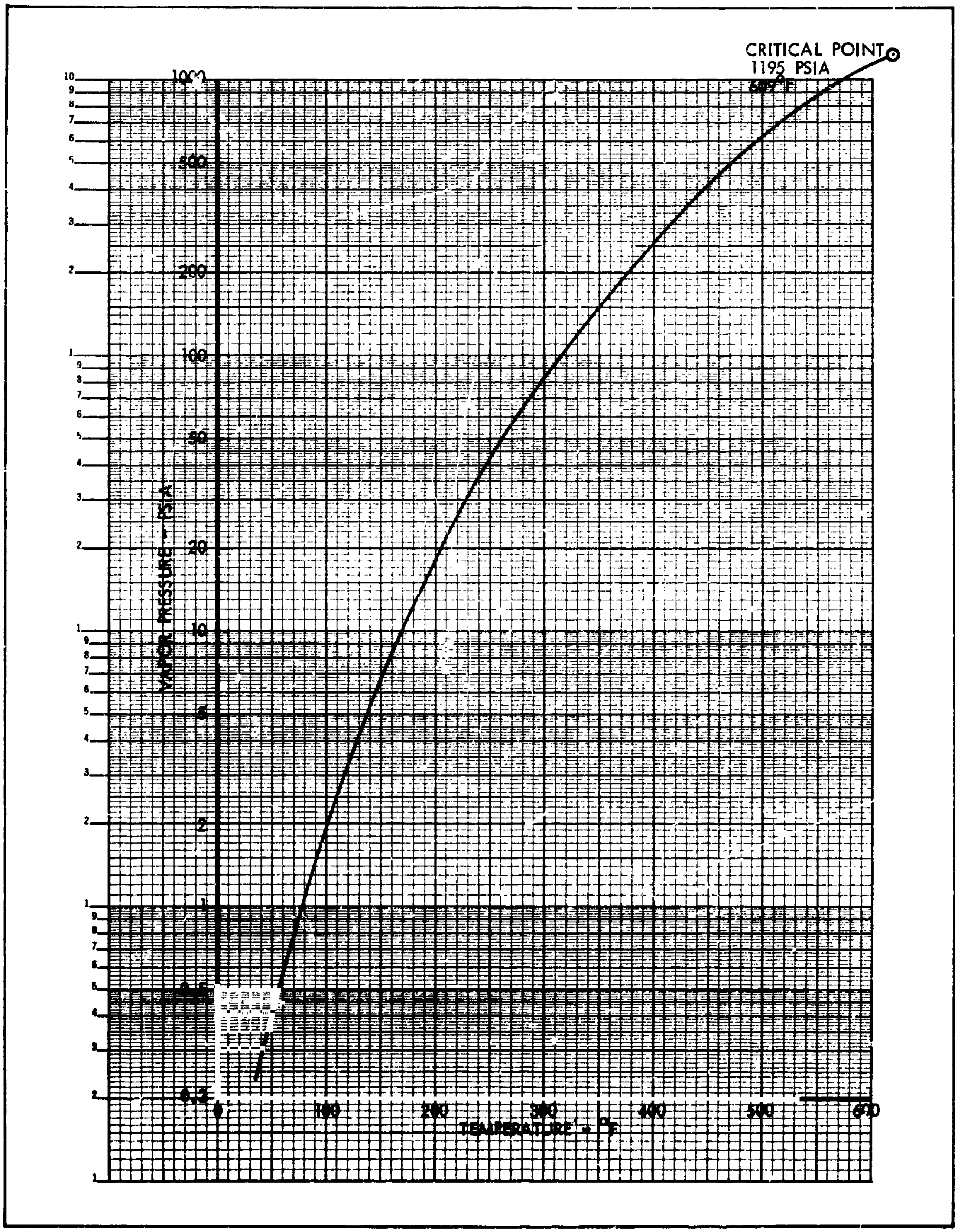

Figure 8-69. Liquid Helium Vapor Pressure vs Temperature

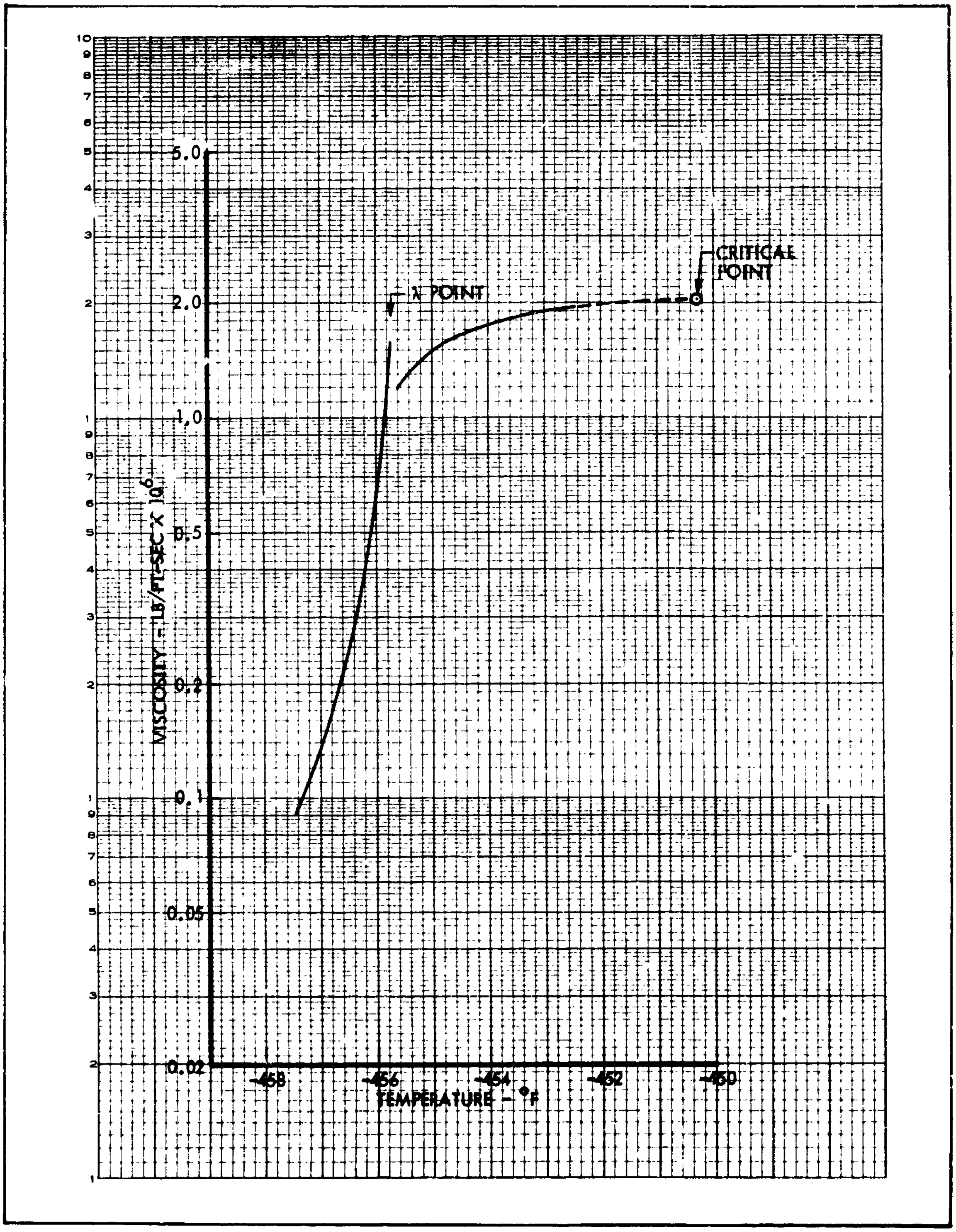

Figure 8-70. Liquid Helium Viscosity vs Temperature

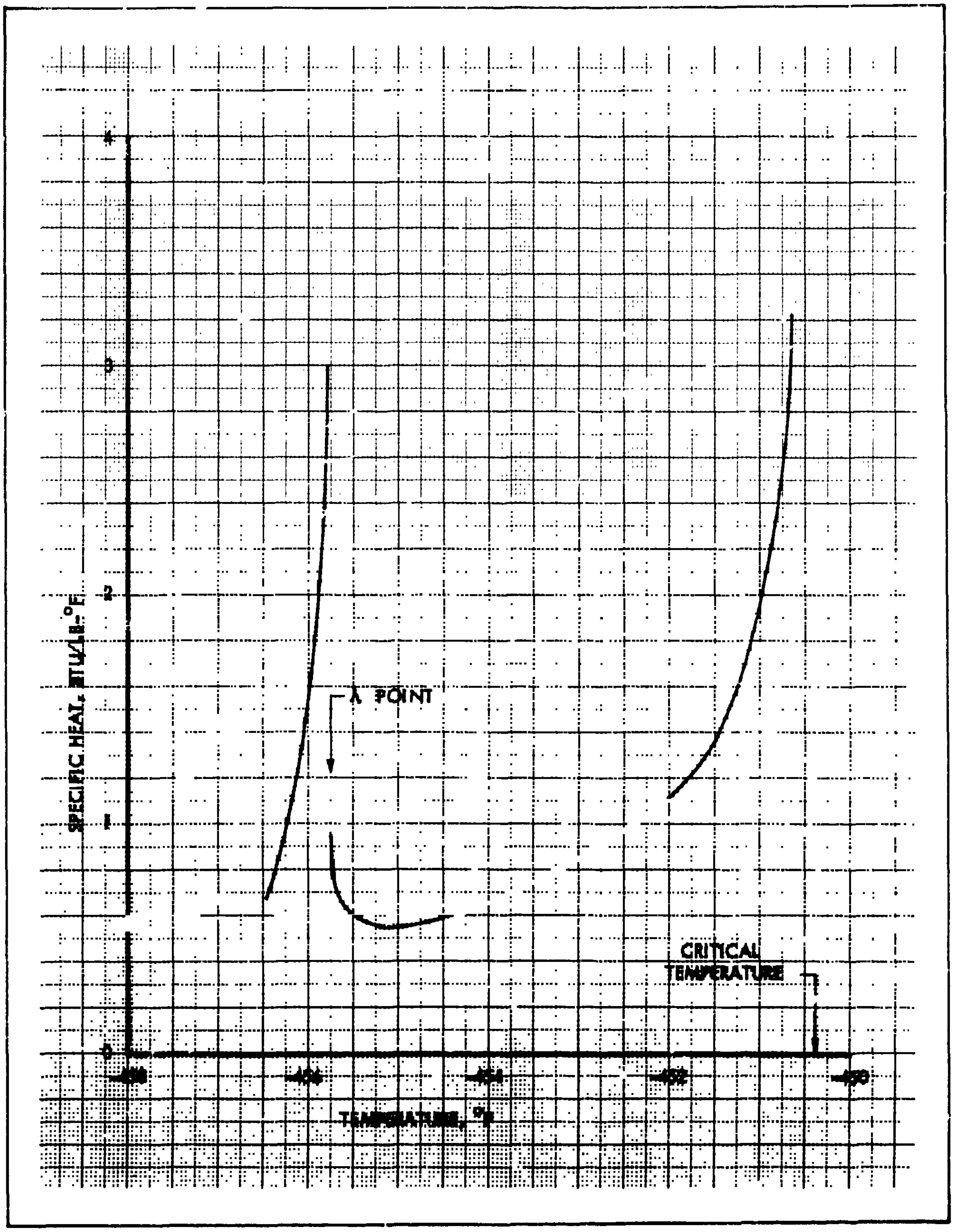

Figure 8-71. Liquid Helium Specific Heat vs Temperature

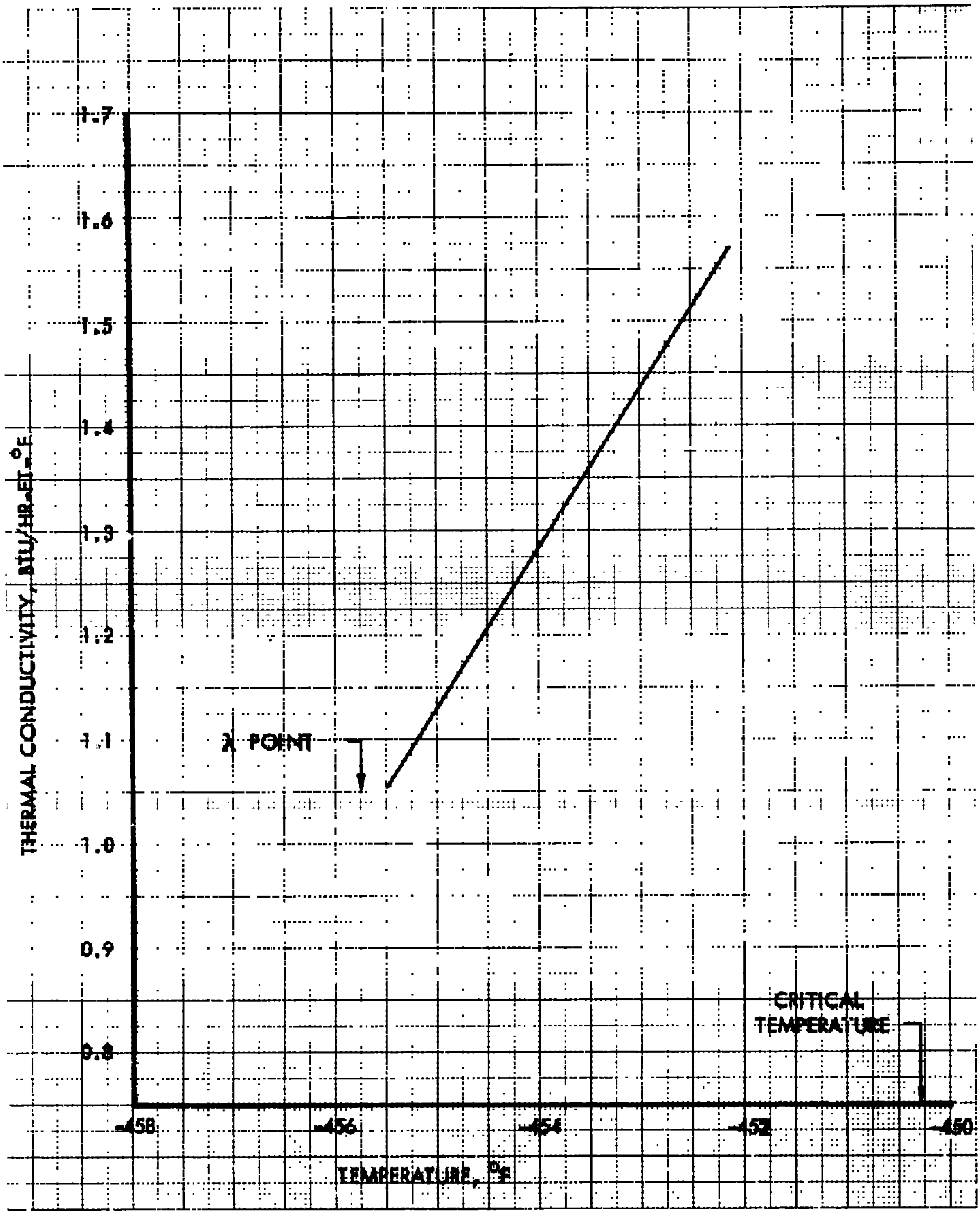

Figure 8-72. Liquid Helium Thermal Conductivity vs Temperature

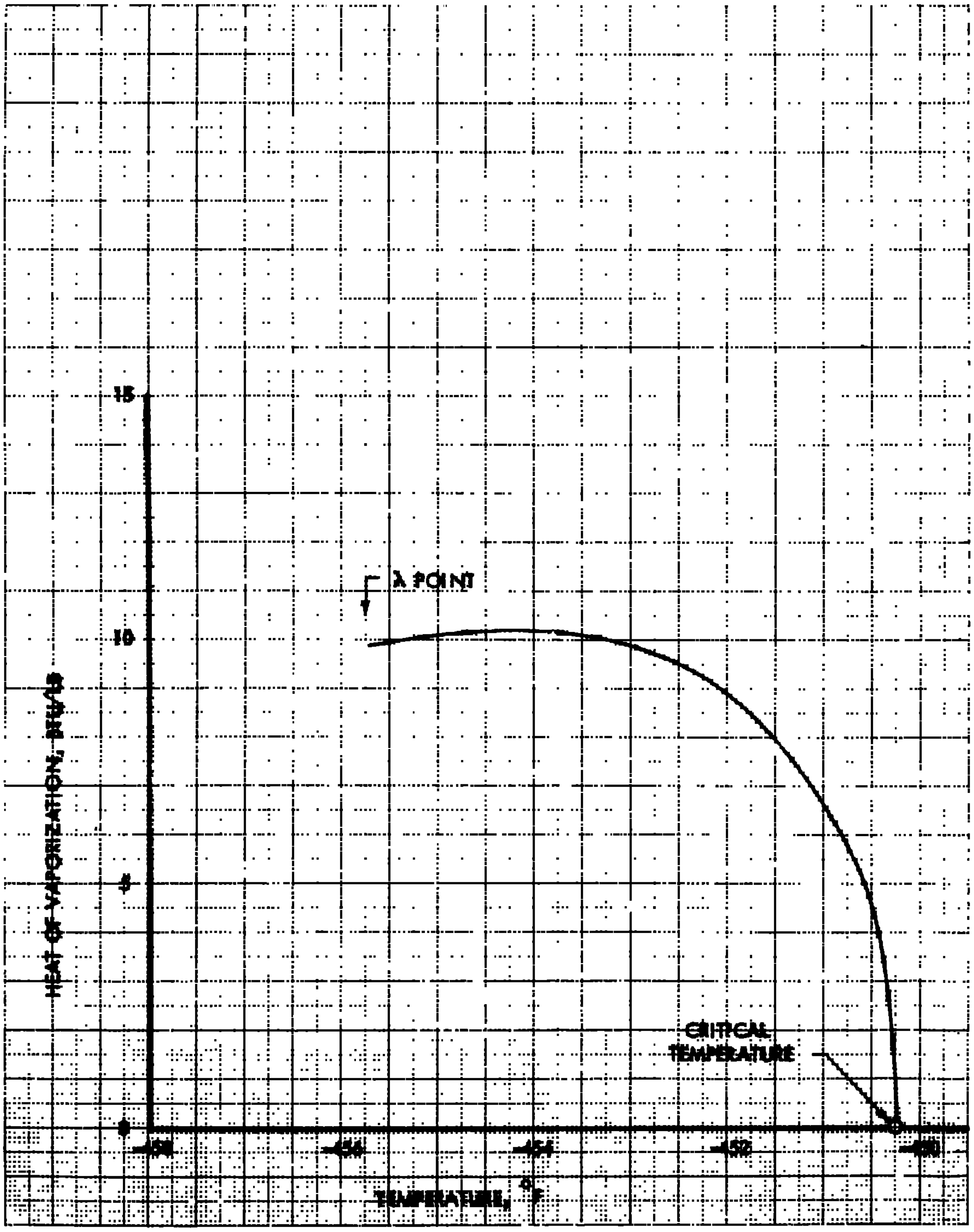

Figure 8-73. Liquid Helium Heat of Vaporization vs Temperature

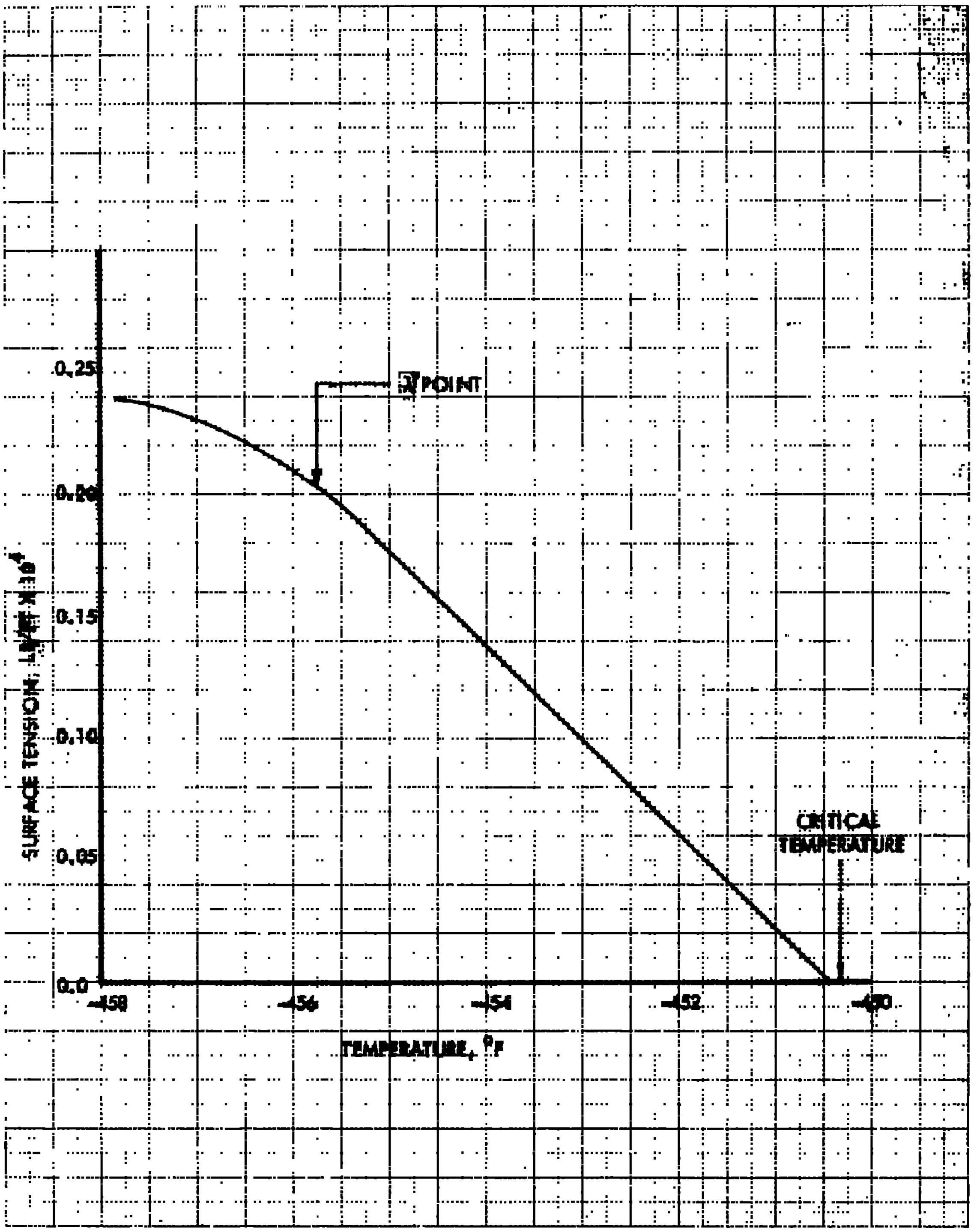

Figure 8-74. Liquid Helium Surface Tension vs Temperature

TABLE 8-18

GASEOUS HELIUM COMPRESSIBILITY FACTOR

Temperature, °F

Pressure, psia	-448.9	-447.1	-443.5	-440	-425	-400	-300	-200	0	+600
14.7	.879	.917	.956	.974	.996	1.001	1.001	1.001	1.001	1.001
43.1	.588	.747	.874	.926	.988	1.004	1.005	1.003	1.002	1.002
147	.619	.608	.720	.835	.980	1.016	1.016	1.011	1.007	1.003
397	1.368	1.229	1.074	1.017	1.037	1.062	1.043	1.030	1.019	1.008
882	2.629	2.251	1.896	1.655	1.295	1.187	1.098	1.068	1.041	1.017
1470	3.992	3.477	2.802	2.386	1.676	1.364	1.166	1.113	1.069	1.028
6000					3.70	2.50	1.598	1.379	1.221	1.106

TABLE 8-19

GASEOUS HELIUM SPECIFIC HEAT
(Btu/lb-°F)
Temperature, °F

Pressure, psia	-448	447	-443	-440	-425	-400	-300	-200	-100	0	+600
14.7	1.42	1.37	1.31	1.285	1.26	1.25	1.24	1.24	1.24	1.24	1.24
43.1	2.06	1.87	1.49	1.386	1.28	1.26	1.24	1.24	1.24	1.24	1.24
147	1.17	1.55	1.96	1.706	1.37	1.28	1.25	1.24	1.24	1.24	1.24
397	0.76	0.89	1.24	1.443	1.45	1.33	1.26	1.25	1.24	1.24	1.24
882	0.60	0.69	0.96	1.123	1.35	1.35	1.27	1.25	1.25	1.24	1.24
1470	0.51	0.60	0.86	1.003	1.22	1.33	1.28	1.26	1.25	1.25	1.24
6000								1.31	1.28	1.26	1.24

TABLE 8-20

GASEOUS HELIUM THERMAL CONDUCTIVITY

(Btu/hr-ft-°F)

Temperature, °F

Pressure, psia	-456	-450	-440	-410	-300	-100	0	+400
14.7	.0022	.0063	.0106	.0186	.0400	.0673	.0792	.1191

TABLE 8-21

THERMAL PROPERTIES OF LIQUID FREON 11

	Temp.	Density	Temp.	Vapor Pressure	Temp.	Specific Heat	Temp.	Thermal Conductivity	Temp.	Heat of Vaporization	Temp.	Viscosity	Temp.	Surface Tension
	(°F)	(gm/cm^3)	(°F)	(psia)	(°F)	(Btu/lb-°F)	(°F)	(Btu/hr-ft-°F)	(°F)	(Btu/lb)	(°F)	(lb/ft-sec)	(°F)	(lb/ft)
Freezing	-168													
	-90	1.68			-90	0.20	-4	0.0605	-90	91.5				
	-40	1.625	-40	0.74	+20	0.21	68	0.055	-40	87.5	-40	6.5×10^{-4}		
	+160	1.365	-30	1.03	160	0.22			+80	78.	0	4.5×10^{-4}	77	13.0×10^{-4}
			-20	1.42					160	70.	60	3.05×10^{-4}		
			0	2.56							140	2.15×10^{-4}		
											240	1.55×10^{-4}		
Critical	388.4	0.554	+20	4.3					388.4	0			388.4	0
			40	7.0										
			60	10.9										
			80	16.3										
			100	23.6										
			120	33.										
			140	46.										
			160	61.										
			200	104.										
			240	163.										
			280	250.										
			320	360.										
			360	500.										
Critical			388.4	635.										

TABLE 8-22

GASEOUS FREON 11 COMPRESSIBILITY FACTOR

Temperature, °F

Pressure, psia	20	50	70	100	130	160	190	290
1	.997	.997	.998	.998	.998	.998	.999	.999
2	.994	.994	.995	.996	.996	.997	.997	.999
4	.988	.990	.991	.992	.993	.994	.995	.998
6	L	.985	.986	.988	.990	.991	.992	.996
8		.961	.981	.984	.986	.988	.990	.994
10		L	.977	.980	.983	.985	.987	.992
20			L	.960	.965	.970	.974	.984
30				L	.947	.955	.961	.976
40					L	.939	.947	.968
50						.923	.934	.960

TABLE 8-23

GASEOUS FREON 11 SPECIFIC HEAT
(Btu/lb-°F)

(Pressure = 14.7 psia)

Temperature (°F)	Specific Heat (Btu/lb-°F)
100	.136
150	.141

TABLE 8-24

GASEOUS FREON 11 THERMAL CONDUCTIVITY
(Btu/hr-ft-°F)

(Pressure = 14.7 psia)

Temperature (°F)	Conductivity (Btu/hr-ft-°F)
86	.0050
194	.0062

TABLE 8-25

THERMAL PROPERTIES OF 60:40 ETHYLENE GLYCOL: WATER

Temp. (°F)	Density (gm/cm^3)	Temp (°F)	Vapor Pressure (psia)	Temp (°F)	Specific Heat (Btu/lb-°F)	Temp (°F)	Thermal Conductivity (Btu/hr-ft-°F)	Temp. (°F)	Viscosity lb /ft-sec
-60	1.099			-60	0.644	-60	0.232	-50	1900×10^{-4}
120	1.057	232	≈15	300	0.902	120	0.221	-40	1050×10^{-4}
274	.993					250	0.205	-30	620×10^{-4}
300	.975					300	0.195	-12	300×10^{-4}
								0	180×10^{-4}
								+10	126×10^{-4}
								30	70×10^{-4}
								62	36×10^{-4}
								122	14×10^{-4}
								172	6×10^{-4}
								250	4×10^{-4}

REFERENCES

8-1. Hydrogen Handbook, A.D. Little, TR60-19, April 1960

8-2. A Compendium of the Properties of Materials at Low Temperature (Phase I) Part I Properties of Fluids, National Bureau of Standards, TR60-56, July 1960

8-3. Design Data for Pressurized Gas Systems, Stanford Research Institute, November 1963

8-4. Nitrogen Tetroxide, Product Bulletin, Allied Chemical Corp., 1960

8-5. Performance and Properties of Liquid Propellants, Aerojet General Corp., Report 8160-68, June 1961

8-6. Liquid Propellants Handbook, Battelle Memorial Institute, 1956 (CONF.)

8-7. Storable Liquid Propellants - Nitrogen Tetroxide/Aerozine 50, Aerojet General Corp., Report LRP 198, June 1962

8-8. Titan II Storable Propellant Handbook, Final Handbook, Revision A, Bell Aerospace Corp., AFBSD TR62-2, March 1962

8-9. Yaffe, B.S. Diborane-Space Storable Fuel, Calley Chemical Co., January 1962

8-10. Oxygen Difluoride, Product Data Sheet, Allied Chemical Corp.

8-11. Fluorine, Product Data Sheet, Allied Chemical Corp., August 1958

REFERENCES (Continued)

8-12. Monomethyl Hydrazine, Product Bulletin, Olin Mathieson Chemical Corp., 1961

8-13. JANAF Thermochemical Data, Dow Chemical Co., 1961

8-14. Research on Rheologic & Thermodynamic Properties of Solid and Slush Hydrogen, Union Carbide Corp., October 1964

8-15 Roder, Diller, Weber, Goodwin "The Orthobaric Densities of Parahydrogen, Derived Heats of Vaporization and Critical Constants, NBS, Boulder, Colo., Cryogenics 3, No. 1, of 20 March 1963

8-16. Schlinger and Sage "Volumetric Behavior of Nitrogen Dioxide," (gas phase) Ind. & Eng. Chem. 42, 1950

8-17. Reamer and Sage "Volumetric Behavior of Nitrogen Dioxide in the Liquid Phase," Ind. & Eng. Chem. 44, 1952

8-18. Physical and Thermodynamic Properties of Helium, Whittaker Controls Div., Telecomputing Corp., Report D-9027, Revised, September 1960

8-19. Mann, D.B. The Thermodynamic Properties of Helium from 6 to 540°R Between 10 and 1500 Atmospheres, NBS Tech. Note 154A, January 1962

8-20. Steward, Hust, McCarty Interim Thermodynamic Properties for Gaseous and Liquid Oxygen at Temperatures from 55 to 300°K and Pressures to 300 Atm., NBS Report 7922, October 1963

8-21. Roder, Weber, Goodwin Thermodynamic and Related Properties of Parahydrogen from the Triple Point to 100°K at Pressures to 340 Atm., NBS Report 7987, 15 November 1963

8-22. Younglove and Diller "The Specific Heat of Saturated Liquid Parahydrogen from 15 to 32°K," NBS, Boulder, Colo., Cryogenics 2, No. 5, September 1962

REFERENCES (Continued)

8-23. Ziegler and Mullins — Calculation of the Vapor Pressure and Heats of Vaporization and Sublimination of Liquids and Solids, Especially Below One Atmosphere No. IV, Nitrogen and Fluorine, Georgia Inst. Tech., NBS Project A-663 TR-1. April 1963

8-24. Strobridge, T.R. — The Thermodynamic Properties of Nitrogen from 114 to 540°R between 1.0 and 3000 Psia, NBS TN 129A, February 1963

8-25. Chlorine Trifluoride and Other Halogen Fluorides, Technical Bulletin TA-8532-2, Allied Chemical Corp.

8-26. Chlorine Trifluoride, LPIA-LPM-1, Unit 3, March 1961

8-27. Fluorine, LPIA-LPM-1 Unit 14, December 1961

8-28. Private Communication from NASA Manned Spacecraft Center, November 1964

8-29. Monomethylhydrazine LPIA-LPM-1 Unit 11, December 1961

8-30. Guide and Data Book, Fundamentals and Equipment, ASHRAE, 1961

8-31. Wright, Johnson, Anderson, and Stake — Thermal Radiators for Space Vehicle Environmental Control Systems, Garrett Corp., Report STC-20-R, July 1962

IX. THERMAL PROPERTIES OF STRUCTURAL MATERIALS AND INSULATIONS

The following properties were sought for ten metal alloys and four insulating materials used in spacecraft design:

- Density
- Specific Heat
- Thermal Conductivity

STRUCTURAL MATERIALS

Table 9-1 lists the ten selected alloys and the weight percentage of each major constituent. Table 9-2 lists the properties of these alloys at 70°F, and indicates the properties table numbers, and each reference source from which the data were obtained. A single value for each density at 70°F is listed, as the slight variation of density with temperature is not considered important. However, point pairs show the variation of specific heat and of thermal conductivity with temperature from -450°F to the initial melting point, or over the range of the available data. Specific heat and thermal conductivity are affected by prior heat treatment of each alloy, but a full account of all such treatments was not attempted as part of this program.

TABLE 9-1

MAJOR ALLOY CONSTITUENTS

Aluminum	2219-T87	Al ≈94	Mn 0.2-0.4	Cu 5.8-6.8						
Aluminum	7075-T6	Al 90	Zn 5.6	Mg 2.5	Cu 1.6	Cr 0.3				
Magnesium	AZ31B-H24	Al 3	Zn 1	Mg 95.5	Mn .5					
Titanium	6Al4V	Ti ≈90	Al 5.5-6.5	V 3.5-4.5						
Titanium	A110AT	Ti ≈92	Al 4-6	Sn 2-3						
Columbium	C-103	Cb ≈88	Hf 9-11	Zr <0.7	Ti 0.7-1.3					
Stainless Steel 321		Fe ≈62	Cr 17-19	Ni 9-12	Mn < 2	Ti < 5	Si < 1			
Inconel X		Fe 5-9	Cr 14-16	Ni 70 min	Mn .3-1.0	Ti 2.25-2.75	Cb .7-1.2	Al .4-1.0		
Rene 41		Fe 5 max	Cr 18-20	Ni ≈ 45	Mn .5 max	Ti 3-3.3	Mo 9-10.5	Co 10-12	Al 1.4-1.6	Si .5 max
Beryllium		Be 98	BeO 2							

NOTE: Amounts given in percent by weight

TABLE 9-2

SUMMARY OF ALLOY PROPERTIES

	Properties (at 70°F unless otherwise noted)						Reference Nos.		
	Density lb/ft^3	Initial Melting °F	Heat of Fusion Btu/lb	Specific Heat Btu/lb-°F	Thermal Conductivity Btu/hr-ft-°F	Table No.	Density	Specific Heat	Thermal Conductivity
Aluminum 2219-T87	176	1010	-	0.19	75	9-4	9-13	9-27	9-27
Aluminum 7075-T6	175	890	162	0.19	75	9-5	9-1	9-7,27	9-1,27
Magnesium AZ31B-H24	110	990	146	0.237	44	9-6	9-6	9-4,18	9-4,18
Titanium 6A14V	278	2800		0.128	4.0	9-7	9-14	9-4,5,7	9-1,5,16
Titanium A11CAT	278	2800		0.125	4.6	9-8	9-14	9-14,15	9-1,14,15,24
Columbium C-103	553	4380		0.065 (1600°F)	22 (1600°F)	9-9	9-13	9-13	9-13
Stainless Steel 321	493	2400		0.112	9.0	9-10	9-1	9-18	9-10,18,26
Inconel X	515	2540	134	0.106	9.9	9-11	9-1	9-1,27,28	9-23,24,28,30
René 41	515	2250	134	0.108	4.2	9-12	9-9	9-22	9-9,18,31
Beryllium	116	2341	470	0.49	102	9-13	9-1	9-20	9-1,7,20

INSULATING MATERIALS

Table 9-3 lists the selected insulations, reference sources, and the properties table numbers. The thermal conductivity versus temperature curves are constructed in a special fashion because of the strong dependence on both the upper and lower boundary termperatures. In order to present one curve for each insulation that can be used for all temperatures, the curves were constructed so that the apparent thermal conductivity is obtained by integrating between the lower and upper temperatures and dividing by ΔT:

$$k_{app} = \frac{1}{T_2 - T_1} \int_{T_1}^{T_2} k_T dT \qquad (9\text{-}1)$$

This was accomplished by measuring the conductivity over narrow temperature ranges and taking the limiting values as ΔT approached zero. For small ΔT's, the values can be used directly without integrating. The Thermal Properties Library (Section 10) is set up so that the linear interpolation routine of the Thermal Analyzer program (Ref. 9-36) automatically performs the required integration.

The NRC-2 conductivity data (Ref. 9-34) were converted to the integrable form by first converting to effective emissivity (radiation barrier concept), solving for k by equating heat transfer by the conventional conduction barrier and the radiation barrier methods, and taking the limit as ΔT approaches zero. This procedure is as follows:

$$Q = \frac{kA\,(T_1 - T_2)}{x} = \sigma \epsilon A\,(T_1^4 - T_2^4)$$

$$k/x' = \sigma \epsilon (T_1 + T_2)(T_1^2 + T_2^2)$$

but $\epsilon_{adj} = 1.8 \times 10^{-3} \frac{D^{0.84}}{n + 1}$ (derived from Ref. 9-34)

where n = number of sheets; $n = Dx'' = 12\ Dx'$

D = number of sheets per inch

for large n, $\epsilon = \frac{1.8 \times 10^{-3} D^{0.84}}{n + 1} \cong \frac{1.8 \times 10^{-3} D(D^{-0.16})}{12 Dx'} = \frac{1.5 \times 10^{-4}}{x'D^{0.16}}$

$$\therefore k_T = \lim_{\Delta T \to 0} \left[\frac{0.1713 \times 10^{-8} \times 1.5 \times 10^{-4} (T_1 + T_2)(T_1^2 + T_2^2) x'}{x'D^{0.16}} \right]$$

$$= \frac{1.04 \times 10^{-6}}{D^{0.16}} \left(\frac{T}{100}\right)^3 \qquad (9\text{-}2)$$

The apparent conductivity is then found by substituting k_T into equation (9-1) and integrating, as before.

TABLE 9-3

SELECTED INSULATING MATERIALS

	Reference Nos.	Table Numbers		
		Density	Specific Heat	Thermal Conductivity
Linde SI-12	9-33	9-15	9-14	9-15
Linde SI-62	9-33	9-16	9-14	9-16
Linde SI-92	9-33	9-17	9-14	9-17
Linde "Flight Weight"	9-33	9-18	9-14	9-18
Linde "High Temperature"	9-33	9-19	9-14	9-19
NRC-2	9-34	9-20	9-20	9-20
Fiberglas	9-35	9-21	9-21	9-21
Micro Quartz	9-35	9-21	9-21	9-21

TABLE 9-4
THERMAL PROPERTIES OF ALUMINUM 2219-T87

Density		Specific Heat		Thermal Conductivity	
(°F)	(lb/ft^3)	(°F)	(Btu/lb°F)	(°F)	(Btu/hr-ft°F)
70	176	-424	0.002	-424	11.2
		-400	.012	-352	28.6
		-360	.039	-316	36.3
		-320	.074	-150	58.
		-280	.111	+100	76.5
		-100	.183	500	87.5
		+100	.198		
		900	.257		
		1010	.268	1010	95.5

TABLE 9-5
THERMAL PROPERTIES OF ALUMINUM 7075-T6

Density (°F)	Density (lb/ft^3)	Specific Heat (°F)	Specific Heat (Btu/lb-°F)	Thermal Conductivity (°F)	Thermal Conductivity (Btu/hr-ft-°F)	Thermal Conductivity (°F)	Thermal Conductivity (Btu/hr-ft-°F)
70	175			As received		Annealed above 550°F	
		-424	0.002				
		-400	.012				
		-360	.039	-388	23.7	-410	54
		-320	.074	-310	38.5	-200	76
		-280	.111	-100	61.0	+40	96
		-100	.183	+100	77.0	340	106
		+100	.198	700	92.0	600	104
		+890	.256	890	94.5	890	94

TABLE 9-6

THERMAL PROPERTIES OF MAGNESIUM AZ31B-H24

Density		Specific Heat		Thermal Conductivity	
(°F)	(lb/ft^3)	(°F)	(Btu/lb - °F)	(°F)	(Btu/hr - ft - °F)
70	110.5	-250	0.18	-310	22
		-50	0.22	-160	32
		+510	0.29	+20	42
		900	0.33	200	50
				500	59
				600	61

TABLE 9-7

THERMAL PROPERTIES OF TITANIUM 6A14V

Density		Specific Heat		Thermal Conductivity	
(°F)	(lb/ft^3)	°F	(Btu/lb-°F)	°F	(Btu/hr-ft-°F)
70	278	-440	.00045	-414	0.92
		-435	.00075	-360	1.60
		-430	.0012	-312	2.08
		-424	.002	-180	3.0
		-418	.003	+50	4.0
		-410	.005	500	5.5
		-400	.008	1600	10.5
		-380	.018		
		-340	.041		
		-300	.062		
		-200	.096		
		-100	.114		
		+100	.130		
		800	.153		
		1200	.185		
		1600	.234		

TABLE 9-8

THERMAL PROPERTIES OF TITANIUM A110AT

Density		Specific Heat		Thermal Conductivity	
(°F)	(lb/ft^3)	(°F)	(Btu/lb-°F)	(°F)	(Btu/hr-ft-°F)
70	278	-440	.00045	-420	1.3
		-435	.00075	-360	2.4
		-430	.0012	-200	3.5
		-424	.002	+600	6.2
		-418	.003	1100	8.4
		-410	.005	1500	10.6
		-400	.008		
		-380	.018		
		-340	.041		
		-300	.062		
		-200	.096		
		-100	.114		
		0	.12		
		900	.15		
		1600	.19		

TABLE 9-9

THERMAL PROPERTIES OF COLUMBIUM C-103

Density		Specific Heat		Thermal Conductivity	
(°F)	(lb/ft^3)	(°F)	(Btu/lb-°F)	(°F)	(Btu/hr-ft-°F)
70	553	1610	0.065	1600	22.0
		2017	0.073	2035	23.5
		2397	0.078	2380	25.8

TABLE 9-10
THERMAL PROPERTIES OF STAINLESS STEEL 321

Density		Specific Heat		Thermal Conductivity	
(°F)	(lb/ft^3)	(°F)	(Btu/lb-°F)	(°F)	(Btu/hr-ft-°F)
70	493	-250	0.08	-459.7	0.0
		+ 80	0.11	-400	2.25
		580	0.13	-350	3.6
		1440	0.15	-200	6.3
		1880	0.18	+120	9.0
				800	12.3
				1800	15.8

TABLE 9-11

THERMAL PROPERTIES OF INCONEL X

Density		Specific Heat		Thermal Conductivity		Thermal Conductivity	
(°F)	(lb/ft^3)	(°F)	(Btu/lb-°F)	(°F)	(Btu/hr-ft-°F)	(°F)	(Btu/hr-ft-°F)
70	515	-410	0.054	-450	0.1	Solution Treated, Aged	
		0	.099	(Gap In Data)		-230	5.5
		+400	.117	-410	3.0	1650	13.7
		1000	.129	-400	4.0		
		1400	.149	-300	6.2		
		1650	.180	0	9.1		
				900	14.1		
				1650	21.5		

TABLE 9-12

THERMAL PROPERTIES OF RENE' 41

Density		Specific Heat		Thermal Conductivity	
($^{\circ}$F)	(lb/ft^3)	($^{\circ}$F)	(Btu/lb-$^{\circ}$F)	($^{\circ}$F)	(Btu/lb-$^{\circ}$F)
70	515	70	0.108	Sol'n. Treated for 2 hr @ 2150°F Aged for 4 hr @ 1650°F	
				200	6.0
				1800	15.8
				Sol'n. Treated for 4 hr @ 1950°F Aged for 16 hr @ 1400°F	
				200	5.2
				1800	12.6

TABLE 9-13

THERMAL PROPERTIES OF BERYLLIUM

Density (°F)	Density (lb/ft^3)	Specific Heat (°F)	Specific Heat (Btu/lb-°F)	Thermal Conductivity (°F)	Thermal Conductivity (Btu/hr-ft-°F)
70	116	-450	0.32×10^{-4}		
		-445	0.64×10^{-4}		
		-440	1.07×10^{-4}		
		-435	1.6×10^{-4}		
		-425	3.2×10^{-4}		
		-415	6.0×10^{-4}		
		-405	.0010		
		-395	.0016		
		-380	.0031		
		-360	.0065		
		-340	.0115		
		-320	.0185	No Reliable Data At Low Temperatures	
		-300	.029		
		-280	.044		
		-260	.063		
		-220	.112	-200	67
		-160	.186	Discontinuity	
		-100	.26	-45	128
		0	.375	200	95
		+200	.50	600	70
		750	.66	1200	52
		2190	.85	1800	42

TABLE 9-14

SPECIFIC HEAT OF LINDE SUPERINSULATIONS - ALL DENSITIES

(Btu/lb-°F)

TEMP. (°F)	SI-12	SI-62	SI-92	Flt. Wt	High Temp.
-435	.002	.009	.002	.009	
-360	.048	.055	.051	.055	
-260	.099	.105	.117	.105	
-210			.142		
-160	.138	.144	.159	.144	
-100					.097
+40	.192	.195	.203	.195	.103
140	.218	.220	.224	.220	
190	.234	.236	.236	.236	
215	.246	.246		.246	
240	.260	.259	.254	.259	
540					.120
1040					.132
2040					.141

TABLE 9-15
THERMAL CONDUCTIVITY OF LINDE SI-12 INSULATION
(Btu/hr-ft-°F)

Layers/in.		8	10	12	14
Density (lb/ft3)		1.296	1.62	1.945	2.27
Temperature, °F	-435	1.4x10^{-6}	2.4x10^{-6}	3.9x10^{-6}	14.6x10^{-6}
	-410	2.1x10^{-6}	3.3x10^{-6}	5.2x10^{-6}	17.0x10^{-6}
	-385	3.1x10^{-6}	4.5x10^{-6}	6.9x10^{-6}	20.x10^{-6}
	-360	4.5x10^{-6}	6.2x10^{-6}	9.1x10^{-6}	23.x10^{-6}
	-310	10.x10^{-6}	11.6x10^{-6}	15.3x10^{-6}	
	-260	20.4x10^{-6}	21.x10^{-6}	25.x10^{-6}	41.x10^{-6}
	-210	38.5x10^{-6}	37.x10^{-6}	41.x10^{-6}	
	-160	67.x10^{-6}	62.x10^{-6}	63.x10^{-6}	71.x10^{-6}
	- 60	155.x10^{-6}	137.x10^{-6}	133.x10^{-6}	112.x10^{-6}
	40	290.x10^{-6}	250.x10^{-6}	230.x10^{-6}	170.x10^{-6}
	140	490.x10^{-6}	410.x10^{-6}	370.x10^{-6}	275.x10^{-6}
	190				370.x10^{-6}
	240	780.x10^{-6}	650.x10^{-6}	560.x10^{-6}	510.x10^{-6}

TABLE 9-16

THERMAL CONDUCTIVITY OF LINDE S1-62 INSULATION

(Btu/hr-ft-°F)

Layers/in.		40	60	80	100
Density (lb/ft^3)		2.88	4.32	5.76	7.20
Temperature, °F	-435	$.22\text{x}10^{-6}$	$.74\text{x}10^{-6}$	$1.65\text{x}10^{-6}$	$4.1\text{x}10^{-6}$
	-410	$.36\text{x}10^{-6}$	$1.02\text{x}10^{-6}$		
	-385	$.56\text{x}10^{-6}$			
	-360	$.86\text{x}10^{-6}$	$1.8\text{x}10^{-6}$	$3.4\text{x}10^{-6}$	$7.57\text{x}10^{-6}$
	-335	$1.28\text{x}10^{-6}$			
	-310	$1.88\text{x}10^{-6}$	$3.05\text{x}10^{-6}$	$5.3\text{x}10^{-6}$	
	-285	$2.70\text{x}10^{-6}$			
	-260	$3.8\text{x}10^{-6}$	$4.95\text{x}10^{-6}$	$8.1\text{x}10^{-6}$	$15.5\text{x}10^{-6}$
	-210	$7.3\text{x}10^{-6}$	$7.9\text{x}10^{-6}$		
	-160	$13.\text{x}10^{-6}$	$12.\text{x}10^{-6}$	$17.\text{x}10^{-6}$	$27.\text{x}10^{-6}$
	- 60	$29.\text{x}10^{-6}$	$24.2\text{x}10^{-6}$	$28.7\text{x}10^{-6}$	
	+ 40	$55.\text{x}10^{-6}$	$43.\text{x}10^{-6}$	$45.\text{x}10^{-6}$	$58.\text{x}10^{-6}$
	140	$93.\text{x}10^{-6}$	$70.\text{x}10^{-6}$	$67.5\text{x}10^{-6}$	
	240	$150.\text{x}10^{-6}$	$110.\text{x}10^{-6}$	$98.\text{x}10^{-6}$	$110.\text{x}10^{-6}$

TABLE 9-17

THERMAL CONDUCTIVITY OF LINDE S1-92 INSULATION

(Btu/hr-ft-°F)

Layers/in.		80	100	120	160
Density (lb/ft^3)		4.992	6.24	7.488	9.984
Temperature, °F	-435	$.14x10^{-6}$	$.31x10^{-6}$	$.70x10^{-6}$	$2.65x10^{-6}$
	-410	$.23x10^{-6}$	$.45x10^{-6}$	$.98x10^{-6}$	
	-385	$.38x10^{-6}$	$.65x10^{-6}$		
	-360	$.59x10^{-6}$	$.94x10^{-6}$	$1.8x\ 10^{-6}$	$4.8x10^{-6}$
	-335	$.92x10^{-6}$			
	-310	$1.38x10^{-6}$	$1.8x10^{-6}$		
	-260	$2.7x10^{-6}$	$3.1x10^{-6}$	$4.5x10^{-6}$	$9.6x10^{-6}$
	-210	$4.7x10^{-6}$	$5.x10^{-6}$		
	-160	$7.7x10^{-6}$	$7.55x10^{-6}$	$9.2x10^{-6}$	
	- 60	$17.x10^{-6}$	$15.x10^{-6}$	$16.8x10^{-6}$	$27.5x10^{-6}$
	+ 40	$33.x10^{-6}$	$28.x10^{-6}$	$29.x10^{-6}$	
	90	$45.x10^{-6}$			$44.x10^{-6}$
	140	$63.x10^{-6}$	$51.x10^{-6}$	$50.x10^{-6}$	
	190	$90.x10^{-6}$			
	240	$130.x10^{-6}$	$89.x10^{-6}$	$82.x10^{-6}$	$52.x10^{-6}$

TABLE 9-18
THERMAL CONDUCTIVITY OF LINDE FLIGHT WEIGHT INSULATION
(Btu/hr-ft-°F)

Layers/in.		40	50	60	80
Density(lb/ft^3)		2.496	3.12	3.744	4.992
Temperature, °F	-435	.8x10^{-6}	.39x10^{-6}	.79x10^{-6}	1.9x10^{-6}
	-410	.285x10^{-6}	.54x10^{-6}	1.03x10^{-6}	
	-385	.44x10^{-6}	.74x10^{-6}		
	-360	.65x10^{-6}	1.0x10^{-6}	1.7x10^{-6}	3.8x10^{-6}
	-310	1.34x10^{-6}	1.8x10^{-6}	2.75x10^{-6}	
	-260	2.54x10^{-6}	3.05x10^{-6}	4.2x10^{-6}	8.x10^{-6}
	-210	4.4x10^{-6}	4.9x10^{-6}		
	-160	7.0x10^{-6}	7.3x10^{-6}	8.4x10^{-6}	14.x10^{-6}
	- 60	14.3x10^{-6}	14.x10^{-6}	14.3x10^{-6}	21.x10^{-6}
	- 10	20.0x10^{-6}	19x10^{-6}	18.5x10^{-6}	
	40	28.5x10^{-6}	26.x10^{-6}	25.x10^{-6}	32.x10^{-6}
	90	44.0x10^{-6}	40.x10^{-6}	38.x10^{-6}	46.x10^{-6}
	115	58.x10^{-6}	53.x10^{-6}	50.x10^{-6}	59.x10^{-6}
	140	81.x10^{-6}	74.x10^{-6}	70.x10^{-6}	81.x10^{-6}
	157		96.x10^{-6}	90.x10^{-6}	
	165	123.x10^{-6}			120.x10^{-6}
	173		128.x10^{-6}	120.x10^{-6}	
	190	200.x10^{-6}	175.x10^{-6}	163.x10^{-6}	182.x10^{-6}
	207	290.x10^{-6}	250.x10^{-6}	235.x10^{-6}	255.x10^{-6}
	224	440.x10^{-6}	375.x10^{-6}	350.x10^{-6}	375.x10^{-6}
	240	680.x10^{-6}	590.x10^{-6}	550.x10^{-6}	590.x10^{-6}

TABLE 9-19

THERMAL CONDUCTIVITY OF LINDE LIGHT WEIGHT HIGH TEMPERATURE INSULATION

(Btu/hr-ft-°F)

Layers/in.		60	120	180
Density(lb/ft^3)		3.384	6.768	10.152
Temperature, °F	-100	$10.x10^{-6}$	$18.x10^{-6}$	$28.5x10^{-6}$
	- 50	$15.2x10^{-6}$	$20.5x10^{-6}$	$32.x10^{-6}$
	0	$19.6x10^{-6}$	$26.3x10^{-6}$	$39.x10^{-6}$
	40	$27.x10^{-6}$	$34.x10^{-6}$	$47.x10^{-6}$
	90	$46.x10^{-6}$	$48.5x10^{-6}$	
	140	$75.x10^{-6}$	$70.x10^{-6}$	$82.x10^{-6}$
	240	$165.x10^{-6}$	$123.x10^{-6}$	$130.x10^{-6}$
	340	$295.x10^{-6}$	$200.x10^{-6}$	$190.x10^{-6}$
	540	$690.x10^{-6}$	$410.x10^{-6}$	$350.x10^{-6}$
	1040	$1900.x10^{-6}$	$1070.x10^{-6}$	
	1540	$3450.x10^{-6}$		
	2040	$5400.x10^{-6}$	$2800.x10^{-6}$	$2000.x10^{-6}$

TABLE 9-20

THERMAL CONDUCTIVITY AND SPECIFIC HEAT OF NRC-2 INSULATION

(Btu/hr-ft-°F)

Layers/in.		40	100	160	Specific Heat Cp Btu/#°F
Density (lb/ft^3)		0.873	2.18	3.49	
Temperature, °F	-430	$0.0156x10^{-6}$	$0.0135x10^{-6}$	$0.01247x10^{-6}$	0.315 at -20°F for all densities
	-418	$0.043x10^{-6}$	$0.0385x10^{-6}$	$0.035x10^{-6}$	
	-410	$0.072x10^{-6}$	$0.063x10^{-6}$	$0.057x10^{-6}$	
	-402	$0.113x10^{-6}$	$0.1x10^{-6}$	$0.09x10^{-6}$	
	-393	$0.168x10^{-6}$	$0.147x10^{-6}$	$0.135x10^{-6}$	
	-377	$0.325x10^{-6}$	$0.28x10^{-6}$	$0.36x10^{-6}$	
	-360	$0.576x10^{-6}$	$0.498x10^{-6}$	$0.462x10^{-6}$	
	-335	$1.18x10^{-6}$	$1.x10^{-6}$	$0.94x10^{-6}$	
	-310	$2.05x10^{-6}$	$1.77x10^{-6}$	$1.65x10^{-6}$	
	-260	$4.61x10^{-6}$	$3.98x10^{-6}$	$3.69x10^{-6}$	
	-210	$8.9x10^{-6}$	$7.7x10^{-6}$	$7.2x10^{-6}$	
	-160	$15.56x10^{-6}$	$13.45x10^{-6}$	$12.47x10^{-6}$	
	-110	$24.2x10^{-6}$	$21.1x10^{-6}$	$19.4x10^{-6}$	
	- 60	$36.x10^{-6}$	$31.4x10^{-6}$	$28.6x10^{-6}$	
	40	$72.x10^{-6}$	$62.3x10^{-6}$	$57.7x10^{-6}$	
	140	$129.x10^{-6}$	$113.x10^{-6}$	$102.x10^{-6}$	
	240	$197.7x10^{-6}$	$170.9x10^{-6}$	$158.3x10^{-6}$	

TABLE 9-21

THERMAL CONDUCTIVITY AND SPECIFIC HEAT OF JOHNS-MANVILLE INSULATIONS

MICRO QUARTZ (Density = 3.5 lb/ft^3)			FIBERGLAS (Density = 4 lb/ft^3)		
Temp. (°F)	Specific Heat (Btu/lb-°F)	Thermal Conductivity (Btu/hr-ft-°F)	Temp. (°F)	Specific Heat (Btu/lb-°F)	Thermal Conductivity (Btu/hr-ft-°F)
-430	0.016	7.16×10^{-3}	-430	0.042	0.83×10^{-3}
-300	0.070	5.83×10^{-3}	-300	0.093	
-150	0.123		-200		0.83×10^{-3}
0	0.163		-150	0.141	1.08×10^{-3}
+100		2.50×10^{-3}	-100		1.67×10^{-3}
150		3.17×10^{-3}	- 50		2.67×10^{-3}
200	0.201	4.17×10^{-3}	0	0.178	3.50×10^{-3}
300		7.50×10^{-3}	+100		4.17×10^{-3}
400		10.00×10^{-3}	200	0.215	4.17×10^{-3}
500		14.16×10^{-3}	250		5.25×10^{-3}
600	0.248		300		6.63×10^{-3}
900		30.82×10^{-3}	400		8.33×10^{-3}
1200	0.280		600	0.257	
			800		20.83×10^{-3}
			1200	0.288	

REFERENCES

9-1. Goldsmith, Waterman and Hirschom — *Handbook of Thermophysical Properties of Solid Materials,* Revised Ed. (6 Vol), MacMillan Co., 1962

9-2. Guybareff, Janssen and Tarborg — *Thermal Radiation Properties Survey,* Second Ed., Honeywell Regulator Co., 1960

9-3. Morrison and Ingle — *Design Data for Aeronautics and Astronautics,* Wiley 1962

9-4. *Aerospace Structural Metals Handbook,* Syracuse Univ., March 1963, Revised December 1963

9-5. Ziegler, Mullins and Hwa — "Specific Heat and Thermal Conductivity of Four Commercial Titanium Alloys from 20° to 300°K," *Advances in Cryogenic Engineering,* Vol. 8, p. 268, Plenum 1963

9-6. *Electrical and Thermal Properties of Magnesium and Magnesium Alloys,* Dow Chemical Co., October 23, 1959

9-7. *Aerospace Applied Thermodynamics Manual,* SAE (revised) January 1962

9-8. *Technical Data Pamphlet on Rene 41,* Cannon Muskagon Corp.

9-9. *Haynes Alloy No. R-41,* Haynes Stellite Co., Div. Union Carbide Corp., April 1963

9-10. "Stainless Steel Type 321, *"Materials Property Manual and Summary Report AL2604,* North American Aviation, October 1957

9-11. *MIL Handbook #5,* Dept. of Defense (revised), August 1962

REFERENCES (Continued)

9-12. Columbium and Tantalum Base Alloys for Structural and Nuclear Applications, Wah Chang Corp., Vol. 1, Rev. 2, 1962

9-13. Products and Facilities Handbook, Wah Chang Corp., Albany, Oregon

9-14. Deem, and Lucks Survey of Physical Property Data for Titanium and Titanium Alloys, Battelle Memorial Institute, TML Report 39, March 30, 1956

9-15. Technical Data Sheets for Titanium Alloys MST 6AL4V and MST5AL2.5Sn, Reactive Metals Corp.

9-16 "Thermal Conductivity of Titanium Alloys," chart from Metalscope Quarterly, Brooks & Perkins Inc., August 1964

9-17. Engineering Properties of Aluminum Alloy 2219, Ryan Astronautical Co., Report 63B049 ARTC Project 19-62, June 1963

9-18. "Physical Properties of Metals and Alloys from Cryogenic to Elevated Temperatures," Special Tech. Pub. 296, ASTM. 1961

9-19. "Thermal Conductivity of Magnesium Alloys and Beryllium," chart from Metalscope Quarterly, Brooks and Perkins, February 1964

9-20. Hodge, W. Berryllium for Structural Applications, Battelle Memorial Inst., DMIC Report 168 Table B-4, May 1962

9-21. "Materials in Design Engineering," Materials Selection Issue, October 1962

9-22. High Temperature Alloys, Allegheny Ludlum Steel, March 1961

9-23. Technical Bull. T-38, Huntington Alloy Prod. Div., International Nichel Co., August 1959

REFERENCES (Continued)

9-24. Cryogenic Materials Data Handbook, NBS Boulder, PB 171809, Colorado, March 1961

9-25. Scott, Russel B. Cryogenic Engineering, NBS, May 1962

9-26. Mechanical and Physical Properties of the Austenitic Chromium-Nickel Stainless Steels at Subzero Temperatures, International Nickel Co., 1963

9-27. Private Communication from Alcoa Research Laboratory, January 1965

9-28. Lucks, C.F., et al Experimental Measurement of Thermal Conductivities Specific Heats, and Densities of Metallic, Transparent and Protective Materials, Battelle Memorial Institute, WADC TR-6145, Part I, DMIC 32891, February 1951, Part III, DMIC 32892, March 1954

9-29. Inconel "X" A High Strength, High Temperature Alloy, R & D Div., International Nickel Corp., January 1949

9-30. King, C.P. "Wrought Nickel Alloys," Astronautics, Vol. 6, No. 7, p. 92, July 1961

9-31. Engineering Properties of Rene 41, unpublished data (DMIC) Pratt Whitney Aircraft Div., United Aircraft Corp., December 1962

9-32. Berryllium Design Data - General Physical Properties, Report LMSD 48472, Lockheed, 1959

9-33. Private Communication from Linde Division, Union Carbide Corporation, February 2, 1965

9-34. NRC-2 Insulation, National Research Corporation, 1962

9-35. Private Communication from Johns-Manville Sales Corporation, February 24, 1965

9-36. Schultz, H.D. Thermal Analyzer Computer Program for the Solution of General Heat Transfer Problems, Lockheed-California Company Report LR 18902, 16 July 1965

BLANK PAGE

X - THERMAL PROPERTIES LIBRARY

The thermal properties library contains tables of data points for the propellants, pressurants, simulated propellants, structural materials, and insulating materials of Sections VIII and IX. This materials library is set up for use with the Thermal Analyzer Program (Ref. 10-1) and the Fluid Storage and Pressurization Program (Ref. 10-2). Special data search and interpolation routines are incorporated into these programs to utilize the library data.

In all cases where data are available, the tables are accurate for linear interpolation within ±5% over the appropriate temperature range. To construct a useful data library, it was necessary to extend some properties data by means of extrapolation and/or estimation into regions where data are unavailable. All such "extended" data are flagged and interpolations based on these data are automatically noted by the special interpolation routines, and suitable explanations will be printed out. These "extended" data are not necessarily accurate to within ±5%, but are included as a convenience.

PROPERTY IDENTIFICATION CODES

Table 10-1 shows the thermal property identification codes that are assigned to the data tables. A flag in the data-block input of the Thermal Analyzer or Pressurization Programs causes the compiler to search the data tape for the specific table called for by the flag. That table is then stored instead of the flag. There must be an exact correspondence between the identification of the library tables and the flags used to call the tables to be used in the program. The table identification consists of six alphameric characters in columns 6-11, preceded by the mnemonic code "TAP" in columns 1-3.

TABLE 10-1

THERMAL PROPERTIES LIBRARY IDENTIFICATION CODE

PROPERTIES CODE *

Property	Liquid	Gas	Solid
Density (lb/ft^3)	-11		-1
Specific heat (Btu/lb-°F)	-12	-22	-2
Conductivity (Btu/hr-ft-°F)	-13	-23	-3
Vapor pressure (lb/in^2)	-14		
Viscosity (lb/ft-sec)	-15		
Heat of vaporization (Btu/lb)	-16		
Surface tension (lb/ft)	-17		
Compressibility factor		-28	

* Note: The property code is added to a 3-letter (liquid or gas) or a 4-letter (solid) material code to form a 6-character property table identification, such as:

NT0-13	(thermal conductivity of liquid N_2O_4)
HYD-23	(thermal conductivity of gaseous H_2)
T6AL-1	(density of titanium 6Al4V)

PROPELLANT CODE

Propellants	Code	Example
Nitrogen tetroxide (N_2O_4)	NT0	NT0-13
Oxygen (O_2)	0XY	0XY-28
Fluorine (F_2)	FLU	FLU-22
Oxygen difluoride (OF_2)	0DF	0DF-15
Chlorine trifluoride (ClF_3)	CTF	CTF-17
Aerozine 50 (50:50 UDMH-N_2H_4)	AER	AER-12

TABLE 10-1 (Continued)

PROPELLANT CODE (Cont.)

Propellants (Cont.)	Code	Example
Monomethyl hydrazine	MMH	MMH-11
Diborane (B_2H_6)	DIB	DIB-14
Hydrogen (H_2)	HYD	HYD-23
Hybaline A5	HA5	HA5-16
Pressurants		
Nitrogen (N_2)	NIT	NIT-22
Helium (He)	HEL	HEL-28
Simulated Propellants		
60% Ethylene Glycol	G60	G60-13
Freon 11	F11	F11-12

MATERIAL CODE

Structural Material	Code	Example
Aluminum 2219-T87	AL22	AL22-2
Aluminum 7075-T6*	AL70	AL70-1
Magnesium AZ31B-H24	MGA3	MGA3-3
Titanium 6Al4V	T6AL	T6AL-1
Titanium A110AT	T110	T110-3
Columbium C-103	C103	C103-2
Stainless steel 321	S321	S321-3

TABLE 10-1 (Continued)

MATERIAL CODE (Cont.)

Structural Material (Cont.)	Code	Example
Inconel X*	INCX	INCX-2
Rene' 41*	RE41	RE41-1
Beryllium	BERL	BERL-2

* Note: Two conductivity curves, identified as -3 and -4, are provided for the following materials:

Aluminum 7075-T6:	as received and annealed
Inconel X:	as received and solution treated, aged
Rene' 41:	solution treated 2 hr, aged 4 hr and solution treated 4 hr, aged 16 hr

Insulation		Code	Example
Linde SI-12,	8 layers/in.	L12A	L12A-3
	10 layers/in.	L12B	L12B-1
	12 layers/in.	L12C	L12C-2
	14 layers/in.	L12D	L12D-1
Linde SI-62,	40 layers/in.	L62A	L62A-3
	60 layers/in.	L62B	L62B-2
	80 layers/in.	L62C	L62C-3
	100 layers/in.	L62D	L62D-1
Linde SI-92,	80 layers/in.	L92A	L92A-2
	100 layers/in.	L92B	L92B-3
	120 layers/in.	L92C	L92C-2
	160 layers/in.	L92D	L92D-1

TABLE 10-1 (Continued)

MATERIAL CODE (Cont.)

Insulation (Cont.)		Code	Example
Linde "Flight Weight,"	40 layers/in.	LFWA	LFWA-1
	50 layers/in.	LFWB	LFWB-3
	60 layers/in.	LFWC	LFWC-1
	80 layers/in.	LFWD	LFWD-2
Linde "High Temp "	60 layers/in.	LHTA	LHTA-2
	120 layers/in.	LHTB	LHTB-3
	180 layers/in.	LHTC	LHTC-1
NRC-2,	40 layers/in.	NRCA	NRCA-2
	100 layers/in.	NRCB	NRCB-1
	160 layers/in.	NRCC	NRCC-3
Fiberglass		FGLS	FGLS-3
Micro Quartz		MQTZ	MQTZ-1

LIBRARY LISTING

Table 10-2 is a complete listing of the thermal properties library for propellants, pressurants, simulated propellants, structural materials, and insulations. Each set of property data consists of an identification card, an extended data classification code (COD), and cards containing the data.

The classification codes are as follows:

COD 0 (or no "code") - No "extended" data
COD 1 - Extrapolated data
COD 2 - Fitted parabola
COD 3 - Estimated values
COD 4 - "Dummy" values
COD 5 - Values for 1 atmosphere pressure
COD 6 - Values for saturation line
COD 7 - Special Bivariate interpolation routine used in vicivity of saturation line (See Ref. 10-1)
COD 15 - 1 plus 5
COD 16 - 1 plus 6
COD 71 - 7 plus 1
COD 73 - 7 plus 3

These codes are utilized only for those portions of the data that are "extended," as indicated by a "-" sign flag attached to the value of the property in question. The special bivariate routine, which applies to gas properties only, is activated when the interpolation requires data for temperatures and pressures that are in the liquid region, as indicated by blanks in the data and the "COD" 7.

Liquid and solid properties are listed in order, the first value of the independent variable (temperature, ^{o}F) followed by the corresponding value of the dependent variable (the property), etc. A final 0. (or -1000. in the case of the final temperature being negative) signifies the end of the data for that property.

Gas properties are in the form of a matrix, giving values as a function of temperature (^{o}F) and pressure (psia). The first row contains a flag indicating the size of the matrix (e.g., 014007. means 14 pressures by 7 temperatures), followed by the temperatures in ascending order. The following rows contain a pressure, followed by the property values at that pressure corresponding to the temperatures in the first row. The rows are listed in an ascending order of pressure.

Note that all "dashes" in the curve identification codes are input as minus signs (11 punch), and <u>not</u> normal dashes (8-4 punch).

TABLE 10-2

THERMAL PROPERTIES LIBRARY LISTING

```
TAP  NTO-11   DENSITY OF LIQUID NITROGEN TETROXIDE                 101012266
COD      0                                                         101022266
DEC06     11.8     94.27      180.     80.53      240.     72.42  101032266
DEC06     280.     63.05      300.     55.56      310.     48.07  101042266
DEC05     316.     39.96     316.8     34.34        0.            101052266
TAP  NTO-12   SPECIFIC HEAT OF LIQUID NITROGEN TETROXIDE           102012266
COD      1                                                         102022266
DEC06     11.8      .355       50.      .361       85.      .377  102032266
DEC06     110.      .402      120.      .418      130.      .438  102042266
DEC05     180.      -.54     316.8   -1.0E20        0.            102052266
TAP  NTO-13   THERMAL CONDUCTIVITY OF LIQUID NITROGEN TETROXIDE    103012266
COD      1                                                         103022266
DEC06     11.8      .085      110.      .070      145.      .062  103032266
DEC06     160.      .056      220.     -.035     316.8      -.01  103042266
DEC01       0.                                                    103052266
TAP  NTO-14   VAPOR PRESSURE OF LIQUID NITROGEN TETROXIDE          104012266
COD      0                                                         104022266
DEC06     11.8       2.7       14.       2.9       20.      3.45  104032266
DEC06      30.       4.7       40.       6.4       50.       8.5  104042266
DEC06      70.      14.8       80.      19.5      100.      30.7  104052266
DEC06     120.      48.2      140.       74.      160.      111.  104062266
DEC06     180.      164.      200.      236.      220.      330.  104072266
DEC06     240.      460.      260.      630.      280.      860.  104082266
DEC06     300.     1160.      310.     1330.     316.8     1470.  104092266
DEC01       0.                                                    104102266
TAP  NTO-15   VISCOSITY OF LIQUID NITROGEN TETROXIDE               105012266
COD      1                                                         105022266
DEC06     11.8   -3.9E-4       40.   3.34E-4      100.   2.27E-4  105032266
DEC06     180.   1.28E-4      240.    .71E-4      280.    .38E-4  105042266
DEC03    316.8   -0.1E-4        0.                                105052266
TAP  NTO-16   HEAT OF VAPORIZATION OF LIQUID NITROGEN TETROXIDE    106012266
COD      2                                                         106022266
DEC06     11.8      145.       25.     -165.       50.     -176.  106032266
DEC06      70.      178.      100.     -173.      125.     -163.  106042266
DEC05     150.     -147.     316.8        0.        0.            106052266
TAP  NTO-17   SURFACE TENSION OF LIQUID NITROGEN TETROXIDE         107012266
COD      1                                                         107022266
DEC06     11.8  -22.5E-4       68.   18.2E-4     316.8        0.  107032266
DEC01       0.                                                    107042266
TAP  NTO-22   SPECIFIC  HEAT OF GASEOUS NITROGEN TETROXIDE         108012266
COD     73                                                         108022266
DEC06  006012.       32.       62.       70.       90.      105.  108032266
DEC06     120.      135.      150.      170.      200.      230.  108042266
DEC01      60.                                                    108052266
DEC06     4.85      -.97      1.55      1.71      2.10       2.2  108062266
DEC06     2.14      1.90      1.54      1.07       .60       .39  108072266
DEC01      .28                                                    108082266
DEC06    10.88                1.14      1.28      1.63      1.89  108092266
DEC06     2.06      2.06      1.90      1.55       .95       .57  108102266
DEC01      .36                                                    108112266
DEC06    14.70                          1.13      1.46      1.71  108122266
DEC06     1.94      2.02      1.97      1.70      1.11       .67  108132266
DEC01      .44                                                    108142266
DEC06      50.                                                    108152266
DEC06    -1.20     -1.39     -1.56     -1.74     -1.42      -.86  108162266
DEC01     -.52                                                    108172266
DEC06     100.                                                    108182266
DEC06                                  -1.22     -1.50     -1.27  108192266
DEC01     -.75                                                    108202266
DEC06     300.                                                    108212266
DEC06                                                       -.92  108222266
```

TABLE 10-2 (Continued)

```
DEC01     -1.13                                                           108232266
TAP  NTO-23   THERMAL CONDUCTIVITY OF GASEOUS NITROGEN TETROXIDE          109012266
COD     5                                                                 109022266
DEC06   002005.       32.      70.07       118.       146.       220.     109032266
DEC06       .01      -.04     -.063      -.088      -.086      -.035     109042266
DEC06      300.      -.04     -.063      -.088      -.086      -.035     109052266
TAP  NTO-28   COMPRESSIBILITY FACTOR OF GASEOUS NITROGEN TETROXIDE       110012266
COD     71                                                                110022266
DEC06   014007.       32.        70.        100.       130.       160.    110032266
DEC02      190.      220.                                                 110042266
DEC06      4.85      -.52       -.59       -.66       -.75       -.86    110052266
DEC02      -.94      -.97                                                 110062266
DEC06      14.7                 .566        .64       .728        .83    110072266
DEC02      .913      .957                                                 110082266
DEC06       20.                             .62       .698        .80    110092266
DEC02      .889      .942                                                 110102266
DEC06       30.                            .594       .659       .755    110112266
DEC02      .851      .917                                                 110122266
DEC06       40.                                       .632       .722    110132266
DEC02      .821      .894                                                 110142266
DEC06       50.                                       .612       .695    110152266
DEC02      .792      .872                                                 110162266
DEC06       60.                                       .597       .673    110172266
DEC02      .767      .855                                                 110182266
DEC06       80.                                                  .637    110192266
DEC02      .725      .824                                                 110202266
DEC06      100.                                                  .609    110212266
DEC02      .693      .797                                                 110222266
DEC06      125.                                                           110232266
DEC02      .660      .768                                                 110242266
DEC06      150.                                                           110252266
DEC02      .632      .742                                                 110262266
DEC06      200.                                                           110272266
DEC02                .696                                                 110282266
DEC06      250.                                                           110292266
DEC02                .653                                                 110302266
DEC06      300.                                                           110312266
DEC02                .608                                                 110322266
TAP   OXY-11    DENSITY OF LIQUID OXYGEN                                  111012266
COD     0                                                                 111022266
DEC06    -361.8     81.78     -240.      60.56      -194.      45.57     111032266
DEC06     -186.     39.33     -181.2     33.71     -181.1      26.84     111042266
DEC01    -1000.                                                           111052266
TAP   OXY-12    SPECIFIC HEAT OF LIQUID OXYGEN                            112012266
COD     1                                                                 112022266
DEC06    -361.8      .335     -240.       .465      -220.        .51     112032266
DEC06     -204.       .61     -192.        .78     -181.1    -1.E20     112042266
DEC01    -1000.                                                           112052266
TAP   OXY-13    THERMAL CONDUCTIVITY OF LIQUID OXYGEN                     113012266
COD     0                                                                 113022266
DEC06    -361.8      .110     -230.       .053      -194.       .040     113032266
DEC03     -184.      .030    -1000.                                       113042266
TAP   OXY-14    VAPOR PRESSURE OF LIQUID OXYGEN                           114012266
COD     0                                                                 114022266
DEC06    -361.8      .022    -360.7       .027     -351.7       .105     114032266
DEC06     -350.       .15     -345.        .25      -340.        .45     114042266
DEC06     -335.       .75     -330.       1.22      -325.        1.9     114052266
DEC06     -320.       3.0     -315.        4.5      -310.        6.5     114062266
DEC06     -305.       9.1     -300.       12.3      -290.        22.     114072266
DEC06     -280.       36.     -270.        56.      -260.        84.     114082266
DEC06     -250.      120.     -240.       165.      -225.       260.     114092266
```

TABLE 10-2 (Continued)

```
DEC06      -210.      380.     -195.      540.    -181.1      736. 114102266
DEC01     -1000.                                                    114112266
TAP   OXY-15   VISCOSITY OF LIQUID OXYGEN                            115012266
COD        0                                                        115022266
DEC06     -361.8   5.87E-4    -360.     5.E-4     -350.    3.5E-4 115032266
DEC06      -336.    2.5E-4    -320.    1.8E-4     -300.    1.3E-4 115042266
DEC06      -280.     1.E-4    -260.    .77E-4     -182.     .6E-4 115052266
DEC01     -1000.                                                    115062266
TAP   OXY-16   HEAT OF VAPORIZATION OF LIQUID OXYGEN                 116012266
COD        0                                                        116022266
DEC06     -361.8      104.     -280.       88.     -230.       69. 116032266
DEC06      -200.       49.    -186.1      29.8    -182.5      21.2 116042266
DEC03     -181.1        0.    -1000.                                116052266
TAP   OXY-17   SURFACE TENSION OF LIQUID OXYGEN                      117012266
COD        0                                                        117022266
DEC06     -361.8   15.2E-4    -300.    9.3E-4     -240.     4.E-4 117032266
DEC05      -200.    1.1E-4    -181.1       0.    -1000.             117042266
TAP   OXY-22   SPECIFIC HEAT OF GASEOUS OXYGEN                       118012266
COD       71                                                        118022266
DEC06    008011.     -332.     -296.     -280.     -260.     -240. 118032266
DEC06      -220.     -200.     -150.     -100.       80.      800. 118042266
DEC06         1.     -.222     -.222     -.222     -.220     -.220 118052266
DEC06      -.220     -.220     -.220     -.220     -.220     -.228 118062266
DEC06       14.7                .225      .225      .222      .220 118072266
DEC06       .220      .220      .220      .220      .220      .228 118082266
DEC06       29.4                          .232      .229      .225 118092266
DEC06       .222      .222      .220      .220      .220      .228 118102266
DEC06       44.1                                    .234      .229 118112266
DEC06       .229      .225      .222      .220      .220      .228 118122266
DEC06       73.5                                    .251      .244 118132266
DEC06       .236      .234      .225      .222      .222      .229 118142266
DEC06       147.                                              .282 118152266
DEC06       .263      .251      .236      .229      .222      .229 118162266
DEC06       221.                                                    118172266
DEC06       .303      .277      .248      .234      .225      .232 118182266
DEC06       294.                                                    118192266
DEC06                 .315      .260      .241      .227      .234 118202266
TAP   OXY-23   THERMAL CONDUCTIVITY OF GASEOUS OXYGEN                119012266
COD       71                                                        119022266
DEC06    003005.     -332.     -292.     -220.      104.      300. 119032266
DEC06         1.     -.004    -.0048     -.007     -.016     -.025 119042266
DEC06       14.7               .0048      .007      .016     -.025 119052266
DEC06       294.                         .0089     .0165     -.026 119062266
TAP   OXY-28   COMPRESSIBILITY FACTOR OF GASEOUS OXYGEN              120012266
COD       71                                                        120022266
DEC06    008011.     -332.     -296.     -280.     -260.     -240. 120032266
DEC06      -220.     -200.     -100.        0.       80.      300. 120042266
DEC06         1.     -.970     -.977     -.983     -.988     -.992 120052266
DEC06      -.995     -.997     -.999       -1.       -1.       -1. 120062266
DEC06       14.7                .969      .976      .982      .987 120072266
DEC06       .990      .992      .997      .999        1.        1. 120082266
DEC06       29.4                          .951      .964      .973 120092266
DEC06       .979      .983      .994      .998      .999        1. 120102266
DEC06       44.1                                    .945      .959 120112266
DEC06       .968      .975      .992      .997      .999        1. 120122266
DEC06       73.5                                    .905      .929 120132266
DEC06       .946      .958      .985      .994      .997        1. 120142266
DEC06       147.                                              .846 120152266
DEC06       .886      .912      .971      .988      .995        1. 120162266
DEC06       221.                                                    120172266
DEC06       .817      .862      .955      .982      .992        1. 120182266
```

TABLE 10-2 (Continued)

```
DEC06       294.                                                         120192266
DEC06       .734      .807      .940       .976       .989           1.  120202266
TAP  FLU-11   DENSITY OF LIQUID FLUORINE                                 121012266
COD       0                                                              121022266
DEC06    -363.3    107.38     -278.      87.40      -228.        69.92  121032266
DEC06     -210.     53.07     -204.      43.70     -201.6        37.46  121042266
DEC01    -1000.                                                          121052266
TAP  FLU-12   SPECIFIC HEAT OF LIQUID FLUORINE                           122012266
COD       1                                                              122022266
DEC06    -363.3      .360     -330.       .357      -307.         .367  122032266
DEC06     -250.      -.42     -225.        -1.     -200.5       -1.E20  122042266
DEC01    -1000.                                                          122052266
TAP  FLU-13   THERMAL CONDUCTIVITY OF LIQUID FLUORINE                    123012266
COD       1                                                              123022266
DEC06    -363.3      .193     -260.       .135      -220.        -.115  123032266
DEC01    -1000.                                                          123042266
TAP  FLU-14   VAPOR PRESSURE OF LIQUID FLUORINE                          124012266
COD       0                                                              124022266
DEC06    -351.6       .22     -339.         1.      -334.          1.8  124032266
DEC06     -330.       2.6     -325.         4.      -320.           6.  124042266
DEC06     -314.        9.     -310.        12.      -302.          19.  124052266
DEC06     -291.       33.     -280.        54.      -270.          80.  124062266
DEC06     -260.      119.     -245.       200.      -230.         330.  124072266
DEC05     -212.      540.    -200.5       808.     -1000.                124082266
TAP  FLU-15   VISCOSITY OF LIQUID FLUORINE                               125012266
COD       1                                                              125022266
DEC06    -363.3    5.1E-4     -347.     3.5E-4      -335.      2.75E-4  125032266
DEC06     -320.   2.05E-4     -305.    1.55E-4      -250.      -.70E-4  125042266
DEC03    -200.5    -.5E-4    -1000.                                      125052266
TAP  FLU-16   HEAT OF VAPORIZATION OF LIQUID FLUORINE                    126012266
COD       0                                                              126022266
DEC06    -363.3       85.     -288.        67.      -235.          47.  126032266
DEC06     -210.       29.     -202.        16.     -200.5           0.  126042266
DEC01    -1000.                                                          126052266
TAP  FLU-17   SURFACE TENSION OF LIQUID FLUORINE                         127012266
COD       0                                                              127022266
DEC06    -363.3   15.3E-4    -313.5     10.E-4      -253.        4.E-4  127032266
DEC03    -200.5        0.    -1000.                                      127042266
TAP  FLU-22   SPECIFIC HEAT OF GASEOUS FLUORINE                          128012266
COD       5                                                              128022266
DEC06   002013.     -306.     -298.      -280.      -262.        -244.  128032266
DEC06     -226.     -136.     -100.       -64.       -28.           8.  128042266
DEC02       44.       77.                                                128052266
DEC06        1.     -.194     -.193      -.190      -.189        -.187  128062266
DEC06    -.1865    -.1865     -.188      -.190      -.192        -.194  128072266
DEC02     -.196     -.198                                                128082266
DEC06      300.     -.194     -.193      -.190      -.189        -.187  128092266
DEC06    -.1865    -.1865     -.188     - .190      -.192        -.194  128102266
DEC02     -.196     -.198                                                128112266
TAP  FLU-23   THERMAL CONDUCTIVITY OF GASEOUS FLUORINE                   129012266
COD      15                                                              129022266
DEC06   002005.     -306.     -280.      -100.        31.         170.  129032266
DEC06        1.     -.004   -.00498     -.0105     -.0143       -.0178  129042266
DEC06      300.     -.004   -.00498     -.0105     -.0143       -.0178  129052266
TAP  FLU-28   COMPRESSIBILITY FACTOR OF GASEOUS FLUORINE                 130012266
COD       4                                                              130022266
DEC03   002002.     -340.      200.                                      130032266
DEC03        1.       -1.       -1.                                      130042266
DEC03      300.       -1.       -1.                                      130052266
TAP  ODF-11   DENSITY OF LIQUID OXYGEN DIFLUORIDE                        131012266
COD       0                                                              131022266
```

TABLE 10-2 (Continued)

```
DEC06    -370.8    119.24     -180.     87.40      -110.      69.92  131032266
DEC06      -80.     52.44      -76.     43.70      -75.5      34.34  131042266
DEC01    -1000.                                                      131052266
TAP  ODF-12   SPECIFIC HEAT OF LIQUID OXYGEN DIFLUORIDE              132012266
COD      1                                                           132022266
DEC06    -370.8      -.35     -296.       .35      -256.        .35  132032266
DEC03     -75.5      -.35    -1000.                                  132042266
TAP  ODF-13   THERMAL CONDUCTIVITY OF LIQUID OXYGEN DIFLUORIDE       133012266
COD      1                                                           133022266
DEC06     -320.      .148     -296.      .140      -75.5       -.07  133032266
DEC01    -1000.                                                      133042266
TAP  ODF-14   VAPOR PRESSURE OF LIQUID OXYGEN DIFLUORIDE             134012266
COD      0                                                           134022266
DEC06     -302.        .1     -296.        .2      -290.        .35  134032266
DEC06     -285.        .5     -280.        .8      -275.       1.15  134042266
DEC06     -265.       2.3     -255.        4.      -245.         7.  134052266
DEC06     -235.      11.6     -220.       22.      -205.        38.  134062266
DEC06     -190.       60.     -175.       94.      -155.       158.  134072266
DEC06     -135.      250.     -115.      370.       -95.       540.  134082266
DEC03     -75.5      728.    -1000.                                  134092266
TAP  ODF-15   VISCOSITY OF LIQUID OXYGEN DIFLUORIDE                  135012266
COD      1                                                           135022266
DEC06     -340.   11.5E-4     -330.    8.5E-4      -316.      6.E-4  135032266
DEC06     -300.    4.4E-4     -280.    3.1E-4      -252.     2.2E-4  135042266
DEC06     -220.   1.65E-4     -180.   1.25E-4      -150.    1.07E-4  135052266
DEC03     -75.5    -.8E-4    -1000.                                  135062266
TAP  ODF-16   HEAT OF VAPORIZATION OF LIQUID OXYGEN DIFLUORIDE       136012266
COD      2                                                           136022266
DEC06    -370.8     -120.    -228.6       89.      -120.       -50.  136032266
DEC03     -75.5        0.    -1000.                                  136042266
TAP  ODF-22   SPECIFIC HEAT OF GASEOUS OXYGEN DIFLUORIDE             138012266
COD     5                                                            138022266
DEC04   002003.    -229.5       80.      300.                        138032266
DEC04        1.      -.15     -.192     -.215                        138042266
DEC04      300.      -.15     -.192     -.215                        138052266
TAP  ODF-28   COMPRESSIBILITY FACTOR OF LIQUID OXYGEN DIFLUORIDE     140012266
COD      4                                                           140022266
DEC03   002002.     -400.      300.                                  140032266
DEC03        1.       -1.       -1.                                  140042266
DEC03      300.       -1.       -1.                                  140052266
TAP  CTF-11   DENSITY OF LIQUID CHLORINE TRIFLUORIDE                 141012266
COD      0                                                           141022266
DEC06    -107.1    130.48      150.    105.51       300.      79.29  141032266
DEC06      335.     64.30      340.     59.31       345.      42.45  141042266
DEC01        0.                                                      141052266
TAP  CTF-12   SPECIFIC HEAT OF LIQUID CHLORINE TRIFLUORIDE           142012266
COD      1                                                           142022266
DEC06    -107.1      .288       50.      .303       200.       .329  142032266
DEC05      300.      -.38      345.    -1.E20         0.             142042266
TAP  CTF-13   THERMAL CONDUCTIVITY OF LIQUID CHLORINE TRIFLUCRIDE    143012266
COD      1                                                           143022266
DEC06    -107.1      .149        0.      .139       .175       .132  143032266
DEC03      345.     -.127        0.                                  143042266
TAP  CTF-14   VAPOR PRESSURE OF LIQUID CHLORINE TRIFLUORIDE          144012266
COD      0                                                           144022266
DEC06      -80.       .19      -70.       .29       -60.        .43  144032266
DEC06      -50.       .63      -40.       .91       -30.       1.28  144042266
DEC06      -20.      1.83        0.       3.5        20.        6.2  144052266
DEC06       40.      10.6       60.       17.        90.        32.  144062266
DEC06      120.       56.      150.       94.       190.       170.  144072266
DEC06      230.      290.      230.      490.       345.       838.  144082266
```

TABLE 10-2 (Continued)

```
DEC01        0.                                                    144092266
TAP  CTF-15   VISCOSITY OF LIQUID CHLORINE TRIFLUORIDE             145012266
COD      0                                                         145022266
DEC06      -50.    7.7E-4      -15.    5.3E-4       50.    3.2E-4  145032266
DEC06      130.     2.E-4      215.   1.25E-4      300.     .7E-4  145042266
DEC01        0.                                                    145052266
TAP  CTF-16   HEAT OF VAPORIZATION OF LIQUID CHLORINE TRIFLUORIDE  146012266
COD      2                                                         146022266
DEC06    -107.1     -140.      53.2      128.      250.      -93.  146032266
DEC05      325.      -40.       345        0.        0.            146042266
TAP  CTF-17   SURFACE TENSION OF LIQUID CHLORINE TRIFLUORIDE       147012266
COD      0                                                         147022266
DEC06    -107.1   26.9E-4      135.    12.E-4      345.        0.  147032266
DEC01        0.                                                    147042266
TAP  CTF-22   SPECIFIC HEAT OF GASEOUS CHLORINE TRIFLUORIDE        148012266
COD      5                                                         148022266
DEC05   002004.     -100.       80.      260.      440.            148032266
DEC05        1.     -.141     -.168     -.184     -.194            148042266
DEC05      300.     -.141     -.168     -.184     -.194            148052266
TAP  CTF-28   COMPRESSIBILITY FACTOR,GASEOUS CHLORINE TRIFLUORIDE  150012266
COD      1                                                         150022266
DEC03   002002.     -100.      500.                                150032266
DEC03        1.     -.968     -.968                                150042266
DEC03      300.     -.968     -.968                                150052266
TAP  AER-11   DENSITY OF LIQUID AEROZINE 50                        151012266
COD      1                                                         151022266
DEC06      18.8     58.06      160.     53.69      300.    -49.01  151032266
DEC01        0.                                                    151042266
TAP  AER-12   SPECIFIC HEAT OF LIQUID AEROZINE 50                  152012266
COD      1                                                         152022266
DEC06      18.8       .68      250.       .74      300.     -.758  152032266
DEC01        0.                                                    152042266
TAP  AER-13   THERMAL CONDUCTIVITY OF LIQUID AEROZINE 50           153012266
COD      1                                                         153022266
DEC06      18.8      .131      100.      .134      146.      .138  153032266
DEC05      200.     -.148      250.      -.16        0.            153042266
TAP  AER-14   VAPOR PRESSURE OF LIQUID AEROZINE 50                 154012266
COD      1                                                         154022266
DEC06      18.8       .63       32.       .92       50.       1.4  154032266
DEC06       70.       2.2       90.       3.6      120.       7.1  154042266
DEC06      150.      13.5      180.      24.5      200.      -41.  154052266
DEC05      250.     -120.      300.     -340.        0.            154062266
TAP  AER-15   VISCOSITY OF LIQUID AEROZINE 50                      155012266
COD      1                                                         155022266
DEC06      18.8   10.4E-4       40.    7.8E-4       70.    5.7E-4  155032266
DEC06      100.    4.5E-4      138.    3.5E-4      160.    3.1E-4  155042266
DEC03      300.    -1.E-4        0.                                155052266
TAP  AER-16   HEAT OF VAPORIZATION OF LIQUID AEROZINE 50           156012266
COD      2                                                         156022266
DEC06      18.8     -270.       77.      264.      300.     -235.  156032266
DEC01        0.                                                    156042266
TAP  AER-17   SURFACE TENSION OF LIQUID AEROZINE 50                157012266
COD      1                                                         157022266
DEC06      18.8  -22.5E-4       68.   20.8E-4      300.  -12.2E-4  157032266
DEC01        0.                                                    157042266
TAP  AER-22   SPECIFIC HEAT OF GASEOUS AEROZINE 50                 158012266
COD      4                                                         158022266
DEC03   002002.        0.      300.                                158032266
DEC03        .5   -1.E-20   -1.E-20                                158042266
DEC03      400.   -1.E-20   -1.E-20                                158052266
TAP  AER-23   THERMAL CONDUCTIVITY OF GASEOUS AEROZINE 50          159012266
```

TABLE 10-2 (Continued)

```
COD      4                                                           159022266
DEC03      002002.        0.      300.                               159032266
DEC03           .5   -1.E-20   -1.E-20                               159042266
DEC03         400.   -1.E-20   -1.E-20                               159052266
TAP  AFR-28   COMPRESSIBILITY FACTOR OF GASEOUS AEROZINE 50          160012266
COD      4                                                           160022266
DEC03      002002.        0.      300.                               160032266
DEC03           .5       -1.       -1.                               160042266
DEC03         400.       -1.       -1.                               160052266
TAP  MMH-11   DENSITY OF LIQUID MONOMETHYL HYDRAZINE                 161012266
COD      0                                                           161022266
DEC06        -62.3     58.68      315.     46.82      450.     40.58 161032266
DEC01           0.                                                   161042266
TAP  MMH-12   SPECIFIC HEAT OF LIQUID MONOMETHYL HYDRAZINE           162012266
COD      0                                                           162022266
DEC05        -62.3      .679      400.      .751        0.           162032266
TAP  MMH-13   THERMAL CONDUCTIVITY OF LIQUID MONOMETHYL HYDRAZINE    163012266
COD      0                                                           163022266
DEC05        -62.3      .152      400.      .120        0.           163032266
TAP  MMH-14   VAPOR PRESSURE OF LIQUID MONOMETHYL HYDRAZINE          164012266
COD      1                                                           164022266
DEC06        -62.3      -.01       30.       .19       40.       .27 164032266
DEC06          50.       .39       60.       .54       80.      1.05 164042266
DEC06         100.       1.9      120.       3.1      140.       5.2 164052266
DEC06         160.        8.      180.       12.      210.       21. 164062266
DEC06         240.       35.      270.       55.      300.       81. 164072266
DEC06         340.      130.      380.      200.      420.      305. 164082266
DEC06         460.      450.      500.      630.      560.      920. 164092266
DEC03         609.     1195.        0.                               164102266
TAP  MMH-15   VISCOSITY OF LIQUID MONOMETHYL HYDRAZINE               165012266
COD      0                                                           165022266
DEC06        -62.3    90.E-4      -50.    50.E-4      -30.    27.E-4 165032266
DEC06         -10.    18.E-4       10.   12.5E-4       40.    8.2E-4 165042266
DEC06          80.    5.4E-4      120.     4.E-4      200.    2.6E-4 165052266
DEC06         300.    1.7E-4      400.   1.15E-4      500.    .74E-4 165062266
DEC01           0.                                                   165072266
TAP  MMH-16   HEAT OF VAPORIZATION OF LIQUID MONOMETHYL HYDRAZINE    166012266
COD      2                                                           166022266
DEC06        -62.3     -400.       77.      377.      400.     -290. 166032266
DEC01           0.                                                   166042266
TAP  MMH-17   SURFACE TENSION OF LIQUID MONOMETHYL HYDRAZINE         167012266
COD      0                                                           167022266
DEC06        -62.3   28.4E-4      150.   20.5E-4      350.   12.5E-4 167032266
DEC03         609.        0.        0.                               167042266
TAP  MMH-22   SPECIFIC HEAT OF GASEOUS MONOMETHYL HYDRAZINE          168012266
COD      4                                                           168022266
DEC03      002002.     -100.      400.                               168032266
DEC03         .005   -1.E-20   -1.E-20                               168042266
DEC03         400.   -1.E-20   -1.E-20                               168052266
TAP  MMH-23   THERMAL CONDUCTIVITY , GASEOUS MONOMETHYL HYDRAZINE    169012266
COD      4                                                           169022266
DEC03      002002.     -100.      400.                               169032266
DEC03         .005   -1.E-20   -1.E-20                               169042266
DEC03         400.   -1.E-20   -1.E-20                               169052266
TAP  MMH-28   COMPRESSIBILITY FACTOR,GASEOUS MONOMETHYL HYDRAZINE    170012266
COD      4                                                           170022266
DEC03      002002.     -100.      400.                               170032266
DEC03         .005       -1.       -1.                               170042266
DEC03         400.       -1.       -1.                               170052266
TAP  DIB-11   DENSITY OF LIQUID DIBORANE                             171012266
COD      0                                                           171022266
```

TABLE 10-2 (Continued)

```
DEC06    -265.9     32.46     -140.     27.47       -7.     19.98  171032266
DEC06       44.     15.61      57.2     13.11      62.1      9.99  171042266
DEC01        0.                                                    171052266
TAP   DIB-12   SPECIFIC HEAT OF LIQUID DIBORANE                    172012266
COD        1                                                       172022266
DEC06    -265.9       .66     -200.       .65      -130       .67  172032266
DEC06      -80.       .71      -40.       .76       10.       .88  172042266
DEC03      62.1    -1.E20        0.                                172052266
TAP   DIB-13   THERMAL CONDUCTIVITY OF LIQUID DIBORANE             173012266
COD        1                                                       173022266
DEC06    -265.9      .078     -200.      .073     -130.      .061  173032266
DEC06     -100.      .053      -50.      -.04      62.1      -.01  173042266
DEC01        0.                                                    173052266
TAP   DIB-14   VAPOR PRESSURE OF LIQUID DIBORANE                   174012266
COD        1                                                       174022266
DEC06    -265.9       -.1    -232.6      .147    -222.7       .29  174032266
DEC06     -215.       .47     -205.       .80     -195.      1.37  174042266
DEC06     -180.       2.8     -165.       5.3     -150.       9.4  174052266
DEC06     -130.       17.     -110.       29.      -90.       48.  174062266
DEC06      -70.       73.      -50.      108.      -20.      180.  174072266
DEC06       10.      280.       40.      490.       62.      580.  174082266
DEC01        0.                                                    174092266
TAP   DIB-15   VISCOSITY OF LIQUID DIBORANE                        175012266
COD        1                                                       175022266
DEC06     -196.   1.64E-4     -170.   1.24E-4     -130.    .92E-4  175032266
DEC06      -94.    .65E-4        0.    -.4E-4      62.1    -.3E-4  175042266
DEC01        0.                                                    175052266
TAP   DIB-16   HEAT OF VAPORIZATION OF LIQUID DIBORANE             176012266
COD        2                                                       176022266
DEC06    -265.9     -250.    -134.5      222.        0.     -140.  176032266
DEC03      62.1        0.        0.                                176042266
TAP   DIB-22   SPECIFIC HEAT OF GASEOUS DIBORANE                   178012266
COD       16                                                       178022266
DEC06   002005.    -265.9     -100.       80.      260.      440.  178032266
DEC06       .05      -.25     -.361     -.483     -.621     -.749  178042266
DEC06      600.      -.25     -.361     -.483     -.621     -.749  178052266
TAP   DIB-28   COMPRESSIBILITY FACTOR OF GASEOUS DIBORANE          180012266
COD        4                                                       180022266
DEC03   002002.     -300.      100.                                180032266
DEC03       .05       -1.       -1.                                180042266
DEC03      600.       -1.       -1.                                180052266
TAP   HYD-11   DENSITY OF LIQUID HYDROGEN                          181012266
COD        0                                                       181022266
DEC06    -434.8      4.81     -414.      4.06     -403.      3.12  181032266
DEC06     -401.      2.62    -400.5      2.31    -400.3      1.94  181042266
DEC01     -1000.                                                   181052266
TAP   HYD-12   SPECIFIC HEAT OF LIQUID HYDROGEN                    182012266
COD        0                                                       182022266
DEC06    -434.8      1.54    -423.7      2.25     -415.      3.03  182032266
DEC06     -411       3.58    -408.5      4.11      405.      5.36  182042266
DEC03    -402.9      6.83    -1000.                                182052266
TAP   HYD-13   THERMAL CONDUCTIVITY OF LIQUID HYDROGEN             183012266
COD        0                                                       183022266
DEC05    -434.8     ,0609    -400.3     .0868    -1000.            183032266
TAP   HYD-14   VAPOR PRESSURE OF LIQUID HYDROGEN                   184012266
COD        0                                                       184022266
DEC06    -434.8      1.02     -433.      1.77     -431.        3.  184032266
DEC06     -429.       4.8     -427.       7.4     -425.       11.  184042266
DEC06     -422.       18.     -419.       27.     -416.       41.  184052266
DEC06     -412.       64.     -408.       96.     -404.      138.  184062266
DEC03    -400.3      188.    -1000.                                184072266
```

TABLE 10-2 (Continued)

```
TAP   HYD-15    VISCOSITY OF LIQUID HYDROGEN                                185012266
COD      1                                                                  185022266
DEC06    -434.8    .169E-4      -430.    .125E-4      -425.    .097E-4     185032266
DEC06     -420.    .079E-4      -415.    .067E-4      -410.    .058E-4     185042266
DEC03    -400.3    .046E-4     -1000.                                       185052266
TAP   HYD-16    HEAT OF VAPORIZATION OF LIQUID HYDROGEN                     186012266
COD      0                                                                  186022266
DEC06    -434.8       195.      -425.       195.      -416.       180.     186032266
DEC06     -408.       145.      -403.        98.     -402.1        81.     186042266
DEC06    -401.4        66.     -400.8        50.     -400.5       30.3     186052266
DEC03    -400.3         0.     -1000.                                       186062266
TAP   HYD-17    SURFACE TENSION OF LIQUID HYDROGEN                          187012266
COD      0                                                                  187022266
DEC06    -434.8    2.08E-4      -423.    1.31E-4     -400.3         0.     187032266
DEC01    -1000.                                                             187042266
TAP   HYD-22    SPECIFIC HEAT OF GASEOUS NORMAL HYDROGEN                    188012266
COD     71                                                                  188022266
DEC06   007021.      -423.      -410.      -405.     -402.5      -400.     188032266
DEC06    -397.5      -395.     -392.5      -390.     -387.5      -385.     188042266
DEC06     -380.      -370.      -360.      -350.      -300.      -200.     188052266
DEC04     -100.       -10.        80.       340.                            188062266
DEC06        0.       2.46       2.46       2.46       2.46       2.46     188072266
DEC06      2.46       2.46       2.46       2.46       2.46       2.46     188082266
DEC06      2.47       2.47       2.48       2.48        2.6       2.95     188092266
DEC04      3.23       3.35       3.42      -3.42                            188102266
DEC06      14.7       2.86       2.67        2.6        2.6       2.59     188112266
DEC06      2.57       2.56       2.55       2.54       2.53       2.53     188122266
DEC06       2.5        2.5        2.5        2.5        2.6       2.95     188132266
DEC04      3.23       3.35       3.42      -3.42                            188142266
DEC06       71.                   4.3        3.5        3.4       3.25     188152266
DEC06       3.1        3.0       2.95        2.9        2.9        2.9     188162266
DEC06       2.8        2.7       2.65        2.6       2.65       2.95     188172266
DEC04      3.23       3.35       3.42      -3.42                            188182266
DEC06      147.                                         8.5        6.2     188192266
DEC06       4.9        4.3        4.0        3.8        3.4        3.3     188202266
DEC06      3.15        3.0       2.85       2.75        2.7        3.0     188212266
DEC04      3.25       3.36       3.42      -3.42                            188222266
DEC06      191.                                                             188232266
DEC06       8.5        6.0        4.9        4.4        4.0       3.95     188242266
DEC06      3.55        3.2        3.0       2.85        2.7        3.0     188252266
DEC04       3.3        3.4       3.45      -3.45                            188262266
DEC06      220.                                                             188272266
DEC06       16.        8.4        6.6        5.3        4.5        4.1     188282266
DEC06       3.8        3.4        3.1        2.9        2.7        3.0     188292266
DEC04       3.3        3.4       3.45      -3.45                            188302266
DEC06      294.                                                             188312266
DEC06                 34.5       12.4        8.6        6.5        5.5     188322266
DEC06       4.5        3.6        3.2        3.0        2.7       3.05     188332266
DEC04       3.3        3.4       3.46      -3.46                            188342266
TAP   HYD-23    THERMAL CONDUCTIVITY OF GASEOUS PARA HYDROGEN               189012266
COD     15                                                                  189022266
DEC06   002005.      -420.      -330.      -190.       -60.        80.     189032266
DEC06        .5       -.01       -.03       -.07       -.09      -.108     189042266
DEC06      200.       -.01       -.03       -.07       -.09      -.108     189052266
TAP   HYD-28    COMPRESSIBILITY FACTOR OF GASEOUS PARA HYDROGEN             190012266
COD      7                                                                  190022266
DEC06   009013.     -429.7     -419.7     -409.7     -399.7      -395.     190032266
DEC06     -390.      -385.      -380.      -370.      -360.      -310.     190042266
DEC02     -260.       340.                                                  190052266
DEC06        1.       .990       .995       .997       .998       .998     190062266
DEC06      .999       .999       .999       .999       .999         1.     190072266
```

TABLE 10-2 (Continued)

```
DEC02       1.        1.                                               190082266
DEC06       6.      .939       .969       .982       .990       .991   190092266
DEC06     .993      .994       .995       .996       .997         1.   190102266
DEC02       1.        1.                                               190112266
DEC06     14.7                 .918       .949       .976       .983   190122266
DEC06     .988      .989       .989       .987       .991       .999   190132266
DEC02       1.        1.                                               190142266
DEC06      30.                            .895       .948       .965   190152266
DEC06     .971      .975       .979       .98[illegible]       .986       .998   190162266
DEC02       1.     1.001                                               190172266
DEC06      60.                                       .890       .915   190182266
DEC06     .932      .944       .954       .966       .975       .995   190192266
DEC02       1.     1.002                                               190202266
DEC06     100.                                       .796       .847   190212266
DEC06     .883      .907       .925       .945       .957       .992   190222266
DEC02    1.001     1.003                                               190232266
DEC06     150.                                       .664       .775   190242266
DEC06     .826      .862       .883       .908       .934       .989   190252266
DEC02    1.002     1.004                                               190262266
DEC06     200.                                       .263       .647   190272266
DEC06     .765      .802       .802       .887       .923       .986   190282266
DEC02    1.002     1.005                                               190292266
DEC06     300.                                       .285       .385   190302266
DEC06     .554      .669       .748       .839       .885       .981   190312266
DEC02    1.004     1.008                                               190322266
TAP  HA5-11   DENSITY OF LIQUID HYBALINE A5                            191012266
COD      0                                                             191022266
DEC06     -59.     48.95        30.      46.70       200.      43.70   191032266
DEC01       0.                                                         191042266
TAP  HA5-12   SPECIFIC HEAT OF LIQUID HYBALINE A5                      192012266
COD      1                                                             192022266
DEC06     -59.      .506       110.        .67       200.      -.756   192032266
DEC01       0.                                                         192042266
TAP  HA5-13   THERMAL CONDUCTIVITY OF LIQUID HYBALINE A5               193012266
COD      1                                                             193022266
DEC06     -59.     -.097        10.       .097        96.         .1   193032266
DEC05     160.      .108       260.       .131         0.              193042266
TAP  HA5-14   VAPOR PRESSURE OF LIQUID HYBALINE A5                     194012266
COD      1                                                             194022266
DEC06     -59.      -.01        10.        .02        40.       .033   194032266
DEC06      70.      .056       100.       .094       130.       .158   194042266
DEC05     160.       .26       200.        .52         0.              194052266
TAP  HA5-15   VISCOSITY OF LIQUID HYBALINE A5                          195012266
COD      0                                                             195022266
DEC06     -59.   680.E-4       -40.    430.E-4       -20.    265.E-4   195032266
DEC06       0.   170.E-4        20.    112.E-4        45.     70.E-4   195042266
DEC06      70.    47.E-4       100.    31.5E-4       130.     23.E-4   195052266
DEC05     160.   18.7E-4       200.    15.6E-4         0.              195062266
TAP  HA5-22   SPECIFIC HEAT OF GASEOUS HYBALINE A5                     198012266
COD      4                                                             198022266
DEC03  002002.      -60.       300.                                    198032266
DEC03     .005   -1.E-20    -1.E-20                                    198042266
DEC03       1.   -1.E-20    -1.E-20                                    198052266
TAP  HA5-23   THERMAL CONDUCTIVITY OF GASEOUS HYBALINE A5              199012266
COD      4                                                             199022266
DEC03  002002.      -60.       300.                                    199032266
DEC03     .005   -1.E-20    -1.E-20                                    199042266
DEC03       1.   -1.E-20    -1.E-20                                    199052266
TAP  HA5-28   COMPRESSIBILITY FACTOR OF GASEOUS HYBALINE A5            200012266
COD      4                                                             200022266
DEC03  002002.      -60.       300.                                    200032266
```

TABLE 10-2 (Continued)

```
DEC03      .005       -1.        -1.                                  200042266
DEC03       1.        -1.        -1.                                  200052266
TAP  NIT-11   DENSITY OF LIQUID NITROGEN                              201012266
COD      0                                                            201022266
DEC06     -346.      54.31     -282.       43.70     -250.     35.59  201032266
DEC06     -235.      28.09     -233.       23.72     -232.6    19.67  201042266
DEC01    -1000.                                                       201052266
TAP  NIT-12   SPECIFIC HEAT OF LIQUID NITROGEN                        202012266
COD      1                                                            202022266
DEC06     -346.       .495     -310.         .49     -284.       .53  202032266
DEC06     -260.       .65      -247.         .80     -244.       .90  202042266
DEC05    -242.7       .98      -232.6     -1.E20    -1000.            202052266
TAP  NIT-13   THERMAL CONDUCTIVITY OF LIQUID NITROGEN                 203012266
COD      0                                                            203022266
DEC06     -346.      .0915     -262.        .055     -232.6     .042  203032266
DEC01    -1000.                                                       203042266
TAP  NIT-14   VAPOR PRESSURE OF LIQUID NITROGEN                       204012266
COD      0                                                            204022266
DEC06     -346.       1.81     -340.8         3.     -335.        5.  204032266
DEC06    -330.8        7.      -326.         10.     -320.4     14.7  204042266
DEC06    -315.2       20.      -308.5        30.     -298.6      50.  204052266
DEC06    -291.2       70.      -282.7       100.     -272.      150.  204062266
DEC06    -263.6      200.      -250.5       300.     -232.6     492.  204072266
DEC01    -1000.                                                       204082266
TAP  NIT-15   VISCOSITY OF LIQUID NITROGEN                            205012266
COD      0                                                            205022266
DEC06     -346.    2.04E-4     -325.     1.16E-4     -300.    .73E-4  205032266
DEC05     -260.     .50E-4     -232.6     .46E-4    -1000.            205042266
TAP  NIT-16   HEAT OF VAPORIZATION OF LIQUID NITROGEN                 206012266
COD      0                                                            206022266
DEC06     -346.        93.     -290.         76.     -252.       50.  206032266
DEC06     -237.        30.     -233.         28.     -232.6       0.  206042265
DEC01    -1000.                                                       206052266
TAP  NIT-17   SURFACE TENSION OF LIQUID NITROGEN                      207012266
COD      0                                                            207022266
DEC06     -346.     8.3E-4     -295.      4.E-4      -260.    1.5E-4  207032266
DEC05     -243.      .5E-4     -232.6        0.     -1000.            207042266
TAP  NIT-22   SPECIFIC HEAT OF GASEOUS NITROGEN                       208012266
COD      71                                                           208022266
DEC06   009012.      -320.     -280.       -230.     -210.     -190.  208032266
DEC06     -160.      -130.     -100         -60.        0.       80.  208042266
DEC01      500.                                                       208052266
DEC06        1.      -.245     -.254       -.251     -.250     -.249  208062266
DEC06     -.249      -.248     -.248       -.248     -.248     -.247  208072266
DEC01     -.247                                                       208082266
DEC06      14.7       .246      .255        .252      .251      .250  208092266
DEC06      .250       .249      .249        .249      .249      .248  208102266
DEC01     -.248                                                       208112266
DEC06      150.                             .296      .284      .276  208122266
DEC06      .293       .263      .260        .257      .254      .252  208132266
DEC01     -.252                                                       208142266
DEC06      400.                              .59      .415      .351  208152266
DEC06      .314       .294      .282        .273      .264      .259  208162266
DEC01     -.259                                                       208172266
DEC06      500.                             2.28       .52      .398  208182266
DEC06      .336       .308      .292        .280      .269      .262  208192266
DEC01     -.262                                                       208202266
DEC06      600.                             1.62       .72      .462  208212266
DEC06      .363       .324      .304        .286      .273      .264  208222266
DEC01     -.264                                                       208232266
DEC06     1000.                              .72       .96       .80  208242266
```

TABLE 10-2 (Continued)

```
DEC06      .494      .393      .347      .315       .29      .276 208232266
DEC01     -.276                                                   208262266
DEC06     1400.                           .61       .66        .7 208272266
DEC06      .576      .455      .388      .342      .306      .284 208282266
DEC01     -.284                                                   208292266
DEC06     3000.                           .52       .50       .47 208302266
DEC06      .468      .456      .433      .393      .349      .314 208312266
DEC01     -.314                                                   208322266
TAP   NIT-23   THERMAL CONDUCTIVITY OF GASEOUS NITROGEN           209012266
COD       71                                                      209022266
DEC06   009010.     -280.     -270.     -243.     -226.     -210. 209032266
DEC05     -190.     -170.     -140.     -100.      500.           209042266
DEC06        1.   -.00546    -.0057    -.0062    -.0070    -.0075 209052266
DEC05    -.0080    -.0087    -.0094    -.0105     -.015           209062266
DEC06      14.7    .00546     .0057     .0062     .0070     .0075 209072266
DEC05     .0080     .0087     .0094     .0105     -.015           209082266
DEC06      123.               .0085      .008      .008     .0085 209092266
DEC05      .009     .0095     .0105     .0115     -.015           209102266
DEC06      247.                         .0128      .009      .009 209112266
DEC05     .0095       .01      .011      .012     -.015           209122266
DEC06      492.                                   .0145     .0115 209132266
DEC05     .0115     .0115      .012     .0125     -.015           209142266
DEC06      739.                                    .026     .0195 209152266
DEC05      .015      .013      .013     .0135     -.015           209162266
DEC06      985.                                    .035     .0265 209172266
DEC05       .02      .017      .015      .015     -.015           209182266
DEC06     1477.                                    .040      .034 209192266
DEC05     .0275      .023     .0195     .0175     -.015           209202266
DEC06     1969.                                   .0435      .038 209212266
DEC05     .0325     .0285     .0235     .0205     -.015           209222266
TAP   NIT-28   COMPRESSIBILITY FACTOR OF GASEOUS NITROGEN         210012266
COD       71                                                      210022266
DEC06   012013.     -300.     -280.     -260.     -240.     -230. 210032266
DEC06     -220.     -210.     -190.     -160.     -110.      -60. 210042266
DEC02       80.      500.                                         210052266
DEC06        1.      -.98      -.99       -1.       -1.       -1. 210062266
DEC06       -1.       -1.       -1.       -1.       -1.       -1. 210072266
DEC02       -1.       -1.                                         210082266
DEC06      14.7       .97       .98       .99       .99       .99 210092266
DEC06       .99       .99        1.        1.        1.        1. 210102266
DEC02        1.       -1.                                         210112266
DEC06       50.                 .93       .95       .96       .97 210122266
DEC06       .97       .98       .98       .99       .99        1. 210132266
DEC02        1.       -1.                                         210142266
DEC06      100.                 .85       .89       .92       .93 210152266
DEC06       .94       .95       .96       .97       .98       .99 210162266
DEC02        1.       -1.                                         210172266
DEC06      200.                                     .83       .86 210182266
DEC06       .88       .89       .92       .94       .97       .98 210192266
DEC02        1.       -1.                                         210202266
DEC06      400.                                     .54       .65 210212266
DEC06       .72       .76       .83       .89       .94       .96 210222266
DEC02        1.       -1.                                         210232266
DEC06      600.                                              .244 210242266
DEC06       .48        .6       .73       .83       .91       .95 210252266
DEC02        1.       -1.                                         210262266
DEC06      800.                                              .284 210272266
DEC06      .327       .43       .63       .77       .88       .94 210282266
DEC02        1.       -1.                                         210292266
DEC06     1000.                                              .334 210302266
DEC06      .358        .4       .55       .72       .86       .93 210312266
```

TABLE 10-2 (Continued)

```
DEC02        1.       -1.                                                  210322266
DEC06     1400.                                                      .44   210332266
DEC06       .45       .47        .53        .67        .83          .91   210342266
DEC02        1.       -1.                                                  210352266
DEC06     2000.                                                      .59   210362266
DEC06       .59       .60        .62        .69        .82          .91   210372266
DEC02      1.02     -1.02                                                  210382266
DEC06     3000.                                                      .83   210392266
DEC06       .82       .82        .76        .84         .9          .96   210402266
DEC02      1.06     -1.06                                                  210412266
TAP  HEL-22   SPECIFIC HEAT OF GASEOUS HELIUM                              218012266
COD       71                                                               218022266
DEC06   008011.    -448.9     -447.1     -443.5      -440.       -425.   218032266
DEC06     -400.     -300.      -200.      -100.         0.        600.   218042266
DEC06        1.     -1.31      -1.29      -1.27      -1.25       -1.24   218052266
DEC06     -1.25     -1.24      -1.24      -1.24      -1.24       -1.24   218062266
DEC06      14.7      1.42       1.37       1.31      1.285        1.26   218072266
DEC06      1.25      1.24       1.24       1.24       1.24        1.24   218082266
DEC06      43.1      2.06       1.87       1.49      1.386        1.28   218092266
DEC06      1.26      1.24       1.24       1.24       1.24        1.24   218102266
DEC06      147.      1.17       1.55       1.96      1.706        1.37   218112266
DEC06      1.28      1.25       1.24       1.24       1.24        1.24   218122266
DEC06      397.       .76        .89       1.24      1.443        1.45   218132266
DEC06      1.33      1.26       1.25       1.24       1.24        1.24   218142266
DEC06      882.       .60        .69        .96      1.123        1.35   218152266
DEC06      1.35      1.27       1.25       1.25       1.24        1.24   218162266
DEC06     1470.       .51        .60        .86      1.003        1.22   218172266
DEC06      1.33      1.28       1.26       1.25       1.25        1.24   218182266
DEC06     6000.                                                            218192266
DEC06                           1.31       1.28       1.26        1.24   218202266
TAP  HEL-23   THERMAL CONDUCTIVITY OF GASEOUS HELIUM                       219012266
COD       5                                                                219022266
DEC06   002008.     -456.      -450.      -440.      -410.       -300.   219032266
DEC03     -100.        0.       400.                                       219042266
DEC06        1.    -.0022     -.0063     -.0106     -.0186        -.04   219052266
DEC03    -.0673    -.0792     -.1191                                       219062266
DEC06     6000.    -.0022     -.0063     -.0106     -.0186        -.04   219072266
DEC03    -.0673    -.0792     -.1191                                       219082266
TAP  HEL-28   COMPRESSIBILITY FACTOR OF GASEOUS HELIUM                     220012266
COD       71                                                               220022266
DEC05   008010.    -448.9     -447.1     -443.5      -440.       -425.   220032266
DEC05     -400.     -300.      -200.         0.       600.                 220042266
DEC06       1.0       -1.        -1.        -1.        -1.         -1.   220052266
DEC05       -1.       -1.        -1.        -1.        -1.                 220062266
DEC06      14.7      .879       .917       .956       .974        .996   220072266
DEC05     1.001     1.001      1.001      1.001      1.001                 220082266
DEC06      43.1      .588       .747       .874       .926        .988   220092266
DEC05     1.004     1.005      1.003      1.002      1.002                 220102266
DEC06      147.      .619       .608       .720       .835        .980   220112266
DEC05     1.016     1.016      1.011      1.007      1.002                 220122266
DEC06      397.     1.368      1.229      1.074      1.017       1.037   220132266
DEC05     1.062     1.043      1.030      1.019      1.008                 220142266
DEC06      882.     2.629      2 251      1.896      1.655       1.295   220152266
DEC05     1.137     1.098      1.068      1.041      1.017                 220162266
DEC06     1470.     3.992      3.477      2.802      2.386       1.676   220172266
DEC05     1.364     1.166      1.113      1.069      1.028                 220182266
DEC06     6000.                                                   3.70   220192266
DEC05      2.50     1.598      1.379      1.221      1.106                 220202266
TAP  G60-11   DENSITY OF LIQUID .6 ETHYLENE GLYCOL                         221012266
COD       0                                                                221022266
DEC06      -60.     68.61       120.      65.99       274.       61.99   221032266
```

TABLE 10-2 (Continued)

```
DEC03        300.       60.87        0.                                      221042266
TAP   G60-12   SPECIFIC HEAT OF LIQUID .6 ETHYLENE GLYCOL                    222012266
COD        0                                                                 222022266
DEC05       -60.        .644       300.        .902          0.              222032266
TAP   G60-13   THERMAL CONDUCTIVITY OF LIQUID .6 ETHYLENE GLYCOL             223012266
COD        0                                                                 223022266
DEC06       -60.        .232       120.        .221        250.        .205  223032266
DEC03       300.        .195         0.                                      223042266
TAP   G60-14   VAPOR PRESSURE OF LIQUID .6 ETHYLENE GLYCOL                   224012266
COD        3                                                                 224022266
DEC06       -60.        -.01        50.         -.5        150.         -2.  224032266
DEC06       232.         15.       265.        -30.        300.        -60.  224042266
DEC01         0.                                                             224052266
TAP   G60-15   VISCOSITY OF LIQUID .6 ETHYLENE GLYCOL                        225012266
COD        0                                                                 225022266
DEC06       -50.   1900.E-4        -40.    1050.E-4        -30.     620.E-4  225032266
DEC06       -12.    300.E-4          0.     180.E-4         10.     126.E-4  225042266
DEC06        30.     70.E-4         62.      36.E-4        122.      14.E-4  225052266
DEC05       172.      6.E-4        250.       4.E-4          0.              225062266
TAP   G60-22   SPECIFIC HEAT OF GASEOUS .6 ETHYLENE GLYCOL                   228012266
COD        4                                                                 228022266
DEC03    002002.        -60.       300.                                      228032266
DEC03        .01    -1.E-20     -1.E-20                                      228042266
DEC03        60.    -1.E-20     -1.E-20                                      228052266
TAP   G60-23   THERMAL CONDUCTIVITY OF GASEOUS .6 ETHYLENE GLYCOL            229012266
COD        4                                                                 229022266
DEC03    002002.        -60.       300.                                      229032266
DEC03        .01    -1.E-20     -1.E-20                                      229042266
DEC03        60.    -1.E-20     -1.E-20                                      229052266
TAP   G60-28   COMPRESSIBILITY FACTOR , GASEOUS .6 ETHYLENE GLYCOL           230012266
COD        4                                                                 230022266
DEC03    002002.        -60.       300.                                      230032266
DEC03        .01         -1.        -1.                                      230042266
DEC03        60.         -1.        -1.                                      230052266
TAP   F11-11   DENSITY OF LIQUID FREON 11                                    231012266
COD        0                                                                 231022266
DEC06       -90.     104.88        -40.      101.45        160.       85.22  231032266
DEC03      388.4      34.59          0.                                      231042266
TAP   F11-12   SPECIFIC HEAT OF LIQUID FREON 11                              232012266
COD        1                                                                 232022266
DEC06       -90.        .20         20.         .21        160.         .22  232032266
DEC03      388.4       -.23          0.                                      232042266
TAP   F11-13   THERMAL CONDUCTIVITY OF LIQUID FREON 11                       233012266
COD        1                                                                 233022266
DEC06       -90.       -.07         -4.       .0605         68.        .055  233032266
DEC03      388.4      -.018          0.                                      233042266
TAP   F11-14   VAPOR PRESSURE OF LIQUID FREON 11                             234012266
COD        0                                                                 234022266
DEC06       -40.        .74        -30.        1.03        -20.        1.42  234032266
DEC06         0.       2.56         20.         4.3         40.         7.0  234042266
DEC06        60.       10.9         80.        16.3        100.        23.6  234052266
DEC06       120.        33.        140.         46.        160.         61.  234062266
DEC06       200.       104.        240.        163.        280.        250.  234072266
DEC06       320.       360.        360.        500.       388.4        635.  234082266
DEC01         0.                                                             234092266
TAP   F11-15   VISCOSITY OF LIQUID FREON 11                                  235012266
COD        0                                                                 235022266
DEC06       -40.     6.5E-4          0.      4.5E-4         60.     3.05E-4  235032266
DEC05       140.    2.15E-4        240.     1.55E-4          0.              235042266
TAP   F11-16   HEAT OF VAPORIZATION OF LIQUID FREON 11                       236012266
COD        0                                                                 236022266
```

TABLE 10-2 (Continued)

```
DEC06       -90      91.5      -40.      87.5       80.       78.  236032266
DEC05      160.       70.     388.4        0.        0.            236042266
TAP   F11-17   SURFACE TENSION OF LIQUID FREON 11                  237012266
COD   1                                                            237022266
DEC06      -90.   -15.E-4        0.  -14.2E-4       77.    13.E-4  237032266
DEC05      200.   -8.8E-4     388.4        0.        0.            237042266
TAP   F11-22   SPECIFIC HEAT OF GASEOUS FREON 11                   238012266
COD   15                                                           238022266
DEC04   002003.       20.      100.      150.                      238032266
DEC04        1.      -.13      .136      .141                      238042266
DEC04       60.      -.13      .136      .141                      238052266
TAP   F11-23   THERMAL CONDUCTIVITY OF GASEOUS FREON 11            239012266
COD   15                                                           239022266
DEC04   002003.       20.       86.      194.                      239032266
DEC04        1.    -.0039      .005     .0062                      239042266
DEC04       60.    -.0039      .005     .0062                      239052266
TAP   F11-28   COMPRESSIBILITY FACTOR OF GASEOUS FREON 11          240012266
COD   71                                                           240022266
DEC06   011008.       20.       50.       70.      100.      130.  240032266
DEC03      160.      190.      290.                                240042266
DEC06        1.      .997      .997      .998      .998      .998  240052266
DEC03      .998      .999      .999                                240062266
DEC06        2.      .994      .994      .995      .996      .996  240072266
DEC03      .997      .997      .999                                240082266
DEC06        4.      .988 [illegible]      .991      .992      .993  240092266
DEC03      .994      .995 [illegible]                                240102266
DEC06        6.                .985      .986      .988      .990  240112266
DEC03      .991      .992      .996                                240122266
DEC06        8.                .961      .981      .984      .986  240132266
DEC03      .988      .990      .994                                240142266
DEC06       10.                          .977      .980      .983  240152266
DEC03      .985      .987      .992                                240162266
DEC06       20.                                    .960      .965  240172266
DEC03      .970      .974      .984                                240182266
DEC06       30.                                              .947  240192266
DEC03      .955      .961      .976                                240202266
DEC06       40.                                                    240212266
DEC03      .939      .947      .968                                240222266
DEC06       50.                                                    240232266
DEC03      .923      .934      .960                                240242266
DEC06       60.                                                    240252266
DEC03     -.908     -.920     -.952                                240262266
TAP   BERL-1   DENSITY OF BERYLLIUM                                291012266
COD   0                                                            291022266
DEC05     -460.      116.     2341.      116.        0.            291032266
TAP   BERL-2   SPECIFIC HEAT OF BERYLLIUM                          292012266
COD   0                                                            292022266
DEC06     -450.    .32E-4     -445.    .64E-4     -440.   1.07E-4  292032266
DEC06     -435.    1.6E-4     -425.    3.2E-4     -415.      .E-4  292042266
DEC06     -405.      .001     -395.     .0016     -380.      0031  292052266
DEC06     -360.     .0065     -340.     .0115     -320.      0185  292062266
DEC06     -300.      .029     -280.      .044     -260.      .063  292072266
DEC06     -220.      .112     -160.      .186     -100.       .26  292082266
DEC06        0.      .375      200.       .50      750.       .66  292092266
DEC05     2190.       .85     2341.       .87        0.            292102266
TAP   BERL-3   THERMAL CONDUCTIVITY OF BERYLLIUM                   293012266
COD   1                                                            293022266
DEC06     -150.     -148.      -45.      128.      200.       95.  293032266
DEC06      600.       70.     1200.       52.     1800.       42.  293042266
DEC03     2341.       37.        0.                                293052266
TAP   AL22-1   DENSITY OF ALUMINUM 2219-T87                        301012266
```

TABLE 10-2 (Continued)

```
COD       0                                                                  301022266
DEC05      -460.        176.       1010.        176.          0.             301032266
TAP  AL22-2   SPECIFIC HEAT OF ALUMINUM 2219-T87                             302012266
COD       0                                                                  302022266
DEC05      -424.        .002       -400.        .012       -360.        .039 302032266
DEC06      -320.        .074       -280.        .111       -100.        .183 302042266
DEC06       100         .198        900.        .257       1010.        .268 302052266
DEC01         0.                                                             302062266
TAP  AL22-3   THERMAL CONDUCTIVITY OF ALUMINUM 2219-T87                      303012266
COD       0                                                                  303022266
DEC06      -424.        11.2       -352.        28.6       -316.        36.3 303032266
DEC06      -150.         58.        100.        76.5        500.        87.5 303042266
DEC03      1010.        95.5          0.                                     303052266
TAP  AL70-1   DENSITY OF ALUMINUM 7075-T6                                    311012266
COD       0                                                                  311022266
DEC05      -460.        175.        890.        175.          0.             311032266
TAP  AL70-2   SPECIFIC HEAT OF ALUMINUM 7075-T6                              312012266
COD       0                                                                  312022266
DEC06      -424.        .002       -400.        .012       -360.        .039 312032266
DEC06      -320.        .074       -280.        .111       -100.        .183 312042266
DEC05       100.        .198        890.        .256          0.             312052266
TAP  AL70-3   THERMAL CONDUCTIVITY OF ALUMINUM 7075-T6,AS RECEIVED           313012266
COD       0                                                                  313022266
DEC06      -388.        23.7       -310.        38.5       -100.         61. 313032266
DEC06       100.         77.        700.         92.        890.        94.5 313042266
DEC01         0.                                                             313052266
TAP  AL70-4   THERMAL CONDUCTIVITY OF ALUMINUM 7075-T6,ANNEALED              314012266
COD       0                                                                  314022266
DEC06      -410.         54.       -200.         76.         40.         96. 314032266
DEC06       340.        105.        600.        104.        890.         94. 314042266
DEC01         0.                                                             314052266
TAP  MGA3-1   DENSITY OF MAGNESIUM AZ31B-H24                                 321012266
COD       0                                                                  321022266
DEC05      -460.       110.5        900.       110.5          0.             321032266
TAP  MGA3-2   SPECIFIC HEAT OF MAGNESIUM AZ31B-H24                           322012266
COD       0                                                                  322022266
DEC06      -250.         .18        -50.         .22        510.         .29 322032266
DEC03       900.         .33          0.                                     322042266
TAP  MGA3-3   THERMAL CONDUCTIVITY OF MAGNESIUM AZ31B-H24                    323012266
COD       0                                                                  323022266
DEC06      -310.         22.       -160.         32.         20.         42. 323032266
DEC06       200.         50.        500.         59.        600.         61. 323042266
DEC01         0.                                                             323052266
TAP  T6AL-1   DENSITY OF TITANIUM 6AL4V                                      331012266
COD       0                                                                  331022266
DEC05      -460.        278.       2800.        278.          0.             331032266
TAP  T6AL-2   SPECIFIC HEAT OF TITANIUM 6AL4V                                332012266
COD       0                                                                  332022266
DEC06      -440.      .00045       -435.      .00075       -430.       .0012 332032266
DEC06      -424.        .002       -418.        .003       -410.        .005 332042266
DEC06      -400.        .008       -380.        .018       -340.        .041 332052266
DEC06      -300.        .062       -200.        .096       -100.        .114 332062266
DEC06       100.        .130        800.        .153       1200.        .185 332072266
DEC03      1600.        .234          0.                                     332082266
TAP  T6AL-3   THERMAL CONDUCTIVITY OF TITANIUM 6AL4V                         333012266
COD       0                                                                  333022266
DEC06      -414.         .92       -360.         1.6       -312.        2.08 333032266
DEC06      -180.          3.         50.          4.        500.         5.5 333042266
DEC03      1600.        10.5          0.                                     333052266
TAP  T110-1   DENSITY OF TITANIUM A110AT                                     341012266
COD       0                                                                  341022266
```

TABLE 10-2 (Continued)

```
DEC05     -460.       278.      2800.       278.          0.            341032266
TAP   T110-2   SPECIFIC HEAT OF TITANIUM A110AT                         342012266
COD        0                                                            342022266
DEC06     -440.    .00045      -435.    .00075       -430.     .0012    342032266
DEC06     -424.      .002      -418.      .003       -410.      .005    342042266
DEC06     -400.      .008      -380.      .018       -340.      .041    342052266
DEC06     -300.      .062      -200.      .096       -100.      .114    342062266
DEC06        0.       .12       900.       .15       1600.       .19    342072266
DEC01        0.                                                         342082266
TAP   T110-3   THERMAL CONDUCTIVITY OF TITANIUM A110AT                  343012266
COD        0                                                            343022266
DEC06     -420.       1.3      -360.       2.4       -200.       3.5    343032266
DEC06      600.       6.2      1100.       8.4       1500.      10.6    343042266
DEC01        0.                                                         343052266
TAP   C103-1   DENSITY OF COLUMBIUM C-103                               351012266
COD        0                                                            351022266
DEC05     -460.       553.      4380.       553.          0.            351032266
TAP   C103-2   SPECIFIC HEAT OF COLUMBIUM C-103                         352012266
COD        1                                                            352022266
DEC06     -400.     -.013         0.     -.025        800.     -.047    352032266
DEC06     1610.      .065      2017.      .073       2397.      .078    352042266
DEC05     2800.     -.083      3200.     -.091          0.              352052266
TAP   C103-3   THERMAL CONDUCTIVITY OF COLUMBIUM C-103                  353012266
COD        1                                                            353022266
DEC06     -400.      -19.         0.     -19.3        800.     -20.3    353032266
DEC06     1600.       22.      2035.      23.5       2380.      25.8    353042266
DEC05     2800.     -29.3      3200.     -33.4          0.              353052266
TAP   S321-1   DENSITY OF STAINLESS STEEL 321                           361012266
COD        0                                                            361022266
DEC05     -460.       493.      2500.       493.          0.            361032266
TAP   S321-2   SPECIFIC HEAT OF STAINLESS STEEL 321                     362012266
COD        0                                                            362022266
DEC06     -250.       .08        80.       .11        580.       .13    362032266
DEC05     1440.       .15      1880.       .18          0.              362042266
TAP   S321-3   THERMAL CONDUCTIVITY OF STAINLESS STEEL 321              363012266
COD        0                                                            363022266
DEC06    -459.7        0.      -400.      2.25       -350.       3.6    363032266
DEC06     -200.       6.3       120.        9.        800.      12.3    363042266
DEC03     1800.      15.8         0.                                    363052266
TAP   INCX-1   DENSITY OF INCONEL X                                     371012266
COD        0                                                            371022266
DEC05     -460.       515.      2540.       515.          0.            371032266
TAP   INCX-2   SPECIFIC HEAT OF INCONEL X                               372012266
COD        0                                                            372022266
DEC06     -410.      .054         0.      .099        400.      .117    372032266
DEC06     1000.      .129      1400.      .149       1650.      .180    372042266
DEC01        0.                                                         372052266
TAP   INCX-3   THERMAL CONDUCTIVITY OF INCONEL X                        373012266
COD        0                                                            373022266
DEC06     -410.        3.      -400.        4.       -300.       6.2    373032266
DEC06        0.       9.1       900.      14.1       1650.      21.5    373042266
DEC01        0.                                                         373052266
TAP   INCX-4   THERMAL CONDUCTIVITY OF INCONEL X, SOLUTION TREATED      374012266
COD        0                                                            374022266
DEC05     -230.       5.5      1650.      13.7          0.              374032266
TAP   RE41-1   DENSITY OF RENE 41                                       381012266
COD        0                                                            381022266
DEC05     -460.       515.      2250.       515.          0.            381032266
TAP   RE41-2   SPECIFIC HEAT OF RENE 41                                 382012266
COD        1                                                            382022266
DEC06     -200.     -.108        70.      .108       1800.     -.108    382032266
```

TABLE 10-2 (Continued)

```
DEC01       0.                                                        382042266
TAP  RE41-3   THERMAL CONDUCTIVITY OF RENE 41, 2HR SOLN TREATED       383012266
COD       1                                                           383022266
DEC06      -400.       -2.4       200.         6.      1800.     15.8 383032266
DEC01       0.                                                        383042266
TAP  RE41-4   THERMAL CONDUCTIVITY OF RENE 41, 4HR SOLN TREATED       384012266
COD       1                                                           384022266
DEC06      -400.       -2.4       200.       5.2      1800.     12.6 384032266
DEC01       0.                                                        384042266
TAP  L12A-1   DENSITY OF LINDE SI-12 (8 LAYERS/INCH)                  401012266
COD       0                                                           401022266
DEC05      -435.      1.296       240.     1.296         0.           401032266
TAP  L12A-2   SPECIFIC HEAT OF LINDE SI-12                            402012266
COD       0                                                           402022266
DEC06      -435.       .002      -360.      .048      -260.      .099 402032266
DEC06      -160.       .138        40.      .192       140.      .218 402042266
DEC06       190.       .234       215.      .246       240.      .260 402052266
DEC01       0.                                                        402062266
TAP  L12A-3   THERMAL CONDUCTIVITY OF LINDE SI-12 (8 LAYERS/INCH)     403012266
DEC06      -435.     1.4E-6      -410.    2.1E-6      -385.    3.1E-6 403022266
DEC06      -360.     4.5E-6      -310.    10.E-6      -260.   20.4E-6 403032266
DEC06      -210.    38.5E-6      -160.    67.E-6       -60.   155.E-6 403042266
DEC06        40.   290.E-6       140.   490.E-6       240.   780.E-6 403052266
DEC01       0.                                                        403062266
TAP  L12B-1   DENSITY OF LINDE SI-12 (10 LAYERS/INCH)                 411012266
COD       0                                                           411022266
DEC05      -435.       1.62       240.      1.62         0.           411032266
TAP  L12B-2   SPECIFIC HEAT OF LINDE SI-12                            412012266
COD       0                                                           412022266
DEC06      -435.       .002      -360.      .048      -260.      .099 412032266
DEC06      -160.       .138        40.      .192       140.      .218 412042266
DEC06       190.       .234       215.      .246       240.      .260 412052266
DEC01       0.                                                        412062266
TAP  L12B-3   THERMAL CONDUCTIVITY OF LINDE SI-12 (10 LAYERS/INCH)    413012266
DEC06      -435.     2.4E-6      -410.    3.3E-6      -385.    4.5E-6 413022266
DEC06      -360.     6.2E-6      -310.   11.6E-6      -260.    21.E-6 413032266
DEC06      -210.     37.E-6      -160.    62.E-6       -60.   137.E-6 413042266
DEC06        40.   250.E-6       140.   410.E-6       240.   650.E-6 413052266
DEC01       0.                                                        413062266
TAP  L12C-1   DENSITY OF LINDE SI-12 (12 LAYERS/INCH)                 421012266
COD       0                                                           421022266
DEC05      -435.      1.945       240.     1.945         0.           421032266
TAP  L12C-2   SPECIFIC HEAT OF LINDE SI-12                            422012266
COD       0                                                           422022266
DEC06      -435.       .002      -360.      .048      -260.      .099 422032266
DEC06      -160.       .138        40.      .192       140.      .218 422042266
DEC06       190.       .234       215.      .246       240.      .260 422052266
DEC01       0.                                                        422062266
TAP  L12C-3   THERMAL CONDUCTIVITY OF LINDE SI-12 (12 LAYERS/INCH)    423012266
DEC06      -435.     3.9E-6      -410.    5.2E-6      -385.    6.9E-6 423022266
DEC06      -360.     9.1E-6      -310.   15.3E-6      -260.    25.E-6 423032266
DEC06      -210.     41.E-6      -160.    63.E-6       -60.   133.E-6 423042266
DEC06        40.   230.E-6       140.   370.E-6       240.   560.E-6 423052266
DEC01       0.                                                        423062266
TAP  L12D-1   DENSITY OF LINDE SI-12 (14 LAYERS/INCH)                 431012266
COD       0                                                           431022266
DEC05      -435.       2.27       240.      2.27         0.           431032266
TAP  L12D-2   SPECIFIC HEAT OF LINDE SI-12                            432012266
COD       0                                                           432022266
DEC06      -435.       .002      -360.      .048      -260.      .099 432032266
DEC06      -160.       .138        40.      .192       140.      .218 432042266
```

TABLE 10-2 (Continued)

```
DEC06      190.      .234      215.      .246      240.      .260 432052266
DEC01        0.                                                   432062266
TAP  L12D-3   THERMAL CONDUCTIVITY OF LINDE SI-12 (14 LAYERS/INCH) 433012266
DEC06     -435.   14.6E-6     -410.    17.E-6     -385.    20.E-6 433022266
DEC06     -360.    23.E-6     -260.    41.E-6     -160.    71.E-6 433032266
DEC06      -60.   112.E-6       40.   170.E-6      140.   275.E-6 433042266
DEC05      190.   370.E-6      240.   510.E-5        0.           433052266
TAP  L62A-1   DENSITY OF LINDE SI-62 (40 LAYERS/INCH)             441012266
COD       0                                                       441022266
DEC05     -435.      2.88      240.      2.88        0.           441032266
TAP  L62A-2   SPECIFIC HEAT OF LINDE SI-62                        442012266
COD       0                                                       442022266
DEC06     -435.      .009     -360.      .055     -260.      .105 442032266
DEC06     -160.      .144       40.      .195      140.      .220 442042266
DEC06      190.      .236      215.      .246      240.      .259 442052266
DEC01        0.                                                   442062266
TAP  L62A-3   THERMAL CONDUCTIVITY OF LINDE SI-62 (40 LAYERS/INCH) 443012266
DEC06     -435.    .22E-6     -410.    .36E-6     -385.    .56E-6 443022266
DEC06     -360.    .86E-6     -335.   1.28E-6     -310.   1.88E-6 443032266
DEC06     -285.    2.7E-6     -260.    3.8E-6     -210.    7.3E-6 443042266
DEC06     -160.    13.E-6      -60.    29.E-6       40.    55.E-6 443052266
DEC05      140.    93.E-6      240.   150.E-6        0.           443062266
TAP  L62B-1   DENSITY OF LINDE SI-62 (60 LAYERS/INCH)             451012266
COD       0                                                       451022266
DEC05     -435.      4.32      240.      4.32        0.           451032266
TAP  L62B-2   SPECIFIC HEAT OF LINDE SI-62                        452012266
COD       0                                                       452022266
DEC06     -435.      .009     -360.      .055     -260.      .105 452032266
DEC06     -160.      .144       40.      .195      140.      .220 452042266
DEC06      190.      .236      215.      .246      240.      .259 452052266
DEC01        0.                                                   452062266
TAP  L62B-3   THERMAL CONDUCTIVITY OF LINDE SI-62 (60 LAYERS/INCH) 453012266
DEC06     -435.    .74E-6     -410.   1.02E-6     -360.    1.8E-6 453022266
DEC06     -310.   3.05E-6     -260.   4.95E-6     -210.    7.9E-6 453032266
DEC06     -160.    12.E-6      -60.   24.2E-6       40.    43.E-6 453042266
DEC05      140.    70.E-6      240.   110.E-6        0.           453052266
TAP  L62C-1   DENSITY OF LINDE SI-62 (80 LAYERS/INCH)             461012266
COD       0                                                       461022266
DEC05     -435.      5.76      240.      5.76        0.           461032266
TAP  L62C-2   SPECIFIC HEAT OF LINDE SI-62                        462012266
COD       0                                                       462022266
DEC06     -435.      .009     -360.      .055     -260.      .105 462032266
DEC06     -160.      .144       40.      .195      140.      .220 462042266
DEC06      190.      .236      215.      .246      240.      .259 462052266
DEC01        0.                                                   462062266
TAP  L62C-3   THERMAL CONDUCTIVITY OF LINDE SI-62 (80 LAYERS/INCH) 463012266
DEC06     -435.   1.65E-6     -360.    3.4E-6     -310.    5.3E-6 463022266
DEC06     -260.    8.1E-6     -160.    17.E-6      -60.   28.7E-6 463032266
DEC06       40.    45.E-6      140.   67.5E-6      240.    98.E-6 463042266
DEC01        0.                                                   463052266
TAP  L62D-1   DENSITY OF LINDE SI-62 (100 LAYERS/INCH)            471012266
COD       0                                                       471022266
DEC05     -435.      7.20      240.      7.20        0.           471032266
TAP  L62D-2   SPECIFIC HEAT OF LINDE SI-62                        472012266
COD       0                                                       472022266
DEC06     -435.      .009     -360.      .055     -260.      .105 472032266
DEC06     -160.      .144       40.      .195      140.      .220 472042266
DEC06      190.      .236      215.      .246      240.      .259 472052266
DEC01        0.                                                   472062266
TAP  L62D-3   THERMAL CONDUCTIVITY OF LINDE SI-62 (100 LAYERS/INCH)473012266
DEC06     -435.    4.1E-6     -360.   7.57E-6     -260.   15.5E-6 473022266
```

TABLE 10-2 (Continued)

```
DEC06     -160.    27.E-6        40.    58.E-6      240.    110.E-6  473032266
DEC01        0.                                                      473042266
TAP  L92A-1   DENSITY OF LINDE SI-92 (80 LAYERS/INCH)                481012266
COD      0                                                           481022266
DEC05     -435.     4.992       240.     4.992        0.             481032266
TAP  L92A-2   SPECIFIC HEAT OF LINDE SI-92                           482012266
COD      0                                                           482022266
DEC06     -435.      .002      -360.      .051     -260.       .117  482032266
DEC06     -210.      .142      -160.      .159       40.       .203  482042266
DEC06      140.      .224       190.      .236      240.       .254  482052266
DEC01        0.                                                      482062266
TAP  L92A-3   THERMAL CONDUCTIVITY OF LINDE SI-92 (80 LAYERS/INCH) 483012266
DEC06     -435.    .14E-6      -410.    .23E-6     -385.     .38E-6  483022266
DEC06     -360.    .59E-6      -335.    .92E-6     -310.    1.38E-6  483032266
DEC06     -260.    2.7E-6      -210.    4.7E-6     -160.     7.7E-6  483042266
DEC06      -60.    17.E-6        40.    33.E-6       90.     45.E-6  483052266
DEC06      140.    63.E-6       190.    90.E-6      240.    130.E-6  483062266
DEC01        0.                                                      483072266
TAP  L92B-1   DENSITY OF LINDE SI-92 (100 LAYERS/INCH)               491012266
COD      0                                                           491022266
DEC05     -435.      6.24       240.      6.24        0.             491032266
TAP  L92B-2   SPECIFIC HEAT OF LINDE SI-92                           492012266
COD      0                                                           492022266
DEC06     -435.      .002      -360.      .051     -260.       .117  492032266
DEC06     -210.      .142      -160.      .159       40.       .203  492042266
DEC06      140.      .224       190.      .236      240.       .254  492052266
DEC01        0.                                                      492062266
TAP  L92B-3   THERMAL CONDUCTIVITY OF LINDE SI-92 (100 LAYERS/INCH)493012266
DEC06     -435.    .31E-6      -410.    .45E-6     -385.     .65E-6  493022266
DEC06     -360.    .94E-6      -310.    1.8E-6     -260.    3.15E-6  493032266
DEC06     -210.     5.E-6      -160.   7.55E-6      -60.     15.E-6  493042266
DEC06       40.    28.E-6       140.    51.E-6      240.     89.E-6  493052266
DEC01        0.                                                      493062266
TAP  L92C-1   DENSITY OF LINDE SI-92 (120 LAYERS/INCH)               501012266
COD      0                                                           501022266
DEC05     -435.     7.488       240.     7.488        0.             501032266
TAP  L92C-2   SPECIFIC HEAT OF LINDE SI-92                           502012266
COD      0                                                           502022266
DEC06     -435.      .002      -360.      .051     -260.       .117  502032266
DEC06     -210.      .142      -160.      .159       40.       .203  502042266
DEC06      140.      .224       190.      .236      240.       .254  502052266
DEC01        0.                                                      502062266
TAP  L92C-3   THERMAL CONDUCTIVITY OF LINDE SI-92 (120 LAYERS/INCH)503012266
DEC06     -435.    .70E-6      -410.    .98E-6     -360.     1.8E-6  503022266
DEC06     -260.    4.5E-6      -160.    9.2E-6      -60.    16.8E-6  503032266
DEC06       40.    29.E-6       140.    50.E-6      240.     82.E-6  503042266
DEC01        0.                                                      503052266
TAP  L92D-1   DENSITY OF LINDE SI-92 (160 LAYERS/INCH)               511012266
COD      0                                                           511022266
DEC05     -435.     9.984       240.     9.984        0.             511032266
TAP  L92D-2   SPECIFIC HEAT OF LINDE SI-92                           512012266
COD      0                                                           512022266
DEC06     -435.      .002      -360.      .051     -260.       .117  512032266
DEC06     -210.      .142      -160.      .159       40.       .203  512042266
DEC06      140.      .224       190.      .236      240.       .254  512052266
DEC01        0.                                                      512062266
TAP  L92D-3   THERMAL CONDUCTIVITY OF LINDE SI-92 (160 LAYERS/INCH)513012266
DEC06     -435.   2.65E-6      -360.    4.8E-6     -260.     9.6E-6  513022266
DEC06      -60.   27.5E-6        90.    44.E-6      240.     52.E-6  513032266
DEC01        0.                                                      513042266
TAP  LFWA-1   DENSITY OF LINDE FT WT (40 LAYERS/INCH)                521012266
```

TABLE 10-2 (Continued)

```
COD      0                                                           521022266
DEC05    -435.     2.496      240.     2.496        0.               521032266
TAP  LFWA-2   SPECIFIC HEAT OF LINDE FLT WT                          522012266
COD      3                                                           522022266
DEC06    -435.     -.009     -360.     -.055     -260.     -.105     522032266
DEC06    -160.     -.144       40.     -.195      140.     -.220     522042266
DEC06     190.     -.236      215.     -.246      240.     -.259     522052266
DEC01       0.                                                       522062266
TAP  LFWA-3   THERMAL CONDUCTIVITY OF LINDE FLT WT (40 LAYERS/INCH)523012266
DEC06    -435.     .18E-6    -410.    .285E-6    -385.     .44E-6    523022266
DEC06    -360.     .65E-6    -310.    1.34E-6    -260.    2.54E-6    523032266
DEC06    -210.     4.4E-6    -160.     7.0E-6     -60.    14.3E-6    523042266
DEC06     -10.     20.E-6      40.    28.5E-6      90.     44.E-6    523052266
DEC06     115.     58.E-6     140.     81.E-6     165.    123.E-6    523062266
DEC06     190.    200.E-6     207.    290.E-6     224.    440.E-6    523072266
DEC03     240.    680.E-6       0.                                   523082266
TAP  LFWB-1   DENSITY OF LINDE FT WT (50 LAYERS(INCH)                531012266
COD      0                                                           531022266
DEC05    -435.      3.12      240.      3.12        0.               531032266
TAP  LFWB-2   SPECIFIC HEAT OF LINDE FLT WT                          532012266
COD      3                                                           532022266
DEC06    -435.     -.009     -360.     -.055     -260.     -.105     532032266
DEC06    -160.     -.144       40.     -.195      140.     -.220     532042266
DEC06     190.     -.236      215.     -.246      240.     -.259     532052266
DEC01       0.                                                       532062266
TAP  LFWB-3   THERMAL CONDUCTIVITY OF LINDE FLT WT (50 LAYERS/INCH)533012266
DEC06    -435.     .39E-6    -410.     .54E-6    -385.     .74E-6    533022266
DEC06    -360.      1.E-6    -310.     1.8E-6    -260.    3.05E-6    533032266
DEC06    -210.     4.9E-6    -160.     7.3E-6     -60.     14.E-6    533042266
DEC06     -10.     19.E-6      40.     26.E-6      90.     40.E-6    533052266
DEC06     115.     53.E-6     140.     74.E-6     157.     96.E-6    533062266
DEC06     173.    128.E-6     190.    175.E-6     207.    250.E-6    533072266
DEC05     224.    375.E-6     240.    590.E-6       0.               533082266
TAP  LFWC-1   DENSITY OF LINDE FT WT (60 LAYERS/INCH)                541012266
COD      0                                                           541022266
DEC05    -435.     3.744      240.     3.744        0.               541032266
TAP  LFWC-2   SPECIFIC HEAT OF LINDE FLT WT                          542012266
COD      3                                                           542022266
DEC06    -435.     -.009     -360.     -.055     -260.     -.105     542032266
DEC06    -160.     -.144       40.     -.195      140.     -.220     542042266
DEC06     190.     -.236      215.     -.246      240.     -.259     542052266
DEC01       0.                                                       542062266
TAP  LFWC-3   THERMAL CONDUCTIVITY OF LINDE FLT WT (60 LAYERS/INCH)543012266
DEC06    -435.     .79E-6    -410.    1.03E-6    -360.     1.7E-6    543022266
DEC06    -310.    2.75E-6    -260.     4.2E-6    -160.     8.4E-6    543032266
DEC06     -60.    14.3E-6     -10.    18.5E-6      40.     25.E-6    543042266
DEC06      90.     38.E-6     115.     50.E-6     140.     70.E-6    543052266
DEC06     157.     90.E-6     173.    120.E-6     190.    163.E-6    543062266
DEC06     207.    235.E-6     224.    350.E-6     240.    550.E-6    543072266
DEC01       0.                                                       543082266
TAP  LFWD-1   DENSITY OF LINDE FT WT (80 LAYERS/INCH)                551012266
COD      0                                                           551022266
DEC05    -435.     4.992      240.     4.992        0.               551032266
TAP  LFWD-2   SPECIFIC HEAT OF LINDE FLT WT                          552012266
COD      3                                                           552022266
DEC06    -435.     -.009     -360.     -.055     -260.     -.105     552032266
DEC06    -160.     -.144       40.     -.195      140.     -.220     552042266
DEC06     190.     -.236      215.     -.246      240.     -.259     552052266
DEC01       0.                                                       552062266
TAP  LFWD-3   THERMAL CONDUCTIVITY OF LINDE FLT WT (80 LAYERS/INCH)553012266
DEC06    -435.     1.9E-6    -360.     3.8E-6    -260.      8.E-6    553022266
```

TABLE 10-2 (Continued)

```
DEC06      -160.     14.E-6      -60.      21.E-6        40.      32.E-6  553032266
DEC06        90.     46.E-6      115.      59.E-6       140.      81.E-6  553042266
DEC06       165.    120.E-6      190.     182.E-6       207.     255.E-6  553052266
DEC05       224.    375.E-6      240.     590.E-6         0.              553062266
TAP  LHTA-1   DENSITY OF LINDE HIGH TEMP (60 LAYERS/INCH)                 561012266
COD       0                                                               561022266
DEC05      -100.      3.384     2040.      3.384          0.              561032266
TAP  LHTA-2   SPECIFIC HEAT OF LINDE HIGH TEMP                            562012266
COD       0                                                               562022266
DEC06      -100.       .097       40.       .103        540.        .120  562032266
DEC05      1040.       .132     2040.       .141          0.              562042266
TAP  LHTA-3   THERMAL CONDUCTIVITY OF LINDE HI TEMP(60 LAYERS/INCH)563012266
DEC06      -100.     10.E-6      -50.     13.2E-6         0.     19.6E-6  563022266
DEC06        40.     27.E-6       90.      46.E-6       140.      75.E-6  563032266
DEC06       240.    165.E-6      340.     295.E-6       540.     690.E-6  563042266
DEC06      1040.   1900.E-6     1540.    3450.E-6      2040.    5400.E-6  563052266
DEC01         0.                                                          563062266
TAP  LHTB-1   DENSITY OF LINDE HIGH TEMP (120 LAYERS/INCH)                571012266
COD       0                                                               571022266
DEC05      -100.      6.768     2040.      6.768          0.              571032266
TAP  LHTB-2   SPECIFIC HEAT OF LINDE HIGH TEMP                            572012266
COD       0                                                               572022266
DEC06      -100.       .097       40.       .103        540.        .120  572032266
DEC05      1040.       .132     2040.       .141          0.              572042266
TAP  LHTB-3   THERMAL CONDUCTIVITY OF LINDE HI TEMP(120 LAYER/INCH)573012266
DEC06      -100.     18.E-6      -50.     20.5E-6         0.     26.3E-6  573022266
DEC06        40.     34.E-6       90.     48.5E-6       140.      70.E-6  573032266
DEC06       240.    123.E-6      340.     200.E-6       540.     410.E-6  573042266
DEC05      1040.   1070.E-6     2040.    2800.E-6         0.              573052266
TAP  LHTC-1   DENSITY OF LINDE HIGH TEMP (180 LAYERS/INCH)                581012266
COD       0                                                               581022266
DEC05      -100.     10.152     2040.     10.152          0.              581032266
TAP  LHTC-2   SPECIFIC HEAT OF LINDE HIGH TEMP                            582012266
COD       0                                                               582022266
DEC06      -100.       .097       40.       .103        540.        .120  582032266
DEC05      1040.       .132     2040.       .141          0.              582042266
TAP  LHTC-3   THERMAL CONDUCTIVITY OF LINDE HI TEMP(180 LAYER/INCH)583012266
DEC06      -100.    28.5E-6      -50.      32.E-6         0.      39.E-6  583022266
DEC06        40.     47.E-6      140.      82.E-6       240.     130.E-6  583032266
DEC06       340.    190.E-6      540.     350.E-6      2040.    2000.E-6  583042266
DEC01         0.                                                          583052266
TAP  NRCA-1   DENSITY OF NRC-2 (40 LAYERS/INCH)                           601012266
COD       0                                                               601022266
DEC05      -430.       .873      240.       .873          0.              601032266
TAP  NRCA-2   SPECIFIC HEAT OF NRC-2                                      602012266
COD       1                                                               602022266
DEC06      -430       -.315      -20.       .315        240.       -.315  602032266
DFC01         0.                                                          602042266
TAP  NRCA-3   THERMAL CONDUCTIVITY OF NRC-2 (40 LAYERS/INCH)              603012266
DEC06      -430.   .0156E-6     -418.    .043E-6       -410.     .072E-6  603022266
DEC06      -402.    .113E-6     -393.    .168E-6       -377.     .325E-6  603032266
DEC06      -360.    .576E-6     -335.    1.18E-6       -310.     2.05E-6  603042266
DEC06      -260.    4.61E-6     -210.     8.9E-6       -160.    15.56E-6  603052266
DEC06      -110.    24.2E-6      -60.      36.E-6        40.      72.E-6  603062266
DEC05       140.    129.E-6      240.    197.7E-6         0.              603072266
TAP  NRCB-1   DENSITY OF NRC-2 (100 LAYERS/INCH)                          611012266
COD       0                                                               611022266
DEC05      -430.       2.18      240.       2.18          0.              611032266
TAP  NRCB-2   SPECIFIC HEAT OF NRC-2                                      612012266
COD       1                                                               612022266
DEC06      -430       -.315      -20.       .315        240.       -.315  612032266
```

TABLE 10-2 (Continued)

```
DEC01          0.                                                    612042266
TAP  NRCB-3   THERMAL CONDUCTIVITY OF NRC-2 (100 LAYERS/INCH)        613012266
DEC06      -430. .0135E-6      -418.  .0385E-6      -410.   .063E-6  613022266
DEC06      -402.     .1E-6     -393.   .147E-6      -377.    .28E-6  613032266
DEC06      -360.   .498E-6     -335.     1.E-6      -310.   1.77E-6  613042266
DEC06      -260.   3.98E-6     -210.    7.7E-6      -160.  13.45E-6  613052266
DEC06      -110.   21.1E-6      -60.   31.4E-6        40.   62.3E-6  613062266
DEC05       140.   113.E-6      240.  170.9E-6         0.            613072266
TAP  NRCC-1   DENSITY OF NRC-2 (160 LAYERS/INCH)                     621012266
COD       0                                                          621022266
DEC05      -430.      3.49      240.      3.49         0.            621032266
TAP  NRCC-2   SPECIFIC HEAT OF NRC-2                                 622012266
COD       1                                                          622022266
DEC06      -430       -.315     -20.      .315       240.     -.315  622032266
DEC01          0.                                                    622042266
TAP  NRCC-3   THERMAL CONDUCTIVITY OF NRC-2 (160 LAYERS/INCH)        623012266
DEC06      -430. .01247E-6     -418.   .035E-6      -410.   .057E-6  623022266
DEC06      -402.    .09E-6     -393.   .135E-6      -377.    .36E-6  623032266
DEC06      -360.   .462E-6     -335.    .94E-6      -310.   1.65E-6  623042266
DEC06      -260.   3.69E-6     -210.    7.2E-6      -160.  12.47E-6  623052266
DEC06      -110.   19.4E-6      -60.   28.6E-6        40.   57.7E-6  623062266
DEC05       140.   102.E-6      240.  158.3E-6         0.            623072266
TAP  FGLS-1   DENSITY OF FIBERGLASS                                  701012266
COD       0                                                          701022266
DEC05      -430.        4.      800.        4.         0.            701032266
TAP  FGLS-2   SPECIFIC HEAT OF FIBERGLASS                            702012266
COD       0                                                          702022266
DEC06      -430.      .042     -300.      .093      -150.      .141  702032266
DEC06         0.      .178      200.      .215       600.      .257  702042266
DEC03      1200.      .288        0.                                 702052266
TAP  FGLS-3   THERMAL CONDUCTIVITY OF FIBERGLASS                     703012266
DEC06      -430.    .83E-3     -200.    .83E-3      -150.   1.08E-3  703022266
DEC06      -100.   1.67E-3      -50.   2.67E-3         0.    3.5E-3  703032266
DEC06       100.   4.17E-3      200.   4.17E-3       250.   5.25E-3  703042266
DEC06       300.   6.66E-3      400.   8.33E-3       800.  20.83E-3  703052266
DEC01          0.                                                    703062266
TAP  MQTZ-1   DENSITY OF MICRO QUARTZ                                751012266
COD       0                                                          751022266
DEC05      -430.       3.5      900.       3.5         0.            751032266
TAP  MQTZ-2   SPECIFIC HEAT OF MICRO QUARTZ                          752012266
COD       0                                                          752022266
DEC06      -430.      .016     -300.      .070      -150.      .123  752032266
DEC06         0.      .163      200.      .201       600.      .248  752042266
DEC03      1200.      .280        0.                                 752052266
TAP  MQTZ-3   THERMAL CONDUCTIVITY OF MICRO QUARTZ                   753012266
DEC06      -430.   7.16E-3     -300.   5.83E-3       100.    2.5E-3  753022266
DEC06       150.   3.17E-3      200.   4.17E-3       300.    7.5E-3  753032266
DEC06       400.   10.0E-3      500.  14.16E-3       900.  30.82E-3  753042266
DEC01          0.                                                    753052266
TAP  000000
```

REFERENCES

10-1. Schultz, H.D. *Thermal Analyzer Computer Program for the Solution of General Heat Transfer Problems,* Lockheed-California Company Report LR 18902, June 1965.

10-2. Hirasawa, P.S., I. Shuldiner, and Josephine Laue *Thermal Analyzer Computer Program for the Solution of Fluid Storage and Pressurization Problems,* Lockheea-California Company Report LR 18903, July 1965.

SECTION 2.0

PHYSICAL PROPERTIES OF 50/50 FUEL BLEND

The fuel blend, comprising a 50/50 mixture of UDMH and N_2H_4, is a clear, colorless, hygroscopic (capable of absorbing moisture readily) liquid having a characteristic ammoniacal odor. When the blend is exposed to air, a distinct fishy odor is evident in addition to the ammonia odor; this is probably caused by the air oxidation of UDMH.

The UDMH and N_2H_4 are miscible in all proportions. When combined, there is an immediate tendency for each to dissolve in the other. However, because of their different densities, they are easily stratified; UDMH above the N_2H_4, especially when UDMH is poured into a vessel containing N_2H_4. Under these conditions, a distinct interface may form (Reference 1).

In the pages that follow, additional physical property data is presented for this fuel blend. The information was obtained from the literature or from laboratory tests conducted at Bell Aerosystems. Table 2.1 summarizes pertinent physical properties of the fuel blend.

TABLE 2.1

PHYSICAL PROPERTIES OF THE 50/50 FUEL BLEND

Structural Formula of the Fuel

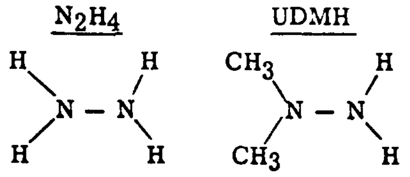

Molecular Weight (ave)	45.0
Melting Point[a]	18.8°F
Boiling Point UDMH[c] at 14.7 psia	146°F
Boiling Point N_2H_4[c] at 14.7 psia	235°F
Physical State	Colorless Liquid
Density of Liquid at 77°F and 14.7 psia[a] ρ	56.1 lb/ft^3
Viscosity of Liquid at 77°F[a] μ	54.9 x 10^{-5} lb/ft-sec = .817 cp
Vapor Pressure at 77°F[b]	2.75 psia
Critical Temperature (calc)	634°F
Critical Pressure (calc)	1696 psia
Heat of Vaporization (calc)	425.8 BTU/lb
Heat of Formation at 77°F (calc)	527.6 BTU/lb
Specific Heat at 77°F (calc)	0.694 BTU/lb-°F
Thermal Conductivity at 77°F (calc)	0.151 BTU/ft-hr-°F
Specific Resistance at 78°F[a]	142 to 161 ohm-cm[d]

All data is from Reference 1 except as noted.

a - Measured on samples of the fuel blend of typical composition (51.0% N_2H_4, 48.2% UDMH, and 0.5% H_2O).

b - Fuel blend composition 51.0% N_2H_4, 48.4% UDMH, and 0.6% H_2O.

c - Fuel blend is not a constant boiling mixture (see Section 2.8).

d - Reference 68.

lbm / ft sec

cP = 6.72 x10^{-4}

2.1 FUEL BLEND SPECIFICATION

The chemical requirements for procuring the fuel blend are taken from specification MIL-P-27402(USAF), dated 25 August 1961. This specification contains a method for performing analyses to fulfill the chemical requirements given in Table 2.2. This method is the salicylaldehyde method which is based upon a differential titration and determines UDMH directly and N_2H_4 indirectly. Water content and other soluble impurities are calculated by difference.

TABLE 2.2
PROPELLANT SPECIFICATION - 50/50 FUEL BLEND

Chemical Requirements	Specification (wt %)
N_2H_4	51.0 ±0.8
UDMH plus Amines	47.0 (min)
H_2O plus Other Soluble Impurities	1.8 (max)
N_2H_4 - UDMH plus Amines	98.2 (min)

2.2 MELTING POINT

Figure 2.1 contains melting point data for various mixtures of UDMH and N_2H_4 obtained from JPL, Aerojet-General Corporation, and Bell Aerosystems Company. The melting point of the fuel blend, as estimated by Aerojet, can range from about 17° to 21°F, thereby meeting the composition requirements of the procurement specification (see Table 2.2).

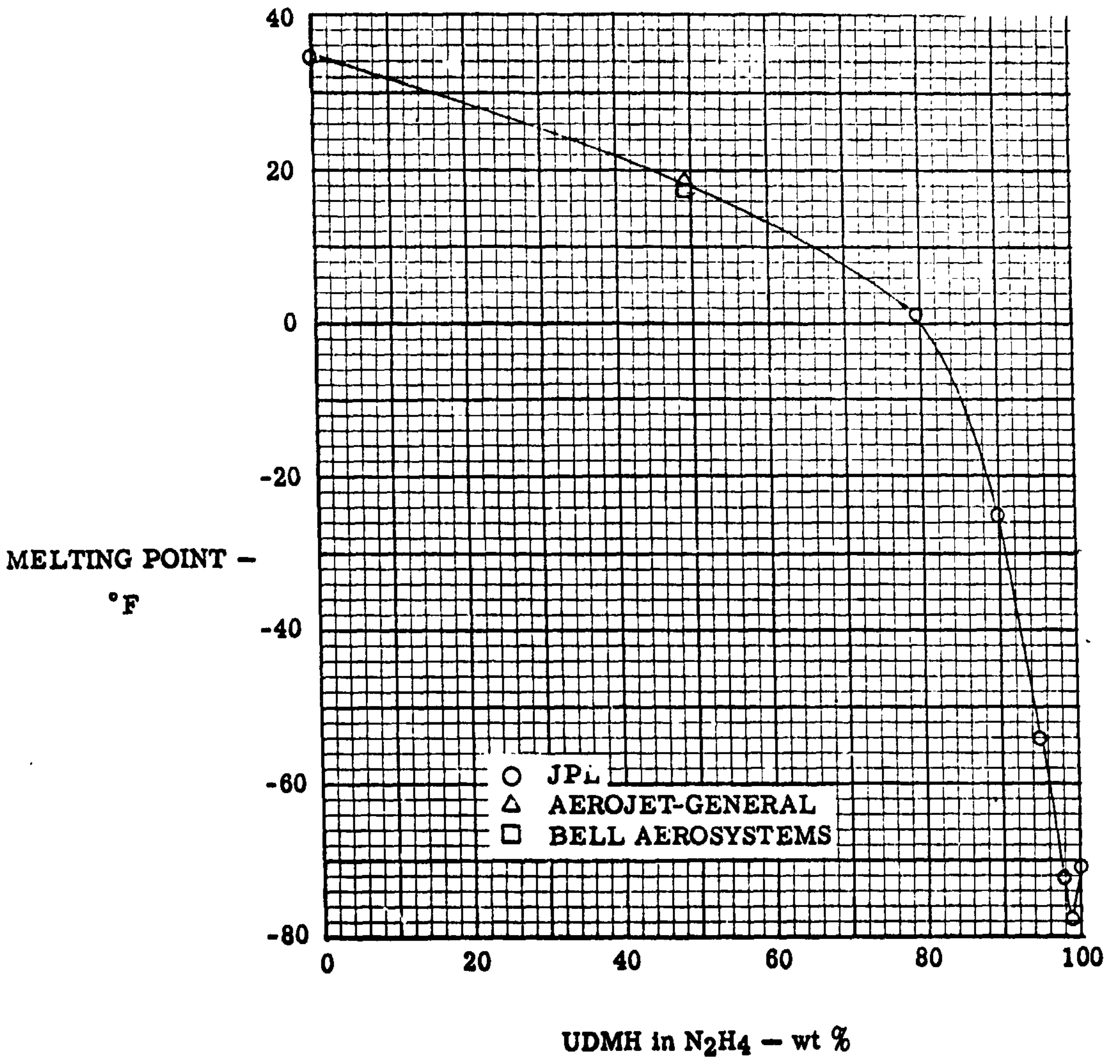

Figure 2.1. Melting Point versus Percent Weight of UDMH in N_2H_4

2.3 DENSITY

Figures 2.2 and 2.3 present density and specific gravity data for the fuel blend at various pressures as reported by Aerojet-General Corporation (References 1 and 35). The specific gravity equation is

$$S.G. = \left[5.1 \times 10^{-4} (114 - T_F) + 0.880\right] + \left[\Delta P (5.9 \times 10^{-6})\right]$$

where:

$S.G.$ = Specific gravity of fuel blend.

T_F = Temperature of fuel blend, °F.

ΔP = Pressure difference between the desired point of measurement and atmospheric pressure, psi.

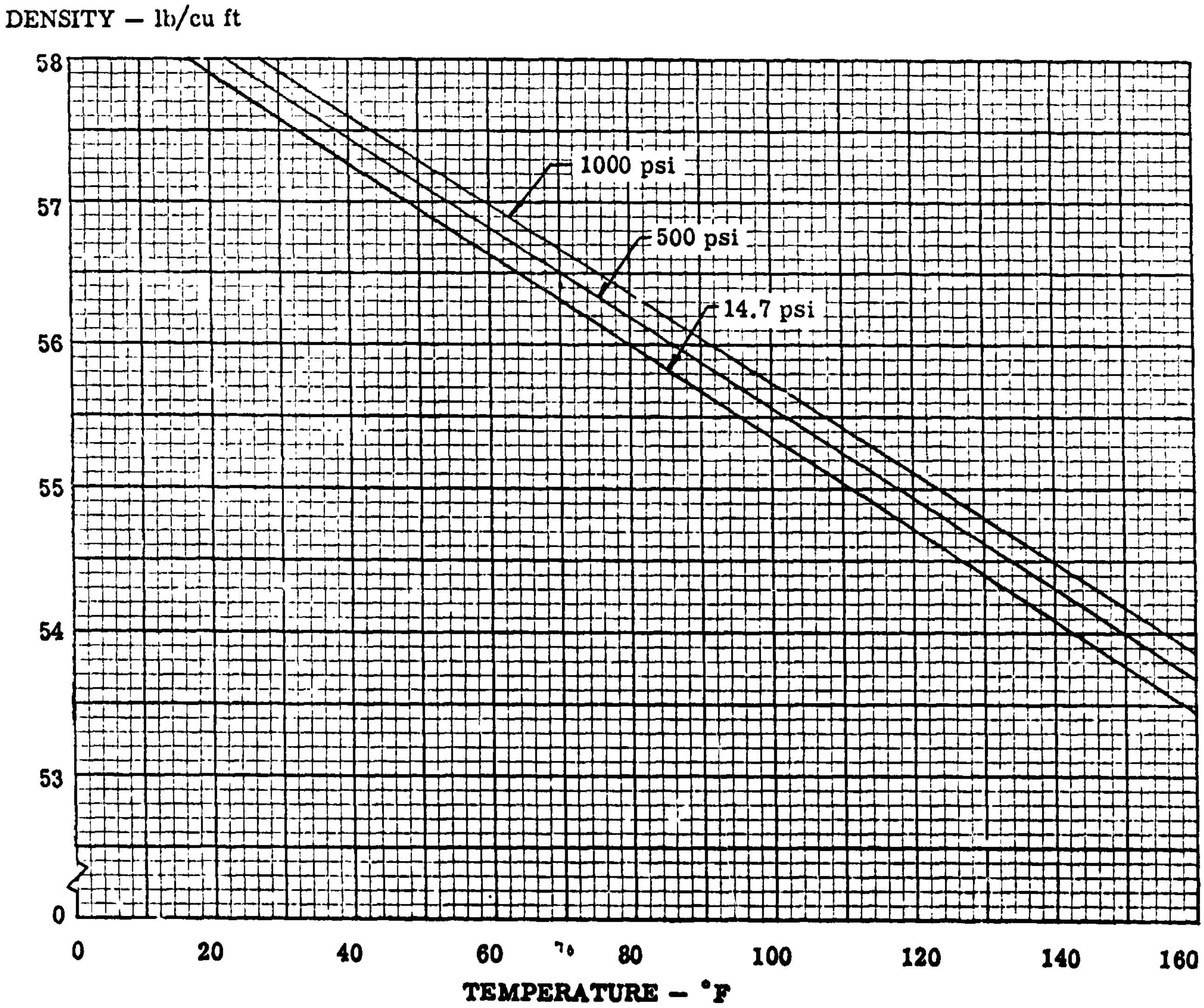

(References 1 and 35) Figure 2.2. Density of 50/50 Fuel Blend at Various Pressures

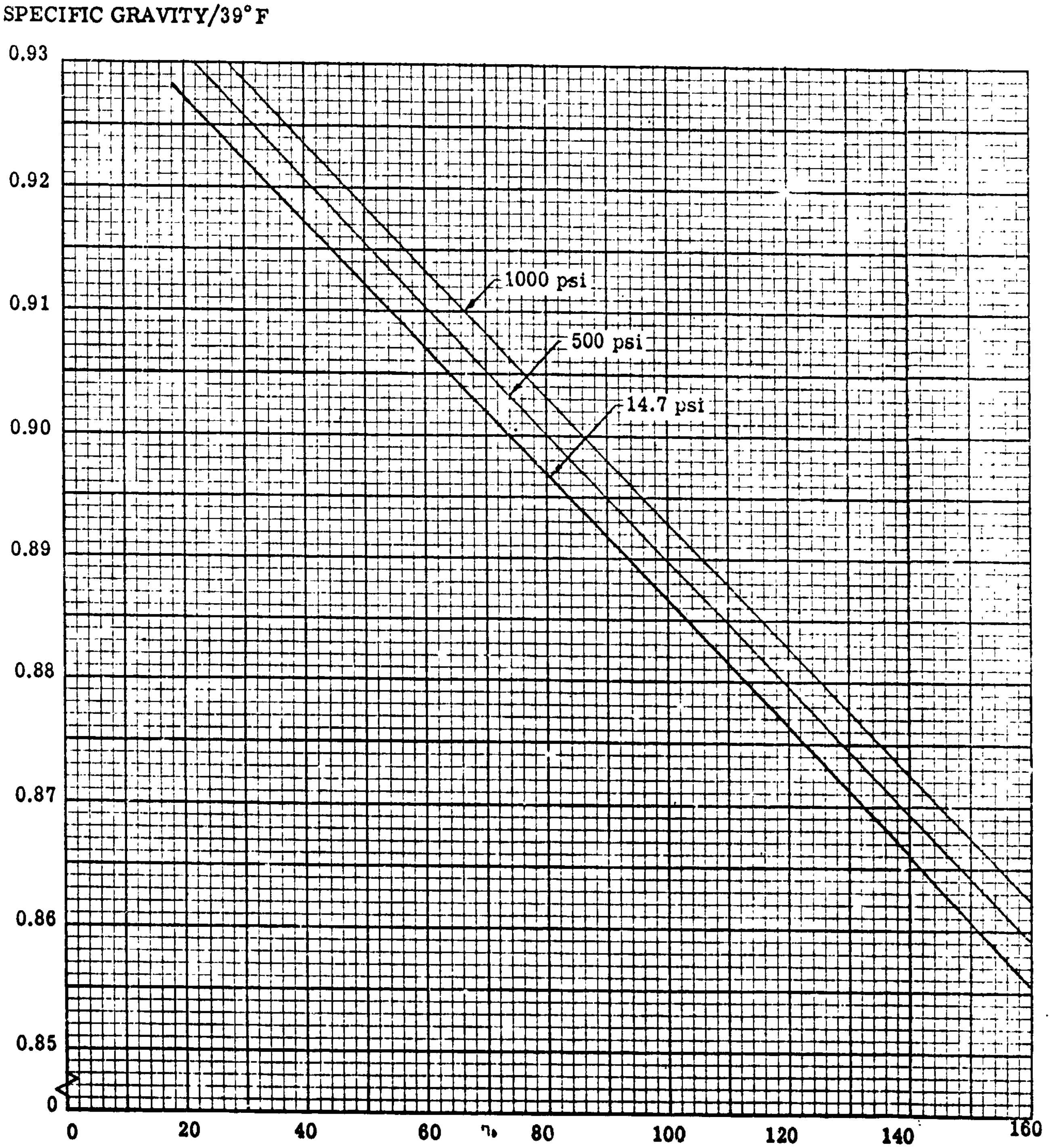

(References 1 and 35)

Figure 2.3. Specific Gravity of 50/50 Fuel Blend at Various Pressures

2.4 VAPOR PRESSURE

This 50/50 fuel blend is a mixture of UDMH and N_2H_4, with UDMH possessing the higher vapor pressure. The vapor pressure of a liquid mixture depends upon the composition of the mixture and temperature and is the sum of the partial pressures of each gas at a constant temperature. However, as one of the more-volatile components vaporizes from a liquid mixture (in this case UDMH into a large volume space (ullage) above it, the vapor pressure of the resulting liquid mixture decreases. Inversely, as the volume space above the liquid mixture decreases, the vapor pressure of the liquid increases. Experiments were conducted at Bell (References 4 and 51) to determine the effect this would have when the vapor pressure of the fuel blend was measured at different ullages employing an all-glass evacuated system and an isoteniscope. At 80°F, the vapor pressure was 3.96 psia at 25% ullage and 3.06 psia at 75% ullage. These measurements demonstrate the effect of ullage on vapor pressure. Also, variations in fuel blend composition will effect vapor pressure at a given ullage and temperature.

Table 2.3 and Figure 2.4 contain the vapor pressure of the 50/50 fuel blend at various temperatures and at 46% ullage. The Bell experimental points were obtained with the apparatus shown and described in Reference 2.

TABLE 2.3

VAPOR PRESSURE OF 50/50 FUEL BLEND

Temperature (°F)	Vapor Pressure (psia)	Pg H_2O
14.0[a]	0.55	0.4593
23.0[a]	0.71	
32.0[a]	0.92	
68.0[a]	2.09	0.3390
77.0[a]	2.75	
80.3[b]	3.08	
86.0[a]	3.42	
104.0[a]	5.00	
108.9[b]	5.30	
122.0[a]	7.30	
135.3[b]	9.29	
140.0[a]	10.50	
159.8[a]	15.10	

a - Aerojet-General Corporation experimental data (Reference 1).

b - Bell Aerosystems Company experimental data (Reference 2).

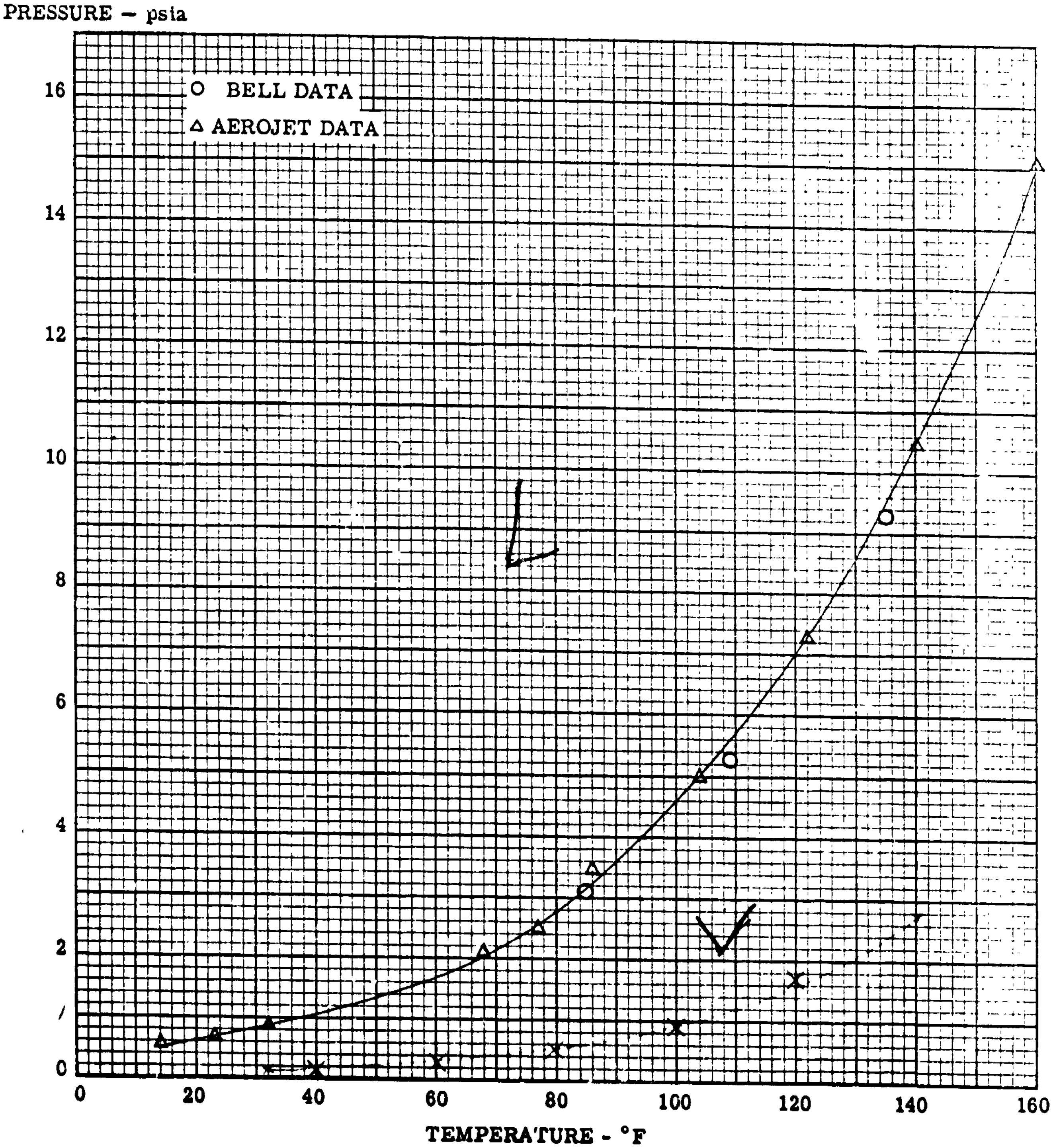

Figure 2.4. Vapor Pressure of 50/50 Fuel Blend

2.5 VISCOSITY

The viscosity of the 50/50 fuel blend was measured by Aerojet-General Corporation over the liquid range (Reference 1). Figure 2.5 is a plot of viscosity in centistokes versus temperature of the fuel blend.

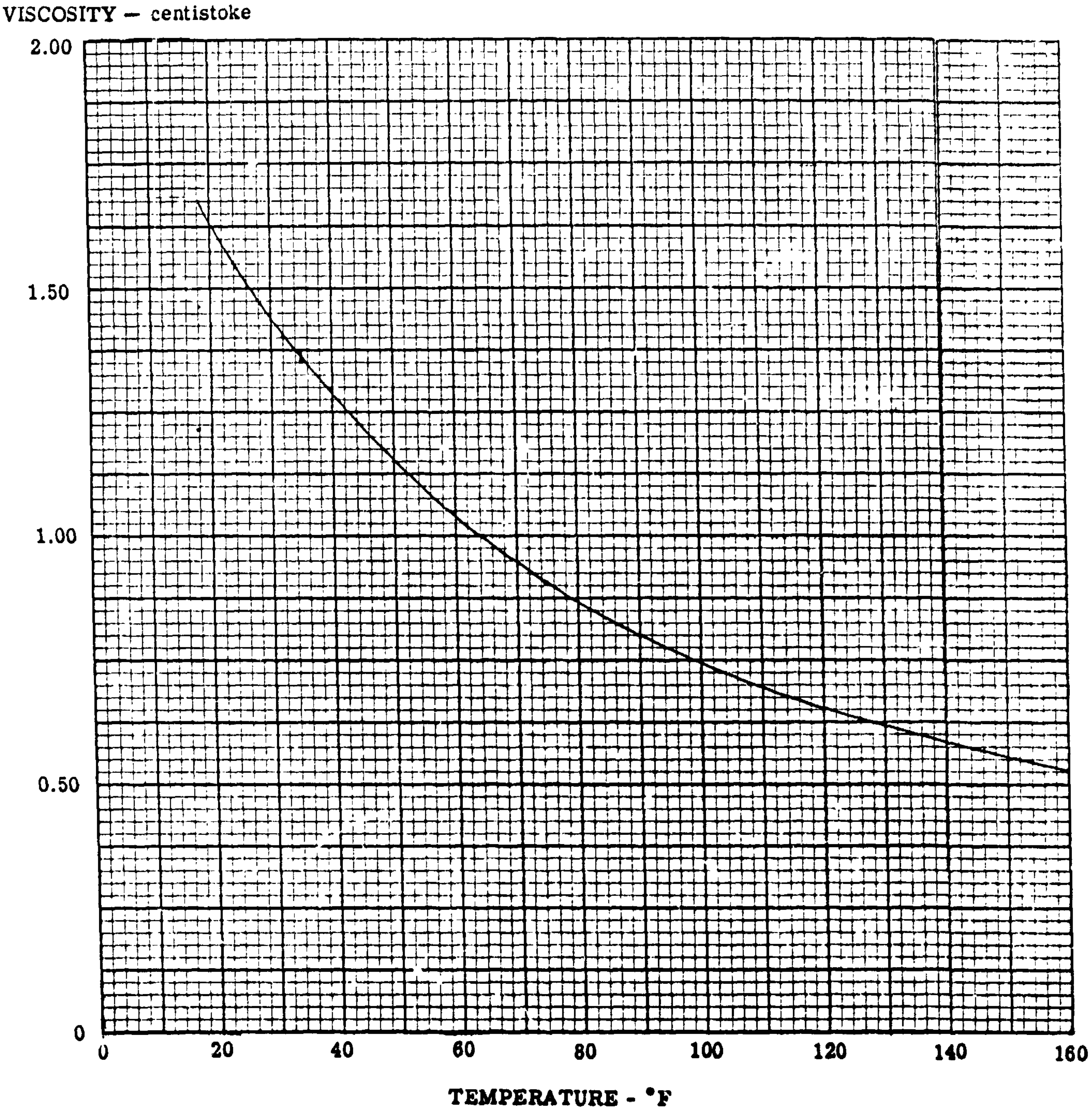

(Reference 1)

Figure 2.5. Viscosity of 50/50 Fuel Blend

2.6 SPECIFIC HEAT

Specific heat data of the 50/50 fuel blend, as calculated by Aerojet-General Corporation, is presented in Table 2.4 and plotted in Figure 2.6. Bell measured the specific heat of the fuel blend at two temperatures using the method of mixtures described in Reference 2. The Bell experimental data agrees within 0.5% of the Aeroject calculated data.

TABLE 2.4
SPECIFIC HEAT OF 50/50 FUEL BLEND
(Calculated by Aerojet-General)

Temperature (°F)	Specific Heat (BTU/lb-°F)
21	0.680
35	0.684
63	0.692
81	0.696
99	0.702
135	0.709
153	0.715
250	0.743
350	0.780
420	0.814

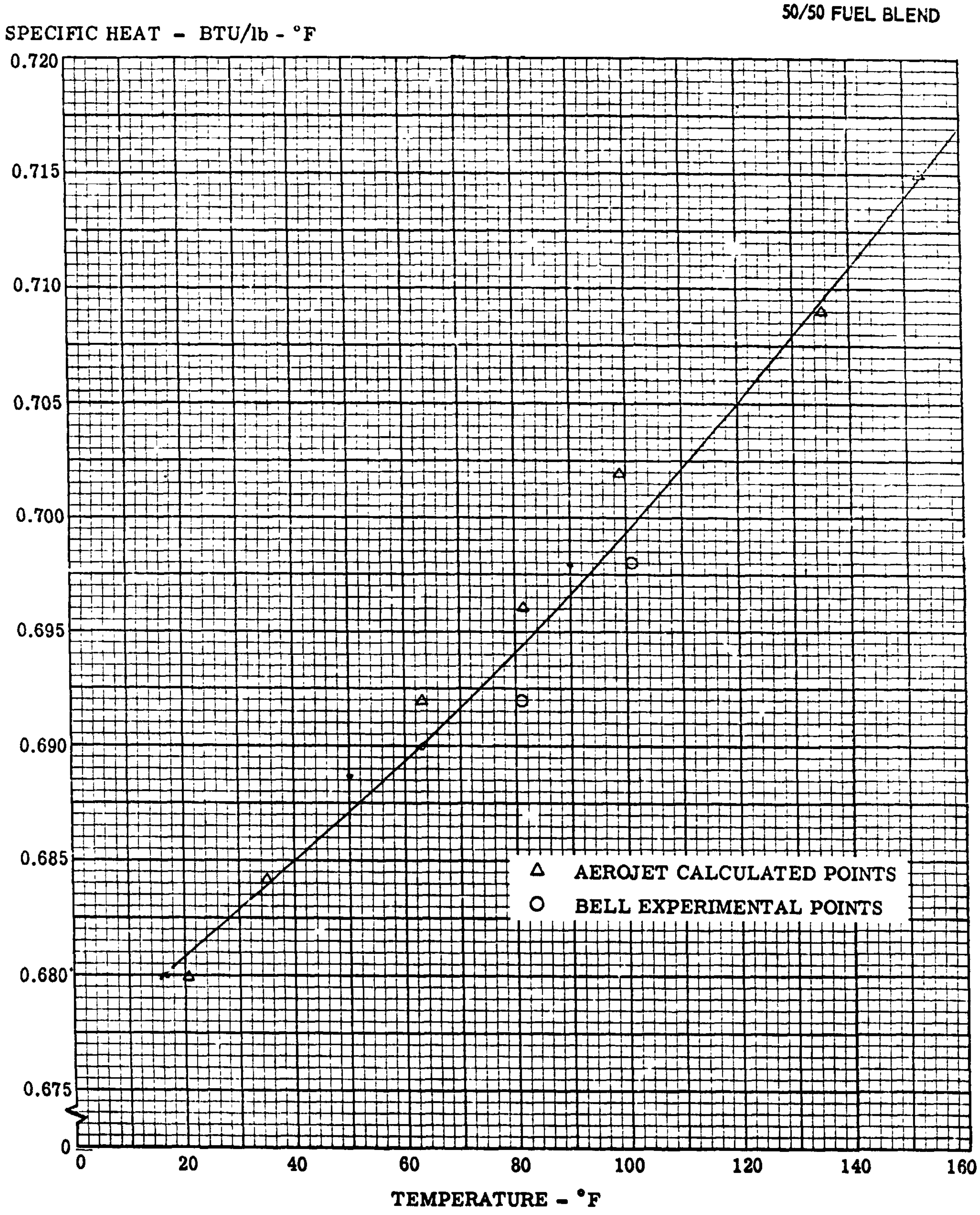

Figure 2.6. Specific Heat of 50/50 Fuel Blend

2.7 FLASH AND FIRE POINTS

Flash and fire point measurements made in duplicate with a modified Cleveland Open-Cup Tester (Reference 51) resulted in the average data presented in Table 2.5 and plotted in Figure 2.7. The tests indicate that the fuel blend must be diluted with at least an equal volume of water before the fire hazard is reduced appreciably. A dilution of three volumes of water to two volumes of fuel blend is required to increase the flash and fire point temperature to 180°F.

TABLE 2.5
FLASH AND FIRE POINTS OF 50/50 FUEL BLEND
WITH VARIOUS WATER DILUTIONS
(Using a Modified Cleveland Open-Cup Tester)

H_2O in Fuel Blend (vol %)	Flash Point (°F)	Fire Point (°F)
Undiluted	34.7	34.7
10	41.9	41.9
20	55.4	55.4
30	82.4	82.4
40	113.9	117.5
50	145.4	153.5
60	178.7	218.3

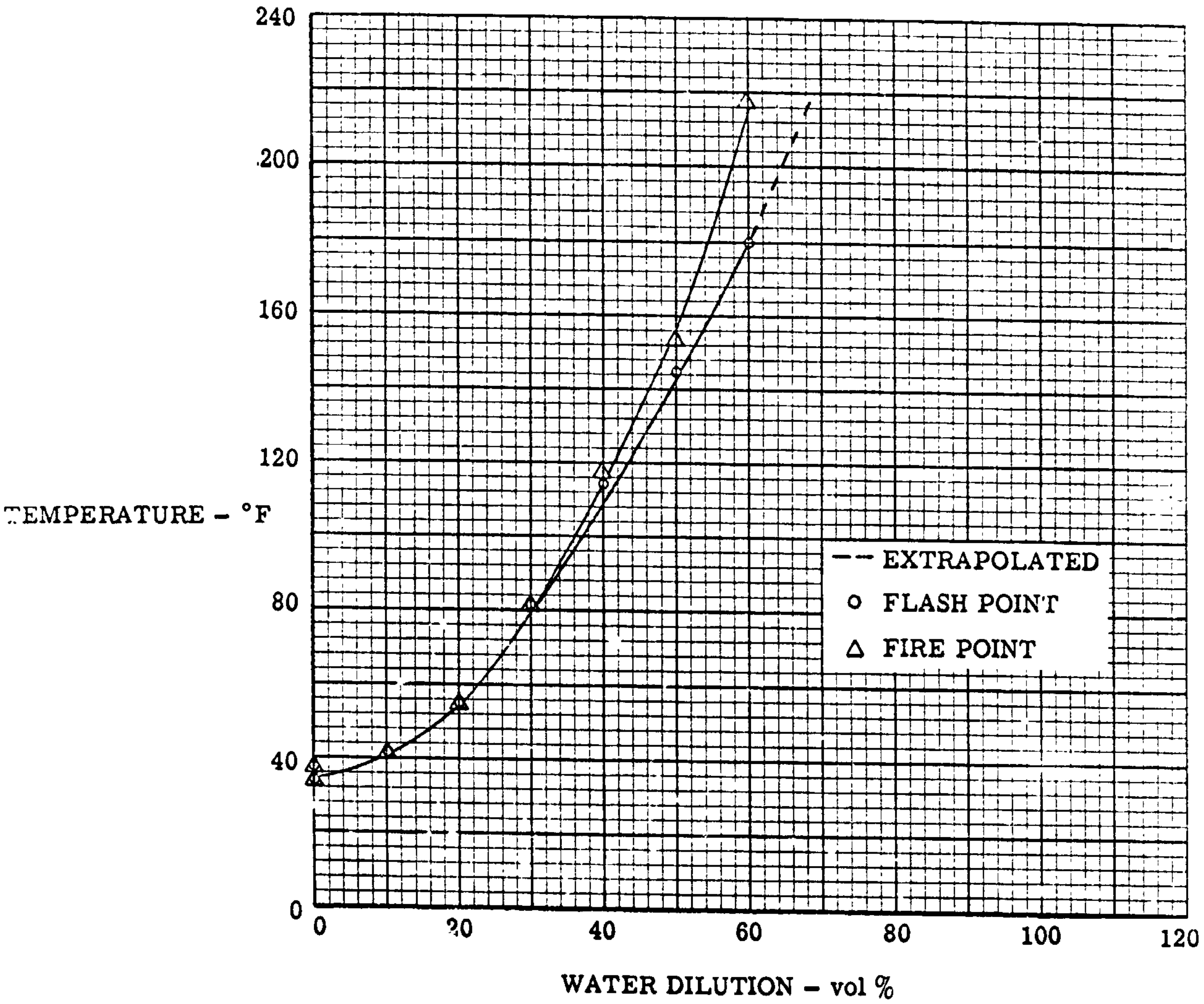

Figure 2.7. Flash and Fire Points of 50/50 Fuel Blend with Various Water Dilutions

2.8 DISTILLATION RANGE

The distillation range of the 50/50 fuel blend, together with analyses of various fractions, is shown in Table 2.6. When the fuel blend is heated, the initial condensed vapors are richer in the more-volatile UDMH; as the distillation process continues with increasing temperature, the condensed distillate becomes richer in the less-volatile N_2H_4.

TABLE 2.6

DISTILLATION RANGE OF THE 50/50 FUEL BLEND
AT 14.7 PSIA

Blend Composition by Weight	%
UDMH	48.7
N_2H_4	50.4
H_2O + impurities	0.9

Temperature (°F)	Volume % (Distilled)	Distillate Analyses
149.0	First Drop Distilled	-
158.0	10	86.0% UDMH, 8.0% N_2H_4
161.6	20	85.0% UDMH, 9.0% N_2H_4
167.0	30	-
170.6	40	-
194.0	50	79.0% UDMH, 16.0% N_2H_4
233.6	60	-
235.4	70	-
235.4	80	100% N_2H_4
239.0	90	95% N_2H_4

NOTE: Fuel fractions were analyzed spectrally employing calibration curves covering the UDMH and N_2H_4 concentration range of 45% to 55% by weight. The analytical results, obtained by extrapolating the calibration curves, are approximate. N_2H_4 at the 90% fraction probably contains hydrazine hydrate.

(Reference 2)

2.9 SOLUBILITY OF PRESSURIZING GASES

The solubility of nitrogen, helium, and ammonia in the 50/50 fuel blend was determined using the apparatus shown in Reference 2 and the procedure described in Reference 3. Results of these tests are shown in Table 2.7.

TABLE 2.7

SOLUBILITY OF VARIOUS GASES IN 50/50 FUEL BLEND

Pressurizing Gas	Temperature (°F)	Solubility (wt %)	Total Gas Pressure (psia)
Nitrogen	70.0	< 0.01	86.0
	32.0	< 0.01	79.4
Helium	71.5	0.012 ± 0.008	63.6
	33.0	< 0.008	60.7
Ammonia	57.5	0.26 ±0.01	38.0
	70.0	0.25 ±0.01	44.4

2.10 SHOCK SENSITIVITY

To determine the shock sensitivity of the 50/50 fuel blend, tests were conducted at room temperature using a drop-weight tester and a procedure developed by Olin Mathieson Chemical Corporation. The procedure is acceptable to the Joint Army-Navy-Air Force Panel on Liquid Propellant Test Methods. Results of these tests show that the liquid fuel blend is not shock sensitive at the highest impact value (8 foot-pounds) produced by the tester (Reference 2).

SECTION 3.0
PHYSICAL PROPERTIES OF N_2O_4

The compound N_2O_4 is an equilibrium mixture of nitrogen tetroxide and nitrogen dioxide ($N_2O_4 \rightleftarrows 2NO_2$).

In the solid state, N_2O_4 is colorless; in the liquid state, the equilibrium mixture is yellow to red-brown; and in the gaseous state, it is red-brown. The fumes exhibit a characteristic pungent and irritating odor.

When exposed to water, N_2O_4 reacts to form nitric acid and nitrous acid. The nitrous acid decomposes immediately to form additional nitric acid and evolve nitric oxide (Reference 30). Also, N_2O_4 is hypergolic with fuels as UDMH, N_2H_4, and aniline.

This section of the handbook contains physical property data for N_2O_4 based upon information obtained from a literature survey. Table 3.1 summarizes the pertinent physical properties of N_2O_4.

TABLE 3.1

PHYSICAL PROPERTIES OF N_2O_4

		Reference	Freon-11	F-113
Empirical Formula	$N_2O_4 \rightleftharpoons 2NO_2$	5		
Structural Formula	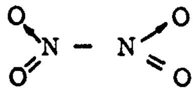	6		
Molecular Weight	92.016	5		
Melting Point	11.84°F	5	-168	-31
Boiling Point at 14.7 psia	70.07°F	5	74.78	117.63
Physical State	Red-brown liquid	5		
Density of Liquid at 77°F and 18.0 psia	89.34 lb/ft^3	5	92.12	97.69
Viscosity of Liquid at 77°F	0 0002796 lb/ft-sec	7		
	0.410 centipoise	7	0.42	0.66
Vapor Pressure at 77°F	17.7 psia	5		
Critical Temperature	316.8°F	5		
Critical Pressure	1469 psia	5		
Heat of Vaporization (equilibrium mixture at 70°F)	178 BTU/lb	5		
Heat of Formation at 77°F (calc for liquid equilibrium mixture)	-87.62 BTU/lb	41		
Specific Heat at 77°F	0.374 BTU/lb °F	8	0.209	0.218
Thermal Conductivity at 77°F and at the bubble point	0.0755 BTU/ft-hr-°F	5		
Heat of Fusion	68.4 BTU/lb	5		

R = 16.8

3.1 N_2O_4 SPECIFICATION

The chemical requirements for procuring N_2O_4 were taken from Specification MIL-P-26539 (USAF) dated 18 July 1960. These requirements are presented in Table 3.2. The specification contains procedures for performing propellant analysis. The N_2O_4 assay is determined directly by titration. The water content is determined directly by evaporating N_2O_4 and weighing the nitric acid remaining. The water equivalent in this acidic non-volatile matter is based upon the assumption that it is 70% nitric acid. Nitrosyl chloride (NOCl) content is determined by colorimetric means. The non-volatile ash is determined by evaporating N_2O_4 to dryness and igniting the residue at high temperatures. The percentage of non-volatile ash is calculated from the ash that remains.

TABLE 3.2

PROPELLANT SPECIFICATION – N_2O_4

Chemical Requirements	Specification (wt %)
N_2O_4 Assay	99.5 (min)
H_2O Equivalent	0.1 (max)
Chloride as NOCl	0.08 (max)
Non-Volatile Ash	0.01 (max)

3.2 N_2O_4 DISSOCIATION

The compound N_2O_4 is an equilibrium mixture of nitrogen tetroxide and nitrogen dioxide ($N_2O_4 \rightleftarrows 2NO_2$). At 68° F and at a pressure of one atmosphere, the vapor consists of 84.2% N_2O_4 in equilibrium with 15.8% NO_2 as shown in Table 3.3 and Figure 3.1.

TABLE 3.3

EQUILIBRIUM VALUES - PERCENT DISSOCIATION OF GASEOUS N_2O_4

$N_2O_4 \rightleftarrows 2NO_2$

Temperature (°F)	Weight Percent NO_2		
	At 7.4 psia	At 14.7 psia	At 73.5 psia
68	19.5	15.8	7.2
104	38.7	31.0	15.1
140	66.0	50.4	28.2
176	85.0	73.8	46.7
212	93.7	88.0	66.5
(Reference 5)			

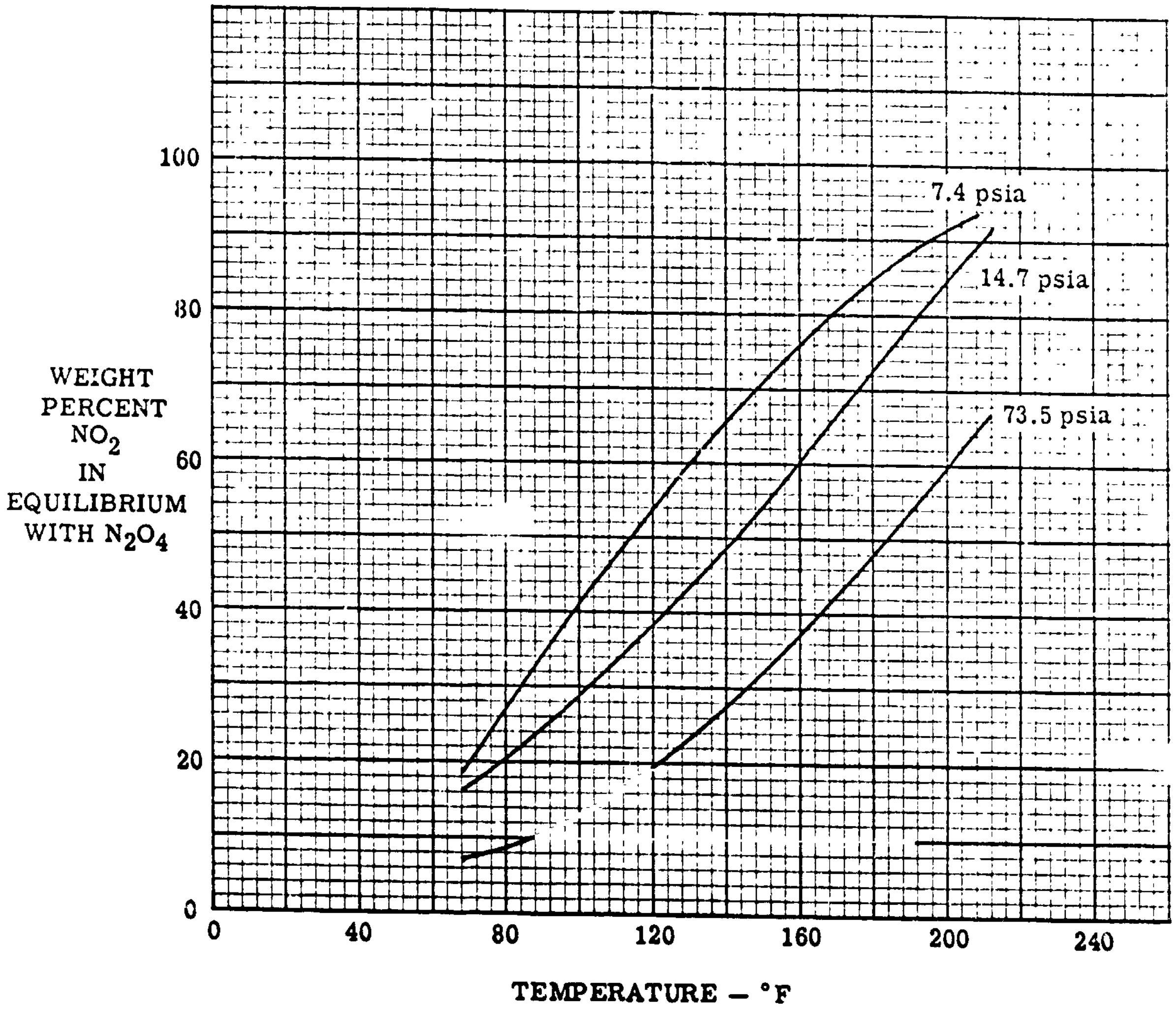

Figure 3.1. Equilibrium Values — Dissociation of Gaseous N_2O_4

3.3 VAPOR PRESSURE

Vapor pressure data, as a function of temperature, is presented in Table 3.4 and plotted in Figure 3.2.

TABLE 3.4

VAPOR PRESSURE OF N_2O_4

Temperature (°F)	Vapor Pressure (psia)	Temperature (°F)	Vapor Pressure (psia)
11.8	2.70	180	163.29
14	2.90	190	196.35
32	5.08	200	235.01
50	8.56	210	281.56
68	13.92	220	332.8
70	14.78	230	393.2
80	18.98	240	463.3
90	24.21	250	543.9
100	30.69	260	636.3
110	38.62	270	732.6
120	48.24	280	864.1
130	59.98	290	1000.5
140	74.12	300	1160.1
150	91.06	310	1336.5[a]
160	111.24	316.8[b]	1469.0[a]
170	135.14		

a - Value extrapolated.

b - Critical pressure estimated from measured critical temperature.

(References 1 and 5)

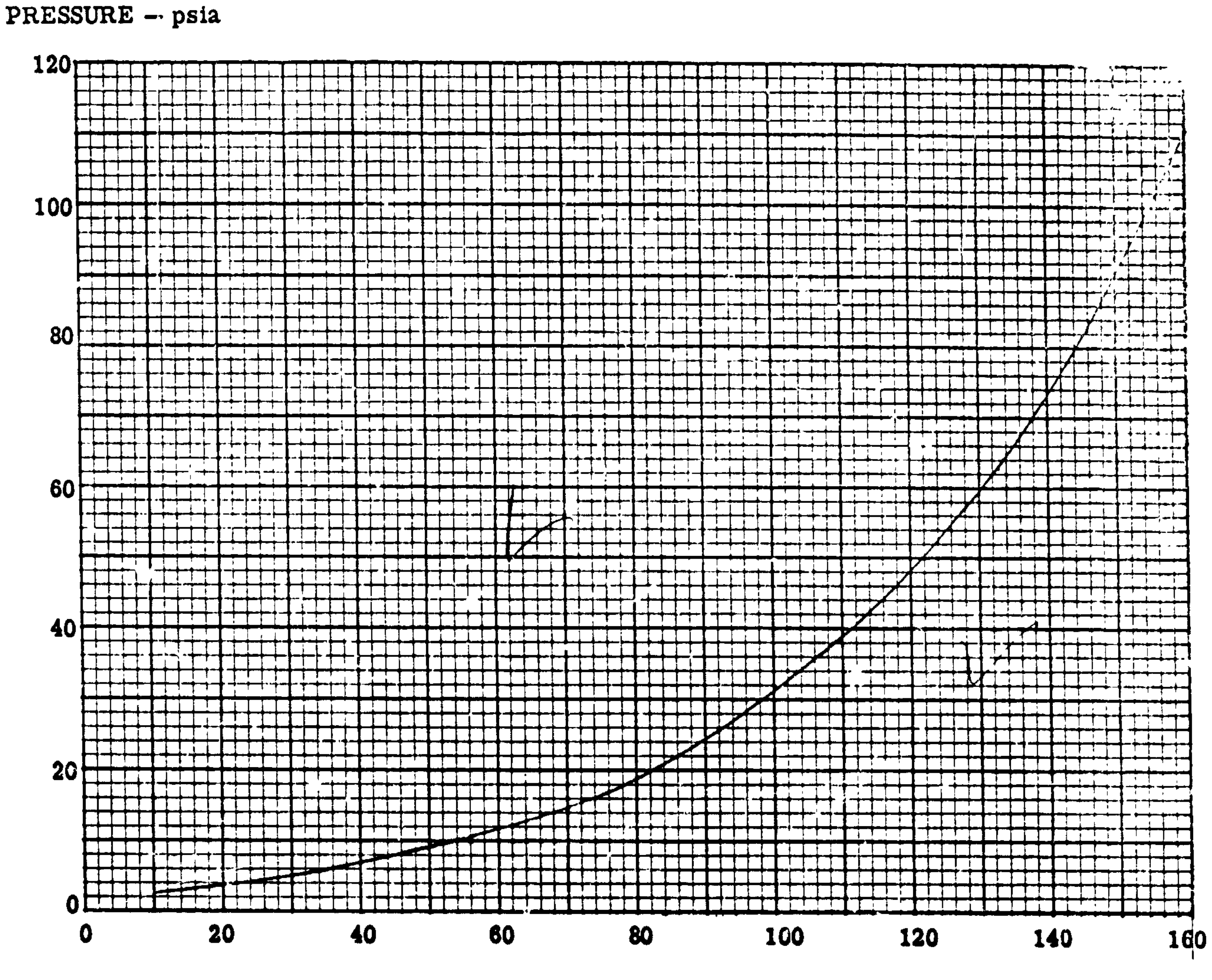

(References 1 and 5)

Figure 3.2. Vapor Pressure of N_2O_4

3.4 DENSITY

Table 3.5 and Figures 3.3 and 3.4 contain density and specific gravity for N_2O_4 at various pressures.

The specific gravity equation reported by Aerojet-General Corporation (Reference 35) is

$$S.G. = \left[12.5 \times 10^{-4}(11.8-T_O) + 1.515\right] + \left[11.2 \times 10^{-6} \ (\Delta P)\right]$$

where:

S.G. = Specific gravity of N_2O_4.

T_O = Temperature of N_2O_4, °F

ΔP = Pressure difference between the desired point of measurement and atmospheric pressure, psi.

TABLE 3.5

DENSITY OF LIQUID N_2O_4

(Under its Own Vapor Pressure)

Temperature (°F)	Specific Gravity	Density (lb/ft^3)	Density (lb/gal)
11.8	1.515	94.54	12.62
32.0	1.490	93.05	12.44
50.0	1.470	91.77	12.27
68.0	1.447	90.34	12.08
77.0	1.431	89.34	11.94
95.0	1.412	88.15	11.76
104.0	1.400	87.40	11.66
113.0	1.388	86.61	11.56
118.4	1.379	86.05	11.49
122.0	1.375	85.80	11.45
129.2	1.363	85.05	11.35

(References 1 and 5)

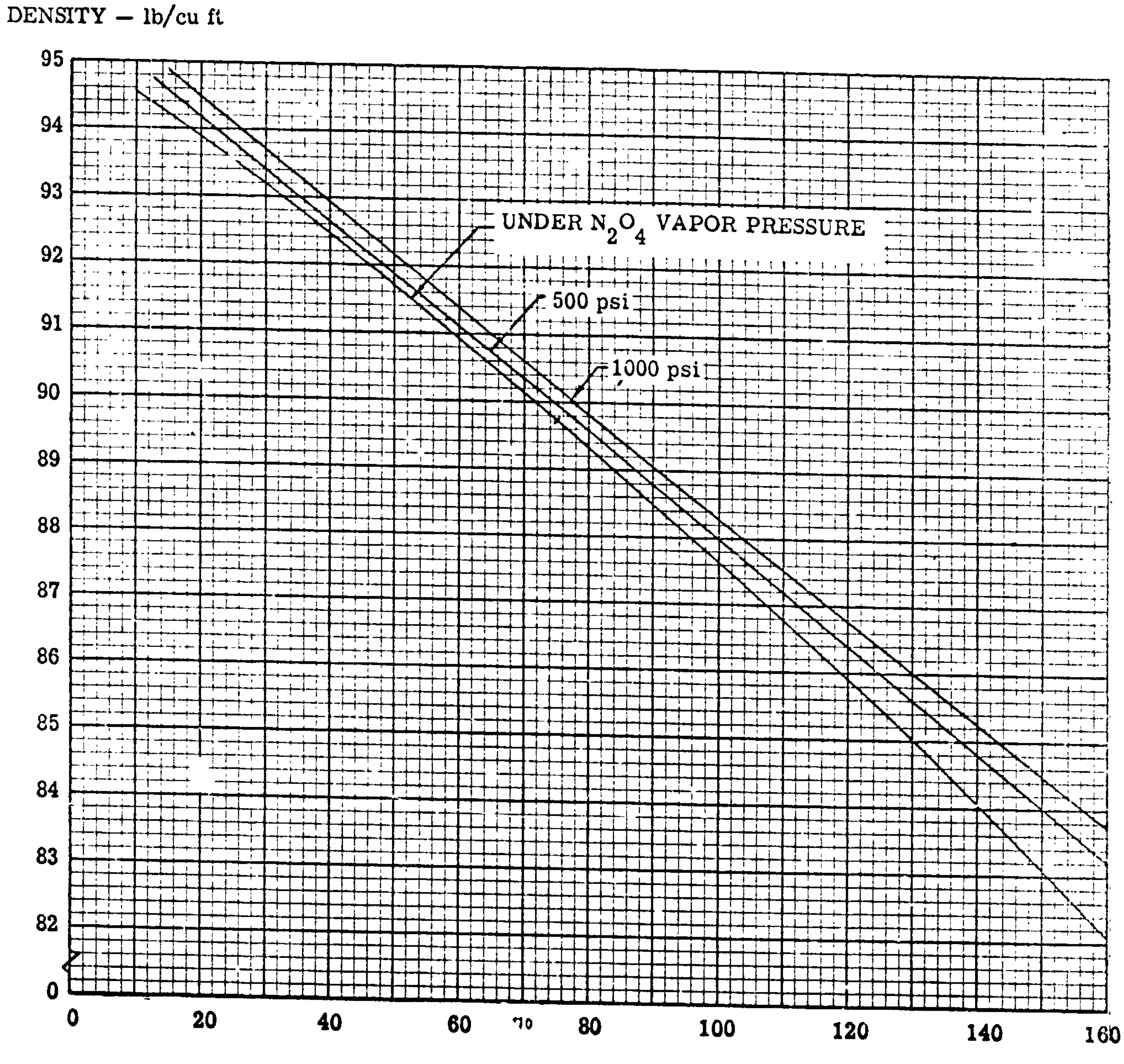

(References 15 and 35)

Figure 3.3 Density of N_2O_4 at Various Pressures

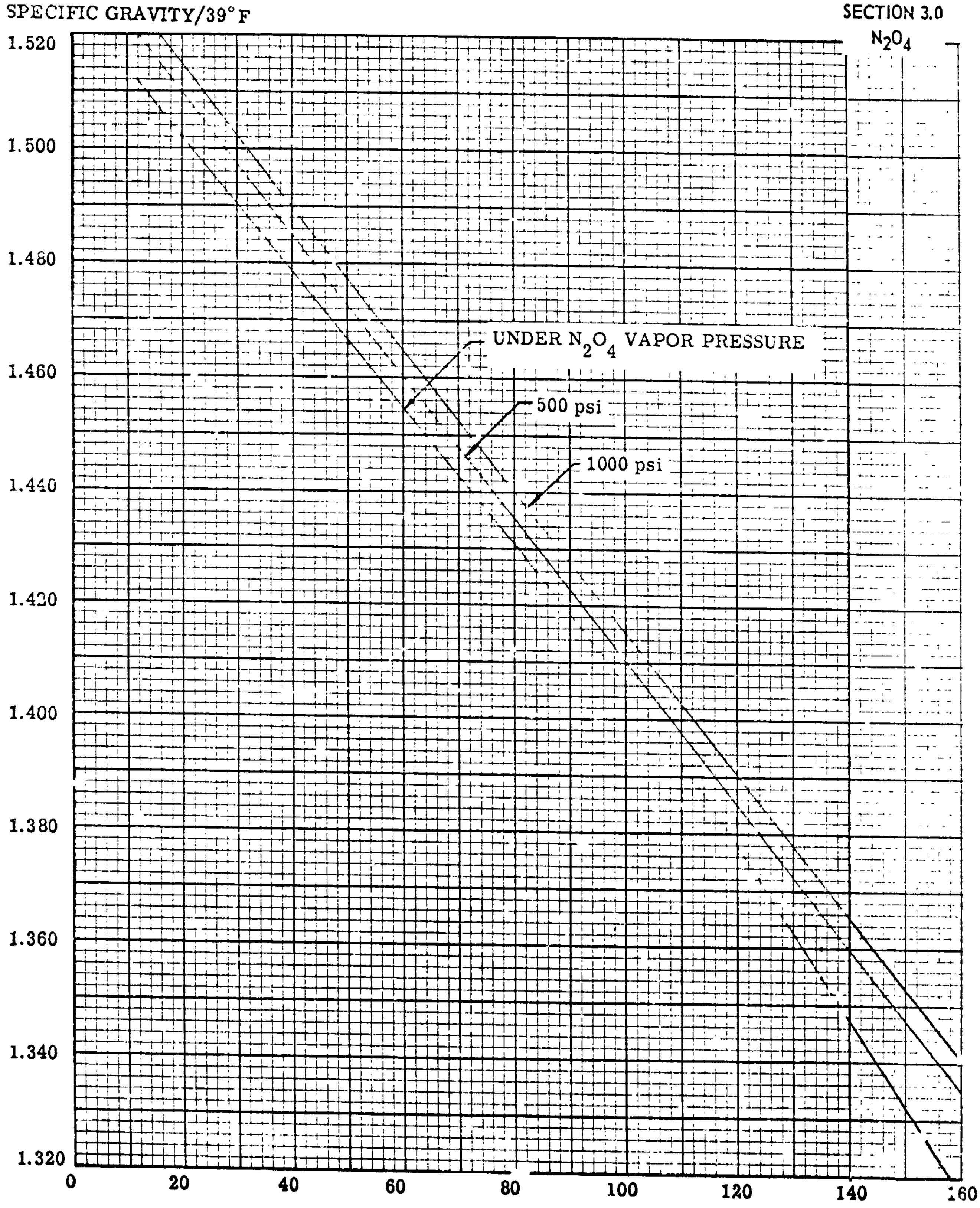

(References 15 and 35)

Figure 3.4 Specific Gravity of N_2O_4 at Various Pressures

3.5 VISCOSITY

The viscosity of N_2O_4 in the liquid phase from 40° to 280°F is presented in Table 3.6 and plotted in Figures 3.5 and 3.6. Figure 3.5 shows the effect of temperature on the viscosity of N_2O_4; Figure 3.6 shows the effect of pressure on viscosity of N_2O_4.

TABLE 3.6

VISCOSITY OF N_2O_4 IN THE LIQUID PHASE

	Temperature (°F)								
	40	70	100	130	160	190	220	250	280
Pressure (psia)	Viscosity (centipoise)								
Bubble Point	0.4990	0.4132	0.3420	0.2784	0.2235	0.1752	0.1325	0.0924	0.0570
200	0.5021	0.4155	0.3441	0.2800	0.2250	0.1753			
400	0.5055	0.4180	0.3470	0.2820	0.2281	0.1804	0.1350		
600	0.5090	0.4208	0.3495	0.2340	0.2310	0.1850	0.1420	0.0948	
800	0.5121	0.4232	0.3520	0.2861	0.2334	0.1896	0.1482	0.1028	
1000	0.5150	0.4260	0.3544	0.2880	0.2355	0.1939	0.1539	0.1100	0.0630
1250	0.5190	0.4297	0.3566	0.2906	0.2380	0.1975	0.1599	0.1179	0.0713
1500	0.5230	0.4330	0.3587	0.2919	0.2400	0.2010	0.1646	0.1252	0.0798
1750	0.5270	0.4366	0.3608	0.2949	0.2420	0.2040	0.1686	0.1319	0.0881
2000	0.5310	0.4400	0.3628	0.2965	0.2440	0.2083	0.1720	0.1370	0.0940
2200	0.5345	0.4433	0.3649	0.2990	0.2459	0.2060	0.1742	0.1400	0.0990
2500	0.5382	0.4470	0.3670	0.3010	0.2480	0.2098	0.1764	0.1430	0.1045
2750	0.5422	0.4502	0.3691	0.3024	0.2496	0.2110	0.1785	0.1444	0.1090
3000	0.5465	0.4535	0.3713	0.3042	0.2510	0.2127	0.1800	0.1470	0.1120
3500		0.4593	0.3753	0.2070	0.2540	0.2151	0.1822	0.1510	0.1170
4000		0.4655	0.3792	0.3095	0.2568	0.2183	0.1850	0.1532	0.1210
4500		0.4714	0.3830	0.3118	0.2600	0.2200	0.1880	0.1555	0.1249
5000		0.4782	0.3869	0.3145	0.2625	0.2229	0.1900	0.1579	0.1280

(Reference 5)

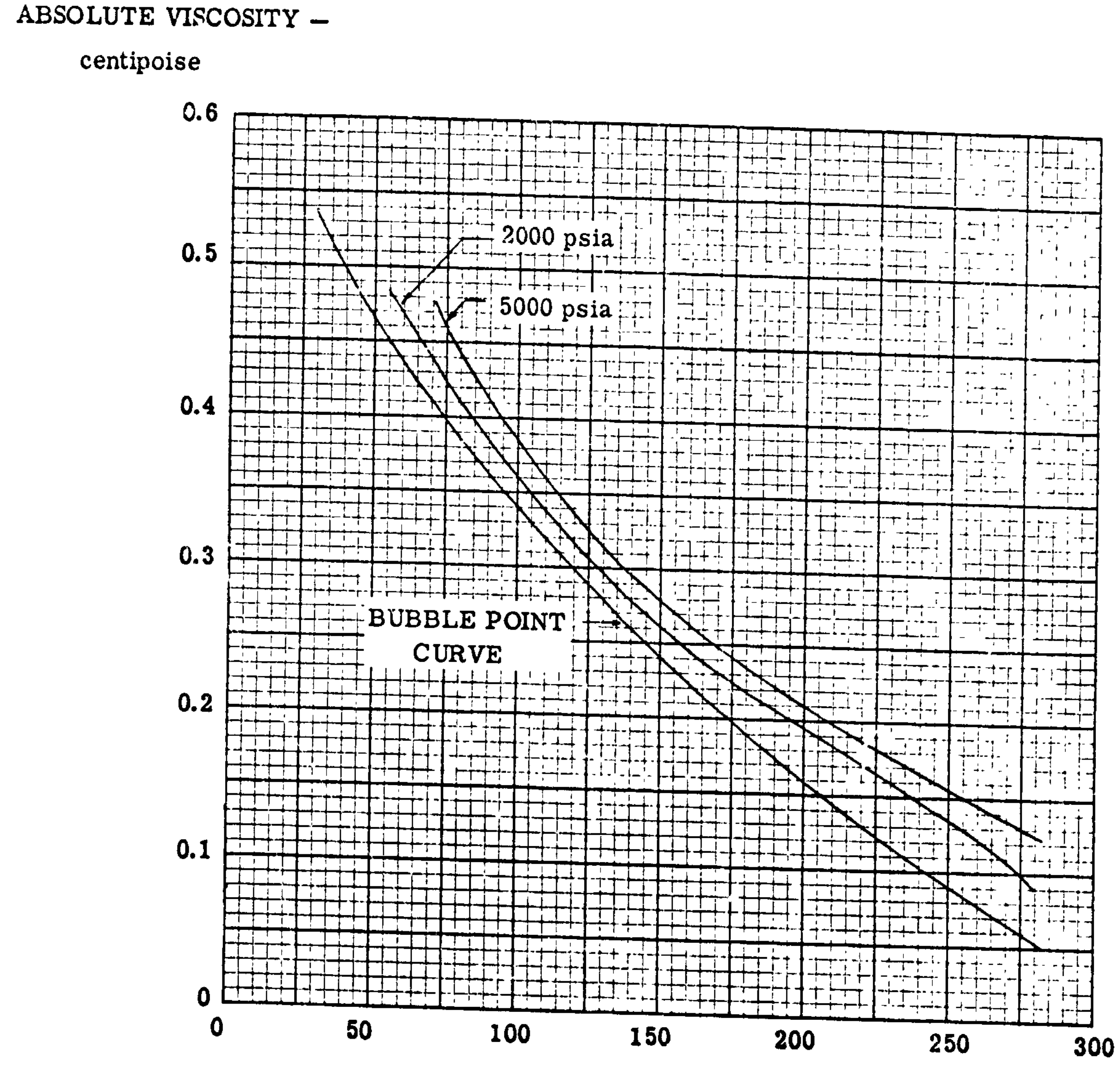

(Reference 5)

Figure 3.5. Effect of Temperature on Viscosity in the Liquid Phase, N_2O_4

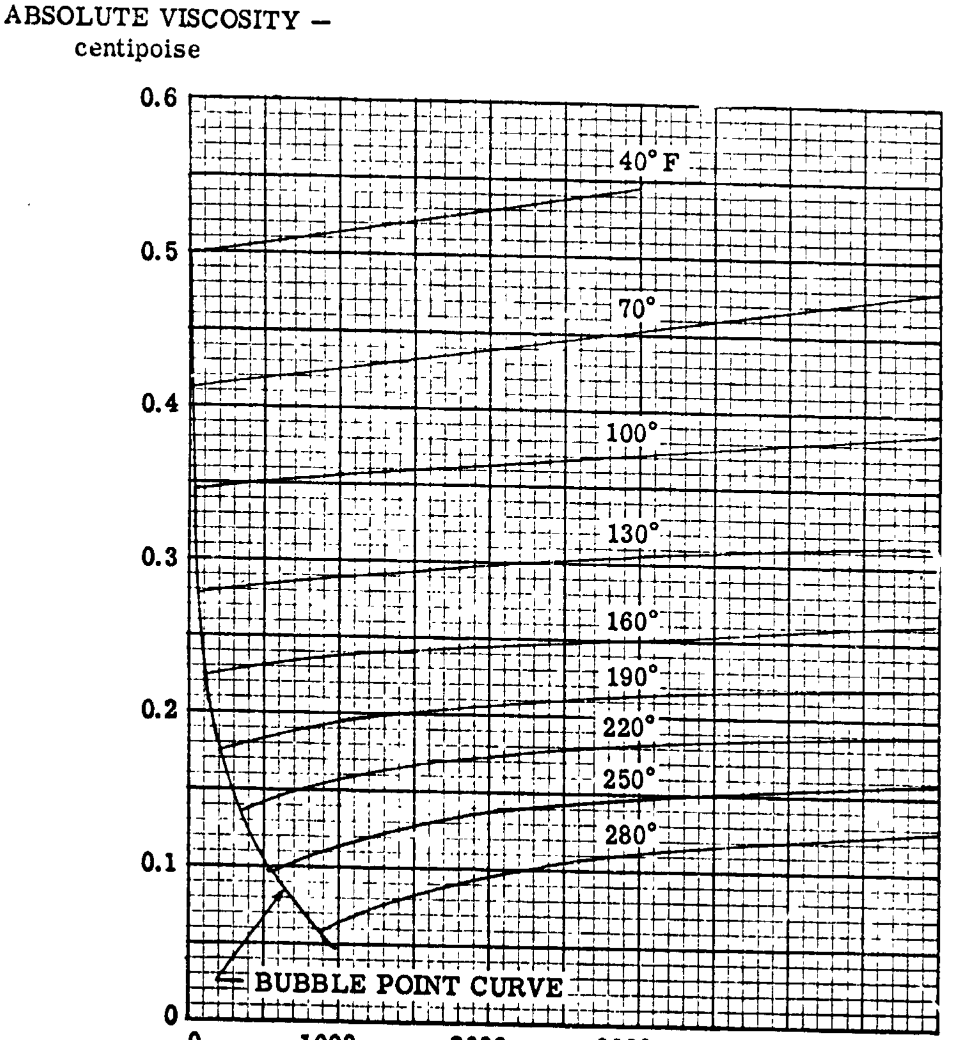

(Reference 5)

Figure 3.6. Effect of Pressure on Viscosity, Liquid N_2O_4

3.6 SPECIFIC HEAT

Table 3.7 contains experimental specific heat data for N_2O_4. Figure 3.7 is a plot of these points, as well as calculated points obtained by T. F. Morey (Reference 9).

TABLE 3.7

SPECIFIC HEAT OF LIQUID N_2O_4

Temperature (°F)	Specific Heat (BTU/lb-°F)
20.5	0.3564
27.0	0.3578
36.1	0.3598
48.6	0.3624
56.8	0.3652
64.8	0.3667

(Reference 8)

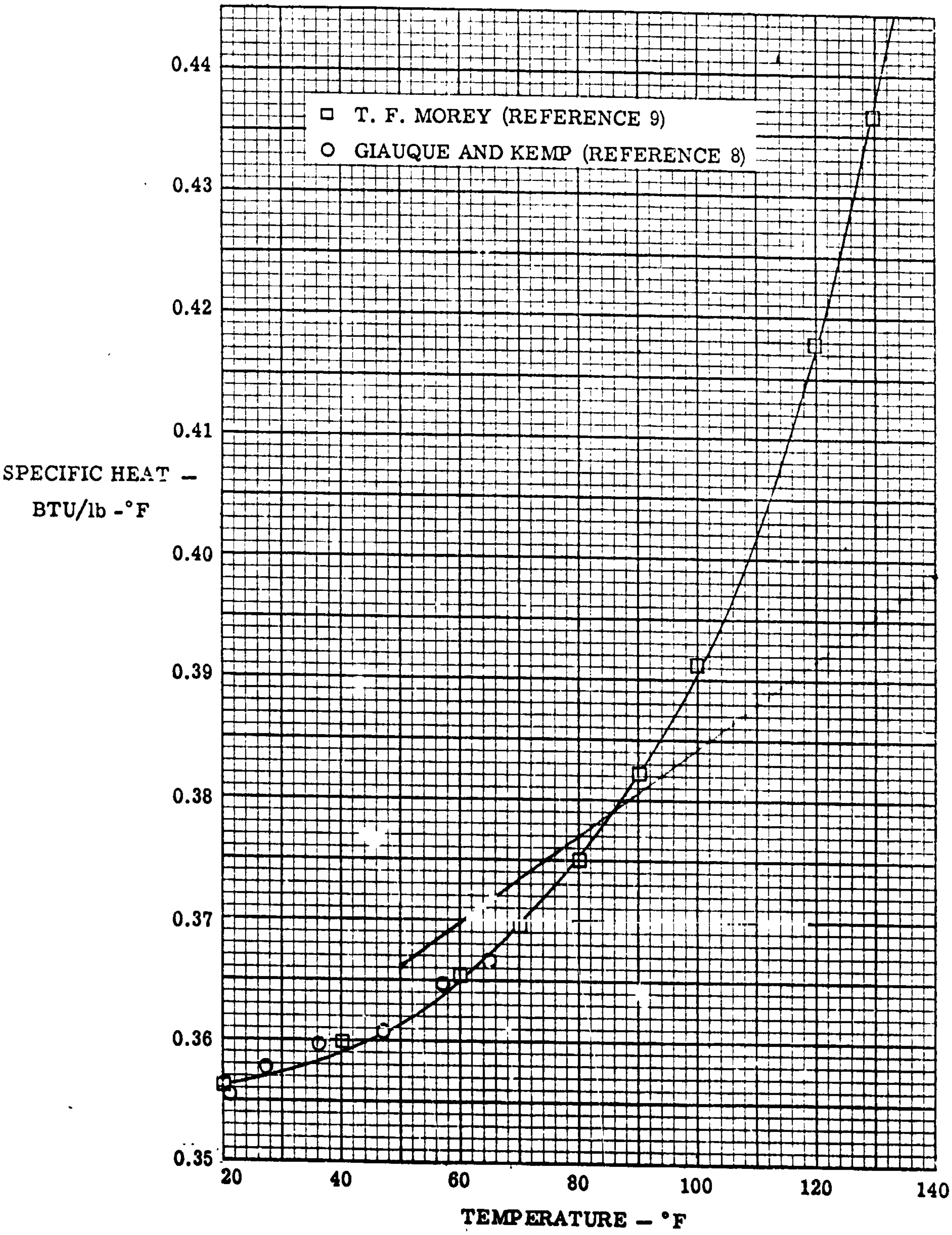

Figure 3.7. Specific Heat of Liquid N_2O_4

3.7 SOLUBILITY OF PRESSURIZING GASES

The solubility of nitrogen and helium in N_2O_4 was determined using the apparatus shown in Reference 2 and the procedure described in Reference 3. Results of these tests are presented in Table 3.8.

TABLE 3.8

SOLUBILITY OF NITROGEN AND HELIUM IN LIQUID N_2O_4

Pressurizing Gas	Temperature (°F)	Solubility (wt %)	Total Gas Pressure (psia)
Nitrogen	70	0.20 ±0.01	63.7
	32	0.14 ±0.01	64.2
Helium	73	0.04 ±0.01	54.3
	32	0.02 ±0.01	55.4

(Reference 4)

(CONT'D)

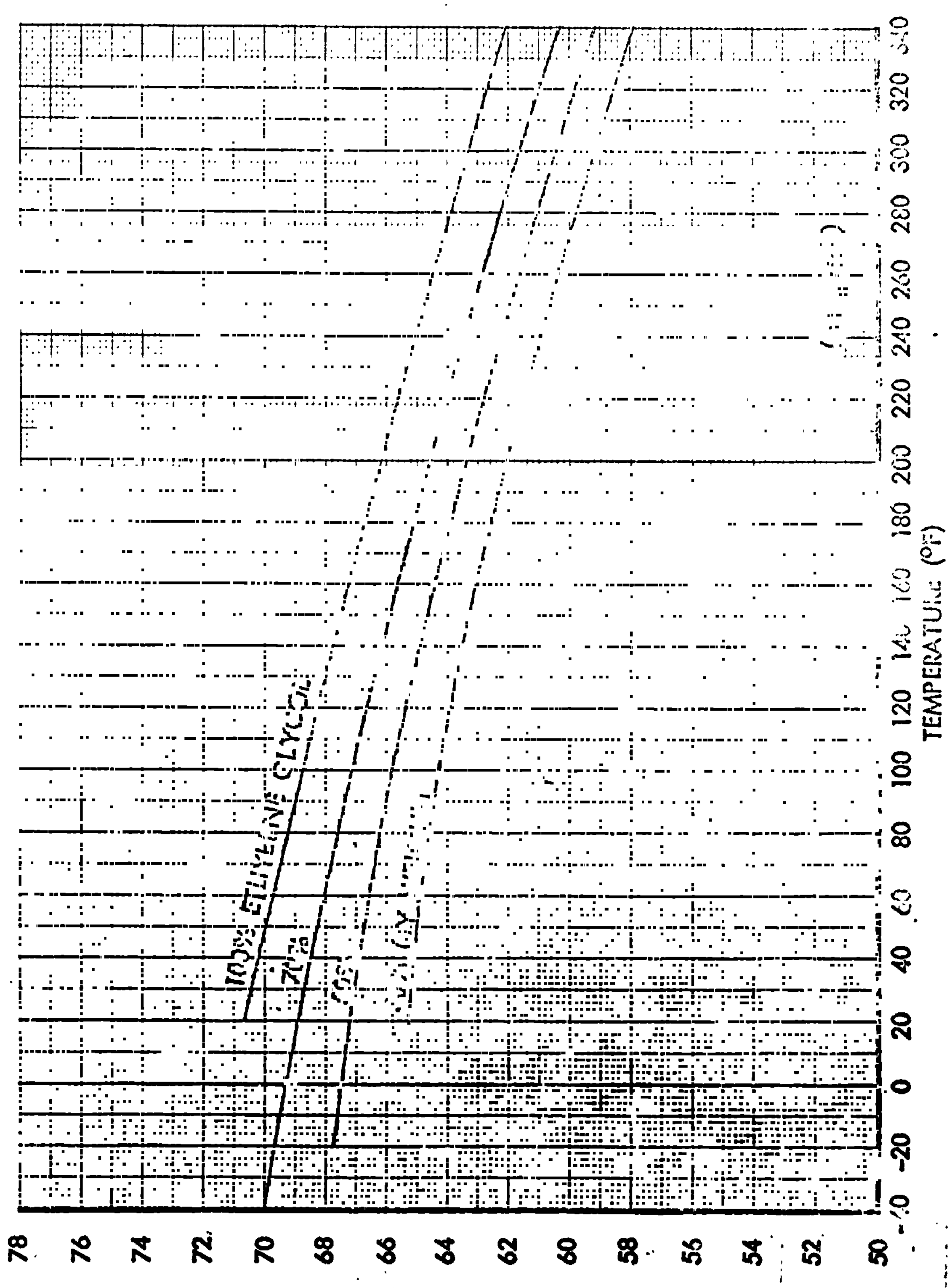

FIGURE 2C-27 AQUEOUS ETHYLENE GLYCOL SOLUTIONS

Part C PROPERTIES OF LIQUIDS
(CONT'D)

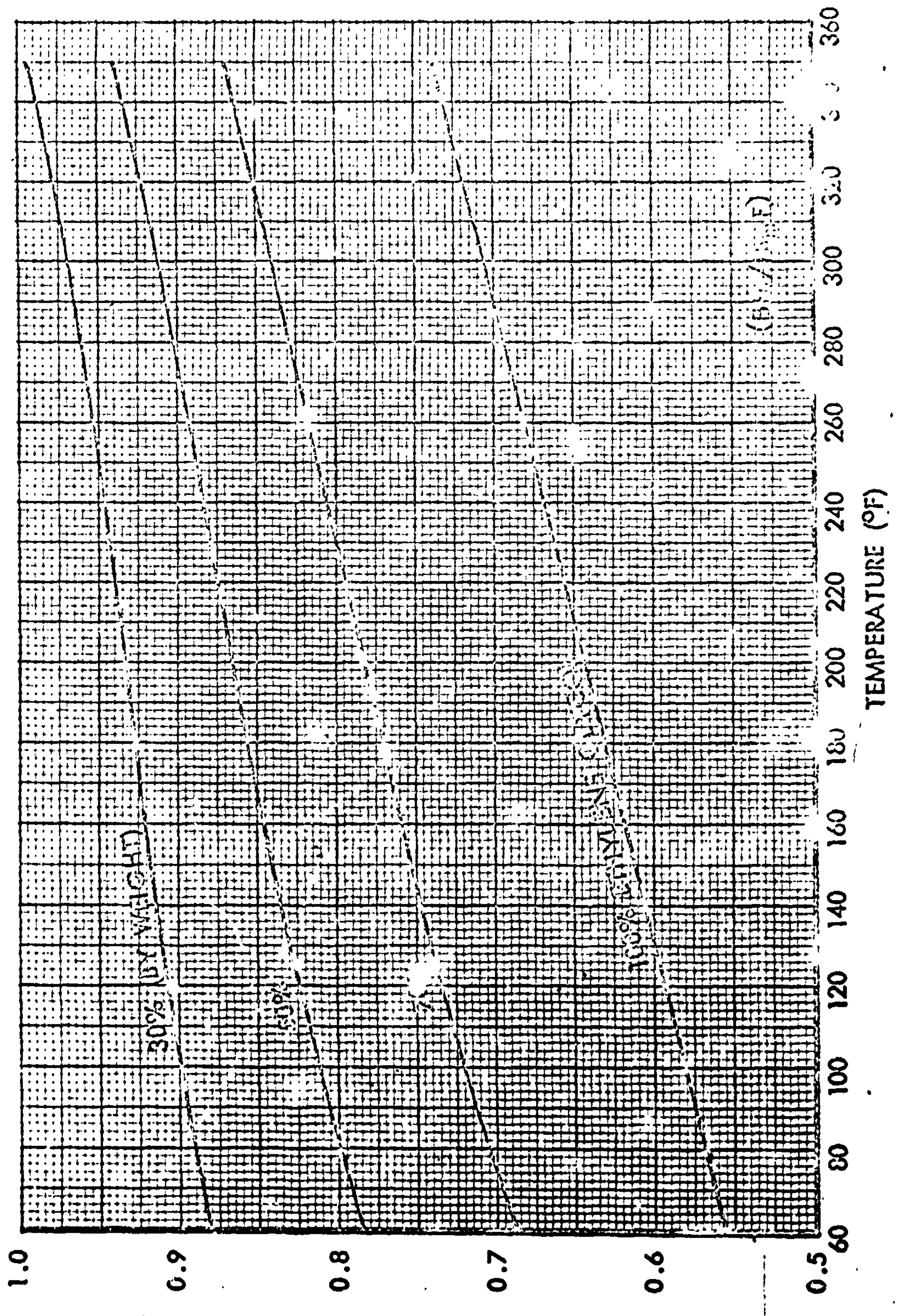

FIGURE 2C-28 SPECIFIC HEAT OF AQUEOUS ETHYLENE GLYCOL SOLUTIONS

C_p

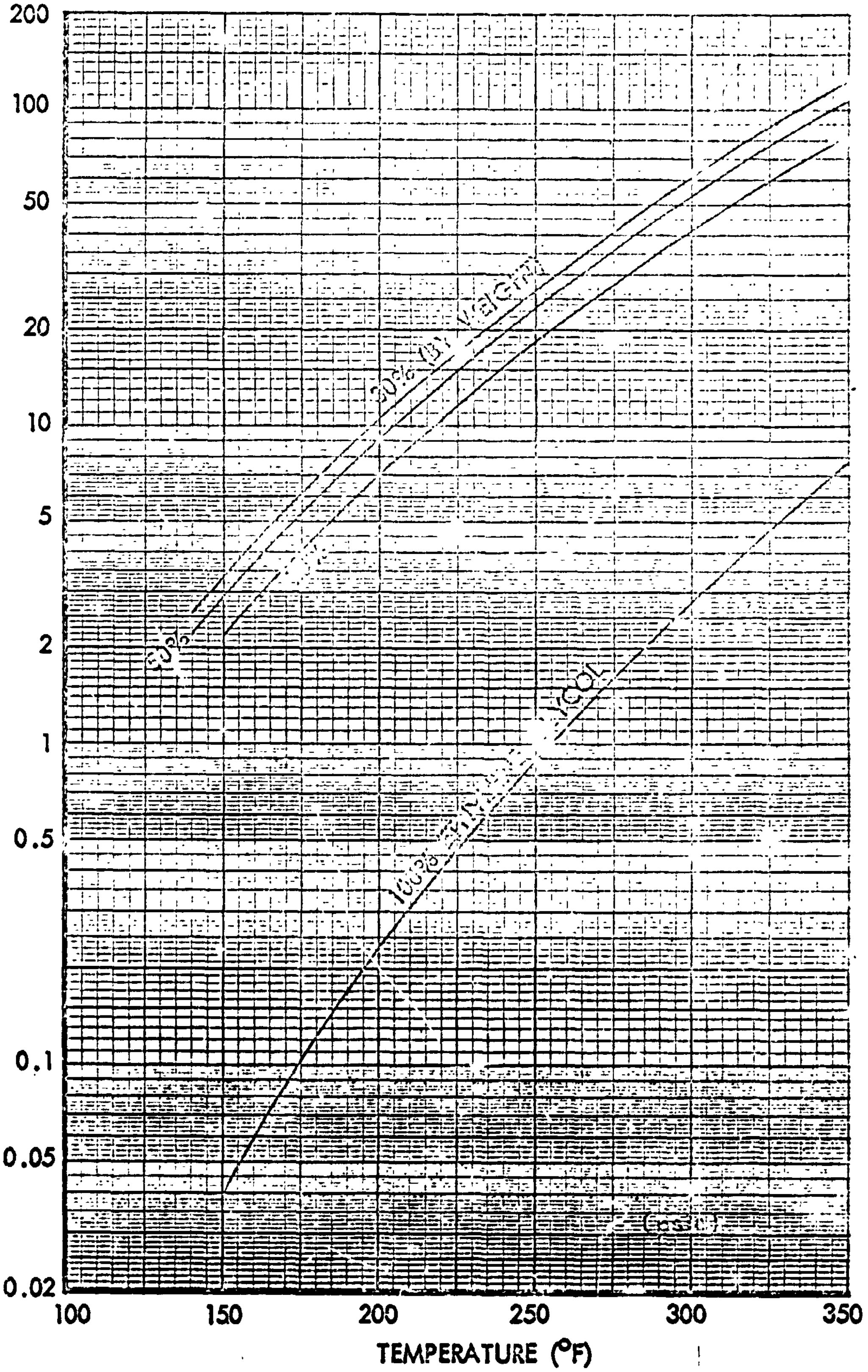

FIGURE 2C-29 VAPOR PRESSURE OF AQUEOUS ETHYLENE GLYCOL SOLUTIONS

(CONT'D)

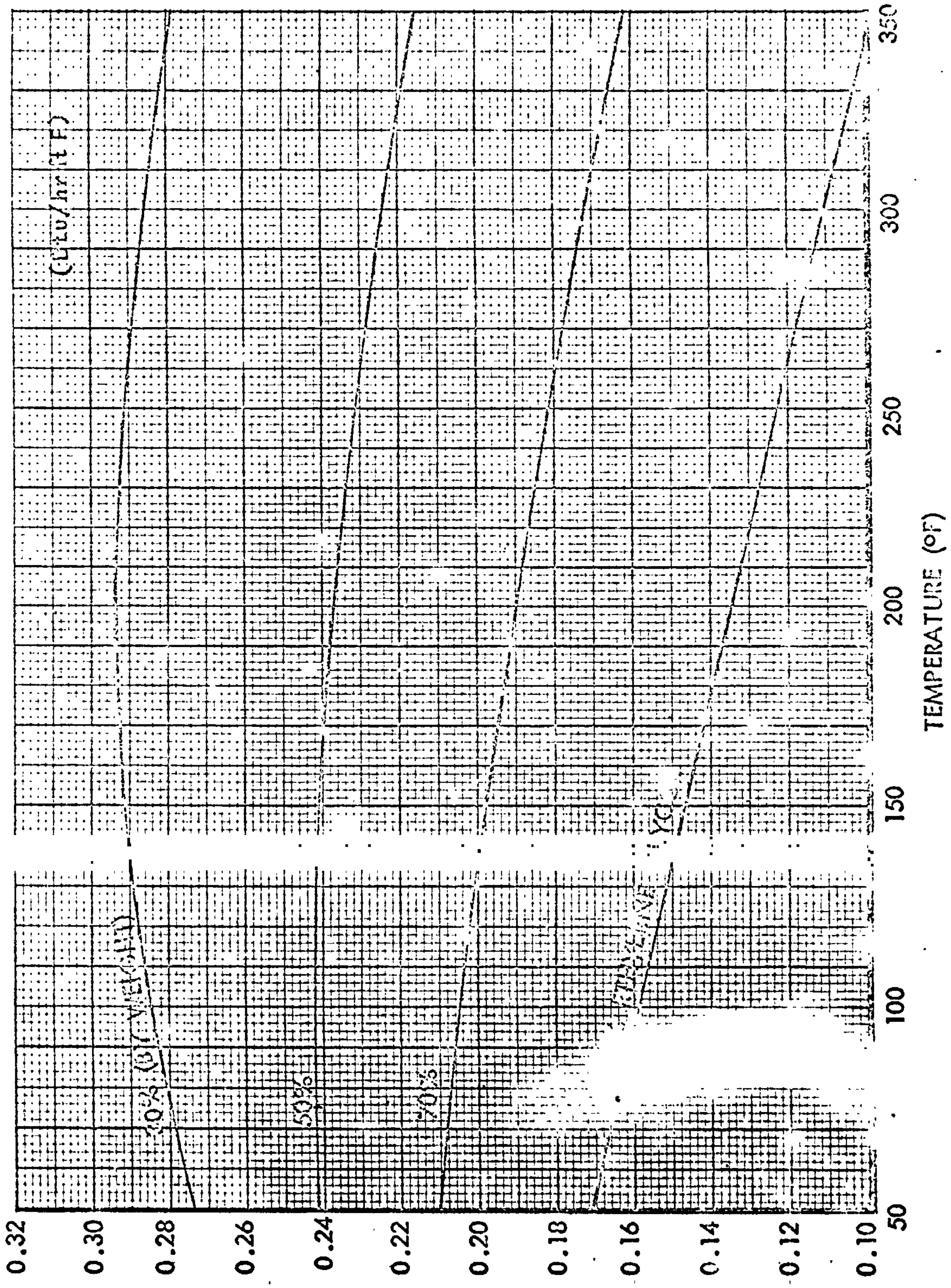

FIGURE 2C-30 THERMAL CONDUCTIVITY OF AQUEOUS ETHYLENE GLYCOL SOLUTIONS

Part C PROPERTIES OF LIQUIDS (CONT'D)

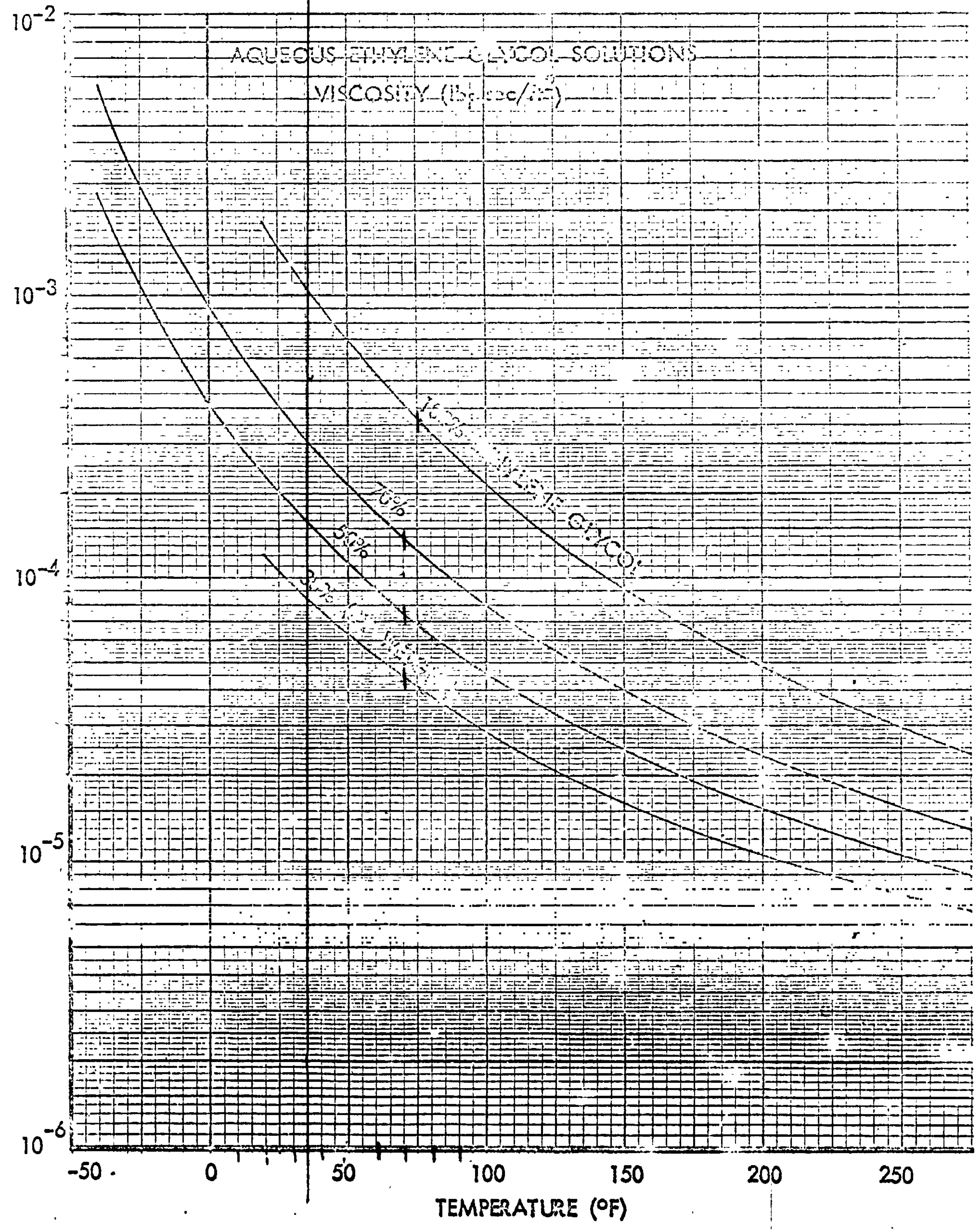

FIGURE 2C-31 VISCOSITY OF AQUEOUS ETHYLENE GLYCOL SOLUTIONS

BLANK PAGE

	Fuel: A-50	Ox: N_2O_4	Freon-11	Freon-113	50% Glycol 50% H_2O	Freon-21	H_2O
$\rho(lb_m/ft^3)$	56.1	89.34	92.12	97.69	66.2	85.28	62
$c_p(Btu/lb_m\text{-}R)$	0.694	0.374	0.209	0.218	0.795	0.256	.98
$\mu(lb_m/ft\text{-}sec)$	5.49×10^{-4}	2.796×10^{-4}	2.82×10^{-4}	4.51×10^{-4}	2.09×10^{-3}	2.29×10^{-4}	6.x10
$k(Btu/hr\text{-}ft\text{-}R)$	0.151	0.0755	0.050	0.038	0.242	0.063	
$\rho c_p(Btu/ft^3\text{-}R)$	39	33.4	19.3	21.3	52.6	21.9	
$\nu(ft^2/sec)$	9.79×10^{-6}	3.13×10^{-6}	3.06×10^{-6}	4.54×10^{-6}	3.16×10^{-5}	2.68×10^{-5}	1×10^{-5}
$a=\frac{k}{\rho c_p}$ (ft^2/hr)	3.87×10^{-3}	2.26×10^{-3}	2.59×10^{-3}	1.78×10^{-3}	4.64×10^{-3}	2.88×10^{-3}	
Cost ($/ft³)	———	———	18.70	53.10	6.40	———	

Table 1. Fluid Properties Evaluated at 1 atm., 77F.

$69.5 \times .56 = 39$

TABLE 3.7. DIELECTRIC CONSTANT OF ETHYLENE GLYCOL-WATER MIXTURES

Ethylene Glycol, % by wt.	Dielectric Constant, 150 meters, esu at				
	20°C.	40°C.	60°C.	80°C.	100°C.
0	80.37	73.12	66.62	60.58	55.10
10	77.49	70.29	63.92	58.02	52.64
20	74.60	67.52	61.20	55.36	50.39
30	71.59	64.51	58.37	52.59	47.56
40	68.40	61.56	55.48	49.81	44.78
50	64.92	58.25	52.30	46.75	41.96
60	61.08	54.53	48.75	43.68	39.13
70	56.30	50.17	44.98	40.19	35.94
80	50.64	45.45	40.72	36.36	32.52
90	44.91	40.43	36.35	32.58	29.27
100	38.66	34.94	31.58	28.45	25.61

commercial product rather than on the pure chemical. A survey of the available data indicates that ethylene glycol has a flash point of 240°F. and a fire point of 250°F. The variations in the results of several investigators[41, 45, 46, 47] do not exceed the tolerance of 5°F. customary for these tests. The flash and fire points of aqueous solutions of ethylene glycol are shown in Table 3.8.[41]

Other flammability data for ethylene glycol and its aqueous solutions have been reported. Thompson[48] determined values ranging from 780 to 975°F. for the "apparent ignition temperature in air" of ethylene glycol. The results of experiments performed by the Bureau of Standards[41] and by Sullivan, Wolfe, and Zisman[47] on the spontaneous ignition temperatures of ethylene glycol and its aqueous solutions are summarized in Table 3.8. Results of spray flammability and incendiary bullet tests by these same investigators[47] are also listed in Table 3.8.

Duggan and Green[49] investigated the flammable characteristics of aqueous ethylene glycol solutions. They found that inhibited ethylene glycol anti-freeze solutions containing as low a concentration of water as 40 per cent by volume (freezing point −62°F.) did not burn when sprayed onto wood or gasoline fires. In fact, such solutions acted as control and extinguishing agents. The National Bureau of Standards[50] found that inhibited ethylene glycol-water solutions were nonflammable when sprayed on a hot engine exhaust manifold.

Freezing Point

The accurate determination of the freezing point of ethylene glycol is

TABLE 3.8. FLAMMABILITY VALUES FOR ETHYLENE GLYCOL AND ITS AQUEOUS SOLUTIONS

Ethylene Glycol, % by wt.	Flash Point, °F.[a]	Fire Point, °F.[b]	Spontaneous Ignition Temperature, °F. Ref. 41		Spontaneous Ignition Temperature, °F. Ref. 47	Spray Flammability Limits, % Oxygen[d]	Incendiary Fire Test Flame Height, Feet[e]
100	245	250	750	1170	856	40	3 to 8
95	260	270					
90	270	280			862		
85	[c]						3
80			770	1200	871	48	
75							1
70					880		
65					885	67	2
60			790	1230	892		no flame
50					903	>80	
40			815	1270			
20			810	1350	956		

[a] Approximately the same results were obtained with two open cup instruments (Cleveland, Tag) and two closed cup instruments (Pensky-Martens, Tag). [b] Determined with a Cleveland open cup instrument. [c] Solutions containing not more than 85 per cent ethylene glycol by weight boil actively on continued heating and the test flame is extinguished. [d] Minimum amount of oxygen required in an oxygen-nitrogen stream to cause the ignition of a fine spray of the solution by means of an electric arc. [e] Height of flame produced by fragments of an incendiary bullet piercing and bursting a 1-gallon container of the liquid.

complicated by the high viscosity of the liquid near the freezing temperature. This condition tends to cause supercooling of the liquid, making equilibrium between liquid and solid phase difficult to attain. The most probable value for the freezing point is − 13°C. (+ 8.6°F.), which is an average of the more reliable values given in the literature[10, 18, 32, 36, 39, 41, 51, 52, 53, 54, 55].

Ethylene glycol and water form a eutectic mixture in the range 58 to 80 per cent glycol by weight, although the exact eutectic composition and temperature have not been accurately defined. Solutions up to 58 per cent by weight form ice crystals on cooling to the freezing point. A nonrigid "slush" formation results. Solutions in the 80 to 100 per cent glycol range form ethylene glycol crystals upon freezing. Such solutions have a pronounced tendency to "supercool" or remain liquid at temperatures below their true freezing point.

Ethylene glycol solutions in the 0 to 58 per cent range in general expand continuously from their freezing points to −54°F. There is some evidence that the more dilute solutions go through a maximum volume and then contract a little on cooling to −54°F. Solutions in the 80 to 100 per cent range contract continuously on cooling below their freezing points.

The average of freezing point values reported by Carbide, Dow, Du Pont, and the National Bureau of Standards is given in Table 3.9. Data are not included for the range 58 to 80 per cent ethylene glycol for the reasons stated above. Figures 3.6 and 3.7 show the relationship between these freezing point data and the specific gravity of aqueous ethylene glycol solutions. "Solution temperature" in Figure 3.7 means the temperature at which the specific gravity of the solution is determined. Such data are commonly used to indicate the protection carried in automotive cooling systems when the temperatures of the sample taken may vary from the freezing point to the boiling point of water.

Mixtures of ethylene glycol and diethylene glycol have been used on a limited scale in anti-freeze preparations. Diethylene glycol is, however, a solvent for the nitrocellulose in auto paint finishes. The glycol mixtures,

TABLE 3.9. Freezing Points of Aqueous Solutions of Ethylene Glycol

Ethylene Glycol		Freezing Point		Ethylene Glycol		Freezing Point	
% by wt.	% by vol.	°C.	°F.	% by wt.	% by vol.	°C.	°F.
0	0.0	0.0	32.0	40	37.8	−24	−11
2	1.8	−0.6	30.9	42	39.8	−26	−15
4	3.6	−1.3	29.7	44	41.8	−28	−18
6	5.4	−2.0	28.4	46	43.8	−31	−23
8	7.2	−2.7	27.0	48	45.8	−33	−27
10	9.1	−3.5	25.6	50	47.8	−36	−32
12	10.9	−4.4	24.0	52	49.8	−38	−37
14	12.8	−5.3	22.4	54	51.9	−41	−42
16	14.6	−6.3	20.6	56	53.9	−44	−48
18	16.5	−7.3	18.8	58	56.0	−48	−54
20	18.4	−8	17	80	78.9	−47	−52
22	20.3	−9	15	82	81.0	−43	−46
24	22.2	−11	12	84	83.1	−40	−40
26	24.1	−12	10	86	85.2	−36	−33
28	26.0	−13	8	88	87.3	−33	−27
30	28.0	−15	5	90	89.4	−29	−21
32	29.9	−17	2	92	91.5	−26	−15
34	31.9	−18	−1	94	93.6	−23	−9
36	33.8	−20	−4	96	95.8	−19	−3
38	35.8	−22	−7	98	97.9	−16	+3
				100	100.0	−13	+9

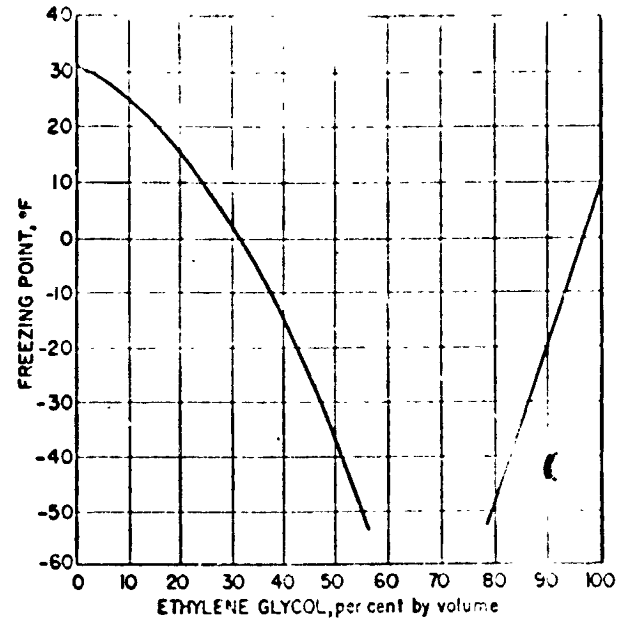

FIGURE 3.6. Freezing point vs. volume per cent for aqueous solutions of ethylene glycol.

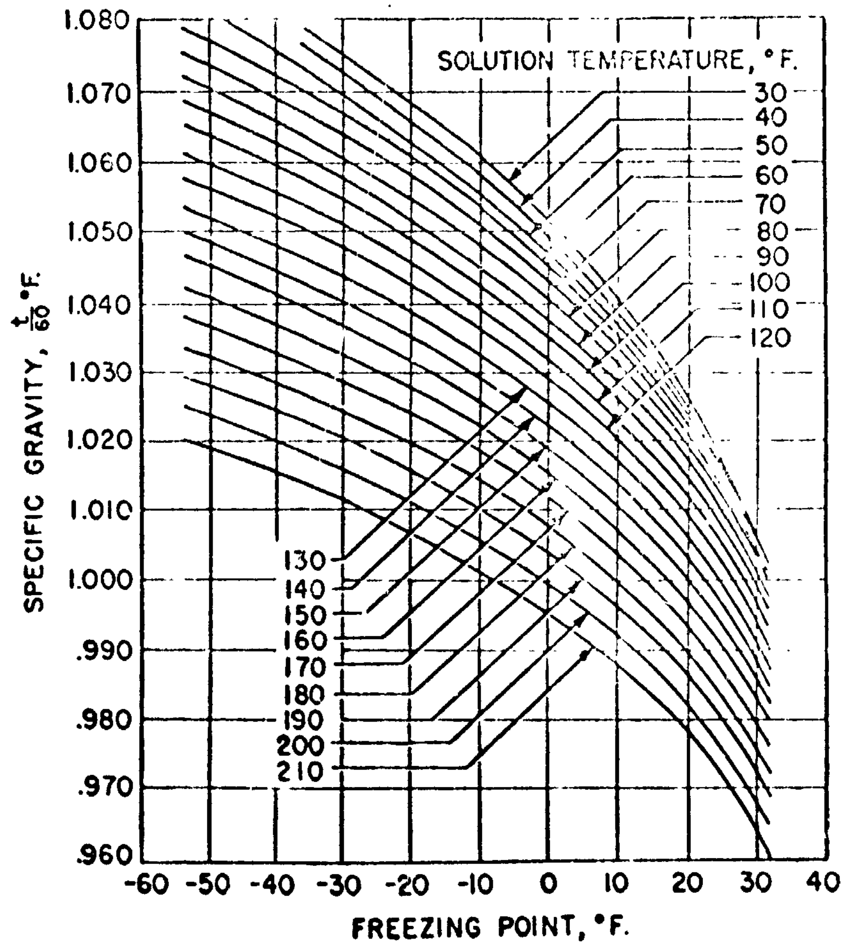

FIGURE 3.7. Freezing points of aqueous ethylene glycol solutions vs. specific gravities at various temperatures.